PETROLOGISCHE UND GEOCHEMISCHE UNTERSUCHUNGEN AN ALKALINEN, PERALKALINEN UND AGPAITISCHEN MAGMATITEN DER MITTELPROTEROZOISCHEN GARDAR-PROVINZ, SÜDGRÖNLAND.

Dissertation

zur Erlangung des Grades eines Doktors der Naturwissenschaften

der Geowissenschaftlichen Fakultät

der Eberhard-Karls-Universität Tübingen

vorgelegt von

MICHAEL MARKS

aus Lahr/Schwarzwald

2003

Tag der mündlichen Prüfung:	22. Dezember 2003
Dekan:	Prof. Dr. Dr. h. c. M. Satir
1. Berichterstatter:	Prof. Dr. G. Markl
2. Berichterstatter:	Prof. Dr. H. Keppler

INHALTSVERZEICHNIS

Einführung 1

Geologischer Rahmen 2

Erweiterte Zusammenfassung der Publikationen 3

Literatur 12

Anhang 19

Kapitel 1: Petrologische und isotopengeochemische Untersuchungen an Ganggesteinen der Isortoq Region

Kapitel 2: Petrologische und isotopengeochemische Untersuchungen an alkalinen bis peralkalinen Gesteinen der Puklen Intrusion

Kapitel 3: Isotopengeochemische Untersuchungen an alkalinen bis agpaitischen Gesteinen der Ilímaussaq Intrusion.

Kapitel 4: Vergleichende petrologische Untersuchungen zwischen Gesteinen der Ilímaussaq Intrusion und einem assoziierten agpaitischen Ganggestein.

Kapitel 5: Spurenelementuntersuchungen an mafischen Mineralen (Amphibole, Pyroxene) dreier verschiedener Alkaligesteinsintrusionen der Gardar Provinz.

DANKSAGUNGEN

An dieser Stelle möchte ich Prof. Gregor Markl danken, der dieses Projekt initiierte und mir dadurch ermöglichte, die Thematik dieser Arbeit in den letzten drei Jahren zu bearbeiten. Viele Ergebnisse der vorliegenden Dissertation gehen auf Anregungen seinerseits zurück. Für eine große Zahl inspirierender Diskussionen bin ich ihm ebenso dankbar, wie für sein immer währendes Interesse an den Ergebnissen und dem Fortgang dieser Arbeit. Prof. Hans Keppler danke ich für die freundliche Übernahme des Koreferats.

Prof. Thorsten Vennemann (Lausanne), Privatdozent Dr. Wolfgang Siebel (Tübingen) und Privatdozent Dr. Thomas Wenzel (Tübingen) danke ich für zahlreiche Diskussionen und Impulse, für ihre kollegiale Hilfe und für ihre kritische Durchsicht der Manuskripte. Für die teils technische, teils fachliche Unterstützung bei der Vorbereitung und Durchführung verschiedener analytischer Verfahren danke ich unter anderem Dr. Mathias Westphal (Mikrosonde), Dr. Bruce Patterson (Laser ICP-MS), Gaby Stoscheck (Stabile Isotope), Elmar Reiter (Radiogene Isotope) und Gisela Bartholomä (Mineralseparation). Für die Herstellung von möglichst reinen Mineralseparaten durch Handauslesen am Binokular danke ich Jasmin Köhler, die mich damit sehr entlastet hat. Ulrich Alt-Epping danke ich für die Hilfe bei verschiedenen Berechnungen mit der MATLAB Software. Bei allen Kollegen und Mitarbeiter am Institut möchte ich mich hiermit für die vielen kleinen und großen Hilfen bedanken die sie mir zukommen ließen. Besonderer Dank gilt Frau Dagmar Dimitrovice.

Ein dickes Dankeschön auch an meinem Mitstreiter Dipl. Geol. Ralf Halama, der mir immer ein angenehmer und freundlicher Zimmerkollege war. Besonders die Geländearbeit im Sommer 2001 zusammen mit ihm war einfach eine tolle Zeit. Ich wünsche ihm alles Gute für seine weitere Zukunft!

Neben diesen kollegialen Hilfe haben meine privaten Freunde ebenso großen Anteil an dem erfolgreichen Abschluss dieser Arbeit. Sie haben mich durch die Jahre begleitet und mich oft - ohne es selbst zu bemerken - immer wieder moralisch unterstützt und gaben mir dadurch neue Kraft. Danke an euch alle. Insbesondere Dir, Babette schulde ich großen Dank für Ablenkung, für Entspannung, für Solidarität und für deine schier unendliche Geduld mit mir in Zeiten, in denen ich mal wieder nicht abschalten konnte. Es gibt viel nachzuholen!

Den größten Dank jedoch möchte ich meinen Eltern aussprechen. Über viele Jahre hinweg helfen sie mir jetzt schon, meine Ideen und Träume zu verwirklichen. Wann immer es ihnen möglich war und ist konnte und kann ich mir ihrer Unterstützung sicher sein. In unzähligen Situationen konnte ich auf sie zählen – danke für dieses bemerkenswertes Maß an Vertrauen!

EINFÜHRUNG

Die vorliegende Arbeit entstand im Rahmen des von der DFG geförderten Projektes *„Differentiationsprozesse alkalischer bis peralkalischer Magmen, untersucht an Intrusivkomplexen der Gardar-Provinz in Südgrönland“* (Antragsteller Prof. G. Markl). Auf der Grundlage einer integrierten Bearbeitung von unterschiedlich stark differenzierten Magmatiten der Gardar-Provinz in Südgrönland sollten mit Hilfe moderner mineralogischer, petrologischer, geochemischer und isotopengeochemischer Methoden unter anderem folgende Fragestellungen bearbeitet werden:

- Welche Phasengleichgewichte bestimmen die Differentiation von alkalibasaltischen zu alkaligranitischen, alkalisyenitischen und agpaitischen Magmen (molares (Na+K)/Al Verhältnis > 1.2; Ussing, 1912; Sørensen, 1997) und wie werden diese von intensiven Parametern wie a_{SiO2}, a_{H2O}, a_{NaCl} und f_{O2} beeinflusst?
- Welchen Einfluss haben die beiden konkurrierenden Prozesse der fraktionierenden Kristallisation und der krustalen Kontamination auf diese Differentiationsprozesse und welche Schmelzen sind die Ursprungsschmelzen für die Alkali-Granitoide der Gardar-Provinz?
- Wie entwickeln sich spätmagmatische, wässrige Fluide in peralkalinen Systemen nach ihrer Entmischung aus der Schmelze? Ist die Fenitisierung bzw. autometasomatische Überprägung um und in Alkali-Komplexen durch magmatische und/oder meteorische Fluide verursacht?

Schließlich lag es nahe, die gewonnenen Ergebnisse mit anderen Granitoid-Typen zu vergleichen und mögliche generelle Grundlagen der Entmischung von Fluidphasen aus granitischen Schmelzen zu erkennen. Durch einen Vergleich und die Vernetzung der Ergebnisse an den verschiedenen Gesteinen und Gesteinskomplexen sollten quantitative Aussagen über die jeweilige Bedeutung der beteiligten Prozesse getroffen werden. Die Ergebnisse dieser Dissertation sind dabei nicht nur von regionaler Bedeutung für die Gardar-Provinz, sondern tragen allgemein zum besseren Verständnis der Genese und Differentiation alkalischer Magmen in Riftzonen bei.

Die vorliegende Arbeit umfasst 5 Kapitel, ein jedes davon entspricht einem zur Veröffentlichung bei einer internationalen Fachzeitschrift eingereichten oder bereits im Druck befindlichen Manuskript. Der nun folgenden erweiterten Zusammenfassung und jedem Einzelkapitel im Anhang ist ein spezifisches Literaturverzeichnis angeschlossen, um das Auffinden der verwendeten Literatur zu erleichtern.

GEOLOGISCHER RAHMEN

Mit dem Ausgang des späten Archaikums und dem damit verbundenen schnellen und massiven Wachstum der kontinentalen Kruste unter Bildung großer kontinentaler Schilde wurden kontinentale Riftzonen mehr und mehr ein prägendes tektonisches Element der kontinentalen Kruste. Mit die frühesten magmatischen Produkte, die auf beginnendes kontinentales Auseinanderbrechen (Rifting) im frühen Proterozoikum hindeuten sind unter anderem der „Great Dyke“ in Zimbabwe (2461 ± 16 Ma; Podmore & Wilson, 1987; Wilson & Prendergast, 1989) und verschiedene mafische Gangschwärme in Schottland und dem südlichen Kanadischen Schild (2.4 bis 2.1 Ga; Nelson et al., 1990; Chapman, 1979; Southwick & Day, 1983). Während des weiteren Verlaufs des Proterozoikums können dann drei Hauptphasen des kontinentalen Riftings zwischen 2.0 und 1.8 Ga, 1.2 und 0.9 Ga und 0.8 und 0.6 Ga unterschieden werden. Im Verlauf des späten Proterozoikums setzte dann eine Phase ein, in der ein weltweites stark verbreitetes Auseinanderbrechen der Kontinente zu verzeichnen ist („continental breakup“), bevor sich dann die einzelnen Fragmente während des Paläozoikums in Gondwanaland und Pangäa wieder reorganisierten.

Südgrönland entwickelte sich in einem kontinentalen Setting, das während der ketilidischen Orogenese (1900-1700 Ma) deformiert wurde. Während der Subduktion ozeanischer Kruste unter den nördlich gelegenen Archaischen Kraton kam es zur Platznahme des I-Typ granitischen Julianehåb Batholiths (Garde et al., 2002), der das heutige Grundgebirge Südgrönlands darstellt. Die Gardar-Provinz in Südgrönland stellt eine Schwächezone innerhalb des ketilidischen Orogens am Südrand des archaischen Kratons dar. Sie repräsentiert eine kontinentale Riftzone, die zeitlich in die zweiten der oben genannten Hauptphasen zu stellen ist. Im Zeitraum zwischen 1350 – 1140 Ma kam es in ca. 120 x 50 km großen Gebiet zu einem intensiven Alkalimagmatismus. Der Aufstieg und die Platznahme der Schmelzen ist zum überwiegenden Teil an ältere ketilidische Strukturen gebunden (Emeleus & Upton, 1976). Die magmatischen Produkte der Gardar Periode bestehen aus alkalibasaltischen bis rhyolitischen subaerischen Vulkaniten mit zwischengeschalteten klastischen Sedimenten (Eriksfjord Formation; Poulsen, 1964), einer Vielzahl vor allem doleritischer bis syenitischer Ganggesteine und zwölf unterschiedlich großer Alkaligesteinsintrusivkomplexe.

Vor allem in den basaltischen Ganggesteinen der Gardar-Provinz tritt eine große Zahl von Feldspatmegakristallen und Anorthosit-Xenolithen auf (Bridgwater, 1967; Bridgwater & Harry, 1968; Halama et al., 2002). Das weit verbreitete Vorkommen solcher Xenolithe in der gesamten

Gardar-Provinz gilt als Hinweis für die Bildung eines großen Anorthosit Körpers in der Tiefe (Bridgwater, 1967; Bridgwater & Hary, 1968; Halama et al., 2002), dessen abgeschätze Größe mit der des ebenfalls mittelproterozoischen Nain Anorthosit-Komplexes in Labrador (Hill, 1988), der ähnlich wie die Gesteine der Gardar-Provinz einem extensionalen Regime zugeschrieben wird (z.B. Emslie, 1980; Morse, 1982), vergleichbar ist. Das etwa zeitgleiche Auftreten von mafischen Gangschwärmen und Alkaligesteinsintrusionen in Nordostkanada und Labrador (z.B. LeCheminant & Heaman, 1989; Cadman et al., 1993; Mitchell & Platt, 1982; Heaman & Machado, 1992) und die vergleichbaren tektonischen Großeinheiten des kanadischen und grönlandischen Präkambriums belegen die enge Beziehung dieser Provinzen zueinander. Druckabschätzungen für die Platznahme der kanadischen Anorthosite schwanken zwischen 3 und 5 kbar (Fuhrmann et al., 1988; Kolker & Lindsley, 1989), während entsprechende Abschätzungen für die Gardar Gesteine etwa 1 kbar anzeigen (Poulsen, 1964; Konnerup-Madsen & Rose-Hansen, 1984). Die Gardar Provinz in Südgrönland kann also als ein in einem höheren Krustenstockwerk aufgeschlossenes Segment des kanadischen Schildes gedeutet werden.

Eine der ersten Arbeiten über die Geologie Südgrönlands lieferte Wegmann (1938). Er prägte den heute noch allgemeingültigen Namen der Gardar Periode, in Ahnlehnung an das alte norwegischen Bistum *Garður*, das sich im Bereich des heutigen Ortes Igaliko in Südgrönland befand. Zusammenfassende Arbeiten über die Gardar Provinz stammen von Upton (1974), Emeleus & Upton (1976), Upton & Emeleus (1987), Kalsbeek et al. (1990) und Upton et al. (2003). Letztere gibt unter anderem einen detaillierten Überblick über die aktuellen geochronologischen Daten der Gardar Gesteine.

ERWEITERTE ZUSAMMENFASSUNG DER PUBLIKATIONEN

Kapitel 1 stellt die Ergebnisse einer petrologischen und isotopengeochemischen Studie an relativ primitiven Ganggesteinen der Isortoq-Region im Westen der Gardar-Provinz zusammen. Die untersuchten Ganggesteine sind Teil eines der beiden großen WSW - ONO streichenden Gardar-Gangschwärme in Südgrönland. Der Gangschwarm besteht aus verschiedenen Generationen gabbroischer bis syenitischer Gänge mit sehr unterschiedlichen Mächtigkeiten zwischen wenigen Zentimetern bis mehreren hundert Metern. Ungewöhnlich ist das Auftreten mehrerer so genannter „Giant Dikes“, die die jüngste Ganggeneration darstellen und Mächtigkeiten bis ca. 800m aufweisen (Bridgwater & Coe, 1969). Diese Giant Dikes treten an verschiedenen Stellen in der Gardar-Provinz auf und sind teilweise über 30 km weit aufgeschlossen (z.B. Upton et al., 1985; Upton & Thomas, 1980). Sie bestehen oft aus recht primitiven gabbroiden Rand- und (Nephelin-

oder Quarz-) syenitischen Zentralbereichen und können daher als Übergang zwischen mafischen Ganggesteinen und den salischen Alkaligesteinsintrusionen angesehen werden. Vergleichbare Beispiele solcher mächtiger Ganggesteine sind weltweit nur sehr selten bekannt. Allenfalls die proterozoischen Giant Dykes Zentralschwedens (Krokström, 1936; Lopez-Montano, 1986) zeigen vergleichbare Charakteristika. Der gesamte Ganggschwarm stellt möglicherweise den Untergrund eines großen vulkanischen Feldes dar, vergleichbar etwa mit den phanerozoischen vulkanischen Lineamenten Äthiopiens (Barbieri & Varet, 1970) und Saudi Arabiens (Camp et al., 1989).

Mafische Gangschwärme sind weit verbreitet im Proterozoikum und zeigen zweifelsohne ein extensionales Regime an (z.B. Tarney & Weaver, 1987). Die Untersuchung solcher rift-gebundener Gangschwärme kann Aufschluss geben über die Prozesse, die zur Bildung und Entwicklung solcher enormen Mengen an mafischen Schmelzen führen und ermöglicht prinzipiell die Identifizierung der beteiligter Mantelquellen (Ernst & Buchan, 1997; 2001; Devey & Cox, 1987; Peng et al., 1994). In verschieden Arbeiten wurde allerdings gezeigt, dass Mantelschmelzen sowohl bei ihrer Fraktionierung in tiefkrustalen Magmenkammern als auch beim Aufstieg durch die Kruste zu einem gewissen Grade chemisch und isotopisch verändert werden können (z.B. Mohr, 1987; Lightfoot et al., 1991; O´Hara & Herzberg, 2002). Da die Ganggesteine der Isortoq-Region ein großes Spektrum an Gesteinen gabbroischer, syenitischer und larvikitischer Zusammensetzung abdecken, sind diese sehr gut dazu geeignet die wechselnde Rolle von fraktionierender Kristallisation und krustaler Assimilation (AFC-Prozesse; DePaolo, 1981) zu studieren und den Einfluss von krustaler Kontamination auf die chemische und isotopische Zusammensetzung der mafischen Mutterschmelzen zu untersuchen.

Die detaillierte Untersuchung der Entwicklung der chemischen Zusammensetzung der wichtigsten Mineralphasen der Isortoq-Ganggesteine (Olivin, Klinopyroxen, Fe-Ti Oxide und Plagioklas) und darauf basierende phasenpetrologischen Berechnungen zeigen, dass fraktionierende Kristallisation dieser Mineralphasen eine bedeutende Rolle bei der Genese der verschiedenen Gesteinstypen spielt. Vor allem für die untersuchten Giant Dikes kann davon ausgegangen werden, dass diese im geschlossenen System von einer randlich ausgebildeten gabbroiden Fazies hin zu einer syenitischen Fazies im Zentrum fraktionierten. Die O-, Sr-, Nd- und Os-isotopische Untersuchungen an Gesamtgesteinen und Mineralseparaten der verschiedenen Ganggesteine zeigen allerdings auch, dass die Mutterschmelzen der Isortoq-Gesteine zwar ursprünglich aus Mantelregionen stammen, diese jedoch durch unterschiedlich starke Assimilation von krustalem Material chemisch und isotopisch verändert wurde. Der dabei in Frage kommende Assimilant war Plagioklas-reich und ist

isotopisch durch sehr niedrige $^{143}Nd/^{144}Nd$ Verhältnisse und niedrige $^{87}Sr/^{86}Sr$ Verhältnisse zu charakterisieren. Außerdem werden geringe Nb-Gehalte, mittlere $\delta^{18}O$-Werte und stark radiogene Os-isotopische Zusammensetzungen für den Assimilant angezeigt. Diese Beobachtungen können mit der Assimilation partieller Schmelzen von Plagioklas-reichen granulitfaziellen Unterkrustengesteine ähnlich derer des weiter nördlich aufgeschlossenen archaischen Kratons erklärt werden. O- und Nd-Isotopendaten deuten außerdem an, dass die Assimilation von granitischen Oberkrustengesteinen während des Aufstieges und der Platznahme der Ganggesteine hingegen, keine bedeutende Rolle spielte. Diese Ergebnisse sind konsistent sowohl mit seismischen Daten (Dahl-Jensen et al., 1998) als auch mit der Vorstellung der Kontamination von Mantelschmelzen mit Unterkrustenmaterial bei der Anorthosit-Genese (z.B. Ashwal, 1993), was wiederum sehr gut mit der Annahme eines großen Anorthositkörpers im Bereich der Kruste-Mantel Grenze unter der Gardar-Provinz im Einklang steht (Bridgwater, 1967). Eine Quantifizierung der Assimilationsvorgänge wurde mit Hilfe von EC-AFC Moddelierungen vorgenommen (Bohrson & Spera, 2001) und ergab maximal etwa 10 % Unterkrusteneinfluß bei den am stärksten kontaminierten Gesteinen.

Aufgrund der krustalen Kontamination sind die Charakteristika der Mantelquelle der Isortoq-Ganggesteine stark überprägt. Ein bedeutender Einfluss einer klassischen MORB-Quelle kann jedoch aufgrund der Sr- und Nd-Isotopendaten und Spurenelementdaten ausgeschlossen werden. Vor allem die SEE Muster der Klinopyroxene unterscheiden sich ganz klar von denen typischer MOR Basalte, ähneln allerdings ganz stark solcher von gabbroischen Gesteinen, die im Zusammenhang mit dem Island-Plume stehen (Bernstein et al., 1998). Die Entscheidung allerdings, ob es sich bei der Quellregion der Isortoq-Ganggesteine um einen an Spurenelementen angereicherten subkontinentalen lithosphärischen Mantel, um einen Plume-beeinflußten Mantel, oder aber um eine Mischung dieser beiden Komponenten handelt, kann an dieser Stelle aufgrund des nachgewiesenen Einflusses von krustaler Kontamination nicht endgültig getroffen werden.

Kapitel 2 bis 4 beschäftigen sich mit der Petrologie und Geochemie der hochfraktionierten Alkaligesteine der Gardar-Provinz. Hauptziele dieser Arbeiten war zum einen die Untersuchung der relevanten Phasengleichgewichte, die die Differentiation von alkalibasaltischen zu alkalisyenitischen, alkaligranitischen und agpaitischen Magmen bestimmen und deren Abhängigkeit von intensiven Parametern wie T, a_{SiO2}, a_{H2O} und f_{O2} zu quantifizieren. Außerdem sollte geklärt werden, welchen Einfluss krustale Kontamination an der Quelle und während des Aufstiegs für

diese Differentiationsprozesse hat. Weiterhin wurden Fragen zu spätmagmatischen Phänomenen in peralkalinen Schmelzen untersucht.

Innerhalb der zwölf aufgeschlossenen plutonischen Komplexe können prinzipiell zwei unterschiedliche Haupttypen unterschieden werden. Solche, die mit zunehmender Entwicklung einen SiO_2-übersättigten Trend von Syeniten über Quarz-Syeniten zu Alkali-Graniten zeigen und eine Gruppe von Intrusionen, die einem SiO_2-untersättigten Trend von Syeniten bis hin zu stark SiO_2-untersättigten agpaitischen Nephelin-Syeniten folgt. Von den beiden oben angesprochenen Fraktionierungstrends wurde jeweils ein Intrusivkomplex ausgewählt: Der Puklen-Komplex (Kapitel 2) ist mit etwa 4 x 2 km eine der kleinsten Intrusionen der Gardar-Provinz und zeigt grundsätzlich mit zunehmender Fraktionierung einen Trend zur SiO_2-Übersättigung (Pulvertaft, 1961; Parsons, 1972). Die Intrusion besteht aus einer Suite verschiedener Syenite, die von einem sehr homogen erscheinenden Alkaligranit intrudiert wird, der stellenweise auch feinkörnige und leukokrate Varianten (Mikro-Granite) ausbildet. Der Süden der Intrusion besteht aus einem größeren Vorkommen von feinkörnigen und leukograten, quarz-reichen granophyrischen Gesteinen. Die Ilímaussaq-Intrusion (Kapitel 3) entstand aus 3 verschiedenen Magmenschüben und zeigt grundsätzlich mit zunehmender Fraktionierung einen Trend zur SiO_2-Untersättigung (Ferguson, 1964; Larsen, 1976). Den ersten Magmenschub stellt ein schwach untersättigter Augit-Syenit dar, der später von einem peralkalinen Granit intrudiert wird. Der überwiegende Teil der Intrusion jedoch besteht aus stark SiO_2-untersättigten agpaitischen Nephelin-Syeniten. Für alle drei Magmenschübe wird angenommen, dass sie aus einer gemeinsamen, tief liegenden Magmenkammer stammen, die unter hohen Drucken fraktionierte und zu unterschiedlichen Zeiten mehrmals hintereinander angezapft wurde (z. B. Larsen & Sørensen, 1987). Kapitel 4 befaßt sich mit einem peralkaline bis agpaitischen Ganggestein, das sehr starke mineralogische und petrologische Gemeinsamkeiten zur nahe gelegenen Ilímaussaq-Intrusion zeigt.

Schon frühe experimentelle Arbeiten haben gezeigt, dass peralkaline Intrusivgesteine über einen sehr großen Temperaturintervall von teilweise über 1000°C bis <400°C kristallisieren und dass die Entmischung einer fluiden Phase von der Restschmelze erst zu einem sehr späten Stadium erfolgt (Piotrowski & Edgar, 1970; Sood & Edgar, 1970; Edgar & Parker, 1974; Kogarko & Romanchev, 1977; 1982; Scaillet & Macdonald, 2001). Die Bedeutung von fluiden Phasen für die chemische und physikalische Entwicklung von alkalinen und peralkalinen Schmelzen ist unumstritten und die Effekte solcher spätmagmatischen bis hydrothermalen Alkalien-reicher Fluide wurden unter anderem von Salvi & Williams-Jones (1990), Parsons et al. (1991), Boily & Williams-Jones (1995),

Finch et al. (1995), Coulson (1997), Markl (2001), Markl et al. (2001), Markl & Baumgartner (2002) und Chakhmouradian & Mitchel (2002) beschrieben. Peralkaline Schmelzen im allgemeinen scheinen eine stark reduzierte magmatische Fluidphase zu besitzen, die meist reich an Methan und ausgesprochen arm an Wasser und CO_2 ist (z.B. Konnerup-Madsen, 1982; Salvi & Williams-Jones, 1997; Potter et al., 1998). Die Frage nach der Quelle dieser Methan-führenden Fluide in solchen Systemen wird stellenweise kontrovers diskutiert (z.B. Sheppard, 1986; Nivin et al., 1995; Potter et al., 1998; Potter & Konnerup-Madsen, 2003).

Am Beispiel der syenitischen Gesteine des Puklen-Komplexes (Kapitel 2) konnte gezeigt werden, dass die Kristallisationsabfolge mit ternärem Feldspat, Olivin, Augit, Fe-Ti Oxiden und Amphibol als fraktionierende Phasen bei 950 – 750°C beginnt und unter sehr reduzierten Bedingungen stattfindet. Vergleichbare Studien and der Ilímaussaq-Intrusion und an anderen Alkali-Intrusionen zeigen, dass stark reduzierende Bedingungen im frühmagmatischen Stadium der alkalinen Schmelzen der Gardar-Provinz typisch sind (Larsen, 1976; Powell, 1978; Marks & Markl, 2001; Markl et al., 2001). Mit zunehmender Fraktionierung und Abkühlung im geschlossenen System entmischt schließlich eine Alkalien-reiche fluide Phase, die primäre teilweise Ca-reiche Minerale (z.B. Augit) angreift, und durch Na-reiche Minerale (Aegirin-Augit, Aenigmatit, Albit) ersetzt. Dadurch werden größere Mengen an Ca freisetzt und es kristallisieren dann bei sehr niedrigen Temperaturen von bis zu etwa 300°C sekundäre Ca-reiche Minerale (Ferro-Aktinolit, Karbonate, Hydro-Andradit, Titanit), die im Gleichgewicht mit den Na-reichen Mineralen stehen. Mit dieser lang anhaltenden Abkühlungsgeschichte und Autometasomatose geht eine starke Oxidation einher. Auch in den peralkalinen Graniten des Puklen-Komplexes kann eine primäre magmatische Paragenese von einer sekundären spätmagmatischen bis hydrothermalen unterschieden werden. Die frühen mafischen Minerale (Na-Amphibole, Ilmenit) kristallisierten während stark reduzierten Bedingungen bei Temperaturen von mindestens 750°C und wurden schließlich bei Temperaturen um 300°C von Ägirin, Astrophyllit und Hämatit ersetzt, was auf stark oxidierte Bedingungen während dieses späten Stadiums schließen lässt.

Ein ausgesprochen langer Kristallisationsbereich mit zunehmend oxidierenden Bedingungen während der Abkühlung wurde auch für ein peralkalines Ganggestein, das in unmittelbarer Nähe zur Ilímaussaq-Intrusion auftritt, gefunden (Kapitel 4). Die genaue mineralchemische und petrologische Analyse dieses Ganggesteines ergab starke Parallelen zur Ilímaussaq-Intrusion. Die Abnahme der Silika-Aktivität und der Anstieg der Sauerstofffugazität und Wasseraktivität mit fortschreitender Fraktionierung und Abkühlung ist auf eine Entwicklung im geschlossenen System

zurückzuführen und verläuft fast identisch zu den Gesteinen der Ilímaussaq-Intrusion (Larsen, 1976; Marks & Markl, 2001; Markl et al., 2001). Die verschieden Mineralparagenesen des Ganggesteines repräsentieren dabei einzelne Gesteinstypen der Ilímaussaq-Intrusion und man kann davon ausgehen, dass die beiden geologischen Einheiten einer gemeinsamen Mutterschmelze entstammen, sich jedoch früh voneinander trennten und trotzdem einer sehr ähnliche Kristallisations- und Abkühlgeschichte folgten. Die ist umso erstaunlicher, wenn man sich den enormen Größenunterschied zwischen der Ilímaussaq-Intrusion (etwa 17 x 8 km) und dem peralkalinen Ganggestein (10 bis 30 m mächtig und etwa 18 km lang) klarmacht. Berechnungen zur Abkühlgeschichte (Peacock, 1989) ergaben, dass das Ganggestein innerhalb einer sehr kurzen Zeitspanne von maximal 100 Jahren von etwa 850°C auf 250°C abkühlte. Diese Zeitspanne ist etwa zwei bis vier Größenordnungen kürzer als was man für Plutonite der Größe der Ilímaussaq-Intrusion annimmt (z.B. Brown and Fletcher, 1999; Vazquez and Reid, 2002; Charlier and Zellmer, 2002). Offensichtlich spielen also weder das beteiligte Schmelzvolumen noch dessen Abkühlgeschwindigkeit eine wesentliche Rolle bei der Fraktionierung.

Demgegenüber ist ein starker Einfluss von krustaler Kontamination auf den Fraktionierungspfad einer Schmelze ersichtlich: Zwar deuten O-isotopische Daten für verschieden Mineralseparate der beiden untersuchten Alkaligesteinskomplexe von Puklen (Kapitel 2) und Ilímaussaq (Kapitel 3) eine prinzipielle Herkunft der Mutterschmelze aus dem Mantel an, doch zeigen die durchgeführten Nd- (und Sr-) isotopischen Untersuchungen, dass es zu signifikanten Unterschieden bei der weiteren Entwicklung dieser Schmelzen, sowohl beim Aufstieg als auch bei der Platznahme kam. Nd-Isotopenuntersuchungen ergaben für die Gesteine der Ilímaussaq-Intrusion eine isotopisch sehr homogene Quelle. Dies gilt sowohl für frühmagmatische Mineralseparate, als auch für spätmagmatische bis hydrothermale Mineraladern und Pegmatite. Die Fraktionierung und Kristallisation der Ilímaussaq Schmelzen fand also prinzipiell in einem geschlossenen System statt und ein wesentlicher Einfluss von krustaler Kontamination kann nur für den Alkali-Granit nachgewiesen werden.

Ein ganz anderes Bild ergeben entsprechende Daten für die Puklen-Gesteine. Nd-isotopische Daten für primäre Minerale verschiedener Syenite dieses relativ kleinen Intrusivkörpers deuten eine isotopisch recht heterogene Quelle für diese Gesteine an, was durch unterschiedlich starke Assimilation krustaler Schmelzen erklärt werden kann. Innerhalb der untersuchten Proben ergibt sich dabei eine Tendenz, dass Quarz-reiche Syenite stärker kontaminiert sind als Quarz-arme bzw.

Quarz-freie Syenite. Die Alkali-Granite und Mikro-Granite des Komplexes fügen sich in diesen Trend ein.

Ein wesentlicher Unterschied zwischen den syenitischen und granitischen Gesteinen ist jedoch ihr Verhalten während dem spätmagmatischen bis hydrothermalen Stadium: Die syenitischen Gesteine scheinen in einem, geschlossenen System abzukühlen. Die weiter oben angesprochenen Umverteilungsprozesse die schließlich zur Bildung sekundärer Minerale führen sind durch eine einzige, höchstwahrscheinlich interne fluide Phase erklärbar. In den Alkali-Graniten allerdings ist mindestens eine externe (eventuell meteorische) fluide Phase notwendig, um die starken Nd-isotopischen Unterschiede zwischen primärem Amphibol und bei tiefen Temperaturen um 300°C gebildetem sekundärem Ägirin zu erklären. Wie bereits weiter oben schon angesprochen wurde, scheinen diese externen Fluidphase(n) eine stark oxidierende Wirkung zu besitzen.

Von einem Anstieg der Sauerstofffugazität während der Abkühlung kann aber auch in dem quasi-geschlossenen System der Ilímaussaq-Intrusion ausgegangen werden. H-isotopen Daten magmatischer bis hydrothermaler Amphibole sind extrem variabel und D-verarmt und liegen deutlich außerhalb der bekannten Variation für „normale“ magmatische Amphibole (Hoefs, 1997), scheinen allerdings typisch für peralkaline Intrusivgesteine zu schein (Sheppard, 1986), was auf einen gemeinsamen Prozess in peralkalinen Gesteinen hindeutet, der zu solch ungewöhnlichen H-isotopischen Zusammensetzungen führt. In völligem Kontrast dazu steht dabei die „normale“ und homogene O-isotopische Zusammensetzung der entsprechenden Minerale, was eigentlich nur durch eine Entkoppelung dieser beiden Isotopensysteme erklärt werden kann. Gängige Erklärungen für solch niedrige H-isotopische Zusammensetzungen wie z.B. der Einfluss meteorischer Fluide (z.B. Taylor, 1974; Brandriss et al., 1995; Nevle et al., 1994; Agemar et al., 1999), starke Entgasungsphänomene (z.B. Nabelek et al., 1983; Taylor et al., 1983) oder die Assimilation biogener Sedimente (Sheppard, 1986) sind im Falle der Ilímaussaq-Intrusion als sehr unwahrscheinlich anzusehen. Die extrem niedrigen δD Werte können letztendlich nur durch die spätmagmatische Oxidation der primären Methan-Fluide erklärt werden. Ein spätmagmatischer Anstieg der Sauerstofffugazität bis in den Bereich des Hämatit-Magnetit-Puffers wird unter anderem durch die Bildung von Ägirin auf Kosten von Na-Amphibole angezeigt (Markl et al., 2001). Das bei der Oxidation freigesetzte Wasser könnte dann sekundär mit den Hydroxyl-Gruppen der Amphibole re-äquilibriert haben, was aufgrund der starken H-Isotopenfraktionierung bei niedrigen Temperaturen zu den beobachteten H-Isotopenzusammensetzungen führte. Alternativ dazu könnten allerdings auch die bisher bekannten experimentell bestimmten Amphibol-Wasser

Fraktionierungen im H-Isotopensystem problematisch sein, vor allem was ihre Abhängigkeit vom Fe-Gehalt der betreffenden Amphibole betrifft (Suzuoki & Epstein, 1976; Graham et al., 1984). Die starke Korrelation zwischen den gemessenen δD Werten der Ilímaussaq Amphibole und ihrem Fe-Gehalt kann als Hinweis dafür gelten. Ohne weitere experimentelle Untersuchungen dieser Problematik kann diese Frage allerdings nicht endgültig beantwortet werden.

Zusammenfassend betrachtet wird die geochemische und isotopische Entwicklung von peralkalinen Pluoniten durch ein komplexes Zusammenspiel verschiedenster Prozesse gesteuert. Fraktionierende Kristallisation und krustale Kontamination sind die beiden wesentlichen Prozesse, die zu einem bedeutenden Maße den Fraktionierungspfad der Mutterschmelze mitbestimmen (AFC-Prozesse, DePaolo, 1981). Das Auftreten von SiO_2-untersättigten und SiO_2-übersättigten Intrusionen innerhalb der Gardar-Provinz ist generell also durch die unterschiedliche Bedeutung von krustaler Kontamination für die einzelnen Intrusivkörper zu erklären. SiO_2-untersättigte Intrusionen entwickeln sich im wesentlichen durch die fraktionierende Kristallisation von alkalibasaltischen Schmelzen im geschlossenen System. Im Gegensatz dazu stellen SiO_2-übersättigte Intrusionen vermutlich stärker kontaminierte Äquivalente der selben Mutterschmelzen dar, für die eine Entwicklung im offenen System angenommen werden muss. Diese Ergebnisse stehen im Einklang mit zahlreichen Studien an vergleichbaren Granitoiden (z.B. Perry et al., 1987; Kramm and Kogarko, 1994; Schmitt et al., 2000; Davies and Macdonald, 1987; Heaman and Machado, 1992; Harris et al., 1990; Harris, 1995; Mingram et al., 2000; Späth et al., 2001). Die primären geochemischen und isotopischen Charakteristika können allerdings sehr stark durch sekundäre Prozesse wie hydrothermale und post-magmatische Alteration, Sub-Solidus Re-äquilibrierung und dem Einfluss externer (meteorischer) Fluidquellen überprägt werden. Aufgrund ihrer unterschiedlichen Anfälligkeit bzw. Resistenz gegenüber solchen Prozessen ist die Kombination von verschiedenen stabilen und radiogenen Isotopensysemen (H, O, Sr, Nd, Os) ein gut geeignetes Werkzeug diese unterschiedlichen magmatischen und post-magmatischen Prozesse zu unterscheiden. In vielen Fällen zeigt die detaillierte Analyse (petrographisch, mineralchemisch und isotopengeochemisch) verschiedener Mineralparagenesen peralkaliner Plutonite eine komplizierte und mehrstufige Entwicklungsgeschichte an. Die Analyse von Gesamtgesteinsproben würde in solchen Fällen nur zu Durchschnittswerten führen und daher eine vernünftige geologische Interpretation nicht zulassen. Nur die genaue Trennung und Analyse der verschiedenen Mineralparagenesen und die dadurch erst mögliche Differenzierung der einzelnen beteiligten Prozesse kann zu verlässlichen Aussagen und Interpretationen zur Magmengenese und zur spätmagmatischen Entwicklung in solchen Gesteinstypen führen.

Im abschließenden Kapitel 5 werden die Ergebnisse einer Spurenelementstudie an mafischen Mineralen (Klinopyroxene und Amphibole) dreier Alkaligesteinsintrusionen der Gardar-Provinz präsentiert. Beide untersuchten Minerale zeigen einen kontinuierlichen Entwicklungstrend in ihrer Hauptelementzusammensetzung von Ca-dominierten über intermediäre bis hin zu Na-dominierten Gliedern. Ähnliche Studien, die sich mit basaltischen Systemen (z.B. Jeffries et al., 1995; Benoit et al., 1996; Coogan et al., 2000; Thompson & Malpas, 2000; Tiepolo et al., 2002) und mit Mantel Mineralen (Nimis & Vanucci, 1995; Blundy & Dalton, 2000, Grégoire et al., 2000; Tiepolo et al., 2000) beschäftigten, finden sich in der Literatur recht häufig. Entsprechende Arbeiten an stärker entwickelten Magmatiten hingegen sind weniger häufig (Wörner et al., 1983; Lemarchand et al. 1987; Wood & Trigila, 2001) und wurden insbesondere an intrusiven Alkaligesteinen bisher nur selten durchgeführt (Larsen 1979; Shearer and Larsen 1994).

Prinzipiell sind alle untersuchten Minerale durch sehr hohe Gehalte an inkompatiblen Spurenelementen gekennzeichnet, die im Vergleich zum durchschnittlichen primitiven Mantel (McDonough & Sun, 1995), teilweise bis zu 10000-fach angereichert sind, was einen hochfraktionierten Charakter der Gesteine impliziert. Die beiden wichtigsten Prozesse, die den Einbau von Spurenelementen in die betreffenden Minerale steuern sind einerseits die chemische Zusammensetzung und die Struktur der Schmelzen oder Fluidphasen, aus denen sie kristallisieren (z.B. Sisson, 1994; Gaetani & Grove, 1995) und zum anderen kristallchemische und strukturelle Voraussetzungen des betreffenden Minerals (z.B. Blundy & Wood, 1991; 1994; Wood & Blundy, 1997; 2001). Die Ergebnisse dieser Studie zeigen, dass diese beiden Faktoren für verschiedene, nach ihrem geochemischen Verhalten verwandte Elementgruppen, von unterschiedlicher Bedeutung sein können:

Die auffällig niedrigen Gehalte an LIL-Elementen (Ba, Sr, Pb, Eu^{2+}) reflektieren vermutlich die Fraktionierung großer Mengen von Feldspat während früherer Entwicklungsstadien der Schmelze, zeigen also eine starke Abhängigkeit von der chemischen Zusammensetzung der Mutterschmelze. Diese Interpretation ist konsistent mit den weiter oben schon angesprochenen Vorstellung eines die Gardar-Provinz unterlagernden großen Anorthositkörpers. Allerdings können Änderungen der Sauerstofffugazität und krustale Kontamination einen ganz erheblichen Einfluss auf den Einbau von Eu^{2+} und Pb haben.

Der Einbau von HFS-Elementen (Ti, Zr, Hf, Sn, Nb, Ta) hingegen scheint vor allem von kristallchemischen und strukturellen Faktoren gesteuert zu werden. Während die effektiven Ionenradien von Zr^{4+} (0.72 Å), Hf^{4+} (0.71 Å) and Sn^{4+} (0.69 Å; Shannon, 1976) sehr gut mit der optimalen Größe von 0.70 Å für die in Frage kommenden Plätze in der Pyroxen- bzw. Amphibolstruktur (Jensen, 1973; Bailey et al., 2001) übereinstimmen, ist Ti^{4+} mit 0.61 Å deutlich kleiner. Daraus resultiert ein nur geringer Effekt auf den Ti-Einbau, ganz im Gegensatz zu starken Konzentrationsänderungen von Zr, Hf und Sn mit sich ändernden Na/Ca-Verhältnissen der Klinopyroxe und Amphibole, was zu leichten Veränderungen in der Größe der entsprechenden Strukturplätze führt. Die in Tiepolo et al. (2000) beschriebene Fraktionierung zwischen Nb und Ta in Amphibolen tritt nach unseren Daten auch in Pyroxenen auf und kann ebenfalls durch minimale Größenunterschiede zwischen Nb^{5+} und Ta^{5+} erklärt werden.

Für die Seltenerd Elemente (SEE) scheinen beide oben genannte Faktoren einen signifikanten Einfluss auf den Einbau in Klinopyroxen und Amphibol zu besitzen. Einerseits zeigt sich eine systematische und kontinuierliche Änderung der Mantel-normierten SEE-Muster von Ca-dominierte bis zu Na-dominierten Glieder, was auf eine kristallchemische Kontrolle des SEE-Einbaus schließen lässt. Andererseits wirkt sich offensichtlich auch die Fraktionierung SEE-reicher Minerale (Eudialyt) sowohl auf die Absolutkonzentrationen, als auch auf das Verhältnis von leichten zu schweren SEE aus und belegt damit den Einfluss der Schmelzzusammensetzung.

Die Verteilung der meisten Spurenelemente zwischen Klinopyroxen und Amphibol scheint relativ unabhängig von der Schmelzzusammensetzung und der Hauptelementzusammensetzung der Minerale zu sein. Im Vergleich mit Literaturdaten aus basaltischen, basanitischen und ultramafischen Systemen (z.B. Vannucci et al., 1991; Chazot et al., 1996; Witt-Eickschen & Harte, 1994; Adam & Green, 1994; Grégoire et al., 2000) zeigt sich eine große Übereinstimmung mit den hier bestimmten Verteilungskoeffizienten, trotz bedeutender Unterschiede in der chemischen Zusammensetzung der Schmelzen und der Kristalle. Für einen Grossteil der Spurenelemente zeigt sich eine leichte Präferenz für Amphibol. Einige Elemente (v. a. Rb, U, Th, Ba) weichen stark von dieser Tendenz ab. Dies wurde jedoch nur in solchen Proben beobachtet, in denen intensive hydrothermale und autometasomatische Prozesse bedeutend waren, was vermutlich zu einer sekundären Umverteilung dieser Elemente führte.

LITERATUR

Adam, J. and Green, T. H. (1994) The effects of pressure and temperature on the partitioning of Ti, Sr and

REE between amphibole, clinopyroxene and basanitic melts. *Chemical Geology* **117**, 219-233.
Agemar, T., Wörner, G., and Heumann, A. (1999) Stable isotopes and amphibole chemistry on hydrothermally altered granitoids in the North Chilean Precordillera: A limited role of meteoric water? *Contributions to Mineralogy and Petrology* **136**, 331-344.
Ashwal, L. D. (1993) Anorthosites. Springer, Berlin Heidelberg
Bailey, J. C., Gwozdz, R., Rose-Hansen, J., and Sørensen, H. (2001) Geochemical overview of the Ilimaussaq alkaline complex, South Greenland. *Geology of Greenland Survey Bulletin* **190**, 35-53.
Barbieri, F. and Varet, J. (1970) The Erta Ale volcanic range (Danakil depression), Northern Afar, Ethiopia. *Bulletin of Volcanology* **34**, 848-917.
Benoit, M., Polvé, M., and Ceuleneer, G. (1996) Trace element and isotopic characterization of mafic cumulates in a fossil mantle diapir (Oman ophiolite). *Chemical Geology* **134** , 199-214.
Bernstein, S., Kelemen, P. B., Tegner, C., Kurz, M. D., Blusztajn, J., and Kent Brooks, C. (1998) Post-breakup basaltic magmatism along the East Greenland Tertiary rifted margin. *Earth and Planetary Science Letters* **160**, 845-862.
Blundy, J. and Dalton, J. (2000) Experimental comparison of trace element partitioning between clinopyroxene and melt in carbonate and silicate systems, and implications for mantle metasomatism. *Contributions to Mineralogy and Petrology* **139**, 356-371.
Blundy, J. and Wood, B. (1994) Prediction of crystal-melt partition coefficients from elastic moduli. *Nature* **372**, 452-454.
Blundy, J. D. and Wood, B. J. (1991) Crystal-chemical controls on the partitioning of Sr and Ba between plagioclase feldspar, silicate melts, and hydrothermal solutions. *Geochimica et Cosmochimica Acta* **55**, 193-209.
Bohrson, W. A. and Spera, F. J. (2001) Energy-constrained open-system magmatic processes; II, Application of energy-constrained assimilation-fractional crystallization (EC-AFC) model to magmatic systems *Journal of Petrology* **42**, 1019-1041.
Boily, M. and Williams-Jones, A. E. (1994) The role of magmatic and hydrothermal processes in the chemical evolution of the Strange Lake plutonic complex, Quebec-Labrador. *Contributions to Mineralogy and Petrology* **118**, 33-47.
Brandriss, M. E., Nevle, R. J., Bird, D. K., and O´Neil, J. R. (1995) Imprint of meteoric water on the stable isotope compositions of igneous and secondary minerals, Kap Edvard Holm complex, East Greenland. *Contributions to Mineralogy and Petrology* **121**, 74-86.
Bridgwater, D. (1967) Feldspathic inclusions in the Gardar igneous rocks of South Greenland and their relevance to the formation of major Anorthosites in the Canadian Shield. *Canadian Journal of Earth Sciences* **4**, 995-1014.
Bridgwater, D. and Coe, K. (1970) The role of stoping in the emplacement of the giant dikes of Isortoq, South Greenland. *Geological Journal, Special issue* **2**, 67-78.
Bridgwater, D. and Harry, W. T. (1968) Anorthosite xenoliths and plagioclase megacrysts in Precambrian intrusions of South Greenland. *Meddelelser om Grønland* **185** , 243.
Brown, S. J. A. and Fletcher, I. R. (1999) SHRIMP U-Pb dating of the preeruption growth history of zircon from the 340 ka Whakamaru ignimbrite, New Zealand: evidence for > 250 ky magma residence times. *Geology* **27**, 1035-1038.
Cadman, A. C., Heaman, L., Tarney, J., Wardle, R., and Krogh, T. E. (1993) U-Pb geochronology and geochemical variation within two Proterozoic mafic dyke swarms, Labrador. *Canadian Journal of Earth Sciences* **30**, 1490-1504.
Camp, V. E., Roobol, M. J., and Hooper, P. R. (1996) Intraplate alcalic volcanism and magmatic processes along the 600 km-long Makkah-Madinah-Nafud volcanic line, western Saudi-Arabia. *IAVCEI General Assembly Bulletin* **131**, 39.
Chadwick, B., Erfurt, P., Frisch, T., Frith, R. A., Garde, A. A., Schønwandt, H. K., Stendal, H., and Thomassen, B. (1994) Sinistral transpression and hydrothermal activity during emplaceement of the Early Proterozoic Julianehåb bathollith, Letilidian orogenic belt, South Greenland. *Rapport Grønlands Geologiske Undersøgelse* **163**, 5-22.
Chakhmouradian, A. R. and Mitchell, R. H. (2002) The mineralogy of Ba- and Zr-rich alkaline pegmatites from Gordon Butte, Crazy Mountains (Montana, USA): comparisons between potassic and sodic agpaitic pegmatites. *Contributions to Mineralogy and Petrology* **143**, 93-114.
Chapman, H. J. (1979) 2390 Myr Rb-Sr whole-rock for the Scourie dyke of North-west Scotland. *Nature* **227**, 642-643.

Charlier, B. L. A. and Zellmer, G. (2000) Some remarks on U-Th mineral ages from igneous rocks with prolonged crystallisation histories. *Earth and Planetary Science Letters* **183**, 457-469.
Chazot, G., Menzies, M., and Harte, B. (1996) Determination of partition coefficients between apatite, clinopyroxene, amphibole, and melt in natural spinel lherzolites from Yemen: Implications for wet melting of the lithospheric mantle. *Geochimica et Cosmochimica Acta* **60**, 423-437.
Coogan, L. A., kempton, P. D., Saunders, A. D., and Norry, M. J. (2000) Melt aggregation within the crust beneath the Mid-Atlantic Ridge: evidence from plagioclase and clinopyroxene major and trace element compositions. *Earth and Planetary Science Letters* **176**, 245-257.
Coulson, I. M. (1997) Post-magmatic alteration in eudialyte from the North Qoroq centre, South Greenland. *Mineralogical Magazine* **61**, 99-109.
Dahl-Jensen, T., Thybo, H., Hopper, J., and Rosing, M. (1998) Crustal structure at the SE Greenland margin from wide-angle and normal incidence seismic data. *Tectonophysics* **288**, 191-198.
Davies, G. R. and Macdonald, R. (1987) Crustal influences in the petrogenesis of the Naivasha basalt-comendite complex: combined trace element and Sr-Nd-Pb isotope constraints. *Journal of Petrology* **28**, 1009-1031.
DePaolo, D. J. (1981) Trace element and isotopic effects of combined wallrock assimilation and fractional crystallisation. *Earth and Planetary Science Letters* **53**, 189-202.
Devey, C. W. and Cox, K. G. (1987) Relationships between crustal contamination and crystallisation in continental flood basalt magmas with special reference to the Deccan Traps of the Western Ghats, India. *Earth and Planetary Science Letters* **84**, 59-68.
Edgar, A. D. and Parker, L. M. (1974) Comparison of melting relationships of some plutonic and volcanic peralkaline undersaturated rocks. *Lithos* **7**, 263-273.
Emeleus, C. H. and Upton, B. G. J. (1976) The Gardar period in southern Greenland. *In: Escher, A. & Watt, W.S. (eds.), Geology of Greenland. Copenhagen: Geological Survey of Greenland.* 152-181.
Emslie, R. F. (1980) Anorthosite massifs, rapakivi granites, and late Proterozoic rifting of North America. *Precambrian Research* **7**, 61-98.
Ernst, R. E. and Buchan, K. L. (1997) Giant Radiating Dyke Swarms: Their Use in Identifying Pre-Mesozoic Large Igneous Provinces and Mantle Plumes. *In: Large Igneous Provinces: Continental, Oceanic, and Planetary Flood Volcanism. Mahoney, J.J. and Coffin, M.E. (editors). Geophysical Monograph.* **100**, 297-333.
Ernst, R. E. and Buchan, K. L. (2001) The use of mafic dike swarms in identifying and locating mantle plumes. *in: Ernst, R.E. and Buchan, K.L. (editors), Mantle Plumes: Their Identification Through Time. Geological Society of America Special Paper* **352**, 247-265.
Ferguson, J. (1964) Geology of the Ilimaussaq alkaline intrusion, South Greenland. *Bulletin Grønlands Geologiske Undersøgelse* **39**, 82.
Finch, A. A., Parsons, I., and Mingard, S. C. (1995) Biotites as indicators of fluorine fugacities in late-stage magmatic fluids: the Gardar Province in South Greenland. *Journal of Petrology* **36**, 1701-1728.
Fuhrman, M. L., Frost, B. R., and Lindsley, D. H. (1988) Crystallization conditions of the Sybille Monzosyenite, Laramie Anorthosite Complex, Wyoming. *Journal of Petrology* **29**, 699-729.
Gaetani, G. A. and Grove, T. L. (1995) Partitioning of rare earth elements betwee clinopyroxene and silicate melt: Crystal-chemical controls. *Geochimica et Cosmochimica Acta* **59**, 1951-1962.
Garde, A. A., Hamilton, M. A., Chadwick, B., Grocott, J., and McCaffrey, K. J. W. (2002) The Ketilidian orogen of South Greenland: geochronology, tectonics, magmatism, and fore-arc accretion during Palaeoproterozoic oblique convergence. *Canadian Journal of Earth Sciences* **39**, 765-793.
Graham, C. M., Harmon, R. S., and Sheppard, S. M. F. (1984) Experimental hydrogen isotope studies: hydrogen isotope exchange between amphibole and water. *American Mineralogist* **69** , 128-138.
Grégoire, M., Moine, B. N., O´Reilly, S. Y., Cottin, J. Y., and Giret, A. (2000) Trace element residence and partitioning in mantle xenoliths metasomatized by highly alkaline, silicate- and carbonate-rich melts (Kerguelen Islands, Indian Ocean). *Journal of Petrology* **41**, 477-509.
Halama, R., Waight, T., and Markl, G. (2002) Geochemical and isotopic zoning patterns of plagioclase megacrysts in gabbroic dykes from the Gardar Province, South Greenland: implications for crystallisation processes in anorthositic magmas. *Contributions to Mineralogy and Petrology* **144**, 109-127.
Harris, C. (1995) Oxygen isotope geochemistry of the Mesozoic anorogenic complexes of Damaraland, northwest Namibia: evidence for crustal contamination and its effects on silica saturation. *Contributions to Mineralogy and Petrology* **122**, 308-321.
Harris, C., Whittingham, A. M., Milner, S. C., and Armstrong, R. A. (1990) Oxygen isotope geochemistry of

the silicic volcanic rocks of the Etendeka/Parana Province: source constraints. *Geology* **18**, 1119-1121.
Heaman, L. M. and Machado, N. (1992) Timing and origin of midcontinent rift alkaline magmatism, North America: evidence from the Coldwell Complex. *Contributions to Mineralogy and Petrology* **110**, 289-303.
Hill, J. D. (1988) Alkalic to transitional ferrogabbro magma associated with Paleohelikian anorthositic plutons in the Flowers River area, southeastern Nain igneous complex, LAbrador. *Contributions to Mineralogy and Petrology* **99**, 113-125.
Hoefs, J. (1997) Stable isotope geochemistry. *Springer, Berlin Heidelberg*
Jeffries, T. E., Perkins, W. T., and Pearce, N. J. G. (1995) Measurements of trace elements in basalts and their phenocrysts by laser probe microanalysis inductively coupled plasma mass sepctrometry (LPMA-ICP-MS). *Chemical Geology* **121**, 131-144.
Jensen, B. B. (1973) Patterns of trace element partitioning. *Geochimica et Cosmochimica Acta* **37**, 2227-2242.
Kalsbeek, F. Larsen L. M. and Bondam, J. (1990) Geological map of Greenland 1:500 000, Sydgrønland Sheet 1 (descriptive text). *Grønlands Geologiske Undersøgelse* 36.
Kogarko, L. N. and Romanchev, B. P. (1977) Temperature, pressure, redox conditions, and mineral equilibria in agpaitic nepheline syenites and apatite-nepheline rocks. *Geochemistry International* **14**, 113-128.
Kogarko, L. N. and Romanchev, B. P. (1982) Phase equilibria in alkaline melts. *International Geology Review* **25**, 534-546.
Kolker, A. and Lindsley, D. H. (1989) Geochemical evolution of the Maloin Ranch pluton, Laramie Anorthosite Complex, Wyoming: petrology and mixing relations. *American Mineralogist* **74**, 307-324.
Konnerup-Madsen, J. and Rose-Hansen, J. (1982) Volatiles associated with alkaline igneous rift activity: Fluid inclusions in the Ilimaussaq intrusion and the Gardar granitic complexes (south Greenland). *Chemical Geology* **37**, 79-93.
Konnerup-Madsen, J. and Rose-Hansen, J. (1984) Composition and significance of fluid inclusions in the Ilimaussaq peralkaline granite, South Greenland. *Bulletin de Minéralogie* **107**, 317-326.
Kramm, U. and Kogarko, L. N. (1994) Nd and Sr isotope signatures of the Khibina and Lovozero agpaitic centres, Kola Province, Russia. *Lithos* **32**, 225-242.
Krokström, T. (1936) The Hellerförs dolerite dyke and some problems of basaltic rocks. *Bull.Ups.Univ.Mineral.-Geol. Inst.* **26**, 113-263.
Larsen, L. M. (1976) Clinopyroxenes and coexisting mafic minerals from the alkaline Ilimaussaq intrusion, south Greenland. *Journal of Petrology* **17**, 258-290.
Larsen, L. M. (1979) Distribution of REE and other trace elements between phenocrysts and peralkaline undersaturated magmas, exemplified by rocks from the Gardar igneous province, South Greenland. *Lithos* **12**, 303-315.
Larsen, L. M. and Sørensen, H. (1987) The Ilimaussaq intrusion-progressive crystallization and formation of layering in an agpaitic magma. In: Fitton, J.G. & Upton, B.G.J. (eds.), Alkaline Igneous Rocks, Geological Society Special Publication **30**, 473-488.
LeCheminant, A. N. and Heaman, L. M. (1989) Mackenzie igneous events, Canada: Middle Proterozoic hotspot magmatism associated with ocean opening. *Earth and Planetary Science Letters* **96**, 38-48.
Lemarchand, F., Villemant, B., and Calas, G. (1987) Trace element distribution coefficients in alkaline series. *Geochimica et Cosmochimica Acta* **51**, 1071-1081.
Lightfoot, P. C., Sutcliffe, R. H., and Doherty, W. (1991) Crustal contamination identified in Keweenawan Osler Group Tholeiites, Ontario: A trace element perspective. *Journal of Geology* **99**, 739-760.
Lopez-Montano, R. (1986) Origin and composition of the Halleförs composite dyke, central Sweden. *Meddel. Stockholms Universitets Geologiska Institution.* **267**, 113.
Markl, G. (2001) Stability of Na-Be minerals in late-magmatic fluids of the Ilimaussaq alkaline complex, South Greenland. *Geology of Greenland Survey Bulletin* **190**, 145-158.
Markl, G. and Baumgartner, L. (2002) pH changes in peralkaline late-magmatic fluids. *Contributions to Mineralogy and Petrology* **144**, 31-346.
Markl, G., Marks, M, Schwinn, G., and Sommer, H. (2001) Phase equilibrium constraints on intensive crystallization parameters of the Ilimaussaq Complex, South Greenland. *Journal of Petrology* **42**, 2231-2258.
Marks, M. and Markl, G. (2001) Fractionation and assimilation processes in the alkaline augite syenite unit of the Ilimaussaq Intrusion, South Greenland, as deduced from phase equilibria. *Journal of Petrology* **42**,

1947-1969.
McDonough, W. F. and Sun, S. S. (1995) The composition of the Earth. *Chemical Geology* **120**, 223-253.
Mingram, B., Trumbull, R. B., Littman, S., and Gerstenberger, H. (2000) A petrogenetic study of anorogenic felsic magmatism in the Cretaceous Paresis ring complex, Namibia: evidence for mixing of crust and mantle-derived components. *Lithos* **54**, 1-22.
Mitchell, R. H. and Platt, R. G. (1982) Mineralogy and petrology of nepheline syenites from the Coldwell Alkaline Complex, Ontario, Canada. *Journal of Petrology* **23**, 186-214.
Mohr, P. A. (1987) Crustal Contamination in Mafic Sheets: a Summary. *In: Mafic dyke swarms; Halls, H.C. and Fahrig, W.C. (eds.). Geological Association of Canada, Special Publication* **34**, 75-80.
Morse, S. A. (1982) A partisan review of Proterozoic anorthosites. *American Mineralogist* **67**, 1087-1100.
Nabelek, P. I., O´Neil, J. R., and Papike, J. J. (1983) Vapour phase exsolution as the controling factor in hydrogen isotope variation in granitic rocks; the Notche Peak granitic stock, Utah. *Earth and Planetary Science Letters* **66**, 137-150.
Nelson, D. O., Morrison, D. A., and Phinney, W. C. (1990) Open-system evolution versus source control in basaltic magmas; Matachewan-Hearst dike swarm, Superior Province, Canada. *Canadian Journal of Earth Sciences* **27**, 767-783.
Nevle, R. J., Brandriss, M. E., Bird, D. K., MacWilliams, M. O., and O´Neil, J. R. (1994) Tertiary plutons monitor climate change in East Greenland. *Geology* **22**, 775-778.
Nimis, P and Vannucci, R. (1995) An ion microprobe study of clinopyroxenes in websteritic and megacrystic xenoliths from Hyblean Plateau (SE Sicily, Italy): constraints on HFSE/REE/Sr fractionation at mantle depth. *Chemical Geology* **124**, 185-197.
O'Hara, M. J. and Herzberg, C. (2002) Interpretation of trace element and isotope features of basalts: relevance of field relations, petrology, major element data, phase equilibria, and magma chamber modeling in basalt petrogenesis. *Geochimica et Cosmochimica Acta* **66**, 2167-2191.
Parsons, I. (1972) Petrology of the Puklen syenite-alkali granite complex, Nunarssuit, South Greenland. *Meddelelser om Grønland* **195**, 73.
Parsons, I., Mason, R. A., Becker, S. M., and Finch, A. A. (1991) Biotite equilibria and fluid circulation in the Klokken Intrusion. *Journal of Petrology* **32**, 1299-1333.
Peacock, S. M. (1989) Thermal modeling of metamorphic pressure-time-temperature paths: a forward approach. In: Spear, F.S. & Peackock, S.M. (eds.), Metamorphic pressure-time-temperature paths. Short course in Geology. Washington: American Geophysical Union 57-112.
Peng, Z. X., Mahoney, J., Hooper, P., Harris, C., and Beane, J. (1994) A role for lower continental crust in flood basalt genesis? Isotopic and incompatible element study of the lower six formations of the western Deccan Traps. *Geochimica et Cosmochimica Acta* **58**, 267-288.
Perry, F. V., Baldridge, W. S., and DePaolo, D. J. (1987) Role of asthenosphere and lithosphere in the genesis of late cenozoic basaltic rocks from the Rio Grande rift and adjacent regions of the Southwestern United States. *Journal of Geophysical Research* **92**, 9193-9213.
Piotrowski, J. M. and Edgar, A. D. (1970) Melting relations of undersaturated alkaline rocks from South Greenland. *Meddelelser om Grønland* **181**, 62.
Podmore, F. and Wilson, A. H. (1987) A reappraisal of the structure, geology, and emplacement of the Grat Dyke, Zibabwe. *In: Halls, H. C. & Fahrig, F. (eds.), Mafic dyke swars; a collection of papers based on proceedings of an international conference. Geological Association of Canada: Special Paper.* **34**, 317-330.
Potter, J. and Konnerup-Madsen, J. (2003) A review of the occurence and origin of hydrocarbons in igneous rocks. *In: Petford, N. & McCaffrey, K.J.W. (eds.), Hydrocarbons in crystalline rocks, Geological Society Special Publication* **214**, 151-173.
Potter, J., Rankin, A. H., Treloar, P. J., Nivin, V. A., ting, W., and Ni, P. (1998) A preliminary study of methane inclusions in alkaline igneous rocks of the Kola igneous province, Russia: implications for the origin of methane in igneous rocks. *European Journal of Mineralogy* **10**, 1167-1180.
Poulsen, V. (1964) The sandstones of the Precambrian Eriksfjord Formation in South Greenland. *Rapport Grønlands Geologiske Undersøgelse* **2**, 16.
Powell, M. (1978) The crystallisation history of the Igdlerfigssalik nepheline syenite intrusion, Greenland. *Lithos* **11**, 99-120.
Pulvertaft, T. C. R. (1961) The Puklen intrusion, Nunarssuit, SW Greenland. *Meddelelser om Grønland* **123**, 35-49.
Salvi, S. and Williams-Jones, A. E. (1990) The role of hydrothermal processes in the granite-hosted Zr, Y,

REE deposit at Strange Lake, Quebec/Labrador: evidence from fluid inclusions. *Geochimica et Cosmochimica Acta* **54**, 2403-2418.
Salvi, S. and Williams-Jones, A. E. (1997) Fischer-Tropsch synthesis of hydrocarbons during sub-solidus alteration of the Strange Lake peralkaline granite, Quebec/ Labrador, Canada *Geochimica et Cosmochimica Acta* **61**, 83-99.
Scaillet, B. and MacDonald, R. (2001) Phase relations of peralkaline silicic magmas and petrogenetic implications. *Journal of Petrology* **42**, 825-845.
Schmitt, A. K., Emmermann, R., Trumbull, R. B., Bühn, B., and Henjes-Kunst, F. (2000) Petrogenesis and 40Ar/39Ar Geochronology of the Brandberg Complex, Namibia: Evidence for a major mantle contribution in metaluminous and peralkaline granites. *Journal of Petrology* **41**, 1207-1239.
Shannon, R. D. (1976) Revised effective ionic radii and systematic studies of interatomic distances in halides and chalcogenides. *Acta Crystallographica* **A32**, 751-767.
Shearer, C. K. and Larsen, L. M. (1994) Sector-zoned aegirine from the Ilimaussaq alkaline intrusion, South Greenland: Implications for trace-element behavior in pyroxene. *American Mineralogist* **79**, 340-352.
Sheppard, S. M. F. (1986) Igneous rocks: III. Isotopic case studies of magmatism in Africa, Eurasia and oceanic island. In: Valley, J.W., Taylor, H.P.Jr and O´Neil, J.R. (eds.): Stable Isotopes. Reviews in Mineralogy. Washington: Mineralogical Society of America. **16**, 319-368.
Sisson, T. W. (1994) Hornblende-melt trace-element partitioning measured by ion microprobe. *Chemical Geology* **117**, 331-344.
Sood, M. K. and Edgar, A. D. (1970) Melting relations of undersaturated alkaline rocks. *Meddelelser om Grønland* **181**, 41.
Sørensen, H. (1997) The agpaitic rocks - an overview. *Mineralogical Magazine* **61**, 485-498.
Southwick, D. L. and Day, W. C. (1983) Geology and petrology of Proterozoic mafic dikes, north central Mineasota and western Ontario. *Canadian Journal of Earth Sciences* **20**, 622-638.
Späth, A., Le Roex, A. P., and Opiyo-Akech, N. (2001) Plume-litosphere interaction and the origin of continental rift-related alkaline volcanism-the Chyulu hills volcanic province, Southern Kenya. *Journal of Petrology* **42**, 765-787.
Suzuoki, T. and Epstein, S. (1976) Hydrogen isotope fractionation between OH-bearing minerals and water. *Geochimica et Cosmochimica Acta* **40**, 1229-1240.
Tarney, J. and Weaver, B. L. (1987) Geochemistry and Petrogenesis of Early Proterozoic Dyke Swarms. In: Mafic dyke swarms; Halls, H.C. and Fahrig, W.C. (eds.). Geological Association of Canada, Special Publication **34**, 81-93.
Taylor, B. E., Eichelberger, J. C., and Westrich, H. R. (1983) Hydrogen isotopic evidence of rhyolitic magma degassing during shallow intrusion and eruption. *Nature* **306**, 541-545.
Taylor, H. P. (1974) The application of oxygen and hydrogen isotope studies to problems of hydrothermal alteration and ore deposition. *Economic Geology* **69**, 843-883.
Thompson, G. M. and Malpas, J. (2000) Mineral/melt partition coefficients of oceanic alkali basalts determined on natural samples using laser ablation-inductively coupled plasma-mass spectrometry (LAM-ICP-MS) *Mineralogical Magazine* **64**, 85-94.
Tiepolo, M., Tribuzio, R., and Vannucci, R. (2002) The compositions of mantle-derived melts developed during the Alpine continental collision. *Contributions to Mineralogy and Petrology* **144**, 1-15.
Tiepolo, M., Vanucci, R., Oberti, R., Foley, S., Bottazzi, P., and Zanetti, A. (2000) Nb and Ta incorporation and fractionation in titanian pargasite and kaersurtite: crystal-chemical constraints and implications for natural systems. *Earth and Planetary Science Letters* **176**, 185-201.
Upton, B. G. J. (1974) The Alkaline province of South-West Greenland. *In: Sørensen, H.. (ed..), The Alkaline Rocks. London: Wiley.* 221-238.
Upton, B. G. J. and Emeleus, C. H. (1987) Mid-Proterozoic alkaline magmatism in southern Greenland: the Gardar province. In: Fitton, J.G. & Upton, B.G.J. (eds.), Alkaline Igneous Rocks, Geological Society Special Publication **30**, 449-471.
Upton, B. G. J., Emeleus, C. H., Heaman, L. M., Goodenough, K. M., and Finch, A. (2003) Magmatism of the mid-Proterozoic Gardar Province, South Greenland: chronology, petrogenesis and geological setting. *Lithos* **68**, 43-65.
Upton, B. G. J., Stephenson, D., and Martin, A. R. (1985) The Tugtutôq older giant dyke complex: mineralogy and geochemistry of an alkali gabbro-augite-syenite-foyaite association in the Gardar Province of South Greenland. *Mineralogical Magazine* **49**, 624-642.
Upton, B. G. J. and Thomas, J. E. (1980) The Tugtutôq younger giant dyke complex, South Greenland:

fractional crystallisation of transitional olivine basalt magma. *Journal of Petrology* **21**, 167-198.
Ussing, N. V. (1912) Geology of the country around Julianehaab, Greenland. *Meddelelser om Grønland* **38**, 426.
Vannucci, R., Tribuzio, R., Piccardo, G. B., Ottolini, L., and Bottazzi, P. (1991) SIMS analysis of REE in pyroxenes and amphiboles from the Proterozoic Ikasaulak intrusive complex (SE Greenland): implications for LREE enrichment processes during post-orogenic plutonism. *Chemical Geology* **92**, 115-133.
Vazquez, J. A. and Reid, M. R. (2002) Time scales of magma storage and differentiation of voluminous high-silica rhyolites at Yellewstone caldera, Wyoming. *Contributions to Mineralogy and Petrology* **144**, 274-285.
Wegmann, C. E. (1938) Geological investigations in Southern Greenland. *Meddelelser om Grønland* **113**, 148.
Wilson, A. H. and Prendergast, M. S. (1989) The Great Dyke of Zimbabwe; I, Tectonic setting, stratigraphy, petrology, structure, emplacement crystallization. In: Prendergast, M.S. & Jones, M.J. (eds.), Magmatic sulfides; the Zimbabwe volume. London: Inst. Min. and Metall. 1-20.
Witt-Eickschen, G. and Harte, B. (1994) Distribution of trace elements between amphibole and clinopyroxene from mantle peridotites of the Eifel (western Germany): An ion-microprobe study. *Chemical Geology* **117**, 235-250.
Wood, B. J. and Blundy, J. D. (1997) A predictive model for rare earth element partioning between clinopyroxene and anhydrous silicate melt. *Contributions to Mineralogy and Petrology* **129**, 166-181.
Wood, B. J. and Blundy, J. D. (2001) The effect of cation charge on crystal-melt partitioning of trace elements. *Earth and Planetary Science Letters* **188**, 59-71.
Wood, B. J. and Trigila, R. (2001) Experimental determination of aluminous clinopyroxene-melt partition coefficients for potasic liquids, with applicatio to the evolution of the Roma province potassic magmas. *Chemical Geology* **172**, 213-223.
Wörner, G., Beusen, J.-M., Duchateau, N., Gijbels, R., and Schmincke, H.-U. (1983) Trace element abundances and mineral/melz distribution coefficients in phonolites from the Laacher See Volcano (Germany) *Contributions to Mineralogy and Petrology* **84**, 152-173.

Kapitel 1: Petrologische und isotopengeochemische Untersuchungen an Ganggesteinen der Isortoq Region

Manuskript-Titel:
Archaean crust below South Greenland: Evidence from a petrological, geochemical and Sr-Nd-Os-O isotopic study of the Proterozoic Isortoq dike swarm.

Autoren:
Ralf Halama[1], Michael Marks[1], Gerhard Brügmann[2], Wolfgang Siebel[1], Thomas Wenzel[1], Gregor Markl[1]

[1] Institut für Geowissenschaften, Eberhard-Karls-Universität Tübingen, Wilhelmstrasse 56, 72074 Tübingen.

[2] Max-Planck-Institut für Chemie, Abteilung Geochemie, Postfach 3060, 55020 Mainz.

Eingereicht bei:
LITHOS

Eigenanteile:

a) Idee	20 %
b) Probenbeschaffung	70 %
c) Datenbeschaffung	20 %
d) Auswertung und Interpretation	20 %
e) Ausarbeitung der Publikation	30 %

Abstract

The mid-Proterozoic Isortoq dike swarm in the Gardar Province, South Greenland, comprises a variety of alkaline rocks ranging from gabbroic to syenitic in composition. Major magmatic mineral phases are olivine, clinopyroxene, Fe-Ti oxides, amphibole, plagioclase and alkali feldspar. Quartz occurs in some samples as a late magmatic phase. Liquidus temperatures of olivine-bearing samples range between 1120-1145 °C and solidus temperatures are 850-930 °C. Calculated silica activities are highly variable between 0.53 and unity. Oxygen fugacities vary from –3 to +1 log units relative to the fayalite-magnetite-quartz buffer.

The rocks have MgO contents < 6 wt.% with Mg# between 53 and 17. Primitive mantle-normalized trace-element patterns show a relative enrichment of LIL elements with Ba peaks and Nb troughs. Clinopyroxenes show a general enrichment in REE relative to chondritic values with variable slightly positive to prominent negative Eu anomalies. Two of the dikes were dated with Sm-Nd 3-point isochrons at 1190 ± 44 Ma and 1187 ± 87 Ma, respectively. Initial $^{87}Sr/^{86}Sr$ ratios of mafic mineral separates range from 0.70289 to 0.70432 and initial ε_{Nd} values vary from +0.3 to -10.7. Whole-rock initial $^{187}Os/^{188}Os$ ratios are highly variable including very radiogenic values of up to 7.967. $\delta^{18}O_{v\text{-}smow}$ values of separated clinopyroxene and amphibole range from +5.2 to +6.2 ‰ and fall within the range of typical mantle-derived rocks, although mixing with a lower crustal component is permitted by the data. Using EC-AFC modeling equations, the Sr-Nd isotope data of the more radiogenic samples can successfully be modeled by addition of up to 10 % lower crustal granulite-facies Archaean gneisses as contaminants. The Os isotopic data also suggest the involvement of old radiogenic crust. In accordance with seismic data, we conclude that a wedge of Archean crust extends from West Greenland further to the south below the present erosion level.

Keywords: Sr-Nd-Os-O isotopes; QUILF; EC-AFC modeling; mafic dike swarm; Gardar Province; South Greenland;

1. Introduction

Mafic dike swarms of Proterozoic age are widespread in many Precambrian cratons and their intrusion indicates a considerable extension of the continental crust (Tarney and Weaver, 1987). Studies of rift-related mafic dike swarms are essential for understanding generation of such extensive mafic magmatism and they may be used to identify mantle plumes (Ernst and Buchan, 1997, 2001). There is general agreement that mafic mantle-derived experience some degree of crustal contamination during ascent and/or residence in crustal magma chambers (Mohr, 1987). The crust is both a density filter and a source of incompatible elements (Lightfoot et al., 1991) and it may act as a site of large-scale contamination and extensive partial crystallization of primitive melts (O'Hara and Herzberg, 2002). However, there is much debate whether the trace element and isotopic characteristics of intracontinental basalts are mantle-derived or due to crustal contamination. Crustal contamination has been shown to be important in the petrogenesis of flood basalts (Devey and Cox 1987; Peng et al., 1992; Chesley and Ruiz 1998; Baker et al., 2000). On the other hand, a mantle source enriched in incompatible trace-elements not influenced by a major crustal input was postulated for some Proterozoic dike swarms (Tarney and Weaver 1987; Condie et al., 1987; Boily and Ludden, 1991) and other flood basalts (Molzahn et al., 1996). If a mantle-derived geochemical signature can be demonstrated, it remains difficult to locate the mantle source, i.e. whether the magmas are predominantly derived from the subcontinental lithospheric mantle (SCLM) (e.g. Gallagher and Hawkesworth 1992; Turner et al., 1996), from an upwelling mantle plume (e.g. LeCheminant and Heaman, 1989; Walker et al., 1997; Puchtel et al., 1999) or from a mixture of both (e.g. Ellam et al., 1992; Gibson et al., 1995; Thompson et al., 1998).

Here we present new petrological, geochemical and isotopic data of the Isortoq dike swarm in the mid-Proterozoic igneous Gardar Province in South Greenland. The Gardar Province represents a failed rift and comprises numerous mafic dikes of different generations. The Isortoq dike swarm is one major Gardar mafic dike swarm which has not been studied in great detail before, although the feldspathic inclusions in some of the dikes were the topic of several investigations (Bridgwater, 1967; Bridgwater and Harry, 1968; Halama et al., 2002). Since the swarm comprises a variety of petrographically diverse dike rocks ranging from gabbroic to syenitic in composition, it is well suited to study the influence of crustal assimilation processes on the composition of intracontinental mafic magmas. For that purpose, we combine petrological with Sr-Nd-O isotopic and whole-rock geochemical data. Additionally, we apply the Re-Os method which is known to have a great potential as tracer of crustal contamination (e.g. Chesley and Ruiz, 1998). The olivine-gabbroic

dikes may provide information on the nature of the mantle sources for the dikes and Gardar magmatism in general.

2. Geological Setting

The mid-Proterozoic Gardar Province in South Greenland represents a rift-related igneous province with magmatic activity lasting from about 1.35 to 1.14 Ga (Emeleus and Upton, 1976; Upton and Emeleus, 1987; Upton et al., 2003) (Fig. 1a). The country rocks mainly consist of I-type calc-alkaline granitoids (Julianehåb batholith) of Early Proterozoic age (van Breemen et al., 1974; Allaart, 1976; Patchett and Bridgwater, 1984; Kalsbeek and Taylor, 1985). Recent work (Garde et al., 2002) indicates that the Julianehåb batholith was emplaced mainly between 1.85 – 1.80 Ga. In the northwestern part of the province, Archean rocks of the Border and Foreland Zones of the craton comprise the basement (Allaart, 1976). Apart from twelve major alkaline igneous complexes and a succession of supracrustal lavas and sediments (Eriksfjord Formation), a large number of dike rocks with variable chemical composition intruded the basement. Two major dike swarms were emplaced into the Julianehåb batholith along WSW-ENE to SW-NE trends in the Tugtutôq-Ilímaussaq and the Nunarssuit-Isortoq zones during the late Gardar period (~ 1.20 - 1.14 Ga). The latter of these is the topic of the present paper.

In the Isortoq area, several generations of gabbroic to intermediate dikes with variable widths from a few centimeters to several hundred meters occur (Bridgwater and Coe 1970, Fig. 1b). The earliest generation of Gardar dikes belongs to a regional dike swarm of early-Gardar olivine dolerites ("Brown Dikes" or "BD_0 dikes") trending WNW-ESE across the Gardar province. They are dated at 1282 ± 5 Ma (Upton et al., 2003), pre-dating the main late-Gardar dike swarm of the Isortoq area. These Brown Dikes can be correlated with major dike swarms within the Canadian shield, namely the Mackenzie swarm (LeCheminant and Heaman, 1989) and the Harp dikes (Cadman et al., 1993).

The late-Gardar dikes of the Nunarssuit-Isortoq region were emplaced along WSW-ENE to SW-NE trends. The most spectacular feature of the dike swarm is the abundance of anorthosite xenoliths and feldspar megacrysts in some of the gabbroic dikes (Bridgwater and Harry, 1968; Halama et al., 2002) that are informally named "Big Feldspar Dikes" (BFDs). The feldspathic material varies from single feldspar crystals (< 1 cm to 1 m in size) to anorthositic bodies up to 30 m long. It is considered as evidence for an anorthosite body underlying South Greenland (Bridgwater, 1967). BFD 1 can be traced for 30 km and is one of the dikes with the greatest volume of feldspathic material in South Greenland (Bridgwater and Harry, 1968). BFD 2 is a composite dike that consists of a 1-2 m wide marginal microsyenite enclosing a feldspathic alkaline gabbro (Bridgwater and Harry, 1968). The amount of feldspathic material is about average in BFD 3, but relatively low in

BFD 4. Olivine-gabbros without excessive feldspathic material also occur. Composite dikes comprising a gabbroic, a syenitic and an intermediate syeno-gabbroic facies with maximum widths of up to 500 metres are called "Giant Dikes". They post-date all other members of the swarm (Bridgwater and Coe, 1970) and represent a connecting link between the mafic dykes and the major intrusions of the Gardar province. Giant Dike 3 is the least altered of the Giant Dikes and was therefore selected for a detailed study. Two further, petrographically distinct dikes investigated in this study include a larvikite and a hornblende-syenite. It is likely that some of the gabbroic dikes of the Isortoq swarm are connected to the Bangs Havn Giant Dike (Bridgwater and Harry, 1968) dated at 1185 ± 22 Ma (Engell and Pedersen, 1974). The swarm pre-dates the 1171 ± 5 Ma old Nunarssuit syenite (Finch et al., 2001).

3. Analytical Methods

Mineral compositions were determined using a JEOL 8900 electron microprobe at the Institut für Geowissenschaften, Universität Tübingen, Germany. An internal φρZ correction of the raw data was applied (Armstrong, 1991). Both synthetic and natural standards were used. Measuring times were 16 s for major elements and 30 s for minor elements. The emission current was 15 nA and the acceleration voltage 15 kV. For feldspar analyses, a beam diameter of 5 µm was used to avoid Na migration. The bulk compositions of oxy-exsolved titanomagnetite grains were reconstructed by combining image processing (NIH Image software) of back-scattered electron images of the exsolved grains with point analyses of exsolved ilmenite and broad beam analyses of exsolved magnetite (Marks and Markl, 2001).

Rare earth element contents (REE) in clinopyroxenes were measured by in-situ laser ablation inductively coupled plasma-mass spectrometry (LA-ICP-MS) at the EU Large-Scale Geochemical Facility (University of Bristol) using a VG Elemental PlasmaQuad 3 + S-Option ICP-MS equipped with a 266 nm Nd-YAG laser (VG MicroProbe II). Details of the method are described by Halama et al. (2002). The precision of trace-element concentrations, based on repeated analyses of standards, is approximately ± 5% for element concentrations >10 ppm and ±10% for concentrations <10 ppm. Typical detection limits for the REE in this study were 0.04 - 0.6 ppm.

Whole-rock analyses were performed by standard X-ray fluorescence (XRF) techniques at the Universität Mainz, using a Philips PW 1404 spectrometer and at the Universität Freiburg, using a Philips PW 2404 spectrometer. Pressed powder pellets and fused glass discs were prepared to measure contents of trace and major elements, respectively. The raw data were processed with the standard XR-55 software of Philips. Natural standards were used for calibration. Detection limits vary between 1 and 10 ppm, depending on the specific trace element and on the instrument used.

For Sr and Nd isotope analyses, about 10 mg of hand-picked mineral separate were spiked with mixed ^{84}Sr -^{87}Rb and ^{150}Nd - ^{149}Sm tracers before dissolution under high pressure in HF at 180°C in poly-tetrafluor-ethylene reaction bombs. Rb, Sr, Sm and Nd were separated and measured as described by Marks et al. (in press). Analyses of the Ames Nd-standard (Geological Survey of Canada, Roddick et al., 1992) gave $^{143}Nd/^{144}Nd = 0.512119 \pm 10$ ($\pm 2\sigma$, n = 42) and analyses of the NBS 987 Sr standard yielded $^{87}Sr/^{86}Sr = 0.710261 \pm 16$ ($\pm 2\sigma$, n = 30). $^{143}Nd/^{144}Nd$ ratios were cross-checked with the La Jolla Nd-standard which gave 0.511831 ± 30 ($\pm 2\sigma$, n = 12). ε_{Nd} values were calculated using present day CHUR values of 0.1967 for $^{147}Sm/^{144}Nd$ (Jacobson and Wasserburg, 1980) and 0.512638 for $^{143}Nd/^{144}Nd$ (Goldstein et al., 1984). The uncertainty in ε_{Nd} based on analytical errors is less than 0.5 ε_{Nd} units.

For Re-Os isotope analyses, 2-3 g of bulk sample powder was dissolved and equilibrated with a ^{185}Re – ^{190}Os mixed spike using aqua regia digestion in sealed Carius tubes (Shirey and Walker, 1998). Details of the further analytical procedures based on the method of Birck et al. (1997) are described by Puchtel et al. (2001). Re and Os isotopic compositions were measured via negative thermal ionization mass spectrometry at the MPI für Chemie at Mainz. Effects of mass fractionation were eliminated by normalizing to $^{192}Os/^{188}Os = 3.082678$. Re isotopic ratios were not corrected for fractionation. Analytical errors were determined by multiple analyses of internal MPI standards. They are ± 0.5% on both Os isotopic composition and Re/Os ratio. Initial $^{187}Os/^{188}Os$ ratios were calculated using the ^{187}Re decay constant of $1.666 * 10^{-11}$ a^{-1} (Shirey and Walker, 1998).

Oxygen isotope compositions of powdered whole-rock basement samples were determined by a conventional method modified after Clayton and Mayeda (1963) and Vennemann and Smith (1990), using BrF_5 as reagent and converting the liberated oxygen to CO_2. The oxygen isotope composition of 0.5 - 2 mg handpicked mineral separates was determined using a laser fluorination method adapted after Sharp (1990) and Rumble and Hoering (1994). Details of the method are described by Marks et al. (in press). Results are given in the standard δ-notation, expressed relative to V-SMOW in per mil (‰). Replicate oxygen isotope analyses of the NBS-28 quartz standard (Valley et. al., 1995) had an average precision of ± 0.1 ‰ for $\delta^{18}O$. In each run, standards were analyzed at the beginning and the end of the sample set. A correction was applied to the data equal to the average of the difference between the mean measured value and the accepted value for the standard (9.64 ‰).

4. Results

4.1. Petrography

Major mineral assemblages of the samples investigated in this study are summarized in Table 1. Abbreviations used there and in text and figures are after Kretz (1983).

Olivine-Gabbro and "Big Feldspar Dikes" (BFDs)

The major magmatic mineral phases in the olivine-gabbro and in BFDs 1, 3 and 4 are subhedral olivine, plagioclase and interstitial clinopyroxene. The excessive feldspathic material characteristic of the BFDs is absent in the olivine-gabbro, but otherwise both rock types are petrographically very similar. In BFD 2, olivine is lacking, but some quartz occurs interstitially. Minor phases are apatite, Fe-Ti oxides and sulphides. Biotite is fairly common and can occur either as single grain or surrounding Fe-Ti oxides or olivine. Titanite, amphibole and chlorite occur as secondary alteration products.

Giant Dikes

The Giant Dikes consist of a gabbroic and a syenitic facies. In the gabbroic samples primary minerals are plagioclase, alkali feldspar, anhedral olivine, interstitial clinopyroxene, titanomagnetite, ilmenite, and in some samples high amounts of apatite. In two samples (GM1761 and GM1762) olivine is rimmed by a second clinopyroxene generation. Biotite and/or chlorite overgrow olivine, clinopyroxene and Fe-Ti oxides, whereas amphibole is absent. The transition from the gabbroic to the syenitic facies is characterized by the disappearance of plagioclase, olivine and primary ilmenite, and the abundant occurrence of amphibole. Additionally, clinopyroxene in syenitic samples is euhedral to subhedral but never occurs as interstitial grains (Fig. 2a). As in the gabbroic samples, primary titanomagnetite is oxy-exsolved to ilmenite and magnetite. The exsolved ilmenite laths are selectively altered to titanite and chlorite. Most oxide grains are rimmed by amphibole, biotite and chlorite. In all syenitic samples, aggregates of sector-zoned epidote, associated with titanite, biotite and interstitial albite can be observed (Fig. 2b). In some places pumpellyite and prehnite occur as breakdown products of epidote. Sample GM1712 from the Giant Dike 1 is intermediate between the two above-mentioned facies. Primary olivine is strongly altered, titanomagnetite is the only primary Fe-Ti oxide, but plagioclase is still present in this sample. As in syenitic samples of Giant dike 3, aggregates of epidote and prehnite occur in this sample.

Larvikite

In the larvikite, olivine is very rare, and is surrounded by orthopyroxene (Fig. 2c). The major magmatic phases are clinopyroxene, plagioclase and alkali feldspar. Plagioclase is less common than alkali feldspar and is rimmed by the latter (Fig. 2d). Accessory phases in the larvikite include euhedral to subhedral amphibole, interstitial quartz, biotite, apatite, Fe-Ti oxides and sulphides. Secondary talc, titanite and chlorite are relatively rare.

Hornblende-syenite

Major minerals of this dike rock are euhedral amphibole, alkali feldspar and quartz. Accessory phases are Fe-Ti oxides, biotite, apatite and zircon. Occasional chlorite and titanite are probably of secondary origin.

4.2. Mineral Chemistry

Feldspars

Representative feldspar analyses are presented in Table 2 and illustrated in Fig. 3. In the olivine-gabbro and the BFDs, plagioclase is normally zoned and its composition varies between $An_{63}Ab_{36}Or_2$ and $An_{12}Ab_{85}Or_3$ (Fig. 3a). Plagioclase megacryst data from BFDs and the anorthosite xenoliths have been presented in Halama et al. (2002).

The gabbroic samples of Giant Dikes contain plagioclase evolving from $An_{59}Ab_{36}Or_5$ to $An_{15}Ab_{73}Or_{11}$ and alkali feldspar with compositions between $An_{14}Ab_{43}Or_{42}$ and $An_6Ab_{27}Or_{67}$ (Fig. 3b). Maximum anorthite content decreases from the margin to the center of the Giant Dike. In the syenitic facies, plagioclase is lacking, and alkali feldspar composition varies between $An_7Ab_{65}Or_{29}$ to $An_2Ab_{38}Or_{61}$ (Fig. 3b).

The larvikite contains plagioclase ($An_{47}Ab_{51}Or_2$ to $An_{20}Ab_{77}Or_3$) and alkali feldspar ($An_{14}Ab_{56}Or_{30}$ to $An_3Ab_{30}Or_{67}$; Fig. 3c). Large areas of alkali feldspar in the larvikite and all feldspar in the hornblende-syenite are completely exsolved to albite and orthoclase.

Olivine

Typical olivine analyses are presented in Table 3. Olivine ranges in composition from Fo_{70} to Fo_{32}, with the most Fo-rich olivine in some BFD samples and the most Fa-rich ones in the larvikite (Fig. 4). In the olivine-gabbro and the BFD samples, the compositional variability can reach 20 mol% Fo within a single grain and can be as large as in the whole sample. Some grains show growth zoning patterns with a decrease in Fo content towards the rims, but most are irregularly zoned. Olivines from Giant Dike 3 and from the larvikite are rather homogeneous with only minor chemical variation within one single grain and sample. In the gabbroic samples of Giant Dyke 3, Fo-contents of olivine decrease systematically from the margin (Fo_{57}) to the center (Fo_{38}) of the dike.

Clinopyroxene

Clinopyroxene of the whole sample suite is subcalcic augite with generally > 90% quadrilateral (Di + Hed + En + Fs) components. End-member components are calculated after Lindsley (1983) and

some typical analyses are presented in Table 4. Aegirine contents in all samples range from 2 to 10 mol %.

Augites in the olivine-gabbro, the BFDs and the matrix of the anorthosite xenoliths have all similar compositions between $En_{43}Fs_{15}Wo_{42}$ and $En_{30}Fs_{31}Wo_{39}$ (Figs. 4a, b). Some rare augite inclusions in feldspar megacrysts are relatively Ca-poor with a compositional range from $En_{51}Fs_{19}Wo_{31}$ to $En_{48}Fs_{19}Wo_{33}$ (Fig. 4a).

Augite in the gabbroic samples of the two Giant dikes is essentially unzoned and shows a relatively small compositional range within the sample suite ($En_{41}Fs_{16}Wo_{42}$ to $En_{34}Fs_{22}Wo_{44}$). Augite rims around olivine are strongly zoned showing an increase in Fs-component with increasing distance from the olivine grain ($En_{42}Fs_{11}Wo_{47}$ to $En_{31}Fs_{22}Wo_{47}$). Augites of the syenitic samples span a large range in composition ($En_{40}Fs_{19}Wo_{41}$ to $En_{8}Fs_{47}Wo_{45}$), partly overlapping with augites of the gabbroic samples. Due to strong chemical zoning, the compositional variation within one single grain may reach as much as 20 mol% (Fig. 4c). Among the investigated syenitic samples, three different zoning patterns can be distinguished: In most cases X_{Fe} (=Fe^{2+}/(Fe^{2+} + Mg), Fe^{3+}, Na and Si increase and Ti and Al(4) decrease more or less continuously from core to rim, whereas the wollastonite component is almost constant (Fig. 5a). Some samples have Mg-rich cores, and display a stepwise increase of X_{Fe} from core to rim (Fig. 5b). In other samples, partly resorbed inner cores of clinopyroxene are Fe- and Si-rich, followed by a homogeneous but significantly Fe-depleted outer rim with a normal increase of X_{Fe} towards the rim. Interestingly, Na, Al(4), Fe^{3+} and Ti contents in these crystals is more or less constant throughout the whole profile (Fig. 5c).

Clinopyroxene in the larvikite is relatively Ca-poor with a compositional range between $En_{44}Fs_{17}Wo_{39}$ and $En_{29}Fs_{32}Wo_{39}$ (Fig. 4d).

Orthopyroxene

Orthopyroxene is only present in the larvikite where it occurs as small rims around olivine (Fig. 2c). It is chemically unzoned with a composition of $En_{52}Fs_{47}Wo_{1}$ to $En_{50}Fs_{49}Wo_{1}$.

Fe-Ti oxides

Typical compositions of exsolved and reintegrated Fe-Ti oxides are presented in Table 5. In most samples, primary titanomagnetite is oxy-exsolved to ilmenite and magnetite (Figs. 6a-d).

The olivine-gabbro contains a single oxy-exsolved titanomagnetite with very Ti-rich compositions ($Usp_{94-95}Sp_{3-4}Mag_{2}$), which is characterized by a very fine trellis-type exsolution texture (terminology after Buddington and Lindsley, 1964 ; Fig. 6a).

In BFD 1 and 3, more coarsely trellis-type oxy-exsolved titanomagnetite is common, but there are also Fe-Ti oxide grains where it is difficult to decide whether they represent a single oxy-exsolved grain with a granule exsolution texture or two coexisting oxides. In those cases, oxides with trellis-type exsolution were preferentially used for reintegration resulting in compositions between $Usp_{89}Sp_3Mag_7$ and $Usp_{65}Sp_4Mag_{31}$ (Fig. 6b). In BFD 4, a two-oxide assemblage comprises $Usp_{71-58}Sp_{9-5}Mag_{24-37}$ coexisting with $Ilm_{98-96}Hem_{2-4}$.

Gabbroic samples of Giant Dike 3 contain a two-oxide assemblage of titanomagnetite ($Usp_{94-70}Sp_3Mag_{4-27}$) coexisting with ilmenite ($Ilm_{99-96}Hem_{1-4}$). The intermediate sample of Giant Dike 1 contains a single exsolved titanomagnetite of the composition $Usp_{93-83}Sp_3Mag_{5-14}$. In syenitic samples primary titanomagnetite compositions could not be recalculated because both exsolved ilmenite and magnetite were strongly altered to titanite/Fe-rich chlorite and chlorite/Fe-hydroxides, respectively (Fig. 6c). However, relics of exsolved magnetite ($Usp_{19-8}Sp_{5-3}Mag_{78-87}$) still have elevated Ti contents indicating an Usp-rich primary composition of titanomagnetite.

The larvikite contains a two-oxide assemblage, but textural evidence suggests that ilmenite was overgrown by later magnetite (Fig. 6d). Both have a relatively constant composition of $Ilm_{97-94}Hem_{6-3}$ and $Usp_{27-21}Sp_{4-3}Mag_{70-76}$, respectively. The hornblende-syenite contains only primary ilmenite of the compositon $Ilm_{98-89}Hem_{2-11}$.

4.3. Calculation of intensive crystallization parameters

Intensive crystallization parameters were calculated because estimates of liquidus and solidus temperatures of the dike magmas are essential for energy constrained – AFC modeling (Spera and Bohrson, 2001) and calculated values of silica activity and oxygen fugacity may provide important constraints on the evolution of the dike magmas. For all calculations, pressure was fixed at 1 kbar, assuming that crystallization of the dikes took place at approximately the same depth as of the Ilímaussaq complex further south in the Gardar Province for which a crystallization pressure of ~ 1 kbar was derived from fluid inclusion data (Konnerup-Madsen and Rose-Hansen, 1984).

Liquidus temperatures were calculated for some olivine-bearing samples, which are considered to be close to liquid compositions (GM 1803, GM 1735, GM 1805 and GD 39) after Sugawara (2000) based on the MgO content in olivine-saturated liquids. They range between 1145 and 1120 °C with an error in calculated temperatures of ± 30 °C.

Feldspar geothermometry using solvus isotherms after Elkins and Grove (1990) indicates minimum crystallization temperatures of ~ 700 °C for BFD 1 as an example for the gabbroic BFDs and the olivine-gabbro (Fig. 3a). Plagioclase-alkali feldspar pairs in the gabbroic samples of Giant Dike 3 and in the larvikite are not in equilibrium. As shown in Fig. 2d, plagioclase has reacted with the

liquid to produce alkali feldspar. Ternary feldspar compositions in gabbroic and syenitic samples of Giant Dike 3 point to minimum temperatures of 950 °C - 1020 °C (Fig. 3b). A zoning profile through an alkali feldspar in the larvikite show continuously decreasing minimum temperatures from > 1000 ° in the core to about 700 °C in the outermost rim (Fig. 3 c).

Solidus temperatures, silica activity and oxygen fugacity were calculated from olivine-pyroxene-Fe-Ti oxide equilibria using the QUILF program of Andersen et al. (1993). The theoretical background for these calculations was given by Frost and Lindsley (1992) and Lindsley and Frost (1992). Temperature and silica activity were calculated based on Fe, Mg and Ca exchange between olivine and clinopyroxene using a range of mineral compositions. Calculated silica activities are based on a reference state of pure SiO_2 at P and T. The oxygen fugacity was calculated from equilibria among Fe-Mg silicates and Fe-Ti oxides using the full range of measured and reintegrated Fe-Ti oxide compositions. Details of the use of QUILF can be found in Marks and Markl (2001).

Calculated equilibrium temperatures for the olivine-gabbro, the BFDs, and for gabbroic samples of the Giant Dike 3 range between 930°C and 850°C. Calculated silica activities are 0.60 in the olivine-gabbro, 0.67 - 0.83 in the quartz-free BFDs, and 0.53 – 0.68 in the Giant Dike profile. The clinopyroxene rims around olivine in two gabbroic samples of Giant Dike 3 indicate an increase in silica activity. In the syenitic samples, olivine has disappeared due to a further increase in silica activity during progressive fractionation. Unreasonably low calculated temperatures (< 650 °C) for the larvikite indicate that very rare olivine is not in chemical equilibrium with clinopyroxene. Using a calculated olivine equilibrium composition of Fo_{56} and a range of early ilmenite compositions, the resulting silica activity is 0.83, which is within the upper range obtained for the gabbroic samples. The orthopyroxene rim around olivine indicates increasing silica activities during later stages. This is in accordance with petrography, as interstitial quartz is present and thus, final solidification of the larvikite took place at $a_{SiO2} = 1$.

Generally, the calculated oxygen fugacity increases with increasing silica activity from about 3 log units below the fayalite-magnetite-quartz (FMQ) buffer in the olivine-gabbro to values slightly above the FMQ buffer in some BFD samples, with the gabbroic samples of Giant Dike 3 in between (Fig. 7). Oxygen fugacity for the syenitic samples of Giant Dike 3 could not be determined because it was not possible to reconstruct the primary composition of titanomagnetite. However, the absence of primary ilmenite indicates that oxygen fugacity in the syenitic samples was higher than in gabbroic samples of Giant Dike 3 (Toplis and Carroll, 1995). For the larvikite, oxygen fugacity was calculated only with ilmenite, as textural relationships (Fig. 6d) indicate that magnetite grew later. It varies between 0 and 0.9 log units below FMQ at T = 853 °C. Oxygen fugacity calculated with the assemblage Fe-rich clinopyroxene + titanomagnetite ± orthopyroxene at temperatures fixed between

850-700 °C to simulate gradual cooling during later stages indicates more oxidizing conditions of 0.6 to 1.0 log units above the FMQ buffer.

4.4. REE data of clinopyroxenes

REE concentrations of average clinopyroxenes from the Isortoq dike rocks are presented in Table 6 and typical chondrite-normalized REE patterns of individual and average analyses are shown in Fig. 8. Since closed-system fractionation can result in considerable fractionation of the REE (Bernstein et al., 1998), rims of clinopyroxenes were avoided for analyses. Clinopyroxenes of all dikes are enriched in REE relative to chondritic values. The patterns generally show an increase in normalized REE contents from La to Nd, followed by a gradual decrease from Sm to Lu. Significant Eu anomalies are lacking in the BFDs, but there is a small negative Eu anomaly in the olivine-gabbro (Eu/Eu* = 0.70). In the Giant Dikes, a negative Eu anomaly is increasing from Eu/Eu* = 0.81 in the relatively primitive gabbroic facies, via 0.65 in an intermediate syenogabbro towards 0.41 in the more fractionated syenitic rocks. A similar evolution can be seen in the larvikite, where the extent of the negative Eu anomaly is positively correlated with the degree of REE enrichment, i.e. fractionation. Taking La_N/Yb_N as a measure for REE fractionation, two observations may be of importance: First, the olivine-gabbro has a less fractionated clinopyroxene REE pattern than the BFDs, but it has a more pronounced negative Eu anomaly. Second, La_N/Yb_N in the low-Ca clinopyroxene inclusions is considerably lower than in any of the dike matrix clinopyroxenes. Clinopyroxenes from all dike rocks have REE patterns similar to gabbros from the rifted East Greenland margin (Bernstein et al., 1998), but distinct from gabbros derived from a MORB-like source.

4.5. Whole-rock geochemistry

XRF whole-rock data of the dike rocks are presented in Table 7 and the compositional variation with respect to Mg# as fractionation index is shown in Fig. 9. Mg-numbers (Mg# = 100 Mg/(Mg + Fe^{2+}) atomic) were calculated using a Fe_2O_3/FeO ratio of 0.2 (Middlemost, 1989) for all rock types as the Ti-rich oxides from all samples indicate relatively reducing conditions even in more fractionated rocks. Mg# between 53 and 18 indicate that the samples do not represent primary melts. SiO_2 contents appear to be relatively scattered, but there is a distinct negative correlation within the BFD and the Giant Dike samples. The positive correlation of CaO/Al_2O_3 with Mg# suggests fractionation of clinopyroxene (Class et al., 1994). The larvikite and the hornblende-syenite are characterized by higher SiO_2 and lower CaO/Al_2O_3 values. The high P_2O_5 and TiO_2

concentrations in Giant Dike sample GM 1760 (Table 7), combined with the high modal apatite content, indicates that this sample was affected by apatite and possibly Fe-Ti oxide accumulation.

Maximum Ni and Cr contents of 87 ppm and 70 ppm, respectively, confirm that the dikes crystallized from relatively fractionated melts. Other trace elements compatible in mafic systems (e.g. V, Sc) also have relatively low concentrations. Ni and Sc are positively correlated with Mg# suggesting fractionation of olivine and clinopyroxene. A positive correlation of Cr contents with Mg# in the BFDs is a further indication that olivine and/or clinopyroxene fractionation operated in the magmas (not shown). V, which is highly compatible in magnetite and slightly compatible in clinopyroxene, is also decreasing with decreasing Mg#, indicating fractionation of Fe-Ti oxides. The larvikite and the hornblende-syenite have compatible trace element contents that lie in general within the trends observed for the other samples, although the latter has relatively low Ni contents. However, due to its distinct mineralogy compared with all the other dikes, the hornblende-syenite should not be combined with the other data to derive conclusions on the geochemical evolution of the magmas. Incompatible trace elements like Zr show a weak negative correlation with Mg# for the Giant Dike samples consistent with increasing degrees of differentiation, but the BFD samples are rather scattered.

Normative mineral compositions were calculated following the CIPW scheme (Cross et al., 1903; Cox et al., 1979) and characteristic normative minerals are listed in Table 7. The olivine-gabbro and the BFDs are variably *ne*- and *hy*-normative. In the Giant Dikes, normative compositions change from *ne*-normative in the gabbros to *hy*-normative in the syenites. The *qz*-normative larvikite and hornblende-syenite both contain modal quartz indicating that the normative compositions accurately reflect the modal mineralogy. However, BFD 2 (GM 1750) and the anorthosite xenolith (GM 1682) have late interstitial quartz, but they are quartz-free in the norm calculation. This might be due to the fact that small errors in the assumed Fe^{2+}/Fe^{3+} ratio can lead to variable normative mineral compositions. In summary, the calculations of the normative mineral compositions demonstrate that the least fractionated rocks are silica undersaturated. The most fractionated rocks, represented by the syenites of the Giant Dikes, evolved towards *hy*-normative compositions. *Qz*-normative compositions of the larvikite and the hornblende-syenite are not coupled to a low Mg#.

Primitive mantle-normalized incompatible trace element diagrams for selected samples are shown in Fig. 10. The patterns are characterized by a general enrichment relative to primitive mantle values and distinct Ba peaks and Nb troughs. The Ba peak in the hornblende-syenite is considerably smaller than in all other dikes. Small negative P and Ti anomalies are present in the two syenitic samples, and the GD 3 syenite has also a negative Sr anomaly. The two BFD samples have fairly

smooth patterns from La to Y with a small positive Sr anomaly in the anorthosite xenolith and a small negative one in BFD 4.

4.6. Sr and Nd isotopic compositions

Sr and Nd isotopic compositions of mineral separates from the dikes and of whole-rocks from the Julianehåb batholith are presented in Table 8. Using the Sm-Nd system on mineral separates of clinopyroxene and plagioclase and whole-rock powder (Table 8, Fig. 11), we dated sample GM 1735 from BFD 1. The age of 1190 ± 44 Ma agrees well with that of the Bangs Havn Giant Dike (1185 ± 22 Ma; Engell and Pedersen, 1974) which is thought to be of the same age. The three clinopyroxene separates from Giant Dike 3 give an age of 1187 ± 87 Ma, consistent with the BFD 1 and the Bangs Havn Giant Dike ages. These ages also agree with field evidence, as the Isortoq swarm is cut by the Nunarssuit syenite, which was dated by the U/Pb method at 1171 ± 5 Ma (Finch et al., 2001), and post-dates the older "Brown dikes" dated at 1280 ± 5 Ma (Upton et al., 2003). The ages of the Isortoq dike swarm overlap with a Rb-Sr age for a dike from the Narsarsuaq area (1206 ± 20 Ma; Winther, 1992), an U-Pb age for the older Giant Dike of Tugtutôq (1184 ± 5 Ma; Upton et al., 2003) and Sm-Nd ages for the Eriksfjord Formation basalts (1170 ± 30 and 1200 ± 30 Ma; Paslick et al., 1993). However, more precise U-Pb dating would be desirable to determine how these magmatic events are related in time.

$^{87}Sr/^{86}Sr$ initial ratios of the dikes at 1.19 Ga range from 0.70289 to 0.70432 and $\varepsilon_{Nd}(i)$ values from + 0.3 to – 10.7 (Table 8). On the Sr-Nd isotope diagram, the data define a relatively steep trend (Fig. 12) with initial $^{87}Sr/^{86}Sr$ ratios of the isotopically more primitive samples similar to Bulk Silicate Earth (BSE). The olivine-gabbro and the Giant Dikes have $\varepsilon_{Nd}(i)$ values clustering around 0 to –2, whereas the BFDs show a clear tendency towards more negative $\varepsilon_{Nd}(i)$ values. None of the samples has $\varepsilon_{Nd}(i)$ values close to those of the depleted MORB mantle (DMM) reservoir, estimated to be between $\varepsilon_{Nd}(i) = + 5.3$ (calculated after DePaolo, 1981) and $\varepsilon_{Nd}(i) = + 7.4$ (calculated after Goldstein et al., 1984).

In comparison with other Sr-Nd data from the Gardar Province, the Isortoq dikes extend the range of $\varepsilon_{Nd}(i)$ towards significantly more negative values than previously reported. The isotopically more primitive dikes overlap with data from the Eriksfjord Formation basalts (Halama et al., in press), but they do not reach the positive $\varepsilon_{Nd}(i)$ values of basaltic, lamprophyric and carbonatitic dikes from Ivittuut (Goodenough et al., 2002) and Igaliko (Pearce and Leng, 1996). The intitial $^{87}Sr/^{86}Sr$ ratios of the Isortoq dikes, however, show a broad overlap with published data.

4.7. Re-Os isotopic analyses

The Os isotopic data presented in Table 9 include 4 samples from the Isortoq dike rocks together with 4 samples from the Eriksfjord Formation basalts (Halama et al., in press) and 2 samples from the Ilímaussaq intrusion (Marks and Markl, 2001). The EF basalt samples were added to the data set because they represent even more primitive Gardar melts than the Isortoq dikes and are therefore more likely to reflect the Os isotopic composition of the mantle source. The augite syenites from Ilímaussaq are the most primitive rocks of one of the major igneous complexes of the Gardar Province. Obtaining reliable geochemical information of these samples proved to be a challenging task because of the very low Os abundances and the potential Re-mobility during secondary alteration, although it has been shown that the Re-Os system can remain resistant during low-degree metamorphism and hydrothermal alteration (Puchtel et al., 1999). One sample (EF 024) was omitted from data analysis because it was overspiked with respect to Os. The other samples show highly variable initial $^{187}Os/^{188}Os$ ratios ranging from –2.428 to 7.967 (Table 9). The negative $(^{187}Os/^{188}Os)_i$ of the olivine-gabbro is probably due to either analytical problems or mobilization of Re. All other $(^{187}Os/^{188}Os)_i$ values are much higher than those assumed for the primitive upper mantle (0.129), the subcontinental lithospheric mantle (0.105-0.129), the depleted MORB mantle (0.123-0.126) or enriched mantle components (0.130–0.152) (Shirey and Walker, 1998). The initial $^{187}Os/^{188}Os$ ratio of the two most radiogenic samples are significantly higher than the estimated average upper crustal value of 1.9256 (Esser and Turekian, 1993) and a range of values from 0.1652 to 1.8138 for lower crustal xenoliths (Saal et al., 1998).

4.8. Oxygen isotope measurements

Oxygen isotope analyses of mineral separates from the dikes and whole-rock powders from the basement rocks are listed in Table 8. $\delta^{18}O$ values of clinopyroxene and amphibole separates from the dikes range from 5.2 to 6.2 ‰. The BFDs show a restricted range in $\delta^{18}O_{cpx}$ from 5.6 - 5.9 whereas the dikes without feldspathic material, i.e. the olivine-gabbro and the Giant Dikes, have lower $\delta^{18}O_{cpx}$ values in the range 5.3 - 5.6 ‰. Most of the $\delta^{18}O_{cpx}$ values from the Isortoq dike swarm overlap with $\delta^{18}O_{cpx}$ values of mantle peridotites (5.25 – 5.90 ‰, Mattey et al., 1994), OIBs (5.3 – 6.1 ‰, Harris et al., 2000) and the spatially associated Eriksfjord Formation basalts (5.2 – 6.0 ‰, Halama et al., in press).

The oxygen isotope equilibration temperature for fractionation between plagioclase and diopside was calculated after Zheng (1993) for sample GM 1735 (BFD 1) using Δ(plagioclase-diopside) = 0.89 and X_{An} = 0.50. The apparent equilibration temperature is 924 °C. Allowing an error of ± 0.15

‰ in Δ, calculated temperatures range from 832 to 1035 °C. This indicates that the equilibration of oxygen isotopes occurred at magmatic temperatures.

Mineral-melt fractionations allow the calculation of the magma oxygen isotopic compositions directly from measured values of minerals (Taylor and Sheppard, 1986). Using a $\Delta_{melt\text{-}cpx}$ value of 0.3, calculated after Kalamarides (1986) for a liquidus temperature of ~ 1130 °C, calculated $\delta^{18}O_{melt}$ values for the Isortoq dike rocks range from 5.5 to 6.5 ‰.

On the $\varepsilon_{Nd}(i)$ - $\delta^{18}O$ diagram (Fig. 12b), the Isortoq dike rocks define a weak trend of slightly increasing $\delta^{18}O$ with decreasing $\varepsilon_{Nd}(i)$. This trend does not approach the trend defined by the Ketilidian basement rocks. Some of the data overlap with comparative data from the Eriksfjord Formation basalts, but none of the Isortoq data plots close to a modeled DMM source.

5. Discussion

5.1. Validity of calculations of intrinsic parameters

Liquidus temperatures calculated for the Isortoq dike samples after Sugawara (2000) (1120-1145 °C) are in agreement with experimental results from Upton (1971) and Upton and Thomas (1980), who obtained liquidus temperatures of about 1190 °C for very similar gabbroic rocks from the Tugtutoq area and assumed that the intrusion of the dike magmas took place between 1160 and 1125 °C. Toplis and Carroll (1995) obtained similar liquidus temperatures for ferro-basaltic melts of ~ 1160 °C. Minimum crystallisation temperatures derived from ternary feldspars yield temperatures in the range 950-1020 °C similar to intrusion temperatures of 1050°C inferred for more differentiated syenitic rock types (Upton and Thomas, 1980).

Temperatures determined by QUILF (Andersen et al., 1993) can be subjected to subsolidus exchange (Markl et al., 1998). Re-equilibration of Fe/Mg in mafic silicates takes place more readily than Na/Ca equilibration in plagioclase (Morse 1984) and restricted zoning may suggest local homogenization (Tegner et al., 1996). Fe/Mg silicates equilibrate fast when liquid is present and temperatures calculated by QUILF might reflect equilibration with a cooler, more fractionated residual melt (Markl and White 1999). Our QUILF-calculated temperatures (930-850 °C) are slightly lower compared to solidus temperatures of hawaiitic magmas (990-965 °C, Upton 1971). Therefore, QUILF temperatures calculated here are believed to reflect partly solidus temperatures and partly sub-solidus exchange temperatures. Thus, the crystallization interval for the gabbroic rocks is assumed to be 1150-900 °C, whereas the syenitic rocks probably crystallized between 1050-800 °C.

The calculated silica activities correlate positively with whole-rock SiO_2 contents, indicating that the results are reliable. Oxygen fugacities indicate conditions below the FMQ buffer curve within

the range of other Gardar magmas. Low oxygen fugacities appear to be a general feature of the Gardar magmas (Powell, 1978; Upton and Thomas, 1980, Larsen and Sørensen, 1987; Marks and Markl, 2001; Marks et al., in press). Albeit the range in calculated log f_{O2} values is relatively large, there appears to be a general tendency of increasing oxygen fugacity with increasing silica activity (Fig. 7), which is confirmed by magnetite overgrowths over ilmenite in the larvikite. This feature may hint at an FMQ-type equilibrium buffering these parameters.

5.2. Evidence for closed-system fractionation in the Giant Dikes

The systematic decrease of X_{Fo} in olivine and X_{An} in plagioclase parallel to the assumed crystallization direction from the margin towards the dike center in GD 3 is interpreted to reflect fractional crystallization in an essentially closed system for the gabbroic facies of the dike. For various intrusions of the Gardar Province, in situ differentiation (e.g. Stephenson and Upton, 1982; Marks and Markl, 2001) and sidewall crystallisation (e.g. Parsons and Brown, 1988) have been proposed as crystallization processes and it seems likely that both of those processes governed the magmatic evolution of the gabbroic facies of the Giant Dikes. Whole-rock geochemical data trends and REE patterns from clinopyroxenes are consistent with a closed-system fractional crystallization in Giant Dike 3. The Nd isotopic data provide evidence that fractionation from gabbroic to syenitic rocks in GD3 took place in a closed-system because the three samples from GD3 do not show any change in $\varepsilon_{Nd}(i)$ at various concentrations of SiO_2 (Fig. 13) and it was demonstrated earlier that they define an isochron age. Thus, the syenitic rocks may represent a more differentiated member of the same parental melt as the gabbroic rocks. However, differentiation did probably not occur in situ as field evidence (Bridgewater and Coe, 1970, and own observations) indicates that stoping was an important emplacement mechanism in the Giant Dikes. Thereby, syenitic rocks differentiated in deeper levels as the magma rose, and intruded the partly solidified gabbroic material. Fe-rich and partly resorbed cores (Fig. 5) of augites from syenitic samples support this assumption. Possibly, these cores represent relics of crystals from gabbroic rocks which where already solidified and were incorporated into the rising magma during emplacement of the syenitic members.

5.3. Evaluation of crustal contamination and mantle heterogeneity

Variations in the Sr-Nd isotopic composition of magmatic rocks can principally be explained by either crustal contamination or heterogeneous mantle sources. Today, the different mantle components have a wide range of isotopic compositions (Hart et al., 1992, Hofmann, 1997), but their projection into the Proterozoic is problematic. Generally speaking, steep trends on Sr-Nd isotope plots could be attributed to mixtures of an isotopically depleted mantle component and an

isotopically enriched mantle component similar to EM-1 (e.g. Milner and Le Roex, 1996). The EM-1 component is characterized by extremely low $^{143}Nd/^{144}Nd$ ratios and negative ε_{Nd} values (Hofmann, 1997). Based on the Sr-Nd data alone, it seems possible that the dike magmas were derived from a source composed of two distinct mantle components, implying that the larvikite is closest to the EM-1-like end-member composition. However, mantle melts with these low initial Nd isotopic values are usually potassic, highly enriched in LREE and do not show any features indicative of crustal influences (e.g. Nelson, 1992, Schmidt et al., 1999). We will show below that there are many signs for a crustal component in the dike compositions and we therefore prefer the alternative view to explain the decrease in initial ε_{Nd} values by increasing amounts of crustal contamination (e.g. Paces and Bell, 1989).

In the Isortoq dikes, the rough negative correlation of a_{SiO2} with Mg# indicates that a_{SiO2} was increasing with fractionation and/or crustal contamination (Fig. 13). One possibility to explain this is that the liquid composition for the dike rocks started on the right-hand side of the thermal boundary in the nepheline-albite-quartz system and therefore differentiation produced quartz-saturated compositions. However, the trend towards higher a_{SiO2} in the Isortoq dikes is not continuous as the most fractionated syenites of Giant Dike 3 are still below SiO_2-saturation, whereas the less fractionated larvikite contains quartz. The negative correlation of a_{SiO2} with ε_{Nd} (Fig. 13) is not compatible with simple fractionation trends, but suggests assimilation of relatively quartz-rich partial melts of crustal rocks that influenced the silica activities in the dikes to different degrees. Normative rock compositions agree well with the Nd isotope and QUILF data. Those rocks with relatively high ε_{Nd} are *ne*-normative, whereas the larvikite with the most negative ε_{Nd} is *qz*-normative, again consistent with assimilation of a SiO_2-rich partial melt. Mixing with SiO_2-rich mantle material is considered as unlikely because typical mantle-derived melts are usually poor in SiO_2 compared to crustal melts.

Geochemical data are in agreement with the assimilation hypothesis. High Ba contents typical of the Isortoq dikes (Fig. 10) resemble those in basaltic-hawaiitic lavas from Mull (Kerr *et al.,* 1995). Based on melting experiments (Thompson, 1981), the latter were explained by addition partial melts derived from Lewisian gneisses containing alkali feldspar as a source of the Ba (Kerr et al., 1995). This scenario is also conceivable for the Isortoq magmas when we consider contamination with Archean lithologies which are present in the craton of southern West Greenland. There, granodioritic K-feldspar-bearing gneisses are quite common (McGregor, 1973; O'Nions and Pankhurst, 1974) and some of the gneisses are relatively Ba-rich (McGregor, 1979). Small negative Nb and Ti anomalies (Fig. 10) are consistent with contamination by crustal material modified or generated by subduction zone magmatism. In fact, they are typcial features of Archean granulites

(Rudnick and Presper, 1990) and negative Nb anomalies in flood basalts were previously explained by crustal contamination (McDonough, 1990). However, the presence of a negative Nb anomaly is no unequivocal evidence for crustal contamination, as it was also proposed to be characteristic for magmas derived from the SCLM (e.g. Hawkesworth et al., 1992; Goodenough et al., 2002).

Recent studies have shown that the Re-Os isotopic system can be particularly useful to distinguish between magmas derived from sublithospheric mantle plumes and lithospheric mantle (e.g. Ellam et al., 1992; Hart et al., 1997; Shirey, 1997). Additionally, Re-Os data can be a powerful tool to decipher crustal assimilation (e.g. Chesley and Ruiz, 1998) as some portions of the lower crust comprise the most radiogenic large-scale Os reservoirs within the Earth (Asmerom and Walker, 1998). Os concentrations in the Isortoq dike rocks are very low, probably because of the compatible behaviour of Os during mantle melting (Shirey and Walker, 1998), prior sulfide separation and/or Os compatibility in olivine (Brügmann et al., 1987). Therefore, small amounts of crustal contamination may have a large impact on the Os isotopic composition of the magmas. On the Re-Os isochron diagram, the data points have a tendency to scatter around the 1.2 Ga reference line, which is an approximate realistic age for all samples (Fig. 14). Excluding the relatively most altered Eriksfjord Formation basalt sample (EF 174), a reasonable fit of the reference line to the data points yields an initial $^{187}Os/^{188}Os$ ratio of ~ 0.8. Despite the large uncertainty in this estimation, this ratio is much higher than $^{187}Os/^{188}Os$ values of all known mantle reservoirs, which have a range in $^{187}Os/^{188}Os$ from 0.105 to 0.152 (Shirey and Walker, 1998). Therefore, the Os isotopic composition does not reflect a primary mantle composition. The only reservoir known to contain significant radiogenic Os is old continental crust (Chesley and Ruiz, 1998) and lower crustal xenoliths with $^{187}Os/^{188}Os$ values as high as 3.5 have been reported (Molzahn et al., 1996). Accordingly, several studies postulated the assimilation of material from the lower crust in the petrogenesis of mafic continental magmas (e.g. Asmerom and Walker, 1998; Sproule et al., 2002). The Os isotopic data are at least compatible with an important role of assimilation of crustal material in the petrogenesis of the Gardar magmas. The high initial $^{187}Os/^{188}Os$ ratio might suggest that almost all Os was crustally derived.

Fractionation of olivine, clinopyroxene, plagioclase and Fe-Ti oxides is known to produce small increases in melt $\delta^{18}O$ values (< 0.3 ‰) and the increase in the $\Delta_{melt\text{-}cpx}$ fractionation factor with decreasing T is about 0.1 ‰ in $\delta^{18}O$ of the clinopyroxene (Baker et al., 2000). Therefore, the increase in $\delta^{18}O$ isotopic values in the Isortoq clinopyroxenes can only partly be accounted for by these processes. Since the EM-1 mantle component does not deviate significantly from average upper mantle values (Eiler et al., 1997), the $\delta^{18}O_{melt}$ in the larvikite is above typcial values for mantle melts and requires another explanation than a heterogeneous mantle source. The weak

positive correlations of $\delta^{18}O$ with ε_{Nd} (Fig. 12b) and Eu/Eu^*_{cpx} (Fig. 15) are consistent with an $\delta^{18}O$ increase due to crustal contamination. The Nd-O data indicate that assimilation of Ketilidian upper crustal basement is unlikely (Fig. 12b). This is supported by field evidence as granitoid xenoliths in the dikes are characterized by sharp contacts, suggesting that they did not react much with the magmas. Lower crustal rocks of igneous origin have an average $\delta^{18}O$ value of +7.5 ± 1.4 ‰ with an overall range from +5.4 ‰ to +12.5 ‰ (Fowler and Harmon, 1990) and contamination with crustal material with oxygen isotopic values of +7.0 ‰ to + 10 ‰ and low ε_{Nd} values is in qualitative agreement with the data.

Having established that the olivine-gabbro and the Giant Dikes are less crustally contaminated than the BFDs, the absence of a negative Eu anomaly in the BFDs needs to be explained. Intuitively, one would expect that the more pronounced the influence of the AFC process is, the larger should the negative Eu anomaly be. However, this is not the case and alternative explanations are required. A significant difference in the oxidation state of the magmas can be excluded because QUILF calculations show negative ΔFMQ values for both. A more viable explanation for the lack of negative Eu anomalies in the BFD clinopyroxenes is resorption of plagioclase in the melt either due to a pressure decrease or due to injection of new, hot magma (Markl and Frost, 1999). BFD magmas could have been mechanically enriched in plagioclase in a magma chamber possibly close to the crust-mantle boundary before the resorption started. Alternatively, interaction with lower crust can even produce positive Eu anomalies in the melts (Mitchell et al., 1995). This explanation is also compatible with the negative correlation of Eu/Eu^*_{max} with ε_{Nd} (Fig. 15) because a larger degree of assimilation as seen in the BFDs would also lead to a relative enrichment in Eu. REE data of amphibolite- and granulite-facies gneisses from the Archean craton of southern West Greenland frequently show a prominent positive Eu anomaly (Compton, 1978) and contamination of the dike magmas with similar material is therefore in agreement with the REE data. In the most primitive clinopyroxenes of the most contaminated rock (the larvikite), an Eu anomaly is also absent (Fig. 8). Negative Eu anomalies occur in more REE-enriched clinopyroxenes of the larvikite, but the size of the anomaly correlates well with the degree of REE fractionation and can therefore be best explained by plagioclase fractionation.

5.4. Quantitative modeling of crustal contamination processes

Mechanisms to explain contamination signatures in mantle-derived mafic magmas include assimilation coupled with fractional crystallization (AFC) (Bowen, 1928; Taylor, 1980; DePaolo, 1981) and assimilation of crust by the most mafic magmas during turbulent ascent (ATA) (Huppert

and Sparks, 1985; Devey and Cox, 1987). Correlations of isotopic ratios and parameters of fractionation can be used to evaluate which process is more likely to have occurred. For the Isortoq magmas, the $\varepsilon_{Nd}(i)$ vs. SiO_2 diagram (Fig. 13) reveals a negative correlation. This indicates that AFC processes were operating because AFC processes result in the most evolved rocks becoming the most contaminated. Quantification of the AFC processes was carried out using an energy-constrained assimilation-fractional crystallization (EC-AFC) model (Spera and Bohrson, 2001; Bohrson and Spera, 2001). Since some of the trace elements analyzed are prone to mobilization (Rb, Ba, K) or influenced by accumulation or fractionation processes (P, Ti, Sr) and the oxygen isotope data show only a limited spread, we constrained this modeling to the Sr-Nd isotopic compositions.

Several studies proposed assimilation of granulite facies gneisses by mafic magmas to explain steep trends on Sr-Nd isotope diagrams (e.g. Carter et al., 1978; Bernstein et al., 1998). A negative correlation between ε_{Nd} and SiO_2 content was suggested as further indication for assimilation of Archean granulite-facies lower crust (Heaman and Machado, 1992). Since our data point towards compositionally similar contaminants and seismic data were interpreted to reflect the existence of a wedge of Archean crust that extends southwards to Lindenow Fjord (Dahl-Jensen et al., 1998), we used an average of five granulite-facies gneisses with low Rb/Sr ratios from the Archaean craton of West Greenland (Taylor et al., 1984) as representative for the lower crustal composition (Table 10). The Julianehåb granitoids, in which the dikes were emplaced and which represents the most abundant country rock, are a second possible contaminant. Thus, the weighted average from the three granitoid samples of the Julianehåb batholith were used as representative for the chemical composition of an upper crustal contaminant. Sr is modeled as compatible in the assimilant because the assimilated material is thought to be plagioclase-rich based on the ε_{Nd} – Eu/Eu^*_{max} correlation (Fig. 15). In the magma, Sr is also modeled as slightly compatible consistent with the influence of plagioclase on the fractionating assemblage. Following Bohrson and Spera (2001), Nd is modeled as incompatible both in the magma and the upper and lower crustal assimilants.

The results indicate that AFC processes involving upper crustal Ketilidian basement cannot explain the steep trend on the Sr-Nd isotope diagram, although an upper crustal component appears to be involved in the petrogenesis of the hornblende-syenite (Fig. 16). On the other hand, assimilation of lower crustal material is consistent with the bulk of the data and indicates a maximum mass of assimilated anatectic melt of ~ 10% (Fig. 16). However, the starting composition, chosen to be similar to the isotopically most primitive samples, might already be contaminated by some crustal material and therefore 10% is not a maximum value. We conclude that AFC processes involving magmas isotopically similar to the most primitive of the Isortoq dikes and up to ~ 10% partial melts

derived from lower crustal rocks similar to Archean granulite-facies gneisses can reasonably explain the bulk of the Sr-Nd isotope data. The hornblende-syenite appears to be contaminated with both upper and lower crustal material, whereas the off-trend position of BFD 2 can be explained by assimilation of isotopically and/or chemically heterogeneous material.

5.5. Regional perspective

Contamination of Gardar magmas with crustal rocks was demonstrated previously at several localities (e.g. Taylor and Upton, 1993; Andersen, 1997; Stevenson et al., 1997; Marks and Markl, 2001). However, there has been no consensus whether the Ketilidian mobile belt, in which the Isortoq dikes are emplaced, is underlain by Archean crust. This hypothesis was rejected based on isotopic and geochemical data of the Ketilidian granites (van Breemen et al., 1974; Kalsbeek and Taylor, 1985), although field evidence suggested the presence of older basement in the mobile belt (van Breemen et al., 1974). On the other hand, seismic data indicate that a wedge of Archean crust underlies the predominant part of the Ketilidian belt (Dahl-Jensen et al., 1998) and recent studies on Gardar rocks suggest an involvement of lower crustal material in their petrogenesis (Marks et al., in press; Halama et al., in press). The ε_{Nd} data reported here are among the most negative for Gardar rocks and together with petrological and Sr-O-Os isotopic data provide compelling evidence for assimilation of partial melts from lower crustal rocks similar to granulite-facies gneisses from the Archean craton. The Nd isotopic composition of the BD_0 Brown Dike, which is roughly about 90 Ma older than the main Isortoq dike swarm, indicates that these assimilation processes in the Gardar magmas occurred already at earlier times. It is also noteworthy that the REE patterns of the clinopyroxenes and the strongly negative ε_{Nd} value of the anorthosite xenolith are compatible with a significant input of crustal partial melts. This is in contrast to previous observations which concluded, based on the alkalic character of the anorthosites and the low initial $^{87}Sr/^{86}Sr$ values, that crustal assimilation was insignificant in the formation of the anorthositic rocks (Patchett et al., 1976). On the other hand, the data from Giant Dike 3 show that closed-system fractional crystallization operated at near-surface levels in magmas that were contaminated prior to emplacement.

6. Conclusions

The importance of mafic rocks as probes of the continental crust they have traversed rather than as probes of the lithospheric mantle was recently stressed by Baker et al. (1998). Our data of the Isortoq dikes indicate that the assimilated material must have been silicic because the increase in a_{SiO2} and SiO_2 content in some dikes is higher than expected from fractional crystallization alone.

REE and Nd isotopic data require the assimilated material to be rich in plagioclase-component. Isotopic characteristics of the crustal component include a very low $^{143}Nd/^{144}Nd$ and a moderately low $^{87}Sr/^{86}Sr$ ratio. Furthermore, low Nb contents, moderate $\delta^{18}O$ values and a highly radiogenic Os isotopic composition of the assimilant are indicated. All these features are compatible with assimilation of partial melts derived from Archean granulite-facies gneisses similar to those present in the Archean craton north of the Ketilidian mobile belt. In agreement with seismic data (Dahl-Jensen et al., 1998), we therefore suggest that Archean rocks occur at depth in the Isortoq region, thus continuing further south than at the present erosion level. Contamination of mafic mantle-derived magmas with lower crustal material is also compatible with models for anorthosite genesis (Ashwal, 1993 and references therein) and therefore in agreement with the assumed existence of anorthosite complexes below the present erosion surface in the Gardar Province (Bridgwater, 1967). Assimilation of upper crustal material was generally insignificant, but might have operated in the petrogenesis of the hornblende-syenite dike.

The Giant Dikes of the Isortoq dike swarm provide evidence for closed-system fractional crystallization processes with olivine, clinopyroxene, plagioclase and Fe-Ti oxides as major fractionating phases. Resorbed clinopyroxene cores in syenitic samples are probably inherited from the gabbro support the idea that stoping was the main emplacement mechanism of the Giant Dikes (Bridgwater and Coe, 1970).

Due to their crustal contamination, mantle source characteristics of the Isortoq dikes are masked. However, the general relative enrichment in incompatible elements and the Sr-Nd isotopic compositions argue against a significant role of depleted MORB mantle in the magma generation. The clinopyroxene REE patterns do also not show any similarity to patterns from MORB-like gabbros, but they are very similar to patterns from cumulus clinopyroxene in gabbroic rocks related to post-breakup magmatism caused by the proximity of the Iceland plume in East Greenland (Bernstein et al., 1998). However, the importance of crustal contamination demonstrated for the Isortoq dikes makes it impossible to distinguish whether the enrichment in incompatible trace elements relative to the primitive mantle was derived from the SCLM, an enriched plume or a mixture of both.

Acknowledgements

We would like to thank Bruce Paterson who provided invaluable help during Laser ICP-MS measurements at the Large-Scale Geochemical Facility supported by the European Community - Access to Research Infrastructure action of the Improving Human Potential Programme, contract number HPRI-CT-1999-00008 awarded to Prof. B.J. Wood (University of Bristol). Gabi Stoschek

and Torsten Vennemann are thanked for their help with oxygen isotope measurements. Elmar Reitter expertly assisted with preparation and measurements of radiogenic isotopes and Mathias Westphal helped with microprobe measurements. Financial funding of this work by the Deutsche Forschungsgemeinschaft (grant Ma-2135/1-2) is gratefully acknowledged.

References

Allaart, J.H., 1976. Ketilidian mobile belt in South Greenland. In: A. Escher W.S. Watt (Editors), Geology of Greenland. Grønlands Geologiske Undersøgelse, Copenhagen, pp. 121-151.

Andersen, D.J., Lindsley, D.H., Davidson, P.M., 1993. QUILF: a PASCAL program to assess equilibria among Fe-Mg-Mn-Ti oxides, pyroxenes, olivine, and quartz. Computers and Geosciences 19: 1333-1350.

Andersen, T., 1997. Age and petrogenesis of the Qassiarsuk carbonatite-alkaline silicate volcanic complex in the Gardar rift, South Greenland. Mineralogical Magazine 61: 499-513.

Armstrong, J.T., 1991. Quantitative elemental analysis of individual microparticles with electron beam instruments. In: K.F.J. Heinrich and D.E. Newbury (Editors), Electron Probe Quantitation. Plenum Press, New York and London, pp. 261-315.

Ashwal, L.D., 1993. Anorthosites. Springer, Berlin Heidelberg.

Asmerom, Y., Walker, R.J., 1998. Pb and Os isotopic constraints on the composition and rheology of the lower crust. Geology 26: 359-362.

Baker, J.A., Menzies, M.A., Thirlwall, M.F., Macpherson, C.G., 1998. Petrogenesis of Quaternary Intraplate Volcanism, Sana'a, Yemen: Implications for Plume-Lithosphere Interaction and Polybaric Melt Hybridization. Journal of Petrology 38: 1359-1390.

Baker, J.A., MacPherson, C.G., Menzies, M.A., Thirlwall, M.F., Al-Kadasi, M., Mattey, D.P., 2000. Resolving crustal and mantle contributions to continental flood volcanism, Yemen; constraints from mineral oxygen isotope data. Journal of Petrology 41: 1805-1820.

Benoit, M., Polvé, M., Ceuleneer, G., 1996. Trace element and isotopic characterization of mafic cumulates in a fossil mantle diapir (Oman ophiolite). Chemical Geology 134: 199-214.

Bernstein, S., Kelemen, P.B., Tegner, C., Kurz, M.D., Blusztajn, J., Kent Brooks, C., 1998. Post-breakup basaltic magmatism along the East Greenland Tertiary rifted margin. Earth and Planetary Science Letters 160: 845-862.

Birck, J.L., Roy Barman, M., Capmas, F., 1997. Re-Os Isotopic Measurements at the Femtomole Level in Natural Samples. Geostandard Newsletters 20: 19-27.

Bohrson, W.A., Spera, F.J., 2001. Energy-constrained open-system magmatic processes; II, Application of energy-constrained assimilation-fractional crystallization (EC-AFC) model to magmatic systems. Journal of Petrology 42: 1019-1041.

Boily, M., Ludden, J.N., 1991. Trace-element and Nd isotopic variations in Early Proterozoic dyke swarms emplaced in the vicinity of the Kapuskasing structural zone: enriched mantle or assimilation and fractional crystallization (AFC) process? Canadian Journal of Earth Sciences 28: 26-36.

Bowen, N.L., 1928. The evolution of the Igneous Rocks. Princeton University Press, Princeton, 332 pp.

Boynton, W.V., 1984. Geochemistry of the rare earth elements: meteorite studies. In: P. Henderson (Editor), Rare earth element geochemistry. Elsevier, Amsterdam, pp. 63-114.

Bridgwater, D., 1967. Feldspathic inclusions in the Gardar igneous rocks of South Greenland and their relevance to the formation of major Anorthosites in the Canadian Shield. Canadian Journal of Earth Sciences 4: 995-1014.

Bridgwater, D., Coe, K., 1970. The role of stoping in the emplacement of the giant dikes of Isortoq, South Greenland. Geological Journal, special issue 2: 67-78.

Bridgwater, D., Harry, W.T., 1968. Anorthosite xenoliths and plagioclase megacrysts in Precambrian intrusions of South Greenland. Meddelelser om Grønland 185.

Brügmann, G.E., Arndt, N.T., Hofmann, A.W., Tobschall, H.J., 1987. Noble metal abundances in komatiite suites from Alexo, Ontario and Gorgona Island, Columbia. Geochimica et Cosmochimica Acta 51:

2159-2169.
Buddington, A.F., Lindsley, D.H., 1964. Iron-titanium oxide minerals and synthetic equivalents. Journal of Petrology 5: 310-357.
Cadman, A.C., Heaman, L., Tarney, J., Wardle, R., Krogh, T.E., 1993. U-Pb geochronology and geochemical variation within two Proterozoic mafic dyke swarms, Labrador. Canadian Journal of Earth Sciences 30: 1490-1504.
Carter, S.R., Evensen, N.M., Hamilton, P.J., O'Nions, R.K., 1978. Neodymium and Strontium Isotope Evidence for Crustal Contamination of Continental Volcanics. Science 202: 743-747.
Chesley, J.T., Ruiz, J., 1998. Crust-mantle interaction in large igneous provinces: Implications from the Re-Os isotope systematics of the Columbia River flood basalts. Earth and Planetary Science Letters 154: 1-11.
Class, C., Altherr, R., Volker, F., Eberz, G., McCulloch, M.T., 1994. Geochemistry of Pliocene to Quarternary alkali basalts from the Huri Hills, northern Kenya. Chemical Geology 113: 1-22.
Clayton, R.N., Mayeda, T.K., 1963. The use of bromine pentafluoride in the extraction of oxygen from oxides and silicates for isotope analysis. Geochimica et Cosmochimica Acta 27: 43-52.
Compton, P., 1978. Rare earth Evidence for the Origin of the Nûk Gneisses, Buksefjorden Region, Southern West Greenland. Contributions to Mineralogy and Petrology 66: 283-293.
Condie, K.C., Bobrow, D.J., Card, K.D., 1987. Geochemistry of Precambrian Mafic Dykes from the Southern Superior Province of the Canadian Shield. In: H.C. Halls and W.C. Fahrig (Editors), Mafic dyke swarms. Geological Association of Canada, Special Publication 34: 95-107.
Cox, K.G., Bell, J.D., Pankhurst, R.J., 1979. The interpretation of igneous rocks. George, Allen and Unwin, London.
Cross, W., Iddings, J.P., Pirsson, L.V., Washington, H.S., 1903. Quantitative classification of igneous rocks. University of Chicago Press, Chicago.
Dahl-Jensen, T., Thybo, T., Hopper, H., Rosing, M., 1998. Crustal structure at the SE Greenland margin from wide-angle and normal incidence seismic data. Tectonophysics 288: 191-198.
DePaolo, D.J., 1988. Neodymium isotope geochemistry: An introduction. Springer Verlag, New York.
DePaolo, D.J., 1981. Trace element and isotopic effects of combined wallrock assimilation and fractional crystallisation. Earth and Planetary Science Letters 53: 189-202.
Devey, C.W., Cox, K.G., 1987. Relationships between crustal contamination and crystallisation in continental flood basalt magmas with special reference to the Deccan Traps of the Western Ghats, India. Earth and Planetary Science Letters 84: 59-68.
Eiler, J.M., Farley, K.A., Valley, J.W., Hauri, E., Craig, H., Hart, S.R., Stolper, E.M., 1997. Oxygen isotope variations in ocean island basalt phenocrysts. Geochimica et Cosmochimica Acta 61: 2281-2293.
Elkins, L.T., Grove, T.L., 1990. Ternary feldspar experiments and thermodynamic models. American Mineralogist, 75, 544-559.
Ellam, R.M., Cox, K.G., 1991. An interpretation of Karoo picrite basalts in terms of interaction between asthenospheric magmas and the mantle lithosphere. Earth and Planetary Science Letters 105: 330-342.
Ellam, R.M., Carlson, R.W., Shirey, S.B., 1992. Evidence from Re-Os isotopes for plume-lithosphere mixing in Karoo flood basalt genesis. Nature 359: 718-721.
Emeleus, C.H. Upton, B.G.J., 1976. The Gardar period in southern Greenland. In: A.Escher and W.S. Watt (Editors), Geology of Greenland. Geological Survey of Greenland, Copenhagen, pp. 152-181.
Engell, J., Pedersen, S., 1974. Rb-Sr whole rock isochron age determination from the Bangs Havn intrusion, South Greenland. Bulletin of the Geological Society of Denmark 23: 130-133.
Ernst, R.E., Buchan, K.L., 1997. Giant Radiating Dyke Swarms: Their Use in Identifying Pre-Mesozoic Large Igneous Provinces and Mantle Plumes. In: J.J. Mahoney and M.E. Coffin (Editors), Large Igneous Provinces: Continental, Oceanic, and Planetary Flood Volcanism. Geophysical Monograph 100: 297-333.
Ernst, R.E., Buchan, K.L., 2001. The use of mafic dike swarms in identifying and locating mantle plumes. In: R.E. Ernst and K.L. Buchan (Editors), Mantle Plumes: Their Identification Through Time. Geological Society of America Special Paper 352: 247-265.
Esser, B.K., Turekian, K.K., 1993. The osmium isotopic composition of the continental crust. Geochimica et Cosmochimica Acta 57: 3093-3104.
Finch, A.A., Mansfeld, J., Andersen, T., 2001. U-Pb radiometric age of Nunarsuit pegmatite, Greenland: constraints on the timing of Gardar magmatism. Bulletin of the Geological Society of Denmark 48: 1-7.

Fowler, M.B. Harmon, R.S., 1990. The oxygen isotope composition of lower crustal granulite xenoliths. In: D. Vielzeuf and P.Vidal (Editors), Granulites and Crustal Evolution. Kluwer Academic Publishers, Dordrecht, pp. 493-506.

Frost, B.R., Lindsley, D.H., 1992. Equilibria among Fe-Ti-oxides, pyroxenes, olivine, and quartz: Part II. Application. American Mineralogist 77: 1004-1020.

Gallagher, K., Hawkesworth, C., 1992. Dehydration melting and the generation of continental flood basalts. Nature 358: 57-59.

Garde, A.A., Hamilton, M.A., Chadwick, B., Grocott, J., McCaffrey, K.J.W., 2002. The Ketilidian orogen of South Greenland: geochronology, tectonics, magmatism, and fore-arc accretion during Palaeoproterozoic oblique convergence. Canadian Journal of Earth Sciences 39: 765-793.

Gibson, S.A., Thompson, R.N., Dickin, A.P., Leonardos, O.H., 1995. High-Ti and Low-Ti mafic potassic magmas: key to plume-lithosphere interactions and continental flood-basalt genesis. Earth and Planetary Science Letters 136: 149-165.

Goldstein, S.L., O´Nions, R.K., Hamilton, P.J., 1984. A Sm-Nd isotopic study of the atmospheric dust and particulates from major river systems. Earth and Planetary Science Letters 70: 221-236.

Goodenough, K.M., Upton, B.G.J., Ellam, R.M., 2002. Long-term memory of subduction processes in the lithospheric mantle: evidence from the geochemistry of basic dykes in the Gardar Province of south Greenland. Journal of the Geological Society of London 159: 705-714.

Halama, R., Waight, T., Markl, G., 2002. Geochemical and isotopic zoning patterns of plagioclase megacrysts in gabbroic dykes from the Gardar Province, South Greenland: implications for crystallisation processes in anorthositic magmas. Contributions to Mineralogy and Petrology 144: 109-127.

Halama, R., Wenzel, T., Upton, B.G.J., Siebel, W., Markl, G., in press. A geochemical and Sr-Nd-O isotopic study of the Proterozoic Eriksfjord Basalts, Gardar Province, South Greenland: Reconstruction of an OIB signature in crustally contaminated rift-related basalts. Mineralogical Magazine.

Harris, C., Smith, H.S., le Roex, A.P., 2000. Oxygen isotope composition of phenocrysts from Tristan da Cunha and Gough Island lavas: variation with fractional crystallization and evidence for assimilation. Contributions to Mineralogy and Petrology 138: 164-175.

Hart, S.R., Hauri, E.H., Oschmann, L.A., Whitehead, J.A., 1992. Mantle Plumes and Entrainment: Isotopic Evidence. Science 256: 517-520.

Hart, W.K., Carlson, R.W., Shirey, S.B., 1997. Radiogenic Os in primitive basalts from the northwestern U.S.A.: Implications for petrogenesis. Earth and Planetary Science Letters 150: 103-116.

Hawkesworth, C.J., Gallagher, K., Kelly, S., Mantovani, M., Peate, D.W., Regelous, M., Rogers, N.W., 1992. Paraná magmatism and the opening of the South Atlantic. In: B.C. Storey, T. Alabaster and R.J. Pankhurst (Editors), Magmatism and the Causes of Continental Break-up. Geological Society of London Special Publication 68: 221-240.

Heaman, L.M., Machado, N., 1992. Timing and origin of midcontinent rift alkaline magmatism, North America: evidence from the Coldwell Complex. Contributions to Mineralogy and Petrology 110: 289-303.

Hofmann, A.W., 1997. Mantle geochemistry: the message from oceanic volcanism. Nature 385: 219-229.

Huppert, H.E., Sparks, R.S.J., 1985. Cooling and contamination of mafic and ultramafic magmas during ascent through continental crust. Earth and Planetary Science Letters 74: 371-386.

Jacobson, S.B., Wasserburg, G.J., 1980. Sm-Nd isotopic evolution of chondrites. Earth and Planetary Science Letters 50: 139-155.

Kalamarides, R.I., 1986. High-temperature oxygen isotope fractionation among the phases of Kiglapait intrusion, Labrador, Canada. Chemical Geology 58: 303-310.

Kalsbeek, F., Taylor, P.N., 1985. Isotopic and chemical variation in granites across a Proterozoic continental margin-the Ketilidian mobile belt of South Greenland. Earth and Planetary Science Letters 73: 65-80.

Kerr, A.C., Kempton, P.D., Thompson, R.N., 1995. Crustal assimilation during turbulent magma ascent (ATA); new isotopic evidence from the Mull Tertiary lava succession, N.W. Scotland. Contributions to Mineralogy and Petrology 119: 142-154.

Konnerup-Madsen, J., Rose-Hansen, J., 1984. Composition and significance of fluid inclusions in the Ilímaussaq peralkaline granite, South Greenland. Bulletin minéralogique 107: 317-326.

Kretz, R., 1983: Symbols for rock-forming minerals. American Mineralogist 68: 277-279.

Larsen, L.M., Sørensen, H., 1987. The Ilimaussaq intrusion-progressive crystallization and formation of layering in an agpaitic magma. In: J.G. Fitton and B.G.J. Upton (Editors), Alkaline Igneous Rocks.

Geological Society of London Special Publication 30: 473-488.
LeCheminant, A.N., Heaman, L.M., 1989. Mackenzie igneous events, Canada: Middle Proterozoic hotspot magmatism associated with ocean opening. Earth and Planetary Science Letters 96: 38-48.
Lightfoot, P.C., Sutcliffe, R.H., Doherty, W., 1991. Crustal contamination identified in Keweenawan Osler Group Tholeiites, Ontario: A trace element perspective. Journal of Geology 99: 739-760.
Lindsley, D.H., 1983. Pyroxene thermometry. American Mineralogist 68: 477-493.
Lindsley, D.H., Frost, B.R., 1992. Equilibria among Fe-Ti-oxides, pyroxenes, olivine, and quartz: Part I. Theory. American Mineralogist 77: 987-1003.
Markl, G., Frost, B.R., 1999. The Origin of Anorthosites and Related Rocks from the Lofoten Islands, Northern Norway: II. Calculation of Parental Liquid Compositions for Anorthosites. Journal of Petrology 40: 61-77.
Markl, G., White, C., 1999. Pigeonite-augite intergrowths from the Graveyard Point sill, Oregon: a record of the interplay between bulk and interstitial liquid fractionation. Contributions to Mineralogy and Petrology 137: 170-183.
Markl, G., Frost, B.R., Bucher, K., 1998. The origin of Anorthosites and related rocks from the Lofoten islands, Northern Norway: I. Field relations and estimation of intrinsic variables. Journal of Petrology 39: 1425-1452.
Marks, M., Markl, G., 2001. Fractionation and assimilation processes in the alkaline augite syenite unit of the Ilimaussaq Intrusion, South Greenland, as deduced from phase equilibria. Journal of Petrology 42: 1947-1969.
Marks, M., Vennemann, T., Siebel, W., Markl, G., in press. Quantification of Magmatic and Hydrothermal Processes in a Peralkaline Syenite-Alkali Granite Complex based on Textures, Phase Equilibria, and Stable and Radiogenic Isotopes. Journal of Petrology.
Mattey, D., Lowry, D., Macpherson, C., 1994. Oxygen isotope composition of mantle peridotite. Earth and Planetary Science Letters 128: 231-241.
McDonough, W.F., 1990. Constraints on the composition of the continental lithospheric mantle. Earth and Planetary Science Letters 101: 1-18.
McDonough, W.F., Sun, S.S., 1995. The composition of the Earth. Chemical Geology 120: 223-253.
McGregor, V.R. 1973. The early Precambrian gneisses of the Godthaab district, West Greenland. Philosophical Transactions of the Royal Society of London A273: 343-358.
McGregor, V.R., 1979. Archean gray gneisses and the origin of the continental crust; evidence from the Godthaab region, West Greenland. In: F. Barker (Editor), Trondhjemites, dacites, and related rocks. Elsevier, Amsterdam, pp. 169-204.
Middlemost, E.A.K., 1989. Iron oxidation ratios, norms and the classification of volcanic rocks. Chemical Geology 77: 19-26.
Milner, S.C., Le Roex, A.P., 1996. Isotope characteristics of the Okenyenya igneous complex, northwestern Namibia: constraints on the composition of the early Tristan plume and the origin of the EM 1 mantle component. Earth and Planetary Science Letters 141: 277-291.
Mitchell, J.N., Scoates, J.S., Frost, C.D., 1995. High-Al gabbros in the Laramie Anorthosite Complex, Wyoming: Implications for the composition of melts parental to Proterozoic anorthosite. Contributions to Mineralogy and Petrology 119: 166-180.
Mohr, P.A., 1987. Crustal Contamination in Mafic Sheets: a Summary. In: H.C. Halls and W.C. Fahrig (Editors), Mafic dyke swarms. Geological Association of Canada, Special Publication 34: 75-80.
Molzahn, M., Reisberg, L., Wörner, G., 1996. Os, Sr, Nd, Pb, O isotope and trace element data from the Ferrar flood basalts, Antarctica: evidence for an enriched subcontinental lithospheric source. Earth and Planetary Science Letters 144: 529-546.
Morse, S.A., 1984. Cation diffusion in Plagioclase Feldspar. Science 225: 505-505.
Nelson, D.R., 1992. Isotopic characteristics of potassic rocks: Evidence for the involvement of subducted sediments in magma genesis. Lithos 28: 403-420.
O'Hara, M.J., Herzberg, C., 2002. Interpretation of trace element and isotope features of basalts: relevance of field relations, petrology, major element data, phase equilibria, and magma chamber modeling in basalt petrogenesis. Geochimica et Cosmochimica Acta 66: 2167-2191.
O'Nions, R.K., Pankhurst, R.J., 1974. Rare-earth element distribution in Archaean gneisses and anorthosites, Godthåb area, West Greenland. Earth and Planetary Science Letters 22: 328-338.
Paces, J.B., Bell, K., 1989. Non-depleted sub-continental mantle beneath the Superior Province of the Canadian Shield: Nd-Sr isotopic and trace element evidence from Midcontinent Rift basalts.

Geochimica et Cosmochimica Acta 53: 2023-2035.
Parsons, I., Brown, W.L., 1988. Sidewall crystallization in the Klokken intrusion: zoned ternary feldspars and coexisting minerals. Contributions to Mineralogy and Petrology 98: 431-443.
Paslick, C.R., Halliday, A.N., Davies, G.R., Mezger, K., Upton, B.G.J., 1993. Timing of proterozoic magmatism in the Gardar Province, southern Greenland. Bulletin of the Geological Society of America 105: 272-278.
Patchett, J., Bridgwater, D., 1984. Origin of continental crust of 1.9-1.7 Ga age defined by Nd isotopes in the Ketilidian terrain. Contributions to Mineralogy and Petrology 87: 311-318.
Patchett, P.J., Hutchinson, J., Blaxland, A.B., Upton, B.G.J., 1976. Origin of anorthosites, gabbros and potassic ultramafic rocks from the Gardar Province, South Greenland: Sr isotopic ratio studies. Bulletin of the Geological Society of Denmark 25: 79-84.
Pearce, N.J.G., Leng, M.J., 1996. The origin of carbonatites and related rocks from the Igaliko Dyke Swarm, Gardar Province, South Greenland: field, geochemical and C-O-Sr-Nd isotope evidence. Lithos 39: 21-40.
Peng, Z.X., Mahoney, J., Hooper, P., Harris, C., Beane, J., 1994. A role for lower continental crust in flood basalt genesis? Isotopic and incompatible element study of the lower six formations of the western Deccan Traps. Geochimica et Cosmochimica Acta 58: 267-288.
Powell, M., 1978. The crystallisation history of the Igdlerfigssalik nepheline syenite intrusion, Greenland. Lithos 11: 99-120.
Puchtel, I.S., Brügmann, G.E., Hofmann, A.W., 1999. Precise Re-Os mineral isochron and Pb-Nd-Os systematics of a mafic-ultramfic sill in the 2.0 Ga Onega plateau (Baltic Shield). Earth and Planetary Science Letters 170: 447-461.
Puchtel, I.S., Brügmann, G.E., Hofmann, A.W., 2001. ^{187}Os-enriched domain in an Archean mantle plume: evidence from 2.8 Ga komatiites of the Kostomuksha greenstone belt, NW Baltic Shield. Earth and Planetary Science Letters 186: 513-526.
Roddick, J.C., Sullivan, R.W., Dudas, F.Ö., 1992. Precise calibration of Nd tracer isotopic composition for Sm-Nd studies. Chemical Geology 97: 1-8.
Rudnick, R.L. Presper, T., 1990. Geochemistry of intermediate/- to high-pressure granulites. In: D. Vielzeuf and P. Vidal (Editors), Granulites and Crustal Evolution. Kluwer Academic Publishers, Dordrecht, pp. 523-550.
Rumble, D., Hoering, T.C., 1994. Analysis of oxygen and sulfur isotope ratios in oxide and sulfide minerals by spot heating with a carbon dioxide laser in a fluorine atmosphrere. Accounts of Chemical Research 27: 237-241.
Saal, A.E., Rudnick, R.L., Ravizza, G.E., Hart, S.R., 1998. Re-Os isotope evidence for the composition, formation and age of the lower continental crust. Nature 393: 58-61.
Schmidt, K.H., Bottazzi, P.V.R., Mengel, K., 1999. Trace element partitioning between phlogopite, clinopyroxene and leucite lamproite melt. Earth and Planetary Science Letters 168: 287-299.
Sharp. Z.D., 1990. A laser-based microanalytical method for the in-situ determination of oxygen isotope ratios of silicates and oxides. Geochimica et Cosmochimica Acta 54: 1353-1357.
Shirey, S.B., 1997. Re-Os isotopic compositions of Midcontinent rift system picrites: implications for plume-lithosphere interaction and enriched mantle sources. Canadian Journal of Earth Sciences, 34, 489-503.
Shirey, S.B., Walker, R.J., 1998. The Re-Os isotope system in cosmochemistry and high-temperature geochemistry. Annual Review of Earth and Planetary Sciences 26: 423-500.
Spera, F.J., Bohrson, W.A., 2001. Energy-constrained open-system magmatic processes I: General model and energy-constrained assimilation and fractional crystallization (EC-AFC) formulation. Journal of Petrology 42: 999-1018.
Sproule, R.A., Lambert, D.D., Hoatson, D.M., 2002. Decoupling of the Sm-Nd and Re-Os Isotopic Systems in Sulphid-Saturated Magmas in the Halls Creek Orogen, Western Australia. Journal of Petrology 43: 375-402.
Stephenson, D., Upton, B.G.J., 1982. Ferromagnesian silicates in a differentiated alkaline complex: Kungnât Fjeld, South Greenland. Mineralogical Magazine 46: 283-300.
Stevenson, R., Upton, B.G.J., Steenfelt, A., 1997. Crust-mantle interaction in the evolution of the Ilimaussaq Complex, South Greenland: Nd isotopic studies. Lithos 40: 189-202.
Sugawara, T., 2000. Empirical relationships between temperature, pressure, and MgO content in olivine and pyroxene saturated liquid. Journal of Geophysical Research 105: 8457-8472.
Tarney, J., Weaver, B.L., 1987. Geochemistry and Petrogenesis of Early Proterozoic Dyke Swarms. In: H.C.

Halls and W.C. Fahrig (Editors), Mafic dyke swarms. Geological Association of Canada, Special Publication 34: 81-93.

Taylor, H.P., 1980. The effects of assimilation of country rocks by magmas on $^{18}O/^{16}O$ and $^{87}Sr/^{86}Sr$ systematics in igneous rocks. Earth and Planetary Science Letters 47: 243-254.

Taylor, H.P.J., Sheppard, S.M.F., 1986. Igneous rocks: I. Processes of isotopic fractionation and isotope systematics. In: J.W. Valley, H.P.J. Taylor and J.R. O'Neil (Editors), Stable Isotopes. Reviews in Mineralogy 16: 227-269.

Taylor, P.N., Upton, B.G.J., 1993. Contrasting Pb isotopic compositions in two intrusive complexes of the Gardar magmatic province of South Greenland. Chemical Geology 104: 261-268.

Taylor, P.N., Jones, N.W., Moorbath, S., 1984. Isotopic assessment of relative contributions from crust and mantle sources to the magma genesis of Precambrian granitoid rocks. Philosophical Transactions of the Royal Society of London A 310: 605-625.

Tegner, C., Robins, B., Sørensen, H.S., 1996: Crystallization from stratified magmas in the Honningsvag intrusive suite, Northern Norway; a reappraisal. Mineralogical Magazine 60: 41-51.

Thompson, R.N., 1981. Thermal aspects of the origin of Hebridean Tertiary acid magmas. I. An experimental study of partial fusion of Lewisian gneisses and Torridonian sediments. Mineralogical Magazine 44: 161-170.

Thompson, R.N., Gibson, S.A., Mitchell, J.G., Dickin, A.P., Leonardos, O.H., Brod, J.A., Greenwood, J.C., 1998. Migrating Cretaceous-Eocene Magmatism in the Serra do Mar Alkaline Province, SE Brazil: melts from the deflected Trindade mantle plume? Journal of Petrology 39: 1493-1526.

Toplis, M.J., Carroll, M.R., 1995. An experimental study of the influence of oxygen fugacity on Fe-Ti oxide stability, phase relations, and mineral-melt equilibria in ferro-basaltic systems. Journal of Petrology 36: 1137-1170.

Turner, S.P., Hawkesworth, C.J., Gallagher, K.G., Stewart, K., Peate, D., Mantovani, M., 1996. Mantle plumes, flood basalts and thermal models for melt generation beneath continents: assessment of a conductive heating model. Journal of Geophysical Research 101: 11503-11518.

Upton, B.G.J., 1971. Melting experiments on chilled gabbros and syenogabbros. Carnegie Institute Washington Year Book, pp. 112-118.

Upton, B.G.J., Emeleus, C.H., 1987. Mid-Proterozoic alkaline magmatism in southern Greenland: the Gardar province. In: J.G. Fitton and B.G.J. Upton (Editors), The Alkaline Rocks. Geological Society of London Special Publication 30: 449-471.

Upton, B.G.J., Thomas, J.E., 1980. The Tugtutôq younger giant dyke complex, South Greenland: fractional crystallisation of transitional olivine basalt magma. Journal of Petrology 21: 167-198.

Upton, B.G.J., Emeleus, C.H., Heaman, L.M., Goodenough, K.M., Finch, A., 2003. Magmatism of the mid-Proterozoic Gardar Province, South Greenland: chronology, petrogenesis and geological setting. Lithos 68: 43-65.

Valley J.W., Kitchen, N., Kohn, M.J., Niendorf, C.R., Spicuzza, M.J., 1995. UWG-2, a garnet standard for oxygen isotope ratios: strategies for high precision and accuracy with laser heating. Geochimica et Cosmochimica Acta 59: 5223-5231.

van Bremen, O., Aftalion, M., Allart, J.H., 1974. Isotopic and Geochronologic Studies on Granites from the Ketilidian Mobile Belt of South Greenland. Bulletin of the Geological Society of America 85: 403-412.

Vennemann, T.W. O´Neil, J.R., 1993. A simple and inexpensive method of hydrogen isotope and water analyses of minerals and rocks based on zinc reagent. Chemical Geology 103: 227-234.

Walker, R.J., Morgan, J.W., Hanski, E.J., Smolkin, V.F., 1997. Re-Os systematics of Early Proterozoic ferropicrites, Pechenga Complex, northwestern Russia: Evidence for ancient ^{187}Os-enriched plumes. Geochimica et Cosmochimica Acta 61: 3145-3160.

Wendt, I., 1986. Radiometrische Methoden in der Geochronologie. Clausthaler Tektonische Hefte Band 23, Pilger Verlag, Clausthal-Zellerfeld.

Winther, K.T., 1992. Feldspar megacryst and anorthosite xenolith-bearing dykes in the Narssarssuaq area, South Greenland. Rapport Grønlands Geologiske Undersøgelse 154: 49-59.

Zheng, Y.-F., 1993. Calculation of oxygen isotope fractionation in anydrous silicate minerals. Geochimica et Cosmochimica Acta 57: 1079-1091.

Figure captions

Fig. 1: a) Map of the Gardar Province (after Upton and Emeleus, 1987); b) Map of the Isortoq region (after Bridgwater and Coe, 1970) with sample localities.

Fig. 2: Back-scatterd electron (BSE) images of a) euhedral clinopyroxene with apatite inclusions in the gabbroic facies of Giant Dike 3, b) sector-zoned epidote associated with titanite, biotite, albite, pumpellyite and prehnite in the syenitic facies of Giant Dike 3, c) olivine, overgrown by orthopyroxene and biotite, in the larvikite and d) plagioclase surrounded by alkali feldspar in the larvikite.

Fig. 3: Feldspar compositions of Isortoq dike rocks in the An-Ab-Or triangle with solvus isotherms after Elkins and Grove (1990).

Fig. 4: Olivine and pyroxene compositions of Isortoq dike rocks in the enstatite-ferrosilite-hedenbergite-diopside (En-Fs-Hd-Di) quadrilateral. Fo = forsterite, Fa = fayalite, Ks = kirschsteinite ($CaFeSiO_4$) and Mo = monticellite ($CaMgSiO_4$).

Fig. 5: Zoning profiles in clinopyroxenes of Giant Dike 3.

Fig. 6: BSE images of Fe-Ti oxides in Isortoq dike rocks. a) fine trellis-type exsolution in the olivine-gabbro; b) coarse trellis-type exsolution in BFD 1; c) alteration of Fe-Ti oxides to titanite in the syenitic facies of Giant Dike 3; d) ilmenite overgrown by magnetite in the larvikite.

Fig. 7: Oxygen fugacity vs. silica activity in Isortoq dike rocks, calculated with QUILF (Andersen et al., 1993). Please note that BFD 2 and the hornblende-syenite were omitted for QUILF calculations due of the lack of suitable mineral parageneses, but they should plot at $a_{SiO2} = 1$.

Fig. 8: REE patterns of clinopyroxenes from Isortoq dike rocks, normalized to chondritic values from Boynton (1984). Individual clinopyroxene analyses are shown in a) and c), all other diagrams show averaged values. REE patterns of clinopyroxenes from MORB-like olivine-gabbro (Benoit et al., 1996) and gabbro from a rifted continental margin (Bernstein et al., 1998) together with whole-rock REE data from two Archean gneisses (Compton, 1978) are shown for comparison.

Fig. 9: Whole-rock variation diagrams for Isortoq dike rocks with Mg# = $Mg/(Mg + Fe^{2+})$ as fractionation index.

Fig. 10: Multi-element plot of selected Isortoq samples normalized to primitive mantle values from McDonough and Sun (1995).

Fig. 11: Isochron diagrams for BFD 1 and Giant Dike 3. Error bars indicate 2σ errors. Errors used in the isochron calculations are ± 0.5% for $^{147}Sm/^{144}Nd$ and 0.002% $^{143}Nd/^{144}Nd$, based on repeated standard analyses. Isochrons were calculated after Wendt (1986).

Fig. 12: a) $\varepsilon_{Nd}(i)$ vs. $(^{87}Sr/^{86}Sr)_i$ diagram for mineral separates of Isortoq dike rocks and whole-rock basement samples. Reference data are from Pearce and Leng (1996), Goodenough et al. (2002) and Halama et al. (in press). The reference line of Bulk Silicate Earth (BSE) for the Sr isotopic composition was calculated after DePaolo (1988) assuming present-day values of 0.0827 for $^{87}Rb/86Sr$ and 0.7045 for $^{87}Sr/^{86}Sr$. b) Oxygen isotopic compositions vs. $\varepsilon_{Nd}(i)$ of separated clinopyroxenes and amphiboles from Isortoq dike rocks and whole-rock country rock samples. Oxygen isotopic composition of clinopyroxene from a DMM source was modeled using an average

mantle olivine $\delta^{18}O$ value of 5.2 ‰ (Eiler et al., 1997) and an average $\Delta^{18}O_{cpx\text{-}olivine}$ fractionation of 0.4 ‰ (Mattey et al., 1994).

Fig. 13: a) $\varepsilon_{Nd}(i)$ vs. SiO_2 (wt.%) diagram with general trends of fractional crystallization and AFC processes (solid arrows). Note the fractional crystallization trend for the three samples of Giant Dike 3 (dashed arrow). b) and c) Silica activities calculated with QUILF (Andersen et al., 1993) vs. $\varepsilon_{Nd}(i)$ and Mg# (symbols as in Fig. 12).

Fig. 14: Maximum Eu anomalies in clinopyroxenes from Isortoq dike rocks vs. $\varepsilon_{Nd}(i)$ and $\delta^{18}O$ (symbols as in Fig. 12).

Fig. 15: Re-Os isotope composition correlation diagram for four Isortoq dikes, three Eriksfjord Formation basalts and two Ilímaussaq augite-syenites.

Fig. 16: Sr-Nd isotope diagram showing the results of the AFC modeling with the parameters from Table 10 (symbols as in Fig. 12). Isotopic compositions of upper crust is an weighted average from the three basement samples and lower crust is represented by an average of 5 Archean granulite facies gneisses with low Rb/Sr ratios from Taylor et al. (1984). Numbers at EC-AFC curves indicate the percentage of mass of assimilated partial melt.

Table 1: Sample description

Dike	Type	Sample	Ol	Cpx	Feldspar	Amph	Qtz	Fe-Ti oxides
BD_0	gabbro	GD 37	⊕	⊕	plag			mag
BFD 1	gabbro	GM 1680	⊕	⊕	plag			mag
	plagioclase megacryst	GM 1681		⊕	plag			
	anorthosite xenolith	GM 1682		⊕	plag	±	±	mag
	gabbro	GM 1729	⊕	⊕	plag			
	gabbro	GM 1735	⊕	⊕	plag			mag
BFD 2	leucogabbro from the dike center	GM 1750		⊕	plag		±	mag
BFD 3	gabbro	GM 1805	⊕	⊕	plag			mag
BFD 4	gabbro	GD 39	⊕	⊕	plag			ilm + mag
Olivine-gabbro	gabbro	GM 1803	⊕	⊕	plag			mag
Giant Dike 1	syeno-gabbro	GM 1712		⊕	plag + alk			mag
Giant Dike 3	sample traverse from center to margin in gabbroic facies	GM 1759 - 1762	⊕	⊕	plag + alk			ilm + mag
	syenite	GM 1768		⊕	alk	±		mag
	sample traverse from margin to margin in syenitic facies	GM 1769 - 1776		⊕	alk	±		mag
	syenite	GM 1778		⊕	alk	±		mag
	syenite	GM 1780		⊕	alk	±		mag
	syenite	GM 1784		⊕	alk	±		mag
Larvikite	larvikite from the dike center	GM 1684	⊕	⊕	plag + alk	±	±	ilm + mag
Hornblende-syenite	syenite	GD 38			alk	⊕	⊕	mag

⊕ = mineral is a major component of the sample, ± = minor amounts of mineral present

Table 2: Representative microprobe analyses of feldspar from Isortoq dike rocks

Dike	Olivine-gabbro	BFD 2	BFD 2	GD 3 gabbro	GD 3 gabbro	GD 3 gabbro	GD 3 gabbro	GD 3 gabbro	GD 3 gabbro	GD 3 syenite	GD 3 syenite	Larvikite	Larvikite	Larvikite
Sample	GM 1803	GM 1750	GM 1749	GM1760	GM 1760	GM 1761	GM 1762	GM 1762	GM 1762	GM 1774	GM 1774	GM 1684	GM 1684	GM 1684
wt.%														
SiO_2	53.87	56.49	62.81	62.88	62.55	56.01	65.35	64.84	62.73	65.17	64.20	57.16	62.42	64.41
TiO_2	0.25	0.08	0.05	0.04	0.05	0.05	0.01	0.00	0.05	0.07	0.01	0.08	0.12	0.03
Al_2O_3	27.78	26.46	21.92	22.50	21.98	27.66	19.10	19.88	22.76	19.42	19.11	26.05	21.52	20.00
FeO	1.66	0.51	0.24	0.25	0.27	0.17	0.13	0.11	0.10	0.14	0.11	0.35	0.36	0.19
MnO	0.04	0.00	0.01	0.00	0.00	0.00	0.02	0.02	0.05	0.00	0.00	0.00	0.00	0.02
MgO	0.56	0.08	0.01	0.03	0.00	0.02	0.00	0.00	0.00	0.01	0.00	0.03	0.01	0.01
BaO	0.00	0.05	0.41	0.17	0.23	0.04	0.08	0.12	0.06	0.28	1.59	0.20	0.93	0.77
SrO	0.23	0.25	0.20	0.31	0.29	0.32	0.12	0.16	0.37	0.21	0.24	0.21	0.21	0.20
CaO	9.88	9.86	4.09	3.94	3.55	9.47	0.57	1.43	4.34	0.85	0.31	8.29	3.04	1.51
Na_2O	4.23	5.49	6.43	7.93	6.16	5.46	4.01	4.94	8.24	6.58	4.12	6.61	7.33	5.84
K_2O	0.93	0.70	3.88	1.95	4.72	0.38	10.61	8.37	0.89	6.76	10.03	0.40	3.33	6.83
Total	99.42	99.97	100.04	99.99	99.79	99.60	99.99	99.89	99.60	99.50	99.72	99.39	99.27	99.82
Formulae based on 8 oxygens														
Si	2.46	2.55	2.82	2.81	2.83	2.53	2.97	2.94	2.80	2.95	2.96	2.59	2.83	2.92
Al	1.50	1.41	1.16	1.18	1.17	1.47	1.02	1.06	1.20	1.04	1.04	1.39	1.15	1.07
Ti	0.01	0.00	0.00	0.00	0.00	0.00	0.00	0.00	0.00	0.00	0.00	0.00	0.00	0.00
Fe^{2+}	0.06	0.02	0.01	0.01	0.01	0.01	0.00	0.00	0.00	0.01	0.00	0.01	0.01	0.01
Mn	0.00	0.00	0.00	0.00	0.00	0.00	0.00	0.00	0.00	0.00	0.00	0.00	0.00	0.00
Mg	0.04	0.01	0.00	0.00	0.00	0.00	0.00	0.00	0.00	0.00	0.00	0.00	0.00	0.00
Ba	0.00	0.00	0.01	0.00	0.00	0.00	0.00	0.00	0.00	0.01	0.03	0.00	0.02	0.01
Sr	0.01	0.01	0.01	0.00	0.00	0.00	0.00	0.00	0.00	0.00	0.00	0.01	0.01	0.01
Ca	0.48	0.48	0.20	0.19	0.17	0.46	0.03	0.07	0.21	0.04	0.02	0.40	0.15	0.07
Na	0.38	0.48	0.56	0.69	0.54	0.48	0.35	0.43	0.71	0.58	0.37	0.58	0.64	0.51
K	0.05	0.04	0.22	0.11	0.27	0.02	0.62	0.48	0.05	0.39	0.59	0.02	0.19	0.39
Total	4.99	5.00	4.99	5.00	4.99	4.98	5.00	4.99	4.98	5.01	5.00	5.01	5.01	5.00
X_{An}	0.53	0.48	0.20	0.19	0.17	0.48	0.03	0.07	0.21	0.04	0.02	0.40	0.15	0.07
X_{Ab}	0.41	0.48	0.57	0.70	0.55	0.50	0.35	0.44	0.73	0.57	0.38	0.58	0.65	0.52
X_{Or}	0.06	0.04	0.23	0.11	0.28	0.02	0.62	0.49	0.05	0.39	0.61	0.02	0.20	0.40

Table 3: Representative microprobe analyses of olivine from Isortoq dike rocks

Dike	Olivine-Gabbro	Olivine-Gabbro	BFD 1	BFD 1	BFD 4	Giant Dike 3 gabbro	Giant Dike 3 gabbro	Giant Dike 3 gabbro	Larvikite	Larvikite
Sample	GM 1803	GM 1803	GM 1735	GM 1729	GD 39	GM1759	GM1761	GM1760	GM 1684	GM 1684
wt. %										
SiO_2	36.26	33.82	37.16	33.55	35.28	33.28	35.42	34.64	32.89	32.88
TiO_2	0.06	0.07	0.03	0.02	0.02	0.05	0.02	0.01	0.02	0.08
Al_2O_3	0.01	0.01	0.10	0.05	0.02	0.01	0.00	0.00	0.01	0.00
NiO	0.03	0.03	0.06	0.03	0.03	—	—	—	0.00	0.05
FeO	33.23	47.09	29.32	48.71	39.67	48.28	37.72	42.61	52.13	51.03
MnO	0.44	0.91	0.25	0.84	0.71	0.53	0.23	0.65	1.24	1.14
MgO	29.92	17.84	32.67	16.82	24.00	17.00	26.51	21.86	14.05	15.15
CaO	0.25	0.51	0.24	0.19	0.36	0.40	0.33	0.38	0.06	0.09
Total	100.20	100.28	99.82	100.20	100.10	99.55	100.23	100.15	100.40	100.42
Formulae based on 4 oxygens:										
Si	1.00	1.00	1.00	1.00	1.00	1.00	0.99	1.00	1.00	0.99
Al	0.00	0.00	0.00	0.00	0.00	0.00	0.00	0.00	0.00	0.00
Ti	0.00	0.00	0.00	0.00	0.00	0.00	0.00	0.00	0.00	0.00
Mg	1.22	0.79	1.31	0.75	1.02	0.76	1.11	0.94	0.64	0.68
Fe	0.76	1.17	0.66	1.22	0.94	1.21	0.89	1.03	1.33	1.29
Mn	0.01	0.02	0.01	0.02	0.02	0.01	0.01	0.02	0.03	0.03
Ni	0.00	0.00	0.00	0.00	0.00	—	—	—	0.00	0.00
Ca	0.01	0.02	0.01	0.01	0.01	0.01	0.01	0.01	0.00	0.00
Sum	3.00	3.00	3.00	3.00	3.00	3.00	3.01	3.00	3.00	3.00
X_{Fo}	0.614	0.400	0.663	0.380	0.516	0.383	0.553	0.475	0.324	0.346
X_{Fa}	0.383	0.592	0.334	0.617	0.478	0.610	0.442	0.519	0.675	0.653
X_{La}	0.004	0.008	0.004	0.003	0.006	0.006	0.005	0.006	0.001	0.001

— = not determined

Table 4: Representative microprobe analyses of pyroxene from Isortoq dike rocks

Dike	Olivine-gabbro	BFD 1	BFD 1	BFD 2	GD 1 syeno-gabbro	GD 3 gabbro	GD 3 gabbro	GD 3 syenite	GD 3 syenite	GD 3 syenite	Larvikite	Larvikite
Sample	GM1803	GM 1729	GM 1681	GM 1749	GM 1712	GM 1760	GM 1761	GM 1769	GM 1769	GM 1772	GM 1684	GM 1684
			Ca-poor inclusion in feldspar				rim around olivine	Fe-rich core	rim		cpx	rim around olivine
wt %												
SiO_2	51.21	52.49	51.11	51.09	51.18	50.90	53.36	49.92	50.13	49.16	51.59	51.57
TiO_2	1.00	0.37	1.34	0.71	0.99	0.75	0.01	0.88	1.00	0.67	0.70	0.06
Al_2O_3	2.34	1.76	3.15	1.27	0.68	2.21	0.51	0.77	0.92	0.65	0.41	0.36
Cr_2O_3	0.04	0.00	0.00	0.04	0.00	0.02	—	—	—	0.00	0.00	0.00
FeO	9.17	9.56	11.79	17.26	12.62	10.89	8.29	18.91	17.54	22.00	17.30	28.81
MnO	0.17	0.29	0.31	0.53	0.28	0.11	0.10	0.48	0.47	0.51	0.53	0.91
MgO	12.67	13.89	16.35	9.54	11.48	12.71	13.95	6.71	8.02	4.23	11.05	17.41
CaO	22.34	20.87	16.18	19.01	21.35	21.01	22.46	21.50	21.35	21.07	18.19	1.39
Na_2O	0.73	0.56	0.43	0.49	0.42	0.52	0.54	0.40	0.36	0.87	0.32	0.01
Total	99.66	99.80	100.65	99.93	99.01	99.11	99.37	99.58	99.79	99.15	100.08	100.52
Formulae based on 4 cations and 6 oxygens												
Si	1.92	1.96	1.88	1.97	1.96	1.93	1.99	1.97	1.95	1.97	1.98	1.98
Al	0.10	0.08	0.14	0.06	0.03	0.10	0.02	0.04	0.04	0.03	0.02	0.02
Ti	0.03	0.01	0.04	0.02	0.03	0.02	0.00	0.03	0.03	0.02	0.02	0.00
Cr	0.00	0.00	0.00	0.00	0.00	0.00	—	—	—	0.00	0.00	0.00
Fe^{3+}	0.06	0.03	0.05	0.00	0.02	0.05	0.04	0.01	0.02	0.06	0.00	0.03
Mg	0.71	0.77	0.90	0.55	0.66	0.72	0.78	0.39	0.47	0.25	0.63	0.99
Fe^{2+}	0.23	0.27	0.31	0.56	0.38	0.30	0.22	0.61	0.56	0.68	0.56	0.89
Mn	0.01	0.01	0.01	0.02	0.01	0.00	0.00	0.02	0.02	0.02	0.02	0.03
Ca	0.90	0.83	0.64	0.79	0.88	0.85	0.90	0.91	0.89	0.90	0.75	0.06
Na	0.05	0.04	0.03	0.04	0.03	0.04	0.04	0.03	0.03	0.07	0.02	0.00
Total	4.00	4.00	4.00	4.00	4.00	4.00	4.00	4.00	4.00	4.00	4.00	4.00
X_{Wo}	0.462	0.420	0.314	0.393	0.449	0.429	0.461	0.459	0.454	0.481	0.374	0.030
X_{En}	0.406	0.430	0.508	0.301	0.348	0.403	0.419	0.212	0.249	0.141	0.333	0.511
X_{Fs}	0.133	0.151	0.177	0.306	0.203	0.168	0.120	0.330	0.296	0.379	0.292	0.460

— = not determined; na = not analyzed

Table 5: Representative analyses of unexsolved magnetite and ilmenite, exsolved magnetite and ilmenite and calculated bulk compositions

Dike	BFD 4		Larvikite		BFD 1			GD 3, gabbro			GD 3, gabbro		
Sample	GD 39		GM 1684		GM 1680			GM1762			GM1762		
	mag	ilm	mag	ilm	mag	ilm	bulk	mag	ilm	bulk	mag	ilm	bulk
Texture	unexs.	unexs.	unexs.	unexs.	exs.	exs.	calc.	exs.	exs.	calc.	exs.	exs.	calc.
wt.%													
SiO_2	0.02	0.00	0.05	0.00	0.00	0.00	0.00	0.00	0.00	0.00	0.03	0.02	0.02
TiO_2	25.07	51.98	7.36	50.15	15.42	53.21	26.44	15.44	51.80	32.95	11.34	51.77	25.12
Al_2O_3	2.52	0.12	1.35	0.02	1.05	0.01	0.74	2.20	0.01	1.15	2.35	0.02	1.56
Cr_2O_3	0.17	0.04	0.18	0.02	0.11	0.06	0.10	0.02	0.00	0.01	0.00	0.00	0.00
ZnO	0.03	0.01	—	—	0.09	0.04	0.07	0.10	0.00	0.05	0.19	0.00	0.12
FeO	68.22	44.47	84.98	47.19	78.81	45.07	68.97	77.56	46.51	62.61	80.77	46.49	69.09
MnO	0.90	0.68	0.45	1.96	0.74	2.28	1.19	0.43	1.39	0.89	0.36	1.42	0.72
MgO	1.05	2.30	0.00	0.00	0.00	0.00	0.00	0.00	0.00	0.00	0.00	0.00	0.00
CaO	0.05	0.03	—	—	0.00	0.00	0.00	0.03	0.03	0.03	0.18	0.04	0.14
Total	98.02	99.63	94.37	99.33	96.22	100.67	97.51	95.77	99.74	97.65	95.22	99.76	96.63
Formulae based on 3 (2) cations and 4 (3) oxygens for mag (ilm)													
Si	0.00	0.00	0.00	0.00	0.00	0.00	0.00	0.00	0.00	0.00	0.00	0.00	0.00
Al	0.11	0.00	0.06	0.00	0.05	0.00	0.03	0.10	0.00	0.05	0.10	0.00	0.07
Ti	0.69	0.97	0.21	0.95	0.44	1.00	0.75	0.44	0.99	0.94	0.32	0.98	0.71
Cr	0.01	0.00	0.01	0.00	0.00	0.00	0.00	0.00	0.00	0.00	0.00	0.00	0.00
Fe^{3+}	0.49	0.05	1.51	0.09	1.08	0.00	0.46	1.03	0.03	0.07	1.25	0.03	0.50
Mg	0.06	0.09	0.00	0.00	0.00	0.00	0.00	0.00	0.00	0.00	0.00	0.00	0.00
Fe^{2+}	1.61	0.87	1.20	0.91	1.41	0.95	1.71	1.42	0.95	1.91	1.30	0.95	1.68
Mn	0.03	0.01	0.01	0.04	0.02	0.05	0.04	0.01	0.03	0.03	0.01	0.03	0.02
Zn	0.00	0.00	—	—	0.00	0.00	0.00	0.00	0.00	0.00	0.01	0.00	0.00
Ca	0.00	0.00	—	—	0.00	0.00	0.00	0.00	0.00	0.00	0.01	0.00	0.01
Sum	3.00	2.00	3.00	2.00	3.00	2.00	3.00	3.00	2.00	3.00	3.00	2.00	3.00
mol%													
Usp/Ilm	0.70	0.97	0.21	0.96	0.44	1.00	0.75	0.44	0.99	0.94	0.32	0.99	0.71
Mag/Hem	0.25	0.03	0.76	0.04	0.54	0.00	0.23	0.51	0.01	0.04	0.63	0.01	0.25
Sp	0.05		0.03		0.02		0.02	0.05		0.03	0.05		0.03
For QUILF													
NTi/NHem	0.697	0.026	0.211	0.043	0.438	0.000	0.751	0.439	0.014	0.938	0.323	0.015	0.716
NMg/NGk	0.056	0.085	0.000	0.000	0.000	0.000	0.000	0.000	0.000	0.000	0.000	0.000	0.000
NMn/NPy	0.028	0.014	0.015	0.042	0.024	0.049	0.038	0.014	0.030	0.029	0.012	0.030	0.023

unexs. = unexsolved, exs. = exsolved, calc. = calculated; NTi, NMn, NMg and NHem, NPy, NGk are QUILF-specific parameters for magnetite and ilmenite, respectively (see Andersen *et al.*, 1993); — = not determined.

Table 6: Average Laser-ICP-MS analyses of REEs in clinopyroxene from Isortoq dike rocks

Dike	Olivine-gabbro	BFD 1	BFD 1	BFD 1	BFD 1	BFD 1	BFD 1	BFD 1 anorthosite xenolith	BFD 3	GD 1 syenogabbro	GD 3 gabbro	GD 3 syenite	Larvikite
Sample	GM 1803	GM 1680	GM 1729	GM 1735	GM 1681 matrix	GM 1681 high-Ca inclusions	GM 1681 low-Ca inclusions	GM 1682	GM 1805	GM 1712	GM 1760	GM 1772	GM 1684
No. of cpx analysed	n = 7	n = 3	n = 3	n = 6	n = 2	n = 4	n = 3	n = 4	n = 4	n = 3	n = 11	n = 11	n = 4
REE concentrations in ppm:													
La	7.58	5.60	6.43	8.02	16.53	10.28	2.59	4.18	10.90	10.25	11.55	18.46	13.38
Ce	32.65	27.72	27.30	32.46	64.06	37.77	12.30	16.84	39.26	38.52	42.36	59.64	52.13
Pr	6.28	4.70	5.30	6.07	12.93	6.99	2.93	3.44	7.58	7.78	8.02	11.14	9.50
Nd	34.60	27.53	29.36	38.96	74.00	40.49	18.40	20.40	45.97	43.07	45.54	59.32	56.88
Sm	10.93	8.29	8.20	11.67	18.27	11.63	6.57	7.04	13.39	13.44	13.44	16.15	14.89
Eu	2.60	2.73	2.75	3.54	4.70	3.39	2.16	2.46	3.90	2.72	3.43	1.85	3.41
Gd	11.61	8.27	7.76	12.06	12.40	11.03	8.11	7.73	12.50	13.35	13.35	14.01	12.70
Tb	1.83	1.30	1.25	1.86	1.76	1.96	1.29	1.08	2.17	2.50	2.12	2.31	1.92
Dy	10.81	7.56	7.22	10.87	11.09	11.07	7.95	5.83	11.94	13.72	12.02	13.17	10.63
Ho	2.05	1.42	1.47	2.12	2.22	2.22	1.63	1.19	2.17	2.78	2.46	2.71	2.01
Er	5.67	3.39	3.54	5.17	6.26	5.85	4.19	2.75	5.55	7.09	6.18	7.19	5.48
Tm	0.78	0.47	0.52	0.74	1.17	0.88	0.66	0.55	0.80	0.94	0.92	1.10	0.77
Yb	5.75	3.43	3.25	5.03	9.31	5.84	4.04	2.78	5.72	7.03	6.18	8.99	5.83
Lu	0.86	0.45	0.49	0.72	1.82	0.92	0.74	0.49	0.76	1.03	0.96	1.80	0.84
La_N/Yb_N	0.89	1.10	1.33	1.07	1.20	1.19	0.43	1.01	1.28	0.98	1.26	1.38	1.55
Eu/Eu*	0.70	1.00	1.07	0.92	0.98	0.92	0.91	1.02	0.93	0.65	0.81	0.41	0.89
Eu/Eu^*_{max}	0.74	1.04	1.13	0.98	1.06	0.93	1.13	1.08	1.16	0.80	0.96	0.78	1.20

$Eu/Eu^* = Eu_N/(Sm_N \times Gd_N)^{0.5}$; Eu/Eu^*_{max} is the maximum value of Eu/Eu* in an individual clinopyroxene of the respective sample.

Table 7: XRF whole-rock analyses of Isortoq dike rocks

Dike	Olivine-gabbro	BFD 1	BFD 1 anorthosite xenolith	BFD 2	BFD 3	BFD 4	GD 1 syeno-gabbro	GD 3 gabbro	GD 3 syenite	GD 3 syenite	Larvikite	Hbl.-syenite
Sample	GM 1803	GM 1735	GM 1682	GM 1750	GM 1805	GD 39	GM 1712	GM 1760	GM 1772	GM 1778	GM 1684	GD 38
Major elements (wt.%)												
SiO_2	44.57	46.46	51.86	53.05	49.88	46.73	47.83	41.69	55.17	55.93	56.34	53.91
TiO_2	2.95	2.25	1.76	1.83	1.93	2.67	2.12	4.19	1.55	1.55	1.28	0.97
Al_2O_3	16.79	16.62	19.32	17.56	15.83	16.03	18.54	14.09	15.41	15.37	16.87	16.62
Fe_2O_3	15.90	14.11	8.82	9.81	12.92	14.92	12.30	17.03	10.50	10.91	8.50	8.57
MnO	0.19	0.17	0.12	0.15	0.17	0.19	0.16	0.22	0.20	0.20	0.14	0.13
MgO	5.08	5.54	2.12	2.17	4.34	5.72	2.59	4.71	1.10	0.99	2.35	4.06
CaO	7.68	7.40	7.62	6.12	6.72	7.77	7.26	8.22	4.16	3.67	4.82	6.11
Na_2O	3.69	3.68	4.58	4.40	4.41	3.74	4.46	3.69	5.18	5.86	4.75	4.01
K_2O	1.12	1.25	1.63	2.78	1.48	1.18	1.89	1.79	4.03	3.34	3.26	2.48
P_2O_5	0.48	0.47	0.45	0.68	0.40	0.56	0.47	2.48	0.44	0.40	0.33	0.43
LOI	0.67	0.64	0.88	0.56	0.66	-0.43	2.09	0.84	0.64	0.86	0.67	1.91
Total	99.12	98.59	99.16	99.11	98.74	99.08	99.71	98.95	98.38	99.08	99.31	99.20
Mg#[*]	43.2	48.3	36.4	34.5	44.4	47.7	33.4	39.7	19.9	17.7	39.7	53.0
Trace elements (ppm)												
Sc	17	21	15	18	20	20	14	17	13	10	16	20
V	173	193	86	83	174	162	96	107	6	3	78	155
Cr	36	54	2	4	44	70	n.d.	n.d.	n.d.	n.d.	29	45
Co	62	78	18	22	60	84	40	47	6	7	55	60
Ni	53	87	11	14	60	71	29	n.d.	3	n.d.	34	33
Cu	37	61	10	12	67	47	26	27	n.d.	n.d.	46	46
Zn	92	105	76	85	109	104	86	96	130	124	101	102
Ga	18	20	20	19	21	19	21	15	19	22	23	19
Rb	19	17	15	35	25	14	33	18	32	36	33	60
Sr	411	629	753	563	510	454	558	421	417	265	535	817
Y	30	24	25	32	31	34	42	39	45	51	27	27
Zr	172	140	137	215	221	171	245	150	271	367	245	163
Nb	12	14	11	14	14	12	18	12	22	25	16	14
Ba	463	750	1022	1740	936	649	899	718	2981	2131	2513	972
Pb	4	5	7	9	7	4	15	7	8	11	15	8
La	—	—	24	41	—	16	—	—	38	42	—	35
Ce	—	—	62	95	—	65	—	—	96	101	—	93
Pr	—	—	4	8	—	6	—	—	9	7	—	7
Nd	—	—	31	52	—	32	—	—	51	49	—	44
Sm	—	—	4	9	—	10	—	—	5	8	—	8
Characteristic normative minerals[**]												
	ne+ol	*ne+ol*	*hy+ol*	*hy+ol*	*hy+ol*	*ne+ol*	*ne+ol*	*ne+ol*	*ne+ol*	*hy+ol*	*q+hy*	*q+hy*

[*] Mg# = 100[Mg/(Mg + Fe^{2+})] with Fe_2O_3/FeO = 0.2; [**] Calculation of normative mineral composition according to the CIPW norm;
n.d. = not detected; — = not determined;

Table 8: Sr, Nd and O isotopic composition of Isortoq dike rocks and adjacent Ketilidian basement rocks

Rock type	**Sample**	**Material**	**Sr (ppm)**	**Rb (ppm)**	**$^{87}Rb/^{86}Sr$**	**$^{87}Sr/^{86}Sr$**	**$^{87}Sr/^{86}Sr$ (i)**	**Sm (ppm)**	**Nd (ppm)**	**$^{147}Sm/^{144}Nd$**	**$^{143}Nd/^{144}Nd$**	**ε_{Nd}(i)**	**$\delta^{18}O$ (V-SMOW)**
Isortoq dikes:													
BFD 1, anorthosite xenolith	GM 1682	cpx	41.60	0.800	0.0556	0.704454 ± 10	0.70351	13.56	47.42	0.1728	0.512165 ± 09	-5.6	5.73
Larvikite	GM 1684	cpx	52.31	1.087	0.0601	0.705016 ± 10	0.70399	14.35	53.20	0.1631	0.511830 ± 10	-10.7	6.20
GD 1, gabbro	GM 1712	cpx	56.42	0.361	0.0185	0.703728 ± 10	0.70341	19.94	66.67	0.1808	0.512484 ± 10	-0.6	5.30
BFD 1	GM 1735	cpx	61.40	3.085	0.1453	0.705773 ± 10	0.70330	16.16	58.51	0.1670	0.512223 ± 10	-3.6	5.72 ± 0.07
BFD 1	GM 1735	whole-rock						5.64	26.06	0.1308	0.511922 ± 10	-3.9	
BFD 1	GM 1735	plagioclase						2.14	11.74	0.1100	0.511780 ± 10	-3.5	6.61 ± 0.08
BFD 2	GM 1750	cpx	51.41	7.337	0.4130	0.709994 ± 10	0.70296	19.03	74.61	0.1542	0.511902 ± 09	-7.9	5.93
GD 3, gabbro	GM 1760	cpx	44.96	0.739	0.0475	0.704151 ± 10	0.70334	14.80	51.87	0.1725	0.512357 ± 10	-1.8	5.62
GD 3, syenite	GM 1772	cpx	44.92	0.973	0.0627	0.704572 ± 10	0.70350	22.06	91.46	0.1458	0.512146 ± 14	-1.8	5.41
GD 3, syenite	GM 1778	cpx	32.87	1.128	0.0993	0.704920 ± 09	0.70323	20.03	82.24	0.1472	0.512163 ± 10	-1.7	
Olivine-gabbro	GM 1803	cpx	49.32	1.177	0.0690	0.704069 ± 10	0.70289	21.09	73.19	0.1742	0.512475 ± 10	0.3	5.54
BFD 3	GM 1805	cpx	58.67	1.399	0.0690	0.704794 ± 09	0.70362	13.45	47.63	0.1706	0.512079 ± 10	-6.9	5.59
Brown Dike (BD_0)	GD 37	cpx	44.61	0.218	0.0141	0.703721 ± 09	0.70346	5.79	16.65	0.2103	0.512619 ± 10	-2.6	
Hornblende-syenite	GD 38	amph	101.10	5.863	0.1677	0.707176 ± 10	0.70432	18.99	83.46	0.1376	0.511959 ± 10	-4.2	5.21
BFD 4	GD 39	cpx	67.57	0.391	0.0167	0.703431 ± 09	0.70315	12.62	41.66	0.1831	0.512479 ± 10	-1.0	
Ketilidian basement:													
Granitoid	BT 03	whole-rock	70.58	186.9	7.8080	0.901275 ± 09	0.76821	8.25	54.67	0.0913	0.511341 ± 10	-9.3	8.2
Granitoid	BT 05	whole-rock	946.4	31.96	0.0977	0.704834 ± 16	0.70317	1.94	10.16	0.1154	0.511785 ± 10	-4.3	7.2
Granitoid	BT 06	whole-rock	422.1	109.2	0.7494	0.721722 ± 10	0.70895	6.45	39.03	0.0999	0.511516 ± 10	-7.2	7.9

$^{87}Sr/^{86}Sr$ and $^{143}Nd/^{144}Nd$ initial ratios were calculated for T = 1.19 Ga except for the BD_0 dike (GD 37) for which an age of 1.28 Ga (Upton *et al*., 2003) was assumed. Standard deviations for $\delta^{18}O$ are given for samples which were analysed twice.

Table 9: Os isotope data of Isortoq dike rocks, Eriksfjord Formation basalts and Ilímaussaq syenites

Rock type	Sample	Age (Ma)*	Re (ng/g)	Os (ng/g)	Re/Os	$^{187}Re/^{188}Os$	$^{187}Os/^{188}Os$	$(^{187}Os/^{188}Os)_i$
Isortoq dikes								
BFD 1	GM 1735	1190	0.353	0.0153	23.13	176.44	4.6635 ± 89	1.131
GD 3, gabbro	GM 1760	1190	0.479	0.0070	68.74	4775.09	103.58 ± 16	7.967
Olivine-gabbro	GM 1803	1190	0.153	0.0021	71.71	2237.83	42.381 ± 58	-2.428
BFD 4	GD 39	1190	0.388	0.0144	26.86	213.58	5.181 ± 11	0.905
Eriksfjord Formation basalts								
Basalt, Mussartût group	EF 024	1200	0.362	0.1490	2.43	11.60	0.10690 ± 1	-0.127
Basalt, Ulukasik group	EF 072	1200	0.343	0.0132	25.94	192.34	4.3238 ± 85	0.440
Basalt, Ilímaussaq group	EF 174	1200	0.207	0.0094	22.13	197.13	6.709 ± 21	2.729
Basalt, Ilímaussaq group	EF 168	1200	0.177	0.0123	14.45	93.49	2.8124 ± 61	0.925
Ilímaussaq intrusion								
Augite-syenite (center)	GM 1857	1160	0.013	0.0041	3.23	17.20	0.9751 ± 24	0.639
Augite-syenite (border)	GM 1858	1160	0.0026	0.00023	11.28	68.22	2.1395 ± 32	0.808

* Age determinations from Paslick *et al.* (1993) for the Eriksfjord Formation basalts and Waight *et al.* (2002) for the Ilímaussaq intrusion.

Table 10: Parameters used in energy-constrained assimilation-fractional crystallization (EC-AFC) modeling

Thermal parameters:		
Liquidus temperature of magma	1190 °C	
Initial temperature of magma	1140 °C	
Solidus temperature	850 °C	
Temperature of equilibration	900 °C	
Compositional parameters:	**Sr**	**Nd**
Magma initial concentration (ppm)	411	32
Magma isotope ratio	0.70289	0.51111
Magma trace element distribution coefficient	1.5	0.25
Upper crustal assimilant initial concentration (ppm)	480	35
Upper crustal assimilant isotope ratio	0.70806	0.51069
Lower crustal assimilant initial concentration (ppm)	747	63
Lower crustal assimilant isotope ratio	0.70670	0.5099
Assimilant trace element distribution coefficient	1.5	0.25

For the upper and lower crustal assimilants, the thermal parameters for the “standard“ upper-crustal and the “standard“ lower-crustal case, respectively, were taken from Bohrson & Spera (2001).

Fig. 1

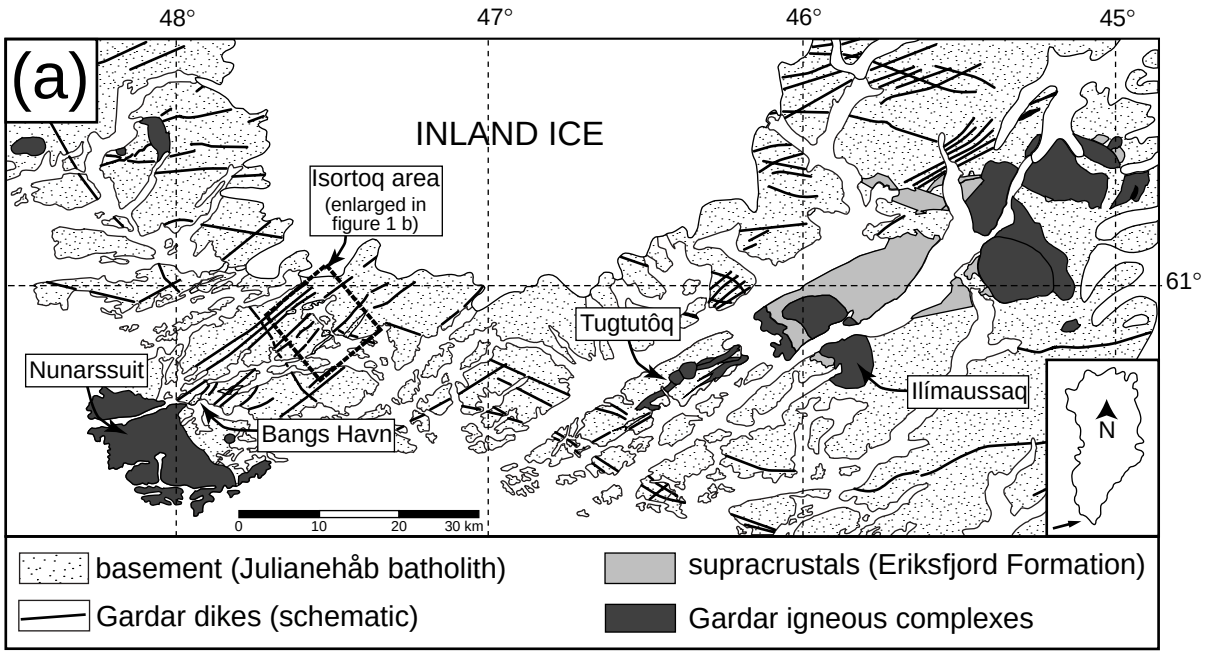
(a)
48°
47°
46°
45°
61°
INLAND ICE
Isortoq area
(enlarged in
figure 1 b)
Tugtutôq
Nunarssuit
Bangs Havn
Ilímaussaq
N
0
10
20
30 km
basement (Julianehåb batholith)
supracrustals (Eriksfjord Formation)
Gardar dikes (schematic)
Gardar igneous complexes

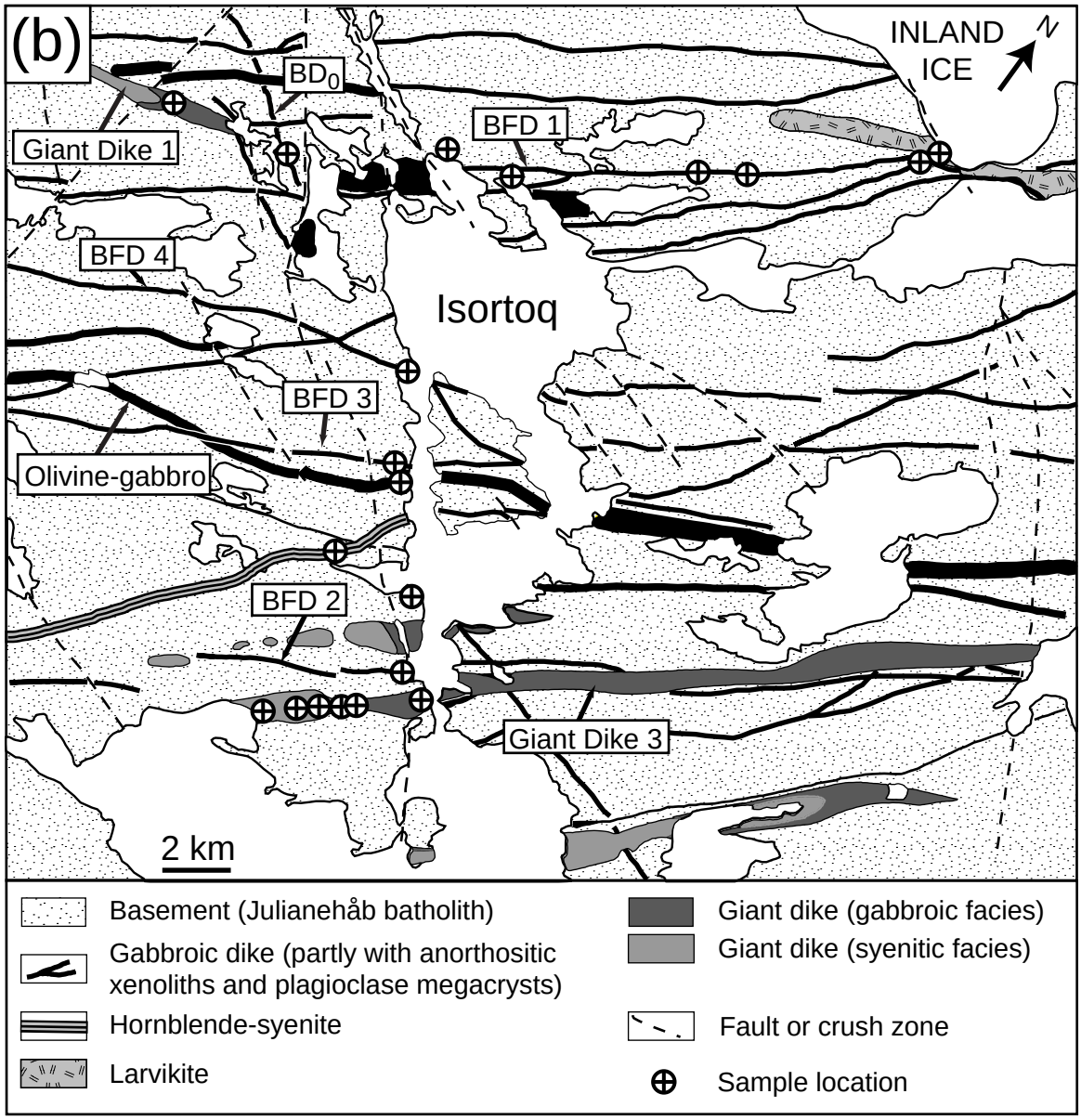
(b)
INLAND
ICE
N
BD0
Giant Dike 1
BFD 1
BFD 4
Isortoq
BFD 3
Olivine-gabbro
BFD 2
Giant Dike 3
2 km
Basement (Julianehåb batholith)
Gabbroic dike (partly with anorthositic
xenoliths and plagioclase megacrysts)
Hornblende-syenite
Larvikite
Giant dike (gabbroic facies)
Giant dike (syenitic facies)
Fault or crush zone
Sample location

Fig. 2

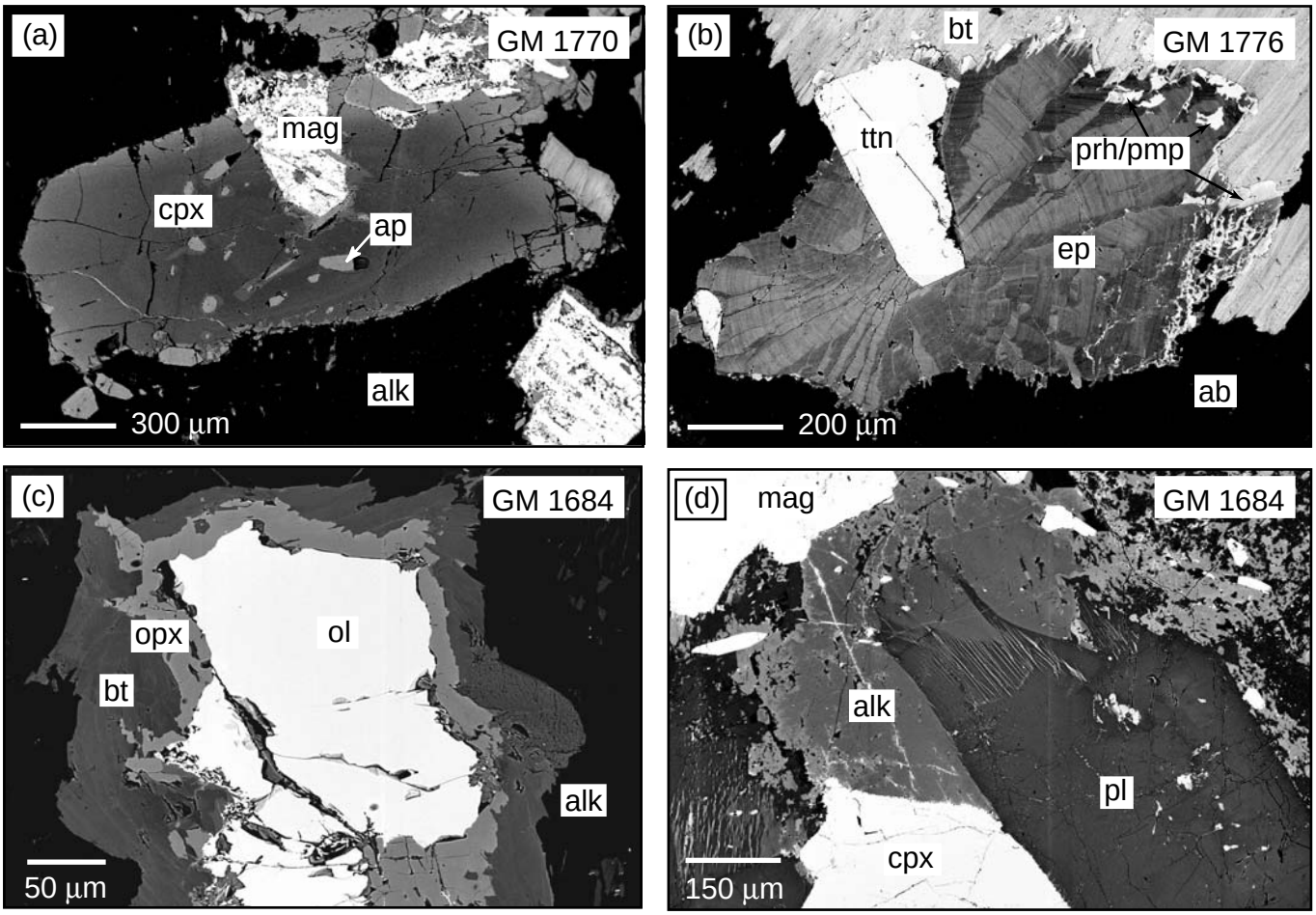
(a)
GM 1770
mag
cpx
ap
alk
300 µm
(b)
bt
GM 1776
ttn
prh/pmp
ep
ab
200 µm
(c)
GM 1684
opx
ol
bt
alk
50 µm
(d)
mag
GM 1684
alk
pl
cpx
150 µm

Fig. 3

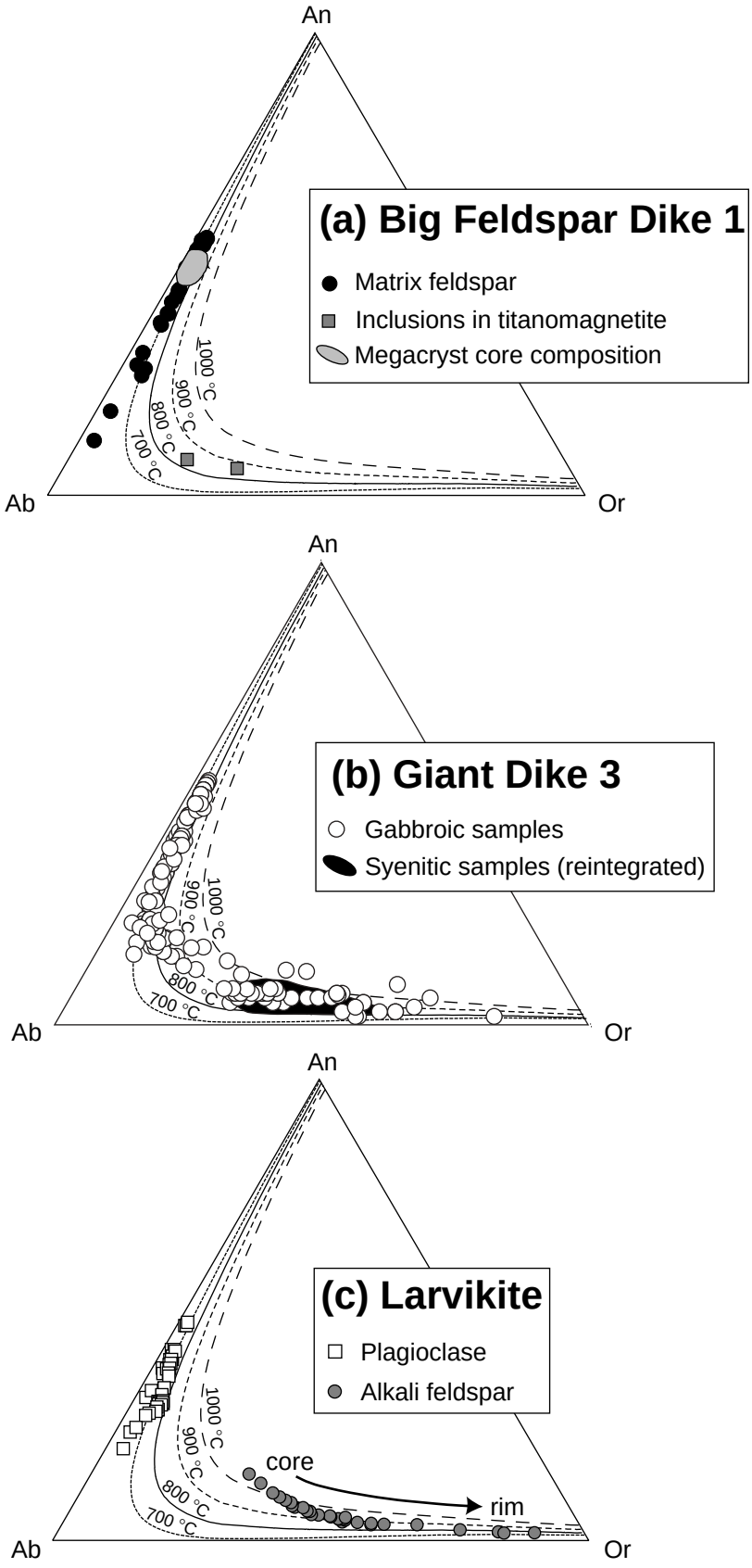
An
Ab
Or
(a) Big Feldspar Dike 1
Matrix feldspar
Inclusions in titanomagnetite
Megacryst core composition
1000 °C
900 °C
800 °C
700 °C
(b) Giant Dike 3
Gabbroic samples
Syenitic samples (reintegrated)
(c) Larvikite
Plagioclase
Alkali feldspar
core
rim

(a) Big Feldspar Dikes (BFDs)

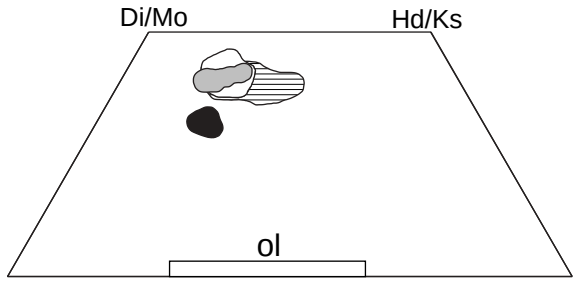

- BFD 1, 3 & 4
- BFD 2
- Anorthosite xenolith (GM1682) in BFD 1
- Ca-poor inclusions in feldspar megacryst in BFD 1 (GM1681)

(b) Olivine-gabbro

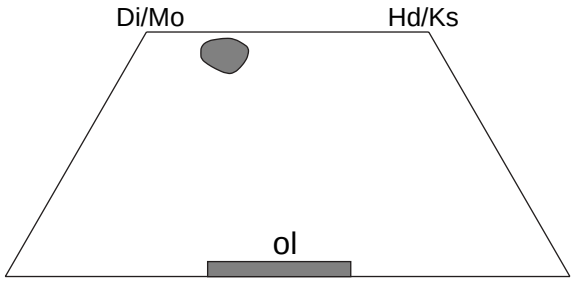

(c) Giant Dikes 1 & 3

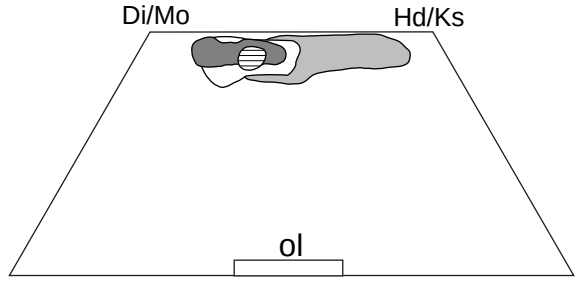

- Giant Dike 1 (GM 1712)
- Giant Dike 3
- Gabbroic samples
- Rims around olivine (GM 1761 & 1762)
- Syenitic samples

(d) Larvikite

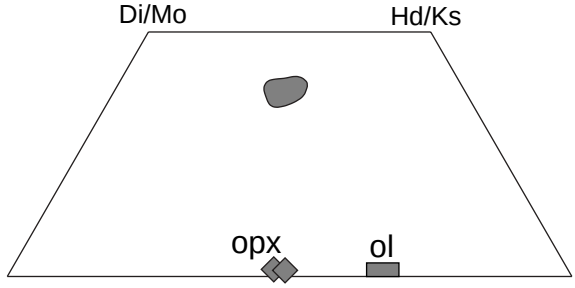

Fig. 5

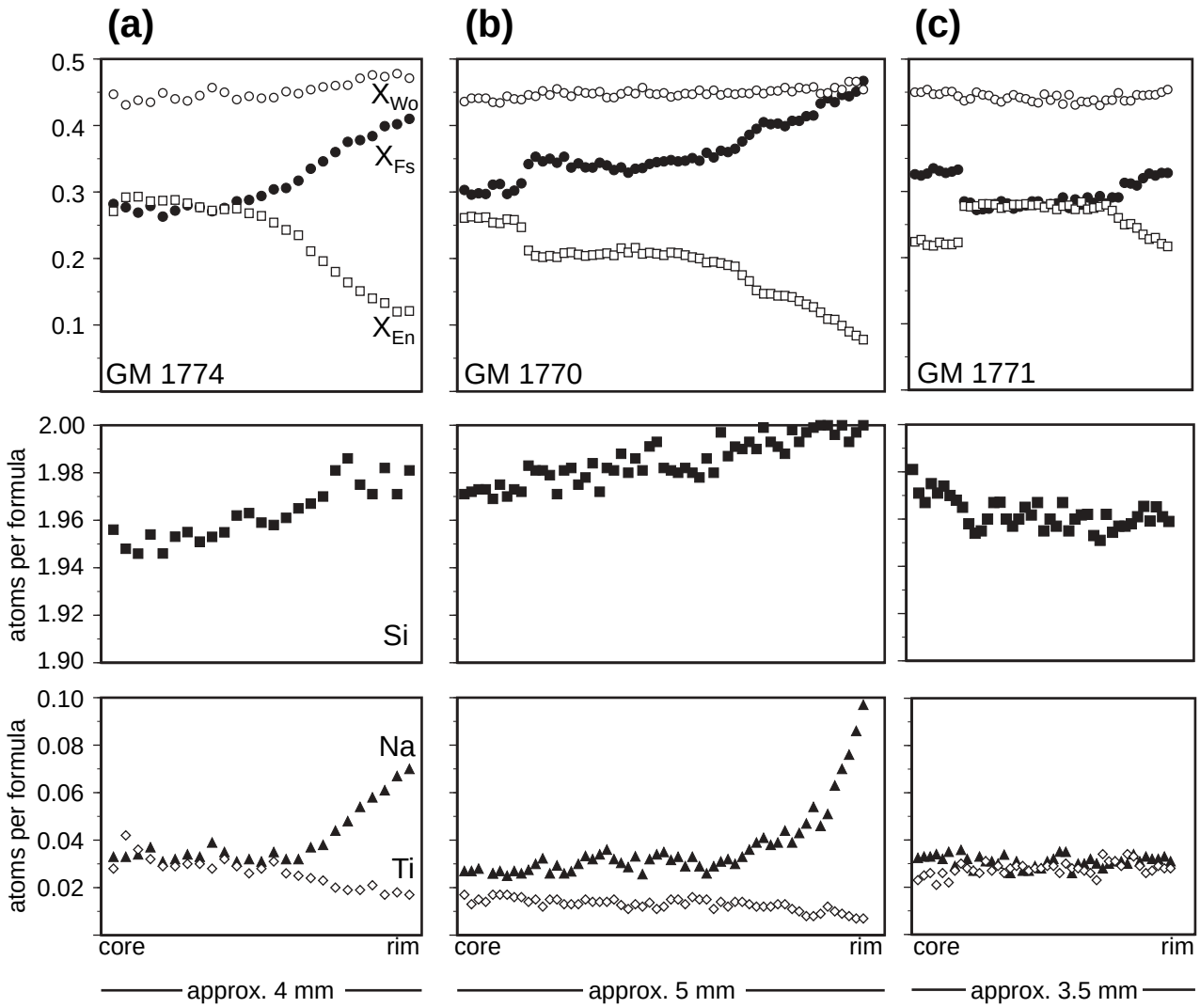
(a)
(b)
(c)
0.5
0.4
0.3
0.2
0.1
X_{Wo}
X_{Fs}
X_{En}
GM 1774
GM 1770
GM 1771
2.00
1.98
1.96
1.94
1.92
1.90
atoms per formula
Si
0.10
0.08
0.06
0.04
0.02
atoms per formula
Na
Ti
core
rim
core
rim
core
rim
approx. 4 mm
approx. 5 mm
approx. 3.5 mm

Fig. 6

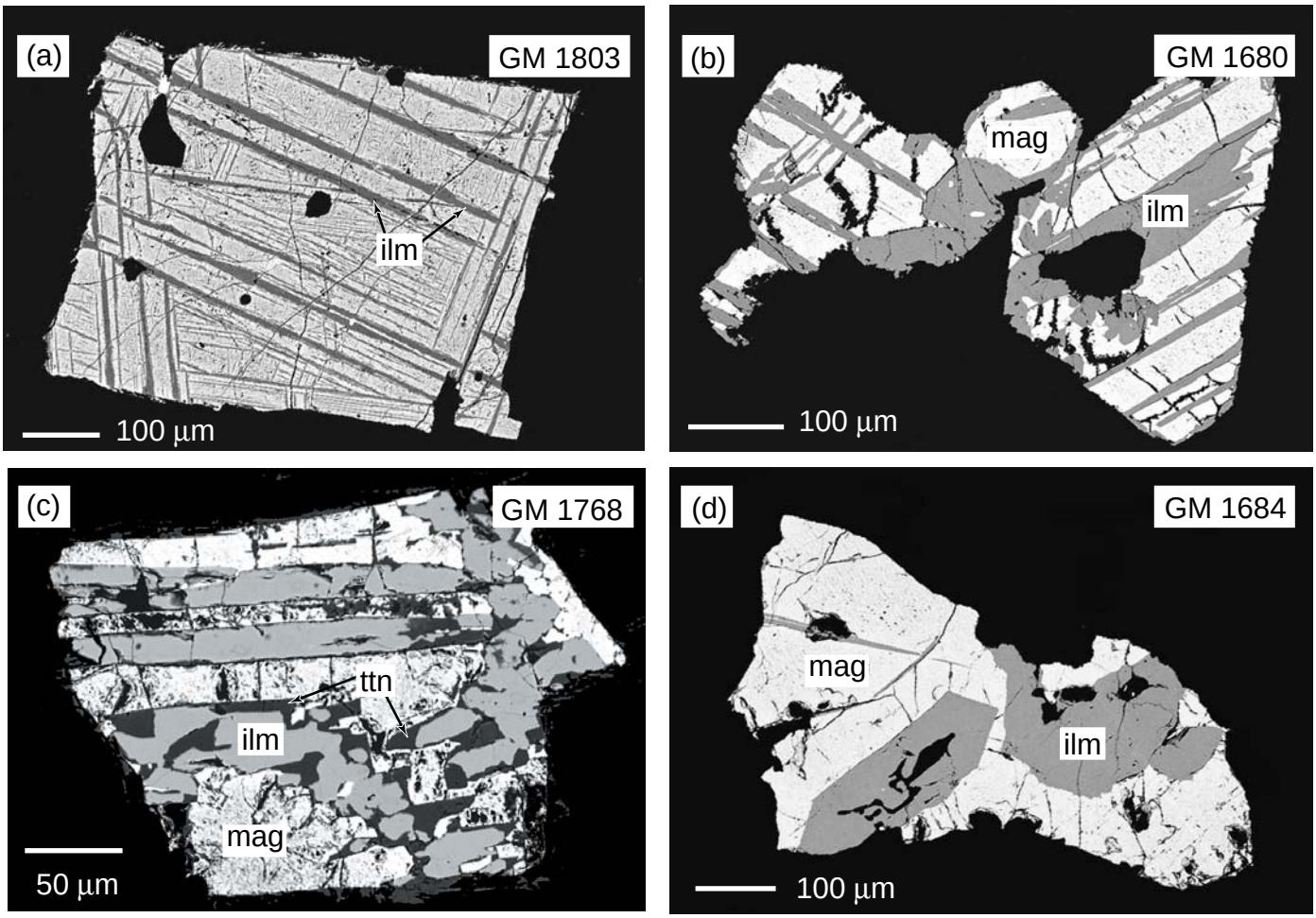
(a)
GM 1803
ilm
100 μm
(b)
GM 1680
mag
ilm
100 μm
(c)
GM 1768
ttn
ilm
mag
50 μm
(d)
GM 1684
mag
ilm
100 μm

Fig. 7

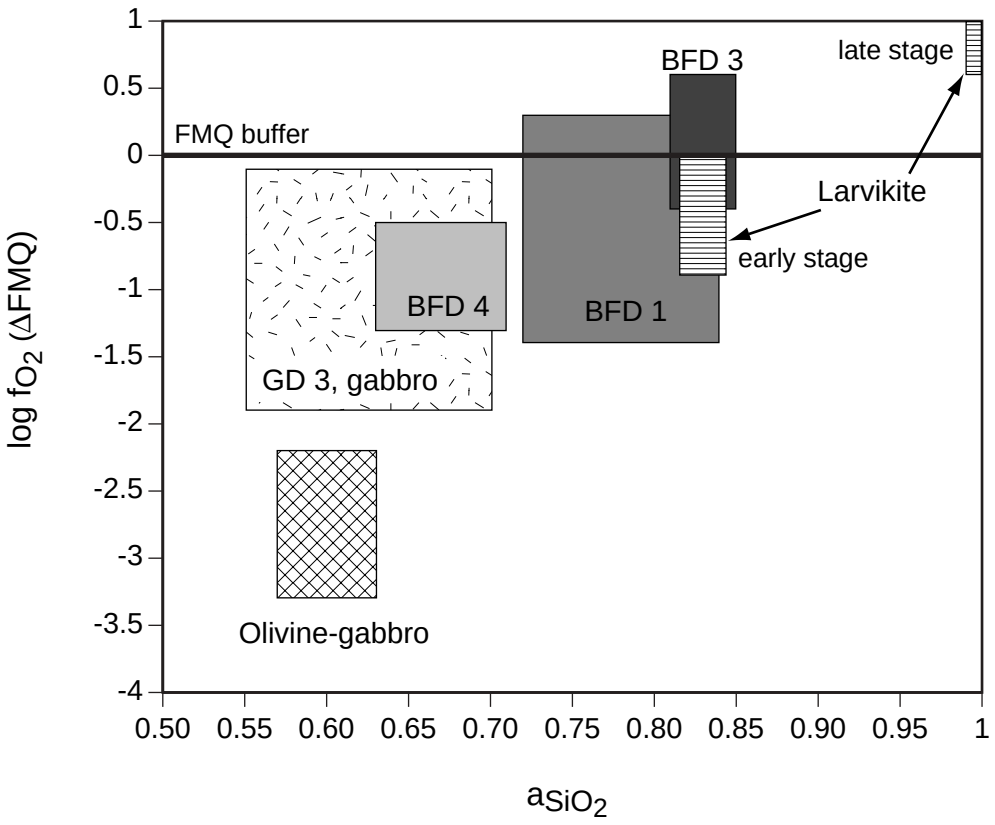
1
0.5
0
-0.5
-1
-1.5
-2
-2.5
-3
-3.5
-4
log f_{O_2} (ΔFMQ)
0.50
0.55
0.60
0.65
0.70
0.75
0.80
0.85
0.90
0.95
1
a_{SiO_2}
FMQ buffer
BFD 3
late stage
Larvikite
early stage
BFD 4
BFD 1
GD 3, gabbro
Olivine-gabbro

Fig. 8

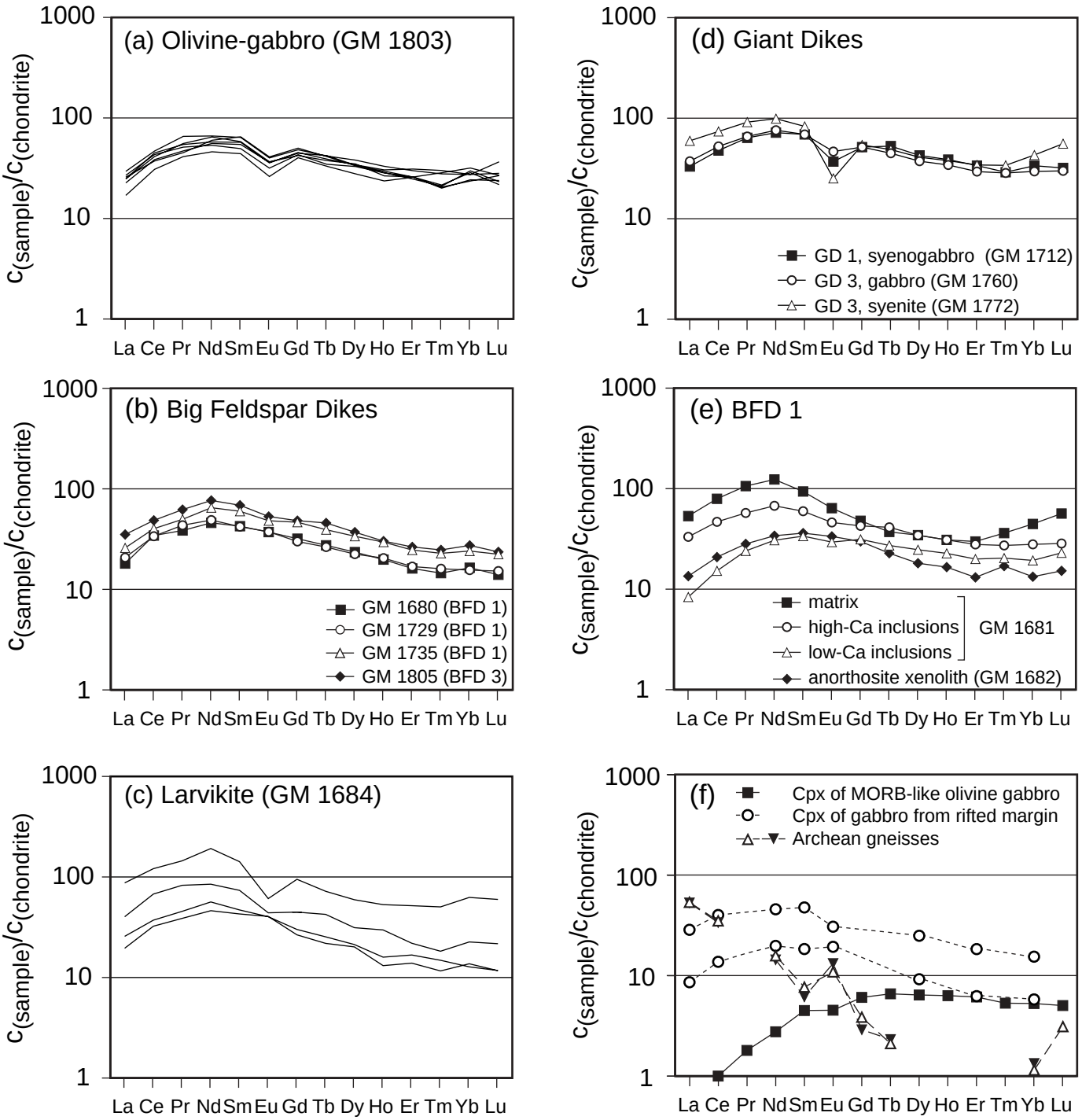
(a) Olivine-gabbro (GM 1803)
(b) Big Feldspar Dikes
GM 1680 (BFD 1)
GM 1729 (BFD 1)
GM 1735 (BFD 1)
GM 1805 (BFD 3)
(c) Larvikite (GM 1684)
(d) Giant Dikes
GD 1, syenogabbro (GM 1712)
GD 3, gabbro (GM 1760)
GD 3, syenite (GM 1772)
(e) BFD 1
matrix
high-Ca inclusions
low-Ca inclusions
GM 1681
anorthosite xenolith (GM 1682)
(f)
Cpx of MORB-like olivine gabbro
Cpx of gabbro from rifted margin
Archean gneisses
c(sample)/c(chondrite)
1000
100
10
1
La Ce Pr Nd Sm Eu Gd Tb Dy Ho Er Tm Yb Lu

Fig. 9

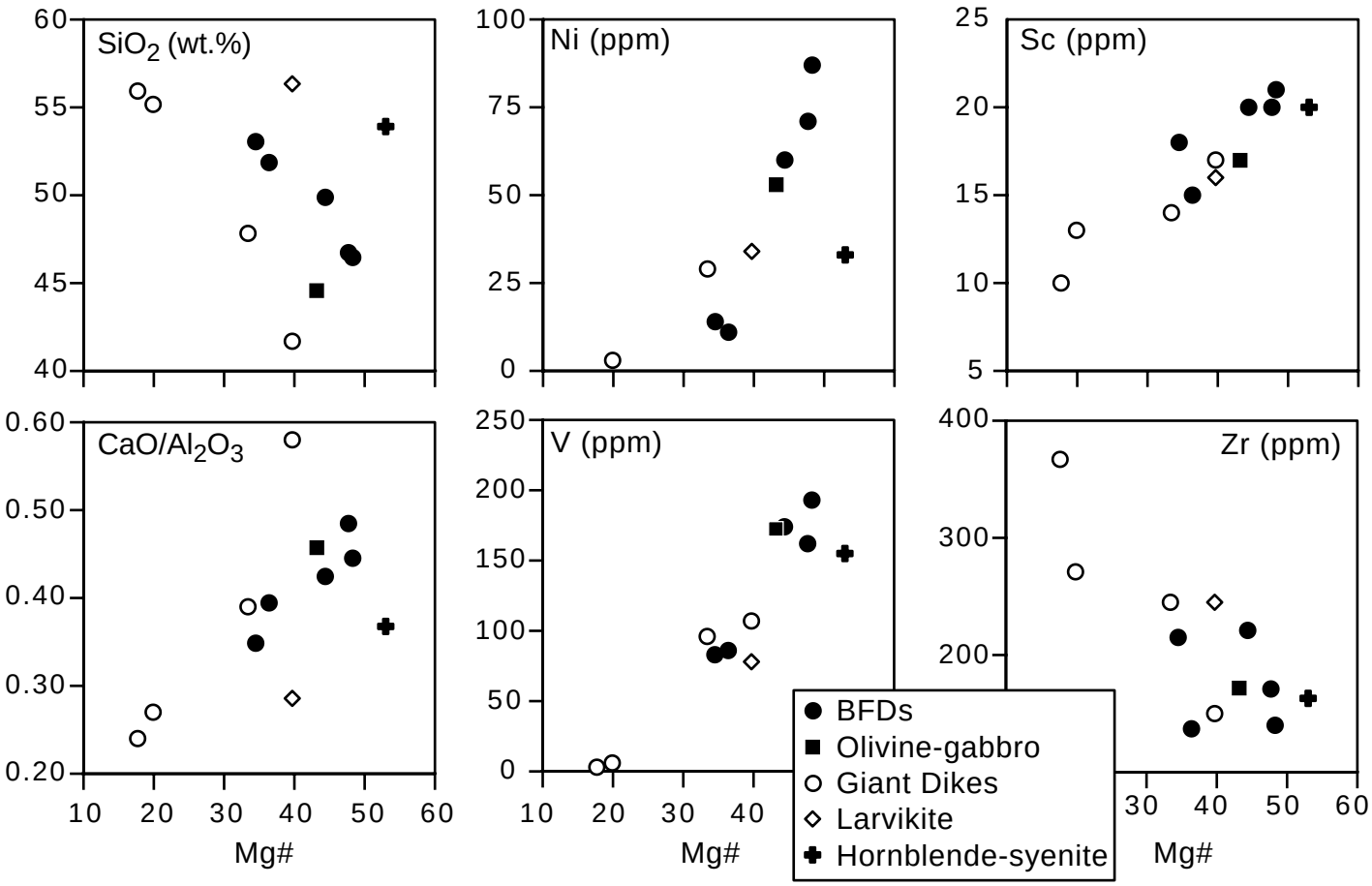
SiO2 (wt.%)
Ni (ppm)
Sc (ppm)
CaO/Al2O3
V (ppm)
Zr (ppm)
Mg#
BFDs
Olivine-gabbro
Giant Dikes
Larvikite
Hornblende-syenite

Fig. 10

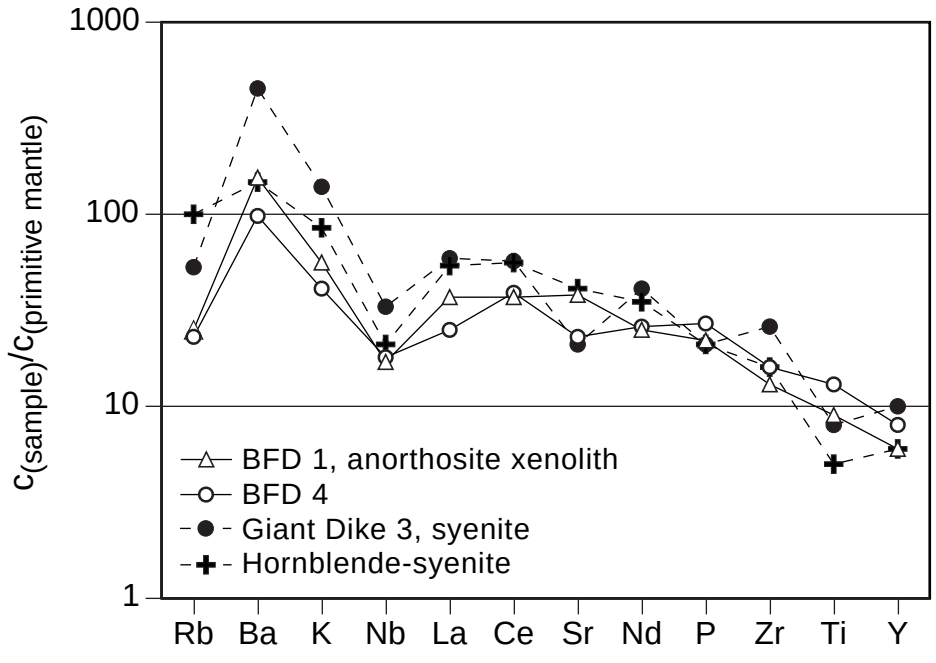
c(sample)/c(primitive mantle)
Rb
Ba
K
Nb
La
Ce
Sr
Nd
P
Zr
Ti
Y
BFD 1, anorthosite xenolith
BFD 4
Giant Dike 3, syenite
Hornblende-syenite

Fig. 11

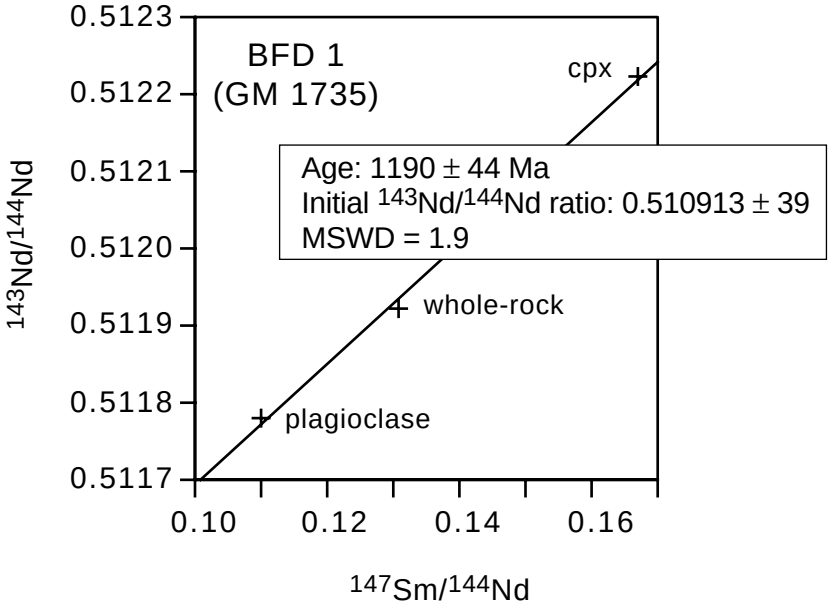
BFD 1
(GM 1735)
cpx
Age: 1190 ± 44 Ma
Initial 143Nd/144Nd ratio: 0.510913 ± 39
MSWD = 1.9
whole-rock
plagioclase
0.5123
0.5122
0.5121
0.5120
0.5119
0.5118
0.5117
0.10
0.12
0.14
0.16
143Nd/144Nd
147Sm/144Nd

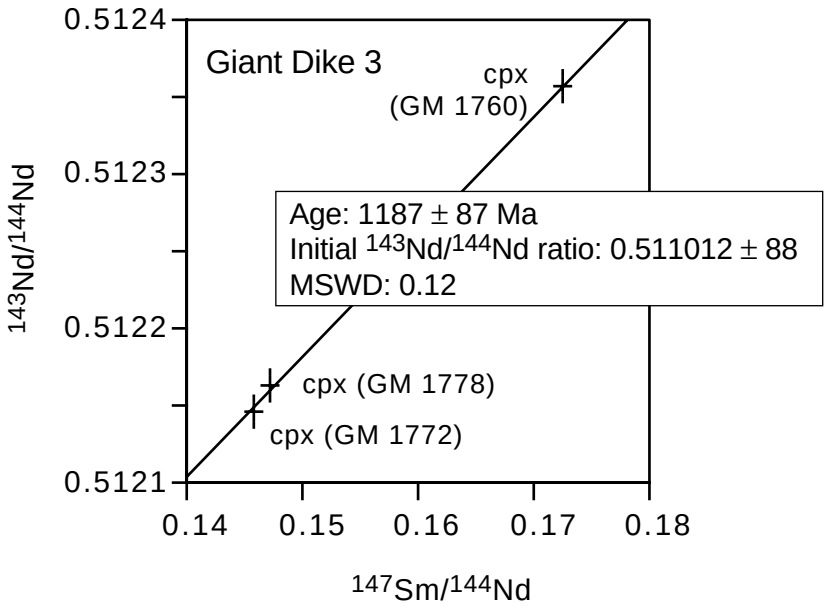
Giant Dike 3
cpx
(GM 1760)
Age: 1187 ± 87 Ma
Initial 143Nd/144Nd ratio: 0.511012 ± 88
MSWD: 0.12
cpx (GM 1778)
cpx (GM 1772)
0.5124
0.5123
0.5122
0.5121
0.14
0.15
0.16
0.17
0.18
143Nd/144Nd
147Sm/144Nd

Fig. 12

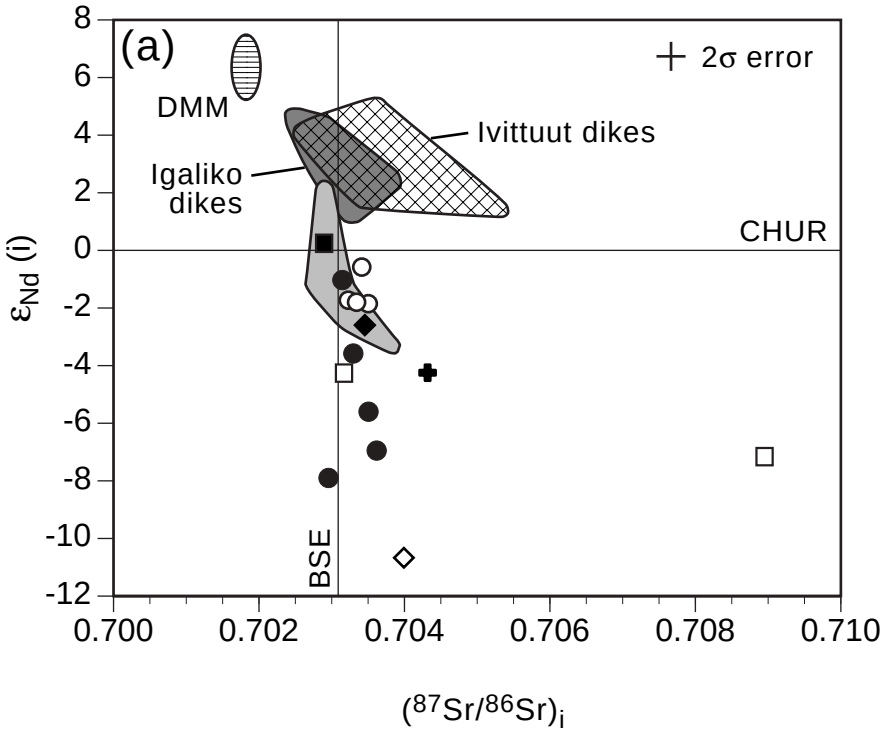
(a)
2σ error
DMM
Ivittuut dikes
Igaliko dikes
CHUR
BSE
ε_{Nd} (i)
$(^{87}Sr/^{86}Sr)_i$
8
6
4
2
0
-2
-4
-6
-8
-10
-12
0.700
0.702
0.704
0.706
0.708
0.710

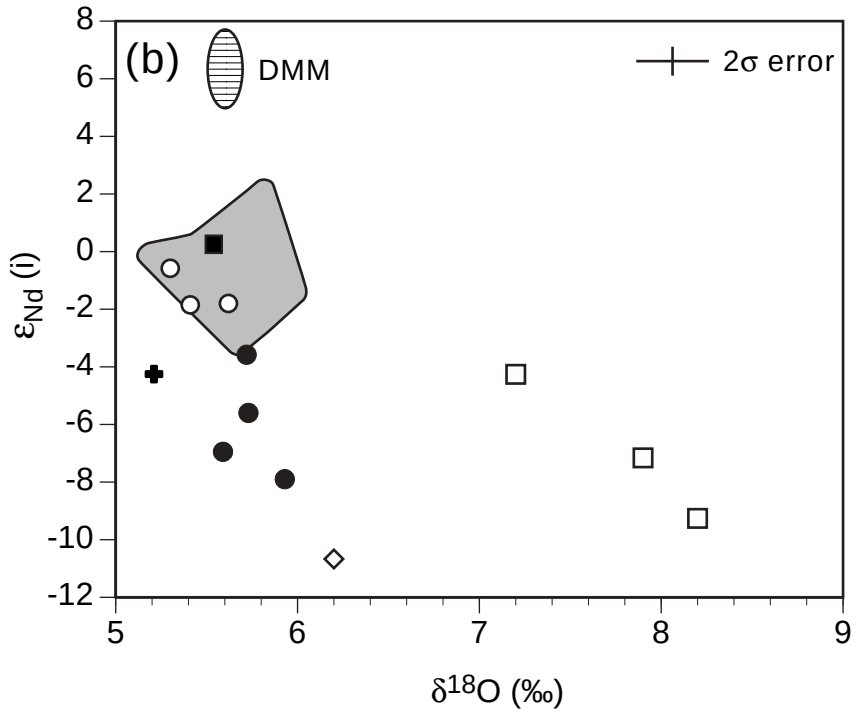
(b)
DMM
2σ error
ε_{Nd} (i)
$\delta^{18}O$ (‰)
8
6
4
2
0
-2
-4
-6
-8
-10
-12
5
6
7
8
9

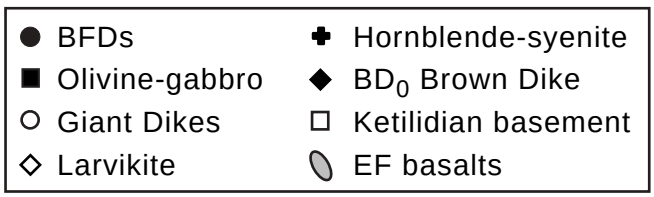
BFDs
Olivine-gabbro
Giant Dikes
Larvikite
Hornblende-syenite
BD_0 Brown Dike
Ketilidian basement
EF basalts

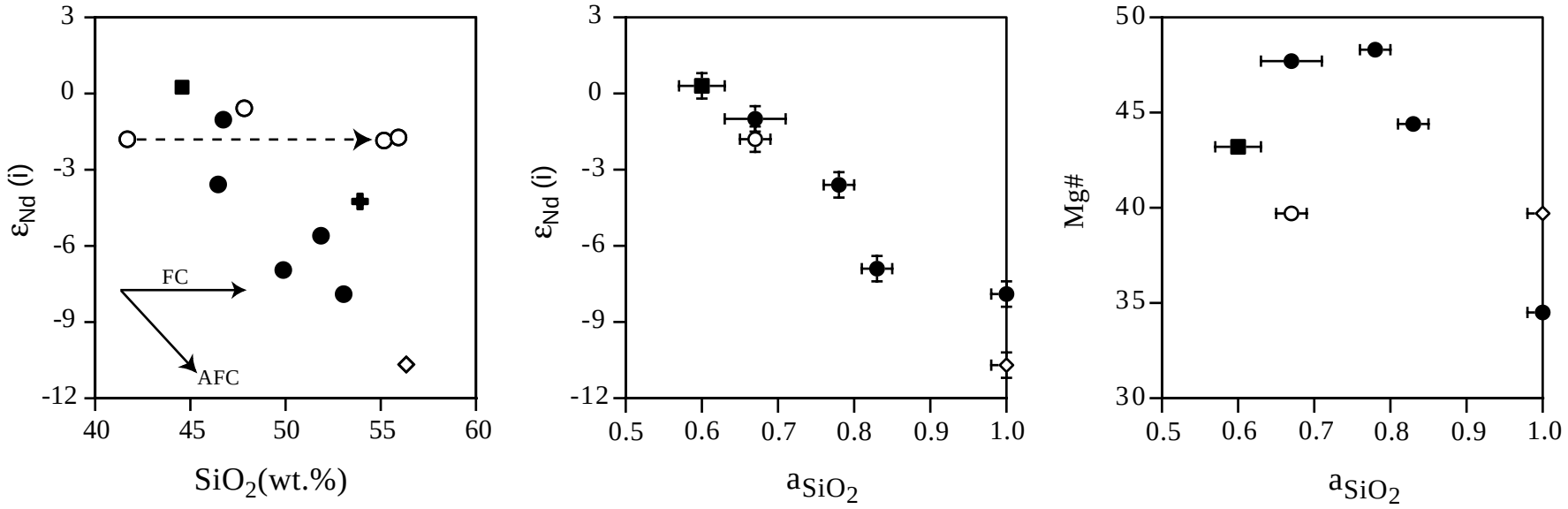
3
0
-3
-6
-9
-12
εNd (i)
FC
AFC
40
45
50
55
60
SiO2(wt.%)
0.5
0.6
0.7
0.8
0.9
1.0
aSiO2
50
45
40
35
30
Mg#

Fig. 13

Fig. 14

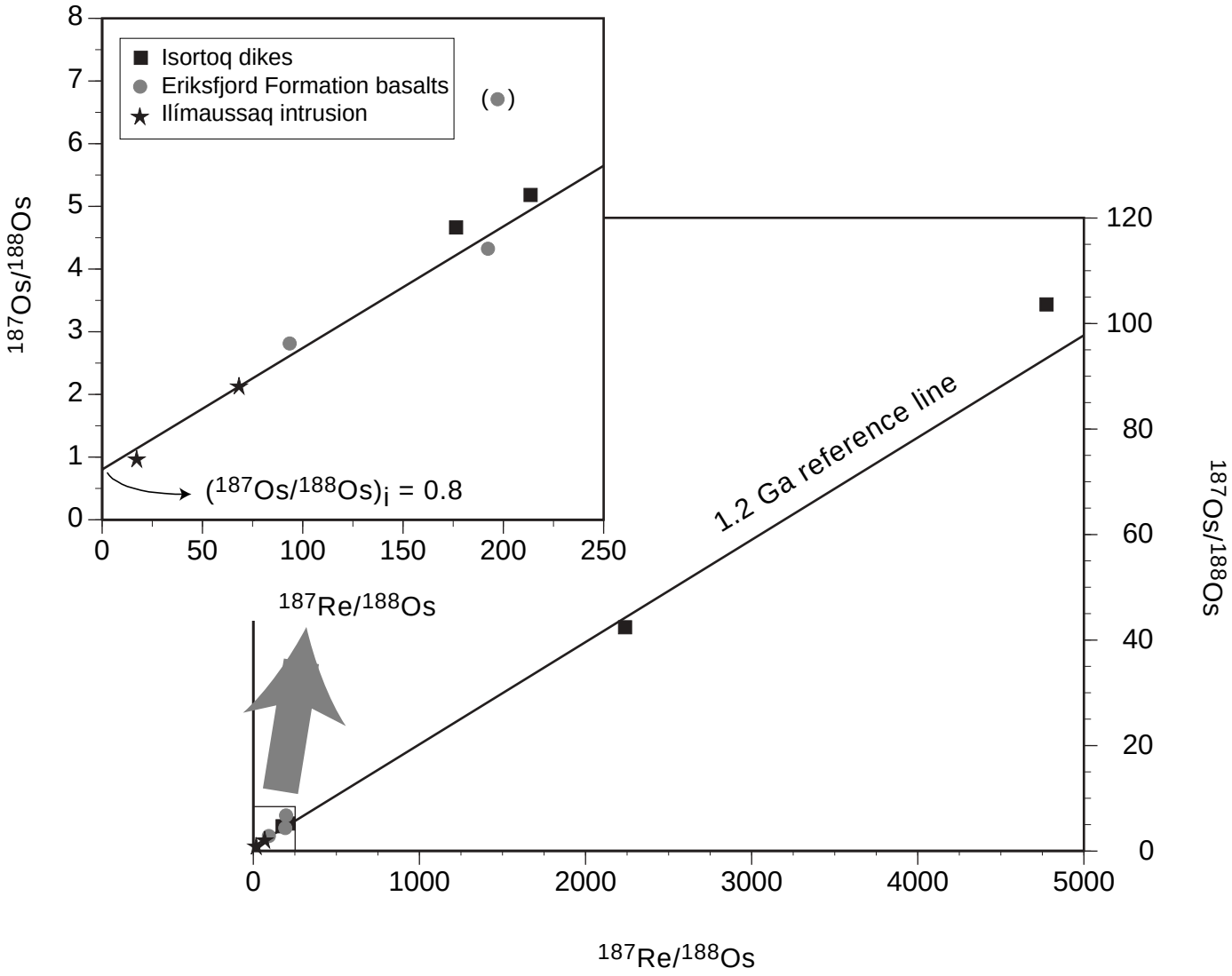
Isortoq dikes
Eriksfjord Formation basalts
Ilímaussaq intrusion
(●)
(187Os/188Os)i = 0.8
1.2 Ga reference line
187Os/188Os
187Re/188Os
187Os/188Os
187Re/188Os

Fig. 15

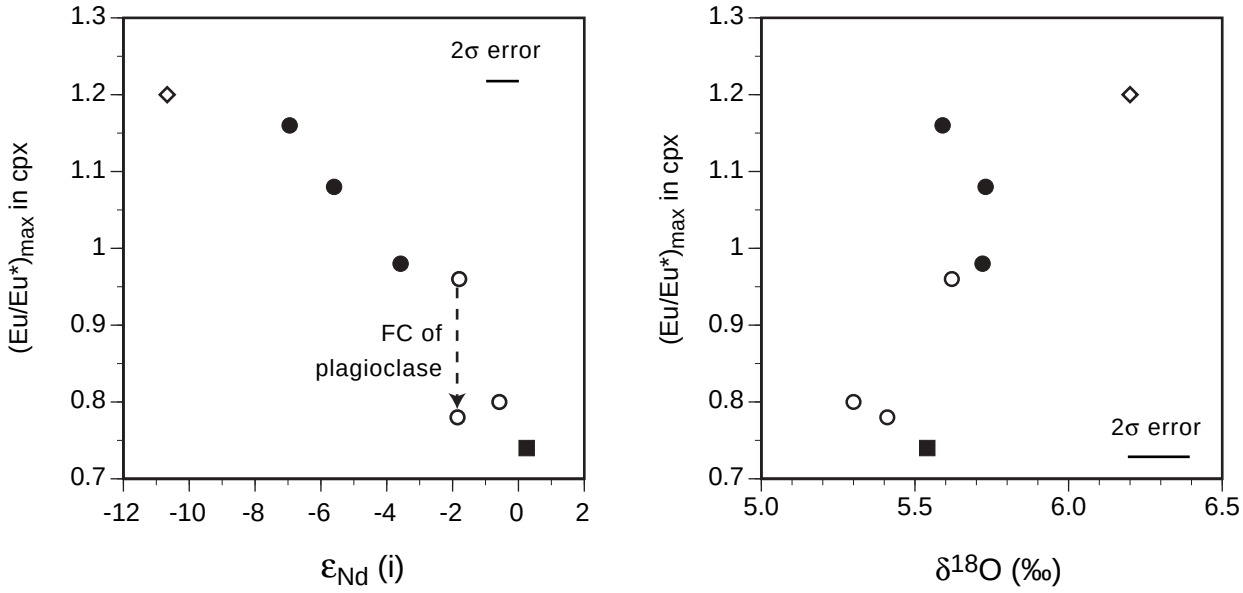
1.3
1.2
1.1
1
0.9
0.8
0.7
(Eu/Eu*)max in cpx
2σ error
FC of
plagioclase
-12
-10
-8
-6
-4
-2
0
2
εNd (i)
5.0
5.5
6.0
6.5
δ18O (‰)

Fig. 16

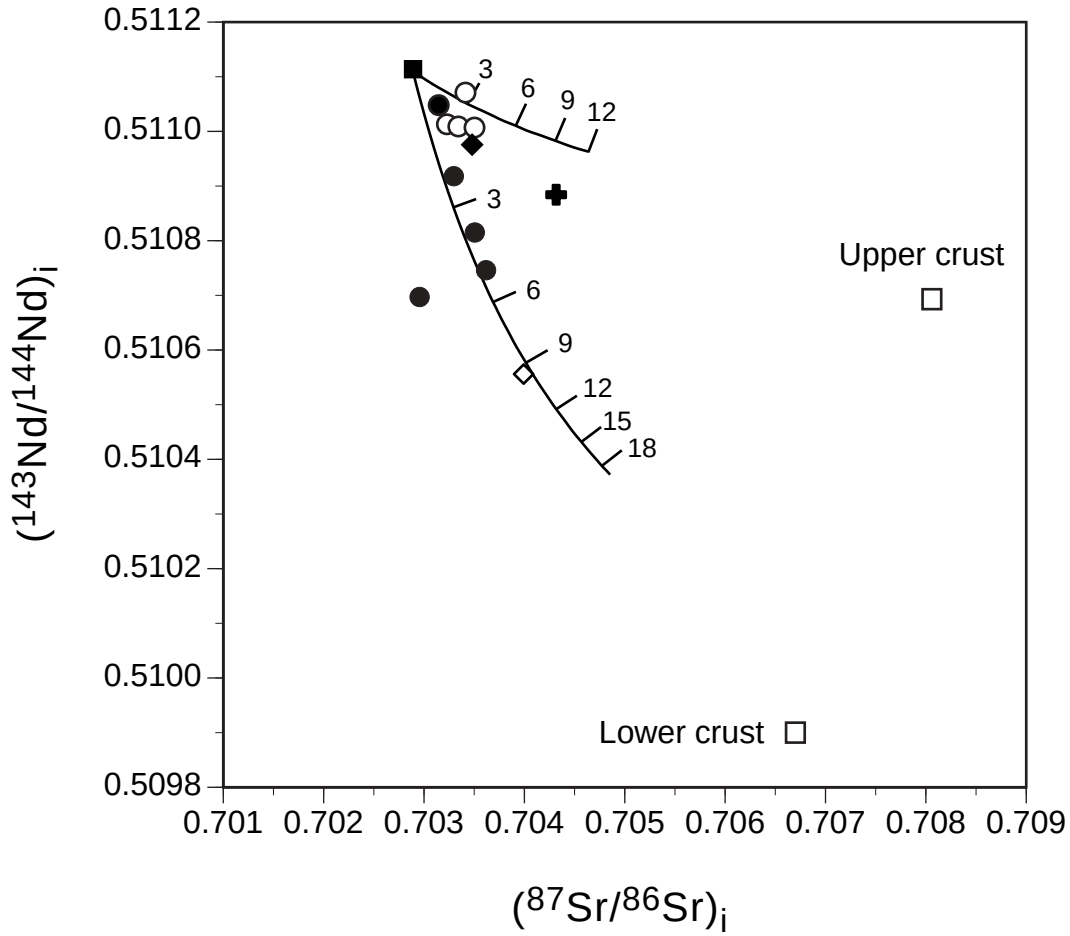
0.5112
0.5110
0.5108
0.5106
0.5104
0.5102
0.5100
0.5098
(143Nd/144Nd)i
3
6
9
12
3
6
9
12
15
18
Upper crust
Lower crust
0.701
0.702
0.703
0.704
0.705
0.706
0.707
0.708
0.709
(87Sr/86Sr)i

Kapitel 2: Petrologische und isotopengeochemische Untersuchungen an alkalinen bis peralkalinen Gesteinen der Puklen Intrusion

Manuskript-Titel:
QUANTIFICATION OF MAGMATIC AND HYDROTHERMAL PROCESSES IN A PERALKALINE SYENITE – ALKALI GRANITE COMPLEX BASED ON TEXTURES, PHASE EQUILIBRIA, STABLE AND RADIOGENIC ISOTOPES.

Autoren:
Michael Marks[1], Torsten Vennemann[2], Wolfgang Siebel[1], Gregor Markl[1]

[1] Institut für Geowissenschaften, Eberhard-Karls-Universität Tübingen, Wilhelmstrasse 56, 72074 Tübingen.

[2] Institut de Minéralogie et Géochimie, Université de Lausanne, BFSH-2, CH-1015 Lausanne, Schweiz.

erschienen in:
Journal of Petrology, 44/7, 1247-1280.

Gutachter:
Prof. D. Barker (Austin), Prof. C. Harris (Kapstadt), Prof I. Parsons (Edinburgh), Prof. R. Trumbull (Potsdam), Prof. M. Wilson (Leeds)

Eigenanteile:

a) Idee	70 %
b) Probenbeschaffung	30 %
c) Datenbeschaffung	100 %
d) Auswertung und Interpretation	90 %
e) Ausarbeitung der Publikation	90 %

ABSTRACT

The Puklen complex of the mid-Proterozoic Gardar province, South Greenland, consists of various silica-saturated to quartz-bearing syenites, which are intruded by a peralkaline granite. The primary mafic minerals in the syenites are augite ± olivine + Fe-Ti oxide + amphibole. Ternary feldspar thermometry and phase equilibria among mafic silicates yield T = 950-750°C, a_{SiO2} = 0.7-1 and an f_{O2} of 1 - 3 log units below the FMQ buffer at 1 kbar. In the granites, the primary mafic minerals are ilmenite and Li-bearing arfvedsonite which crystallized at temperatures >750°C and at f_{O2} values around the FMQ buffer. In both rock types, a secondary post-magmatic assemblage overprints the primary magmatic phases. In syenites, primary Ca-bearing minerals are replaced by Na-rich minerals such as aegirine-augite and albite, resulting in the release of Ca. Accordingly, secondary minerals include ferro-actinolite, $(calcite\text{-}siderite)_{ss}$, titanite and andradite in equilibrium with the Na-rich minerals. Phase equilibria indicate that formation of these minerals took place over a long temperature interval from near-magmatic temperatures down to about 300°C. In the course of this cooling, oxygen fugacity rose in most samples. For example, late-stage aegirine in granites formed at the expense of arfvedsonite at temperatures <300°C and at an oxygen fugacity above the HM buffer.

The calculated $\delta^{18}O_{melt}$ value for syenites (+5.9 to +6.3 ‰) implies a mantle origin, whereas the inferred $\delta^{18}O_{melt}$ value of <+5.1 ‰ for the granitic melts is significantly lower. Thus, granites require an additional low-$\delta^{18}O$ contaminant, which was not involved in the genesis of the syenites. Rb/Sr data for minerals of both rock types indicate open system behavior for Rb and Sr during post-magmatic metasomatism. Neodymium isotope compositions (εNd_{1170Ma} = -3.8 to -6.4) of primary minerals in syenites are highly variable, and suggest that assimilation of crustal rocks occurred to variable extents. Homogeneous ε_{Nd} values of -5.9 and -6.0 of magmatic amphibole of granites lie within the range of the syenites. Because of the very similar neodymium isotopic compositions of magmatic and late- to post-magmatic minerals from the same syenite samples a principally closed-system behavior during cooling is implied. In contrast, for the granites an externally derived fluid phase is required to explain the extremely low ε_{Nd} values of about -10 and low $\delta^{18}O$ between +2.0 and +0.5 ‰ for late-stage aegirine indicating an open system in the late-stage history. In this study we show that the combination of phase equilibria with stable and radiogenic isotopes on mineral separates can provide much more constraints on magma evolution during emplacement and crystallization than conventional whole rock studies.

Key words: peralkaline, phase equilibria, assimilation, hydrothermal, Li-amphiboles

INTRODUCTION

Felsic alkaline igneous rocks can be divided into two principal groups: i) quartz- and feldspar-bearing, silica-oversaturated rocks and ii) feldspar- and feldspathoid-bearing, silica-undersaturated rocks. The genesis and origin of these two groups is believed to be different: Silica-undersaturated, alkaline, intrusive complexes commonly have isotopic compositions that reflect a magma source in the mantle (e.g., Perry et al., 1987; Kramm & Kogarko, 1994; Dunworth & Bell, 2001). In many cases, contamination or assimilation processes seem to be of minor importance and, consequently, undersaturated alkaline rocks are often interpreted as differentiated residues of benmoreitic or nephelinitic magmas formed in the upper mantle (Larsen & Sørensen, 1987; Kramm & Kogarko, 1994; Stevenson et al., 1997; Frisch & Abdel-Rahman, 1999) under relatively dry conditions and low oxygen fugacities (Harris, 1983; Caroff et al., 1993).

In contrast, based on the close spatial association of silica-undersaturated and silica-oversaturated rocks in many alkaline igneous provinces worldwide, the origin of silica-oversaturated alkaline to peralkaline rocks is often explained by crustal contamination of mantle-derived undersaturated magmas (e.g., Davies & Macdonald, 1987; Foland et al., 1993; Harris, 1995; Mingram et al., 2000; Schmitt et al., 2000; Späth et al., 2001). Studies on alkaline rocks of the midcontinental rift system in North America demonstrated that not only upper crust, but also granulite facies rocks of the lower crust might interact with alkaline melts (Heaman & Machado, 1992).

Various experimental studies (e.g. Piotrowski & Edgar, 1970; Sood & Edgar, 1970; Edgar & Parker, 1974; Kogarko & Romanchev, 1977; 1982; Scaillet & Macdonald, 2001) showed that silica-understaurated and oversaturated peralkaline melts have a crystallization interval down to temperatures of about 400°C and the exsolution of a fluid phase from a residual melt is believed to take place in the very late stages of magmatic evolution. There is general consensus that volatiles play a major role in the evolution of alkaline to peralkaline magmas, for both their chemical and physical evolution. Effects of late-stage fluids in some alkaline to peralkaline intrusions of the Gardar Province have been described by Parsons et al. (1991), Finch et al. (1995), Coulson (1997), Markl (2001), Markl et al. (2001) and Markl & Baumgartner (2002). The late-stage fluids expelled from alkaline to peralkaline intrusions are highly enriched in alkalis and incompatible elements. This may result in the formation of aureoles of fenite around alkaline intrusions by interaction with the surrounding country rocks

(e.g. Rock, 1976; Kunzendorf et al., 1982; Kresten, 1988; Morogan, 1989) or the autometasomatic formation of secondary mineral assemblages at the expense of primary magmatic minerals within the solididied part of the intrusion itself (e.g. Salvi & Williams-Jones, 1990; Boily & Williams-Jones, 1995; Chakhmouradian & Mitchell, 2002). Recent studies indicate that the sources and isotopic compositions of such a fluid phase may be highly variable (e.g., Boily & Williams-Jones, 1994; Bea et al., 2001) and different isotope systems show a variable behavior with regard to late- or post-magmatic alteration. The resulting isotopic disequilibria between different minerals within a single rock sample may be used to distinguish between primary magmatic and secondary late- to post-magmatic processes.

The Puklen complex of the Gardar Province, South Greenland, is an example of a silica-oversaturated alkaline to peralkaline intrusion comprising a heterogeneous suite of mostly quartz-bearing syenites to quartz-rich peralkaline granite. Petrographically, all rock types show a primary magmatic and a secondary late- to post-magmatic mineral assemblage. The present study is focused on the phase equilibrium constraints on crystallization parameters, on whole-rock geochemistry and on stable and radiogenic isotope compositions of mineral separates, which are used to constrain the magma sources and to decipher the magmatic and late- to post-magmatic processes in the Puklen complex. We show that whole-rock isotope data for these peralkaline rocks would be difficult to interpret and inadequate for derivation of genetic models.

REGIONAL GEOLOGY

The Gardar Igneous Province (Fig. 1a) in South Greenland represents a failed rift structure of Mid-Proterozoic (1.1 – 1.3 Ga) age (Upton and Emeleus, 1987). Early Proterozoic (1.7 – 1.8 Ga) basement granites and gneisses (Emeleus and Upton, 1976) are in places overlain by a sequence of early Gardar basalts and sandstones (Eriksfjord Formation; Poulsen, 1964). A large number of Gardar dike rocks and about twelve major alkaline to peralkaline igneous complexes intrude the Ketilidian basement. Fluid inclusion data (Poulsen, 1964; Konnerup-Madsen & Rose Hansen, 1984) and the preserved contacts between sediments and lavas of the Eriksfjord Formation and intrusions indicate that at least the Ilímaussaq intrusion, but most likely the others as well were intruded at a high crustal level of 3 - 5 km. The plutonic complexes are comprised of (in order of decreasing abundance) syenites, nepheline syenites,

alkali granites, gabbros, syenogabbros and carbonatites. With one exception (the granitic to agpaitic Ilímaussaq intrusion), the major plutonic complexes follow either a SiO_2-undersaturated trend from just saturated syenites to foyaites and peralkaline or agpaitic nepheline syenites, or an oversaturated trend from augite syenites to peralkaline granites. The Puklen complex belongs to the second group.

The Puklen complex (Fig. 1b) is a relatively small body (4 x 2 km), which intrudes Ketilidian basement granite and early Gardar dolerite dikes. It is cut by northwest trending basic post-Gardar dike rocks (Pulvertaft, 1961). Hence, the Puklen complex is of late Gardar age (Pulvertaft, 1961). Zircons from a pegmatite in the nearby Nunarssuit complex have been dated at 1171 ± 5 Ma (Finch et al., 2001). Fig. 1b shows a generalized geological map of the complex. The field geology was described by Parsons (1972). The first magma pulse formed a suite of coarse-grained, fine-grained and porphyritic varieties of silica-saturated to oversaturated augite syenites. Contacts between the different syenite types are in most cases gradual. Hence, the intrusion of the various syenites probably took place more or less contemporaneously. In the southern part of the intrusion, a fine-grained and leucocratic granophyre cuts the adjoining syenite. A second pulse of magma produced a homogeneous, coarse-grained peralkaline granite, which grades into or may be locally intruded by fine grained and leucocratic microgranite.

SAMPLES AND ANALYTICAL METHODS

Six syenites, two granophyres, three coarse alkali granites, and two microgranites were analyzed for mineral chemical composition, whole rock chemical compositions and $\delta^{18}O$ values, and mineral separates of clinopyroxene and amphibole from selected samples were analyzed for O, Sr and Nd isotope compositions. The samples were selected to cover the range of textural varieties of the different rock types in a representative way. The sample localities are shown on Figure 1b. Additionally, two samples of hydrothermal quartz were analyzed for their $\delta^{18}O$ values: sample Q-M is from a cm-thick quartz vein and sample Q-D from a cavity containing cm-sized euhedral quartz crystals. Both samples were collected from the same locality as sample GM1635.

Minerals were analyzed using a JEOL 8900 electron microprobe at the Institut für Geowissenschaften at the Universität Tübingen, Germany. For calibration both natural and

synthetic standards were used. The beam current was 15 nA and the acceleration voltage was 15 kV. The counting time on the peak was 16 s for major elements, and 30-60 s for minor elements (Mn, Ti, Zr, F, Cl). Background counting times were half of the peak counting times. The peak overlap between the Fe Lβ and F Kα lines was corrected for. To avoid Na migration under the electron beam, feldspar was analyzed using a defocused beam of 15µm diameter. Data reduction was performed using the internal ϕρZ procedures of JEOL (Armstrong, 1991).

Bulk compositions of coarsely exsolved feldspars and titanomagnetites were recalculated by combining image processing (NIH Image software) of BSE-images of the exsolved minerals with point analyses of the exsolved phases (see Marks & Markl, 2001, for a more detailed description of the technique). Bulk compositions for each mineral and sample were calculated from 3 to 5 different grains.

Trace element contents were measured by in-situ laser ablation inductively coupled plasma-mass spectrometry (LA-ICP-MS) at the EU Large Scale Geochemical Facility (University of Bristol) using a method similar to that described by Halama et al. (2002). The precision of trace element concentrations, based on repeated analyses of standards, was approximately ±5 %. The detection limit for Li was typically 150-250 ppm, for Rb and Sr 0.1 - 1 ppm, and for REE < 0.1 ppm.

Whole rock analyses were performed by standard X-ray fluorescence (XRF) techniques at the Institut für Mineralogie, Petrologie und Geochemie at the Universität Freiburg, Germany, using a Philips PW 2404 spectrometer. Pressed powder and Li-borate fused glass discs were prepared to measure contents of trace and major elements, respectively. The raw data were processed with the standard XR-55 software of Philips. Relative standard deviations are < 1 % and < 4% for major and trace elements, respectively. Detection limits vary between 1 and 10 ppm, depending on the specific trace element.

Oxygen isotope compositions of powdered whole rock samples were determined by a conventional method modified after Clayton & Mayeda (1963) and Vennemann & Smith (1990), using BrF_5 as reagent and converting the liberated oxygen to CO_2.

The oxygen isotope composition of hand-picked mineral separates was measured using a method similar to that described by Sharp (1990) and Rumble and Hoering (1994). Between 0.5 and 2 mg of sample were loaded onto a small Pt-sample holder and pumped down to a vacuum of about 10^{-6} mbar. After prefluorination of the sample chamber overnight, the samples were heated with a CO_2-laser in an atmosphere of 50 mbars of pure F_2. Excess F_2 was separated from O_2 by exchange with KCl held at 150°C. The extracted O_2 was collected on a molecular sieve (13X). Oxygen isotopic compositions were measured on O_2 using a Finnigan MAT 252 mass spectrometer. The results are given in the standard δ-notation, expressed relative to VSMOW in permil (‰). Replicate oxygen isotope analyses of the standards (12 loads of NBS-28 quartz and 10 loads of UWG-2 garnet; Valley et. al., 1995) had an average precision of ± 0.1‰ for $\delta^{18}O$ (± 2σ error of the mean). The accuracy of $\delta^{18}O$ values was better than 0.2‰ compared to accepted $\delta^{18}O$ values for NBS-28 of 9.64 ‰ and UWG-2 of 5.8 ‰.

For Sr and Nd isotope analyses, about 10 mg of hand-picked mineral separate were spiked with mixed ^{84}Sr -^{87}Rb and ^{150}Nd - ^{149}Sm tracers before dissolution under high pressure in HF at 180°C in poly-tetrafluor-ethylene (PTFE) reaction bombs. Rb and Sr were separated in quartz columns containing a 5 ml resin bed of AG50W-X12, 200 – 400 mesh, equilibrated with 2.5N HCl. Sm and Nd separation was performed in quartz columns using 1.7 ml Teflon powder coated with HDEHP (Di-Ethyl Hexyl Phosphate) as cation exchange medium, equilibrated with 0.18N HCl. All analyses were made with a Finigan MAT 262 thermal ionization mass spectrometer (TIMS) in static collection mode. Sr was loaded with a Ta-HF activator and measured on a single W filament. Rb, Sm, and Nd were measured with a double Re-filament configuration. The $^{87}Sr/^{86}Sr$ ratios were normalized to $^{86}Sr/^{88}Sr = 0.1194$, the $^{143}Nd/^{144}Nd$ ratios to $^{146}Nd/^{144}Nd = 0.7219$, and the Sm isotopic ratios to $^{147}Sm/^{152}Sm = 0.56081$. Repeated analyses of Ames metal (Geological Survey of Canada, Roddick et al., 1992) gave a $^{143}Nd/^{144}Nd$ ratio of 0.512142 ± 22 (± $2\sigma_m$, n = 10) and of the NBS 987 Sr standard yielded a $^{87}Sr/^{86}Sr$ ratio of 0.710264 ± 16 (± $2\sigma_m$, n = 8). Total procedural blanks (chemistry and loading) were < 200 pg for Sr and < 100 pg for Nd. A decay constant of 1.42 x 10^{-11} a^{-1} for ^{87}Rb (Steiger & Jäger, 1977) and of 6.54 x 10^{-12} a^{-1} for ^{147}Sm (Lugmair & Marti, 1978) were used. ε_{Nd} values were calculated using present day CHUR values of 0.1967 for $^{147}Sm/^{144}Nd$ (Jacobson & Wasserburg, 1980) and 0.512638 for $^{143}Nd/^{144}Nd$ (Goldstein et al., 1984). Initial Sr and Nd isotope ratios were calculated for an age of 1170 Ma, on the basis of U-Pb ages on zircons from the Nunarssuit intrusion, which is close to the Puklen complex and

consists of similar rock types (Finch et al., 2001). Calculated uncertainty in ε_{Nd} units based on analytical errors is not more than 0.5. The error based on age uncertainty is in the order of 0.5 to 1.0 εNd unit for ages, which are 100 Ma younger or older respectively, depending on the Sm/Nd ratio.

PETROGRAPHY

The following description of the different rock types is a brief summary. Detailed and comprehensive petrographic descriptions are given by Parsons (1972). The mineralogy of the investigated samples is summarized in Table 1. Abbreviations used in the text and figures are given in the appendix.

Syenite suite

Syenites are highly variable with respect to color, grain size, texture and modal mineralogy. Most varieties are equigranular; porphyritic types with subhedral feldspar phenocrysts are less common. The syenites are highly variable in quartz content, but nepheline-bearing syenites do not occur. In some places euhedral cm-sized quartz crystals in miarolitic cavities can be found. The dominant matrix feldspar is mesoperthite. In some large feldspar grains, unexsolved cores are still preserved. Some of the quartz-free samples contain interstitial albite. Primary mafic minerals are olivine, clinopyroxene (augite), Fe-Ti oxides, amphibole (amphibole I), apatite, and zircon. Olivine, which is now replaced by orange to red iddingsite, is restricted to quartz-free samples. Parsons (1972) noted the rarity of fresh olivine. Subhedral augitic clinopyroxene is gray to green and some grains are strongly zoned. The primary Fe-Ti oxide in most syenites is ilmenite. Some samples show a magmatic two-oxide assemblage of ilmenite and titanomagnetite, and in two samples, titanomagnetite is the only primary Fe-Ti oxide. Primary titanomagnetite is always oxy-exsolved to ilmenite and magnetite in both trellis and less frequently sandwich-type forms (terminology after Buddington & Lindsley, 1964). Dark brown to dark green amphibole (amphibole I) (Figs. 2a and 2b) occurs as interstitial crystals or as overgrowths on augite (Fig. 2b). Apatite is found as inclusions in alkali feldspar, augite and amphibole I. Zircon forms small subhedral crystals enclosed in alkali feldspar. In virtually all syenite samples, the primary magmatic phase assemblage is overprinted by a late-stage peralkaline phase assemblage. Augite may show green patches or rims of aegirine-rich pyroxene (Fig. 3). Amphibole I is overgrown by a later pale green

amphibole (amphibole II; Fig. 2a) and the primary feldspars developed fine-grained albite along grain boundaries (Fig. 2c).

Two samples without primary quartz (GM1615 and GM1616) bear aenigmatite. Within these samples, augite, ilmenite, and amphibole I form clusters in the feldspar matrix. Albite, secondary quartz II and Ca-Fe carbonates are common as interstitial mineral phases. Aenigmatite forms rims around ilmenite (Fig. 2d). Cracks within aenigmatite are filled with fine-grained titanite and Fe-hydroxides. Titanite also occurs along the contact between ilmenite and aenigmatite. Augite close to aenigmatite is converted to bright green aegirine-augite (Fig. 3).

In sample GM1635, a green rim of aegirine-augite has a distinct grain boundary against the primary augite core (Fig. 3b). The rim can be divided into an inner (aegirine-augite I) and outer part (aegirine-augite II). The inner part contains rounded relics of primary augite (white dashed line on Fig. 3b) and shows patchy irregularities in color. The boundary between inner and outer parts probably marks the former grain boundary of the primary augite (red dashed line on Fig. 3b). The aegirine-augite rim is overgrown by subhedral hydroandradite with oscillatory zoning patterns, which is associated with subhedral titanite and Ti-free magnetite. Primary ilmenite occurs as inclusions within augite or is overgrown by titanite. The matrix consists of recrystallized quartz and albite.

In sample GM1611, primary augite is entirely replaced by aegirine (Fig. 2e), calcite-siderite$_{ss}$, quartz and hematite pseudomorp after former augite. Coarse-grained albite and calcite-siderite$_{ss}$ are arranged around aegirine. Neither amphibole I nor amphibole II is present. The matrix feldspar is mesoperthite.

Granophyres

The rock is highly leucocratic and fine-grained. It consists mainly of euhedral perthitic alkali feldspars overgrown by graphic intergrowths of quartz and alkali feldspar (Fig. 2f). Mafic minerals are rare and comprise augite, ilmenite and amphibole I and II. Textures of the mafic minerals are similar to those in syenites. Interstitial zircon and especially fluorite are abundant accessory phases.

Alkali granites

Primary magmatic minerals in this rock are alkali feldspar, quartz, ilmenite and amphibole. Minor minerals and accessories are aegirine, astrophyllite, apatite, zircon, fluorite and titanite. Feldspar is mesoperthitic and graphic intergrowths of quartz and feldspar are common. Grain boundaries between quartz and alkali feldspar may be filled with granular masses of fine anhedral albite (Fig. 2c), in some cases associated with tiny needles of aegirine. Ilmenite occurs as inclusions in amphibole or aegirine. Amphibole is subhedral deep blue to dark gray arfvedsonite. Commonly it is overgrown and replaced by bottle-green aegirine (Fig. 2g). Aegirine also occurs interstitially, forming radially arranged aggregates that are partly associated with astrophyllite (Fig. 2h). Apatite is enclosed in feldspar and in amphibole. Zircon forms small subhedral grains that may be clustered into bigger groups. In some samples, titanite is an interstitial phase. Fluorite occurs as anhedral inclusions in aegirine. In some samples small veinlets of quartz cut the early magmatic minerals. This feature corresponds to field observations of some about 10 cm-thick quartz veins and lenses in or close to the granite.

Microgranites

This rock is leucocratic and fine-grained. Primary magmatic minerals are alkali feldspar, quartz, magnetite, and arfvedsonite. Aegirine occurs as radiating aggregates or overgrows deep blue amphibole. However, in the same samples, amphibole may overgrow aegirine, implying that the two mafic minerals crystallized alternatively or even may have coexisted in parts of the microgranites. In some of the microgranitic veins, zircon and astrophyllite are remarkably common. The latter forms fringes of small yellow needles around aegirine. Zircon occurs interstitially or as inclusions in quartz. In one of the microgranitic dikes (about 2 cm thick), compositional zoning is marked by the occurrence of amphibole and zircon in the inner parts of the dike, whereas the margins are rich in aegirine.

RESULTS

Mineral chemistry

Feldspar

Measured and recalculated bulk feldspar compositions of the different Puklen rocks are shown in Figs. 4a - c. Some typical analyses are reported in Table 2. Feldspar phenocrysts in syenites are partly chemically zoned and range in composition between $Ab_{74}An_{7}Or_{19}$ and $Ab_{53}An_{2}Or_{45}$. Feldspar phenocrysts in samples GM1615 and GM1616 are lower in An-component compared to the other syenite samples (Fig. 4a). In one sample (GM1580), early ternary feldspar is essentially unzoned, but shows a strong and steep enrichment of Ab-component with almost unchanged An-component at the rim (Fig. 4b). The most common matrix feldspar in syenites is almost Ca-free patchily exsolved alkali feldspar with bulk compositions between $Ab_{69}An_{0}Or_{31}$ and $Ab_{43}An_{0}$ Or_{57}. Late-stage albite in syenites has nearly end-member composition. The low Ca content clearly distinguish these fine-grained aggregates from the Ab-rich rims around phenocrysts in sample GM1580 (see above).

Feldspar compositions in granophyres range from $Ab_{57}An_{0}$ Or_{43} to $Ab_{44}An_{0}Or_{56}$ and are more Or-rich compared to the syenites.

In one sample (GM1605) of coarse alkali granite, the composition of the unexsolved core of an alkali feldspar was determined as $Ab_{69}An_{4}Or_{27}$ – $Ab_{65}An_{2}Or_{23}$ (Fig. 4c). Compositions of matrix feldspars in coarse granites are similar to those in syenites and range between $Ab_{63}An_{1}Or_{26}$ and $Ab_{49}An_{0}Or_{51}$. As in syenites, late-stage albite shows almost end-member composition.

Feldspar compositions in the microgranites ($Ab_{72}An_{1}Or_{27}$ – $Ab_{49}An_{0}Or_{51}$) extend the range towards more albite-rich compositions. As in granophyres, late-stage albite is lacking.

Olivine

The composition of olivine could not be determined by microprobe, as it is altered to red-orange iddingsite. Olivine in such rock types is expected to be fayalite-rich (e.g. Stephenson, 1974, Larsen, 1976, Powell, 1978, Upton et al., 1985, Marks & Markl, 2001).

Pyroxene

The primary pyroxene in syenites and granophyres is augite with >90 mol% quadrilateral (Di+Hed+En+Fs) components (Fig. 5, Table 3). The Na content of the primary augite varies

between 0.03 and 0.15 atoms per formula unit (a.p.f.u.) but exceeds in some analyses Fe^{3+}, which was calculated based on stoichiometry (4 cations, 6 oxygens). This indicates the presence of small amounts of the jadeite molecule (up to 6 mol%) in addition to the aegirine component. Some augites show chemical zonation (Fig. 5b). X_{Fe} and Mn increase from core to rim, continuously in some crystals, but stepwise in others. The Wo-component is more or less constant, Na shows a continuous and smooth enrichment, and Ti decreases. In cracks or rims in augite, the aegirine component rises up to about 40 mol% (Figs. 5a). In such areas, augite is enriched in Na, whereas Ca, Mg and Ti are depleted.

In the texture of Fig. 3b, the inner aegirine-augite I shows patchy irregularities in chemical composition. Similar to the other samples, it is enriched in Na and depleted in Ca, Mg, and Ti. The outer aegirine-augite II shows oscillatory zoning with respect to Na and other elements and is enriched in Al compared to the primary augite (not shown).
In syenite sample GM1611 (Fig. 2e), the chemical composition of the aegirine varies between $Aeg_{72}Di_{3}Hed_{25}$ and $Aeg_{95}Di_{0}Hed_{5}$ and lies within the range observed in the granites (see below).

Pyroxene in coarse granites and microgranites is aegirine with compositions between $Aeg_{76}Di_{4}Hed_{20}$ and $Aeg_{92}Di_{0}Hed_{8}$ (Fig. 5a, Table 3). Aegirine is essentially unzoned and there is no significant compositional difference between aegirine in the coarse granites and in microgranites. Al is the most important minor element; the jadeite component makes up as much as 6 mol%.

Fe-Ti oxides

Table 4 reports some typical analyses of ilmenite and titanomagnetite of the different rock types. The composition of primary ilmenite in syenites varies between $Ilm_{80}Hem_{6}Pyr_{14}$ and $Ilm_{95}Hem_{1}Pyr_{4}$. Recalculated compositions of primary Ti-magnetite grains in syenites range between $Usp_{72}Mag_{28}$ and $Usp_{97}Mag_{3}$. Such Ti-rich compositions have already been reported from the augite syenite of the Ilímaussaq intrusion (Marks & Markl, 2001). Granophyric samples contain ilmenite with compositions between $Ilm_{84}Hem_{5}Pyr_{11}$ and $Ilm_{95}Hem_{2}Pyr_{3}$. Ilmenite in coarse granites is rich in MnO and varies between $Ilm_{91}Hem_{0}Pyr_{9}$ and $Ilm_{64}Hem_{6}Pyr_{30}$. The only primary Fe-Ti oxide observed in microgranites is magnetite with Usp-contents less than 5 mol%.

Secondary Fe-Ti oxides in late- to post-magmatic textures are essentially Ti-free magnetite in some syenite samples and end-member hematite in granites.

Amphibole

Amphibole I in syenites is ferro-richteritic to ferro-edenitic in composition (Table 5). X_{Fe} in the entire suite ranges from 0.72 to 0.99. Fluorine (up to 3.5 wt%) always dominates over chlorine (<0.5 wt%). Some grains show a pronounced chemical zonation. X_{Fe}, Si, Na and Cl increase from core to rim, whereas Al, Ca and F decrease (Fig. 6a). Amphibole I in fluorite-bearing granophyres is ferro-edenite and essentially fluorine-free. The chlorine content is in the same range as in the syenites.

Amphibole II is a ferro-actinolite. X_{Fe} varies in the same manner as in amphibole I (Table 5). Figure 6a shows a zonation profile starting in the core of an amphibole I crystal and extending into a rim of amphibole II. Compared to amphibole I, these late-stage amphiboles are lower in Na, K, Mn, and Ti, and they are also depleted in halogens. Cl is always < 0.1 wt %. and F is below microprobe detection limit.

Amphibole in coarse granites and microgranites is a member of the arfvedsonite - ferro-leakeite series (Table 5). X_{Fe} varies between 0.69 and 0.98. Lithium contents vary from less than 0.1 to 1.0 wt% Li_2O. Li is negatively correlated with Fe^{2+} and Al(VI), but positively with Fe^{3+} (Fig. 6b). The main incorporation mechanisms for Li in the Puklen arfvedsonites is $Li + Fe^{3+} <-> 2(Fe^{2+}, Mg, Mn)$ and $Li + Fe^{3+} <-> Al(VI) + Na$. Cl is always <0.05 wt% whereas F reaches up to 3.5 wt%. F is negatively correlated with X_{Fe}.

Aenigmatite

According to the scheme of Kunzmann (1999), the Puklen aenigmatites vary in composition between $Aen_{78}Wilk_{18}Rhö_4$ and $Aen_{93}Wilk_4Rhö_3$ (Aenigmatite-Wilkinsonite-Rhönite). The main inferred substitution mechanisms are $Fe^{2+} + Ti^{4+} <-> 2\ Fe^{3+}$ and $Ca^{2+} + Al^{3+} <-> Na^{+} + Si^{4+}$. With increasing distance from precursor ilmenite, Ca and Al contents decrease, whereas Na, Si and Mn increase.

Carbonates

Carbonates are essentially Mg-free calcite-siderite-rhodochrosite solid solutions. Tiny carbonate inclusions in replaced augite are calcite-rich and vary in composition between $Cc_{97}Sid_2Rhod_1$ and $Cc_{87}Sid_5Rhod_8$. Large interstitial carbonate coexisting with albite is more siderite-rich ($Cc_{72}Sid_{25}Rhod_7$ – $Cc_{64}Sid_{30}Rhod_6$)

Andradite

Hydroandradite shows oscillatory zoning (Fig. 3b) and varies in composition between $Andr_{67}Gr_{32}Sp_1Alm_0Py_0$ and $Andr_{91}Gr_6Sp_1Alm_2Py_0$.

Trace element data for metasomatized augite of sample GM1616

Figure 7 shows selected trace element data for an augite crystal of sample GM1616. On the basis of petrographic observations and mineral compositions it was suggested, that late-stage metasomatic fluids have affected augites of this sample. The unaffected core region (left side of Fig. 7b) has low Rb/Sr ratios between 0.1 and 0.4. In contrast, in the aegirine-rich metasomatized areas (right side of Fig. 7b), both Sr and Rb are enriched by about one and two orders of magnitude, respectively. Rb/Sr ratios increase with increasing Na (i.e. increasing metasomatism) to >1 in metasomatized parts of the crystal. Concentrations of Sm and Nd and Sm/Nd ratios are shown in Figure 7c for the same analysed points. Both elements are enriched in the metasomatized areas of the crystal, but less significantly than Rb and Sr. Enrichment factors compared to unaffected core regions are about 1.2 for Sm and 1.7 for Nd, resulting in lower Sm/Nd ratios in the metasomatized areas than in unaffected core regions.

Whole rock geochemistry

Major and trace element analyses of the different Puklen rocks are given in Table 6. Some analyses show fairly low totals, which may be attributed to the presence of H_2O^+, CO_2, and halogens, which were not measured. Most samples are peralkaline with an agpaitic index (molar $Na_2O + K_2O / Al_2O_3$) between 0.97 and 1.25. The samples have low contents of MgO and CaO, and high concentrations of iron and alkalis. A significant gap in SiO_2 content exists within the Puklen rock series, between syenites and the other rock types (see also Parsons (1972)).

Contents of Al_2O_3, CaO, FeO_t, TiO_2, MnO, and P_2O_5 decrease with increasing SiO_2 content from syenites to the other rock types (Fig. 8a). This may suggest fractional crystallization of plagioclase, olivine, augite, magnetite/ilmenite, and apatite. However, changes in element concentrations are not always systematic. For example, microgranites, which clearly postdate the coarse alkali granites, have higher contents of CaO and Al_2O_3 than coarse alkali granites.

In general, concentrations of compatible trace elements like Sc, V, Cr, Co, and Ni are low. Of the high field strength elements, Zr is strongly enriched in alkali granites. The concentrations of Zr and Zn correlate positively with the agpaitic index, whereas Sr and Ba concentrations correlate negatively with the agpaitic index (Fig. 8b), which may be attributed to extensive feldspar fractionation.

Oxygen isotope data

Whole-rock and mineral $\delta^{18}O$ values are given in Table 7 and plotted in Figure 9. The $\delta^{18}O$ values of syenites span a large range between +4.8 and +6.9 ‰. The two analyzed granophyres have +4.6 and +5.0 ‰, the three coarse alkali granites vary between +5.0 and +5.8 ‰ and the two microgranites have +4.9 and +5.5 ‰.

In syenites and granophyres, the $\delta^{18}O$ values of mineral separates of individual samples decrease in the order quartz - augite - amphibole I - amphibole II. $\delta^{18}O$ values of quartz (+7.9 to +8.1 ‰), amphibole I (+3.9 to +4.6 ‰) and amphibole II (+2.5 to +2.8 ‰) in syenites are rather homogeneous and significantly higher than in granophyres (+6.4 to 6.7 ‰, +2.5 to +2.7 ‰ and +1.0 to +1.7 ‰, respectively). An explanation for the homogeneous $\delta^{18}O$ values of quartz but the heterogeneous whole-rock $\delta^{18}O$ values will be given later. With the exception of syenite sample GM1616 (+4.7 ‰), augite from syenites is also homogeneous, varying between +5.3 and +5.5 ‰. Augite of the granophyric sample GM1593 (+5.4 ‰) has a $\delta^{18}O$ value in the range of those from syenites. Two separates of perthitic feldspar from syenites have low $\delta^{18}O$ values of +3.5 and +3.9 ‰.

In coarse alkali granites, the decreasing order of $\delta^{18}O$ values is quartz - amphibole - aegirine. The range in measured $\delta^{18}O$ values for all three minerals is large (quartz: +5.1 to

+7.3 ‰, amphibole: +2.2 to + 3.5 and aegirine: +0.5 to + 2.0 ‰) compared to those in syenites.

In microgranites, the $\delta^{18}O$ values of quartz (+6.7 and +7.2 ‰) and aegirine (+1.8 ‰) are in the same range as those in coarse alkali granites, but amphibole has slightly lower values (+1.7 and +1.9 ‰). Both quartz and amphibole have significantly lower $\delta^{18}O$ compared to the same minerals in syenites. The two samples of late-stage quartz veins have $\delta^{18}O$ values similar to quartz in granites (+7.0 and +7.2 ‰).

Nd isotope data

Thirteen mineral separates from eight samples were analyzed for their Sm and Nd concentrations and their Nd isotopic compositions (Table 8). The calculated ε_{Nd} values are all negative and highly variable. The minerals in the syenites cover a fairly large range between -3.8 and -6.4, whereas those in alkali granites show lower and more variable values between -5.9 and -9.6. Intermediate values of -6.5 for a microgranite amphibole and -7.2 for a granophyre augite were determined. Syenites and the two alkali granites show contrasting Nd isotope behavior. Although in a particular syenitic sample, augite and amphibole have approximately homogeneous ε_{Nd}, the variability of the minerals between samples is large. In the two alkali granite samples, the opposite is observed: amphibole and aegirine show almost identical values in the two samples.

Sr isotope data

Six mineral separates from two syenites and two coarse alkali granites were analyzed for Rb and Sr contents and Sr isotopic compositions (Table 8). Rb/Sr ratios of late-stage aegirine (samples GM1605 and GM1606) and metasomatized augite of sample GM1616 are higher compared to primary and unaffected minerals. Augite from sample GM 1590 yielded a highly radiogenic initial Sr value of 0.730, whereas augite from sample GM1616 has the lowest value of 0.590. Despite the higher Rb/Sr and $^{87}Rb/^{86}Sr$ ratios of GM1616, the present day $^{87}Sr/^{86}Sr$ value is low. Amphiboles from alkali granites have low initial Sr isotope ratios between 0.699 and 0.696. Late-stage aegirine has even lower values of 0.642 to 0.631. If ages younger than 1170 Ma are assumed, the calculated initial Sr ratios change only slightly. Only ages younger than about 900 Ma, which are not known from the Gardar Province (Upton & Emeleus, 1987) lead to geologically realistic initial Sr ratios of >0.700 – 0.703 for depleted

sources or >0.703 for isotopically enriched sources (bulk earth at 1170 Ma = 0.703). This indicates that the calculated low initial Sr ratios are not an effect of a wrong age assumption, but reflect disturbance of the Rb-Sr system.

CONDITIONS DURING THE MAGMATIC STAGE

Based on fluid inclusion studies (Konnerup-Madsen & Rose-Hansen, 1984; Markl et al., 2001) and on the reconstruction of the sedimentary and extrusive igneous overburden (Poulsen, 1964; Emeleus & Upton, 1976; Upton, 1962; Harry & Pulvertaft, 1963) the pressure of emplacement of the Ilímaussaq complex was estimated to be about 1 kbar. In the lack of better estimates, we use this value as an approximation for the Puklen complex as well.

Syenites and granophyres

Temperature and silica activity

The composition of early ternary feldspar phenocrysts in some syenite samples can be used to constrain near-liquidus conditions in the parental melt. The minimum crystallization temperature of the microperthites was determined by Parsons (1972) to be in excess of 715°C. Fig. 4 shows feldspar compositions plotted on the temperature-dependent feldspar solvus after Elkins & Grove (1990). Estimated minimum temperatures range from 750° to about 950°C. Equilibria between olivine, pyroxene and melt constrain silica activity of the olivine-bearing samples, which were originally quartz-free. Unfortunately, no primary olivine was preserved in the investigated samples. The QUILF program (Andersen et al., 1993) calculates equilibria involving olivine, augite, quartz, magnetite, and ilmenite and was used to estimate the composition of olivine in equilibrium with the measured augite at temperatures between 750° and 950°C. For detailed information on the theory and application of QUILF see Frost & Lindsley (1992), Lindsley & Frost (1992) and Marks & Markl (2001). Calculated olivine compositions range from $Fa_{67}Fo_{31}La_2$ to $Fa_{96}Fo_3La_1$. Because this range is similar to olivines from other augite syenites of the Gardar province (Stephenson, 1974; Larsen, 1976; Powell, 1978; Upton et al., 1985; Marks & Markl, 2001) we believe that these calculations are reliable and can be used to estimate silica activity for these samples.

Calculated silica activities are based on the reference state of pure quartz at P and T. Silica activity evolved systematically from about 0.70 in the syenite samples with the lowest X_{Fe} in augite to 0.98 in those which contain nearly end-member hedenbergite (Fig. 10). This systematic relationship between X_{Fe} in augite and calculated silica activity in the olivine-bearing syenites indicates that an originally quartz-undersaturated melt evolved by fractionation of olivine, augite and Fe-Ti oxide along a displaced FMQ buffer towards quartz-saturation. All other syenites and granites are quartz-bearing but lack olivine. The above-mentioned trend of the quartz-free samples (Fig. 10) is not applicable to the quartz-bearing ones. In contrast to what one would expect in a closed-system, the quartz-bearing syenites do not contain the Fe-Mg silicates with the highest X_{Fe}, but quartz-bearing syenites show the same range of X_{Fe} in augite as quartz-free samples.

Oxygen fugacity

Oxygen fugacity (f_{O2}) was calculated from equilibria among Fe-Ti oxides and Fe-Mg silicate minerals (olivine, augite) with the QUILF program (Andersen et al., 1993). For each sample, calculations were performed for the whole compositional range observed and consequently, they yielded a range of f_{O2} values. Estimated f_{O2} is always below the synthetic FMQ buffer and varies between 0.8 and 2.3 log units below the FMQ buffer. These and even more reduced conditions seem to be typical for the Gardar syenites (Powell, 1978; Marks & Markl, 2001). Oxygen fugacity in granophyres was estimated to be around or slightly above FMQ at temperatures between 650° and 750°C.

Granites

Temperature

In coarse granites, the rarely preserved homogeneous cores of alkali feldspar indicate minimum temperatures of 750°C (Fig. 4c). The upper stability limit for F-free arfvedsonite is about 700°C (Bailey, 1969). F-rich arfvedsonite is an early liquidus phase in the Puklen granites and F is expected to raise the thermal stability of arfvedsonite significantly because experimental data for richteritic compositions (Gilbert and Briggs, 1974) show a difference in the F- and OH-stabilities of about 300°C in the low-pressure range. Thus, the crystallization of the magmatic assemblage of granites occurred at temperatures ≥750°C.

Oxygen fugacity

The only constraint on oxygen fugacity for the magmatic stage of the coarse granites is the occurrence of arfvedsonite. End-member arfvedsonite is only stable at conditions below the synthetic FMQ buffer (Bailey, 1969).

LATE-STAGE PROCESSES IN SYENITES

Formation of aegirine-augite and aenigmatite in syenites

Crystallization of anhydrous minerals like alkali feldspar, olivine, augite, and Fe-Ti-oxides under relatively reduced conditions (see above) led to the enrichment of Na, Fe, Si, halogens and H_2O in the residual melt. Due to increasing H_2O activity, amphibole I began to crystallize as a late magmatic phase. Enrichment of Na and depletion of Al during fractionation is also indicated by the rise of (Na+K)/Al ratio from core to the rim in augite and amphibole (Figs. 6a & 11). Upon reaching fluid saturation, fluid phase (a presumably H_2O-CO_2) must have been exsolved, which is suggested by the formation of carbonate minerals. Based on petrographical observations that late- to post-magmatic reactions mainly took place along cracks or grain boundaries and carbonates precipitated at the same time, we conclude that this fluid phase was responsible for these reactions. Because one of the most important replacement textures in our samples is the growth of aegirine at the expense of augite (Fig. 3), we assume this fluid phase was very probably Na-dominated. The replacement reaction can be described as follows:

$$4\ CaFeSi_2O_6 + 4\ Na^+ + O_2 + 2\ H_2O \rightarrow 4\ NaFeSi_2O_6 + 4\ Ca^{2+} + 4\ OH^- \quad (1)$$

The Ca released led to the formation of ferro-actinolite (amphibole II), other secondary Ca-silicates and, in some places, interstitial calcite-siderite$_{ss}$. For example, the texture in Fig. 2e (sample GM1611) may be modeled by the schematic reaction:

$$4\ CaFeSi_2O_6 + 2\ Na^+ + 2\ OH^- + O_2 + 4\ CO_2 \rightarrow$$
$$2\ NaFeSi_2O_6 + 4\ CaCO_3 + 4\ SiO_2 + Fe_2O_3 + H_2O \quad (2)$$

During these replacement reactions, fluid composition changed. This can be inferred in sample GM1635, where the oscillatory zoning patterns in aegirine-augite II (Fig. 3b) suggest

discontinuous changes of fluid composition. This might be caused by the complex interplay of dissolution of augite and precipitation of aegirine-augite and the several Ca-phases involved.

The formation of aenigmatite at the expense of ilmenite was observed in the two samples (GM1615 and GM1616) showing most extensive growth of Na-pyroxene (Fig. 2d and 5a). The following schematic reaction describes this process:

$$4\ FeTiO_3 + 20\ CaFeSi_2O_6 + 12\ Na^+ + 12\ OH^- + O_2 + 20\ CO_2 \rightarrow$$
$$4\ Na_2Fe_5TiSi_6O_{20} + 4\ NaFeSi_2O_6 + 20\ CaCO_3 + 8\ SiO_2 + 6\ H_2O \qquad (3)$$

The formation of aegirine-augite and/or aenigmatite indicates an increased oxidation state of the late-magmatic fluid compared to the early magmatic stage and high amounts of Na dissolved in the fluid. An inverse relationship between aenigmatite and Fe-Ti oxides is often observed (e.g. Marsh, 1975; Larsen, 1977; Grapes et al., 1979; Ike, 1985; Birkett et al., 1996) and led Nicholls & Carmichael (1969) to postulate the existence of a so-called “non-oxide” field for quartz-saturated systems in T - f_{O2} space where aenigmatite and aegirine coexist in the absence of Fe-Ti oxides. This non-oxide field is shown on Fig. 12 (gray field) and is bounded by the labeled reactions (a) to (c). Note that reaction curves in Fig. 17 are for constant unit activities of aegirine, magnetite, ilmenite, aenigmatite, and sodium-disilicate. Following Nicholls & Carmichael (1969), point A in Fig. 17 represents the intersection of reactions (a) – (c) for an aegirine activity of 0.5, and the dashed line indicates the intersection of reactions (a) and (b) depending on the activity of sodium-disilicate. Incorporation of Fe^{3+} into aenigmatite shifts reaction (a) to more oxidized conditions and thus expands the non-oxide field to the vicinity of the HM buffer curve. In summary, the formation of aenigmatite and stabilization of aegirine-augite in some of the Puklen syenites indicates an increase of oxygen fugacity as a consequence of cooling (curved arrow on fig. 12).

Formation of late stage Ca-minerals in syenites

Replacement of early magmatic Ca-bearing minerals in syenites by late-stage Na-rich minerals led to the release of Ca into the fluid phase and subsequently to the formation of the secondary Ca-bearing minerals ferro-actinolite, $(calcite\text{-}siderite)_{ss}$, andradite and titanite. In some samples Ti-free magnetite and quartz are associated with these minerals. Three different associations can be distinguished:

$(calcite\text{-}siderite)_{ss}$ + titanite + magnetite + quartz

titanite + hydroandradite + magnetite + quartz
ferro-actinolite

Temperature constraints

Carbonate-bearing samples GM1615 & GM1616. Large interstitial Fe-rich carbonates associated with aenigmatite in samples GM1615 and GM1616 were used for solvus thermometry after Goldsmith et al. (1962) and the re-evaluation of Anovitz & Essene (1987). The inferred minimum temperatures for these compositions are not well constrained and range between 650° and 750°C depending on the solvus used. However, these temperatures probably mark the beginning of fluid activity at relatively high temperatures.

Sample GM1611. Carbonates which were found as tiny inclusions in completely metasomatized augite in sample GM1611 indicate minimum temperatures as low as 360° - 320°C and are better constrained because the solvus curve for such Fe-poor compositions is reasonably well determined (Anovitz & Essene, 1987).

Carbonate-free samples. The upper stability limit of ferro-actinolite (at 1 kbar) has been experimentally determined by Hellner and Schürman (1996) to be about 550°- 600°C. This is the maximum temperature for the beginning of amphibole II formation during cooling.
The above-mentioned temperature constraints indicate that the formation of secondary Ca-minerals occurred within a wide temperature range starting at temperatures close to the magmatic stage of about 750°C and continuing down to temperatures of about 300°C.

Ca-mineral constraints on f_{O2} and a_{CO2}

Although the principle process of replacement of an early Ca-bearing assemblage by a late Na-bearing one appears to be the same in all samples, the secondary Ca-mineral assemblages are not. We assume that local variations in f_{O2}, a_{H2O} or a_{CO2} were responsible for this fact. In order to investigate this, we calculated an $f_{O2} – a_{CO2}$ diagram in the Ca-Fe-Si-O-H-C system involving hedenbergite, magnetite, andradite (as an approximation for hydro-andradite), ferro-actinolite, calcite, quartz, CO_2 and H_2O using the GEOCALC software of Berman et al. (1987) and Lieberman & Petrakakis (1990) and the database of Berman (1988). New thermodynamic data for ferro-actinolite (Ghiorso & Evans, 2002) were added to this database. A set of isothermal log f_{O2} – log a_{CO2} diagrams was calculated from 300° - 600°C. Magnetite

was regarded as a pure end-member in accordance with microprobe analyses. For the calculation of end-member component activities we used the solution models of Holland (1990) for hedenbergite and Cosca et al. (1986) for andradite. For calcite and ferro-actinolite, a “mixing on site” model was used. As an example, the topologic relations for reactions among these minerals are shown for 500°C on Fig. 13. Between 300° and 600°C the topologic relations between reactions are similar but the position of the invariant point [Fe-Act] shifts with falling temperature from $\log f_{O2}$(600°C) = –22 to $\log f_{O2}$(300°C) = –38 and from $\log a_{CO2}$ = -0.3 to –2.4 (black dots and dashed lines on Fig. 13). However, it is important to note that the position of the invariant point relative to the FMQ buffer is generally independent of temperature and lies at about ΔFMQ= +1 log unit at all temperatures. The f_{O2} - a_{CO2} diagram can be used to interpret the various Ca-mineral assemblages:

1. The occurrence of andradite in sample GM 1635 formed by oxidation of hedenbergite points to a fluid phase with $a_{CO2} < 0.25$ ($\log a_{CO2} < -0.6$) (gray area in Fig. 13) if a temperature of 500°C is assumed. Oxygen fugacity in this rock increased from magmatic values (ΔFMQ= -1 to -2) to above ΔFMQ= +1.
2. The two aenigmatite- and carbonate-bearing samples GM1615 and GM1616 indicate even higher f_{O2} and a_{CO2} values (stippled pattern in Fig. 13).
3. Ferro-actinolite-bearing (amphibole II) samples were less oxidized and had lower a_{CO2} (dotted pattern in Fig. 13) or - if oxygen fugacity was higher than in sample GM1635 - they coexisted with a fluid phase unusually rich in CO_2, which is considered unlikely.

Occurrence of titanite

In the two samples GM1615 and GM1616 titanite occurs along grain boundaries between ilmenite and aenigmatite (see reaction (3)) and as fine-grained fillings of small cracks within aenigmatite. These textures indicate that titanite formed at the expense of aenigmatite:

$$Ca^{2+} + Na_2Fe_5TiSi_6O_{20} + O_2 + 2\ OH^- \rightarrow$$
$$CaTiSiO_5 + 2\ NaFeSi_2O_6 + SiO_2 + Fe_3O_4 + H_2O \qquad (4)$$

This reaction separates a more oxidized titanite-aegirine-magnetite-quartz assemblage from a more reduced hedenbergite-aenigmatite assemblage.

In the andradite-bearing sample GM1635, titanite coexists with Ti-free magnetite and quartz (Fig. 3b) as overgrowth on ilmenite. This can be expressed by the classical reaction (Wones, 1989)

$$3\ CaFeSi_2O_6 + 3\ FeTiO_3 + O_2 + \rightarrow 3\ CaTiSiO_5 + 3\ SiO_2 + 2\ Fe_3O_4 \quad (5)$$

Thus, similar to the formation of aegirine-augite and aenigmatite, the occurrence of titanite together with magnetite and quartz implies an increase in oxygen fugacity above the FMQ buffer during sub-solidus cooling.

SIGNIFICANCE OF LI-AMPHIBOLES IN PERALKALINE GRANITES

Similar to Mn, Zn or Zr, Li can be an important component in igneous alkali amphiboles, especially in peralkaline granites (Hawthorne et al., 1993, 1994). Compared to other published analyses (e.g., Bailey et al., 1993; Hawthorne et al., 2001) Li contents in amphiboles of the Puklen granite (0.1 wt% - 1.0 wt% Li_2O) are relatively high, but variable. Comparison to the detailed studies of Hawthorne et al. (1993, 1994, 2001) shows that the dominant substitution mechanism for Li in the alkali amphiboles of the Puklen peralkaline granite is $^{M3}Fe^{2+} + Fe^{2+} <-> {}^{M3}Li + Fe^{3+}$ giving rise to the ideal end-member ferro-leakeite. The Puklen amphiboles contain up to 60 mol% of this component.

Strong and Taylor (1984) distinguished two different compositional trends in amphibole from silica-saturated peralkaline igneous rocks. A magmatic to subsolidus trend is characterized by a change in composition from barroisite to richterite to arfvedsonite. The most important substitution here is $^{[4]}AlCa <-> SiNa$. This substitution involves amphiboles with full A sites and this trend is proposed to occur under reducing conditions. Second, the so-called oxidation trend reaches riebeckite composition and takes place under the influence of oxidizing fluids. This also produces amphiboles with vacancies on the A site. The $Fe^{3+}/(Fe^{3+} + Fe^{2+})$ ratio of the two end-members of both trends are 0.20 and 0.40, respectively. As discussed by Hawthorne et al. (1993), the incorporation of Li by the mechanism mentioned above increases the $Fe^{3+}/(Fe^{3+} + Fe^{2+})$ ratio from 0.20 in Li-free arfvedsonite to 0.50 in ferro-leakeite, which is even more oxidized than the oxidation trend of Strong and Taylor (1984). The relatively high $Fe^{3+}/(Fe^{3+} + Fe^{2+})$ ratios and high Li contents found in the Puklen arfvedsonites imply an extension of the stability field for these amphiboles to higher

oxygen fugacities - even above the FMQ buffer - compared to Li-free arfvedsonite, suggesting that these amphiboles presumably crystallized above the FMQ buffer.

LATE-STAGE FORMATION OF AEGIRINE IN PERALKALINE GRANITES

The formation of aegirine in the Puklen peralkaline granites is a late-stage process and is a well-known phenomenon in peralkaline granites. Most commonly, primary arfvedsonite is replaced by granular aegirine (Fig. 2g), which shows many small inclusions of quartz, fluorite, and hematite. This can be described by the following reaction:

$$Na_3Fe_5Si_8O_{22}(OH)_2 + O_2 \rightarrow 3\ NaFeSi_2O_6 + Fe_2O_3 + 2\ SiO_2 + H_2O \quad (6)$$

Inclusions of fluorite in aegirine are attributed to the release of Ca and F during decomposition of Ca- and F-bearing arfvedsonite and represent an important distinction from the syenites. Some textures indicate the formation of aegirine at the expense of magmatic ilmenite:

$$4\ FeTiO_3 + 8\ SiO_2 + 4\ Na^+ + O_2 + 6\ H_2O \rightarrow 4\ NaFeSi_2O_6 + 4\ Ti^{4+} + 12\ OH^- \quad (7)$$

This reaction was proposed by Nielsen (1979) to represent an important f_{O2}-buffer in peralkaline rocks. In some samples, both reactions took place:

$$Na_3Fe_5Si_8O_{22}(OH)_2 + 4\ FeTiO_3 + 6\ SiO_2 + 4\ Na^+ + 2\ O_2 + 5\ H_2O \rightarrow 7\ NaFeSi_2O_6 + Fe_2O_3 + 4\ Ti^{4+} + 12\ OH^- \quad (8)$$

However, some needle-shaped, radially arranged aegirine seems to have precipitated without interaction with, or decomposition of, arfvedsonite or ilmenite. These aggregates may have formed directly from the fluid phase. In some places, they are associated with astrophyllite (Fig. 2h). Similar mineral associations with astrophyllite from other peralkaline granites have been reported by e.g. Marsh (1975), Abdel-Rahman (1992) and Schmitt et al. (2000).

T- f_{O2} constraints on aegirine formation

The stability of aegirine with water is restricted to conditions between the FMQ and HM buffer curve (Bailey, 1969). The occurrence of Ti-free hematite, and relatively Ti-poor aegirine indicates oxidized conditions at or above the HM-buffer. The decomposition of arfvedsonite into aegirine, quartz and hematite was reported in the Puklen rocks by Parsons (1972), and in other peralkaline granites by e.g. Boily & Williams-Jones (1994) and Schmitt et al. (2000). Reaction (6) represents an f_{O2}-buffer in peralkaline rocks and may be used to estimate the conditions of aegirine formation. Fig. 14 shows the T-f_{O2}- dependence of this reaction at 1 kbar using thermodynamic data for aegirine, hematite, quartz and water from Robie and Hemingway (1995). $\Delta_f H^0$ and S^0 for arfvedsonite were estimated using the methods of Chermak & Rimstidt (1989) and Robinson & Haas (1983). The molar volume from Hawthorne (1976) of arfvedsonite (28.17 J/bar) was used. Temperature-dependent fugacity coefficients for water are from Burnham et al. (1969). Activities for aegirine, hematite, quartz and water were assumed to be unity. The activity of arfvedsonite varied between 0.1 and 0.15 using a “mixing on site” model. Uncertainty of these calculations is mainly based on the estimation of $\Delta_f H^0$. It is believed to be in the range of 0.2 % (Chermak & Rimstidt, 1989). The gray field around the calculated curves on Fig. 14 marks the uncertainty if an error of ± 0.2 % for $\Delta_f H^0$(arf) is assumed. The intersection with the HM-buffer curve divides this curve into a metastable (high-temperature) and a stable (low-temperature) branch. Assuming a stable formation of aegirine, these intersections should reflect maximum crystallization temperatures of about 260° - 280°C. If the assumed uncertainty is taken into account, formation of aegirine took place at temperatures below 450°C.

Popp and Gilbert (1972) showed that the solubility of jadeite in aegirine at constant pressure increases with falling temperature if aegirine coexists with albite and quartz (which is the case for the Puklen aegirines). They investigated the stability of aegirine-jadeite solid solutions at low pressures for temperatures between 300° and 600°C. Assuming a pressure of 1 kbar, temperatures below about 350°C are indicated which is in good agreement with the calculations above.

Whereas Bonin (1986) proposed temperatures of 600° - 625°C for conversion of arfvedsonite into aegirine + quartz + hematite + H_2O, Boily & Williams-Jones (1994) could show, based on oxygen isotope data, that aegirine formed at significantly lower temperatures, in agreement with our estimate.

RETENTION AND ALTERATION OF PRIMARY ISOTOPE SYSTEMATICS

Oxygen isotope fractionation

In this section, we discuss whether the measured oxygen isotope compositions of minerals represent primary magmatic values or the effects of hydrothermal alteration or re-equilibration during slow cooling.

In syenites, oxygen isotope fractionations between different minerals within the same sample are: $\Delta_{qtz\text{-}aug}$ = +2.6 to +2.8 ‰; $\Delta_{qtz\text{-}am\ I}$ = +3.5 to +4.2 ‰; $\Delta_{qtz\text{-}am\ II}$ = +5.1 to +5.6 ‰. The fractionations between quartz and augite indicate equilibrium at magmatic temperatures of 750° to 700°C using the fractionation factors of Zheng (1993a, 1993b). This is in good agreement with the results obtained from feldspar thermometry. The only exception is sample GM1616, with a remarkably large $\Delta_{qtz\text{-}aug}$ of +3.3 ‰, which is due to the exceptionally low $\delta^{18}O$ value of augite from this sample (+4.7 ‰). This low value can be explained by the fact that augite in this sample is strongly affected by late-stage peralkaline fluids. From early magmatic augite to later amphibole I and amphibole II, fractionation increases giving rise to lower apparent equilibrium temperatures (640° to 570°C and 500° to 465°C, respectively).

In granophyres, the measured fractionations between quartz and amphibole I (+3.7 and +4.2 ‰) and quartz - amphibole II (+5.0 and +5.4 ‰) are almost identical to those of the syenites, but is very small for quartz – augite (+1.0 ‰) in sample GM1593. This low value and the resulting high calculated equilibrium temperature of >1300°C indicates non-equilibrium conditions for the two minerals in this sample. Since fractionations between quartz, amphibole I and amphibole II show similar values as in syenites, it can be concluded that augites of sample GM1593 are xenocrysts or that quartz and amphiboles equilibrated with a distinctly different fluid/melt at lower temperatures, while augite did not. Based on their major element and oxygen isotope composition, we assume that these augites are early crystals and were incorporated from the syenites.

In alkali granite and microgranites, quartz - amphibole fractionations vary between +3.6 and +5.3 ‰ yielding low apparent equilibrium temperatures of 640° to 480°C. It appears that quartz and amphibole are not in isotopic equilibrium at the magmatic temperatures of

about 700°C. Possibly, a late closure to oxygen diffusion of quartz caused by low cooling rates may have caused an increase in Δqtz-amph. Differences in $\delta^{18}O$ values between late-stage aegirine and quartz are high (+4.6 to +6.1 ‰) and indicate low apparent equilibrium temperatures of less than 250°C (Zheng, 1993a).

Different effects on the Rb-Sr and the Sm-Nd system during metasomatism

As mentioned above, the Rb-Sr isotope system has been disturbed and no longer reflects primary magmatic values. Disturbance of the Rb-Sr system is common because Rb and Sr are highly mobile in metasomatic fluids. This has been shown in many whole-rock studies (e.g. Stevenson et al., 1997; and Ashwal et al., 2002). The extremely low calculated initial $^{87}Sr/^{86}Sr$ values indicate either loss of radiogenic Sr and/or the addition of Rb. Trace element data for augite of sample GM1616 (Fig. 7) indicate that probably the latter was the case. Additionally, despite the high present-day $^{87}Rb/^{86}Sr$ ratio, a relatively low present-day $^{87}Sr/^{86}Sr$ ratio was measured for augite of sample GM1616. This indicates that the $^{87}Sr/^{86}Sr$ ratio of the infiltrating late-stage fluid must have been significantly lower than that of the primary magmatic fluid and metasomatism changed both the $^{87}Rb/^{86}Sr$ and $^{87}Sr/^{86}Sr$ ratios of the system.

In contrast to the Rb/Sr system, Sm is positively correlated with Nd and samples with high Sm/Nd and $^{147}Sm/^{144}Nd$ ratios consequently have high present-day $^{143}Nd/^{144}Nd$ ratios (Table 8). These observations suggest that the Sm-Nd system was not as strongly affected by metasomatism as the Rb-Sr system. As shown in Fig. 7c, the concentrations for both Sm and Nd in metasomatized augite increased by a factor of about 2 compared to unaffected core regions. This effect is relatively small compared to the Rb/Sr system, where the enrichment of Rb and Sr is between 10 and 100. Probably, the similar atomic sizes and resulting physico-chemical characteristics of Sm and Nd are responsible for the similar behavior of Sm and Nd during late-magmatic processes compared to the drastic differences between Rb and Sr. Therefore, we conclude that the Nd isotopic compositions can be used for geological interpretations.

Figure 15 summarizes the Nd isotopic data in a conventional isochron diagram. The most obvious feature is that the data do not define a single isochron but a trend line at best. The two separates of aegirine from alkali granites show the most pronounced deviation from the general trend. Omitting the aegirine data, a late Gardar age of 1111 ± 95 Ma is obtained.

This is in agreement with the assumption that the Puklen rocks intruded pene-contemporaneously with the Nunarssuit complex (Pulvertaft, 1961; Finch et al., 2001). The large uncertainty and high MSWD-value (Mean of squared weighted deviations) of the isochron could result from the relatively low variation in $^{147}Sm/^{144}Nd$ ratios, from analytical errors, from a post-magmatic modification of the Sm-Nd system as mentioned above (e.g. Andersen, 1984), or from heterogeneous initial isotopic compositions of the samples as discussed below. However, in three syenitic samples (GM1590, GM1600 and GM1616), two minerals were analyzed and in all three cases the calculated ε_{Nd} values of these separates agree well within error (Table 8). Two-point isochrons defined by these samples agree with the above-mentioned age within error (Fig. 15). This supports the petrological and oxygen isotopic results that suggest an essentially closed-system behaviour for each syenite sample after contamination and during cooling (see below).

MELT SOURCE AND CONTAMINATION

Mineral-melt fractionations allow the calculation of the magma oxygen isotopic compositions directly from measured values of minerals (Taylor & Sheppard, 1986). We used $\Delta_{quartz\text{-}melt}$ and $\Delta_{pyroxene\text{-}melt}$ of Taylor & Sheppard (1986), Harris (1995) and Kalamarides (1986) to calculate $\delta^{18}O_{melt}$ values for the Puklen syenites. For granophyres, only $\Delta_{quartz\text{-}melt}$ was used, since the augite of sample GM1593 is not believed to be in equilibrium with quartz because of unreasonably low $\Delta_{quartz\text{-}augite}$. For the coarse alkali granites and microgranites, only $\Delta_{quartz\text{-}melt}$ was used because aegirine is of hydrothermal origin.

The estimates of $\delta^{18}O_{melt}$ versus wt% SiO_2, showing broadly a negative correlation, are plotted in Figure 16. Syenites have $\delta^{18}O_{melt}$ values (+5.9 to +6.3 ‰) and granophyres are slightly lower (+5.4 and +5.7 ‰). Coarse alkali granites (+5.1 and +5.3 ‰) are significantly lower in $\delta^{18}O_{melt}$ than the syenites. If it is considered that $\delta^{18}O_{melt}$ estimates for granites are maxima since $\Delta_{qtz\text{-}amphibole}$ in the alkali granites (see above) indicates a late closure of quartz to oxygen diffusion, the measured $\delta^{18}O$ values for quartz in granites are likely to be higher than values calculated at the crystallization temperatures of quartz. It is well known that the closure temperature for quartz is - depending on grain size - about 500°C (e.g., Giletti & Yund, 1984; Jenkin et al., 1991). During closed-system cooling, the $\delta^{18}O$ value of quartz will

increase relative to other minerals. Therefore, $\delta^{18}O_{melt}$ values for granites are possibly even lower than calculated. Microgranites yielded the lowest $\delta^{18}O_{melt}$ values (+4.7 and +5.2 ‰).

The calculated $\delta^{18}O_{melt}$ value of +5.9 to +6.3 ‰ for syenites essentially supports a mantle derivation of the magma (Kyser, 1986). The analyzed mineral separates from syenites span a large range in ε_{Nd} values between –3.8 and –6.4 (Table 8). These differences probably indicate that different magma batches derived from the same source experienced variable amounts of crustal contamination with country rocks during emplacement. Consequently, sample GM1600 (ε_{Nd} = -6.4) may represent a strongly contaminated magma, whereas sample GM1616 possibly reflects the least contaminated magma with an ε_{Nd} value of –3.8 for primary augite. The high quartz content of sample GM1600 is therefore believed to be due to a high amount of contamination with silicic country rock of this sample and not due to the effects of fractional crystallization.

The differences in inferred $\delta^{18}O_{melt}$ values between syenites and the other Puklen rocks cannot be due to closed-system fractionation processes (Kalamarides, 1986; Baker et al., 2000). Moreover, the present data indicate at least two isotopically different sources and possibly a mixing between these two. The low $\delta^{18}O_{melt}$ values of coarse alkali granites and granophyres can only be explained if the magma was derived from a source rock with a low $\delta^{18}O$ value, or contamination with material of low $\delta^{18}O$ has occurred. Three whole rock $\delta^{18}O$ analyses for basement rocks of the Isortoq area (Fig. 1b) have a mean of +7.8 ± 0.5 ‰ (Halama, unpublished data). Consequently, the upper granitic crust of the Gardar province is not a significant contaminant for the Puklen granites. Other contaminants or sources with low $\delta^{18}O$ - for example lower crustal rocks (Valley, 1986) or sources which were already altered by meteoric fluids prior to melting (Harris & Ashwall, 2002) - are necessary to explain the oxygen isotopic differences between syenites and the other Puklen rocks.

EFFECTS OF LATE-STAGE PROCESSES ON OXYGEN ISOTOPE COMPOSITIONS

Late-stage minerals from the syenites (amphibole II) and alkali granites (aegirine) have much lower $\delta^{18}O$ values compared to the primary magmatic minerals. Petrologic criteria indicate that amphibole II in syenites formed at temperatures below about 550°C and aegirine at even

lower temperatures, possibly < 300°C (see above). Principally, two contrasting explanations for these low $\delta^{18}O$ values are possible: i) the late-stage minerals formed in the presence of a low-$\delta^{18}O$ fluid, or ii) the low values reflect increasing fractionation at lower temperatures between minerals open to oxygen exchange.

In order to evaluate these two possibilities, changes in the $\delta^{18}O$ values of minerals and coexisting fluid phase during cooling were modelled for both rock types. For the calculation of the closed-system evolution in syenites, the following assumptions were made:

1. Quartz, augite and amphibole I were in isotopic equilibrium at magmatic temperatures of 700° to 800°C. Using the fractionation factors of Bottinga & Javoy (1975) and Zheng (1993a), the calculated feldspar composition at the magmatic stage would have been between +6.5 and +7.5 ‰.
2. The calculated oxygen isotope composition of coexisting water (which is used as an approximation for the water-dominated fluid phase in amphibole II-bearing syenites) at these temperatures ranges from +6.3 to +7.5 ‰ based on fractionation factors of Zheng (1993a & b).
3. During cooling and amphibole II formation, oxygen exchange was possible only between amphibole II, feldspar and the coexisting fluid phase. Quartz, augite and amphibole I closed to oxygen diffusion at temperatures below 500°C (Giletti et al., 1978; Giletti & Yund, 1984; Farver & Giletti, 1985; Farver, 1989).
4. Fluid/rock ratios are small enough, so that the fluid does not represent an inexhaustible reservoir that would retain a constant oxygen isotopic composition, independent of temperature or minerals it is in equilibrium with.
5. As a simplification, the oxygen content of amphibole and feldspar is assumed to be equal. Feldspar modally dominates over amphibole. From thin sections, the modal ratio between feldspar and amphibole II was estimated to be about 95 : 5.

Given the above assumptions, the $\delta^{18}O$ value of the system open to exchange at any temperature is defined by:

$$\delta^{18}O_{system} = 0.95\ \delta^{18}O_{fsp} + 0.05\ \delta^{18}O_{am} \qquad (1)$$

Using temperature dependent fractionation factors of Bottinga & Javoy (1975), $\delta^{18}O_{fsp}$ is given by the following equation:

$$\delta^{18}O_{fsp}(\text{at a given temperature}) = e^{\left(\frac{1000 \ln \alpha \text{ fsp-am}}{1000}\right)}(\delta^{18}O_{am} + 1000) - 1000 \qquad (2)$$

Solving equations (1) and (2) simultaneously allows the calculation of $\delta^{18}O_{am}$ and $\delta^{18}O_{fsp}$. Figure 17 illustrates the results of these calculations. Calculated and measured $\delta^{18}O$ values for amphibole II are equal at temperatures of about 400°C. This fits well with the petrological results. Hence, the low $\delta^{18}O$ values measured for amphibole II in syenites can be explained by a closed system cooling model. Feldspar should have an oxygen isotope composition of +6.5 to +7.5 ‰ at a temperature of about 400°C, which is in agreement with a published $\delta^{18}O$ value of about +6.5 ‰ for fresh feldspar from the Puklen complex (Sheppard, 1986).

However, measured values of altered perthitic feldspar are much lower, between about +3 and +4 ‰, indicating a late hydrothermal alteration in the presence of low-$\delta^{18}O$ fluids. Since the dominant mineral in syenites is alkali feldspar, this mineral dominates the whole-rock oxygen isotopic composition. A rough estimate, assuming 15 vol% quartz (with constant values of about +8 ‰), about 15 % mafic minerals (average of about +5 ‰) and about 70 vol % feldspar indicates, that the inhomogeneous whole-rock $\delta^{18}O$ values measured for syenites (+4.8 to +6.9 ‰) must largely be due to variation of the oxygen isotope composition of the alkali feldspar. Calculated $\delta^{18}O$ values of the altered feldspar thus vary between about +2.8 and +5.0 ‰. This is in agreement with two measured values of altered feldspar (+3.5 and +3.9 ‰, Table 7). Whether the $\delta^{18}O$ value of a rock (mineral) increases or decreases during fluid-rock interaction is a function of temperature of alteration, the $\delta^{18}O$ value of the fluid, and of the fluid-rock ratio. At temperatures less than about 100 °C it is possible that the whole rock $\delta^{18}O$ value actually increases even if fluids with very low $\delta^{18}O$ values (-10‰ or lower) are involved, simply because the mineral-water O-isotope fractionation factors are very high at these temperatures. However, at higher temperatures this is not the case as mineral-water fractionation factors decrease with increasing temperatures. It is therefore suggested that the heterogeneity of whole-rock $\delta^{18}O$ values is mainly caused by alteration of feldspars by low-$\delta^{18}O$ fluids, probably dominated by meteoric water at temperatures in excess of 100°C. Such alteration has been described from a number of plutonic rocks (e.g., Criss & Taylor, 1986; Lutz et al., 1988).

Applying a similar closed system model as described above to the alkali granites for possible feldspar-aegirine exchange, the low $\delta^{18}O$ values of aegirine cannot be explained. If a

closed system is assumed, calculated $\delta^{18}O$ values of aegirine are much higher than the measured values. Thus, an influx of low $\delta^{18}O$ fluids is necessary to explain the isotopic compositions of late-stage aegirine in alkali granites (Fig. 17b). The measured aegirines are in oxygen isotopic equilibrium with late-stage quartz veins at temperatures of about 250°C, which is in good agreement with the petrological results for aegirine formation. The calculated fluid oxygen isotopic composition at these low temperatures is about -3 ‰, which is more than 7 ‰ lower than the late-stage, closed-system fluid modelled to be in equilibrium with syenites. This low-$\delta^{18}O$ fluid could be of meteoric origin. The inferred palaeolatitude for South Greenland during late-Gardar times is 30 – 60° N (Piper, 1992). By comparison to the present-day distribution of isotopic compositions of meteoric waters (e.g., Rozanski et al., 1993), it is likely that meteoric waters were even lower than our estimate of -3‰. The chemical and isotopic composition of this meteoric fluid may well have been buffered by interaction with the country rocks. During this process it may have also picked up significant quantities of Nd or at least changed its Nd-isotopic composition significantly, resulting in the remarkably low ε_{Nd}-values for aegirines. Additionally, this meteoric fluid may also be responsible for the inferred low-temperature alteration of alkali feldspar in syenites and alkali granites. While not strictly required, it is also possible that such a fluid has contributed to the decrease of the $\delta^{18}O$ values of amphibole II, a possibility that cannot be excluded on the basis of the present data.

SUMMARY AND CONCLUSIONS

In the alkaline to peralkaline rocks of the Puklen Complex two different phase assemblages can be distinguished: A primary magmatic and a secondary late- to postmagmatic assemblage. The primary magmatic assemblage in the syenites consists of alkfsp ± qtz + aug ± ol + Fe-Ti oxides and interstitial Na-Ca amphibole. Solvus thermometry of early ternary feldspar phenocrysts indicates minimum crystallization temperatures of about 950° - 750°C. Oxygen fugacity during this stage was low and ranged from 0.8 - 2.3 log units below the FMQ buffer. Mineral- and whole-rock geochemical data suggest that fractional crystallization of feldspar, olivine, augite, magnetite/ilmenite, and apatite of a silica-undersaturated parental magma led to an increase of silica activity from about 0.7 in quartz-free samples towards unity in quartz-bearing ones. The magmatic assemblage in the granites (alkfsp + qtz + amph I + ilm) crystallized at temperatures >750° and redox conditions around the FMQ buffer.

A number of processes including fractional crystallization, assimilation of country rocks, post-magmatic alteration and sub-solidus reequilibration played a significant role in the complex geochemical and isotopic evolution of the Puklen rocks. The O, Sr and Nd isotopic data presented here for the Puklen complex can be used to distinguish between magmatic and post-magmatic processes. This is particularly caused by the fact that the three isotope systems investigated here (O, Rb/Sr, Sm/Nd) are affected to variable degrees during late-stage metasomatism and alteration. Isotopic compositions of different minerals from the same sample indicate a multi-source genesis for the Puklen rocks. Whole-rock analyses in similar cases would be inadequate and lead to complex results and wrong geologic interpretations. Even mineral separates may be problematic if adequate conclusions on magma genesis and late-stage history are desired, since some of the processes mentioned above may overlap each other.

Oxygen isotope compositions indicate that the magmas parental to the syenitic melts of the Puklen complex are compatible with derivation from a mantle source. During ascent of syenites, variable degrees of contamination with upper crustal material occurred, which is shown by the large range of ε_{Nd} values in syenites. In contrast, the oxygen isotopic compositions of the primary minerals and estimated magma compositions are homogeneous (Figs. 9 and 16). This may be a consequence of mass balance considerations: since oxygen is a major constituent of silicate rocks, a large contrast in oxygen isotopic composition between primary melt and contaminant is needed to produce significant differences in oxygen isotopic composition. The similar oxygen isotopic composition and the quite different Nd isotope characteristics of the granitic upper crust of the Gardar province fits well with a model where Puklen syenites are explained by variable contamination of a mantle-derived melt by granitic upper crust.

Calculated $\delta^{18}O_{melt}$ values for alkali granites are significantly lower compared to those of the syenites (Figs. 9 & 18). These low $\delta^{18}O$ values are believed to be a source feature and not an effect of low-temperature oxygen diffusion. However, the ε_{Nd} values for two separates of magmatic amphibole from alkali granites fall well within the range of ε_{Nd} values from syenites. Based on Nd isotopic results, a common source for syenites and alkali granites may be accepted, but the low oxygen isotopic composition of granites compared to syenites

requires a different contaminant or source with low $\delta^{18}O$ composition, which was not involved in the genesis of syenites.

Late-stage fluids, which were retained by syenites, caused the replacement of the primary assemblage by secondary silicates: Augite was replaced by aegirine-augite, aenigmatite formed at the expense of ilmenite and, due to the release of Ca during this process, secondary autometasomatic minerals such as ferro-actinolite, carbonates, hydroandradite and titanite formed. The formation of these secondary Ca-minerals took place over a wide temperature range between about 700° and 300°C. During this cooling, oxygen fugacity rose in most samples to values around the FMQ buffer. It is remarkable that the latest minerals in the syenites are not of a typical peralkaline composition, but are Ca-rich like the primary assemblage. The restriction to the syenites and their absence in granites implies either a short transport capacity of the fluid phase for these elements or that late-stage autometasomatism in syenites and granites worked differently. Oxygen and neodymium isotope data of these secondary Ca-phases indicate that syenites generally experienced closed-system behavior during cooling only. A few syenitic samples (GM1611, GM1615 and GM1616) reflect f_{O2} conditions and temperatures similar to the granites. This may indicate that fluids from the granites influenced these samples, since they were collected close to the granite body.

The late-stage formation of aegirine at the expense of arfvedsonite in granites was shown to be a low-temperature process, which took place at conditions around the HM-buffer at temperatures possibly around 300°C. Thus, granites became more oxidized than syenites, which possibly implies a different fluid source for the granites. The large oxygen and neodymium isotopic differences between primary amphibole and late-stage aegirine in granites indicate that the source of the aegirine-forming fluids was isotopically different from the one that formed the primary amphiboles. A major influx of a second, meteoric fluid, with low oxygen and neodymium isotope composition, was probably responsible for this. The widespread alteration of feldspar in all rock types of the Puklen complex, which is reflected by the low ^{18}O isotopic composition of the whole rocks may correlate with this latest meteoric fluid circulation.

ACKNOWLEDGEMENTS

Laser ICP-MS measurements were carried out at the Large Scale Geochemical Facility supported by the European Community - Access to Research Infrastructure action of the

Improving Human Potential Programme, contract number HPRI-CT-1999-00008 awarded to Prof. B. J. Wood (University of Bristol) which is gratefully acknowledged. Bruce Paterson provided invaluable help during these measurements. M. Westphal is thanked for his help during microprobe measurements, Elmar Reitter for his careful help during Sr and Nd isotope measurements, Gaby Stoschek for her help with sample preparation for mass spectrometry and oxygen isotope analysis, and Jasmin Köhler for patient hand picking of mineral separates. Thomas Wenzel helped to improve an earlier version of this manuscript. Extremely thorough reviews and constructive comments by D. Baker, C. Harris, I. Parsons, R. Trumbull, and M. Wilson (editor) improved the quality of this work substantially. A. Lumsden is thanked for his helpful editorial work. Financial support for this work was provided by the Deutsche Forschungsgemeinschaft (grant Ma-2135/1-2).

REFERENCES

Abdel-Rahman, A. M. (1992). Mineral chemistry and paragenesis of astrophyllite from Egypt. *Mineralogical Magazine* **56**, 17-26.

Andersen, T. (1984). Secondary processes in carbonatites: petrology of "rodberg" (hematite-calcite-dolomite carbonatite) in the Fen central complex, Telemark (South Norway). *Lithos* **17**, 227-245.

Andersen, D. J., Lindsley, D. H. & Davidson, P. M. (1993). QUILF: a PASCAL program to assess equilibria among Fe-Mg-Mn-Ti oxides, pyroxenes, olivine, and quartz. *Computers and Geosciences* **19**, 1333-1350.

Anovitz, L. M. & Essene, E. J. (1987). Phase equilibria in the system $CaCO_3$-$MgCO_3$-$FeCO_3$. *Journal of Petrology* **28**, 389-414.

Armstrong, J. T. (1991). Quantitative elemental analysis of individual microparticles with electron beam instruments. *In: Heinrich, K.F.J. & Newbury, D.E. (eds.), Electron Probe Quantitation. New York & London: Plenum Press*. 261-315.

Ashwal, L. D., Demaiffe, D. & Torsvik, T.H. (2002). Petrogenesis of Neoproterozoic granitoids and related rocks from the Seychelles: the case for an Andean-type arc origin. *Journal of Petrology* **43**, 45-83.

Bailey, D. K. (1969). The stability of acmite in the presence of H_2O. *American Journal of Science* **267-A**, 1-16.

Bailey, J. C., Bohse, H., Gwodzdz, R. & Rose-Hansen, J. (1993). Li in minerals from the Ilímaussaq alkaline intrusion, South Greenland. *Bulletin of the Geological Society of Denmark* **40**, 288-299.

Baker, J. A., MacPherson, C. G., Menzies, M. A., Thirlwall, M. F., Al-Kadasi, M. & Mattey, D. P. (2000). Resolving crustal and mantle contributions to continental flood volcanism, Yemen; constraints from mineral oxygen isotope data. *Journal of Petrology* **41**, 1805-1820.

Bea, F., Arzamastsev, A., Montero, P. & Arzamastseva, L. (2001). Anomalous alkaline rocks of Soustov, Kola: evidence of mantle-derived metasomatic fluids affecting crustal materials. *Contributions to Mineralogy and Petrology* **140**, 554-566.

Berman, R. (1988). Internally consistant thermodynamic data for minerals in the system Na_2O-K_2O-CaO-MgO-FeO-Fe_2O_3 -Al_2O_3-SiO_2-TiO_2-H_2O-CO_2. *Journal of Petrology* **29**,

445-522.
Berman, R. G., Brown, T. H. & Perkins, E. H. (1987). Geo-Calc; software for calculation and display of P-T-X phase diagrams. *American Mineralogist* **72**, 861-862.
Birkett, T. C., Trzcienski, W. E. & Stirling, J. A. R. (1996). Occurrence and compositions of some Ti-bearing minerals in the Strange Lake Intrusive Complex, Quebec-Labrador Boundary. *Canadian Mineralogist* **34**, 779-801.
Boily, M. & Williams-Jones, A. E. (1994). The role of magmatic and hydrothermal processes in the chemical evolution of the Strange Lake plutonic complex, Quebec-Labrador. *Contributions to Mineralogy and Petrology* **118**, 33-47.
Bottinga, Y. & Javoy, M. (1975). Oxygen Isotope partitioning among the minerals in igneous and metamorphic rocks. *Reviews of Geophysics and Space Physics* **13**, 401-418.
Bonin, B. (1986). Ring complex granites and anorogenic magmatism. *New York: Elsevier.* pp. 188.
Brooks, C., Hart, S. R. & Wendt, I. (1972). Realistic use of two-error regression treatments as applied to rubidium-strontium data. *Reviews in Geophysics and Space Physics* **10**, 551-577.
Buddington, A. F. & Lindsley, D. H. (1964). Iron-titanium oxide minerals and synthetic equivalents. *Journal of Petrology* **5**, 310-357.
Burnham, C. W., Holloway, J. R. & Davis, N. F. (1969). Thermodynamic properties of water to 1000°C and 10000 bars. *Geological Society of America Special Paper* **132**.
Caroff, M., Maury, R. C., Leterrier, J., Joron, J. L., Cotten, J. & Guille, G. (1993). Trace element behavior in the alkali basalt-comenditic trachyte series from Mururoa atoll, French Polynesia. *Lithos* **30**, 1-22.
Chakhmouradian, A. R. & Mitchell, R. H. (2002). The mineralogy of Ba- and Zr-rich alkaline pegmatites from Gordon Butte, Crazy Mountains (Montana, USA): comparisons between potassic and sodic agpaitic pegmatites. *Contributions to Mineralogy and Petrology* **143**, 93-114.
Chermak, J. A. & Rimstidt, J. D. (1989). Estimating the thermodynamic properties (ΔG^0_f and ΔH^0_f) of silicate minerals at 298 K from the sum of polyhedral contributions. *American Mineralogist* **74**, 1023-1031.
Clayton, R. N. & Mayeda, T. K. (1963). The use of bromine pentafluoride in the extraction of oxygen from oxides and silicates for isotope analysis. *Geochimica et Cosmochimica Acta* **27**, 43-52.
Cosca, M. A., Moecher, D. P. & Essene, E. J. (1986). Activity-composition relations for the join grossular-andradite and application to calc-silicate assemblages. *Abstracts with Programs - Geological Society of America* **18**, 572.
Coulson, I. M. (1997). Post-magmatic alteration in eudialyte from the North Qoroq centre, South Greenland. *Mineralogical Magazine* **61**, 99-109.
Criss, R. E. & Taylor, H. P. Jr. (1986). Meteoric-hydrothermal systems. *In: Valley, J.W., Taylor, H.P.Jr and O´Neil, J.R. (eds.): Stable Isotopes. Reviews in Mineralogy. Washington: Mineralogical Society of America.* **16**, 373-422.
Davies, G. R. & Macdonald, R. (1987). Crustal influences in the petrogenesis of the Naivasha basalt-comendite complex: combined trace element and Sr-Nd-Pb isotope constraints. *Journal of Petrology* **28**, 1009-1031.
Dunworth, E. A. & Bell, K. (2001). The Turiy massif, Kola peninsula, Russia: Isotopic and geochemical evidence for multi-source evolution. *Journal of Petrology* **42**, 377-405.
Edgar, A. D. & Parker, L. M. (1974). Comparison of melting relationships of some plutonic and volcanic peralkaline undersaturated rocks. *Lithos* **7**, 263-273.
Elkins, L. T. & Grove, T. L. (1990). Ternary feldspar experiments and thermodynamic models. *American Mineralogist* **75**, 544-559.
Emeleus, C. H. & Upton, B. G. J. (1976). The Gardar period in southern Greenland. *In:*

Escher, A. & Watt, W.S. (eds.), Geology of Greenland. Copenhagen: Geological Survey of Greenland. 152-181.
Escher, A. & Watt, W.S. (eds.) (1976). Geology of Greenland. *Copenhagen: Geological Survey of Greenland.* pp603.
Farver, J.R. (1989). Oxygen self-diffusion in diopside with application to cooling rate determinations. *Earth and Planetary Science Letters* **92**, 386-396.
Farver, J.R. & Giletti, B.J. (1985). Oxygen diffusion in amphiboles. *Geochimica et Cosmochimica Acta* **49**, 1403-1411.
Finch, A. A., Parsons, I. & Mingard, S. C. (1995). Biotites as indicators of fluorine fugacities in late-stage magmatic fluids: the Gardar Province in South Greenland. *Journal of Petrology* **36**, 1701-1728.
Finch, A. A., Mansfeld, J. & Andersen, T. (2001). U-Pb radiometric age of Nunarsuit pegmatite, Greenland: constraints on the timing of Gardar magmatism. *Bulletin of the Geological Society of Denmark* **48**, 1-7.
Foland, K. A., Landoll, J. D., Henderson, C. M. B. & Jiangfeng, C. (1993). Formation of cogenetic quartz and nepheline syenites. *Geochimica et Cosmochimica Acta* **57**, 697-704.
Frisch, W. & Abdel-Rahman, A. M. (1999). Petrogenesis of the Wadi Dib alkaline ring complex, Eastern Desert of Egypt. *Mineralogy and Petrology* **65**, 249-275.
Frost, B. R. & Lindsley, D. H. (1992). Equilibria among Fe-Ti-oxides, pyroxenes, olivine, and quartz: Part II. Aplication. *American Mineralogist* **77**, 1004-1020.
Ghiorso, M. S. & Evans, B. W. (2002). Thermodynamics of the amphiboles: Ca-Mg-Fe^{2+} Quadrilateral. *American Mineralogist* **87**, 79-98.
Gilbert, M. C. & Briggs, D. F. (1974). Comparison of the stabilities of OH- and F-potassic richterites; a preliminary report. *EOS, Transactions, American Geophysical Union.* **55**, 480-481.
Giletti, B.J. & Yund, R.A. (1984). Oxygen diffusion in quartz. *Journal of geophysical research.* **89**, 4039-4046.
Giletti, B.J.; Semet, M.P. & Yund, R.A. (1978). Studies in diffusion-III. Oxygen in feldspars: an ion microprobe determination. *Geochimica et Cosmochimica Acta* **42**, 45-57.
Goldsmith, J. R., Graf, D. L., Witters, J. & Northtrop, D. A. (1962). Studies in the system $CaCO_3$-$MgCO_3$-$FeCO_3$: 1. Phase relations; 2. A method for major-element spectrochemical analysis; 3.Compositions of some ferroan dolomites. *Journal of Geology* **70**, 659-688.
Goldstein, S. L., O´Nions, R. K. & Hamilton, P. J. (1984). A Sm-Nd isotopic study of the atmospheric dust and particulates from major river systems. *Earth and Planetary Science Letters* **70**, 221-236.
Grapes, R., Yagi, K. & Okumura, K. (1979). Aenigmatite, sodic pyroxene, arfvedsonite and associated minerals in syenites from Morotu, Sakhalin. *Contributions to Mineralogy and Petrology* **69**, 97-103.
Halama, R., Waight, T. & Markl, G. (2002). Geochemical and isotopic zoning patterns of plagioclase megacrysts in gabbroic dykes from the Gardar Province, South Greenland: implications for crystallization processes in anorthositic magmas. *Contributions to Mineralogy and Petrology* **144**, 109-127.
Harris, C. (1983). The petrology of lavas and associated plutonic inclusions of Ascension island. *Journal of Petrology* **24**, 424-470.
Harris, C. (1995). Oxygen isotope geochemistry of the Mesozoic anorogenic complexes of Damaraland, northwest Namibia: evidence for crustal contamination and its effects on silica saturation. *Contributions to Mineralogy and Petrology* **122**, 308-321.
Harris, C. & Ashwal, L. D. (2002). The origin of low $\delta^{18}O$ granites and related rocks from the Seychelles. *Contributions to Mineralogy and Petrology* **143**, 366-376.
Harry, W. T. & Pulvertaft, C. T. R. (1963). The Nunarssuit intrusive complex, South Greenland. *Bulletin Grønlands Geologiske Undersøgelse* **36**, pp. 136.

Hawthorne, F. C. (1976). The crystal chemistry of the amphiboles; V, The structure and chemistry of arfvedsonite. *Canadian Mineralogist* **14**, 346-356.
Hawthorne, F. C., Oberti, R., Cannillo, E. & Ottolini, L. (2001). Li-bearing arfvedsonitic amphiboles from the Strange Lake peralkaline granite, Quebec. *Canadian Mineralogist* **39**, 1161-1170.
Hawthorne, F. C., Ungaretti, L., Oberti, R. & Bottazzi, P. (1993). Li: An important component in igneous alkali amphiboles. *American Mineralogist* **78**, 733-745.
Hawthorne, F. C., Ungaretti, L., Oberti, R. & Cannillo, E. (1994). The mechanisms of [6]Li incorporation in amphiboles. *American Mineralogist* **79**, 443-451.
Heaman, L. M. & Machado, N. (1992). Timing and origin of midcontinent rift alkaline magmatism, North America: evidence from the Coldwell Complex. *Contributions to Mineralogy and Petrology* **110**, 289-303.
Hellner, E. & Schürmann, K. (1966). Stability of metamorphic amphiboles: the tremolite-ferroactinolite series. *Journal of Geology* **74**, 332-331.
Holland, T. J. B. (1990). Activities of components in omphacitic solid solutions; an application of Landay theory of mixtures. *Contributions to Mineralogy and Petrology* **105**, 446-453.
Ike, E. C. (1985). Postmagmatic arfvedsonite-aenigmatite paragenesis in the ring-dyke of the Burra Centre, Ningi-Burra complex, Nigeria. *Journal of African Earth Sciences* **3**, 101-105.
Jacobson, S. B. & Wasserburg, G. J. (1980). Sm-Nd isotopic evolution of chondrites. *Earth and Planetary Science Letters* **50**, 139-155.
Jenkin, G. R. T., Linklater, C. & Fallick, A. E. (1991). Modeling of mineral $\delta^{18}O$ values in an igneous aureole: Closed-system model predicts apparent open-system $\delta^{18}O$ values. *Geology* **19**, 1185-1188.
Kalamarides, R. I. (1986). High-temperature oxygen isotope fractionation among the phases of Kiglapait intrusion, Labrador, Canada. *Chemical Geology* **58**, 303-310.
Kogarko, L. N. & Romanchev, B. P. (1977). Temperature, pressure, redox conditions, and mineral equilibria in agpaitic nepheline syenites and apatite-nepheline rocks. *Geochemistry International* **14**, 113-128.
Kogarko, L. N. & Romanchev, B. P. (1982). Phase equilibria in alkaline melts. *International Geology Review* **25**, 534-546.
Konnerup-Madsen, J. & Rose-Hansen, J. (1984). Composition and significance of fluid inclusions in the Ilímaussaq peralkaline granite, South Greenland. *Bull.minéral.* **107**, 317-326.
Kramm, U. & Kogarko, L. N. (1994). Nd and Sr isotope signatures of the Khibina and Lovozero agpaitic centres, Kola Province, Russia. *Lithos* **32**, 225-242.
Kresten, P. (1988). The chemistry of fenitization, examples from Fen, Norway. *Chemical Geology* **68** , 329-349.
Kunzendorf, H., Nyegaard, P. & Nielsen, B. L. (1982). Distribution of characteristic elements in the radioactive rocks of the northern part of Kvanefjeld, Ilimaussaq intrusion, South Greenland. *Rapport Grønlands Geologiske Undersøgelse* **109**, pp. 32.
Kunzmann, T. (1999). The aenigmatite-rhönite mineral group. *European Journal of Mineralogy* **11**, 743-756.
Larsen, L. M. (1976). Clinopyroxenes and coexisting mafic minerals from the alkaline Ilímaussaq intrusion, south Greenland. *Journal of Petrology* **17**, 258-290.
Larsen, L. M. (1977). Aenigmatites from the Ilímaussaq intrusion, south Greenland: Chemistry and petrological implications. *Lithos* **10**, 257-270.
Larsen, L. M. & Sørensen, H. (1987). The Ilímaussaq intrusion-progressive crystallization and formation of layering in an agpaitic magma. *In: Fitton, J.G. & Upton, B.G.J. (eds.), Alkaline Igneous Rocks, Geological Society Special Publication* **30**, 473-488.

Leake, B.E., Wooley, A.R., Arps, C.E.S., Birch, W.D., Gilbert, M.C., Grice, J.D., Hawthorne, F.C., Kato, A., Kisch, H.J., Krivovichev, V.G., Linthout, K., Laird, J., Mandarino, J.A., Maresch, W.V., Nickel, E.H., Rock, N.M.S., Schumacher, J.C., Smith, D.C., Stephenson, N.C.N., Ungaretti, L., Whittaker, E.J.W. & Youzhi, G. (1997). Nomenclature of amphiboles: Report of the Subcommittee on Amphiboles of the International Mineralogical Association, Commission on New Minerals and MIneral Names. *American Mineralogist* **82**, 295-321.

Liebermann, J. & Petrakakis, K. (1990). TWEEQU thermobarometry, analysis of uncertainties and applications to granulites from western Alaska. *Canadian Mineralogist* **29**, 857-887.

Lindsley, D. H. (1983). Pyroxene thermometry. *American Mineralogist* **68**, 477-493.

Lindsley, D. H. & Frost, B. R. (1992). Equilibria among Fe-Ti-oxides, pyroxenes, olivine, and quartz: Part I. Theory. *American Mineralogist* **77**, 987-1003.

Lugmair, G. W. & Marti, K. (1978). Lunar initial $^{143}Nd/^{144}Nd$: differential evolution of the lunar crust and mantle. *Earth and Planetary Science Letters* **39**, 349-357.

Lutz, T. M., Foland, K.A., Faul, H. & Srogi, L.A. (1988). The strontium and oxygen isotopic record of hydrothermal alteration of syenites from the Abu Khruq complex, Egypt. *Contributions to Mineralogy and Petrology* **98**, 212-223.

Markl, G., (2001). Stability of Na-Be minerals in late-magmatic fluids of the Ilímaussaq alkaline complex, South Greenland. *Geology of Greenland Survey Bulletin* **190**, 145-158.

Markl, G. & Baumgartner, L. (2002). PH changes in peralkaline late magmatic fluids. *Contributions to Mineralogy and Petrology* **144**, 331-346.

Markl, G., Marks, M., Schwinn, G. & Sommer, H. (2001). Phase equilibrium constraints on intensive crystallization parameters of the Ilímaussaq Complex, South Greenland. *Journal of Petrology* **42**, 2231-2258.

Marks, M. & Markl, G. (2001). Fractionation and assimilation processes in the alkaline augite syenite unit of the Ilímaussaq Intrusion, South Greenland, as deduced from phase equilibria. *Journal of Petrology* **42**, 1947-1969.

Marsh, J. S. (1975). Aenigmatite stability in silica-undersaturated rocks. *Contributions to Mineralogy and Petrology* **50**, 135-144.

Mingram, B., Trumbull, R. B., Littman, S. & Gerstenberger, H. (2000). A petrogenetic study of anorogenic felsic magmatism in the Cretaceous Paresis ring complex, Namibia: evidence for mixing of crust and mantle-derived components. *Lithos* **54**, 1-22.

Morogan, V. (1989). Mass transfer and REE mobility during fenitization at Alnö, Sweden. *Contributions to Mineralogy and Petrology* **103**, 25-34.

Nicholls, J. & Carmichael, I. S. E. (1969). Peralkaline acid liquids: A petrological study. *Contributions to Mineralogy and Petrology* **20**, 268-294.

Nielsen, T. F. D. (1979). The occurence and formation of Ti-aegirines in peralkaline syenites; an example from the Tertiary ultramafic alkaline Gardiner complex, East Greenland. *Contributions to Mineralogy and Petrology* **69**, 235-244.

Parsons, I. (1972). Petrology of the Puklen syenite-alkali granite complex, Nunarssuit, South Greenland. *Meddelelser om Grønland* **195**, pp. 73.

Parsons, I. (1979). The Klokken gabbro-syenite complex, South Greenland: Cryptic variation and origin of inversely graded layering. *Journal of Petrology* **20**, 653-694.

Parsons, I., Mason, R. A., Becker, S. M. & Finch, A. A. (1991). Biotite equilibria and fluid circulation in the Klokken Intrusion. *Journal of Petrology* **32**, 1299-1333.

Piotrowski, J. M. & Edgar, A. D. (1970). Melting relations of undersaturated alkaline rocks from South Greenland. *Meddelelser om Grønland* **181**(9), pp. 62.

Piper, J. D. A. (1992). The palaeomagnetism of major (Middle Proterozoic) igneous complexes, South Greenland and the Gardar apparent polar wander track. *Precambrian Research* **54**, 153-172.

Popp, R. K. & Gilbert, M. C. (1972). Stability of acmite-jadeite pyroxenes at low pressure. *American Mineralogist* **57**, 1210-1231.

Poulsen, V. (1964). The sandstones of the Precambrian Eriksfjord Formation in South Greenland. *Rapport Grønlands Geologiske Undersøgelse* **2**, pp. 16.

Powell, M. (1978). The crystallisation history of the Igdlerfigssalik nepheline syenite intrusion, Greenland. *Lithos* **11**, 99-120.

Pulvertaft, T. C. R. (1961). The Puklen intrusion, Nunarssuit, SW Greenland. *Meddelelser om Grønland* **123**(6), 35-49.

Robie, R. A. & Hemingway, B. S. (1995). Thermodynamic properties of minerals and related substances at 298.15 K and 1 bar (10^5 Pascals) pressure and at higher temperatures. *U.S. Geological Survey Bulletin* **2131**, pp. 461.

Robinson, G. R. Jr. & Haas, J. L. Jr. (1983). Heat capacity, relative enthalpy, and calorimetric entropy of silicate minerals: An empirical method of prediction. *American Mineralogist* **68**, 541-553.

Rock, N. M. S. (1976). Fenitisation around the Monchique alkaline complex, Portugal. *Lithos* **9**, 263-279.

Roddick, J. C., Sullivan, R. W. & Dudas, F. Ö. (1992). Precise calibration of Nd tracer isotopic composition for Sm-Nd studies. *Chemical Geology* **97**, 1-8.

Rozanski K., Araguás-Araguás L. & Gonfiantini, R. (1993). Isotopic patterns in modern global precipitation. *In: Swart P. K., Lohmann K. C., Mckenzie J. A. & Savin S. (eds.): Climate change in continental isotopic records. American Geophysical Union. Geophysical Monograph Series.* **78**, 1-36.

Rumble, D. & Hoering, T. C. (1994). Analysis of oxygen and sulfur isotope ratios in oxide and sulfide minerals by spot heating with a carbon dioxide laser in a fluorine atmosphrere. *Accounts of Chemical Research* **27**, 237-241.

Salvi, S. & Williams-Jones, A. E. (1990). The role of hydrothermal processes in the granite-hosted Zr, Y, REE deposit at Strange Lake, Quebec/Labrador: evidence from fluid inclusions. *Geochimica et Cosmochimica Acta* **54**, 2403-2418.

Scaillet, B. & MacDonald, R. (2001). Phase relations of peralkaline silicic magmas and petrogenetic implications. *Journal of Petrology* **42**, 825-845.

Schmitt, A. K., Emmermann, R., Trumbull, R. B., Bühn, B. & Henjes-Kunst, F. (2000). Petrogenesis and $^{40}Ar/^{39}Ar$ geochronology of the Brandberg Complex, Namibia: Evidence for a major mantle contribution in metaluminous and peralkaline granites. *Journal of Petrology* **41**, 1207-1239.

Sharp. Z.D. (1990). A laser-based microanalytical method for the in-situ determination of oxygen isotope ratios of silicates and oxides. *Geochimica et Cosmochimica Acta* **54**, 1353-1357.

Sheppard, S. M. F. (1986). Igneous rocks: III. Isotopic case studies of magmatism in Africa, Eurasia and oceanic island. *In: Valley, J.W., Taylor, H.P.Jr and O´Neil, J.R. (eds.): Stable Isotopes. Reviews in Mineralogy. Washington: Mineralogical Society of America.* **16**, 319-368.

Sood, M. K. & Edgar, A. D. (1970). Melting relations of undersaturated alkaline rocks. *Meddelelser om Grønland* **181**, pp. 41.

Späth, A., Le Roex, A. P. & Opiyo-Akech, N. (2001). Plume-lithosphere interaction and the origin of continental rift-related alkaline volcanism-the Chyulu hills volcanic province, Southern Kenya. *Journal of Petrology* **42**, 765-787.

Steiger, R. H. & Jäger, E. (1977). Subcommission on geochronology: conventions of the use of decay constants in geo- and cosmochronology. *Earth and Planetary Science Letters* **36**, 359-362.

Stephenson, D. (1972). Alkali clinopyroxenes from nepheline syenites of the South Qoroq Centre, south Greenland. *Lithos* **5**, 187-201.

Stephenson, D. (1974). Mn and Ca enriched olivines from nepheline syenites of the South Qoroq Centre, south Greenland. *Lithos* **7**, 35-41.

Stevenson, R., Upton, B. G. J. & Steenfelt, A. (1997). Crust-mantle interaction in the evolution of the Ilímaussaq Complex, South Greenland: Nd isotopic studies. *Lithos* **40**, 189-202.

Strong, D. F. & Taylor, R. P. (1984). Magmatic-subsolidus and oxidation trends in composition of amphiboles from silica-saturated peralkaline igneous rocks. *Tschermaks mineralogisch-petrologische Mitteilungen.* **32**, 211-222.

Taylor, H. P. J. & Sheppard, S. M. F. (1986). Igneous rocks: I. Processes of isotopic fractionation and isotope systematics. *In: Valley, J.W., Taylor, H.P.Jr and O´Neil, J.R. (eds.): Stable Isotopes. Reviews in Mineralogy. Washington: Mineralogical Society of America.* **16**, 227-269.

Upton, B. G. J. (1962). Geology of Tugtutôq and neighbouring islands, South Greenland. I. *Bulletin Grønlands Geologiske Undersøgelse* **34**, pp. 60.

Upton, B. G. J. & Emeleus, C. H. (1987). Mid-Proterozoic alkaline magmatism in southern Greenland: the Gardar province. *In: Fitton, J.G. & Upton, B.G.J. (eds.): Alkaline Igneous Rocks, Geological Society Special Publication.* **30**, 449-471.

Upton, B. G. J., Stephenson, D. & Martin, A. R. (1985). The Tugtutôq older giant dyke complex: mineralogy and geochemistry of an alkali gabbro-augite-syenite-foyaite association in the Gardar Province of South Greenland. *Mineralogical Magazine* **49**, 624-642.

Valley, J. W. (1986). Stable isotope geochemistry of metamorphic rocks. *In: Valley, J.W., Taylor, H.P.Jr and O´Neil, J.R. (eds.): Stable Isotopes. Reviews in Mineralogy. Washington: Mineralogical Society of America.* **16**, 445-486.

Valley J.W., Kitchen, N., Kohn, M. J., Niendorf, C. R. & Spicuzza, M. J. (1995). UWG-2, a garnet standard for oxygen isotope ratios: strategies for high precision and accuracy with laser heating. *Geochimica et Cosmochimica Acta* **59**, 5223-5231.

Vennemann, T. W. & Smith, H. S. (1991). The rate and temperature of reaction of ClF_3 with silicate minerals, and their relevance to oxygen isotope analysis. *Chemical Geology* **86**, 83-88.

Wones, D.R. (1989). Significance of the asssemblage titanite + magnetite + quartz in granitic rocks. *American Mineralogist* **74**, 744-749.

Zheng, Y.-F. (1993a). Calculation of oxygen isotope fractionation in anydrous silicate minerals. *Geochimica et Cosmochimica Acta* **57**, 1079-1091.

Zheng, Y.-F. (1993b). Calculation of oxygen isotope fractionation in hydroxyl-bearing silicates. *Earth and Planetary Science Letters* **120**, 247-263.

Appendix: Mineral abbreviations used in figures and text

Mineral	Abbreviation
Ab	albite
Aeg	aegirine
Aeg-aug	aegirine-augite
Aen	aenigmatite
Alkfsp	alkali feldspar
Alm	almandine
Am	amphibole
An	anorthite
Andr	(hydro)andradite
Ap	apatite
Arf	arfvedsonite
Astr	astrophyllite
Aug	augite
Cc	calcite
Di	diopside
En	enstatite
Fa	fayalite
Fe-Act	ferro-actinolite
Fl	fluorite
Fo	forsterite
Fs	ferrosilite
Gro	grossular
Hed	hedenbergite
Hem	hematite
Ilm	ilmenite
La	larnite
Mag	magnetite
Ol	olivine
Or	orthoclase
Py	pyrope
Qtz	quartz
Rhö	rhönite
Rhod	rhodochrosite
Sid	siderite
Sp	spessartine
Tit	titanite
Ti-mag	titanomagnetite
Usp	ulvøspinel
Wilk	wilkinsonite
Wo	wollastonite
Zrn	zircon

Figure captions

Fig.1:
(a) Sketch map of the alkaline Gardar Province, South Greenland (modified after Escher and Watt, 1976). The Puklen Complex is situated in the western part of the province. Nunarssuit and Ilímaussaq are other alkaline complexes referred to in the text. (b) Enlarged detail of figure 1 a. Generalized geological map of the Puklen Complex, South Greenland (based on Parsons, 1972). Black dots mark sample localities.

Fig. 2:
Photomicrographs (plane-polarized light), BSE images and sketches of mineral textures observed in the Puklen rocks. (a) Autometasomatic ferro-actinolite (am II) overgrowing interstitial ferro-richterite (am I) in syenite. (b) Primary augite, which is overgrown by interstitial amphibole I in syenite. (c) BSE image of granular late-stage albite in granite. (d) Two sketches of aenigmatite textures in syenite. (e) Secondary aegirine with small inclusions of quartz, $(calcite\text{-}siderite)_{ss}$ and hematite (not visible). (f) Graphic intergrowths of quartz and alkali feldspar in granophyre. (g) BSE image of arfvedsonite, which is replaced by aegirine in granite. Inclusions of fluorite are also visible. (h) Late-stage, radially arranged aegirine aggregate associated with astrophyllite in granite.

Fig. 3:
(a) Top: Photomicrograph (plane polarized light) of augite, which is metasomatized along cracks and grain boundaries by a fluid phase (sample GM1616). Bottom: BSE image (left) and element map for Na (right) of a typical Na-enriched area. (b) Top: BSE image of aegirine-augite II rim around primary augite (sample GM1635). Secondary phases include hydroandradite, titanite, Ti-free magnetite and quartz. The dashed red line represents the assumed former grain boundary of primary augite. The dashed white line outlines a relic of primary augite. Bottom: BSE image (left) and element maps for Na (left) of an aegirine-augite II rim, which shows oscillatory zonation.

Fig. 4:
Feldspar compositions observed in the Puklen rocks. (a) In syenitic rocks (b) Composition and zoning profile of a ternary feldspar phenocryst of syenite sample GM1580 (c) In granitic rocks. Feldspar solvus after Elkins & Grove (1990).

Fig. 5:
(a) Clinopyroxene compositional trend in the investigated samples plotted in the ternary system diopside (Di), hedenbergite (Hed) and aegirine (Aeg). Published trends from other Gardar intrusions are shown for comparison. (b) Representative zoning profiles through augite grains of two syenite samples. Formulae are based on four cations and six oxygens. End member components were calculated after the projection method of Lindsley (1983).

Fig. 6:
Amphibole compositions (a) Zoning profile starting in the core of an interstitial amphibole I through a rim of later amphibole II in syenite. Note the logarithmic scale of the y-axis. (b) Li versus Fe^{3+}, Al(VI) and Fe^{2+} for the Li-amphiboles in alkali granites. For amphibole I of syenites and amphibole of granites, calculated formulae are based on 16 cations and 23 oxygens, assuming a completely filled A site. Formulae for amphibole II of syenites are calculated after the method of Schumacher, described in Leake et al. (1997).

Fig.7:

Trace element data for augite of sample GM1616, which is metasomatized along cracks and grain boundaries by a late-stage fluid phase (compare Fig. 3a). (a) BSE image with data points indicated as white circles. (b) Rb and Sr concentrations plotted against Na p.f.u., which is used as an indicator for increasing metasomatism. The dashed gray line separates measurements in virtually unaffected core regions (left) from metasomatized areas (right) of the same grain. (c) Sm and Nd data for the same data points. Note the logarithmic scale of the y-axis.

Fig.8:
(a) Major element variation diagrams for the Puklen rocks. SiO_2 is used as x-axis. Note the logarithmic scale of the y-axis. (b) Minor element variation diagrams for the Puklen rocks, with A.I. (agpaitic index = molar ratio of $(Na_2O+K_2O) / Al_2O_3$) as x-axis. The syenite sample with the exceptionally high A.I. of 1.2 is sample GM1611, which is a totally metasomatized sample.

Fig.9:
Oxygen isotope composition of whole rock samples and mineral separates of the Puklen complex.

Fig. 10:
X_{Fe} in augite versus calculated a_{SiO2} for samples lacking primary quartz.

Fig. 11:
Profiles from core to rim in pyroxene and amphibole I illustrating the observed increase of molar (Na + K)/Al ratio.

Fig. 12:
Stability field of aenigmatite (gray) in a $\log f_{O2}$ – T diagram (after Nicholls & Carmichael, 1969). Dotted field = calculated magmatic conditions for some syenites. The curved black arrow describes the formation of aenigmatite in samples GM1615 and GM1616. Point A represents the intersection of the labeled reactions (a) – (c) for an aegirine activity of 0.5, and the dashed line indicates the intersection of reactions (a) and (b) depending on the activity of sodium-disilicate. See text for further explanations.

Fig 13:
Log f_{O2} – log a_{CO2} diagram (1 kbar) for the system Ca-Fe-Si-O-H-C involving hedenbergite, magnetite, quartz, ferro-actinolite, andradite and calcite. Black dots represent the position of the invariant point [Fe-Act], thick dashed lines show the position of the FMQ buffer curve at specified temperatures. The gray, dotted and stippled fields represent the inferred conditions of formation of secondary Ca-mineral assemblages for syenite samples. See text for further explanations.

Fig14:
Log f_{O2} – T diagram showing the position of reaction (6). The FMQ and the HM buffer curves are shown as well. The gray field marks the uncertainty if an error of ± 0.2 % for D_fH^0(arf) is assumed.

Fig.15:
Sm-Nd isotope diagram for all analyzed mineral separates. Note that the line of best fit of 1111 ± 95 Ma was calculated after the method of Brooks et al. (1972) neglecting the data for

late-stage aegirine separates. Two point isochrons are shown for syenite samples GM1590, GM1600, and GM1616.

Fig.16:
Calculated oxygen isotopic compositions for the Puklen melts after the methods of Taylor & Sheppard (1986), Harris (1995), and Kalamarides (1986). Note the homogeneous values for the syenitic parental melt which is in contrast to significantly lower and rather inhomogeneous values for the other rock types. The calculated $\delta^{18}O_{melt}$ values for coarse alkali granites are maximum estimates. See text for further explanations.

Fig.17:
(a) Variation of $\delta^{18}O$ versus temperature (°C) for the closed-system model for syenites, illustrating the oxygen isotope evolution of minerals and the coexisting fluid phase during cooling. Modeled values are compared to measured data. The black dot represents a published $\delta^{18}O$ value for fresh feldspar from the Puklen complex (Sheppard, 1986). (b) An influx of low-$\delta^{18}O$ fluids during late-stage evolution of granites may explain the low $\delta^{18}O$ values of aegirine. See text for further explanations.

Fig.18:
Correlation diagram of neodymium and oxygen isotopic composition for mineral separates of the Puklen complex.

Table 1: Mineralogy of the investigated samples from the Puklen intrusion

sample	rock type	primary magmatic minerals	secondary, late- to post-magmatic minerals
GM 1580	syenite	ol + aug + ilm + mag + alkfsp + am I + ap + zrn	am II + ab + tit
GM1583	syenite	ol + aug + ilm + mag + alkfsp + am I + ap + zrn	am II + ab + tit
GM1586	syenite	ol + aug + ilm + mag + alkfsp + am I + ap + zrn	ab
GM1587	alkali granite	am + ilm + alkfsp + qtz I + ap + zrn	aeg + ab + fl + hem + qtz II + astr
GM1589	syenite	ilm + am I + alkfsp + qtz + zrn	am II
GM1590	syenite	aug + ilm + am I + alkfsp + ap	am II + tit + ab
GM1592	granophyre	ilm + mag + am I + qtz + ap + fl	am II
GM1593	granophyre	aug + ilm + mag + am I + qtz + ap + fl	am II
GM1600	syenite	aug + ilm + am I + alkfsp + qtz + ap + zrn	am II + ab + tit
GM1603	syenite	aug + ilm + am I + alkfsp + qtz + ap + zrn	am II + bio
GM1605	alkali granite	am + ilm + alkfsp + qtz I + ap + zrn	aeg + ab + fl + hem + qtz II + astr
GM1606	alkali granite	am + ilm + alkfsp + qtz I + ap + zrn	aeg + ab + fl + hem + qtz II
GM1608	alkali granite	am + ilm + alkfsp + qtz I + ap + zrn	aeg + ab + fl + hem + qtz II
GM1611	syenite	ol + aug (?) + ilm + alkfsp + ap + zrn	aeg + ab + cc
GM1615	syenite	ol + aug + ilm + alkfsp + am I + ap + zrn	aen + ab + qtz II + cc + $Fe(OH)_x$ + tit
GM1616	syenite	ol + aug + ilm + alkfsp + am I + ap + zrn	aen + ab + qtz II + cc + $Fe(OH)_x$ + tit
GM1620	microgranite	am + mag + alkfsp + qtz + ap + zrn	aeg + ab + astr
GM1625	syenite	aug + mag + am I + alkfsp + ap + zrn	bio
GM1627	microgranite	am + mag + alkfsp + qtz + ap + zrn	aeg + ab
GM1634	syenite	ol + aug + mag + alkfsp + am I + ap	am II + bio
GM1635	syenite	aug + ilm + alkfsp (?)+ qtz + am I + ap	aeg-aug + ab + andr + tit + mag + qtz

Table 2: Representative microprobe analyses of feldspars

sample	GM1615	GM1580	GM1580	GM1600	GM1605
rock type	syenite	syenite	syenite	syenite	granite
feldspar type	phenocryst	phenocryst	ab rim	ab interstitial	phenocryst
wt%					
SiO_2	66.52	65.57	67.81	67.91	65.15
Al_2O_3	18.91	20.48	20.37	20.28	20.25
FeO	0.20	0.15	0.15	0.05	0.09
MnO	0.04	0.02	0.01	0.08	0.20
MgO	0.01	0.00	0.00	0.02	0.01
CaO	0.26	1.06	1.01	0.09	0.84
Na_2O	6.92	7.93	10.57	11.69	7.53
K_2O	6.57	4.22	0.45	0.10	5.16
Total	99.44	98.94	99.88	100.17	99.23
	Formulae based on 8 oxygens				
Si	2.99	2.93	2.96	2.96	2.93
Al	1.00	1.08	1.05	1.04	1.07
Mg	0.00	0.00	0.00	0.00	0.00
Fe	0.01	0.01	0.01	0.00	0.00
Mn	0.00	0.00	0.00	0.00	0.01
Ca	0.01	0.05	0.05	0.00	0.04
Na	0.60	0.69	0.89	0.99	0.66
K	0.38	0.24	0.03	0.01	0.30
Sum	5.00	4.99	4.98	5.01	5.01
Ab	61	70	93	99	66
An	1	5	5	0	4
Or	38	25	3	1	30

Table 3: Representative microprobe analyses of pyroxenes from the different rock types

sample	GM1593	GM1600	GM1586	GM1616	GM1616	GM1635	GM1605	GM1608	GM1620
rock type	granophyre	syenite	syenite	syenite	syenite	syenite	coarse granite	coarse granite	microgranite
mineral	augite	augite	augite	augite	aeg-augite	aeg-augite	aegirine	aegirine	aegirine
wt%									
SiO_2	52.99	49.80	48.85	48.55	48.78	52.05	52.03	51.70	51.18
TiO_2	0.19	0.17	0.43	0.56	0.34	0.02	0.50	0.08	0.13
Al_2O_3	0.70	0.38	0.38	0.23	0.18	0.24	0.37	0.30	0.24
FeO	12.65	24.23	26.56	29.43	29.59	20.08	30.51	31.00	27.32
MnO	0.52	0.59	0.49	0.67	0.66	0.87	0.06	0.19	0.37
MgO	13.61	5.65	2.73	0.81	0.39	4.09	0.10	0.42	1.69
ZrO_2	0.01	0.00	0.01	0.01	0.02	0.00	0.00	0.00	0.00
CaO	19.72	18.78	19.73	19.10	16.59	14.48	0.04	0.90	4.90
Na_2O	0.23	0.35	0.59	0.61	2.49	6.52	13.17	12.24	10.41
Total	100.62	99.95	99.77	99.97	99.04	98.34	96.87	96.82	96.26
	Formulae based on 4 cations and 6 oxygens								
Si	1.98	1.98	1.98	2.00	1.99	2.00	2.00	2.00	1.99
Al	0.03	0.02	0.02	0.01	0.01	0.01	0.02	0.01	0.01
Ti	0.01	0.01	0.01	0.02	0.01	0.00	0.01	0.00	0.00
Fe^{3+}	0.01	0.03	0.04	0.01	0.18	0.48	0.95	0.90	0.78
Mg	0.76	0.34	0.17	0.05	0.03	0.23	0.01	0.02	0.10
Fe^{2+}	0.39	0.78	0.86	1.00	0.83	0.17	0.03	0.10	0.11
Mn	0.02	0.02	0.02	0.02	0.02	0.03	0.00	0.01	0.01
Zr	0.00	0.00	0.00	0.00	0.00	0.00	0.00	0.00	0.00
Ca	0.79	0.80	0.86	0.84	0.73	0.60	0.00	0.04	0.20
Na	0.02	0.03	0.05	0.05	0.20	0.49	0.98	0.92	0.79
Sum	4.00	4.00	4.00	4.00	4.00	4.00	4.00	4.00	4.00

Table 4: Representative microprobe analyses and recalculations of Fe-Ti oxides

sample	GM1580	GM1603	GM1580	GM1586	GM1593	GM1606	GM1605	GM1620
rock type	syenite	syenite	syenite	syenite	granophyre	coarse granite	coarse granite	microgranite
mineral	ilm	ilm	usp (calc.)	usp (calc.)	ilm	ilm	ilm	mag
wt%								
TiO_2	47.31	50.38	27.17	32.53	51.63	50.75	51.58	0.06
Al_2O_3	0.00	0.00	0.00	0.03	0.00	0.00	0.00	0.14
FeO	49.25	45.68	68.93	65.20	46.58	42.15	42.62	92.15
MnO	2.52	3.36	1.70	1.26	1.69	5.96	5.32	0.02
MgO	0.01	0.00	0.00	0.00	0.00	0.00	0.00	0.08
Total	99.09	99.42	97.80	99.03	99.90	98.86	99.52	92.45
	Formulae based on 3 (2) cations and 4 (3) oxygens for mag (ilm)							
Al	0.00	0.00	0.00	0.00	0.00	0.00	0.00	0.01
Ti	0.90	0.96	0.77	0.92	0.98	0.97	0.98	0.00
Fe^{3+}	0.20	0.08	0.46	0.17	0.04	0.05	0.03	1.99
Mg	0.00	0.00	0.00	0.00	0.00	0.00	0.00	0.00
Fe^{2+}	0.85	0.89	1.72	1.88	0.94	0.84	0.87	1.00
Mn	0.05	0.07	0.05	0.04	0.04	0.13	0.11	0.00
Sum	2.00	2.00	3.00	3.00	2.00	2.00	2.00	3.00

Table 5: Representative microprobe analyses of amphiboles of the different rock types

sample	GM1586	GM1615	GM1590	GM1600	GM1600	GM1634	GM1586	GM1606	GM1587	GM1605
rock type	syenite	syenite	syenite	syenite	syenite	syenite	syenite	granite	granite	granite
mineral	amph I	amph I	amph I	amph I	amph II	amph II	amph II	amph	amph	amph
wt%										
SiO_2	45.41	49.27	48.60	44.08	50.15	48.31	50.42	50.67	50.37	51.56
TiO_2	0.20	1.21	1.66	0.83	0.08	0.04	0.06	1.60	1.84	0.31
Al_2O_3	1.64	0.46	1.96	5.00	0.51	0.40	0.74	1.23	1.12	0.75
ZnO	0.00	0.01	0.01	0.02	0.00	0.00	0.00	0.32	0.22	0.18
Li_2O	0.00	0.00	0.00	0.00	0.00	0.00	0.00	0.25	0.20	1.10
FeO	29.60	34.21	32.16	29.51	31.10	34.98	33.42	30.80	30.52	31.94
MnO	0.18	0.55	0.56	0.34	0.40	0.89	0.41	0.47	0.69	0.51
MgO	3.52	0.45	1.26	4.03	3.60	0.55	2.45	1.51	1.32	0.74
CaO	9.81	3.16	5.59	9.62	9.95	10.45	10.54	0.34	0.43	0.64
Na_2O	2.52	6.63	4.69	2.86	0.99	0.47	0.85	8.42	8.43	7.84
K_2O	0.78	1.50	1.35	0.99	0.41	0.16	0.26	1.50	1.58	1.48
ZrO_2	0.00	0.01	0.00	0.01	0.00	0.00	0.00	0.11	0.15	0.08
Cl	0.12	0.02	0.07	0.30	0.02	0.01	0.01	0.01	0.02	0.01
F	3.44	0.00	0.10	1.57	0.00	0.00	0.00	1.70	1.61	0.69
Total	97.22	97.48	98.01	99.15	97.21	96.26	99.15	98.93	98.50	97.84
	Formulae based on 23 oxygens									
Si	7.73	7.99	7.92	7.15	7.91	7.89	7.88	7.98	7.98	7.99
Al	0.33	0.09	0.38	0.95	0.09	0.08	0.14	0.23	0.21	0.14
Ti	0.03	0.15	0.20	0.10	0.01	0.01	0.01	0.19	0.22	0.04
Zn	0.00	0.00	0.00	0.00	0.00	0.00	0.00	0.04	0.03	0.02
Li*	0.00	0.00	0.00	0.00	0.00	0.00	0.00	0.16	0.13	0.69
r_-^{3+}	0.00	0.02	0.00	0.00	0.29	0.30	0.20	0.45	0.41	1.14
Mg	0.89	0.11	0.31	0.97	0.85	0.13	0.57	0.35	0.31	0.17
r_-^{2+}	4.21	4.62	4.38	4.00	3.81	4.47	4.17	3.60	3.64	3.00
Mn	0.03	0.08	0.08	0.05	0.05	0.12	0.05	0.06	0.09	0.07
Ca	1.79	0.55	0.98	1.67	1.68	1.83	1.77	0.06	0.07	0.11
Na	0.83	2.08	1.48	0.90	0.30	0.15	0.26	2.57	2.59	2.35
K	0.17	0.31	0.28	0.20	0.08	0.03	0.05	0.30	0.32	0.29
Zr	0.00	0.00	0.00	0.00	0.00	0.00	0.00	0.01	0.01	0.01
Cl	0.03	0.01	0.02	0.08	0.00	0.00	0.00	0.00	0.00	0.00
F	1.85	0.00	0.05	0.80	0.00	0.00	0.00	0.85	0.81	0.34
Sum	16.00	16.00	16.00	16.00	15.08	15.01	15.09	16.00	16.00	16.00

* Li was determined by La-ICP-MS

Table 6: Major and trace element compositions of the Puklen rocks. A.I. = agpaitic index (molar ($Na_2O + K_2O$) /Al_2O_3). Total Fe is expressed as FeO (FeO_t).

rock type	syenites						alkali granites			granophyres		microgranites	
sample	GM 1589	GM 1590	GM1600	GM 1603	GM 1611	GM 1616	GM 1605	GM 1606	GM 1608	GM 1592	GM 1593	GM 1620	GM 1627
SiO_2 (wt%)	64.48	59.94	66.79	65.68	61.15	62.11	74.66	74.11	74.21	72.76	70.26	73.38	71.88
TiO_2	0.69	1.10	0.48	0.78	0.66	0.82	0.28	0.28	0.32	0.24	0.31	0.32	0.47
Al_2O_3	14.28	15.09	13.11	13.79	13.04	13.68	11.17	10.26	11.62	12.28	12.52	12.45	13.25
FeO_t	6.69	8.15	3.80	6.46	8.53	8.23	3.30	4.54	3.08	1.66	2.47	2.92	2.76
MnO	0.15	0.17	0.08	0.14	0.17	0.18	0.04	0.06	0.05	0.04	0.05	0.06	0.05
MgO	0.28	0.53	0.42	0.36	0.14	0.18	0.06	0.03	0.06	0.21	0.14	0.20	0.38
CaO	1.48	2.26	1.18	1.76	2.32	2.21	0.33	0.11	0.25	0.45	0.70	0.41	0.98
Na_2O	5.32	5.58	5.02	4.70	6.33	5.44	4.42	4.72	6.40	4.09	4.15	4.71	4.39
K_2O	5.66	5.62	4.56	5.36	4.78	5.26	4.82	4.66	2.22	5.04	5.18	4.84	5.19
P_2O_5	0.08	0.25	0.09	0.14	0.11	0.09	0.01	0.01	0.01	0.03	0.03	0.04	0.09
Total	99.11	98.69	97.44	99.17	97.23	98.20	99.09	98.78	98.22	96.80	95.81	99.33	99.44
A.I.	1.04	1.01	1.01	0.98	1.20	1.07	1.12	1.25	1.11	0.99	0.99	1.04	0.97
Sc (ppm)	5	9	< 5	5	< 5	< 5	< 5	< 5	< 5	< 5	< 5	< 5	< 5
V	9	13	17	12	12	9	8	6	14	13	12	13	23
Cr	19	< 10	68	< 10	< 10	64	106	45	155	31	235	< 10	< 10
Co	< 5	< 5	< 5	< 5	< 5	< 5	< 5	< 5	< 5	< 5	< 5	< 5	< 5
Ni	< 10	< 10	< 10	< 10	< 10	< 10	< 10	< 10	< 10	< 10	< 10	< 10	< 10
Cu	< 5	7	9	8	< 5	10	10	6	< 5	5	7	5	6
Zn	114	137	69	119	151	151	187	189	209	39	67	71	50
Ga	31	27	21	23	30	31	30	31	28	18	21	20	18
Rb	92	112	121	118	137	119	248	206	79	177	194	174	158
Sr	44	95	165	65	43	31	25	16	26	110	91	88	138
Y	82	74	47	53	74	97	116	66	88	38	68	49	30
Zr	774	483	504	302	572	790	1421	1563	1073	291	510	584	338
Nb	37	30	24	29	32	43	64	71	61	21	38	34	15
Ba	301	752	712	361	121	128	150	136	157	651	405	522	761
Hf	14	9	10	7	9	13	27	27	17	9	13	13	9
Ta	< 5	< 5	< 5	< 5	< 5	< 5	< 5	5	< 5	< 5	< 5	< 5	< 5
Pb	19	18	30	18	18	18	40	40	11	20	28	39	21
Th	7	4	8	4	4	7	15	16	15	14	17	13	5
U	< 5	< 5	< 5	< 5	< 5	< 5	6	5	5	5	5	7	< 5

Table 7: Oxygen isotope compositions of whole rock samples and mineral separates from the Puklen intrusion ($\delta^{18}O$ values given in ‰).

sample	whole rock	qtz	aug	aeg	am I	am II	altered fsp
GM 1589	4.8	7.9	-	-	4.1	2.8	3.9
GM 1590	5.8	-	5.5	-	4.3	2.5	-
GM 1600	5.9	8.1	5.5	-	3.9	2.5	3.5
GM 1603	6.9	8.1	5.3	-	4.6	2.7	-
GM 1611	5.8	-	-	0.2	-	-	-
GM 1616	6.5	8.0 (qtz II)	4.7	-	4.4	-	-
GM 1605	5.5	7.3	-	1.2	2.2	-	-
GM 1606	5.8	7.1	-	2.0	3.5	-	-
GM 1608	5.0	5.1	-	0.5	3.3	-	-
GM 1592	5.0	6.7	-	-	2.5	1.7	-
GM 1593	4.6	6.4	5.4	-	2.7	1.0	-
GM 1620	4.9	6.7	-	1.8	1.7	-	-
GM 1627	5.5	7.2	-	-	1.9	-	-
Q-D	-	7.0	-	-	-	-	-
Q-M	-	7.2	-	-	-	-	-

Table 8: Rb-Sr and Sm-Nd data for mineral separates of the Puklen complex.

sample	rock type	mineral	Rb (ppm)	Sr (ppm)	Rb/Sr	$^{87}Rb/^{86}Sr$	$^{87}Sr/^{86}Sr$	$^{87}Sr/^{86}Sr_i$	Sm (ppm)	Nd (ppm)	Sm/Nd	$^{147}Sm/^{144}Nd$	$^{143}Nd/^{144}Nd$	$^{143}Nd/^{144}Nd_i$	ε_{Nd}
GM1589	syenite	am II							32.07	145.5	0.2204	0.1332	0.511881(07)	0.510858	-5.3
GM1590	syenite	aug	7.06	18.02	0.392	1.138	0.749407(10)	0.73035	39.56	201.6	0.1962	0.1186	0.511787(08)	0.510876	-4.9
GM1590	syenite	am I							19.97	80.90	0.2469	0.1492	0.512037(09)	0.510891	-4.6
GM1600	syenite	am I							50.20	213.2	0.2355	0.1424	0.511895(07)	0.510801	-6.4
GM1600	syenite	am II							21.86	100.9	0.2167	0.1310	0.511806(09)	0.510800	-6.4
GM1616	syenite	aug	19.22	7.59	2.532	7.330	0.712627(10)	0.58982	44.30	205.1	0.2160	0.1306	0.511938(10)	0.510935	-3.8
GM1616	syenite	am I							22.26	120.7	0.1844	0.1115	0.511749(10)	0.510893	-4.6
GM1605	alkali granite	am	30.77	75.16	0.409	1.186	0.719392(13)	0.69953	16.42	79.43	0.2067	0.1250	0.511781(09)	0.510821	-6.0
GM1605	alkali granite	aeg	19.22	10.17	1.890	5.481	0.734249(10)	0.64242	23.21	82.01	0.2830	0.1711	0.511973(08)	0.510659	-9.2
GM1606	alkali granite	am	32.37	62.57	0.517	1.499	0.721153(09)	0.69604	17.82	90.43	0.1971	0.1191	0.511742(10)	0.510827	-5.9
GM1606	alkali granite	aeg	29.41	12.98	2.266	6.580	0.740842(09)	0.63061	37.67	132.5	0.2843	0.1720	0.511958(09)	0.510637	-9.6
GM1620	microgranite	am							21.72	110.4	0.1967	0.1189	0.511710(7)	0.510797	-6.5
GM1593	granophyre	aug							64.59	327.5	0.1972	0.1192	0.511673(8)	0.510757	-7.2

Errors of measured $^{87}Sr/^{86}Sr$ and $^{143}Nd/^{144}Nd$ are given as 2σ-values and are indicated in brackets. Initial $^{87}Sr/^{86}Sr$, $^{143}Nd/^{144}Nd$ and ε_{Nd} are recalculated for 1170 Ma.

Fig.1

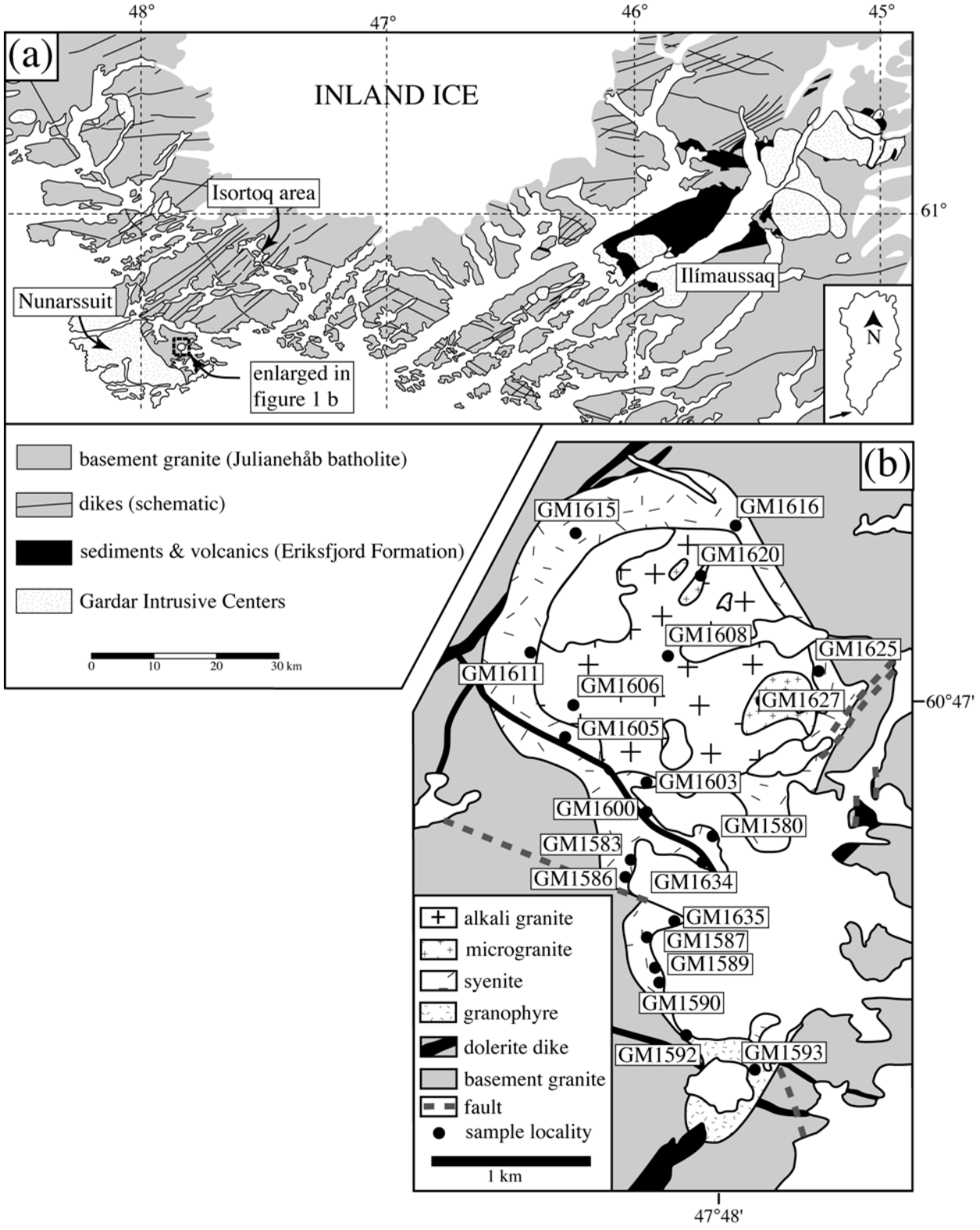
48°
47°
46°
45°
(a)
INLAND ICE
Isortoq area
Nunarssuit
enlarged in
figure 1 b
Ilímaussaq
61°
N
basement granite (Julianehåb batholite)
dikes (schematic)
sediments & volcanics (Eriksfjord Formation)
Gardar Intrusive Centers
0
10
20
30 km
(b)
GM1615
GM1616
GM1620
GM1608
GM1625
GM1611
GM1606
GM1627
GM1605
GM1603
GM1600
GM1580
GM1583
GM1586
GM1634
GM1635
GM1587
GM1589
GM1590
GM1592
GM1593
60°47'
alkali granite
microgranite
syenite
granophyre
dolerite dike
basement granite
fault
sample locality
1 km
47°48'

Fig.2

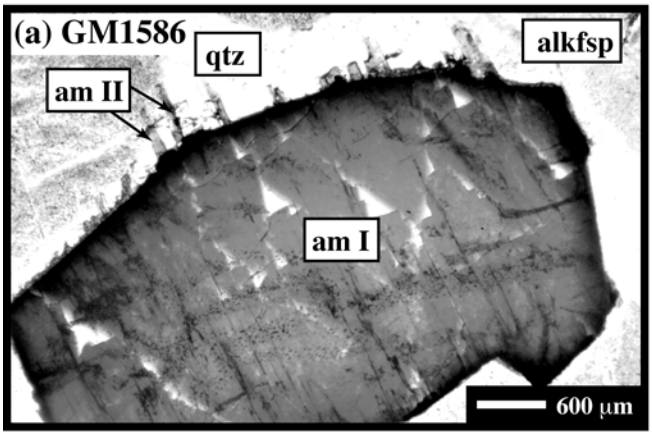
(a) GM1586
qtz
alkfsp
am II
am I
600 μm

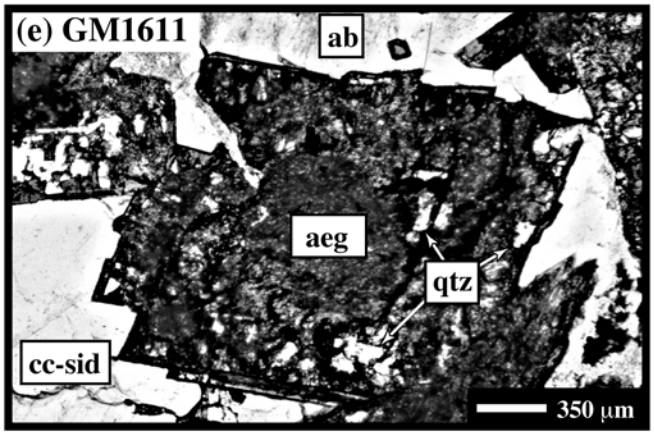
(e) GM1611
ab
aeg
qtz
cc-sid
350 μm

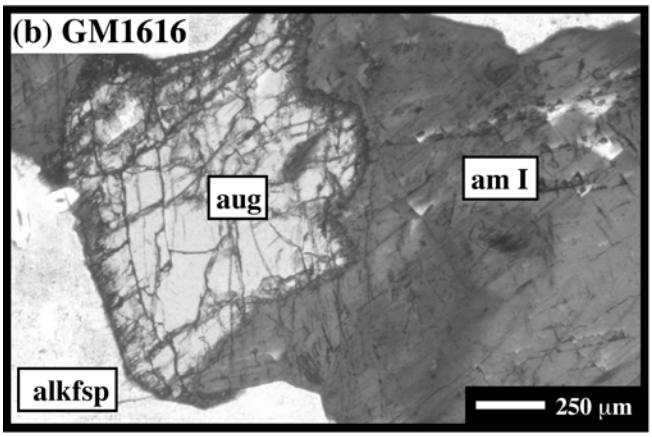
(b) GM1616
aug
am I
alkfsp
250 μm

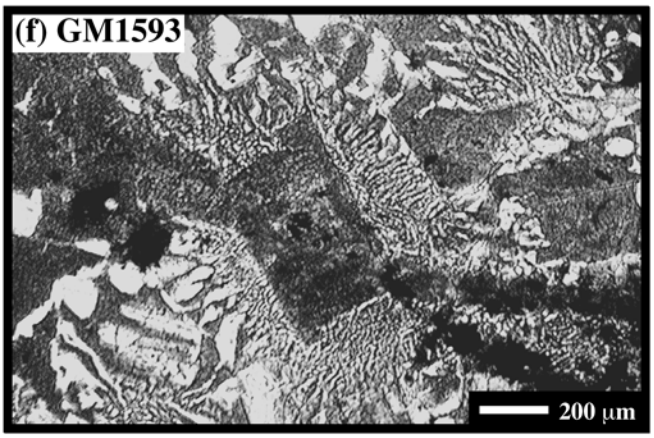
(f) GM1593
200 μm

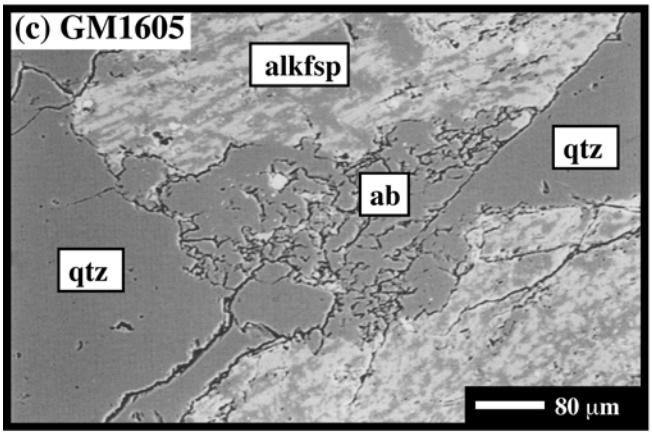
(c) GM1605
alkfsp
qtz
ab
qtz
80 μm

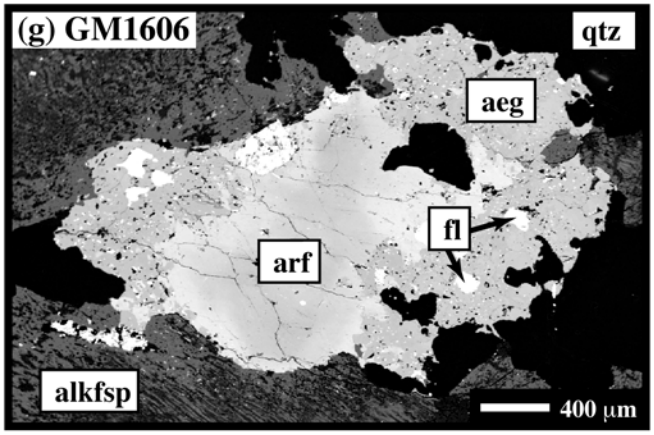
(g) GM1606
qtz
aeg
fl
arf
alkfsp
400 μm

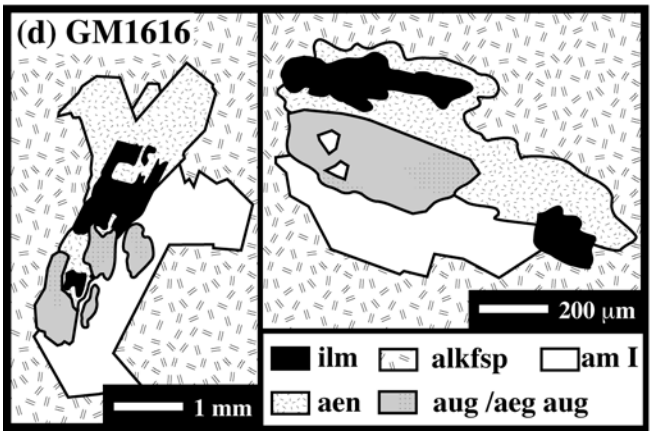
(d) GM1616
200 μm
ilm
alkfsp
am I
aen
aug /aeg aug
1 mm

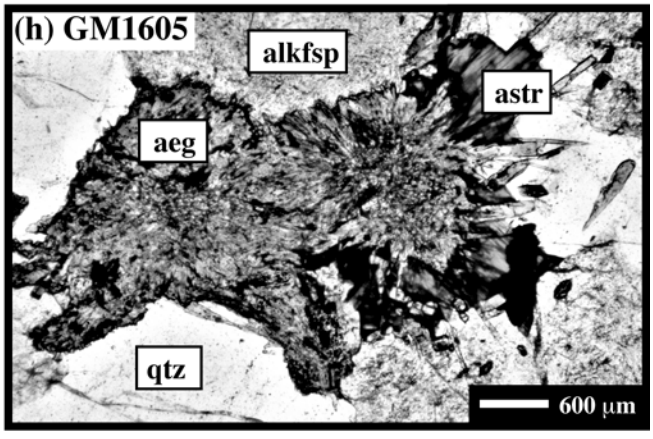
(h) GM1605
alkfsp
astr
aeg
qtz
600 μm

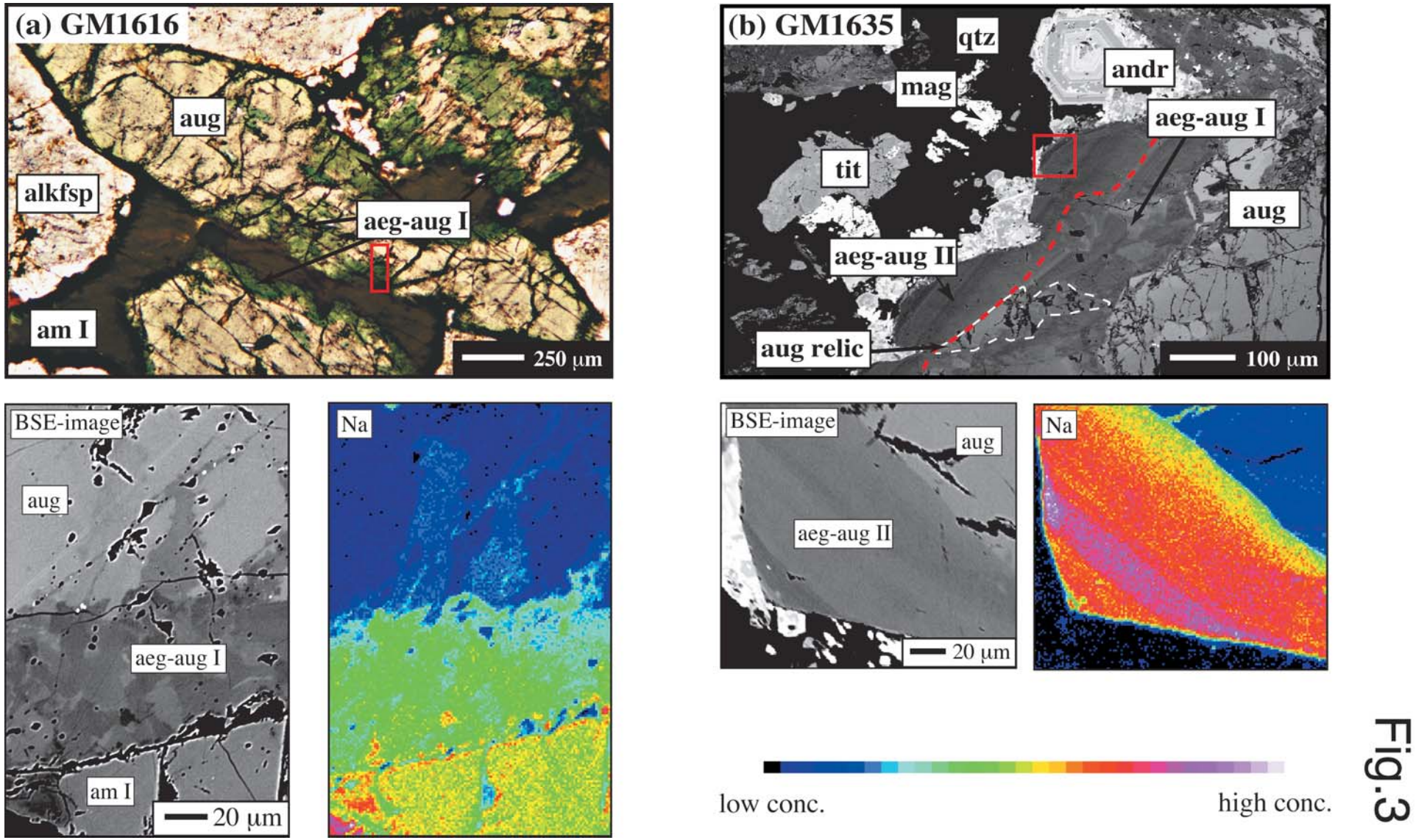
(a) GM1616
aug
alkfsp
aeg-aug I
am I
250 µm
BSE-image
aug
aeg-aug I
am I
20 µm
Na
(b) GM1635
qtz
mag
andr
aeg-aug I
tit
aug
aeg-aug II
aug relic
100 µm
BSE-image
aug
aeg-aug II
20 µm
Na
low conc.
high conc.

Fig.3

Fig.4

(a) syenitic rocks

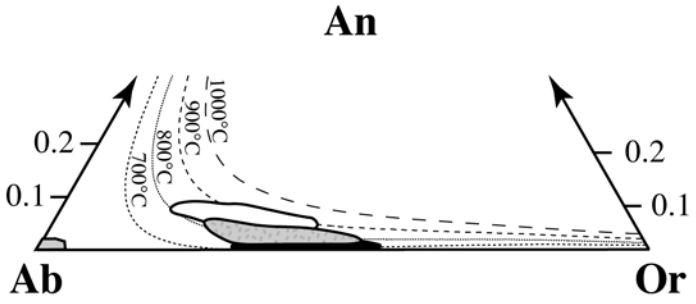

early phenocrysts
early phenocrysts in GM1615/16
late cloudy feldspar (reintegrated)
interstitial albite

(b) sample GM1580 (syenite)

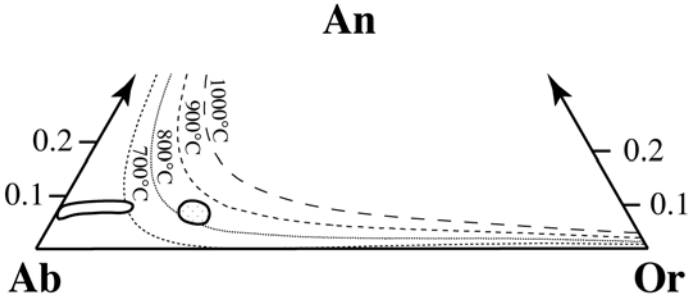

core of phenocryst in GM1580
rim of phenocryst in GM1580

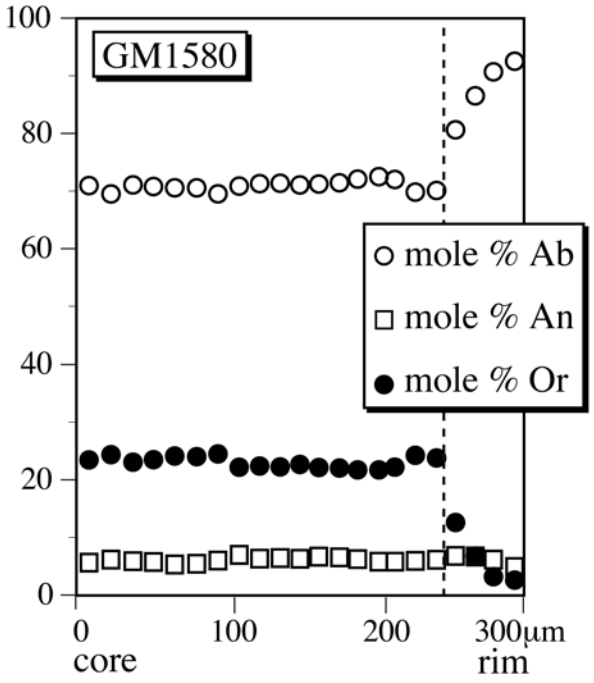

(c) granitic rocks

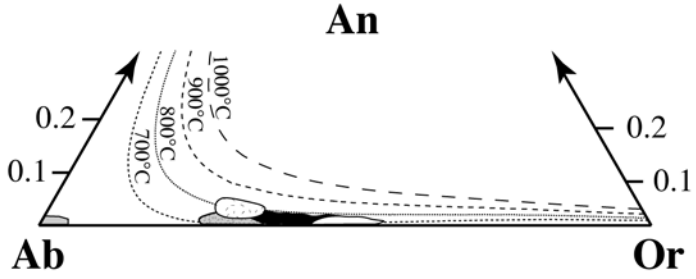

alkali granites
microgranites
granophyres
late albite
feldspar core in GM1605

Fig.5

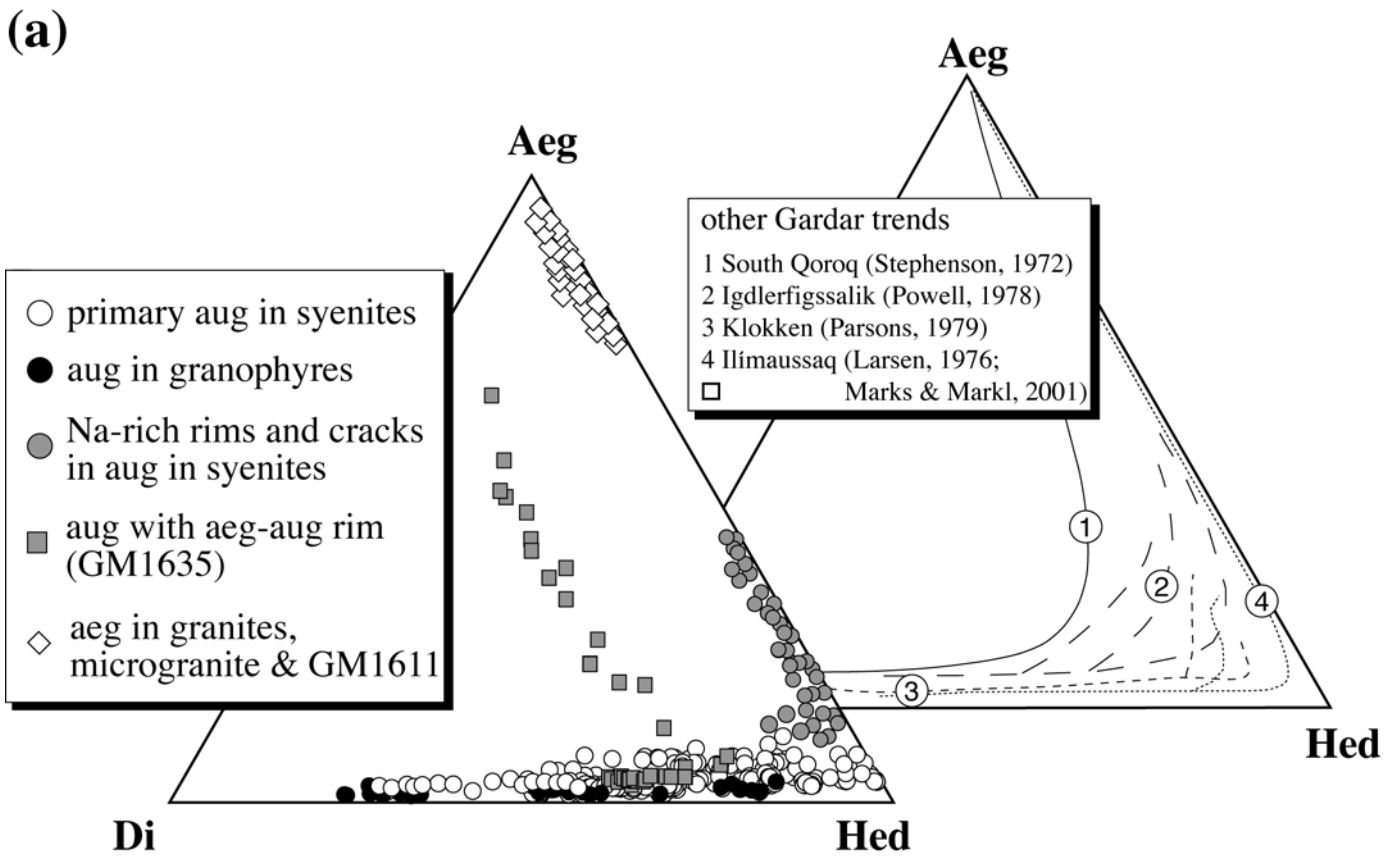
(a)
Aeg
Aeg
Di
Hed
Hed
primary aug in syenites
aug in granophyres
Na-rich rims and cracks in aug in syenites
aug with aeg-aug rim (GM1635)
aeg in granites, microgranite & GM1611
other Gardar trends
1 South Qoroq (Stephenson, 1972)
2 Igdlerfigssalik (Powell, 1978)
3 Klokken (Parsons, 1979)
4 Ilímaussaq (Larsen, 1976; Marks & Markl, 2001)
1
2
3
4

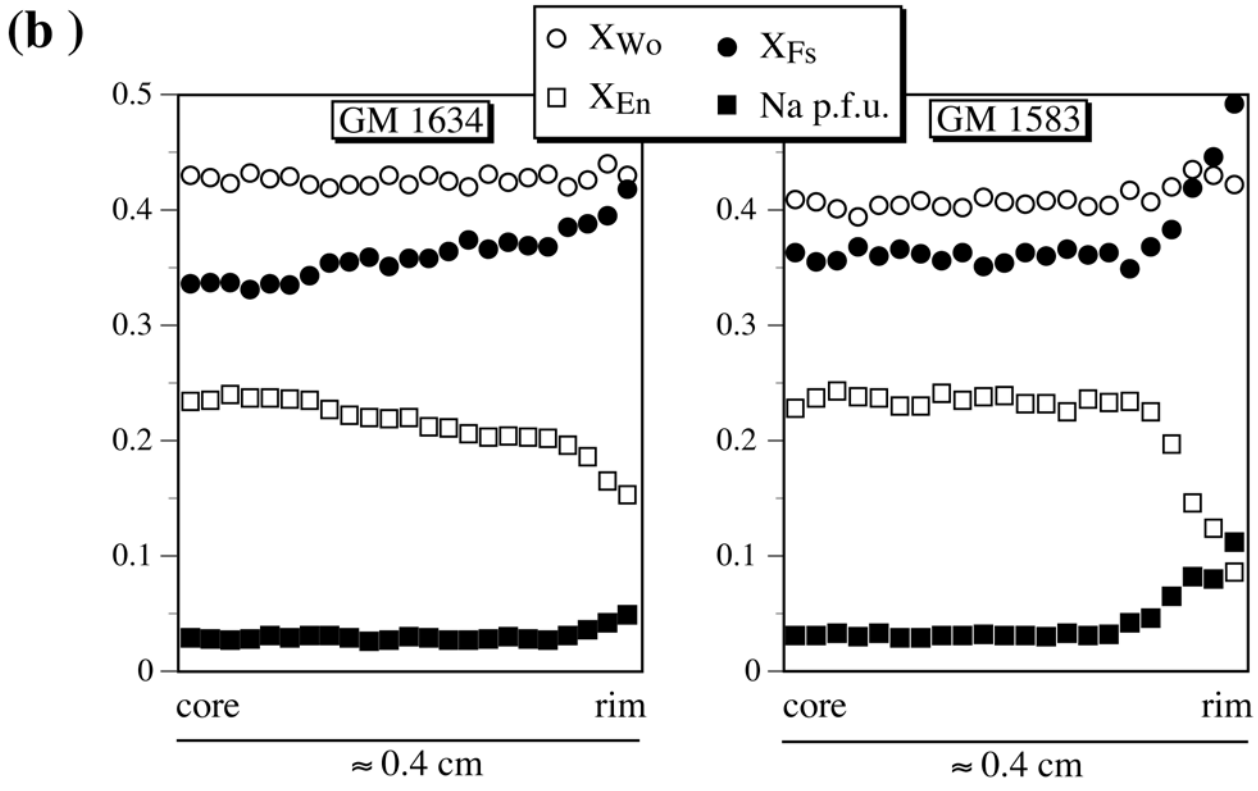
(b)
XWo
XFs
XEn
Na p.f.u.
GM 1634
GM 1583
0.5
0.4
0.3
0.2
0.1
0
core
rim
≈ 0.4 cm
core
rim
≈ 0.4 cm

Fig.6

(a) syenites

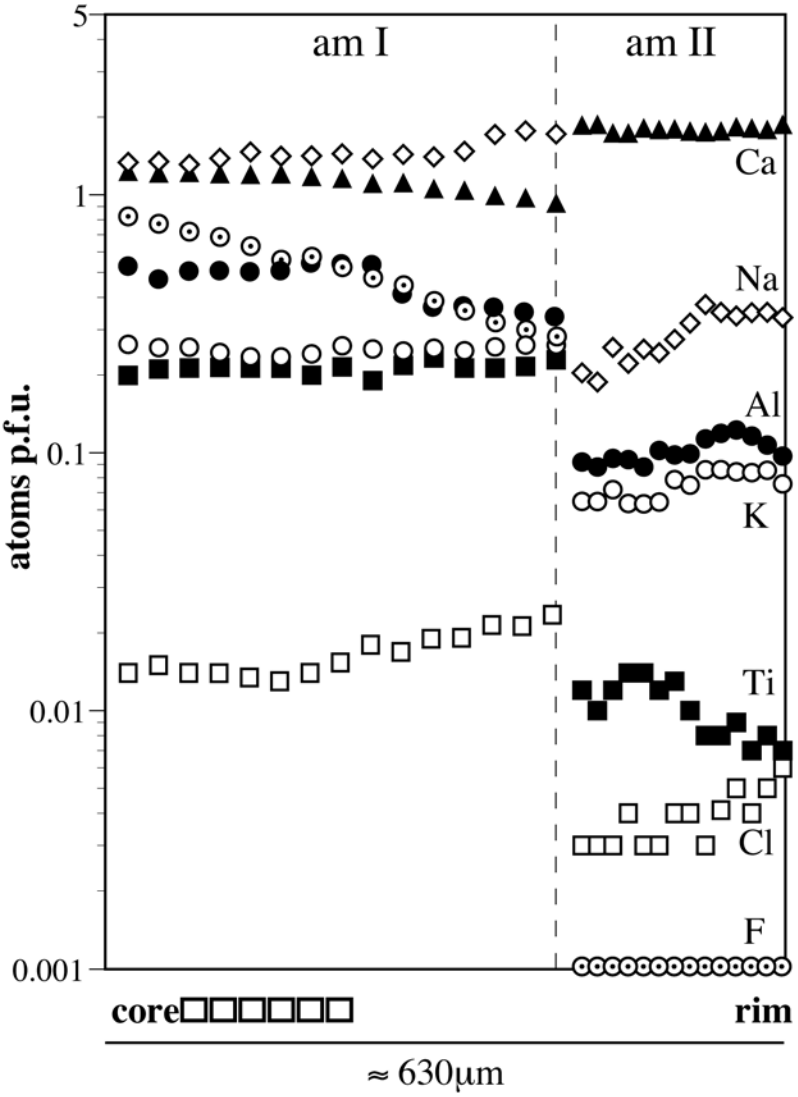

(b) alkali granites

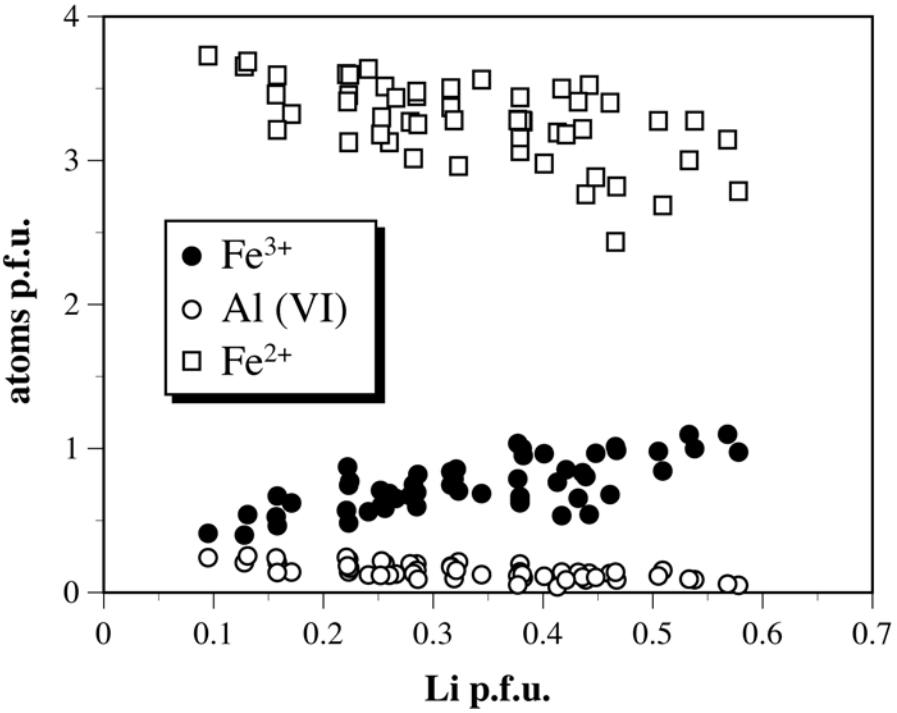

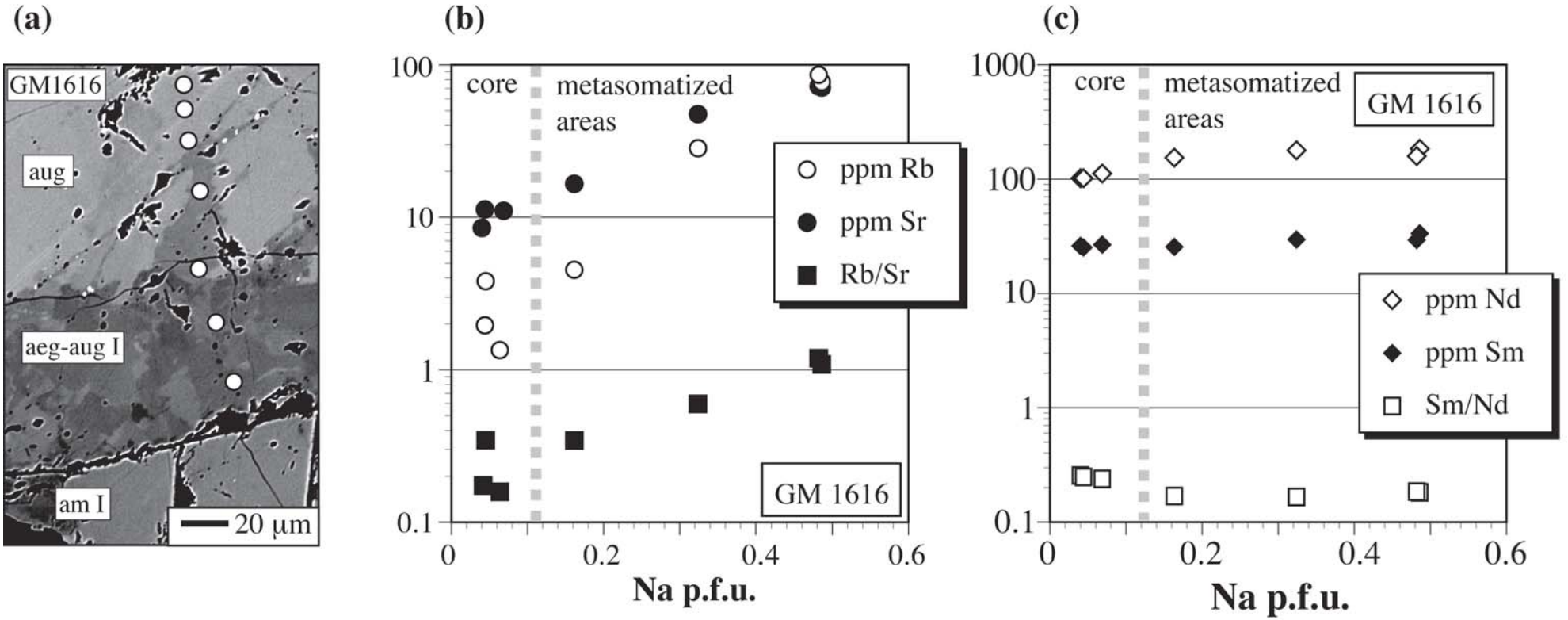
(a)
GM1616
aug
aeg-aug I
am I
20 µm
(b)
core
metasomatized areas
ppm Rb
ppm Sr
Rb/Sr
GM 1616
100
10
1
0.1
0
0.2
0.4
0.6
Na p.f.u.
(c)
core
metasomatized areas
GM 1616
ppm Nd
ppm Sm
Sm/Nd
1000
100
10
1
0.1
0
0.2
0.4
0.6
Na p.f.u.

Fig.7

Fig.8

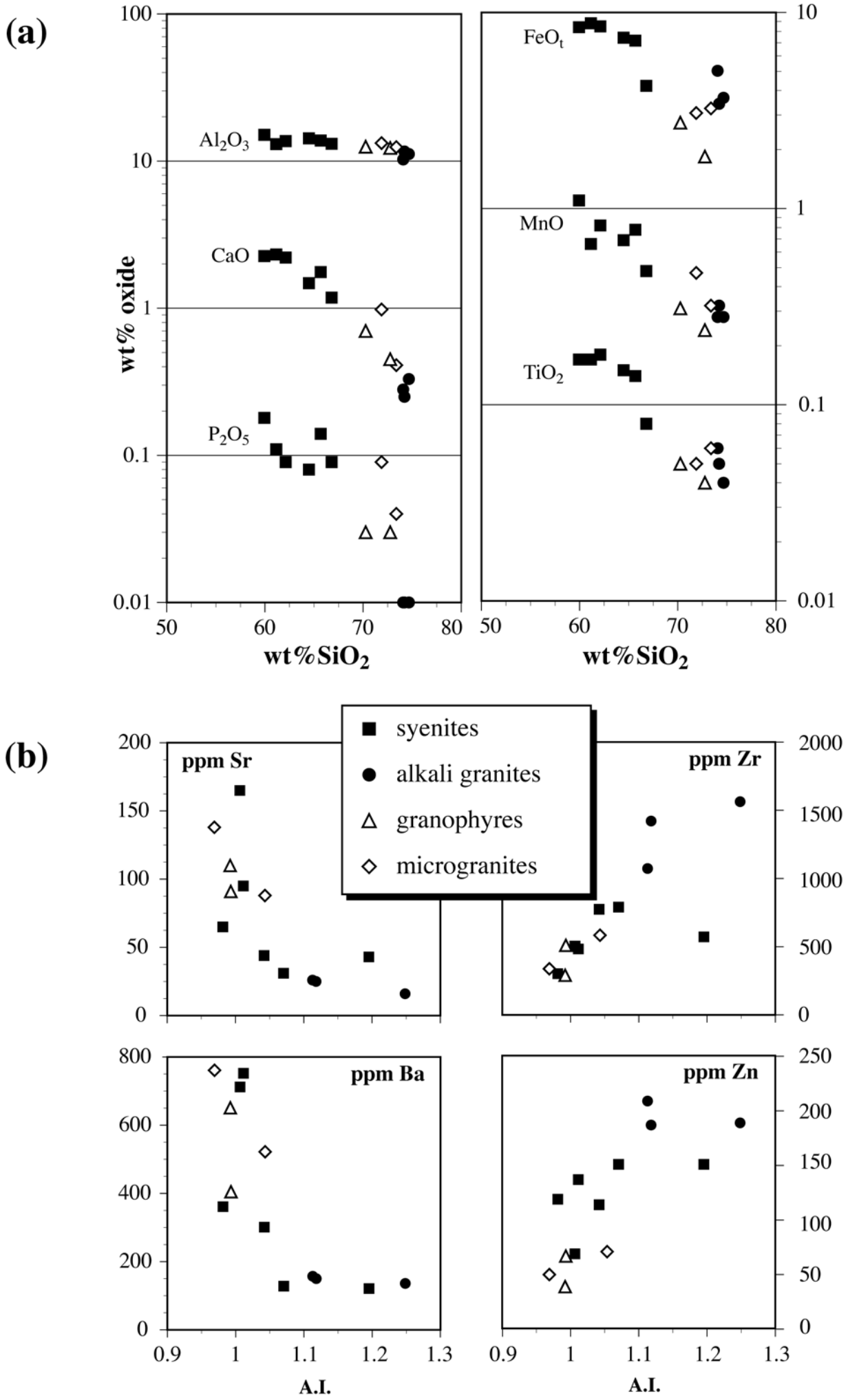
(a)
wt% oxide
Al2O3
CaO
P2O5
FeOt
MnO
TiO2
wt%SiO2
wt%SiO2
(b)
syenites
alkali granites
granophyres
microgranites
ppm Sr
ppm Zr
ppm Ba
ppm Zn
A.I.
A.I.

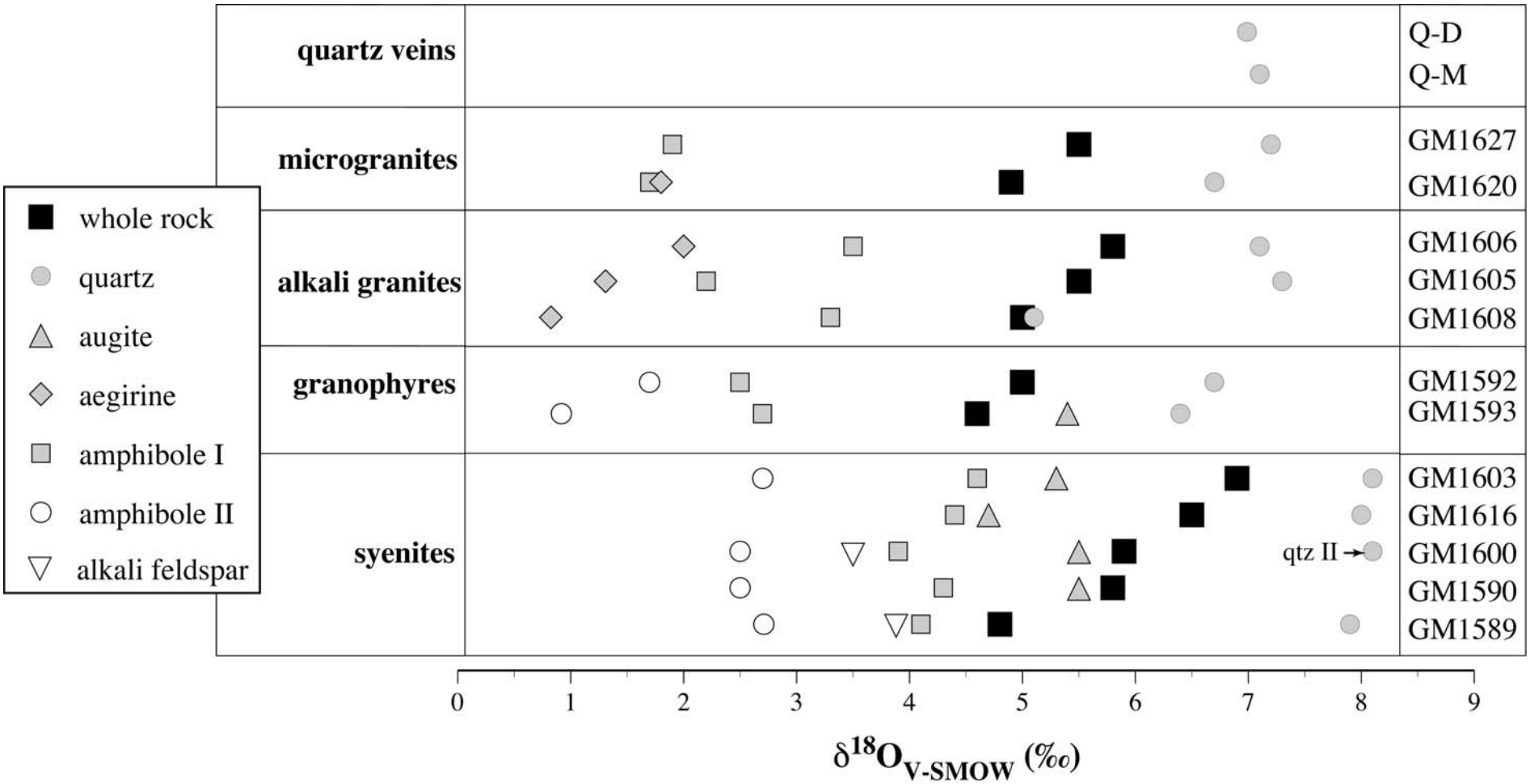
quartz veins
microgranites
alkali granites
granophyres
syenites
Q-D
Q-M
GM1627
GM1620
GM1606
GM1605
GM1608
GM1592
GM1593
GM1603
GM1616
GM1600
GM1590
GM1589
qtz II
whole rock
quartz
augite
aegirine
amphibole I
amphibole II
alkali feldspar
0
1
2
3
4
5
6
7
8
9
δ18OV-SMOW (‰)

Fig.9

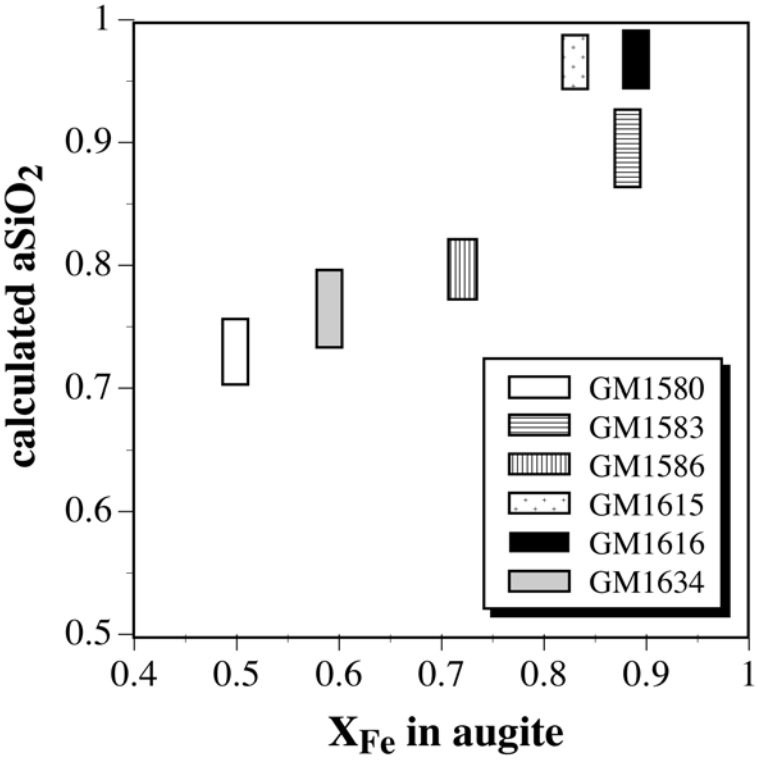
calculated aSiO2
XFe in augite
1
0.9
0.8
0.7
0.6
0.5
0.4
0.5
0.6
0.7
0.8
0.9
1
GM1580
GM1583
GM1586
GM1615
GM1616
GM1634

Fig.10

Fig.11

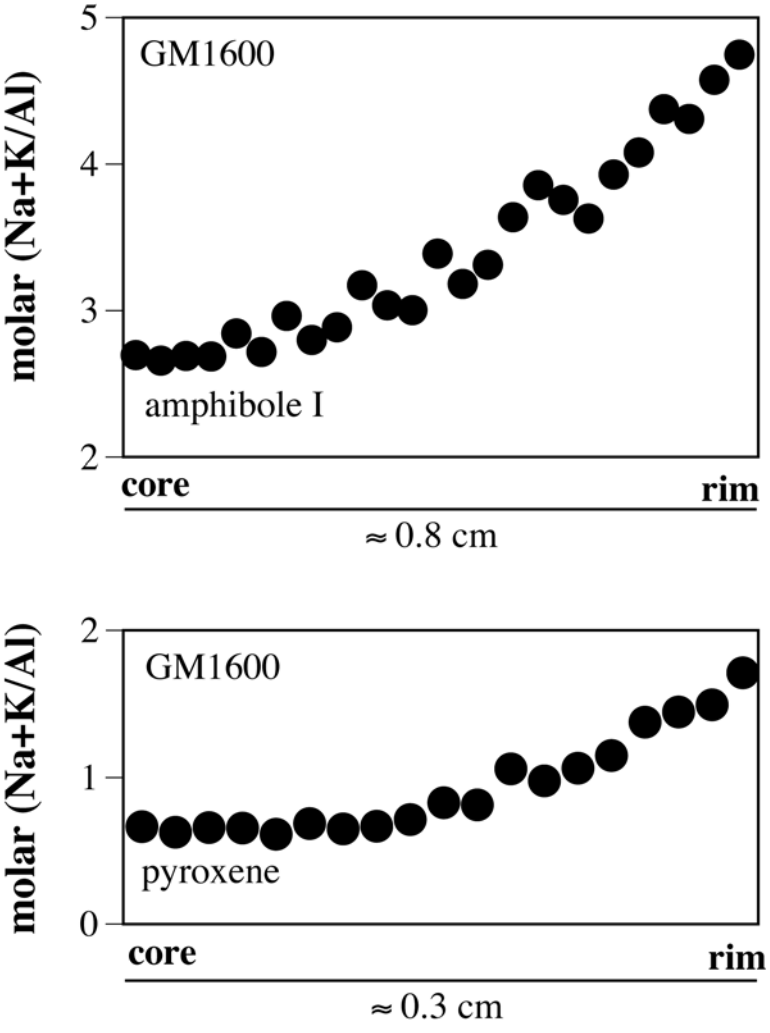
molar (Na+K/Al)
5
4
3
2
GM1600
amphibole I
core
rim
≈ 0.8 cm
molar (Na+K/Al)
2
1
0
GM1600
pyroxene
core
rim
≈ 0.3 cm

Fig.12

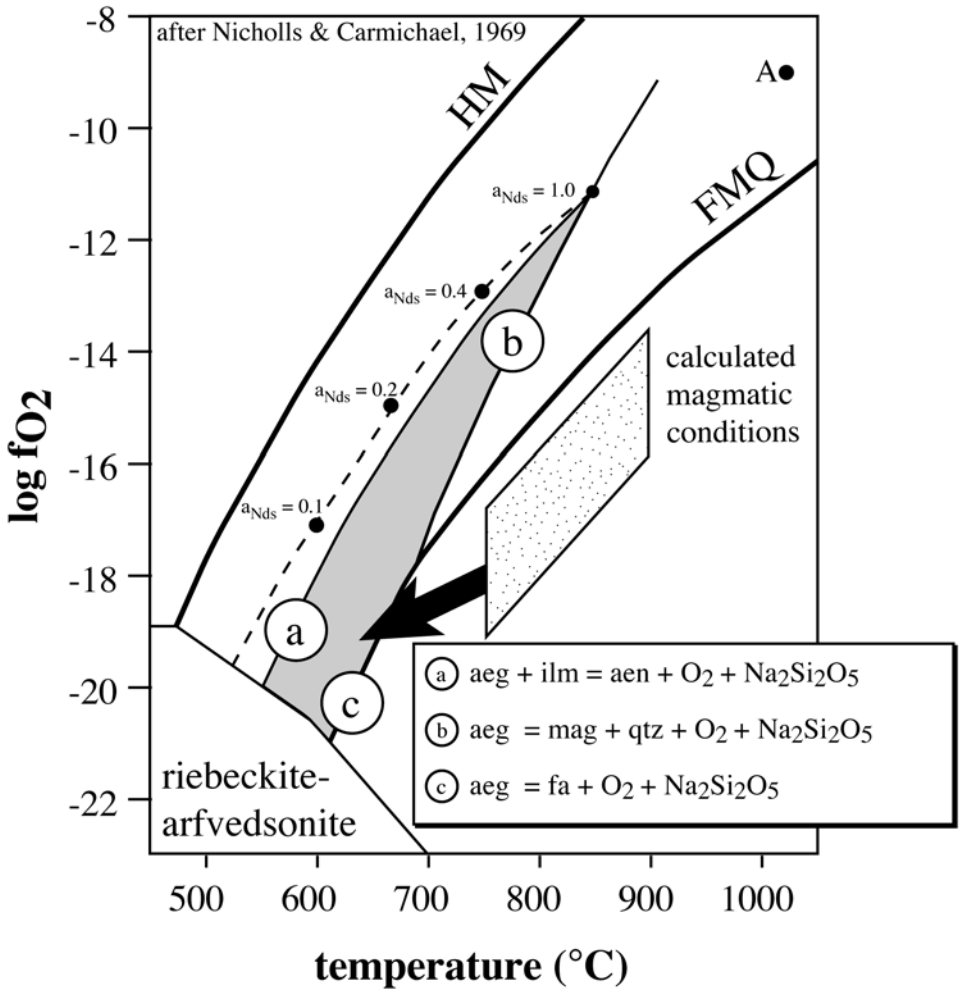
after Nicholls & Carmichael, 1969
HM
FMQ
A
a_{Nds} = 1.0
a_{Nds} = 0.4
a_{Nds} = 0.2
a_{Nds} = 0.1
a
b
c
calculated magmatic conditions
riebeckite-arfvedsonite
a aeg + ilm = aen + O_2 + $Na_2Si_2O_5$
b aeg = mag + qtz + O_2 + $Na_2Si_2O_5$
c aeg = fa + O_2 + $Na_2Si_2O_5$
log fO_2
-8
-10
-12
-14
-16
-18
-20
-22
500
600
700
800
900
1000
temperature (°C)

Fig.13

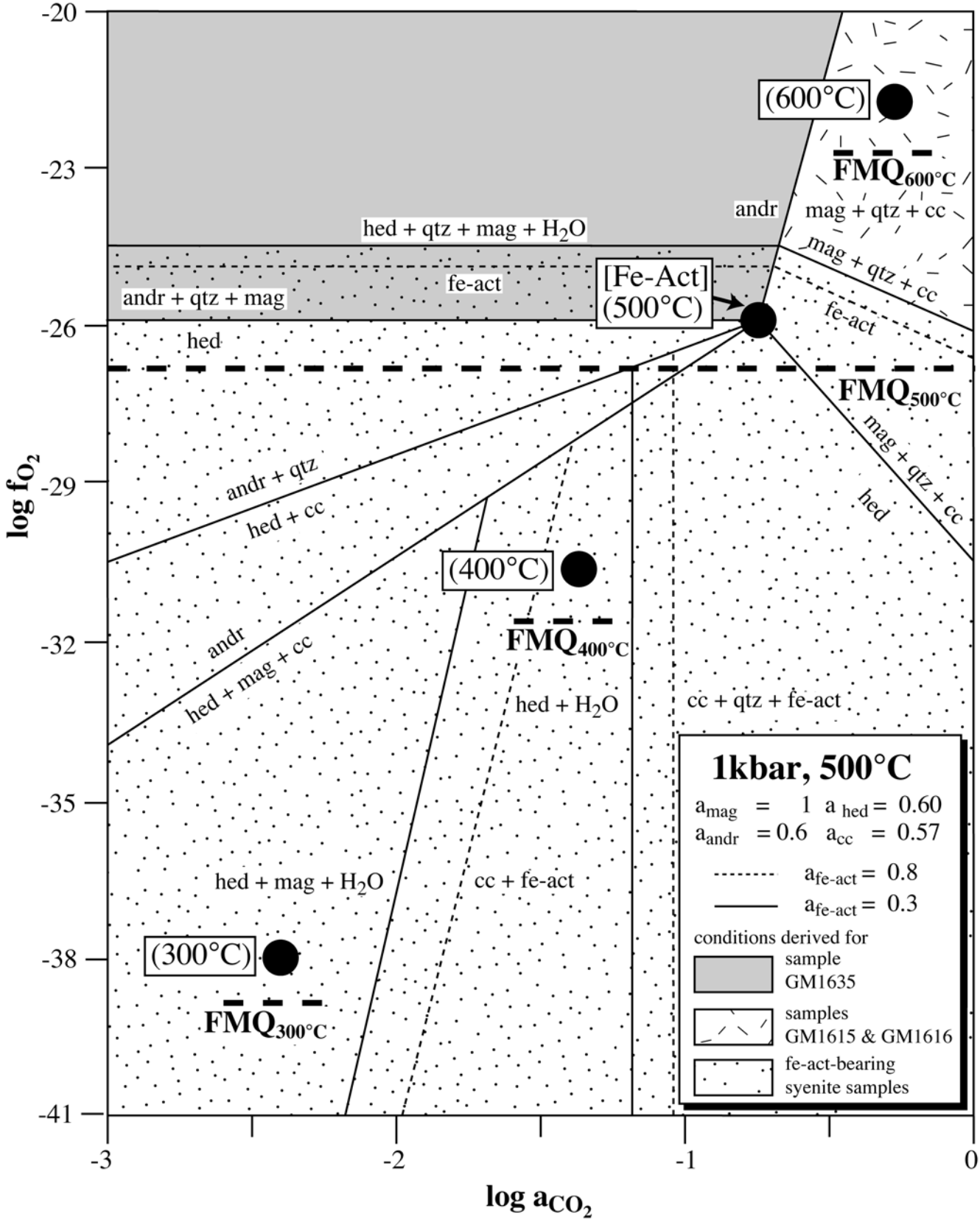
-20
-23
-26
-29
-32
-35
-38
-41
log fO_2
-3
-2
-1
0
log a_{CO_2}
(600°C)
$FMQ_{600°C}$
andr
mag + qtz + cc
hed + qtz + mag + H_2O
fe-act
andr + qtz + mag
[Fe-Act]
(500°C)
mag + qtz + cc
fe-act
hed
$FMQ_{500°C}$
andr + qtz
hed + cc
mag + qtz + cc
hed
(400°C)
andr
hed + mag + cc
$FMQ_{400°C}$
hed + H_2O
cc + qtz + fe-act
hed + mag + H_2O
cc + fe-act
(300°C)
$FMQ_{300°C}$
1kbar, 500°C
a_{mag} = 1 a_{hed} = 0.60
a_{andr} = 0.6 a_{cc} = 0.57
$a_{fe\text{-}act}$ = 0.8
$a_{fe\text{-}act}$ = 0.3
conditions derived for
sample GM1635
samples GM1615 & GM1616
fe-act-bearing syenite samples

Fig.14

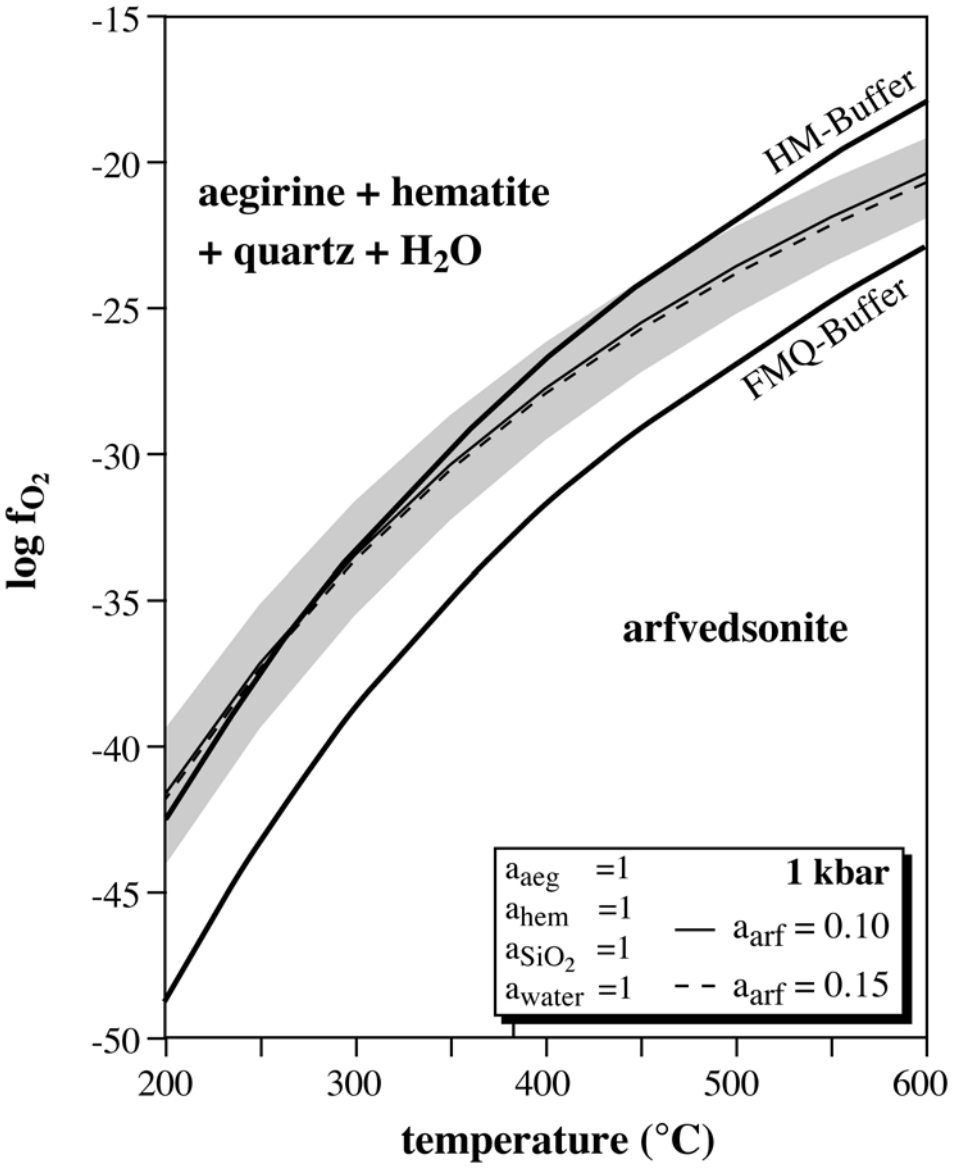
-15
-20
-25
-30
-35
-40
-45
-50
200
300
400
500
600
log f_{O_2}
temperature (°C)
HM-Buffer
FMQ-Buffer
aegirine + hematite
+ quartz + H_2O
arfvedsonite
a_{aeg} =1
a_{hem} =1
a_{SiO_2} =1
a_{water} =1
1 kbar
a_{arf} = 0.10
a_{arf} = 0.15

Fig.15

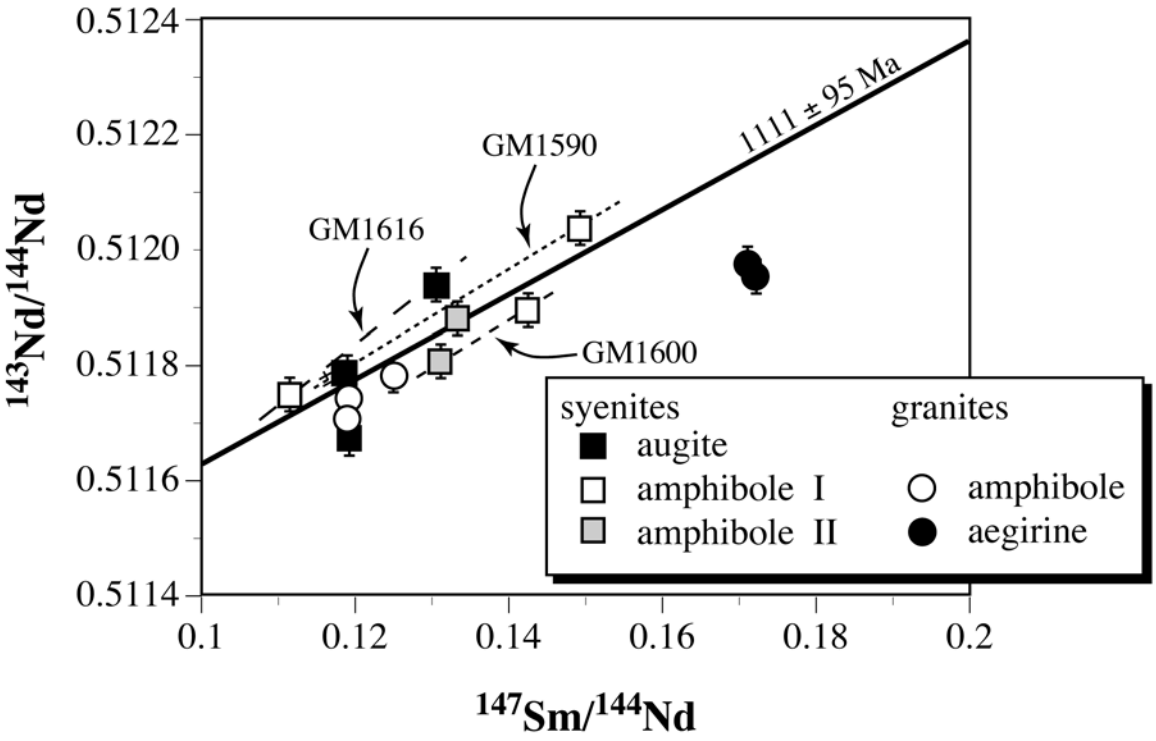
0.5124
0.5122
0.5120
0.5118
0.5116
0.5114
0.1
0.12
0.14
0.16
0.18
0.2
143Nd/144Nd
147Sm/144Nd
1111 ± 95 Ma
GM1590
GM1616
GM1600
syenites
augite
amphibole I
amphibole II
granites
amphibole
aegirine

Fig.16

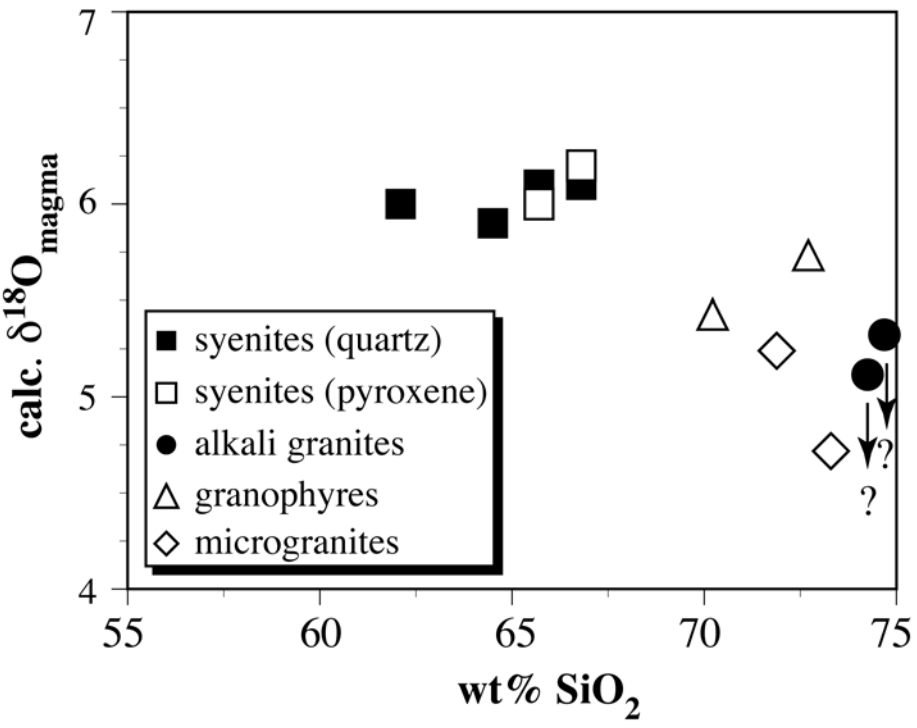
7
6
5
4
55
60
65
70
75
calc. $\delta^{18}O_{magma}$
wt% SiO_2
syenites (quartz)
syenites (pyroxene)
alkali granites
granophyres
microgranites
?
?

Fig.17

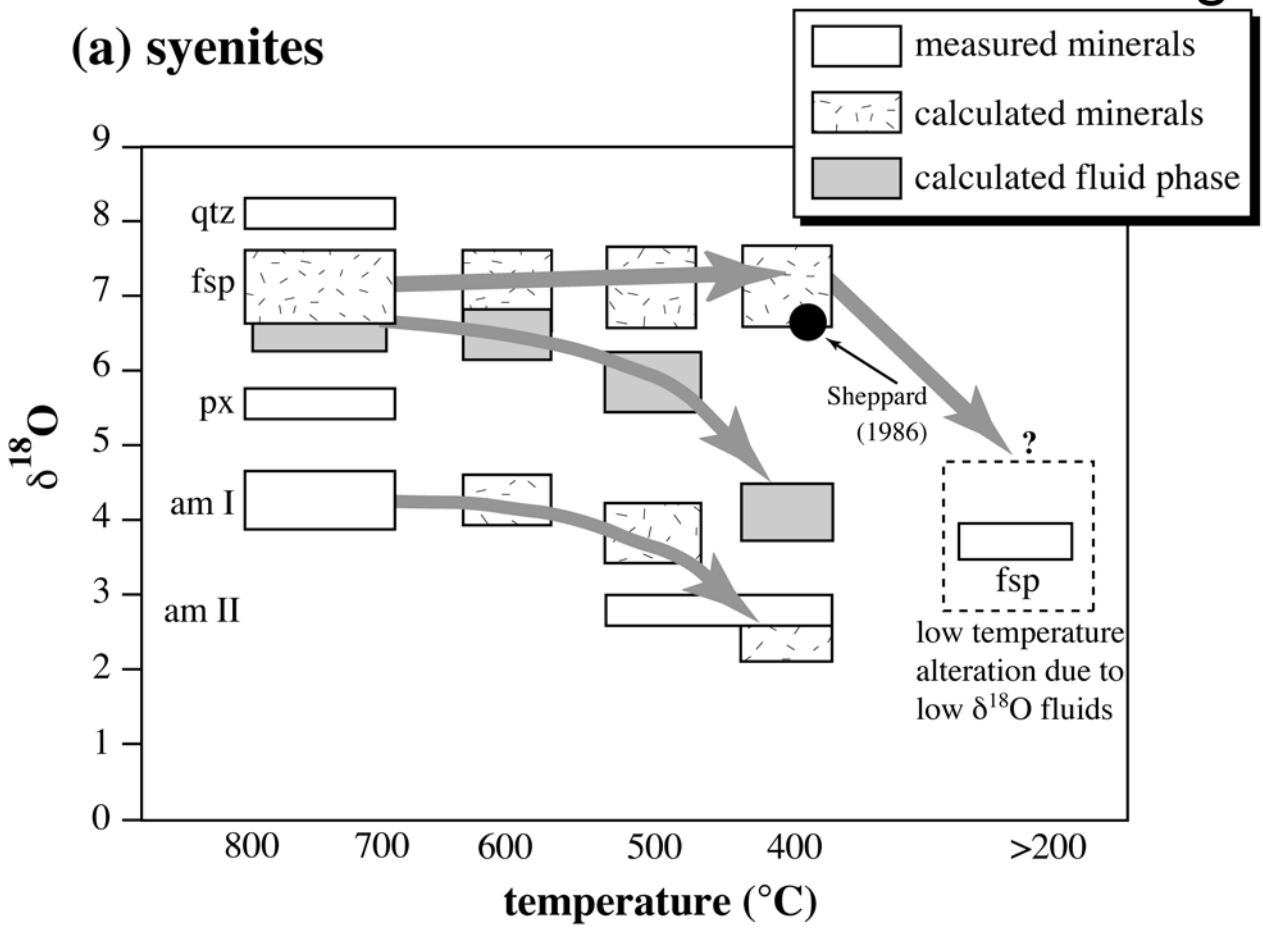
(a) syenites
measured minerals
calculated minerals
calculated fluid phase
qtz
fsp
px
am I
am II
Sheppard
(1986)
?
fsp
low temperature
alteration due to
low δ18O fluids
δ18O
temperature (°C)
800
700
600
500
400
>200

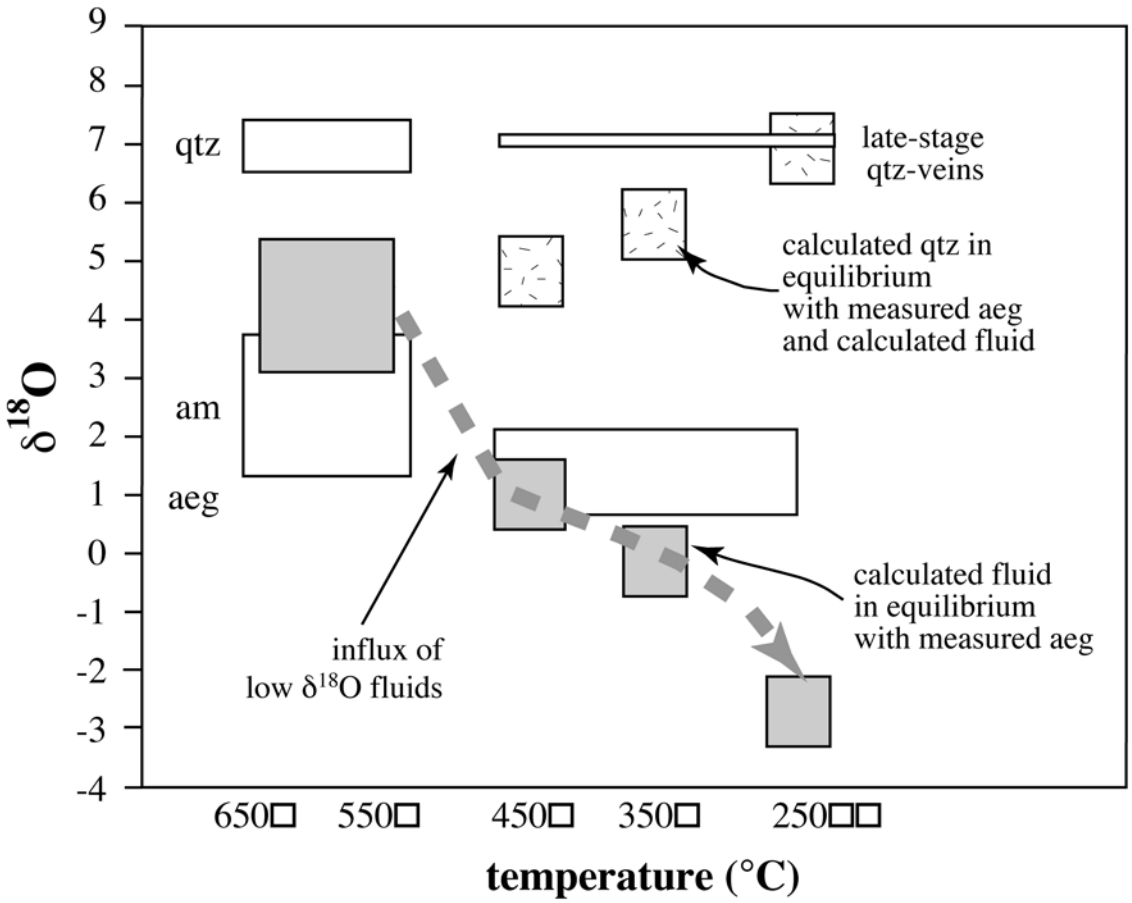
(b) alkali granites
qtz
late-stage
qtz-veins
calculated qtz in
equilibrium
with measured aeg
and calculated fluid
am
aeg
calculated fluid
in equilibrium
with measured aeg
influx of
low δ18O fluids
δ18O
temperature (°C)
650
550
450
350
250

Fig.18

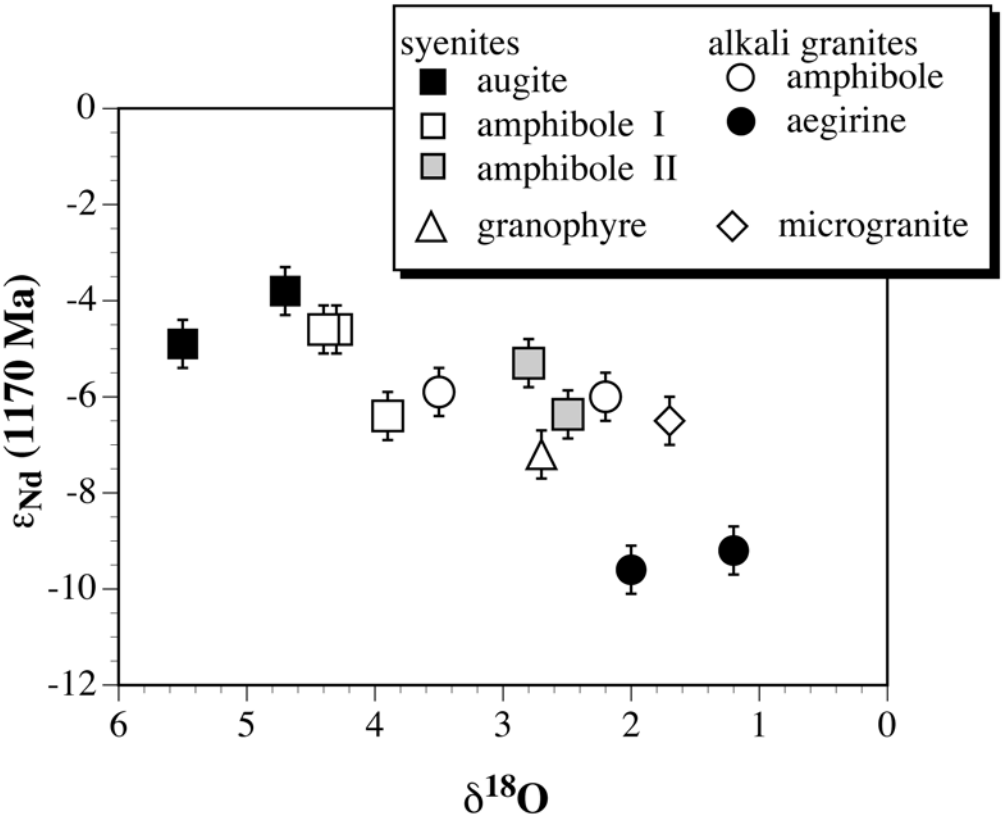
syenites
augite
amphibole I
amphibole II
granophyre
alkali granites
amphibole
aegirine
microgranite
0
-2
-4
-6
-8
-10
-12
6
5
4
3
2
1
0
εNd (1170 Ma)
δ18O

Kapitel 3: Isotopengeochemische Untersuchungen an alkalinen bis agpaitischen Gesteinen der Ilímaussaq Intrusion.

Manuskript-Titel:
DECOUPLING OF O AND H ISOTOPES IN FE-RICH AMPHIBOLES AND STRONG D-DEPLETION DURING MAGMATIC PROCESSES: AN EXAMPLE FROM THE PERALKALINE ILÍMAUSSAQ INTRUSION, SOUTH GREENLAND.

Autoren:
Michael Marks[1], Torsten Vennemann[2], Wolfgang Siebel, Gregor Markl[1]

[1] Institut für Geowissenschaften, Eberhard-Karls-Universität Tübingen, Wilhelmstrasse 56, 72074 Tübingen.

[2] Institut de Minéralogie et Géochimie, Université de Lausanne, BFSH-2, CH-1015 Lausanne, Schweiz.

Eingereicht bei:
Geochimica et Cosmochimica Acta

Eigenanteile:

a) Idee	50 %
b) Probenbeschaffung	80 %
c) Datenbeschaffung	100 %
d) Auswertung und Interpretation	80 %
e) Ausarbeitung der Publikation	80 %

Abstract - Homogeneous oxygen isotope compositions of amphibole, clinopyroxene, and olivine separates (+5.2 and +5.7 ‰ relative to VSMOW) and neodymium isotope compositions ($\varepsilon_{Nd(T)}$ = –0.9 to –1.8 for primary magmatic minerals and $\varepsilon_{Nd(T)}$ = –0.1 and –0.5 for mineral separates from late-stage pegmatites and hydrothermal veins) from the alkaline to agpaitic rocks of the Ilímaussaq intrusion, South Greenland, indicate a closed system evolution of this igneous complex and support a mantle derivation of the magma.

In contrast to the homogeneous oxygen and neodymium isotopic data, δD values for the amphibole separates vary between –92 and –232 ‰ and are among the most deuterium-depleted values measured in igneous amphiboles. Furthermore, the δD values positively correlate with total Fe-contents and Fe^{3+}/Fe^{2+} ratios of the minerals. The calculated fluid phase coexisting with these amphiboles has a homogeneous oxygen isotopic composition within the normal range of magmatic waters, but extremely heterogeneous and low D/H ratios, implying a decoupling of the oxygen- and hydrogen isotope systems. In view of these data and other published data of δD values of minerals and fluids (CH_4 and H_2) from Ilímaussaq, its country rocks, and other alkaline complexes, possible explanations for these extremely low δD values could be:

- They do not reflect primary magmatic values but have been influenced by secondary interaction and re-equilibration with D-depleted H_2O either assimilated from small amounts of organic-rich sediments or obtained through late-stage oxidation of internally generated CH_4 and H_2.
- The measured δD values of the amphiboles reflect the hydrogen isotopic composition of the primary magmatic fluid, but the presently known amphibole-water fractionation factors are in serious error for the $Fe_{(tot)}$- and Fe^{3+}-rich amphiboles that may have formed late and at low pressures.

It is shown that oxidation of magmatic methane to water and re-equilibration of amphiboles with this secondary formed H-depleted water is the most likely explanation for the heterogeneous and extreme δD depletion found.

Keywords: peralkaline, assimilation, hydrogen, oxygen, neodymium, δD depletion, amphiboles, Ilímaussaq

1. INTRODUCTION AND GEOLOGICAL SETTING

Combined studies of oxygen and hydrogen isotope variations in magmatic rocks and minerals can be used to estimate the isotopic compositions and to decipher the origin and evolution of the corresponding melts or fluid phases (e.g., Agemar et al., 1999; Harris and Ashwal, 2002; Dallai et al., 2003). The hydrogen isotopic compositions of hydrous minerals are particularly sensitive indicators of the isotopic composition of the last fluid with which they equilibrated, because most of the hydrous minerals contain relatively small amounts of hydrogen relative to the interacting fluid, except at very small fluid-rock ratios (Gregory and Criss, 1986).

In order to calculate the composition of a fluid phase, which has subsequently been removed from the original mineral-fluid system, it is necessary to know the isotopic fractionation factors between hydrous minerals and fluid. Variables which influence the magnitude of fractionation factors include temperature, pressure, mineral composition, and fluid composition (c.f. Chacko et al., 2001, and references therein). Experimentally determined mineral-water fractionation factors exist for a large variety of important rock-forming minerals (cf. O´Neil, 1986, and references therein). However, for some important mineral-water systems major discrepancies exist between different experimental calibrations and raise questions about the validity of some of the published fractionation curves if extrapolated to extreme compositions, temperatures or pressures.

Although the data base is restricted, it has long been recognized that hydrosilicates of peralkaline igneous rocks typically show very D-depleted isotopic compositions (e.g. Sheppard, 1986a). The reasons for their D-depleted composition are not yet fully understood (Potter et al., 1998). Peralkaline igneous rocks appear to have a magmatic fluid phase, which is commonly rich in methane, but poor in water and the origin of methane-bearing fluids in such systems is a matter of some controversy (e.g., Konnerup-Madsen & Rose-Hansen, 1982; Salvi & Williams-Jones, 1997; Potter et al., 1998).

The Ilímaussaq intrusion, South Greenland is an example for a peralkaline to agpaitic (molar (Na+K)/Al ratio > 1.2) igneous complex, where molecular hydrogen, methane and other hydrocarbons dominate the magmatic fluid phase (e.g. Konnerup-Madsen & Rose-Hansen, 1982). Since the geology, geochemistry, mineral chemistry and petrology of the complex is known in great detail (e.g. Ferguson, 1964; Larsen, 1976; Bailey, et al., 2001; Sørensen, 2001; Markl et al., 2001), we chose this igneous complex to study which processes could be responsible for such extreme D-depletion in magmatic systems.

The Gardar Province of South Greenland (Fig. 1) represents a Mid-Proterozoic (1.1 – 1.3 Ga) failed continental rift structure (Upton and Emeleus, 1987). The Early-Proterozoic (1.80 – 1.85 Ga) basement rocks (I-type calc-alkaline plutonic rocks; Julianehåb batholith; e.g., Kalsbeek and Taylor, 1985; Garde et al., 2002) are in places overlain by a sequence of basalts and sandstones (Eriksfjord Formation; Poulsen, 1964). A large number of dike rocks and twelve major alkaline to peralkaline igneous complexes intrude the basement. The igneous complexes intruded into shallow crustal levels (< 5 km) and they are believed to have had surface expressions (Emeleus and Upton, 1976; Upton et al., 2003). Among these complexes, principally two different sub-groups can be distinguished: those evolving from silica-saturated syenites to alkali granites, following a silica-oversaturated trend, and those following a silica-undersaturated trend, evolving towards nepheline syenites.

The 1.16 Ga old Ilímaussaq complex (Waight et al., 2002) is the only intrusive complex of the Gardar province where both silica-undersaturated and silica-oversaturated rocks occur in significant quantities (Fig. 2). The formation of the complex involved three magma batches, which intruded successively to 3-4 km depth (1 kbar; Larsen and Sørensen, 1987; Konnerup-Madsen and Rose-Hansen, 1984). The earliest melt batch consisted of augite syenite, followed by alkali granite and different varieties of agpaitic syenites (foyaite, sodalite foyaite, naujaite, kakortokite, lujavrite), which comprise the major part of the complex. It is believed that all Ilímaussaq rocks were derived from one parental alkali basaltic magma that fractionated in a deep-seated magma chamber (Nielsen and Steenfelt, 1979; Larsen and Sørensen, 1987; Stevenson et al., 1997). The Sm-Nd whole-rock study and AFC calculations of Stevenson et al. (1997) showed that all of the Ilímaussaq rocks could principally have been derived from the same reservoir through fractional crystallization of a basaltic melt whilst assimilating granitic crust. However, extensive contamination took place only at the margins of the complex (Stevenson et al., 1997; Ferguson, 1964; Marks and Markl, 2001). The petrology and mineral chemistry of the major rock-forming minerals in the various rock types have been presented by Larsen (1976, 1977, 1981), Markl et al. (2001a, b), and Marks and Markl (2001). The fractionation trend found in the Ilímaussaq complex appears to be governed by low water activity and low SiO_2 activity in the parental melt. This results in low oxygen fugacity allowing the co-existence of two immiscible fluids (a methane-dominated gaseous and a saline aqueous fluid phase) during most of the crystallization history (Larsen, 1976; Konnerup-Madsen et al., 1979; Konnerup-Madsen and Rose-Hansen, 1984; Konnerup-Madsen et al., 1988; Konnerup-Madsen, 2001; Markl et al., 2001a; Marks and Markl, 2001).

We present a detailed Nd-, O-, and H-isotopic study on mineral separates of the major rock types and late-stage hydrothermal veins of the Ilímaussaq intrusion. The oxygen and neodymium data are used to show that the complex largely represents an isotopic homogeneous magma, which evolved in a principally closed system. Oxygen and hydrogen isotope data are used to characterize the fluid evolution and to decipher the processes taking place during late- to post-magmatic cooling, which could be responsible for the unusually low hydrogen isotopic compositions found in some peralkaline to agpaitic igneous rocks.

2. PETROGRAPHY AND MINERAL CHEMISTRY

(this section in small type)

2.1. Sample description

From each of the major rock types of the complex, one representative sample was selected for mineral chemical, oxygen, hydrogen, and neodymium isotope analyses. Additional samples were selected from late-stage pegmatites, dikes and mineralized veins. The sample localities are shown on Fig. 2. Detailed descriptions of the major rock types have been given in many publications (e.g. Ferguson, 1964). Therefore, only brief descriptions of the investigated samples of this study are given with special focus on amphibole and aegirine textures, since most Nd, O, and H isotope analyses were performed on separates of these minerals. The mineral chemistry and petrology of some of the samples analyzed here have already been discussed in Markl (2001b), Markl et al. (2001a), and Marks and Markl (2001).

2.1.1. Augite syenite (GM1330)

Early magmatic phases are alkali feldspar, apatite, baddeleyite, olivine, augite, Ti-magnetite, and less abundant amphibole (Fig. 3a). Nepheline occurs as an interstitial phase. Fine-grained biotite and amphibole form small rims around olivine, augite or Ti-magnetite and are believed to be of late-stage origin (Fig. 3b). Magmatic and late-stage amphibole can be distinguished by their different grain size: magmatic amphibole can reach a size of up to 2 mm, whereas late-stage amphibole rims are less than a few hundreds of micrometers thick.

2.1.2. Alkali granite (GM1303)

The sample is coarse-grained and equigranular. Euhedral amphibole, alkali feldspar, and zircon are early magmatic phases, abundant quartz occurs interstitially. In some places, late-stage aegirine aggregates overgrow early magmatic amphibole (Fig. 3c).

2.1.3. Agpaitic syenites (GM1214, GM1370, GM1335, GM1337)

Early magmatic phases in the medium- to coarse-grained nepheline-syenites are alkali feldspar, nepheline, sodalite, amphibole, olivine and augite. The latter two occur only as rare relics in sample GM1214 (sodalite foyaite). Depending on the type of agpaitic syenite, interstitial phases are aegirine-augite, aenigmatite, fluorite, eudialyte, amphibole, sodalite and nepheline (Figs. 3d-g). Late-stage minerals are biotite, aegirine, and analcime. One fine-grained agpaitic rock type (lujavrite, GM1843) shows fluidal textures. Early mineral phases in this sample are euhedral nepheline, eudialyte, and sodalite, which are enclosed in a fine-grained mixture of albite, microcline, and later generations of aegirine and arfvedsonite (for more details see e.g., Ferguson, 1964).

2.1.4. Agpaitic dike rock (GM1849)

Southeast of the Ilímaussaq intrusion, an agpaitic dike, several meters in thickness, is believed to be closely related to the Ilímaussaq rocks and can be traced for about 18 km. (Allaart, 1969; Larsen and Steenfelt, 1974). Phenocrysts in the analyzed sample are olivine, augite, magnetite, alkali feldspar and nepheline (Fig. 3l). The groundmass consists of aegirine, aenigmatite, arfvedsonite, albite, microcline, nepheline, and sodalite. A detailed study on the petrology of this dike rock is presented elsewhere (Marks and Markl, submitted). Similar dike rocks from other parts of the Ilímaussaq intrusion have been described by Rose-Hansen and Sørensen (2001).

2.1.5. Agpaitic dike with ocelli textures (GM1212)

Some agpaitic dikes exhibit spectacular features of macroscopically visible liquid immiscibility. They can be found at several places distributed over the whole intrusion. These dikes are up to several hundreds of meters in length, but less than a meter in width. They consist of a fine-grained black matrix and light grayish to greenish rounded and partly deformed ocelli (Fig. 3i). A detailed description and discussion of these rocks is given by Markl (2001b). The sample analyzed for this study consists of splits from the black and fine-grained matrix of sample GM1212, which is modally dominated by tiny euhedral amphibole.

2.1.6. Agpaitic pegmatite (GM1390)

Sample GM 1390 is an agpaitic pegmatite (Fig. 3j). It consists of cm-to dm-sized K-feldspar and arfvedsonitic amphibole. The latter is overgrown by some mm-thick coatings of aegirine.

2.1.7. Aegirine vein (GM1257)

Millimeter- to cm-thick veins of aegirine, albite and analcime are abundant in the whole complex. They crosscut all other rock types and are therefore believed to represent products of late-stage hydrothermal fluids. Sample GM1257 is a compositionally zoned aegirine vein, which crosscuts naujaite (Fig. 3k). The margins of the vein are dominated by bottle-green needle-shaped aegirine growing towards the center of the vein, where albite and analcime are the dominant minerals. Similar

aegirine-rich veins are known from other localities in the Gardar Province and have been described by Ranløv and Dymek (1991).

2.2. Chemical composition of the Ilímaussaq amphiboles

Major element compositions of amphiboles were determined using a JEOL 8900 electron microprobe at the Institut für Geowissenschaften of the Universität Tübingen, Germany. Details of working conditions and standards used are given in Marks et al. (in press). Li, Zn, and Zr contents were measured by in-situ laser ablation inductively coupled plasma-mass spectrometry (LA-ICP-MS) at the EU Large Scale Geochemical Facility (University of Bristol) using a VG Elemental PlasmaQuad 3 + S-Option ICP-MS equipped with a 266 nm Nd:YAG laser (VG MicroProbe II). Details of the method are described in Halama et al. (2002).

Amphibole occurs in all major rock types as an early magmatic or interstitial mineral phase. This was the reason why we chose it for Nd, O and H isotope analyses. Representative microprobe analyses of amphiboles from the different Ilímaussaq rocks are shown in Table 1. Mineral formulae are based on 16 cations and 23 oxygens, assuming a completely filled A site. Amphibole analyses from sample GM1212 have been published by Markl (2001b). Some further amphibole analyses from the Ilímaussaq rocks are found in Larsen (1976). Amphibole composition ranges from almost pure Ca-amphibole (ferro-edenite, ferro-pargasite) in the early augite syenite via Na-Ca amphibole (katophorite, ferro-richterite) to Na-amphibole (nyböite, arfvedsonite) in the agpaitic rocks (Fig. 4). In the more evolved agpaites, amphibole has high contents of Li (up to 2500 ppm), Zn (5600 ppm), and Zr (5000 ppm) and evolves towards ferro-leakeite composition. The major substitutions observed in this comagmatic suite are $CaAl^{[IV]}$ ‹-› NaSi and Fe^{3+} ‹-› $Na^{[A]}Fe^{2+}$ with a filling of the A site. Incorporation of Li occurs mainly according to Li + Fe^{3+} ‹-› 2(Fe^{2+}, Mg, Mn) and Li + Fe^{3+} ‹-› $Al^{[IV]}$ + Na.

3. ISOTOPE GEOCHEMISTRY

3.1. methods

(this section in small type)

Nd isotopic analyses were performed on about 10 mg of handpicked mineral separates. They were spiked with ^{150}Nd - ^{149}Sm tracers before dissolution under high pressure in HF acid at 180°C in poly-tetrafluor-ethylene (PTFE) reaction bombs. Sm and Nd were separated and measured as described in Marks et al. (in press). The $^{143}Nd/^{144}Nd$ ratios were normalized to $^{146}Nd/^{144}Nd = 0.7219$, the Sm isotopic ratios to $^{147}Sm/^{152}Sm = 0.56081$. Analyses of 11 separate loads of Ames metal (Geological Survey of Canada, Roddick et al., 1992) during this study, gave a $^{143}Nd/^{144}Nd$ ratio of 0.512145 ± 24 (± 2σ error of the mean), 11 loads of the La Jolla standard yielded a $^{143}Nd/^{144}Nd$ ratio of 0.511829 ± 30. Total procedural blanks (chemistry and loading) were < 100 pg for Nd. A decay constant of 6.54 x 10^{-12} a^{-1} for ^{147}Sm (Lugmair and Marti, 1978) was used. $\varepsilon_{Nd(T)}$ values were calculated

using present day CHUR values of 0.1967 for $^{147}Sm/^{144}Nd$ (Jacobson and Wasserburg, 1980) and 0.512638 for $^{143}Nd/^{144}Nd$ (Goldstein et al., 1984). Calculated uncertainty in $\varepsilon_{Nd(T)}$ units based on analytical errors is not more than 0.5. Initial Nd isotope ratios of minerals were corrected for an age of 1160 Ma.

The oxygen isotope composition of the whole-rock sample GM1212 was determined using a modified version of the conventional method after Clayton and Mayeda (1963), with BrF_5 as reagent and converting the liberated oxygen to CO_2 prior to mass spectrometric analyses. The oxygen isotope composition of handpicked mineral separates was determined using a method adapted after Sharp (1990) and Rumble and Hoering (1994). Details of the method are described in Marks et al. (in press). The D/H ratios of amphibole separates and sample GM1212 were determined from about 100 to 200 mg of sample according to the method of Vennemann and O´Neil (1993).

Oxygen and hydrogen isotopic compositions were measured on a Finnigan MAT 252 isotope ratio mass spectrometer. The results are given in the standard δ-notation, expressed relative to VSMOW in permil (‰). Replicate oxygen isotope analyses of the standards (NBS-28 quartz and UWG-2 garnet; Valley et. al., 1995) had an average precision of ± 0.1 ‰ for $\delta^{18}O$. The precision of the in-house kaolinite standard for hydrogen isotope analyses was better than ± 2 ‰.

3.2. Sm-Nd systematics

12 mineral separates from 10 samples and one whole-rock sample (GM1212) were analyzed for their Sm and Nd concentrations and their Nd isotopic compositions (Table 2). The range in Sm (0.4 to 84 ppm in amphibole, 596 ppm in whole-rock) and Nd (3.9 to 432 ppm in amphibole, 4760 ppm in whole-rock) concentrations is relatively large. The lowest concentrations were found in minerals of an agpaitic pegmatite (GM1390), the highest concentrations were measured in the agpaitic dike whole rock sample (GM1212).

Fig. 5 shows the Sm-Nd isotopic data in a conventional isochron diagram. The data define a single isochron. Two separates of amphibole from alkali granites and the agpaitic dike rock show the most pronounced deviations from the general trend in that they are shifted to significantly lower and higher $^{143}Nd/^{144}Nd$ ratios, respectively. Omitting these data, an age of 1160±30 Ma is obtained for the remaining data, which is in agreement with previous datings (see above).

Overall, the Ilímaussaq samples range from $\varepsilon_{Nd(T)}$ = -0.1 to -3.1 with the lowest value for the alkali granite (Fig. 6). Two mineral separates of the augite syenite (augite, amphibole) yield indistinguishable values of about –1. The calculated $\varepsilon_{Nd(T)}$ values for agpaites are identical within analytical error and span a small range between $\varepsilon_{Nd(T)}$ = -1.1 and -1.8. Minerals from the late-stage samples GM1257 and GM1390 have relatively high $\varepsilon_{Nd(T)}$ values between -

0.1 and -0.5. Amphibole from the micro-kakortokite dike (GM1849) has a positive $\varepsilon_{Nd(T)}$ value of +0.7. Nd-model ages (Liew and Hofmann, 1988) range between 1.65 and 1.96 Ga with the youngest value for amphibole from the agpaitic dike (GM1849) and the oldest value for amphibole from the alkali granite (GM1303).

3.3. Oxygen and hydrogen isotope compositions

Measured $\delta^{18}O$ and δD values are presented in Table 2. The $\delta^{18}O$ values of all samples are between +4.6 and +5.7 ‰ with the lowest value obtained for amphibole of the agpaitic dike rock GM1849. All other amphiboles have similar values between +5.3 and +5.7 ‰ (Fig. 6). $\delta^{18}O$ values measured for aegirine, olivine, augite, and the whole-rock sample GM1212 fall in the range of measured values for amphiboles.

δD values for amphibole separates and the whole-rock sample GM1212 are between -232 and -92 ‰. The lowest value was measured for amphibole from the alkali granite, the highest for amphibole from the augite syenite; the agpaitic samples fall within this range. With the exception of amphibole from the augite syenite, the hydrogen isotope compositions are among the most D-depleted igneous amphiboles yet recorded (c.f. Sheppard, 1986a).

4. DISCUSSION

4.1. Magma source and evolution

Excluding the amphibole from the agpaitic dike (GM1849), the similarity in oxygen isotope compositions of the minerals implies a parental melt homogeneous with respect to oxygen isotopes. The small fractionation between augite (+5.6 ‰) and olivine (+5.3 ‰) in the augite syenite is typical for high temperature equilibrium. Because mineral-melt fractionations at magmatic temperatures are small for olivine, augite, and amphibole (Taylor and Sheppard, 1986; Mattey et al., 1994) and because these minerals are known to have high closure temperatures for oxygen diffusion (Farver and Giletti, 1985; Farver, 1989; Gérard and Jaoul, 1989), the estimated $\delta^{18}O_{melt}$ values for all Ilímaussaq melt(s) is about 6.0 ‰. This value is well within the range typical for syenitic bodies (e.g., Taylor and Sheppard, 1986; Lutz et al., 1988; Harris, 1995; Dallai et al., 2003) and supports a principle mantle derivation of the magmas (c.f., Kyser, 1986; Eiler, 2001).

A similar homogeneity is observed in the Nd isotope compositions (Fig. 6). With the exception of amphibole from the alkali granite and from the agpaitic dike, the initial $\varepsilon_{Nd(T)}$ values overlap within analytical error and are similar to most of the whole-rock data from Stevenson et al. (1997). Furthermore, there is no significant difference in $\varepsilon_{Nd(T)}$ values between

amphibole separates of the major rock types and amphibole of late-stage samples. The observed homogeneity implies a closed system during the evolution of the Ilímaussaq melts. Even during late-stage crystallization in pegmatites and hydrothermal veins, no major influence of an external source can be detected. The occurrence of contaminated samples at the margins of the complex shows that greater amounts of assimilation of country rock occurred only on a local scale (Ferguson, 1964; Stevenson et al., 1997; Marks and Markl, 2001). Assuming a homogeneous mantle source and closed system behavior during crystallization for most of the Ilímaussaq melts and late-stage pegmatites and veins, our Nd data would indicate a mantle source slightly enriched in ^{18}O and depleted in ^{147}Sm compared to the bulk mantle. In contrast to Stevenson et al. (1997), who believe that the parental melt for the Ilímaussaq rocks was derived from a depleted mantle, we favor a model where the Ilímaussaq rocks are derived from a mantle source depleted in ^{147}Sm compared to normal mantle values, either because of mantle metasomatism prior to melting (Upton, 1987; Goodenough et al., 2002) or because the mantle source has been modified by plume material (Nicholson and Shirey, 1990; Zindler and Hart, 1986; Halama et al., in press).

There are two significant outliers in the present data set: amphibole from the alkali granite has a lower $\varepsilon_{Nd(T)}$ value of -3.1, whereas amphibole from the agpaitic dike rock has a positive $\varepsilon_{Nd(T)}$ value of +0.7. The origin of the alkali granite can be explained by significant amounts of crustal contamination (see below). A discussion of the relevance of the agpaitic dike rock is presented elsewhere (Marks and Markl, submitted).

The less radiogenic $\varepsilon_{Nd(T)}$ value of the alkali granite has been explained by extensive contamination of the basaltic or syenitic magma with country rock melts (Stevenson et al., 1997). Potential contaminants to explain the quartz-saturated alkali granite include sandstones of the Eriksfjord formation, the surrounding Julianehåb granite, or lower crustal rocks that, however, are not exposed at the present surface but may occur beneath the Julianehåb batholith (Dahl-Jensen et al., 1998). Table 3 shows oxygen and neodymium isotopic data as well as Nd concentrations for possible contaminants. A concentration of 80 ppm Nd (Bailey et al., 2001) is used as an approximation for the augite syenite melt. For the granitic upper crust a typical Julianehåb granite sample from the vicinity of the complex is taken (Halama, unpublished data). Neodymium and oxygen isotope data for sandstones of the Eriksfjord Formation are from Andersen (1997) and from Halama (unpublished data), respectively. For a potential lower crust, oxygen data from Fowler and Harmon (1990) and neodymium data from siliceous Archaean gneisses (Taylor et al., 1984) are used as an approximation. If we apply a two-component mixing model (Pushkar et al., 1972), the amount of these potential

contaminants necessary to explain the neodymium isotopic composition of the alkali granite via contamination of the augite syenitic melts can be calculated using the following equation:

$$\%\ \text{amount of contaminant} = \frac{C_{Nd}^{augitesyenite} * (\varepsilon_{Nd}^{alkaligranite} - \varepsilon_{Nd}^{augitesyenite})}{C_{Nd}^{contaminant} * (\varepsilon_{Nd}^{contaminant} - \varepsilon_{Nd}^{alkaligranite})} \qquad (1)$$

Using this formula, it appears, that sandstones of the Eriksfjord Formation are not valid as a potential contaminant because of their very low Nd concentration. For the granitic upper crust the amount of bulk assimilation was calculated to be about 60 %, which appears un-realistic on energetic reasons. Furthermore, such high amounts of assimilation would result in $\delta^{18}O_{melt}$-values of about 7 ‰, which is not compatible with the present data for the minerals. However, bulk assimilation of about 13 % of lower crust would explain the neodymium isotopic composition of the alkali granite and would result in a $\delta^{18}O_{melt}$-value of 6.2 ‰, which is in the range of calculated $\delta^{18}O_{melt}$-values. Our preferred interpretation is therefore, that during ascent of the augite syenite magma, parts of it became more contaminated with lower crustal melts than others and thereby reached quartz-saturation.

However, for the discussion of the H-isotope data below, the important conclusion is, that the whole complex (with the exception of the alkali granite) evolved from a rather homogeneous magma in a closed system without any significant sign of contamination during ascent, emplacement, cooling, and final crystallization of the different melt batches.

4.2. Discussion of the hydrogen isotope compositions

With the exception of amphibole from the augite syenite, our reported hydrogen isotope compositions are well off the range typical for amphiboles in igneous rocks (δD= -90 to -50 ‰; Hoefs, 1997) and are among the most D-depleted igneous amphiboles yet recorded (c.f. Sheppard, 1986a). Similarly low δD values from igneous amphiboles have been reported for one arfvedsonite of the peralkaline Red Wine Complex, Labrador, (-160 ‰) and for two samples of arfvedsonite from nepheline syenites of the Norra Kärr Intrusive Complex, Sweden (-130 ‰ and -150 ‰; Sheppard, 1986a). These low values may hint to a common process that controls the hydrogen isotope compositions of amphiboles in peralkaline to agpaitic rocks. Typical for such agpaitic igneous rocks is their extreme Fe-enrichment during fractionation under relatively reduced conditions and the existence of an exsolved CH_4-dominated fluid phase. Various fluid inclusion studies (Larsen, 1976; Konnerup-Madsen et al., 1979; Konnerup-Madsen and Rose-Hansen, 1984; Konnerup-Madsen et al., 1988;

Konnerup-Madsen, 2001; Markl et al., 2001) showed that, with the exception of the alkali granite, primary fluid inclusions of the Ilímaussaq rocks are methane-dominated with lesser amounts of H_2 and higher hydrocarbons, but only with traces of H_2O and CO_2. Similar hydrocarbon-rich fluids have been described from other peralkaline complexes worldwide (e.g. Salvi and Williams-Jones, 1997; Potter et al., 1998) of which, however amphibole δD data are lacking (Potter, pers. comm.).

The measured oxygen and hydrogen isotopic compositions of the amphiboles (Table 2) can be used to calculate the isotopic composition of a coexisting fluid phase. Amphibole-water oxygen isotope fractionation between 500° and 800°C is approximately -1 to -2 ‰ (Zheng, 1993), indicating a relatively homogeneous oxygen isotopic composition of the fluid of between +6.3 and +7.6 ‰ in equilibrium with the amphiboles of this study. The calculated fluid of the agpaitic dike, has a relatively low $\delta^{18}O$ value of between +5.4 and +6.4 ‰.

For the very Fe-rich amphiboles of Ilímaussaq (Table 1) amphibole-water hydrogen isotope fractionation at final equilibration temperatures of 350°C can be as large as about -65 to -77 ‰ (expressed as $1000ln\alpha_{amph\text{-}water}$) according to the calibration of Suzuoki and Epstein (1976) for the given mineral compositions (Table 1), or as low as -23‰ according to the calibration of Graham et al. (1984). Using, as a maximum estimate for the D/H ratios of water, the amphibole-water hydrogen isotope fractionations of Suzuoki and Epstein (1976), the δD values calculated for water in equilibrium with the amphiboles of this study are extremely heterogeneous: -12 ‰ (augite syenite), -43 to -116 ‰ (agpaitic rocks) and -154 ‰ (alkali granite). Fig. 7 shows the calculated $\delta^{18}O_{fluid}$ and δD_{fluid} values relative to ranges typical for ocean water, meteoric waters, primary magmatic waters, metamorphic waters, and waters that exchanged with or originated from organic matter (Sheppard, 1986b). The observed heterogeneity and the exceptionally low calculated δD_{fluid} values are in direct contrast to the rather homogeneous $\delta^{18}O$ values. This indicates that these two isotope systems are decoupled and may suggest, that H-bearing molecules other than water are responsible for their existence.

Stable isotope measurements of methane extracted from fluid inclusions provided δD values between -132 and -145 ‰ (Konnerup-Madsen and Rose-Hansen, 1988; Konnerup-Madsen, 2001), which are very similar to isotopic compositions measured for fluid inclusions from the alkaline igneous rocks of the Lovozero Massif (δD values of methane between -132 and –167 ‰; Nivin et al., 1995). Water calculated to be in equilibrium with this methane has a δD value of about -65 to -75 ‰ (Richet et al., 1977; Horibe and Craig, 1995), which is within the range of values typical for magmatic water (Konnerup-Madsen and Rose-Hansen,

1988). The discrepancy between the hydrogen isotopic composition of amphiboles and methane from fluid inclusions is a further indication for the above-mentioned decoupling of the H- and O-isotope system.

We will now explore first the various possibilities, how the very low δD values of the Ilímaussaq amphiboles could be generated. Then we will discuss the significance of the decoupling of the O and H isotope system and lastly, we will propose a process that could account for both of these features.

One possibility to generate such low δD values would be a late-stage exchange with low δD meteoric waters (e.g. Taylor, 1974; Brandriss et al., 1995; Nevle et al., 1994; Agemar et al., 1999). For Ilímaussaq rocks considered in this study, however, there is no mineralogical evidence for an extensive meteoric low-temperature alteration. There is also no indication of such an exchange for the oxygen isotopic composition of the amphiboles studied, even for the most H-depleted amphibole of the alkali granite (Fig. 7), nor do the whole-rock stable isotope compositions of the surrounding volcanic rocks of the Eriksfjord Formation have any unusual δD values that could argue for hydrothermal circulation of meteoric fluids (Sheppard, 1986a; values of around –80 ‰).

Another possibility, which has been shown to result in low δD values of rocks and minerals is an extreme degassing of magmatic fluids (e.g., Nabelek et al., 1983; Taylor et al., 1983). However, such a process would destabilize the formation of late-formed amphibole and would require almost complete degassing in order to lower the δD-values to those measured in this study. Preferential degassing of molecular H_2, in contrast, is a common mechanism for the oxidation of magmatic liquids (Sato, 1978; Mathez, 1984). An increase of the oxidation state of the melt may occur by redox reactions such as:

$$2\ Fe^{2+}_{(melt)} + 2\ H_2O \qquad 2\ Fe^{3+}_{(melt)} + 2\ OH^- + H_2 \qquad (2)$$

Fig. 8 shows the range of $Fe_{(tot)}$ and Fe^{3+}/Fe^{2+} ratios observed in amphiboles of the different rock types versus the measured δD value. With the exception of amphiboles from the alkali granite, these parameters show inverse correlations. If the Fe^{3+}/Fe^{2+} ratio of the amphiboles directly reflects the oxidation state of the parental melt, the augite syenite melt was more reduced than the agpaitic and the alkali granite melts. This is in good accordance with petrological results (Larsen, 1976; Markl et al., 2001) and fluid inclusion studies (Konnerup-Madsen et al., 1979; Konnerup-Madsen and Rose-Hansen, 1984; Konnerup-Madsen et al., 1988; Konnerup-Madsen, 2001). During fractionation and cooling of the melt, the water

content increased supporting progress of reaction (2). The oxidation of ferrous iron into its ferric state released molecular hydrogen, which was depleted in deuterium relative to water (around 200 ‰ at 700°C; Horibe and Craig, 1995). An amphibole crystallizing from the melt can be expected to be in hydrogen and oxygen isotope equilibrium with the coexisting magmatic water. Hence, if significant degassing of H_2 occurs during melt crystallization and formation of amphibole at increasingly oxidizing conditions, δD values of amphibole should actually increase with increasing Fe^{3+}/Fe^{2+} ratios. This is not observed, however, suggesting that this internal buffering mechanism and accompanying loss of H_2 is not a viable process to account for the change in δD values.

A third explanation for the low δD values found in the amphiboles from different peralkaline igneous rocks could be the assimilation of organic-rich sediments (Sheppard, 1986a). This suggestion would be compatible with the lowest δD values measured for the alkali granite. However, a number of arguments argue against this interpretation in the case of the Ilímaussaq intrusion. First, in the whole Gardar province, no organic-rich sediments are known, and hence, the possible contaminant is lacking. Furthermore, based on our oxygen and neodymium isotope data, upper crustal contamination in most samples appears to be limited, allowing relatively small amounts of a H-rich contaminant only. A net addition of H_2, possibly sourced from the decay of organic matter to the amphiboles is also not supported by the negative correlation between calculated Fe^{3+}/Fe^{2+} ratios and the δD values for the amphiboles of this study (Fig. 8). The strongest arguments against the organic contaminant hypothesis, however, is provided by the observed distribution and type of hydrocarbon inclusions (Konnerup-Madsen, 2001) combined with their stable isotope composition isotopic data from methane of fluid inclusions, which point to an abiogenic origin of methane with a H-isotopic composition typical for magmatic water (Konnerup-Madsen and Rose-Hansen, 1988).

A further possibility to explain the low δD values of the Ilímaussaq amphiboles would be the oxidation of magmatic methane. This process will be explored below in the context of the following discussion.

Now we discuss several possibilities that may account for the apparent discrepancy in H-isotopic composition of water calculated to be in equilibrium with the amphiboles and that calculated to be in equilibrium with methane:

- Analytical problems of the measurements of the hydrogen isotope compositions of methane or amphibole.

- The amphibole-water or methane-water fractionation factors as given by Suzuoki and Epstein (1976), Graham et al. (1984), and Richet et al. (1977), Horibe and Craig (1995) are not applicable to the Fe-rich system studied here.
- Methane in fluid inclusions and water incorporated as hydroxyl-groups in amphiboles has never been in isotopic equilibrium.
- Methane in fluid inclusions and water incorporated as hydroxyl-groups in amphiboles have been in isotopic equilibrium, but at least one of them changed its primary isotopic composition by a secondary process.

The first possibility is difficult to evaluate. However, given that measurements of isotopic compositions from different populations of fluid inclusions and different amphiboles, both measured for rocks from different alkaline complexes using different analytical techniques in different laboratories have very similar results, suggests that the measurements are representative. Furthermore, if we use data from Konnerup-Madsen et al. (1981) we can roughly estimate the molar effect of hydrogen from methane and molecular hydrogen from the fluid inclusions on the total hydrogen extracted from hydroxyl-groups of amphibole to be in the order of 0.1 to 0.8 %. Consequently, despite the relatively large fractionation factors between H_2, CH_4 and H_2O, we can treat this amount as negligible and thus, our measured δD values for amphiboles reflect the isotopic composition of structural water in the analyzed amphiboles and, not the composition of water derived from fluid inclusions. The possibility that the investigated amphiboles are OH-free but H-bearing, could also result in low amphibole δD values because of the large water-H_2 hydrogen isotope fractionation factors. However, the totals of the microprobe analyses as well as infrared measurements that demonstrated the characteristic OH-stretching bands at wave numbers between 3650 and 3660 cm^{-1} in all investigated samples argue against this possibility.

The second possibility covers the application of methane-water and amphibole-water fractionation factors. The present theoretical and experimental calibrations of the methane-water hydrogen isotope fractionations (Richet et al., 1977; Horibe and Craig, 1995) are in reasonable agreement with maximum differences of less than 12 ‰ between the calibrations. In contrast, the amphibole-water hydrogen isotope fractionations as given by Suzuoki and Epstein (1976) and Graham et al. (1984) are in obvious disagreement especially on the effects of Fe on mineral-water fractionations. The reasons for the disagreement are not directly known, but at least some of the differences may relate to differences in pressures used for the experiments (Driesner, 1997; Horita et al., 1999; Chacko et al., 2001). Using a maximum pressure correction for the Ilímaussaq samples, which may be applicable, as the intrusion

depths are fairly shallow, calculated δD values of water in equilibrium with the amphiboles would shift by +30 ‰ (Driesner, 1997; Horita et al., 1999), still extending towards values unlike those for typical magmatic waters (Fig. 7). The rough negative correlation between $Fe_{(tot)}$ and Fe^{3+}/Fe^{2+} ratios of amphiboles and the measured δD values (Fig. 8) supports the conclusions on effects of Fe on D-H fractionations between minerals and water by Suzuoki and Epstein (1976) in principle. However, given the general mineral-water calibration of Suzuoki and Epstein (1976), which relates the fractionation factor to the composition of the minerals, the calculated variation in $1000ln\alpha_{amph\text{-}water}$ for the present minerals amounts to about 13 ‰ only. This is much smaller than the observed variation in δD values of the amphiboles and, unless the effect of Fe is much stronger than previously thought (cf. Vennemann and O'Neil, 1996), would still argue for significant heterogeneity in the H-isotopic composition of the fluid. More experimental work on pressure effects and the Fe-dependency of mineral-water fractionation factors under specified pressures is needed to solve this discrepancy.

The third possibility of disequilibrium between the isotopic compositions of amphibole and fluid inclusion methane could be related to temporal differences in their formation. A number of authors suggested that the formation of hydrocarbons could be related to late- or post-magmatic alteration of Fe-rich minerals resulting in the production of H_2 (e.g., Salvi and Williams-Jones, 1997; Potter et al., 1998). For the Strange Lake peralkaline complex (Salvi and Williams-Jones, 1997) and for Khibina and Lovozero (Potter et al., 1998; Potter, 2002) textural evidence was interpreted to support a secondary origin of CH_4-dominated fluid inclusions, leading to the suggestion that these reduced fluids formed during late hydrothermal activity. The released molecular hydrogen is strongly depleted in D compared to methane or water. If secondary re-equilibration between released hydrogen and primary amphibole occurs (Vennemann and O´Neil, 1996), this process could easily explain the analyzed δD compositions, since fractionation between hydrogen and water is several hundreds of permil even at moderate temperatures (Horibe and Craig, 1995). For the Ilímaussaq rocks, however, fluid inclusions are at least partly of primary origin and there is no evidence for disequilibrium between host minerals and enclosed fluid inclusions (Konnerup-Madsen and Rose-Hansen, 1988, Konnerup-Madsen, 2001).

Fourth, if methane in fluid inclusions and amphiboles once have been in isotopic equilibrium, either methane ore amphibole must have changed its isotopic composition by a secondary process. Diffusive loss of H_2 from fluid inclusions (e.g., Hollister and Roedder, 1984) could principally change the mass balance in the CH_4-H_2 system and hence the bulk δD of the system. In the temperature range between 500° and 200°C, the fractionation between

methane and molecular hydrogen is between about 200 and 500 ‰ (Horibe and Craig, 1995). Thus, the preferential loss of H_2 from fluid inclusions would change the δD-value of the system towards an enrichment in D. Konnerup-Madsen et al. (1979) have suggested that higher hydrocarbons found within the majority of the investigated fluid inclusions of the Ilímaussaq rocks are explained by condensation reactions of the type

$$2\ CH_4 = C_2H_6 + H_2 \qquad (3).$$

Mass balance considerations using data for Ilímaussaq fluid inclusions (Konnerup-Madsen et al., 1988; Konnerup-Madsen, 2001) indicate that there is more H_2 in fluid inclusions than what could have been produced according to condensation reactions of methane. Collectively, this implies that the fluid phase contained significant amounts of molecular hydrogen before the condensation reactions and that not all hydrogen was lost from the system.

To explain our data, we favor a process, where during late-magmatic cooling the oxidation state of the whole system increases and primary magmatic methane is oxidized according to the following schematic reaction.

$$CH_4 + 2\ O_2 = CO_2 + 2\ H_2O \qquad (4)$$

An increase in the oxidation state for the Ilímaussaq rocks to values as high as the hematite-magnetite buffer during late-magmatic conditions is indicated e.g. by the formation of aegirine at the expense of arfvedsonite (Markl et al., 2001). The formation of aegirine in similar rocks of the Puklen intrusion, South Greenland (Marks et al., in press) was shown to occur at temperatures down to 300°C. If CH_4 is quantitatively oxidized, the water formed from such methane would have the H-isotopic composition of the precursor methane, which was analyzed to be about -140 ‰. Re-equilibration in this temperature range of primary arfvedsonite with this H-depleted water would result in H-isotopic compositions for amphibole down to about -220 ‰ (using the fractionations of Suzuoki and Epstein at 350°C for the given amphibole compositions), which covers most of the range of measured δD values. This process is the only one that can account for both the low δD amphibole values and the observed decoupling of the O and H isotope system.

5. CONCLUSIONS

On the basis of stable as well as radiogenic isotope studies, the petrogenesis of undersaturated and oversaturated peralkaline igneous rocks is believed to be different: Alkaline silica-undersaturated intrusive rocks are commonly explained by closed system fractional crystallization of mildly alkalic or transitional basalts with only minor or without crustal contamination (e.g., Perry et al., 1987; Larsen and Sørensen, 1987; Kramm and Kogarko, 1994; Schmitt et al., 2000). In contrast, for alkaline silica-oversaturated intrusive rocks an open-system behavior is often indicated by contamination with crustal material during emplacement (e.g., Davies and Macdonald, 1987; Heaman and Machado, 1992; Harris, 1995; Mingram et al., 2000; Schmitt et al., 2000; Späth et al., 2001; Marks et al., 2003). For example, studies on silica-undersaturated, silica-oversaturated, and mixed complexes of the Damaraland, Namibia (Harris et al., 1990; Harris, 1995; Mingram et al., 2000; Schmitt et al., 2000), demonstrated a fundamentally different origin for the silica-oversaturated and the undersaturated alkaline igneous complexes of Namibia. These studies support the assumption of Foland et al. (1993) that alkaline silica-oversaturated magmas evolved from undersaturated magma via crustal contamination, or that they are products of crustal anatexis. For the agpaitic rocks of the intrusive complexes of Khibina and Lovozero (Russia), it has been shown that they are residues formed in the upper mantle by fractional crystallization from nephelinites, basanites or nepheline benmoreites. They have isotopic compositions similar to those of a depleted melt source, but there is no sign of any assimilation of crustal melts in these rocks (Kramm and Kogarko, 1994). In contrast, the silica-saturated to -oversaturated Puklen complex in the western part of the Gardar Province indicates the importance of a crustal component for the genesis of the complex (Marks et al., in press). Nd isotope compositions for primary minerals are highly variable, and show that assimilation of crustal rocks occurred to different extents. Furthermore, isotopic compositions of different minerals from the same sample indicate a multi-source genesis and a major late-stage influx and circulation of an externally derived fluid phase in the Puklen magma chamber.

In summary, the neodymium and oxygen isotope data of mineral separates of the Ilímaussaq intrusion indicate that most of the Ilímaussaq melts are derived from an isotopically homogeneous mantle source. Because there are no significant differences in $\delta^{18}O$ values and Nd isotopic composition between magmatic and late-stage to hydrothermal minerals, a closed system behavior during crystallization and cooling can be assumed for the Ilímaussaq melts. The neodymium isotope data are interpreted to reflect a mantle source with initial ε_{Nd} values of about -1 to -2. The oxygen isotope composition of the Ilímaussaq melts is estimated to be around +5.7 to 6.0 ‰. The alkali granite unit of the Ilímaussaq complex has

the same oxygen isotopic composition but a less radiogenic neodymium isotope composition ($\varepsilon_{Nd(T)}$ = -3.1) compared to the other samples. Higher amounts of assimilation of granitic basement rocks or sandstones are ruled out on the basis of the presently known Nd- and O-isotope compositions and Nd concentrations in these rocks compared to those from the Ilimaussaq intrusion. Contamination with lower crustal rocks during ascent of the alkali granite is probably responsible for this contrast.

The wide variation in δD values is in contrast to the homogeneous O- and Nd-isotopic compositions and the correlation of δD values with total Fe-content and Fe^{3+}/Fe^{2+}, in combination with published δD values for late-stage methane in fluid inclusions of these rocks and the δD values published for the wall rocks, a major influx of low-δD meteoric fluids and major degassing processes are believed to be unlikely. Influence of assimilation of an external sedimentary, organic-rich reservoir in the source region of the Ilímaussaq melts is possible, but must have been very limited in volume and cannot account for the methane and molecular hydrogen in the fluid inclusions. One process that may explain the low δD values for the amphiboles could be a late-magmatic cooling accompanied by an increase in the oxidation state of the whole system and oxidation of magmatic methane. Comparison to data from other alkaline complexes indicates, that such a process may occur not only in the Ilímaussaq complex, but also in many other peralkaline igneous complexes worldwide. Alternatively, amphibole-water fractionation factors as presently known are in serious error, either because of effects of pressure on hydrogen partitioning in the amphibole-water system or because the dependency of mineral-water fractionation on Fe in amphibole is stronger than previously thought.

Acknowledgments. Laser ICP-MS measurements were carried out at the Large Scale Geochemical Facility supported by the European Community - Access to Research Infrastructure action of the Improving Human Potential Programme, contract number HPRI-CT-1999-00008 awarded to Prof. B. J. Wood (University of Bristol) which is gratefully acknowledged. Bruce Paterson provided invaluable help during these measurements. Elmar Reitter is thanked for his careful help during Nd isotope measurements, Gabi Stoschek for her help with the mass spectrometer and the oxygen and hydrogen isotope analyses. Constructive comments by E. Krogstad and two anonymous reviewers helped to improve the quality of this work. Thomas Wenzel helped to improve an earlier version of this manuscript. Financial

support for this work was funded by the Deutsche Forschungsgemeinschaft (grant Ma-2135/1-2).

This is Contribution to the mineralogy of Ilímaussaq No. 118.

REFERENCES

Agemar, T., Wörner, G., and Heumann, A. (1999) Stable isotopes and amphibole chemistry on hydrothermally altered granitoids in the North Chilean Precordillera: A limited role of meteoric water? *Contrib. Mineral. Petr.* **136**, 331-344.

Allaart, J. H. (1969) The chronology and petrography of the Gardar dykes between Igaliko Fjord and Redekammen, South Greenland. *Rapp. Grønl. Geol. Under.* **25** , 26.

Andersen, T. (1997) Age and petrogenesis of the Qassiarsuk carbonatite-alkaline silicate volcanic complex in the Gardar rift, South Greenland. *Mineral. Mag.* **61**, 499-513.

Bailey, J. C., Gwozdz, R., Rose-Hansen, J., and Sørensen, H. (2001) Geochemical overview of the Ilimaussaq alkaline complex, South Greenland. *Geol. Greenl. Surv. Bull.* **190**, 35-53.

Brandriss, M. E., Nevle, R. J., Bird, D. K., and O´Neil, J. R. (1995) Imprint of meteoric water on the stable isotope compositions of igneous and secondary minerals, Kap Edvard Holm complex, East Greenland. *Contrib. Mineral. Petr.* **121**, 74-86.

Chacko T., Cole D.R., and Horita J. (2001) Equilibrium oxygen, hydrogen and carbon isotope fractionation factors applicable to geologic systems. *In: Valley, J.W. and Cole, D.R. (eds.): Stable Isotope Geochemistry. Reviews in Mineralogy. Mineral. Soc. America*. **43**, 1-82.

Clayton, R. N. and Mayeda, T. K. (1963) The use of bromine pentafluoride in the extraction of oxygen from oxides and silicates for isotope analysis. *Geochim. Cosmochim. Acta* **27**, 43-52.

Dahl-Jensen, T., Thybo, H., Hopper, J., and Rosing, M. (1998) Crustal structure at the SE Greenland margin from wide-angle and normal incidence seismic data. *Tectonophysics* **288**, 191-198.

Dallai, L., Ghezzo, C., and Sharp, Z. D. (2003) Oxygen isotope evidence for crustal assimilation and magma mixing in the Granite Harbour intrusives, Northern Victoria Land, Antarctica. *Lithos* **67**,

Davies, G. R. and Macdonald, R. (1987) Crustal influences in the petrogenesis of the Naivasha basalt-comendite complex: combined trace element and Sr-Nd-Pb isotope constraints. *J. Petrol.* **28**, 1009-1031.

Eiler, J. M. (2001) Oxygen isotope variations of basaltic lavas and upper mantle rocks. *In: Valley, J.W. and Cole, D.R. (eds.): Stable Isotope Geochemistry. Reviews in Mineralogy. Washington: Mineral. Soc. America.* **43**, 319-364.

Emeleus, C. H. and Upton, B. G. J. (1976) The Gardar period in southern Greenland. *In: Escher, A. & Watt, W.S. (eds.), Geology of Greenland. Copenhagen: Geological Survey of Greenland.* 152-181.

Escher, A. and Watt, W. S. (1976) Geology of Greenland. Copenhagen: Geological Survey of Greenland. 603 pp.

Farver, J. R. (1989) Oxygen self diffusion in diopside with application to cooling rate determinations. *Earth Planet. Sci. Lett.* **92**, 386-396.

Farver, J. R. and Giletti, B. J. (1985) Oxygen diffusion in amphiboles. *Geochim. Cosmochim. Acta* **49**, 1403-1411.

Ferguson, J. (1964) Geology of the Ilimaussaq alkaline intrusion, South Greenland. *Bull. Grønl. Geol. Under.* **39**, 82.

Foland, K. A., Landoll, J. D., Henderson, C. M. B., and Jiangfeng, C. (1993) Formation of cogenetic quartz and nepheline syenites. *Geochim. Cosmochim. Acta* **57**, 697-704.

Fowler, M. B. and Harmon, R. S. (1990) The oxygen isotope composition of lower crustal granulite xenoliths. *In: Vielzeuf, D. and Vidal, P. (eds.): Granulites and Crustal Evolution.* Kluwer Academic Publishers, Dordrecht, The Netherlands, 493-506.

Garde, A. A., Hamilton, M. A., Chadwick, B., Grocott, J., and McCaffrey, K. J. W. (2002) The Ketilidian orogen of South Greenland: geochronology, tectonics, magmatism, and fore-arc accretion during Palaeoproterozoic oblique convergence. *Can. J. Earth Sci.* **39**, 765-793.

Gérard, O. and Jaoul, O. (1989) Oxygen diffusion in San Carlos olivine. *J. Geophys. Res.* **94**, 4119-4128.

Goldstein, S. L., O´Nions, R. K., and Hamilton, P. J. (1984) A Sm-Nd isotopic study of the atmospheric dust and particulates from major river systems. *Earth Planet. Sci. Lett.* **70**, 221-236.

Goodenough, K. M., Upton, B. G. J., and Ellam, R. M. (2002) Long-term memory of subduction processes in the lithospheric mantle: evidence from the geochemistry of basic dykes in the Gardar Province of south Greenland. J. *Geol. Soc. London* **159**, 705-714.

Graham, C. M., Harmon, R. S., and Sheppard, S. M. F. (1984) Experimental hydrogen isotope studies: hydrogen isotope exchange between amphibole and water. *Am. Mineral.* **69** , 128-138.

Gregory, R. T. and Criss, R.E. (1986) Isotopic exchange in open and closed systems. *In: Valley, J.W., Taylor, H.P.Jr and O´Neil, J.R. (eds.): Stable Isotopes. Reviews in Mineralogy. Washington: Mineral. Soc. America.* **16**, 91-128.

Halama, R., Wenzel, T., Markl, G., Upton, B. G. J., and Siebel, W. (in press) Reconstruction of OIB-signature in crustally contaminated rift-related basalts: A geochemical and Sr-Nd-O isotopic study of the Proterozoic Eriksfjord Basalts, Gardar Province, South Greenland. *Mineral. Mag. special volume*

Harris, C. (1995) Oxygen isotope geochemistry of the Mesozoic anorogenic complexes of Damaraland, northwest Namibia: evidence for crustal contamination and its effects on silica saturation. *Contrib. Mineral. Petr.* **122**, 308-321.

Harris, C. and Ashwal, L.D. (2002) The origin of low $\delta^{18}O$ granites and related rocks fom the Seychelles. *Contrib. Mineral. Petr.* **143**, 366-376.

Harris, C., Marsh, J. S., and Milner, S. C. (1999) Petrology of the alkaline core of the Messum igneous complex, Namibia: Evidence for the progressively decreasing effect of crustal contamination. *J. Petrol.* **40**, 1377-1397.

Harris, C., Whittingham, A. M., Milner, S. C., and Armstrong, R. A. (1990) Oxygen isotope geochemistry of the silicic volcanic rocks of the Etendeka/Parana Province: source constraints. *Geology* **18**, 1119-1121.

Heaman, L. M. and Machado, N. (1992) Timing and origin of midcontinent rift alkaline magmatism, North America: evidence from the Coldwell Complex. *Contr. Mineral. Petrol.* **110**, 289-303.

Hoefs, J. (1997) Stable isotope geochemistry. *Springer, Berlin Heidelberg*

Horibe, Y. and Craig, H. (1995) D/H fractionation in the system methane-hydrogen-water. *Geochim. Cosmochim. Acta* **59**, 5209-5217.

Horita, J., Driesner, T., and Cole, D. R. (1999) Pressure effect on hydrogen isotope fractionation between brucite and water at elevated temperatures. *Science* **286**, 1545-1547.

Jacobson, S. B. and Wasserburg, G. J. (1980) Sm-Nd isotopic evolution of chondrites. *Earth Planet. Sci. Lett.* **50**, 139-155.

Kalsbeek, F. and Taylor, P. N. (1985) Isotopic and chemical variation in granites across a Proterozoic continental margin-the Ketilidian mobile belt of South Greenland. *Earth Planet. Sci. Lett.* **73**, 65-80.

Konnerup-Madsen, J. (2001) A review of the composition and evolution of hydrocarbon gases during solidification of the Ilimaussaq alkaline complex, South Greenland. *Geol. Greenl. Surv. Bull.* **190**, 159-166.

Konnerup-Madsen, J., Kreulen, R., and Rose-Hansen, J. (1988) Stable isotope characteristics of hydrocarbon gases in the alkaline Ilimaussaq complex, South Greenland. *Bull. minéral.* **111**, 567-576.

Konnerup-Madsen, J., Larsen, E., and Rose-Hansen, J. (1979) Hydrocarbon-rich fluid inclusions in minerals from the alkaline Ilimaussaq intrusion, South Greenland. *Bull. minéral.* **102**, 642-653.

Konnerup-Madsen, J. and Rose-Hansen, J. (1984) Composition and significance of fluid inclusions in the Ilimaussaq peralkaline granite, South Greenland. *Bull. minéral.* **107**, 317-326.

Kramm, U. and Kogarko, L. N. (1994) Nd and Sr isotope signatures of the Khibina and Lovozero agpaitic centres, Kola Province, Russia. *Lithos* **32**, 225-242.

Kyser, T. K. (1986) Stable isotope variations in the mantle. *In: Valley, J.W., Taylor, H.P.Jr and O´Neil, J.R. (eds.): Stable Isotopes. Reviews in Mineralogy. Washington: Minera. Soc. America.* **16**, 141-162.

Larsen, L. M. (1976) Clinopyroxenes and coexisting mafic minerals from the alkaline Ilimaussaq intrusion, south Greenland. *J. Petrol.* **17**, 258-290.

Larsen, L. M. (1977) Aenigmatites from the Ilimaussaq intrusion, south Greenland: Chemistry and petrological implications. *Lithos* **10**, 257-270.

Larsen, L. M. (1981) Chemistry of feldspars in the Ilímaussaq augite syenite with additional data on some other minerals. *Rapp. Grønl. Geol. Under.* **103**, 31-37.

Larsen, L. M. and Sørensen, H. (1987) The Ilimaussaq intrusion-progressive crystallization and formation of layering in an agpaitic magma. *In: Fitton, J.G. & Upton, B.G.J. (eds.), Alkaline Igneous Rocks, Geol. Soc. Sp. Publ.* **30**, 473-488.

Larsen, L. M. and Steenfelt, A. (1974) Alkali loss and retention in an iron-rich peralkaline phonolite dyke from the Gardar province, south Greenland. *Lithos* **7**, 81-90.

Liew, T. C. and Hofmann, A. W. (1988) Precambrian crustal components, plutonic associations, plate environment of the Hercynian Fold Belt of central Europe: Indications from a Nd and Sr isotopic study. *Contrib. Mineral. Petr.* **98**, 129-138.

Lugmair, G. W. and Marti, K. (1978) Lunar initial 143Nd/144Nd: differential evolution of the lunar crust and mantle. *Earth Planet. Sci. Lett.* **39**, 349-357.

Lutz, T. M., Foland, K. A., Faul, H., and Srogi, L. A. (1988) The strontium and oxygen isotopic record of hydrothermal alteration of syenites from the Abu Khruq complex, Egypt. *Contrib. Mineral. Petr.* **98**, 212-223.

Macdonald, R., Davies, G. R., Bliss, C. M., Leat, P. T., Bailey, D. K., and Smith, R. L. (1987)

Markl, G. (2001a) Stability of Na-Be minerals in late-magmatic fluids of the Ilimaussaq alkaline complex, South Greenland. *Geol. Greenl. Surv. Bull.* **190**, 145-158.

Markl, G. (2001b) A new type of silicate liquid immiscibility in peralkaline nepheline syenites (lujavrites) of the Ilimaussaq complex, South Greenland. *Contr. Mineral. Petrol.* **141**, 458-472.

Markl, G. and Baumgartner, L. (2002) pH changes in peralkaline late-magmatic fluids. *Contrib. Mineral. Petr.* **144**, 31-346.

Markl, G., Marks, M, Schwinn, G., and Sommer, H. (2001a) Phase equilibrium constraints on intensive crystallization parameters of the Ilimaussaq Complex, South Greenland. *J. Petrol.* **42**, 2231-2258.

Markl, G., Marks, M., and Wirth, R. (2001b) The influence of T, aSiO2, fO2 on exsolution textures in Fe-Mg olivine: an example from augite syenite of the Ilimaussaq Intrusion, South Greenland. *Am. Mineral.* **86**, 36-46.

Marks, M. and Markl, G. (2001) Fractionation and assimilation processes in the alkaline

augite syenite unit of the Ilimaussaq Intrusion, South Greenland, as deduced from phase equilibria. *J. Petrol.* **42**, 1947-1969.

Marks, M., Vennemann, T. W., Siebel, W., and Markl, G. (in press) Evolution of textures and variation of O, Sr and Nd isotope ratios during magmatic and hydrothermal processes in the Puklen syenite-alkali granite complex, South Greenland. *J. Petrol.*

Mathez E.A. (1984) Influence of degassing on oxidation states of basaltic magmas. *Nature* **310**, 371-375.

Mattey, D., Lowry, D., and Macpherson, C. (1994) Oxygen isotope composition of mantle peridotite. *Earth Planet. Sci. Lett.* **128**, 231-241.

Mingram, B., Trumbull, R. B., Littman, S., and Gerstenberger, H. (2000) A petrogenetic study of anorogenic felsic magmatism in the Cretaceous Paresis ring complex, Namibia: evidence for mixing of crust and mantle-derived components. *Lithos* **54**, 1-22.

Mitchell, R.H. (1990) A review of the compositional variation of amphiboles in alkaline plutonic complexes. *Lithos* **26**, 135-156

Nabelek, P. I., O´Neil, J. R., and Papike, J. J. (1983) Vapour phase exsolution as the controling factor in hydrogen isotope variation in granitic rocks; the Notche Peak granitic stock, Utah. *Earth Planet. Sci. Lett.* **66**, 137-150.

Nevle, R. J., Brandriss, M. E., Bird, D. K., MacWilliams, M. O., and O´Neil, J. R. (1994) Tertiary plutons monitor climate change in East Greenland. *Geology* **22**, 775-778.

Nicholson, S. W. and Shirey, S. B. (1990) Midcontinent Rift Volcanism in the Lake Superior Region: Sr, Nd, and Pb isotopic evidence for a mantle plume origin. *J. Geophys. Res.* **95**, 10851-10868.

Nielsen, B. L. and Steenfelt, A. (1979) Intrusive events at Kvanefjeld in the Ilimaussaq igneous complex. *Bull. Geol. Soc. Denmark* **27**, 143-155.

Nivin, V. A., Devirts, A. L., and Lagutina, Y. P. (1995) The origin of the gas phase in the Lovozero massif based on hydrogen-isotope data. *Geochem. Intern.* **32**, 65-71.

O´Neil, J.R. (1986) Theoretical and experimental aspects of isotopic fractionation. *In: Valley, J.W., Taylor, H.P.Jr and O´Neil, J.R. (eds.): Stable Isotopes. Reviews in Mineralogy. Washington: Mineral. Soc. America.* **16**, 1-40.

Perry, F. V., Baldridge, W. S., and DePaolo, D. J. (1987) Role of asthenosphere and lithosphere in the genesis of late cenozoic basaltic rocks from the Rio Grande rift and adjacent regions of the Southwestern United States. *J. Geophys. Res.* **92**, 9193-9213.

Potter, J. (2002) Textural and compositional evidence for the origin of hydrocarbons in alkaline igneous rocks. *Beih. Europ. J. Mineral.* **14**, 132.

Potter, J., Rankin, A. H., Treloar, P. J., Nivin, V. A., ting, W., and Ni, P. (1998) A preliminary study of methane inclusions in alkaline igneous rocks of the Kola igneous province, Russia: implications for the origin of methane in igneous rocks. *Europ. J. Mineral.* **10**, 1167-1180.

Poulsen, V. (1964) The sandstones of the Precambrian Eriksfjord Formation in South Greenland. *Rapp. Grønl. Geol. Under.* **2**, 16.

Pushkar, P., McBirney, A. R., and Kudo, A. M. (1972) The isotopic composition of strontium in Central American ignimbrites. *Bull. Volcanol.* **35**, 265-294.

Ranløv, J. and Dymek, R. F. (1991) Compositional zoning in hydrothermal aegirine from fenites in the Proterozoic Gardar Province, South Greenland. *Europ. J. Mineral.* **3**, 837-853.

Richet, P., Bottinga, Y., and Javoy, M. (1977) A review of hydrogen, carbon, nitrogen, oxygen, sulphur, and chlorine stable isotope fractionation among gaseous molecules. *Ann. Rev. Earth and Planet.* Sci. **5**, 65-110.

Roddick, J. C., Sullivan, R. W., and Dudas, F. Ö. (1992) Precise calibration of Nd tracer isotopic composition for Sm-Nd studies. *Chem. Geol.* **97**, 1-8.

Rose-Hansen, J. and Sørensen, H. (2001) Minor intrusions of peralkaline microsyenite in the Ilimaussaq alkaline complex, South Greenland. *Bull. Geol. Soc. Denmark* **48**, 9-29.

Rumble, D. and Hoering, T. C. (1994) Analysis of oxygen and sulfur isotope ratios in oxide and sulfide minerals by spot heating with a carbon dioxide laser in a fluorine atmosphrere. *Acc. Chem. Res.* **27**, 237-241.

Salvi, S. and Williams-Jones, A. E. (1997) Fischer-Tropsch synthesis of hydrocarbons during sub-solidus alteration of the Strange Lake peralkaline granite, Quebec/ Labrador, Canada *Geochim. Cosmochim. Acta* **61**, 83-99.

Sato, M. (1978) Oxygen fugacity of basaltic magmas and the role of gas-forming elements. *Geophys. Res. Lett.* **5**, 447-449.

Schmitt, A. K., Emmermann, R., Trumbull, R. B., Bühn, B., and Henjes-Kunst, F. (2000) Petrogenesis and 40Ar/39Ar Geochronology of the Brandberg Complex, Namibia: Evidence for a major mantle contribution in metaluminous and peralkaline granites. *J. Petrol.* **41**, 1207-1239.

Sharp. Z.D. (1990) A laser-based microanalytical method for the in-situ determination of oxygen isotope ratios of silicates and oxides. *Geochim. Cosmochim. Acta* **54**, 1353-1357.

Sheppard, S. M. F. (1986a) Igneous rocks: III. Isotopic case studies of magmatism in Africa, Eurasia and oceanic island. *In: Valley, J.W., Taylor, H.P.Jr and O´Neil, J.R. (eds.): Stable Isotopes. Reviews in Mineralogy. Washington: Mineral. Soc. America.* **16**, 319-368.

Sheppard, S. M. F. (1986b) Characterization and isotopic variations in natural waters. *In: Valley, J.W., Taylor, H.P.Jr and O´Neil, J.R. (eds.): Stable Isotopes. Reviews in Mineralogy. Washington: Mineral. Soc. America.* **16**, 165-181.

Sørensen, H. (2001) Brief introduction to the Geology of the Ilimaussaq alkaline complex, South Greenland. *Geol. Green. Surv. Bul.* **190**, 7-24.

Späth, A., Le Roex, A. P., and Opiyo-Akech, N. (2001) Plume-litosphere interaction and the origin of continental rift-related alkaline volcanism-the Chyulu hills volcanic province, Southern Kenya. *J. Petrol.* **42**, 765-787.

Stevenson, R., Upton, B. G. J., and Steenfelt, A. (1997) Crust-mantle interaction in the evolution of the Ilimaussaq Complex, South Greenland: Nd isotopic studies. *Lithos* **40**, 189-202.

Suzuoki, T. and Epstein, S. (1976) Hydrogen isotope fractionation between OH-bearing minerals and water. *Geochim. Cosmochim. Acta* **40**, 1229-1240.

Taylor, H. P. (1974) The application of oxygen and hydrogen isotope studies to problems of hydrothermal alteration and ore deposition. *Econ. Geol.* **69**, 843-883.

Taylor, H. P. Jr and Sheppard, S. M. F. (1986) Igneous rocks: I. Processes of isotopic fractionation and isotope systematics. *In: Valley, J.W., Taylor, H.P.Jr and O´Neil, J.R. (eds.): Stable Isotopes. Reviews in Mineralogy. Washington: Mineral. So. America.* **16**, 227-269.

Taylor, B. E., Eichelberger, J. C., and Westrich, H. R. (1983) Hydrogen isotopic evidence of rhyolitic magma degassing during shallow intrusion and eruption. *Nature* **306**, 541-545.

Taylor, P. N., Jones, N. W., and Moorbath, S. (1984) Isotopic assessment of relative contributions from crust and mantle sources to the magma genesis of Precambrian granitoid rocks. *Phil. Trans. R. Soc. Lond.* **A 310**, 605-625.

Upton, B. G. J. (1987) Gardar mantle xenoliths: Igdlutalik, South Greenland. *Rapp. Grønl. Geol. Under.* **150**, 37-43.

Upton, B. G. J. and Emeleus, C. H. (1987) Mid-Proterozoic alkaline magmatism in southern Greenland: the Gardar province. *In: Fitton, J.G. & Upton, B.G.J. (eds.), The Alkaline Rocks, Boston: Blackwell Scientific.* **30**, 449-471.

Upton, B. G. J., Emeleus, C. H., Heaman, L. M., Goodenough, K. M., and Finch, A. (2003) Magmatism of the mid-Proterozoic Gardar Province, South Greenland: chronology,

petrogenesis and geological setting. *Lithos* **68**, 43-65.
Valley J.W., Kitchen, N., Kohn, M. J., Niendorf, C. R., and Spicuzza, M. J. (1995) UWG-2, a garnet standard for oxygen isotope ratios: strategies for high precision and accuracy with laser heating. *Geochim. Cosmochim. Acta* **59**, 5223-5231.
Vennemann, T. W. and O´Neil, J. R. (1993) A simple and inexpensive method of hydrogen isotope and water analyses of minerals and rocks based on zinc reagent. *Chem. Geol.* **103**, 227-234.
Vennemann, T. W. and O´Neil, J. R. (1996) Hydrogen isotope exchange reactions between hydrous minerals and molecular hydrogen: I. A new approach for the determination of hydrogen isotope fractionation at moderate temperatures. *Geochim. Cosmochim. Acta* **60**, 2437-2451.
Waight, T., Baker, J., and Willigers, B. (2002) Rb isotope dilution analyses by MC-ICPMS using Zr to correct for mass fractionation: towards improved Rb-Sr geochronology? *Chem. Geol.* **186**, 99-116.
Zheng, Y.-F. (1993) Calculation of oxygen isotope fractionation in hydroxyl-bearing silicates. *Earth Planet. Sci. Lett.* **120**, 247-263.
Zindler, A. and Hart, S. R. (1986) Chemical geodynamics. *Ann. Rev. Earth Planet. Sci.* **14**, 493-571.

Figure captions

Fig.1:
Geological sketch map of the alkaline Gardar Province, South Greenland (modified after Escher and Watt, 1976). Note the outcrop of Archaean rocks in the northwestern part of the province. The Ilímaussaq intrusion is demonstrated in the dashed frame and illustrated enlarged in Fig. 2. The Puklen complex and the Ivittut area are locations referred to in the text.

Fig. 2:
Geological sketch map of the Ilímaussaq intrusion after Ferguson (1964), showing sample localities.

Fig. 3:
Micro-textures and field relations observed for the different rock types. (a) Subhedral amphibole in a matrix of feldspar in augite syenite. (b) Fayalitic olivine rimmed by amphibole and biotite in augite syenite. (c) Subhedral amphibole in a matrix of feldspar and quartz in alkali granite. (d) Amphibole together with biotite in sodalite foyaite. (e) Interstitial amphibole in naujaite. (f) Interstitial amphibole in black kakortokite. (g) Euhedral and chemically zoned amphibole together with aenigmatite and natrolite in red kakortokite. (h) Euhedral amphibole in lujavrite. (i) Exsolved lujavrite consisting of a fine-grained black matrix, and gray, partly deformed ocelli. Pocketknife for scale. (j) Agpaitic pegmatite consisting of huge crystals of feldspar and amphibole. The latter is partly overgrown by aegirine coatings (not visible). The head of the hammer is about 12 cm in size. (k) Late-stage aegirine-albite-analcime vein intruding naujaite. Length of hammer is approximately 40 cm. (l) Porphyritic texture in an agpaitic dike rock in the vicinity of the Ilímaussaq intrusion. Abbreviations: aeg = aegirine, aen = aenigmatite, amph = amphibole, bt = biotite, fsp = feldspar, ne = nepheline, ntr = natrolite, ol = olivine, qtz = quartz.

Fig. 4:
Compositional range observed in the Ilímaussaq amphiboles plotted in a Ca p.f.u. vs. Si p.f.u. diagram according to Mitchell (1990).

Fig. 5:
Sm-Nd isotope diagram for all analyzed mineral separates (amphibole, aegirine, augite) and whole rock sample GM1212. Note that an isochron age of 1160±30 Ma was calculated omitting the data for amphibole separates from the alkali granite (GM1303) and the agpaitic dike rock (GM1849).

Fig. 6:
Calculated $\delta^{18}O$ versus $\varepsilon_{Nd(1160)}$ values for Ilímaussaq mineral separates. Note the two outliers (alkali granite and agpaitic dike rock) from the majority of the data set.

Fig. 7:
Calculated $\delta^{18}O_{fluid}$ and δD_{fluid} values for the Ilímaussaq complex based on present mineral-H_2O fractionations (see discussion). Fields for ocean water, meteoric waters, primary magmatic waters, metamorphic waters, and organic waters are from Sheppard (1986b) and shown for comparison.

Fig. 8:

(a) Range of observed Fe^{3+}/Fe^{2+} ratios versus δD value for amphiboles of the different rock types. With the exception of amphiboles from the alkali granite these parameters show an inverse correlation. (b) $Fe_{(tot)}$ a.p.f.u.(atoms per formula unit) of amphiboles versus δD values of the different rock types. A rough correlation between these two parameters can be recognized.

Table 1: Representative microprobe analyses of amphiboles of the different rock types. n.d. = not detected.

sample	GM1330		GM1303		GM1214		GM1370		GM1337		GM1843		GM1849	
rock type	augite syenite		alkali granite		sodalite foyaite		naujaite		kakortokite (black)		lujavrite		agpaitic dike	
wt%														
SiO_2	40.82	39.13	49.22	49.88	46.68	48.27	49.07	50.74	48.13	47.32	50.76	50.74	48.79	48.49
TiO_2	0.35	3.10	1.52	0.55	0.58	0.64	0.50	0.50	0.75	0.71	0.54	0.82	0.38	0.46
Al_2O_3	9.11	10.76	0.29	0.21	3.05	1.83	2.18	0.91	2.68	3.20	0.65	0.70	2.30	2.33
ZnO	0.06	0.07	0.39	0.28	n.d.	n.d.	0.45	0.37	0.16	0.48	0.28	0.22	n.d.	n.d.
Li_2O	0.01	0.01	0.18	0.10	n.d.	n.d.	0.30	0.37	0.13	0.13	0.38	0.39	n.d.	n.d.
FeO	29.00	27.17	32.96	35.19	34.62	35.37	33.30	32.87	32.81	32.80	32.37	31.22	33.10	33.54
MnO	0.50	0.48	0.78	0.48	0.84	0.74	0.93	0.95	0.70	0.63	1.26	1.22	1.00	1.06
MgO	3.12	2.57	0.00	0.10	0.36	0.03	0.08	0.14	1.00	1.00	0.01	0.02	0.50	0.49
CaO	10.26	10.39	0.25	0.22	2.39	1.62	1.00	0.64	1.18	1.50	0.15	0.16	1.08	1.23
Na_2O	3.04	3.19	8.55	8.66	7.33	7.70	9.61	8.73	8.63	8.38	8.67	8.85	7.30	7.31
K_2O	1.69	1.63	1.46	1.17	1.95	1.86	2.02	2.90	2.14	1.92	3.00	3.08	2.71	2.54
ZrO_2	0.32	0.38	0.14	0.11	0.20	0.01	0.07	0.04	0.20	0.65	1.12	1.55	0.04	0.02
Cl	0.06	0.13	0.03	0.03	0.00	0.00	0.00	0.00	0.00	0.01	0.02	0.01	0.00	0.00
F	1.04	0.33	3.29	1.37	0.79	0.56	0.00	0.00	0.07	0.03	0.00	0.00	0.04	0.03
Total	98.99	98.88	99.05	98.36	98.79	98.65	98.69	98.38	98.43	98.25	99.20	98.96	97.23	97.47
	Formulae based on 6 cations and 23 oxygens													
Si	6.50	6.21	7.98	8.00	7.45	7.71	7.50	7.82	7.50	7.41	7.88	7.87	7.82	7.76
Al	1.71	2.01	0.06	0.04	0.57	0.34	0.39	0.16	0.49	0.59	0.12	0.13	0.43	0.44
Ti	0.04	0.37	0.18	0.07	0.07	0.08	0.06	0.06	0.09	0.08	0.06	0.10	0.05	0.06
Zn	0.01	0.01	0.05	0.03	n.d.	n.d.	0.05	0.04	0.02	0.06	0.03	0.03	n.d.	n.d.
Li	0.01	0.01	0.12	0.06	n.d.	n.d.	0.19	0.23	0.08	0.08	0.24	0.24	n.d.	n.d.
Fe^{3+}	0.44	0.08	0.71	0.80	1.02	0.85	1.90	1.48	1.42	1.34	1.24	1.19	0.66	0.72
Mg	0.74	0.61	0.00	0.02	0.09	0.01	0.02	0.03	0.23	0.23	0.00	0.00	0.12	0.12
Fe^{2+}	3.42	3.53	3.76	3.92	3.60	3.87	2.35	2.76	2.85	2.96	2.95	2.86	3.78	3.77
Mn	0.07	0.06	0.11	0.06	0.11	0.10	0.12	0.12	0.09	0.08	0.17	0.16	0.14	0.14
Ca	1.75	1.77	0.04	0.04	0.41	0.28	0.16	0.11	0.20	0.25	0.02	0.03	0.18	0.21
Na	0.94	0.98	2.69	2.69	2.27	2.38	2.85	2.61	2.61	2.54	2.60	2.66	2.27	2.27
K	0.34	0.33	0.30	0.24	0.40	0.38	0.39	0.57	0.43	0.38	0.59	0.61	0.55	0.52
Zr	0.02	0.03	0.01	0.01	0.02	0.00	0.01	0.00	0.02	0.05	0.08	0.12	0.00	0.00
Cl	0.02	0.04	0.01	0.01	0.00	0.00	0.00	0.00	0.00	0.00	0.00	0.00	0.00	0.00
F	0.52	0.17	1.69	0.70	0.40	0.28	0.00	0.00	0.04	0.02	0.00	0.00	0.02	0.02
Sum	16.00	16.00	16.00	16.00	16.00	16.00	16.00	16.00	16.00	16.00	16.00	16.00	16.00	16.00

Table 2: Sm-Nd data and oxygen and hydrogen isotope compositions for mineral separates and one whole rock sample of the Ilímaussaq Intrusion. Errors of measured $^{143}Nd/^{144}Nd$ are given as 2σ-values and are indicated in brackets. Calculation of Nd-model ages according to Liew & Hofmann (1988).

sample	rock type	mineral	Sm (ppm)	Nd (ppm)	$^{147}Sm/^{144}Nd$	$^{143}Nd/^{144}Nd$	$\varepsilon_{Nd(1160)}$	T_{DM} (Ga)	$\delta^{18}O$ (‰)	δD (‰)
GM1330	augite syenite	amphibole	83.67	431.6	0.1172	0.511987(08)	-0.9	1.78	5.7	-92
GM1330	augite syenite	augite	22.1	91.23	0.1464	0.512193(10)	-1.2	1.80	5.6	
GM1330	augite syenite	olivine							5.3	
GM1303	alkali granite	amphibole	13.43	72.6	0.1119	0.511832(09)	-3.1	1.96	5.6	-232
GM1214	sodalite foyaite	amphibole	8.602	58.19	0.0894	0.511765(09)	-1.1	1.79	5.7	-150
GM1370	naujaite	amphibole	10.47	63.61	0.0995	0.511847(12)	-1.0	1.79	5.4	-198
GM1335	kakortokite (red)	amphibole	6.115	35.74	0.1034	0.511838(09)	-1.8	1.85	5.3	-171
GM1337	kakortokite (black)	amphibole	4.190	26.76	0.0947	0.511783(07)	-1.5	1.83	5.5	-171
GM1843	lujavrite	amphibole	14.23	80.1	0.1074	0.511884(10)	-1.4	1.82	5.5	-132
GM1257	aegirine vein	aegirine	7.970	41.99	0.1148	0.511991(10)	-0.5	1.74	5.6	
GM1212	exsolved lujavrite	whole rock	595.5	4763	0.0756	0.511648(10)	-1.3	1.81	5.6	-173
GM1390	agpaitic pegmatite	aegirine	0.822	5.390	0.0922	0.511835(12)	-0.1	1.72	5.2	
GM1390	agpaitic pegmatite	amphibole	0.401	3.898	0.0622	0.511587(14)	-0.5	1.75	5.4	-189
GM1849	agpaitic dike	amphibole	15.46	90.51	0.1033	0.511965(08)	+0.7	1.65	4.5	-151
GM1849	agpaitic dike	olivine							5.6	

Table 3: Oxygen and neodymium isotopic compositions and Nd concentrations of possible contaminants for the Ilímaussaq alkali granite.

potential contaminant	$\delta^{18}O$ (‰)	ε_{Nd}(1160 Ma)	Nd (ppm)	reference
Julianehåb batholith	+7.8	-8.3	62	Halama (in press)
Eriksfjord sandstones	+11.5	-7	7	Andersen (1997); Halama (in press)
Archaean lower crust	+7.5	-23.4	63	Taylor et al. (1984); Fowler and Harmon (1990)

Fig.1

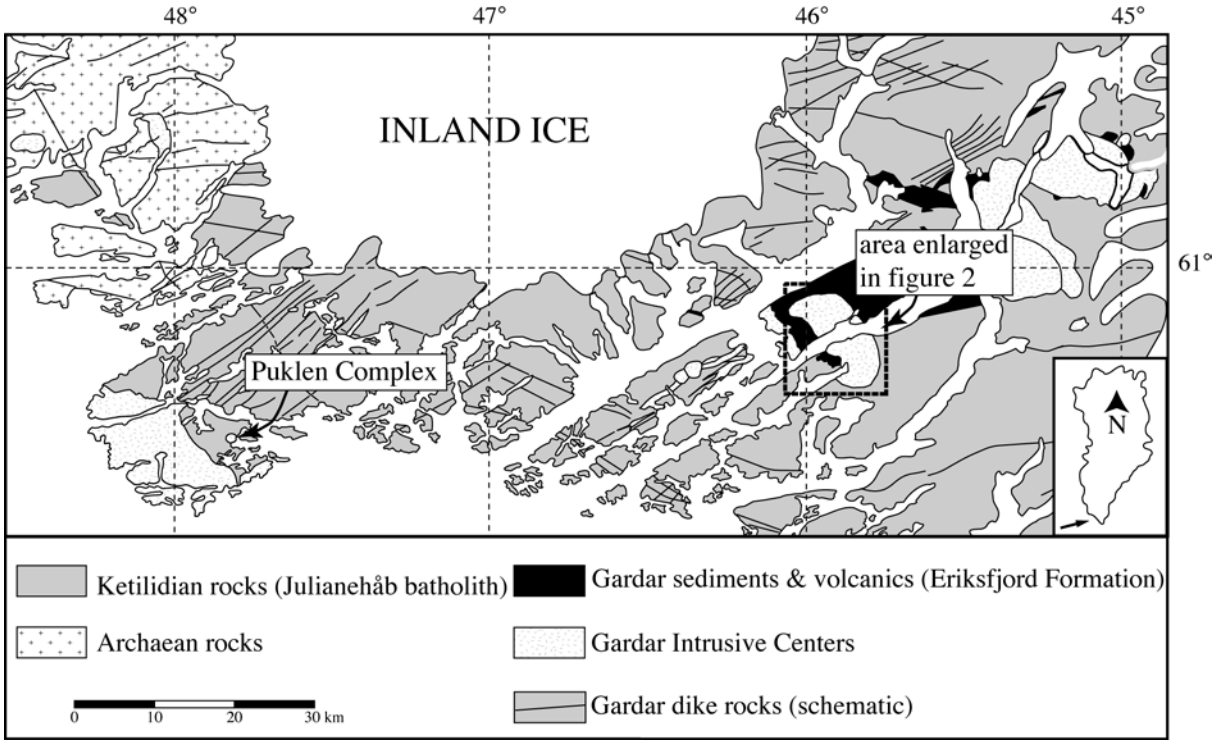
48°
47°
46°
45°
61°
INLAND ICE
area enlarged
in figure 2
Puklen Complex
N
Ketilidian rocks (Julianehåb batholith)
Archaean rocks
Gardar sediments & volcanics (Eriksfjord Formation)
Gardar Intrusive Centers
Gardar dike rocks (schematic)
0
10
20
30 km

Fig.2

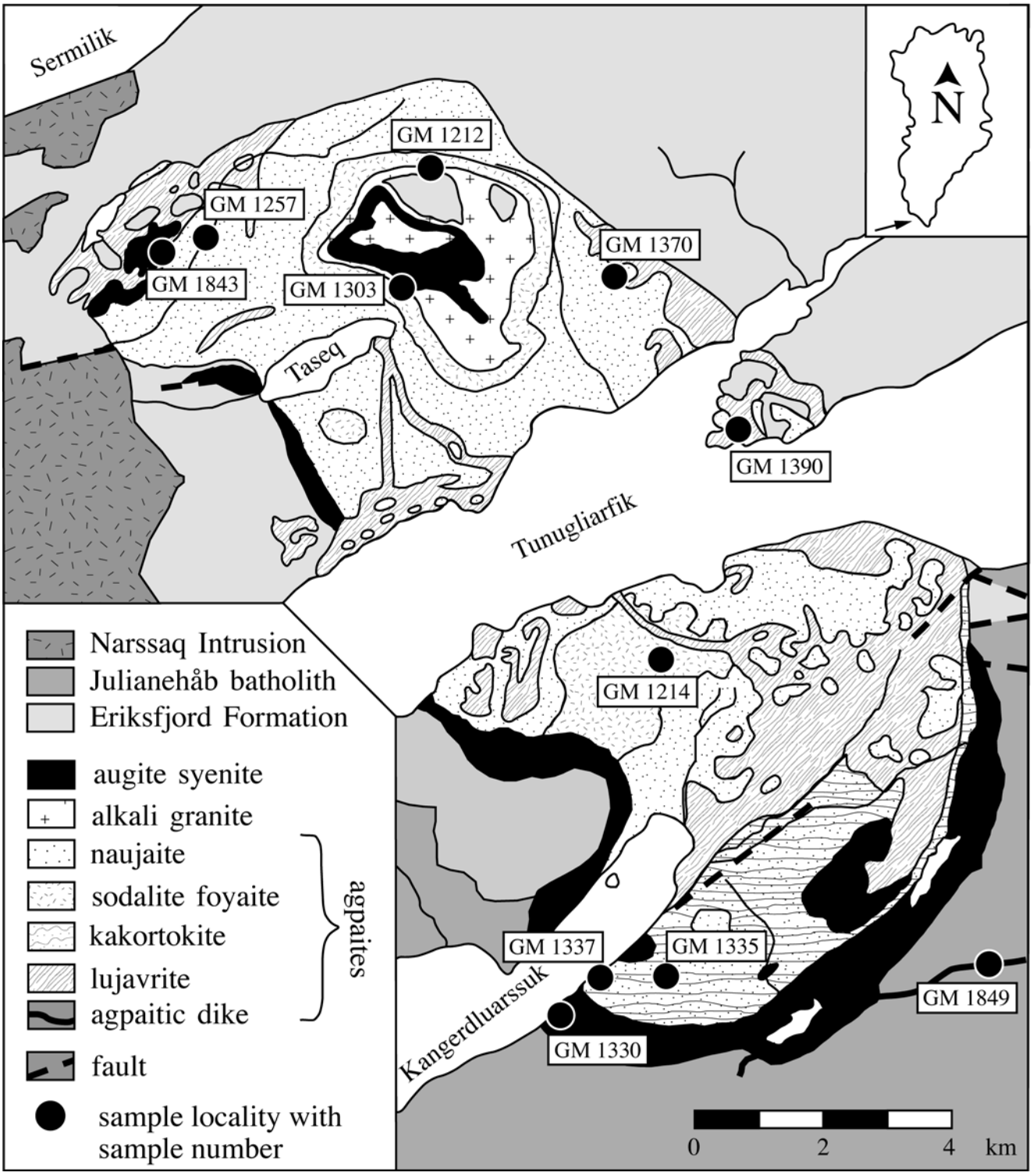
Sermilik
N
GM 1212
GM 1257
GM 1843
GM 1303
GM 1370
Taseq
GM 1390
Tunugliarfik
GM 1214
GM 1337
GM 1335
GM 1849
GM 1330
Kangerdluarssuk
Narssaq Intrusion
Julianehåb batholith
Eriksfjord Formation
augite syenite
alkali granite
naujaite
sodalite foyaite
kakortokite
lujavrite
agpaitic dike
agpaites
fault
sample locality with sample number
0
2
4
km

Fig.3

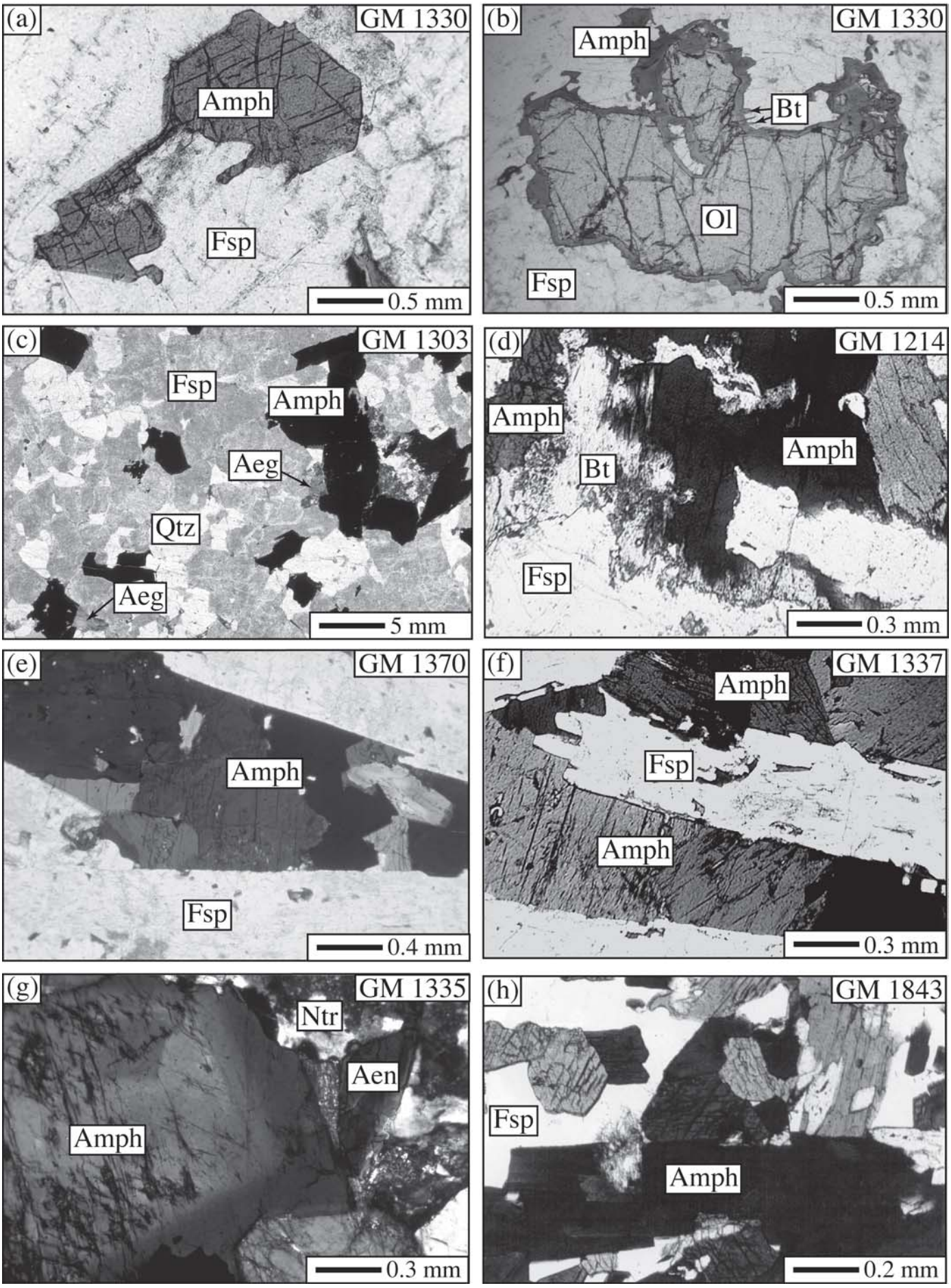
(a)
GM 1330
Amph
Fsp
0.5 mm
(b)
GM 1330
Amph
Bt
Ol
Fsp
0.5 mm
(c)
GM 1303
Fsp
Amph
Aeg
Qtz
Aeg
5 mm
(d)
GM 1214
Amph
Amph
Bt
Fsp
0.3 mm
(e)
GM 1370
Amph
Fsp
0.4 mm
(f)
GM 1337
Amph
Fsp
Amph
0.3 mm
(g)
GM 1335
Ntr
Aen
Amph
0.3 mm
(h)
GM 1843
Fsp
Amph
0.2 mm

Fig.3
(continued)

Fig. 4

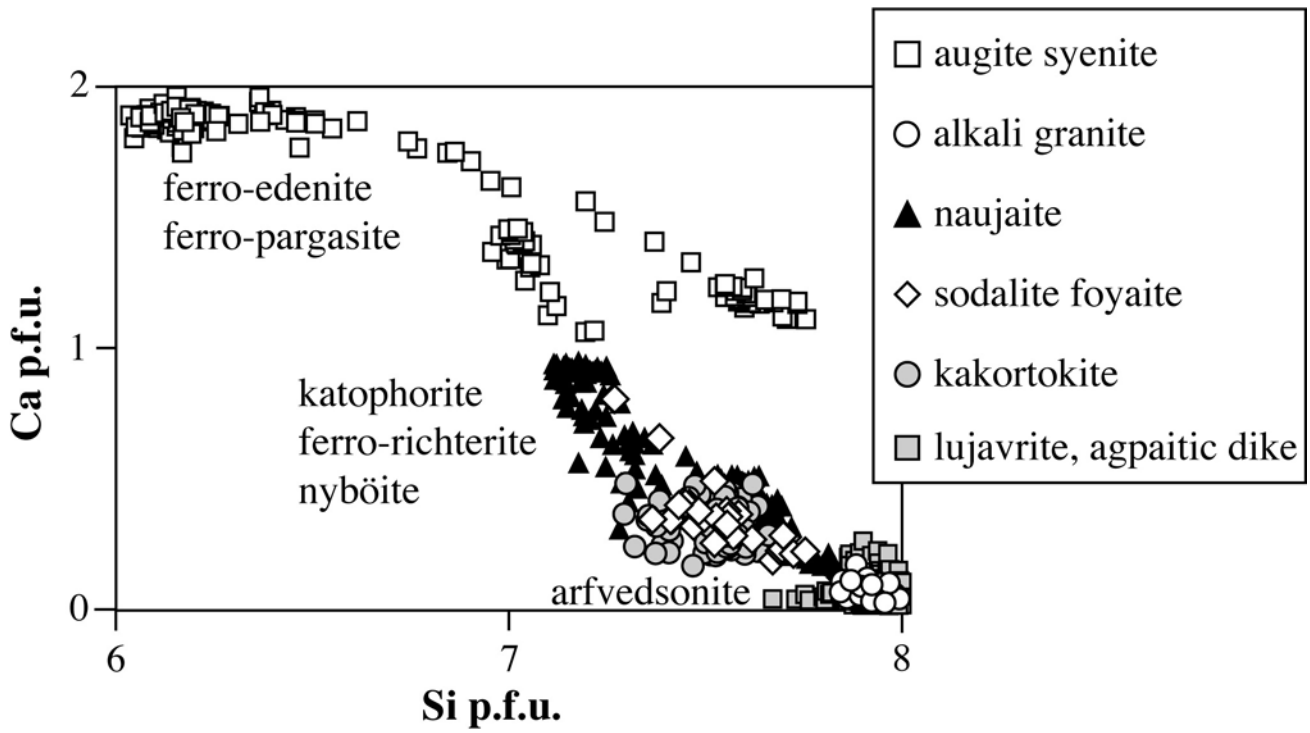
augite syenite
alkali granite
naujaite
sodalite foyaite
kakortokite
lujavrite, agpaitic dike
ferro-edenite
ferro-pargasite
katophorite
ferro-richterite
nyböite
arfvedsonite
Ca p.f.u.
Si p.f.u.
2
1
0
6
7
8

Fig. 5

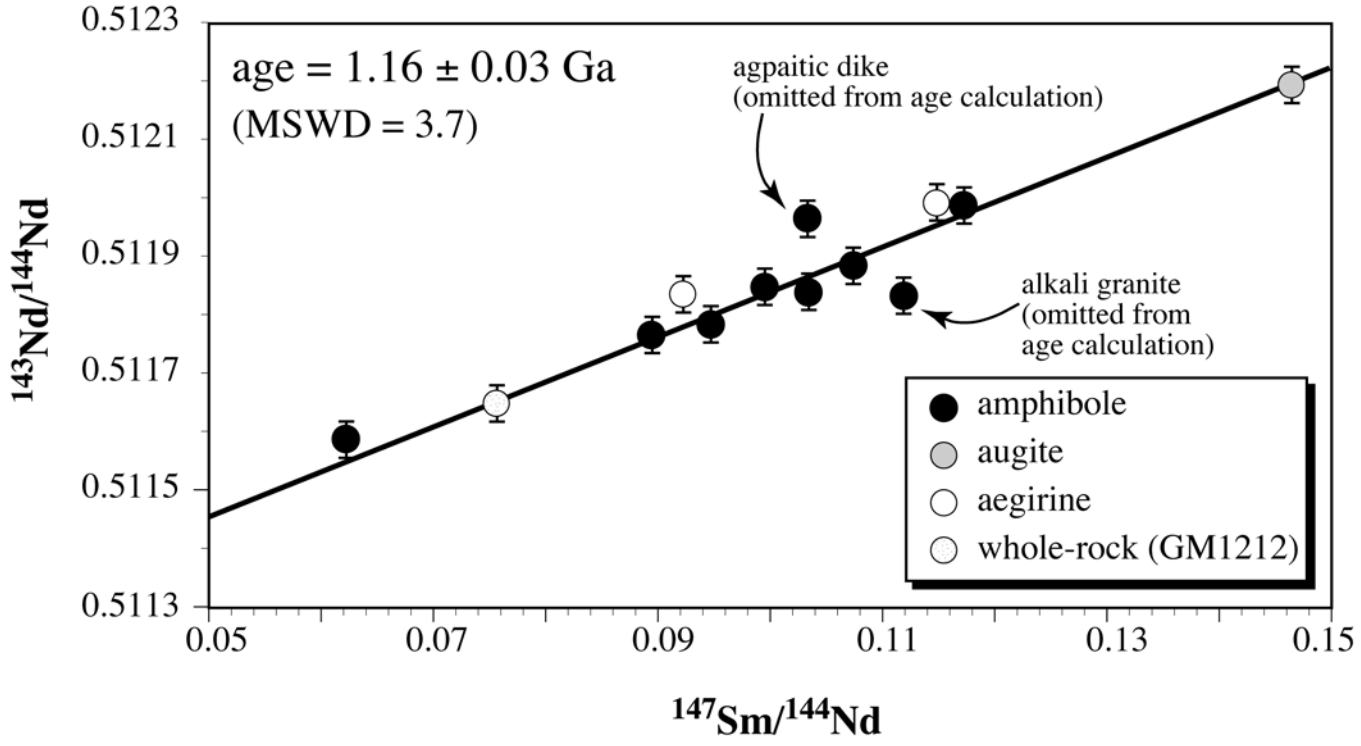
age = 1.16 ± 0.03 Ga
(MSWD = 3.7)
agpaitic dike
(omitted from age calculation)
alkali granite
(omitted from
age calculation)
amphibole
augite
aegirine
whole-rock (GM1212)
0.5123
0.5121
0.5119
0.5117
0.5115
0.5113
0.05
0.07
0.09
0.11
0.13
0.15
143Nd/144Nd
147Sm/144Nd

Fig. 6

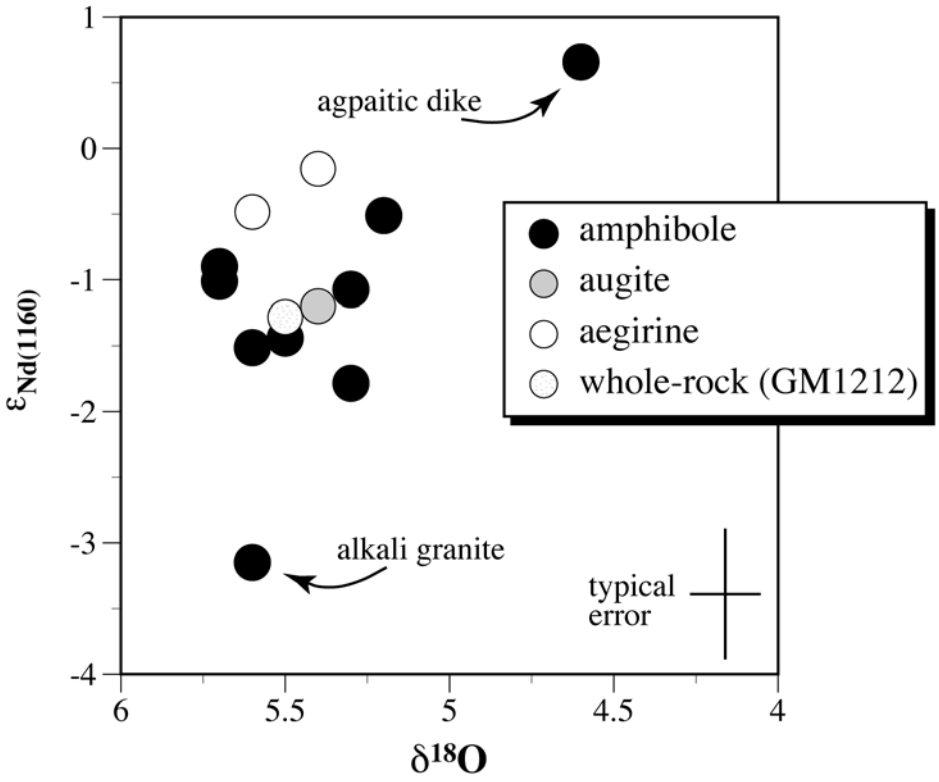
1
0
-1
-2
-3
-4
6
5.5
5
4.5
4
$\varepsilon_{Nd(1160)}$
$\delta^{18}O$
agpaitic dike
alkali granite
amphibole
augite
aegirine
whole-rock (GM1212)
typical
error

Fig. 7

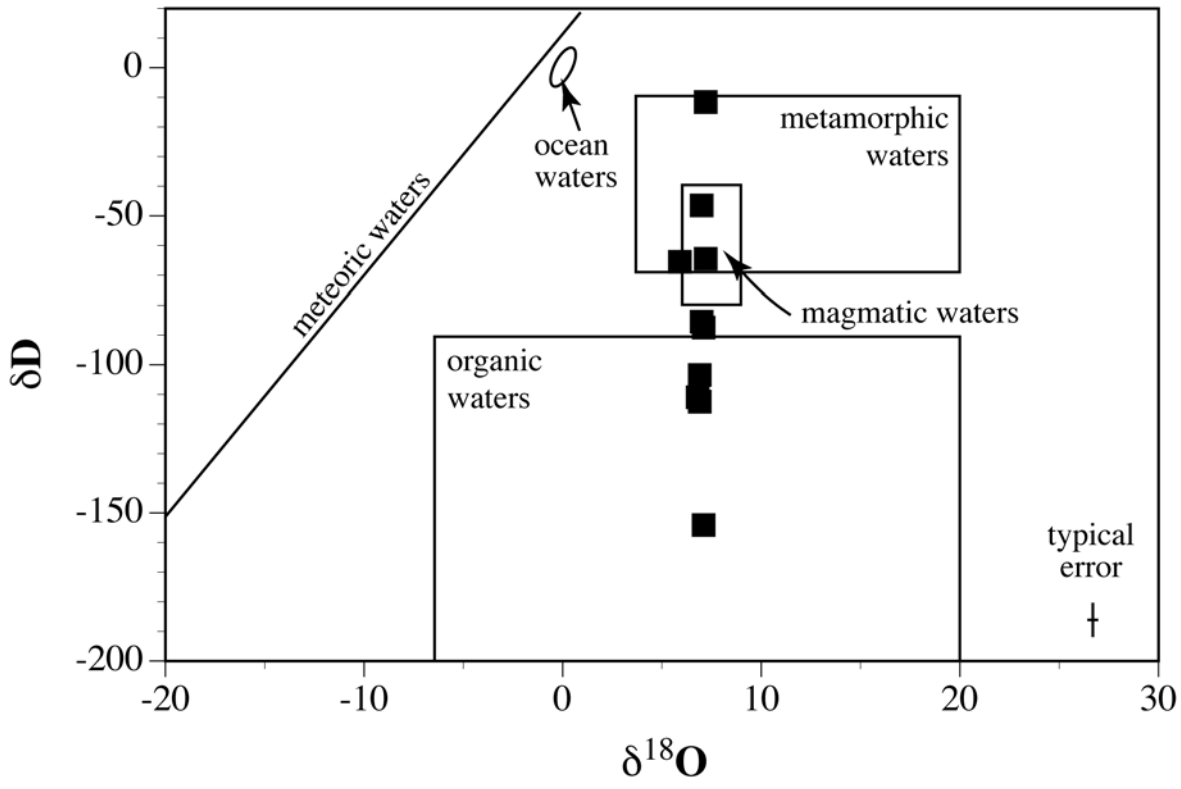
0
-50
-100
-150
-200
δD
-20
-10
0
10
20
30
δ18O
meteoric waters
ocean waters
metamorphic waters
magmatic waters
organic waters
typical error

Fig. 8

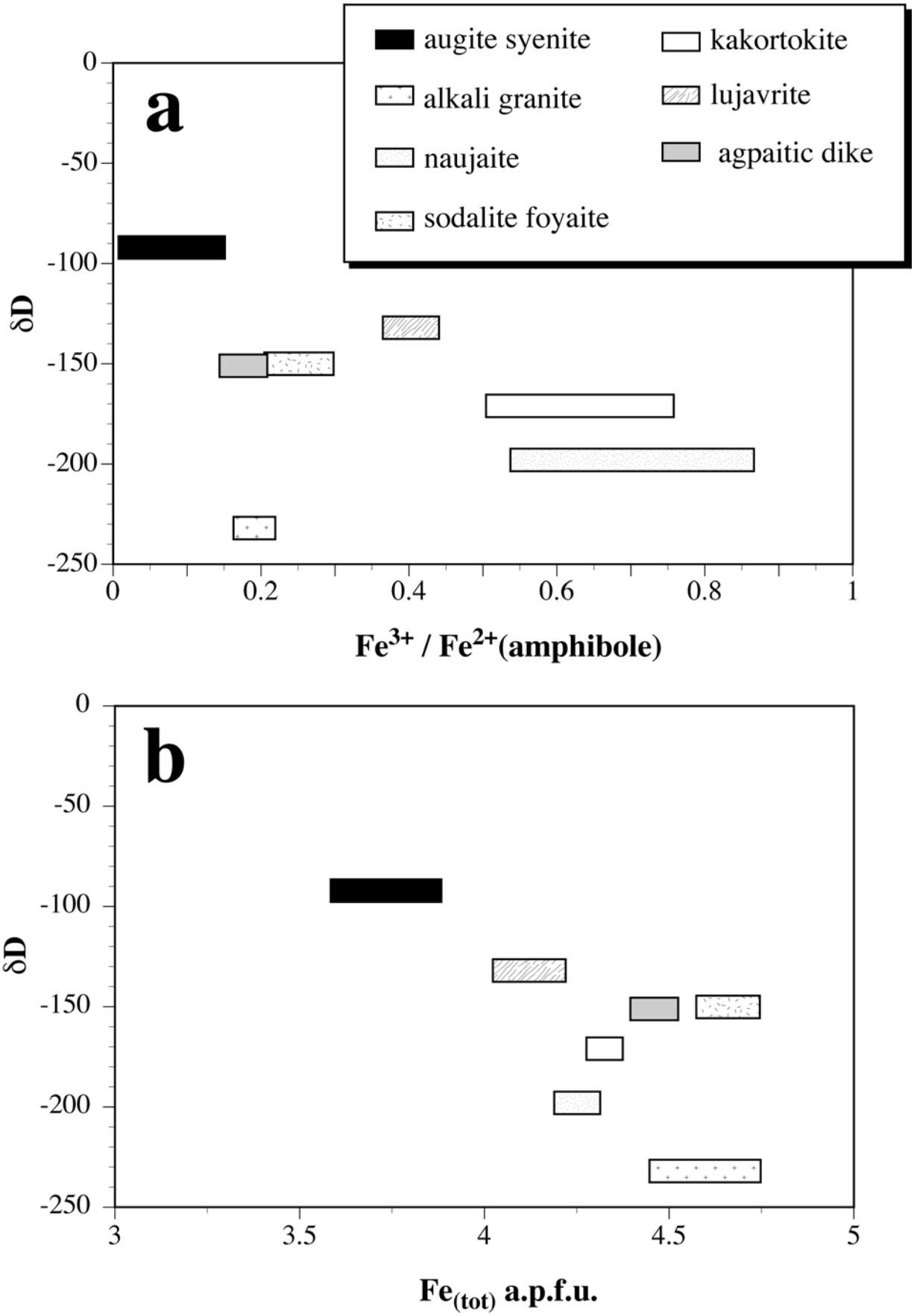
a
augite syenite
alkali granite
naujaite
sodalite foyaite
kakortokite
lujavrite
agpaitic dike
δD
0
-50
-100
-150
-200
-250
0
0.2
0.4
0.6
0.8
1
Fe3+ / Fe2+(amphibole)
b
δD
0
-50
-100
-150
-200
-250
3
3.5
4
4.5
5
Fe(tot) a.p.f.u.

Kapitel 4: Vergleichende petrologische Untersuchungen zwischen Gesteinen der Ilímaussaq Intrusion und einem assoziierten agpaitischen Ganggestein.

Manuskript-Titel:
ILÍMAUSSAQ "EN MINIATURE": CLOSED-SYSTEM FRACTIONATION IN AN AGPAITIC DYKE ROCK FROM THE GARDAR PROVINCE, SOUTH GREENLAND.

Autoren:
Michael Marks[1], Gregor Markl[1]

[1] Institut für Geowissenschaften, Eberhard-Karls-Universität Tübingen, Wilhelmstrasse 56, 72074 Tübingen.

Im Druck bei:
Mineralogical Magazine (Special Volume über Alkaligesteine)

Gutachter:
Prof C.H. Emeleus (Durham), ein anonymer Gutachter, Prof. I. Coulson (Regina)

Eigenanteile:

a) Idee	50 %
b) Probenbeschaffung	100 %
c) Datenbeschaffung	100 %
d) Auswertung und Interpretation	80 %
e) Ausarbeitung der Publikation	90 %

Abstract

Based on petrography, mineral chemistry, and petrology, the physico-chemical evolution of an agpaitic dyke was found to be very similar to that of the neighbouring Ilímaussaq complex. Various mineral assemblages were used to reconstruct the crystallization conditions of the dyke rock for different stages during cooling. The early magmatic phenocryst assemblage is alkali feldspar + nepheline + augite + olivine + magnetite and indicates liquidus temperatures of around 850°C, silica activities of about 0.5, and oxygen fugacities of FMQ -1.5 to -3. The groundmass assemblage albite + microcline + nepheline + sodalite + arfvedsonite + aegirine + aenigmatite + astrophyllite indicates lower temperatures of between 600° and 450°C, at silica activities of 0.25, and oxygen fugacities around the FMQ buffer. Amphibole composition strongly responds to fluorite saturation and proves crystallization occurred in a system closed to oxygen. Late-stage hydrothermal conditions are indicated by the conversion of nepheline and sodalite to analcime and the growth of aegirine on arfvedsonite. These late-stage reactions are constrained to temperatures of <300°C, water activities of between 0.5 and unity, and oxygen fugacities above MH. The dyke has to be regarded as a small equivalent of the larger Ilímaussaq complex, in which identical differentiation processes proceeded at a scale very different in terms of magma volume and cooling times.

Keywords: peralkaline, agpaitic, closed-system fractionation, Ilímaussaq, South Greenland.

Introduction

Based on their molar (Na+K)/Al ratio, alkaline igneous rocks are subdivided into peralkaline (>1.0) and agpaitic (>1.2) rocks (Ussing, 1912). The term agpaitic is restricted to nepheline syenites, which are additionally characterized by the occurrence of complex Zr- and Ti-silicate minerals, such as eudialyte (Sørensen, 1997). Based on the type of rare-metal silicates and accessory minerals present, a further subdivision into miaskitic, low agpaitic, medium agpaitic, highly agpaitic and hyperagpaitic rocks has been introduced by Khomyakov (1995). Geochemically, agpaitic rocks are characterized by high contents of alkali metals, halogens, and rare elements such as Li, Be, Rb, Ga, Zr, Zn, REE and by the presence of aegirine and sodium di-silicate in the norm (Sørensen, 1997). They have low contents of compatible elements like Mg, Ca, Cr, Sc, Co, Ni. Whole rock and mineral ratios of Mg/Fe, Mg/Li, K/Na, Ca/(Na+K) approach zero, whereas others like Zr/Hf or Cl/Br increase to exceptionally high levels. Based on all these characteristics, agpaitic rocks represent the most differentiated plutonic rocks known.

The genesis of agpaitic rocks is generally explained by prolonged fractional crystallization of alkali basaltic or nephelinitic mantle-derived magmas (Larsen and Sørensen, 1987; Kramm and

Kogarko, 1994; Stevenson *et al.*, 1997; Frisch and Abdel-Rahman, 1999). Contamination with crustal material during emplacement has been shown to play a significant role, mainly in the genesis of silica oversaturated peralkaline rocks (Davies and Macdonald, 1987; Heaman and Machado, 1992; Harris, 1995; Mingram *et al.*, 2000; Schmitt *et al.*, 2000; Späth *et al.*, 2001; Marks *et al.*, 2003), whereas closed-system fractionation without significant contamination has been postulated for the evolution of the agpaitic Ilímaussaq intrusion (Markl *et al.*, 2001).

Experimental results have demonstrated that agpaitic rocks have an unusually long crystallization interval, down to temperatures of less than 400°C (Piotrowski and Edgar, 1970; Sood and Edgar, 1970, Edgar and Parker, 1974; Kogarko and Romanchev, 1977; 1982; Scaillet and MacDonald, 2001). This long crystallization interval is mainly explained by the retention of volatiles and alkali metals in the melt by prohibiting their exsolution into a residual fluid phase. Therefore, a continuous transition from peralkaline volatile-rich silicate melts to hydrothermal sodium-oversaturated solutions is assumed (Kogarko, 1974; Khomyakov, 1995; Sørensen, 1997). The late separation of a sodium-rich fluid phase causes late- to post-magmatic alteration of the primary mineral assemblage (e.g. Salvi and Williams-Jones, 1990; Boily and Williams-Jones, 1995; Markl, 2001; Markl *et al.*, 2001a; Chakhmouradian and Mitchell, 2002; Markl and Baumgartner, 2002). At some localities, these residual fluids give rise to the formation of ore deposits of high economic potential (Sørensen, 1992).

The effects of retained and circulating fluids have been studied in some peralkaline intrusions of the alkaline Gardar Province of South Greenland (Parsons *et al.*, 1991; Finch *et al.*, 1995; Coulson, 1997; Markl, 2001; Markl *et al.*, 2001a; and Marks *et al.*, 2003). Probably the best-known and most extensively studied of these intrusions is the Ilímaussaq intrusion. Field geology, geochemistry, systematic mineralogy and the economic potential of the intrusion have been extensively discussed, and are reviewed in Sørensen (2001). Based on mineral chemistry and phase petrology it has been shown that the extreme fractionation trend, found in the Ilímaussaq complex, is governed by low water activity, low SiO_2 activity, low oxygen fugacity and a principally closed-system evolution (Larsen, 1976; 1977; 1981; Markl *et al.*, 2001a, b; Marks and Markl, 2001).

The agpaitic dyke rock, which is the focus of this work, was first described by Allaart (1969). It was found to be the youngest member of a dyke swarm southeast of the Ilímaussaq intrusion. Based on petrographic similarities to some of the layered nepheline syenites (kakortokites) of the Ilímaussaq complex, he termed the dyke a micro-kakortokite (MiKa) and proposed it to represent a hypabyssal extension of the main Ilímaussaq kakortokites. We will show that this hypothesis is not in full agreement with our detailed petrographic and isotopic data. Larsen and Steenfelt (1974) presented some mineral and whole rock geochemical data on the dyke, based

on which, they also concluded that the dyke formed from the Ilímaussaq magmas. Furthermore they suggested that high temperatures in the country rocks due to the vicinity of the Ilímaussaq intrusion, led to a loss of alkalis, water and halogens, in some parts of the dyke. The present study investigates the fractionation mechanisms in this volumetrically small dyke as compared to its larger neighbour (the Ilímaussaq magma chamber) and tries to delimit the time of separation of the two.

Geology

South Greenland is characterized by extensive mid-Proterozoic rift-related alkaline magmatism (e.g. Upton *et al.*, 2003). Interlayered lavas and sedimentary rocks (Eriksfjord Formation; Poulsen, 1964), numerous dyke rocks of variable composition, and about ten alkaline plutonic centres intruded the Ketilidian basement, which consists of Early-Proterozoic granites and gneisses (Emeleus and Upton, 1976). It is believed that magmatism during the Gardar Period (1.30 to 1.12 Ga) involved three principal cycles of activity (Early, Mid and Late; Upton and Blundell, 1978). Each extensional phase commenced with the uprise of olivine basaltic to hawaiitic magmas and terminated with the emplacement of highly fractionated alkaline plutonic centres (Upton and Blundell, 1978).

During the Late-Gardar period (about 1.20 – 1.12 Ga), two WSW-ENE to SW-NE trending dyke swarms intruded in two main areas, which are separated by a zone in which Gardar-aged dykes are rare (Upton and Emeleus, 1987). The southerly swarm, of which the micro-kakortokite is a part, occurs on the Tugtutôq islands and the Narsaq peninsula and can be traced northeastwards to Mellemlandet and the G. F. Holm Nunataq, where it disappears under the ice cover. The dyke compositions of the swarm range from primitive olivine basalt through hawaiitic and benmoreitic to phonolitic, trachytic, and alkali rhyolitic compositions. Lamprophyres and carbonatitic dykes are less abundant (e.g. Scharbert, 1967; Allaart, 1969; Macdonald, 1966; Upton and Fitton, 1985). Some basaltic dykes of the swarm (“Big Feldspar Dykes”) contain plagioclase megacrysts, which are interpreted to stem from anorthosite xenoliths (Bridgwater, 1967; Bridgewater and Harry, 1968; Watt, 1968; Halama *et al.*, 2002). The dykes are remarkable in their size and lateral extension: widths of 5 – 20 m are common and many of them can be traced over several tens of kilometres. The plutonic complexes of Tugtutoq, Ilímaussaq and Igaliko are situated within this dyke swarm, which is more than 100 km long and has a track of about 15 km wide. Fluid inclusion data from the Ilímaussaq complex (Konnerup-Madsen and Rose Hansen, 1984; Markl *et al.*, 2001a), and estimates of the overburden sedimentary rocks and lavas (Poulsen, 1964) indicate that the plutonic complexes, and by analogy the dykes, intruded at a high crustal level (3 - 5 km) and probably had surface expression (Emeleus and Upton, 1976; Upton *et al.*, 2003).

Field observations and petrography

The MiKa dyke has a total length of about 18 km and a variable width of between 10 and 30 m. The contacts with the basement granite are always sharp. Towards its western termination, it appears to cut the marginal augite syenite of the Ilímaussaq intrusion (Larsen and Steenfelt, 1974). However, at outcrop evidence is inconclusive as to whether there is a connection between the dyke sections on either side of the intrusion. (Fig. 1). On the basis of petrography and whole rock geochemistry, Larsen and Steenfelt (1974) distinguished two different facies of the dyke: a high-alkali facies and a low-alkali facies, the latter being explained by loss of alkalis, water, and halogens, which they attributed to the thermal effect of the Ilímaussaq intrusion. The low-alkali facies of the dyke is restricted to its westernmost part, in the vicinity of the Ilímaussaq intrusion, and will not be discussed further here. All samples of this study are taken from the high-alkali facies and sample localities are shown in Fig. 1. At each locality, a sampling profile from the margin towards the centre of the dyke (e.g. approximately parallel to the assumed direction of crystallization) was collected. Most samples were taken from approximately the same stratigraphic height of between 600 and 800 m above sea level. The dyke rock is dark green to dark grey and cm-scale feldspar and nepheline phenocrysts, in a fine-grained matrix (Fig. 2a), are abundant throughout. The feldspar phenocrysts are aligned parallel to the contacts of the dyke. At some localities, the dyke is marginally “chilled” with no phenocrysts in the outer 15 – 30 cm. Some samples contain additional phenocrysts of olivine, augite, and magnetite up to some mm in size. The major groundmass minerals are albite, microcline, nepheline, sodalite, aegirine, arfvedsonite, and aenigmatite. Minor and accessory minerals are eudialyte, astrophyllite, zircon, hjordahlite, monazite, titanite, apatite, fluorite, and various sulphides. Late-stage or secondary minerals include analcime, natrolite, and Fe-hydroxides. Table 1 shows the mineral abbreviations used in the text and figures; Table 2 summarizes the mineral assemblages found in the samples studied.

Feldspar phenocrysts are cryptoperthitic alkali feldspar (Fig. 2b). In one sample from the margin of the dyke (GM1846), µm-sized Ba-rich patches occur within one perthitic feldspar phenocryst (Fig. 2c and 2d). Groundmass feldspars are discrete grains of albite and microcline. In some samples, microcline forms small euhedral laths and albite occurs as anhedral grains (Fig. 2e). In other samples, the opposite is the case. Albite is partly altered to analcime.

Nepheline phenocrysts are present in most samples (Fig. 2a). In some samples, nepheline is found as euhedral to subhedral inclusions in feldspar phenocrysts (Fig. 2b). These crystals have slightly corroded margins and are associated with aegirine aggregates occurring at the margins of

the nepheline. In the groundmass, small nepheline crystals are rarely euhedral but mostly subhedral, interstitial grains (Fig. 2f), which are partly altered to analcime.

Sodalite forms anhedral crystals in the groundmass. In some places, euhedral microcline laths occur as inclusions in sodalite (Fig. 2e). At the rims, along cracks and, locally, at the contact to microcline, sodalite has been replaced by analcime.

Olivine phenocrysts are in most cases rimmed by arfvedsonite or aegirine (Fig. 3a). In samples GM1846 - GM1852, olivine is replaced by orange to red iron hydroxides ("iddingsite"), whereas in most other samples, relics of olivine are still present. Rarely, olivine was found as an inclusion in alkali feldspar phenocrysts.

Magnetite occurs as anhedral inclusions in augite (Fig. 3a) or as subhedral to anhedral phenocrysts rimmed by arfvedsonite, astrophyllite, aegirine, aenigmatite or an intergrowth of these phases (Fig. 3b).

Augite forms subhedral phenocrysts, which are commonly associated with olivine and magnetite (Fig. 3a). It is strongly zoned with colourless to grey cores and grass green poikilitic aegirine-rich rims. Along cracks, augite has typically been converted to aegirine (Fig. 3c).

Aegirine, arfvedsonite and aenigmatite occur as mafic groundmass minerals in different modal proportions. Texturally, they are clearly later than olivine, augite, and magnetite. Samples from the margin of the dyke are dominated by aegirine. Towards the centre of the dyke, the modal contents of arfvedsonite and aenigmatite increase (Fig. 3d). In most samples, aegirine, arfvedsonite, and aenigmatite appear to coexist (Fig. 3e). However, each can be observed to overgrow or replace the others, often within the same sample (Figs. 3f). Where arfvedsonite is replaced by aegirine, secondary fluorite and Fe-hydroxides occur. Additional interstitial (i.e. magmatic) fluorite occurs only in samples GM1846-GM1851. Eudialyte occurs as an interstitial groundmass phase; more rarely it is included in aegirine. Hjordahlite, zircon, apatite, titanite, monazite, and various sulphides occur as inclusions in groundmass feldspar, aegirine, amphibole, and aenigmatite.

Mineral chemistry

Analytical methods

Some mineral data have been presented by Larsen and Steenfelt (1974). Here we augment these analyses with detailed microprobe data on a variety of mineral phases from the dyke.

Electron microprobe measurements of minerals were performed using a JEOL 8900 electron microprobe at the Institut für Geowissenschaften at the Universität Tübingen, Germany. The emission current was 15 nA and acceleration voltage, 15 kV. Peak counting times were 16 s for major and 30-60 s for minor elements. Background counting times were half of the peak counting

times. Natural (albite, baryte, sanidine, diopside, hematite, rhodochrosite, fluorite, tugtupite) and synthetic ($SrTiO_3$, MgO, Al_2O_3, Zr) standards were used for calibration. To avoid Na migration under the electron beam, feldspar, nepheline, analcime, and sodalite were analysed using a defocused beam of 15 μm diameter. The peak overlap between the Fe Lβ and F Kα lines and the Ba Lα1(3) and AlKα lines has been corrected. Data reduction was performed using internal ϕρZ procedures of JEOL (Armstrong, 1991).

Bulk compositions of perthitic feldspars were recalculated by combining image processing (NIH Image software) of BSE-images of the perthitic minerals with point analyses of the exsolved phases (see Marks and Markl, 2001, for a detailed description of the technique). Bulk feldspar compositions in each sample were calculated from the average of 3 to 5 different re-integrated grains.

Feldspar

Euhedral alkali feldspar phenocrysts in sample GM1846 are exsolved into pure albite and K-feldspar. One phenocryst contains small Ba-rich areas within the exsolved K-feldspar phase (Figs. 2c and 2d). In this phenocryst, the exsolved K-feldspar varies in composition between $Or_{93}Ab_7$ and $Or_{99}Ab_1$, and the exsolved albite phase has almost end-member composition ($Ab_{98}Or_2$-Ab_{100}). Both phases are essentially Ba- and Ca-free (<0.05 wt. % BaO and CaO, respectively). Among the two Ba-bearing feldspar phases, which show sharp borderlines against each other, two compositional ranges occur: $Ab_2Or_{96}Cs_2$ – $Ab_{10}Or_{85}Cs_5$ and $Ab_{10}Or_{70}Cs_{20}$ – $Ab_9Or_{49}Cs_{42}$. Tiny grains of extremely celsian-rich feldspar have compositions of about $Ab_{10}Or_{17}Cs_{73}$ (Fig. 4).

The recalculated magmatic composition of feldspar in all other samples varies between $Ab_{41}Or_{59}$ and $Ab_{60}Or_{40}$ and is invariably Ca-free (Fig. 4). Ba contents are below 0.1 wt. %. The feldspar in the groundmass consists of separate grains of end-member albite and end-member microcline with no measurable amounts of Ca and Ba. Sr contents in all types of feldspar reach about 0.6 wt. % SrO, but show no systematic behaviour with any of the other elements. Representative analyses are shown in Table 3.

Nepheline

Nepheline phenocrysts show a wide range of compositions between $Ne_{67}Ks_{12}Qtz_{21}$ and $Ne_{75}Ks_{21}Qtz_4$. Some phenocrysts are chemically zoned with increasing Ks component and decreasing Qtz component towards the rim. The composition of groundmass nepheline overlaps with that of phenocrysts but shows a clear tendency to more Ks-rich and Qtz-poor compositions (Fig. 5, Table 4). CaO is in all cases < 0.5 wt. %.

Sodalite

Sodalite approaches an end-member composition, with SO_3 contents of below 1.5 wt. % (Table 5). In some chemically zoned crystals, SO_3 contents decrease from core to rim.

Olivine

Olivine ranges in composition from $Fo_{12}Fa_{81}Tp_5La_2$ to $Fo_1Fa_{92}Tp_6La_1$ (Table 6). It is not zoned and there is only a small compositional range within one specific sample. Mn reaches up to 4.2 wt. % MnO and is positively correlated with Fe content (Fig. 6). CaO varies between 0.6 and 1.6 wt. % and is positively correlated with Fe. An exception is sample MiKa 28, which displays a low Ca content (Fig. 6).

Clinopyroxene

Clinopyroxene phenocrysts range in composition of between $Aeg_9Jd_0Di_{35}Hed_{56}$ and $Aeg_{82}Jd_{12}Di_0Hed_6$ (Fig. 7, Table 7). They have Ca-rich cores ($Aeg_9Jd_0Di_{35}Hed_{56}$ to $Aeg_{14}Jd_6Di_7Hed_{73}$), but show a strong Na-enrichment at the rim of and along cracks within the mineral grains. The compositional range found by Larsen and Steenfelt (1974) displays more Mg-rich compositions of $Aeg_6Di_{48}Hed_{46}$. Figure 8a shows zoning profiles from the core to the rim of a phenocryst, illustrated in Figure 3a. Fe^{3+} contents are calculated based on stoichiometry (4 cations and 6 oxygens). After a smooth enrichment of Na and Fe^{3+} towards the rim of the crystal, a sudden increase of Na, Fe^{3+}, and Al^{VI} at the outermost rim can be detected, whereas Ca, Fe^{2+}, Mg, Al^{IV}, Mn, Ti and Zr decrease. At the rim, Na contents exceed Fe^{3+}. This indicates the presence of significant amounts of the jadeite molecule (up to 12 mol%), in addition to aegirine.

In rare cases, hedenbergite phenocrysts with older and partially rounded cores (Fig. 2c) show strong enrichment of Fe^{2+} and Mn and depletion of Mg in the core region (Fig. 8b). Ti and Al^{IV} are relatively high, whereas Al^{VI} is low. Ca, Na, Fe^{3+}, and Zr are rather constant and have concentrations comparable to the normal phenocrysts.

The groundmass pyroxene in all samples is aegirine with a compositional range of between $Aeg_{73}Jd_0Di_2Hed_{25}$ and $Aeg_{88}Jd_{12}Di_0Hed_0$ (Fig. 7, Table 7). Aegirine is essentially unzoned. The most important minor element is Al reaching 3.2 wt. %, resulting in a jadeite component of up to 12 mol%. In many cases, Na content exceeds total Fe^{3+} and Al^{VI}. This indicates the presence of other Na-bearing components such as $NaTiAlSiO_6$ as proposed by Larsen (1976) for the Ilímaussaq pyroxenes. The CaO content is negatively correlated with aegirine component. CaO is low in samples from the outer parts of the dyke (< 2 wt. %), but relatively high (up to 8 wt. %) in samples

from central parts. TiO_2, MnO, and ZrO_2 are below 1.6 wt. %, 0.6 wt. %, and 0.2 wt. %, respectively, with the highest Ti and Zr and the lowest Mn contents in aegirine of marginal samples.

Fe-Ti oxides

Magnetite ranges in composition between $Mt_{40}Usp_{57}Sp_3$ and $Mt_{21}Usp_{78}Sp_1$. Despite the Ti-rich composition, no signs of later oxy-exsolution have been observed. MgO contents are less than 0.1 wt. % and ZnO contents less than 0.6 wt. %. Al_2O_3 reaches around 2 wt. % and MnO around 5.5 wt. %. Representative analyses are shown in Table 8.

Amphibole

Amphibole in all samples is arfvedsonite with X_{Fe} (Fe^{2+} / (Mg + Fe^{2+})) of between 0.96 and 0.99. Some typical analyses are reported in Table 9. Fe^{3+} contents are calculated based on stoichiometry (16 cations and 23 oxygens). On the basis of F and Ca content, two groups of amphiboles can be distinguished. Group 1 is F- and Ca-rich and comes from the eastern samples MiKa 13, 14, 24 and 28, group 2 is Ca- and F-poor from samples the western samples GM1847 – GM1851, which were collected close to the Ilímaussaq intrusion (Figs. 1 and 9a). In group 1 amphiboles, F reaches up to 2.2 wt. %. In group 2 amphiboles, F contents do not exceed 0.2 wt. %. Cl in all samples is <0.03 wt. %. Si varies between 7.6 a.p.f.u. and 8 a.p.f.u., with the lowest Si contents occurring in amphiboles of group 1. Zoned crystals of group 1 amphiboles show an increase of Si and Fe^{2+} and a decrease of Fe^{3+} from core to rim, whereas the other elements are more or less constant. Group 2 amphiboles less zoned. At the same Si content, group 1 amphiboles are relatively high in Fe^{2+}, Ca, and F and low in Fe^{3+}, Na, Ti and Mg compared to group 2 amphiboles (Fig. 9b). For Al and Mn, there is no significant difference. In both groups, Si is positively correlated with Fe^{2+} and negatively with Fe^{3+}, but on a different level (Fig. 9b). A positive correlation between Si and Ca and a negative one with Na is clear for group 2, but less obvious for group 1 amphiboles (Fig. 9b). Hence, the most important substitution for both groups is 2 Fe^{3+} <-> Fe^{2+} + Si, whereas the substitution Na_B + Fe^{3+} <-> Ca + Fe^{2+} is significant only in group 2 amphiboles.

Aenigmatite

According to the classification scheme of Kunzmann (1999), aenigmatites in the dyke belong to the aenigmatite subgroup and are dominated by the aenigmatite-wilkinsonite cation exchange (Fe^{2+} + Ti^{4+} <-> 2 Fe^{3+}). A substitution towards the rhönite subgroup (Na^+ + Si^{4+} <-> Ca^{2+} + Al^{3+}) is of only minor importance (Fig. 10, Table 10). Overall, the observed compositions vary between $Aen_{95}Wilk_5Rhö_0$ and $Aen_{52}Wilk_{42}Rhö_6$. Minor elements are Mn (up to 3.2 wt. % MnO), Zr (up to 1.1

wt. % ZrO_2), and Mg (up to 0.13 wt. % MgO). Some aenigmatites show distinct chemical zoning with a decrease of rhönite component and an increase of wilkinsonite component from core to rim.

Phase petrology

The mineral assemblages observed were used to constrain the conditions of crystallization of the dyke rock and allow the reconstruction of their changes during emplacement and cooling. The early magmatic stage is represented by the phenocryst assemblage alkali feldspar – nepheline – augite – olivine – magnetite. The groundmass assemblage albite - microcline– nepheline – sodalite – arfvedsonite – aegirine – aenigmatite-astrophylite represents a later stage of crystallization. Still later hydrothermal conditions are indicated by the conversion of nepheline and sodalite to analcime. Parameters to be calculated are T, a_{SiO2}, f_{O2}, a_{H2O}, and a_{NaCl}.

Early magmatic conditions

The following equilibria among nepheline, albite, and jadeite (components in nepheline, alkali feldspar and clinopyroxene solid solution) were used to constrain T and a_{SiO2} for the early magmatic conditions:

albite	=	jadeite + SiO_2	(1)
albite	=	nepheline + 2 SiO_2	(2)
nepheline	=	jadeite + SiO_2	(3)

We used the range of nepheline, clinopyroxene, and alkali feldspar compositions observed in phenocrysts. Additionally, equilibria among olivine, clinopyroxene and magnetite were used to calculate T, a_{SiO2} and f_{O2} during crystallization of these mafic phenocrysts.

Late magmatic conditions

Crystallization conditions of the groundmass assemblage were calculated based on compositions of the groundmass minerals albite, nepheline, and aegirine. With the following equilibria, it is possible to constrain T, a_{SiO2}, a_{H2O}, and a_{NaCl} during late-stage conditions:

6 nepheline + 2 NaCl	=	sodalite	(4)
nepheline + SiO_2 + H_2O	=	analcime	(5)
sodalite + 6 SiO_2 + 6 H_2O	=	6 analcime + 2 NaCl	(6)

The groundmass assemblage aegirine-arfvedsonite-aenigmatite buffers oxygen fugacity by equilibria of the general type (related to observed textures, but not stoichiometrically balanced except for eq. (9)):

arfvedsonite + O_2	=	aegirine + aenigmatite	(7)
aenigmatite + O_2	=	aegirine	(8)

Late-stage decomposition of arfvedsonite is constraint by the following equilibrium:

arfvedsonite + O_2	=	3 aegirine + hematite + 2 SiO_2	(9)

In principle, equilibria (7) and (8) would allow calculation of the oxygen fugacity for the assemblage aegirine-arfvedsonite-aenigmatite, if reliable thermodynamic data of arfvedsonite and aenigmatite existed. Unfortunately, this is not the case.

Methods of calculation

Phase diagrams in the system Na-Al-Si-O-Cl-H were calculated using the GEOCALC software of Berman *et al.* (1987) and Lieberman and Petrakakis (1990) with the database of Berman (1988). Thermodynamic data for analcime and sodalite were taken from Sharp *et al.* (1989) and Johnson *et al.* (1992). End-member component activities from mineral formulae were calculated using the solution model of Fuhrman and Lindsley (1988) for feldspar and the model of Holland (1990) for clinopyroxene. For nepheline, a mixing on site model was used, analcime and sodalite were treated as pure phases. Unit activity of SiO_2 was referred to a standard state of a pure SiO_2 modification at P and T. Equilibria among olivine, clinopyroxene and magnetite were calculated using the QUILF program of Andersen *et al.* (1993). For a discussion of the theoretical background of the QUILF calculations see Frost and Lindsley (1992) and Lindsley and Frost (1992). Markl *et al.* (1998) showed that clinopyroxene tends to become enriched in Mg during later re-equilibration. In order to minimize these effects, the average olivine composition and the most Fe-rich core composition of clinopyroxene were used for these calculations. Details of the procedure are given in Marks and Markl (2001). The uncertainty of these calculations are estimated at about ± 50°C for temperature and ± 0.05 for silica activity.

Evolution of crystallization conditions during cooling

Pressure

Based on fluid inclusion data (Konnerup-Madsen and Rose-Hansen, 1984; Markl *et al.*, 2001a) and estimated overburden (Poulsen, 1964), the pressure of emplacement of the Ilímaussaq intrusion was estimated to be about 1 kbar. By analogy, all calculations for the MiKa were performed for a fixed pressure of 1 kbar.

Temperature and silica activity

The results of nepheline liquidus thermometry after Hamilton (1961) are illustrated on Fig. 5. Nepheline phenocrysts indicate temperatures between about 900°C and < 500°C, whereas groundmass nepheline temperatures are invariably below 775°C.

Equilibration temperatures between 840° and 690°C at silica activities from 0.5 to 0.25 where deduced from the olivine-augite-magnetite assemblage with the QUILF program (Andersen *et al.*, 1993) (Fig. 11). There is a fairly good correlation between degree of fractionation (expressed as X_{Fe} in olivine) and calculated T and a_{SiO2}.

Equilibria (1) – (3) among nepheline, albite, and jadeite (components in nepheline, alkali feldspar and clinopyroxene solid solution) for the early magmatic phenocrysts indicate liquidus temperatures of between 720° and 780°C and silica activities of between 0.5 and 0.4 (Fig. 12 a). The same calculations for groundmass nepheline, albite and aegirine indicate temperatures between 450° and 600°C and lower silica activities of about 0.4 to 0.25 (Fig. 12 b). Sodalite crystallized at temperatures of less than 400°C (Fig. 13 a). The late-stage formation of analcime at the expense of nepheline and sodalite was calculated to occur at temperatures of below about 300°C, assuming a low silica activity of about 0.2 (Fig. 13 b). This low value was assumed because a decrease in silica activity during cooling was shown to occur in similar phase assemblages in the Ilímaussaq intrusion (Markl *et al.*, 2001) and because of the significant decrease in a_{SiO2} from early to late-magmatic conditions. In summary, the different mineral assemblages in the dyke record the complete history of crystallization from early magmatic conditions at 850°-900°C down to late-stage hydrothermal fluid activity, at below 300°C. During this process, silica activity decreases from about 0.5 to at least 0.25, and possibly, even lower values.

Oxygen fugacity

Relative oxygen fugacities during early magmatic conditions were calculated using the assemblage olivine-augite-magnetite. In the early magmatic stage, relative oxygen fugacity

decreases from about FMQ -1.5 to about FMQ -3. The stabilization of aenigmatite-aegirine-arfvedsonite assemblages at the expense of the olivine-augite-magnetite assemblage during late magmatic conditions indicates that after evolving along a lower f_{O2} displaced FMQ buffer, during early magmatic conditions, oxygen fugacity reached and possibly exceeded that of the synthetic FMQ buffer value (Nicholls and Carmichael, 1969; Marsh, 1975; Marks *et al.*, 2003). The destabilization of arfvedsonite and the formation of aegirine (Reaction (9)) associated with Fe-hydroxides indicates a further rise in oxygen fugacity during hydrothermal activity. The T-f_{O2}-dependency of this equilibrium was calculated for similar mineral activities by Marks *et al.* (2003). They showed that this reaction occurs at low temperatures of around 300°C and at oxygen fugacities slightly above the HM buffer.

Water and NaCl activity

Equilibrium (5) constrains the formation of analcime at the expense of nepheline at low silica activities of about 0.2 and temperatures between 200° and 300°C, and at water activities of between 0.5 and unity (Fig. 13 b). Equilibrium of sodalite with groundmass nepheline buffers NaCl activity and was calculated to occur at temperatures of below about 400°C. According to the calculated T-a_{NaCl} dependency of equilibrium (4), higher temperatures would prevent the stable formation of sodalite. Using equilibria (4) – (6) among nepheline, sodalite, and analcime, the activity of NaCl during late-stage conditions is estimated to range between 0.1 and 0.4 (Fig. 13 b).

Discussion

Interpretation of mineral chemistry

The compositional variation of the rock-forming minerals reflect typical fractional crystallization processes. With increasing Fe content (degree of fractionation) olivine becomes more Mn- and Ca-rich. The high Mn-contents are comparable to other silica-undersaturated suites (e.g. Stephenson, 1974) and reflect the highly fractionated state of the parent magma. High contents of Ca in a relatively Ca-poor magma are indicative of low silica activities and low pressure, during crystallization (Stormer, 1972; Markl *et al.*, 2001 b). Because Ca is known to have fast diffusion rates in olivine (e.g. McKay *et al.*, 1998), the exceptionally low Ca contents in olivine from sample MiKa 28 may be due to post-magmatic diffusional re-equilibration related to lower cooling rates of this sample, which is from the central part of the dyke.

There are two different types of augite phenocrysts present in the dyke (Fig. 8). Augite of sample MiKa 14 (Figs. 3a and 8b) reflects an early stage of fractional crystallization with a relatively Mg-rich and Mn-poor core, whereas augite of sample GM1852 (Figs. 3c and 8a)

crystallized later (but still during the early magmatic stage), since the Fe and Mg content in the core of this crystal is approximately the same as at the rim of the MiKa 14 augite. Further fractional crystallization led to a progressive enrichment of Na and Fe^{3+}. The sudden increase of Na, Fe^{3+}, and Al^{VI} at the outermost rim, and along cracks, may be due to the later activity of a sodium-rich and oxidizing residual melt or fluid phase. According to equilibrium (1), relatively high contents of Al^{VI} in pyroxene, at this stage, may be due to low silica activities in this residual melt/fluid. The sudden decrease of minor elements (Mn, Ti, Zr) in augite may be ascribed to precipitation of eudialyte, which acts as a sink for these elements (Larsen, 1976; Markl *et al.*, 2001a).

Amphibole compositions vary along the strike of the dyke: the westernmost samples (GM1847-GM1851) are Ca- and F-poor, the more easterly samples (MiKa 13, 14, 24, 28) are Ca- and F-rich. In view of these chemical differences, it is tempting to look for a relation with fluorite occurrence. Indeed, detailed petrography showed that interstitial (i.e. magmatic) fluorite occurs only in samples with low-Ca and low-F amphiboles but not in samples with Ca- and F-rich amphiboles. Thus, amphibole chemistry is governed by fluorite saturation in the melt, which obviously was reached only in the westernmost part of the dyke, close to the Ilímaussaq intrusion. This may reflect inhomogeneities in the melt, the thermal effect caused by the hot pluton, or slightly different outcrop levels with respect to original crystallization in the dyke. Since amphibole is, apart from fluorite, the only major F-bearing mineral phase in these rocks, it is an important tracer for such effects.

Another important feature to be explained is the increase of Si and the decrease of Fe^{3+} in the amphiboles with progressive fractionation, which is governed by the substitution mechanism 2 Fe^{3+} <-> Fe^{2+} + Si. This effect can be seen both in amphibole core-rim zoning patterns and in the comparison of samples from the margin and from the centre of the dyke. This compositional evolution results in a decrease of the Fe^{3+}/Fe^{2+} ratio of the amphiboles during fractionation, which may be explained by crystallization in a system closed with respect to oxygen (see Philpotts, 1990, page 210). Once early amphibole crystallized with a high Fe^{3+}/Fe^{2+} ratio, the absolute oxygen fugacity in the system decreases and results in later amphibole having a lower Fe^{3+}/Fe^{2+} ratio. This process works, despite the fact that relative oxygen fugacity increased during cooling of the magma (see later), because amphibole crystallization probably occurred over a relatively small temperature interval.

Comparison with the Ilímaussaq rocks

Asite from their close proximity, the petrographical and mineralogical similarities, specifically their principal mineral assemblages, mineral chemistry and the evolutionary trends, of the intrinsic

parameters between the MiKa and the agpaitic nepheline syenites of the Ilímaussaq intrusion, imply a close relationship between the dyke rock and the intrusive complex (Allaart, 1969; Larsen and Steenfelt, 1974). The most obvious similarities between the investigated MiKa samples and the agpaitic Ilímaussaq complex are as follows:

- The early mafic minerals of the MiKa are olivine, Ti-rich magnetite, and augite. The same is the case in the early alkaline member of the Ilímaussaq complex, the augite syenite (Larsen, 1976; Marks and Markl, 2001). In both rocks, olivine approaches end-member fayalite and augite, hedenbergite composition, and the latter shows a pronounced Na-enrichment towards the rim (Fig. 8). Relics of this mineral assemblage are preserved in the early agpaitic sodalite foyaite of the Ilímaussaq complex (Larsen, 1976; Markl *et al.*, 2001a) and are overgrown or resorbed by aegirine and arfvedsonite. The same can be seen in the MiKa samples.
- In the agpaites of the Ilímaussaq intrusion and in the MiKa, aegirine, arfvedsonite, aenigmatite, sodalite and eudialyte are stable phases in the later stages of fractionation.
- Feldspar in both the agpaites of the Ilímaussaq complex and the MiKa are invariably Ca-free (Markl *et al.*, 2001a). Early feldspar phenocrysts in the MiKa are albite-K-feldspar solid solutions, which is also the case for all Ilímaussaq agpaites except for the late lujavrites (e.g. Ferguson, 1964; Larsen, 1976). These lujavrites contain two separate feldspars (albite and K-feldspar), which are mirrored by the groundmass feldspars of the MiKa.
- The textures resulting from the late-stage replacement of nepheline, albite, and sodalite by analcime and natrolite in the MiKa show remarkable similarities to the late-stage assemblages in the Ilímaussaq rocks (Markl *et al.*, 2001a; Markl and Baumgartner, 2002).
- Oxygen isotope composition of olivine from the MiKa dyke and the augite syenite of the Ilímaussaq intrusion are remarkably similar (Marks *et al.*, unpublished data).

Similar mineral assemblages and similar mineral compositions reflect similar petrological evolutionary trends: Phase equilibria in the MiKa record early magmatic temperatures of about 850° and hydrothermal fluid activity at temperatures less than 300°C, a systematic decrease of silica activity from early magmatic to late-stage hydrothermal assemblages, and a change in redox conditions from very reduced, in the early rocks, to oxidized in the later stages. The same can be seen in the Ilímaussaq rocks (Larsen, 1976; Markl *et al.*, 2001a; Marks and Markl, 2001). Neglecting the Ilímaussaq alkali granite, all the different magma batches of the Ilímaussaq intrusion can be correlated to specific phase assemblages of the MiKa. Hence, the fractionation processes known from the Ilímaussaq rocks can be observed in the MiKa in a surprisingly similar way,

despite the large difference in size. Obviously, magma volume is not a crucial factor in determining fractionation trends.

However, some differences between the MiKa and the Ilímaussaq rocks should be emphasized:

- Sodalite in the Ilímaussaq rocks is, in some agpaites, a primary magmatic phase crystallized at temperatures around 800°C (Markl *et al.*, 2001a). In contrast, sodalite occurs only as an anhedral groundmass phase in the MiKa. It crystallized at significantly lower temperatures, governed by the lower nepheline activities in the MiKa compared to the Ilímaussaq rocks.
- Given the same X_{Fe}, early magmatic olivine in the MiKa is more Mn-rich and hedenbergite phenocrysts are more Na-rich than in the Ilímaussaq augite syenite. Additionally, magnetite is more Mn- and Fe^{3+}-rich. (Marks and Markl, 2001). Furthermore, aenigmatite and aegirine clearly dominate in most MiKa samples over Na-amphibole, which is in contrast to most Ilímaussaq agpaites.
- Nd isotope data (Marks *et al.*, unpublished data) show the MiKa to be slightly different from the Ilímaussaq rocks. A positive $\varepsilon_{Nd(T)}$ value of +0.7 compared to the negative values for the plutonic agpaites of the Ilímaussaq complex ($\varepsilon_{Nd(T)}$ between -0.1 and -3.1) implies less contamination with low ε_{Nd} material for the MiKa dyke.

The assumption of Allaart (1969) that the MiKa represents a hypabyssal extension of the kakortokites (layered agpaitic nepheline syenites) of the Ilímaussaq intrusion is not strictly correct because of the significant neodymium isotopic differences. Two kakortokite samples have $\varepsilon_{Nd(T)}$ values of -1.5 and -1.8, respectively (Marks *et al.*, unpublished data), which contrasts the positive $\varepsilon_{Nd(T)}$ value of +0.7 for a MiKa sample. Moreover, the plutonic kakortokites lack early magmatic olivine, hedenbergite and Ti-magnetite. The occurrence of these minerals as early magmatic phases in the MiKa dyke implies that a separation of the dyke from the Ilímaussaq magma must have occurred at the latest during the sodalite foyaite stage (or possibly earlier) of the Ilímaussaq intrusion because olivine, hedenbergite and Ti-magnetite are early magmatic phases only in the early Ilímaussaq rocks (augite syenite and sodalite foyaite) and not in the later agpaites (e.g. kakortokites). Furthermore, the differences in the composition of the early mafic minerals (olivine, augite, magnetite) imply, that the MiKa melt was slightly more evolved and more oxidized than the Ilímaussaq melt. The late crystallization of sodalite, may be explained by lower Cl contents and therefore later crystallization of sodalite in the MiKa magma.

It may well be that this, and the other small compositional and petrographic differences between the dyke and the intrusion, are the result of different amounts of contamination after separation of the two magmas. Petrography clearly suggests an early separation of the dyke from the Ilímaussaq magma and an independent, but remarkably similar, evolution after this separation. However, a

common melt source can be assumed because of the great petrographic and petrologic similarities and the similar oxygen isotopic composition of early magmatic olivine. Based on Nd isotope data, no major contamination of the dyke took place during intrusion and fast ascent through the granitic upper crust (Julianehåb Batholith). We propose that the small heat capacity, and resultant low potential for assimilation of the dyke, was the reason for this. This indicates that the MiKa dyke rock is a less contaminated equivalent of the Ilímaussaq rocks.

Time constraints on dyke cooling

Using the one dimensional stationary heat flow equations of Peacock (1989), we modelled the cooling history of the MiKa dyke rock using MATLAB software. Based on the calculations above, we chose a liquidus temperature of 850°C. The average thermal conductivity for syenites of $k = 8*10^{-7}$ m^2s^{-1} was taken from Landolt-Börnstein (1982) and the half-thickness of the dyke was fixed at 15 m. Assuming a depth of emplacement of 3-5 km and a typical temperature gradient of about 30°C/km, the temperature of the basement was assumed to be below 150°C. With these parameters, we calculated that the dyke cooled down from 850°C to 250°C in less than 10 years. If we consider the thermal effect of the nearby Ilímaussaq intrusion and therefore allow the basement to be as hot as 500°C, the final cooling of the dyke occurred within a time span of about 100 years. A further indication for the fast cooling history is provided by the Ba-rich patches within feldspar phenocryst (Figs. 2c and 2d). Assuming that the Ba-rich patches in the feldspar phenocryst of sample GM1846 represent primary magmatic and not later metasomatic features, they would have been erased if the dyke had remained at temperatures around 800°C for between 2000 and 9000 years (Cherniak, 2002). Hence, the dyke cooled faster than the maximum constraints. This simple calculation shows, that the observed fractionation trends may occur in extraordinarly short time intervals, which are two to four orders of magnitude shorter than for plutonic rocks (e.g. Brown and Fletcher, 1999; Vazquez and Reid, 2002; Charlier and Zellmer, 2002). Obviously, neither the volume in which the fractionation takes place, nor the time span during which it occurs plays a significant role.

Summary

The various mineral assemblages of the agpaitic micro-kakortokite dyke represent different stages of magma evolution and allows the re-construction of the evolution of intrinsic parameters (T, a_{SiO2}, f_{O2}, a_{NaCl}, a_{H2O}) during cooling.

The phenocryst assemblage alkali feldspar + nepheline + olivine + augite + magnetite constrain early magmatic conditions to about 850°C, silica activity to about 0.5 and a relatively reduced condition of ΔFMQ = -1.5 to -3. The agpaitic groundmass assemblage indicates lower

temperatures (600° to 450°C) and lower silica activity (down to about 0.25) but higher relative oxygen fugacity around or slightly above the FMQ buffer. In some parts of the dyke, magmatic fluorite saturation occurred, which is strongly reflected in the crystallization of Ca- and F-poor amphiboles in contrast to Ca- and F-rich amphiboles in the fluorite-devoid parts of the dyke. The evolution of the amphiboles is indicative of crystallization in a system closed to oxygen. The retention of Cl and water down to low temperatures is indicated by the formation of groundmass sodalite at temperatures of <400°C, at NaCl activities of between 0.1 and 0.4. While the late-stage formation of analcime, at the expense of nepheline and sodalite, occurred at temperatures of <300°C, silica activities of about 0.25 and water activities of between 0.5 and unity. The consumption of arfvedsonite by aegirine indicates oxygen fugacities above the HM buffer, during late-stage conditions.

Mineral assemblages and chemical evolution are very similar to the rocks of the Ilímaussaq intrusion, with specific phase assemblages of the MiKa representing specific rock types of the Ilímaussaq complex. Petrography, mineral chemistry and isotope data indicate a common magma source but an early separation of the MiKa from the Ilímaussaq magma and less contamination with country rocks for the MiKa. The very similar fractionation processes observed in the MiKa occured in a comparatively small magma volume and within a short time interval. Thus, these two parameters have no influence on the course of fractionation.

Acknowledgements

M. Westphal and T. Wenzel are thanked for their help during microprobe measurements, R. Halama for the pleasant time during fieldwork, and U. Alt-Epping for his assistance with the MATLAB software. T. Wenzel helped to improve an earlier version of this manuscript. This work was funded by the Deutsche Forschungsgemeinschaft (grant Ma-2135/1-2), which is gratefully acknowledged. Helpful reviews by C.H. Emeleus, Ian Coulson, and one anonymous reviewer helped to improve the quality of this paper.

This is contribution to the mineralogy of Ilímaussaq No. 117.

References

Allaart, J. H. (1969) The chronology and petrography of the Gardar dykes between Igaliko Fjord and Redekammen, South Greenland. *Rapport Grønlands Geologiske Undersøgelse*, **25**, 20.

Andersen, D. J., Lindsley, D. H. and Davidson, P. M. (1993) QUILF: a PASCAL program to assess equilibria among Fe-Mg-Mn-Ti oxides, pyroxenes, olivine, and quartz. *Computers and Geosciences*, **19**, 1333-1350.

Armstrong, J. T. (1991) Quantitative elemental analysis of individual microparticles with electron beam instruments. Pp. 261-315 in: *Electron Probe Quantitation* (K.F.J. Heinrich and D.E. Newbury, editors). Plenum Press, New York & London.

Bailey, D. K. (1969) The stability of acmite in the presence of H_2O. *American Journal of Science*, **267-A**, 1-16.

Berman, R. (1988) Internally consistant thermodynamic data for minerals in the system Na_2O-K_2O-CaO-MgO-FeO-Fe_2O_3-Al_2O_3-SiO_2-TiO_2-H_2O-CO_2. *Journal of Petrology*, **29**, 445-522.

Berman, R. G., Brown, T. H. and Perkins, E. H. (1987) Geo-Calc; software for calculation and display P-T-X phase diagrams. *American Mineralogist*, **72**, 861-862.

Boily, M. & Williams-Jones, A. E. (1994). The role of magmatic and hydrothermal processes in the chemical evolution of the Strange Lake plutonic complex, Quebec-Labrador. *Contributions to Mineralogy and Petrology*, **118**, 33-47.

Bridgwater, D. (1967) Feldspathic inclusions in the Gardar igneous rocks of South Greenland and their relevance to the formation of major Anorthosites in the Canadian Shield. *Canadian Journal of Earth Sciences*, **4**, 995-1014.

Bridgwater, D. and Harry, W. T. (1968) Anorthosite xenoliths and plagioclase megacrysts in Precambrian intrusions of South Greenland. *Meddelelser om Grønland*, **185** , 243.

Brown, S.J.A. and Fletcher, I. R. (1999) SHRIMP U-Pb dating of the preeruption growth history ofzircons from the 340 ka Whakamaru ignimbrite, New Zealand: evidence for > 250 ka magma residence time. *Geology*, **27**, 1035-1038.

Chakhmouradian, A. R. and Mitchell, R. H. (2002) The mineralogy of Ba- and Zr-rich alkaline pegmatites from Gordon Butte, Crazy Mountains (Montana, USA): comparisons between potassic and sodic agpaitic pegmatites. *Contributions to Mineralogy and Petrology*, **143**, 93-114.

Charlier, B. L. A. and Zellmer, G. (2000) Some remarks on U-Th mineral ages from igneous rocks with prolonged crystallisation history. *Earth and Planetary Science Letters*, **183**, 457-469.

Cherniak, D. J. (2002) Ba diffusion in feldspar. *Geochimica et Cosmochimica Acta*, **66**, 1641-1650.

Coulson, I. M. (1997) Post-magmatic alteration in eudialyte from the North Qôroq centre, South Greenland. *Mineralogical Magazine*, **61**, 99-109.

Davies, G. R. and Macdonald, R. (1987) Crustal influences in the petrogenesis of the Naivasha basalt-comendite complex: combined trace element and Sr-Nd-Pb isotope constraints. *Journal of Petrology*, **28**, 1009-1031.

Edgar, A. D. and Parker, L. M. (1974) Comparison of melting relationships of some plutonic and volcanic peralkaline undersaturated rocks. *Lithos*, **7**, 263-273.

Emeleus, C. H. and Upton, B. G. J. (1976) The Gardar period in southern Greenland. Pp. 152-181 in: *Geology of Greenland* (A. Escher and W.S Watt, editors), Geological Survey of Greenland, Copenhagen.

Ferguson, J. (1964) Geology of the Ilímaussaq alkaline intrusion, South Greenland. *Bulletin Grønlands Geologiske Undersøgelse*, **39**, 82.

Finch, A. A., Parsons, I. and Mingard, S. C. (1995) Biotites as indicators of fluorine fugacities in late-stage magmatic fluids: the Gardar Province in South Greenland. *Journal of Petrology*, **36**, 1701-1728.

Frisch, W. and Abdel-Rahman, A. M. (1999) Petrogenesis of the Wadi Dib alkaline ring complex, Eastern Desert of Egypt. *Mineralogy and Petrology*, **65**, 249-275.

Frost, B. R. and Lindsley, D. H. (1992) Equilibria among Fe-Ti-oxides, pyroxenes, olivine, and quartz: Part II. Aplication. *American Mineralogist*, **77**, 1004-1020.

Fuhrman, M. L. and Lindsley, D. H. (1988) Ternary-feldspar modeling and thermometry. *American Mineralogist*, **73**, 201-205.

Halama, R., Waight, T. and Markl, G. (2002) Geochemical and isotopic zoning patterns of plagioclase megacrysts in gabbroic dykes from the Gardar Province, South Greenland: implications for crystallisation processes in anorthositic magmas. *Contributions to Mineralogy and Petrology*, **144**, 109-127.

Hamilton, D. L. (1961) Nephelines as crystallisation temperature indicators. *Journal of Geology*, **69**, 321-

329.
Harris, C. (1995) Oxygen isotope geochemistry of the Mesozoic anorogenic complexes of Damaraland, northwest Namibia: evidence for crustal contamination and its effects on silica saturation. *Contributions to Mineralogy and Petrology*, **122**, 308-321.
Heaman, L. M. and Machado, N. (1992) Timing and origin of midcontinent rift alkaline magmatism, North America: evidence from the Coldwell Complex. *Contributions to Mineralogy and Petrology*, **110**, 289-303.
Holland, T. J. B. (1990) Activities of components in omphacitic solid solutions; an application of Landay theory of mixtures. *Contributions to Mineralogy and Petrology*, **105**, 446-453.
Johnson, J. W., Oelkers, E. H. and Helgeson, H. (1992) SUPCRT92: A software package for calculating the standard molal thermodynamic properties of minerals, gases, aqueous species, and reactions from 1 to 5000 bars and 0 to 1000°C. *Computers and Geosciences*, **18**, 899-947.
Khomyakov, A. P. (1995) Mineralogy of hyperagpaitic alkaline rocks. Pp. 222 in: *Oxford Scientific Publications*. Clarendon Press, Oxford.
Kogarko, L. N. (1974) Rôle of Volatiles. Pp. 474-487 in: *The Alkaline Rocks.* (H. Sørensen, editor.), John Wiley and Sons, London.
Kogarko, L. N. and Romanchev, B. P. (1977) Temperature, pressure, redox conditions, and mineral equilibria in agpaitic nepheline syenites and apatite-nepheline rocks. *Geochemistry International*, **14**, 113-128.
Kogarko, L. N. and Romanchev, B. P. (1982) Phase equilibria in alkaline melts. *International Geology Review*, **25**, 534-546.
Konnerup-Madsen, J. and Rose-Hansen, J. (1984) Composition and significance of fluid inclusions in the Ilímaussaq peralkaline granite, South Greenland. *Bulletin de Minéralogie*, **107**, 317-326.
Kramm, U. and Kogarko, L. N. (1994) Nd and Sr isotope signatures of the Khibina and Lovozero agpaitic centres, Kola Province, Russia. *Lithos*, **32**, 225-242.
Kunzmann, T. (1999) The aenigmatite-rhönite mineral group. *European Journal of Mineralogy*, **11**, 743-756.
Landolt-Börnstein (1982) *Physical Properties of Rocks* Pp. 373, In: Angenhuster, G. (ed.), Springer, Heidelberg & New York.
Larsen, L. M. (1976) Clinopyroxenes and coexisting mafic minerals from the alkaline Ilímaussaq intrusion, south Greenland. *Journal of Petrology*, **17**, 258-290.
Larsen, L. M. (1977) Aenigmatites from the Ilímaussaq intrusion, south Greenland: Chemistry and petrological implications. *Lithos*, **10**, 257-270.
Larsen, L. M. (1981) Chemistry of feldspars in the Ilímaussaq augite syenite with additional data on some other minerals. *Rapport Grønlands Geologiske Undersøgelse*, **103**, 31-37.
Larsen, L. M. and Sørensen, H. (1987) The Ilímaussaq intrusion-progressive crystallization and formation of layering in an agpaitic magma. Pp. 473-488 in: *Alkaline Igneous Rocks* (J.G. Fitton, J.G. and B.G.J. Upton, editors). Geological Society Special Publication, **30**.
Larsen, L. M. and Steenfelt, A. (1974) Alkali loss and retention in an iron-rich peralkaline phonolite dyke from the Gardar province, south Greenland. *Lithos*, **7**, 81-90.
Liebermann, J. and Petrakakis, K. (1990) TWEEQU thermobarometry, analysis of uncertainties and applications to granulites from western Alaska. *The Canadian Mineralogist*, **29**, 857-887.
Lindsley, D. H. and Frost, B. R. (1992) Equilibria among Fe-Ti-oxides, pyroxenes, olivine, and quartz: Part I. Theory. *American Mineralogist*, **77**, 987-1003.
McKay, G. A., Miyamoto, M., Mikouchi, T. and Ogapa, T. (1998) The cooling history of the Lewis Cliff 86010 angrite as inferred from kirschsteinite lamellae in olivine. *Meteoritics and Planetary Science*, **33**, 977-983.
Macdonald, R. (1966) Petrological studies of some alkalic and peralkalic dyke rocks from the Tugtutoq-Narssaq area. *Rapport Grønlands Geologiske Undersøgelse*, **11**, 44-47.
Markl, G. (2001) Stability of Na-Be minerals in late-magmatic fluids of the Ilímaussaq alkaline complex, South Greenland. *Geology of Greenland Survey Bulletin*, **190**, 145-158
Markl, G. and Baumgartner, L. (2002) pH changes in peralkaline late-magmatic fluids. *Contributions to Mineralogy and Petrology*, **144**, 31-346.
Markl, G., Frost, B. R. and Bucher, K. (1998) The origin of Anorthosites and related rocks from the Lofoten islands, Northern Norway: I. Field relations and estimation of intrinsic variables. *Journal of Petrology*, **39**, 1425-1452.
Markl, G., Marks, M, Schwinn, G. and Sommer, H. (2001a) Phase equilibrium constraints on intensive

crystallization parameters of the Ilímaussaq Complex, South Greenland. *Journal of Petrology*, **42**, 2231-2258.

Markl, G., Marks, M. and Wirth, R. (2001b) The influence of T, aSiO2, fO2 on exsolution textures in Fe-Mg olivine: an example from augite syenite of the Ilímaussaq Intrusion, South Greenland. *American Mineralogist*, **86**, 36-46.

Marks, M. and Markl, G. (2001) Fractionation and assimilation processes in the alkaline augite syenite unit of the Ilímaussaq Intrusion, South Greenland, as deduced from phase equilibria. *Journal of Petrology*, **42**, 1947-1969.

Marks, M., Vennemann, T., Siebel, W. and Markl, G. (2003) Quantification of magmatic and hydrothermal processes in a peralkaline syenite – alkali granite complex based on textures, phase equilibria, and stable and radiogenic isotopes. *Journal of Petrology*, **44**, 1247-1280.

Marsh, J. S. (1975) Aenigmatite stability in silica-undersaturated rocks. *Contributions to Mineralogy and Petrology*, **50**, 135-144.

Mingram, B., Trumbull, R. B., Littman, S. and Gerstenberger, H. (2000) A petrogenetic study of anorogenic felsic magmatism in the Cretaceous Paresis ring complex, Namibia: evidence for mixing of crust and mantle-derived components. *Lithos*, **54**, 1-22.

Nicholls, J. and Carmichael, I. S. E. (1969) Peralkaline acid liquids: A petrological study. *Contributions to Mineralogy and Petrology*, **20**, 268-294.

Parsons, I., Mason, R. A., Becker, S. M. and Finch, A. A. (1991) Biotite equilibria and fluid circulation in the Klokken Intrusion. *Journal of Petrology*, **32**, 1299-1333.

Peacock, S. M. (1989) Thermal modeling of metamorphic pressure-time-temperature paths: a forward approach. Pp. 57-112 in: *Metamorphic pressure-time-temperature paths. Short course in* Geology (F.S. Spear, F.S. and S.M. Peackock, editors). American Geophysical Union, Washington.

Piotrowski, J. M. and Edgar, A. D. (1970) Melting relations of undersaturated alkaline rocks from South Greenland. *Meddelser om Grønland*, **181**, 62.

Philpotts, A. R. (1990) Principles of igneous and metamorphic petrology. Prentice Hall, New Jersey 498.

Poulsen, V. (1964) The sandstones of the Precambrian Eriksfjord Formation in South Greenland. *Rapport Grønlands Geologiske Undersøgelse*, **2**, 16.

Salvi, S. and Williams-Jones, A. E. (1990). The role of hydrothermal processes in the granite-hosted Zr, Y, REE deposit at Strange Lake, Quebec/Labrador: evidence from fluid inclusions. *Geochimica et Cosmochimica Acta*, **54**, 2403-2418.

Scaillet, B. and MacDonald, R. (2001) Phase relations of peralkaline silicic magmas and petrogenetic implications. *Journal of Petrology*, **42**, 825-845.

Scharbert, H. G. (1967) Microsyenitic Dykes from the northern part of the Ilímaussaq Peninsula, Southern Greenland. 443-462.

Schmitt, A. K., Emmermann, R., Trumbull, R. B., Bühn, B. and Henjes-Kunst, F. (2000) Petrogenesis and 40Ar/39Ar Geochronology of the Brandberg Complex, Namibia: Evidence for a major mantle contribution in metaluminous and peralkaline granites. *Journal of Petrology*, **41**, 1207-1239.

Sharp, Z. D., Helffrich, G. R., Bohlen, S. R. and Essene, E. J. (1989) The stability of sodalite in the system $NaAlSiO_4$-NaCl. *Geochimica et Cosmochimica Acta*, **53**, 1934-1954.

Sood, M. K. and Edgar, A. D. (1970) Melting relations of undersaturated alkaline rocks. *Meddelser om Grønland*, **181**, 41.

Sørensen, H. (1992) Agpaitic nepheline syenites: a potential source of rare elements. *Applied Geochemistry*, **7**, 417-427.

Sørensen, H. (1997) The agpaitic rocks - an overview. *Mineralogical Magazine*, **61**, 485-498

Späth, A., Le Roex, A. P. and Opiyo-Akech, N. (2001) Plume-litosphere interaction and the origin of continental rift-related alkaline volcanism-the Chyulu hills volcanic province, Southern Kenya. *Journal of Petrology*, **42**, 765-787.

Stephenson, D. (1974) Mn and Ca enriched olivines from nepheline syenites of the South Qoroq Centre, south Greenland. *Lithos*, **7**, 35-41.

Stevenson, R., Upton, B. G. J. and Steenfelt, A. (1997) Crust-mantle interaction in the evolution of the Ilímaussaq Complex, South Greenland: Nd isotopic studies. *Lithos*, **40**, 189-202.

Stormer, J. C. (1972) Calcium zoning in olivine and its relationship to silica activity and pressure. *Geochimica et Cosmochimica Acta*, **37**, 1815-1821.

Upton, B. G. J. and Blundell, D. J. (1978) The Gardar igneous province: evidence for Proterozoic continental rifting. Pp. 163-172 in: *Petrology and geochemistry of continental* rifts (E.R. Neumann and I.B. Ramberg,

editors). NATO Advanced Study Institute Series C: Mathematical and Physical Sciences. Reidel Publishing Company, Dortrecht.

Upton, B. G. J. and Emeleus, C. H. (1987) Mid-Proterozoic alkaline magmatism in southern Greenland: the Gardar province. Pp. 449-471 *in: The Alkaline Rocks* (J.G. Fitton and B.G.J. Upton, editors). Blackwell Scientific, Boston.

Upton, B. G. J. and Fitton, J. G. (1985) Gardar dykes north of the Igaliko syenite complex, southern Greenland. *Rapport Grønlands Geologiske Undersøgelse*, **127**, 24.

Upton, B. G. J., Emeleus, C. H., Heaman, L. M., Goodenough, K. M. and Finch, A. (2003) Magmatism of the mid-Proterozoic Gardar Province, South Greenland: chronology, petrogenesis and geological setting. *Lithos*, **68**, 43-65.

Ussing, N. V. (1912) Geology of the country around Julianehaab, Greenland. *Meddelelser om Grønland*, **38**, 426.

Watt, W. S. (1968) Petrology and Geology of the Precambrian Gardar Dykes on Qaersuarssuk, South Greenland. *Rapport Grønlands Geologiske Undersøgelse*, **14**, 51.

Vazquez, J. A. and Reid, M. R. (2002) time scales of magma storage and differentiation of voluminous high-silica rhyolites at Yellowstone caldera, Wyoming. *Contributions to Mineralogy and Petrology*, **144**, 274-285.

Figure captions

Fig. 1: Sketch map of part of the Igaliko Peninsula showing the agpaitic Ilímaussaq intrusion and the investigated micro-kakortokite dyke (MiKa) with sample localities indicated. Map is redrawn from Larsen and Steenfelt (1974)

Fig. 2: Photomicrograph (plane-polarized light) and back-scattered electron (BSE) images of textures among the felsic minerals. (a) Photomicrograph of sample MiKa 14 with phenocrysts of alkali feldspar and nepheline in a fine-grained groundmass. (b) Euhedral inclusion of nepheline in an alkali feldspar phenocryst. Note the small aegirine crystals aligned along the margin of nepheline. (c) + (d) BSE images of Ba-rich areas in an alkali feldspar phenocryst of sample GM1846. (e) Euhedral laths of microcline partly as inclusions in anhedral sodalite. (f) Nepheline and sodalite partly replaced by later analcime.

Fig. 3: BSE images of textures among the mafic minerals. (a) Augite phenocryst with Mg-rich core, inclusions of magnetite and associated olivine, which is rimmed by aegirine. (b) Primary magnetite rimmed by aegirine and astrophyllite. (c) Augite phenocryst with poikilitic margins consisting of aegirine-rich pyroxene. Along cracks, augite is converted to aegirine as well. (d) Aggregate of arfvedsonite with small inclusions of euhedral hjordahlite. (e) Stable mafic groundmass assemblage of aegirine, arfvedsonite, and aenigmatite. (f) Aenigmatite partly rimmed and resorbed by aegirine.

Fig. 4: Feldspar compositions observed in MiKa samples in the ternary system Ab-Or-Cs. Ba-rich compositions only occur in alkali feldspar phenocryst of sample GM1846.

Fig. 5: Ne-Ks-SiO_2 triangle (wt. %) showing the compositions of nepheline phenocrysts and groundmass nepheline. Isotherms are after Hamilton (1961).

Fig. 6: Correlation diagram of Ca and Mn with Fe content. Both show a positive correlation, except for Ca in sample MiKa 28.

Fig. 7: Clinopyroxene compositional trend in the investigated samples plotted in the ternary system diopside (Di), hedenbergite (Hed) and aegirine (Aeg). Published trends for the Ilímaussaq intrusions are shown for comparison (from Larsen, 1976; Marks and Markl, 2001).

Fig. 8: Zoning profiles through augite grains of two different samples. (a) GM1852 (see also Fig. 3c). (b) MiKa 14 (Fig. 3a).

Fig. 9: Amphibole chemistry. (a) Ca versus F in amphiboles, distinguishing two groups of amphiboles in MiKa samples. (b) Correlation diagrams of several elements with Si atoms per formula for amphibole.

Fig. 10: Composition of measured aenigmatite in the system aenigmatite-wilkinsonite-rhönite. Analyses of aenigmatites from the Ilímaussaq Intrusion (Larsen, 1977) and from the Puklen complex (Marks *et al.*, 2003) are shown for comparison.

Fig. 11: Temperature-silica activity diagram showing the results of QUILF calculations.

Fig. 12: Temperature-silica activity diagrams showing equilibria among nepheline, albite, and jadeite. (a) Phenocryst phases. (b) Groundmass phases. End-member activities were calculated for the range of mineral composition observed.

Fig. 13: (a) Temperature-log a_{NaCl} diagram showing phase equilibria in the system Na-Al-Si-O-H-Cl. (b) Temperature-a_{H2O} diagram for the equilibrium Ne + SiO_2 + H_2O = Anl.

Tables

Table 1: Mineral abbreviations used in text, figures, and tables

abbreviation	mineral	abbreviation	mineral
Ab	albite	Jd	jadeite
Aeg	aegirine	Ks	kalsilite
Aen	aenigmatite	La	larnite
Alkfsp	alkali feldspar	Mt	magnetite
Am	amphibole	Mz	monazite
An	anorthite	Ne	nepheline
Anl	analcime	Ntr	natrolite
Ap	apatite	Ol	olivine
Arf	arfvedsonite	Or	K-feldspar
Astr	astrophyllite	Qtz	quartz
Aug	augite	Rhö	rhönite
Cs	celsian	Sod	sodalite
Di	diopside	Sp	spinel
Eud	eudialyte	Sph	sphalerite
Fa	fayalite	Tit	titanite
Fl	fluorite	Tp	tephroite
Fo	forsterite	Usp	ulvøspinel
Hed	hedenbergite	Wilk	wilkinsonite
Hj	hjortdahlite	Zrn	zircon

Table 2: Mineral assemblages in micro-kakortokite dike rock samples

sample	approximate distance from dyke margin	phenocrystals	major groundmass minerals	accessories	secondary minerals
GM 1846	0.1 m	Alkfsp	Ab, Or, Ne, Sod, Aeg	Eud, Fl, Astr, Hj, Ap, Sp,	Anl, Ntr
GM 1847	1.0 m	-	Ab, Or, Ne, Sod, Aeg, Aen, Arf	Eud, Fl, Astr, Hj, Ap, FeS	Anl, Ntr
GM 1848	4.5 m	Alkfsp, Ne	Ab, Or, Ne, Sod, Aeg, Aen, Arf	Eud, Fl, Astr, Ap, FeS, Tit	Anl, Ntr
GM 1849	7.5 m	Alkfsp, Ne, Hed	Ab, Or, Ne, Sod, Aeg, Aen, Arf	Eud, Fl, Astr, FeS, Tit	Anl, Ntr, $FeOOH_x$
GM 1850	0.2 m	-	Ab, Or, Ne, Sod, Aeg, Aen, Arf	Eud, Fl, Astr, Sp, FeS, Tit	Anl
GM 1851	0.1 m	Alkfsp, Ne	Ab, Or, Mt, Aeg, Arf	Fl, Ap, Sp, Zrn, Mz	Anl, $FeOOH_x$
GM 1852	6.5 m	Akfsp, Ne, Hed, Mt	Ab, Or, Ne, Sod, Aeg, Aen	Astr, Hj, Ap, Sp, FeS, Zrn,	Anl, $FeOOH_x$
Mika 13	1.5 m	Alkfsp, Ne, Hed, Ol, Mt	Ab, Or, Ne, Sod, Aeg, Aen, Arf	Fl, Ap, Sp, FeS, Zrn, Mz	Anl, $FeOOH_x$
Mika 14	5.5 m	Alkfsp, Ne, Hed, Ol, Mt	Ab, Or, Ne, Sod, Aeg, Aen, Arf	Fl, Ap, Sp, FeS, Zrn, Mz	Anl, $FeOOH_x$
Mika 24	8.0 m	Alkfsp, Ne, Hed, Ol, Mt	Ab, Or, Ne, Sod, Aeg, Aen, Arf	Fl, Ap, Sp, FeS, Zrn, Mz	Anl, $FeOOH_x$
Mika 28	4.0 m	Alkfsp, Ne, Hed, Ol, Mt	Ab, Or, Ne, Sod, Aeg, Aen, Arf	Fl, Ap, Sp, FeS, Zrn, Mz	Anl, $FeOOH_x$

Table 3: Representative microprobe analyses and reintegrated compositions (reint.) of feldspar

sample	GM1846 ab	GM1846 ab	GM1846 or	GM1846 or	GM1846 Ba-Fsp 1	GM1846 Ba-Fsp 1	GM1846 Ba-Fsp 2	GM1846 Cs	GM1848 (reint.)	MiKa 14 (reint)
wt%										
SiO_2	64.14	64.25	68.04	68.79	64.04	62.50	57.38	38.32	65.98	66.64
Al_2O_3	18.22	18.02	19.55	19.19	18.66	18.96	20.69	25.41	18.75	19.11
FeO	0.13	0.15	0.00	0.01	0.02	0.03	0.00	0.00	0.05	0.02
MnO	0.00	0.01	0.00	0.00	0.00	0.00	0.00	0.00	0.00	0.00
MgO	0.00	0.00	0.01	0.00	0.00	0.01	0.01	0.00	0.00	0.01
BaO	0.02	0.00	0.05	0.00	0.94	2.53	10.44	32.48	0.02	0.01
SrO	0.17	0.15	0.15	0.13	0.15	0.17	0.14	0.27	0.09	0.10
CaO	0.00	0.00	0.00	0.00	0.01	0.13	0.00	0.01	0.00	0.00
Na_2O	0.33	0.62	11.53	11.57	0.27	0.31	1.01	0.82	5.12	6.73
K_2O	16.08	16.34	0.14	0.09	15.73	15.20	10.88	2.43	9.07	6.85
Total	99.09	99.54	99.47	99.79	99.81	99.84	100.53	99.73	99.98	99.47
	Formulae based on 8 oxygens									
Si	3.00	3.00	2.99	3.01	2.98	2.95	2.81	2.24	3.00	2.99
Al	1.00	0.99	1.01	0.99	1.02	1.05	1.19	1.75	1.00	1.01
Mg	0.00	0.00	0.00	0.00	0.00	0.00	0.00	0.00	0.00	0.00
Fe	0.01	0.01	0.00	0.00	0.00	0.00	0.00	0.00	0.00	0.00
Mn	0.00	0.00	0.00	0.00	0.00	0.00	0.00	0.00	0.00	0.00
Ba	0.00	0.00	0.00	0.00	0.02	0.05	0.20	0.75	0.00	0.00
Sr	0.00	0.00	0.00	0.00	0.00	0.00	0.00	0.00	0.00	0.00
Ca	0.00	0.00	0.00	0.00	0.00	0.01	0.00	0.00	0.00	0.00
Na	0.03	0.06	0.98	0.98	0.02	0.03	0.10	0.09	0.46	0.59
K	0.96	0.97	0.01	0.01	0.93	0.91	0.68	0.18	0.54	0.39
Sum	5.00	5.02	5.00	4.99	4.98	5.00	4.98	5.02	5.00	4.99
Ab	3.0	5.4	99.1	99.5	2.5	2.9	9.8	9.1	46.2	60.0
Or	96.9	94.6	0.8	0.5	95.7	92.4	69.7	17.8	53.8	40.0
Cs	0.0	0.0	0.1	0.0	1.7	4.7	20.5	73.1	0.0	0.0

Table 4: Representative microprobe analyses of nepheline

sample	GM1848 phenocryst	GM1852 phenocryst	GM1847 phenocryst	GM1849 groundmass	GM1849 groundmass
wt%					
SiO_2	42.79	45.68	43.91	45.46	43.32
Al_2O_3	33.15	31.90	32.51	32.26	33.32
FeO	0.38	0.54	0.59	0.62	0.50
MnO	0.00	0.02	0.03	0.01	0.00
MgO	0.00	0.02	0.00	0.00	0.00
CaO	0.00	0.01	0.00	0.01	0.00
Na_2O	15.81	16.12	16.02	16.54	16.85
K_2O	7.17	5.25	6.46	5.07	6.35
Total	99.30	99.54	99.51	99.97	100.34
	Formulae based on 32 oxygens				
Si	8.32	8.73	8.48	8.66	8.32
Al	7.60	7.18	7.40	7.24	7.54
Mg	0.00	0.00	0.00	0.00	0.00
Fe	0.06	0.09	0.09	0.10	0.08
Mn	0.00	0.00	0.00	0.00	0.00
Ca	0.00	0.00	0.00	0.00	0.00
Na	5.96	5.97	6.00	6.11	6.28
K	1.78	1.28	1.59	1.23	1.56
Sum	23.72	23.26	23.57	23.34	23.78

Table 5: Representative microprobe analyses of sodalite

sample	GM1852	GM1850	GM1849	GM1847	GM1849
wt%					
SiO_2	38.24	37.43	37.80	37.23	37.58
Al_2O_3	30.67	30.61	30.49	30.37	30.54
FeO	0.08	0.21	0.21	0.15	0.18
MnO	0.06	0.00	0.00	0.00	0.24
MgO	0.00	0.00	0.00	0.01	0.00
CaO	0.03	0.07	0.00	0.00	0.02
Na_2O	23.52	24.06	23.57	24.69	23.77
K_2O	0.03	0.06	0.03	0.03	0.03
SO_3	0.33	0.61	0.90	1.05	1.07
Cl	6.87	6.98	6.74	6.53	6.67
Total	99.83	100.03	99.74	100.06	100.10
	Formulae based on 25 oxygens				
Si	6.19	6.08	6.11	6.02	6.06
Al	5.85	5.86	5.81	5.79	5.80
Fe	0.01	0.03	0.03	0.02	0.02
Mg	0.00	0.00	0.00	0.00	0.00
Mn	0.01	0.00	0.00	0.00	0.03
Ca	0.01	0.01	0.00	0.00	0.00
Na	7.38	7.58	7.39	7.74	7.43
K	0.01	0.01	0.01	0.01	0.01
SO_3	0.04	0.07	0.11	0.13	0.13
Cl	1.88	1.92	1.85	1.79	1.82
Sum	21.28	21.56	21.31	21.50	21.30

Table 6: Representative microprobe analyses of olivine

sample	MiKa 24	MiKa 24	MiKa 14	MiKa 13	MiKa 28
wt%					
SiO_2	30.78	30.41	29.76	29.41	29.80
TiO_2	0.03	0.06	0.04	0.08	0.07
Al_2O_3	0.01	0.00	0.00	0.00	0.00
FeO	59.25	60.22	63.64	64.67	64.86
MnO	3.67	3.58	3.84	3.97	3.93
MgO	4.70	4.48	1.00	0.65	0.46
CaO	1.33	1.36	1.50	1.09	0.84
Total	99.76	100.10	99.77	99.88	99.96
	Formulae based on 4 oxygens				
Si	1.00	0.99	1.00	0.99	1.00
Ti	0.00	0.00	0.00	0.00	0.00
Al	0.00	0.00	0.00	0.00	0.00
Mg	0.23	0.22	0.05	0.03	0.02
Fe	1.62	1.64	1.79	1.82	1.83
Mn	0.10	0.10	0.11	0.11	0.11
Ca	0.05	0.05	0.05	0.04	0.03
Sum	3.00	3.00	3.00	3.00	2.99
Fo	11.5	10.9	2.5	1.6	1.2
Fa	81.1	81.9	89.3	90.8	91.5
Tp	5.1	4.9	5.5	5.6	5.6
La	2.3	2.4	2.7	2.0	1.2

Table 7: Representative microprobe analyses of clinopyroxene

sample	MiKa 14	MiKa 14	MiKa 28	MiKa 28	GM1852	GM1848	GM1848	GM1846	GM1846	GM1847
	augite phenocryst						groundmass aegirine			
wt%										
SiO_2	50.15	48.52	49.09	48.96	52.30	50.35	50.70	51.49	51.94	52.25
TiO_2	0.51	0.84	0.31	0.54	0.10	0.49	0.41	1.11	0.71	0.44
Al_2O_3	1.41	1.80	0.51	0.74	2.49	0.95	1.09	0.33	0.34	2.25
FeO	18.92	20.89	26.27	25.71	27.82	27.74	28.35	28.54	28.93	27.61
MnO	0.82	0.75	0.69	0.93	0.08	0.39	0.29	0.23	0.29	0.41
MgO	5.90	4.37	1.38	1.59	0.02	0.14	0.10	0.36	0.57	0.03
ZrO_2	0.31	0.22	0.17	0.13	0.05	0.04	0.03	0.05	0.04	0.03
CaO	21.29	20.72	20.37	20.32	12.60	7.65	4.74	2.54	0.87	0.03
Na_2O	1.20	1.18	1.15	1.29	0.02	9.65	11.14	12.03	12.90	13.40
Total	100.51	99.29	99.94	100.21	96.85	97.40	96.85	96.68	96.59	96.45
	Formulae based on 4 cations and 6 oxygens									
Si	1.95	1.92	1.99	1.97	2.00	1.96	1.97	1.99	2.00	1.99
Al	0.06	0.08	0.02	0.04	0.12	0.04	0.05	0.02	0.02	0.10
Ti	0.01	0.03	0.01	0.02	0.00	0.01	0.01	0.03	0.02	0.01
Fe^{3+}	0.09	0.09	0.07	0.08	0.82	0.73	0.83	0.84	0.91	0.88
Mg	0.34	0.26	0.08	0.10	0.00	0.01	0.01	0.02	0.03	0.00
Fe^{2+}	0.53	0.59	0.82	0.78	0.07	0.18	0.09	0.08	0.01	0.00
Mn	0.03	0.03	0.02	0.03	0.00	0.01	0.01	0.01	0.01	0.01
Zr	0.00	0.00	0.00	0.00	0.00	0.00	0.00	0.00	0.00	0.00
Ca	0.89	0.87	0.88	0.88	0.06	0.32	0.20	0.11	0.04	0.00
Na	0.09	0.09	0.09	0.10	0.93	0.73	0.84	0.90	0.96	0.99
Sum	4.00	4.00	4.00	4.00	4.00	4.00	4.00	4.00	4.00	4.00
Aeg	9.4	10.6	7.1	8.2	82.0	79.3	88.3	84.0	91.0	88.9
Jd	0.0	0.0	2.0	2.0	11.0	0.0	1.1	6.0	5.0	11.1
Di	35.4	29.8	8.1	10.2	0.00	1.1	1.1	2.0	3.0	0.0
Hed	55.2	59.6	82.8	79.6	7.00	19.6	9.5	8.0	1.0	0.0

Table 8: Representative microprobe analyses of magnetite

sample	MiKa 24	MiKa 24	MiKa 14	MiKa 24	MiKa 28
wt%					
SiO_2	0.08	0.02	0.06	0.06	0.05
TiO_2	21.42	22.61	24.78	25.98	27.54
Al_2O_3	0.81	1.29	0.52	0.29	0.51
FeO	71.40	72.51	67.60	66.70	67.85
MnO	3.83	1.37	4.94	5.23	2.46
MgO	0.00	0.00	0.00	0.00	0.00
ZnO	0.32	0.24	0.20	0.12	0.14
CaO	0.03	0.06	0.04	0.08	0.06
Total	97.89	98.09	98.14	98.46	98.60
	Formulae based on 3 cations and 4 oxygens				
Si	0.00	0.00	0.00	0.00	0.00
Al	0.04	0.06	0.02	0.01	0.02
Ti	0.60	0.63	0.70	0.73	0.77
Fe^{3+}	0.76	0.68	0.58	0.52	0.43
Mg	0.00	0.00	0.00	0.00	0.00
Fe^{2+}	1.47	1.58	1.54	1.56	1.69
Mn	0.12	0.04	0.16	0.17	0.08
Zn	0.01	0.01	0.01	0.00	0.00
Ca	0.00	0.00	0.00	0.00	0.00
Sum	3.00	3.00	3.00	3.00	3.00
Usp	60.3	63.3	69.8	73.1	77.5
Mt	37.9	33.8	29.0	26.2	21.4
Sp	1.8	2.8	1.1	0.6	1.1

Table 9: Representative microprobe analyses of amphibole

sample	GM1848	GM1847	GM1846	MiKa 13	MiKa 28	MiKa 14
wt%						
SiO_2	49.18	48.87	48.49	47.00	48.70	47.20
TiO_2	0.42	0.39	0.46	0.17	0.07	0.16
Al_2O_3	2.26	2.23	2.33	2.00	0.93	2.43
FeO	32.50	33.22	33.54	33.81	34.26	34.03
MnO	0.95	1.05	1.06	1.33	1.31	1.06
MgO	0.62	0.48	0.49	0.38	0.33	0.37
CaO	1.70	1.18	1.23	3.17	3.21	2.62
Na_2O	6.73	7.09	7.31	6.16	6.05	6.76
K_2O	2.77	2.70	2.54	2.19	2.03	1.97
ZrO_2	0.01	0.03	0.02	0.05	0.01	0.02
Cl	0.00	0.00	0.00	0.01	0.02	0.01
F	0.00	0.03	0.03	1.94	1.83	2.01
Total	97.16	97.26	97.47	98.95	99.54	99.42
	Formulae based on 16 cations and 23 oxygens					
Si	7.91	7.85	7.76	7.71	7.96	7.67
Al	0.43	0.42	0.44	0.39	0.18	0.47
Ti	0.05	0.05	0.06	0.02	0.01	0.02
Fe^{3+}	0.32	0.54	0.72	0.58	0.22	0.70
Mg	0.15	0.11	0.12	0.09	0.08	0.09
Fe^{2+}	4.05	3.92	3.77	4.06	4.46	3.92
Mn	0.13	0.14	0.14	0.18	0.18	0.15
Ca	0.29	0.20	0.21	0.56	0.56	0.46
Na	2.10	2.21	2.27	1.96	1.92	2.13
K	0.57	0.55	0.52	0.46	0.42	0.41
Zr	0.00	0.00	0.00	0.00	0.00	0.00
Cl	0.00	0.00	0.00	0.00	0.01	0.00
F	0.00	0.02	0.02	1.01	0.95	1.03
Sum	16.00	16.00	16.00	16.00	16.00	16.00

Table 10: Representative microprobe analyses of aenigmatite

sample	GM1848	MiKa 13	GM1850	GM1849	MiKa 28	GM1847
wt%						
SiO_2	41.88	40.51	39.76	39.57	39.84	40.10
TiO_2	8.56	7.81	7.60	6.40	7.87	6.98
Al_2O_3	0.03	0.96	1.33	1.06	1.46	1.56
FeO	40.62	40.46	39.86	42.94	39.66	40.43
MnO	1.63	1.89	3.21	1.57	3.12	1.92
MgO	0.06	0.04	0.12	0.09	0.11	0.05
ZrO_2	0.00	0.57	0.49	0.16	0.20	0.68
CaO	0.02	0.44	0.49	0.53	0.59	0.71
Na_2O	7.28	6.99	7.00	7.01	6.91	6.86
Total	100.09	99.67	99.86	99.32	99.76	99.29
	Formulae based on 14 cations and 20 oxygens					
Si	5.99	5.83	5.70	5.70	5.71	5.78
Al	0.00	0.16	0.23	0.18	0.25	0.27
Ti	0.92	0.84	0.82	0.69	0.85	0.76
Fe^{3+}	0.21	0.45	0.68	1.00	0.56	0.59
Mg	0.01	0.01	0.02	0.02	0.02	0.01
Fe^{2+}	4.65	4.42	4.10	4.16	4.20	4.29
Mn	0.20	0.23	0.39	0.19	0.38	0.23
Zr	0.00	0.04	0.03	0.01	0.01	0.05
Ca	0.00	0.07	0.08	0.08	0.09	0.11
Na	2.02	1.95	1.95	1.96	1.92	1.92
Sum	14.00	14.00	14.00	14.00	14.00	14.00
Rhö	89.8	75.8	67.5	54.6	71.3	66.9
Aen	10.1	21.0	29.2	42.0	24.7	27.9
Wilk	0.1	3.1	3.2	3.4	4.0	5.2

Fig. 1

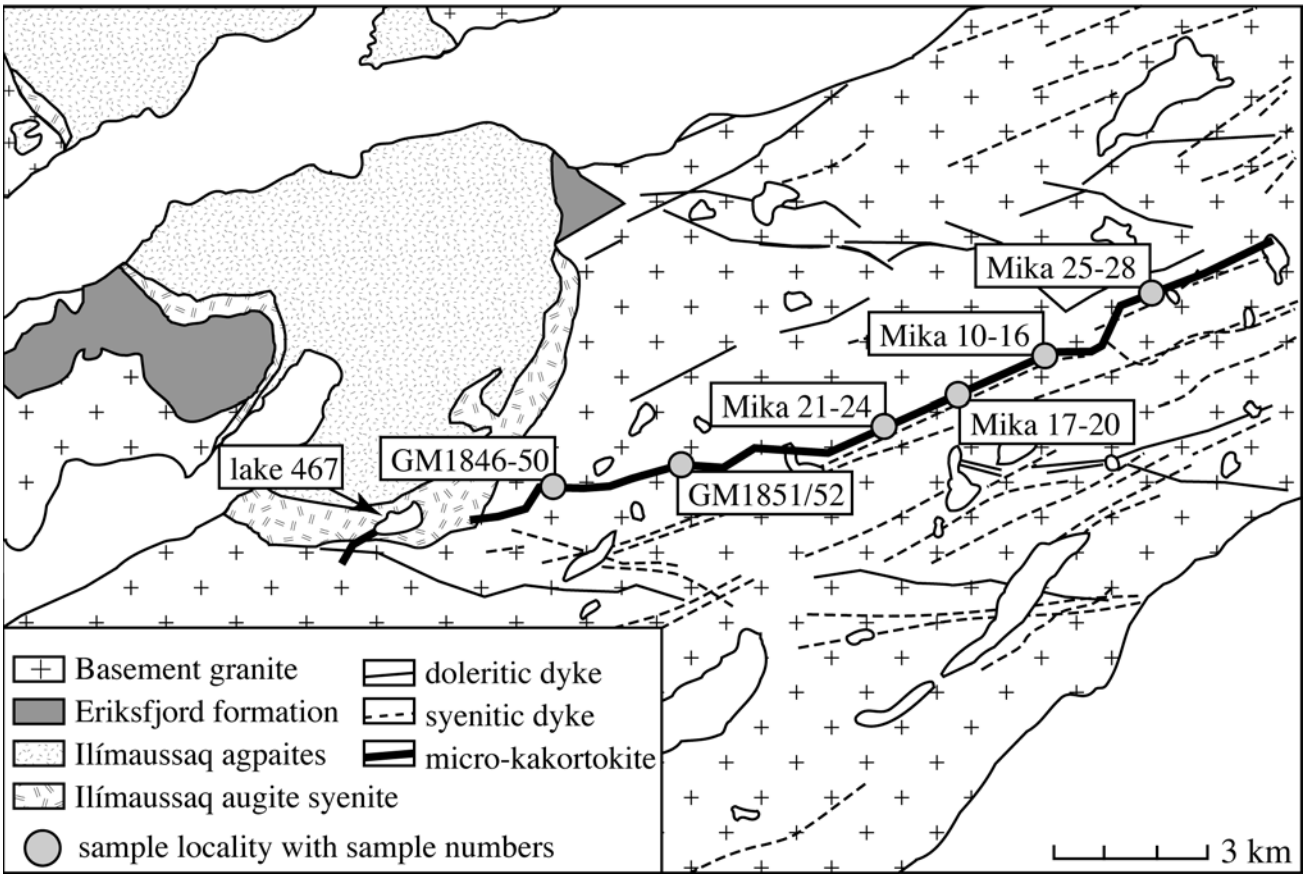
Mika 25-28
Mika 10-16
Mika 21-24
Mika 17-20
lake 467
GM1846-50
GM1851/52
Basement granite
Eriksfjord formation
Ilímaussaq agpaites
Ilímaussaq augite syenite
sample locality with sample numbers
doleritic dyke
syenitic dyke
micro-kakortokite
3 km

Fig. 2

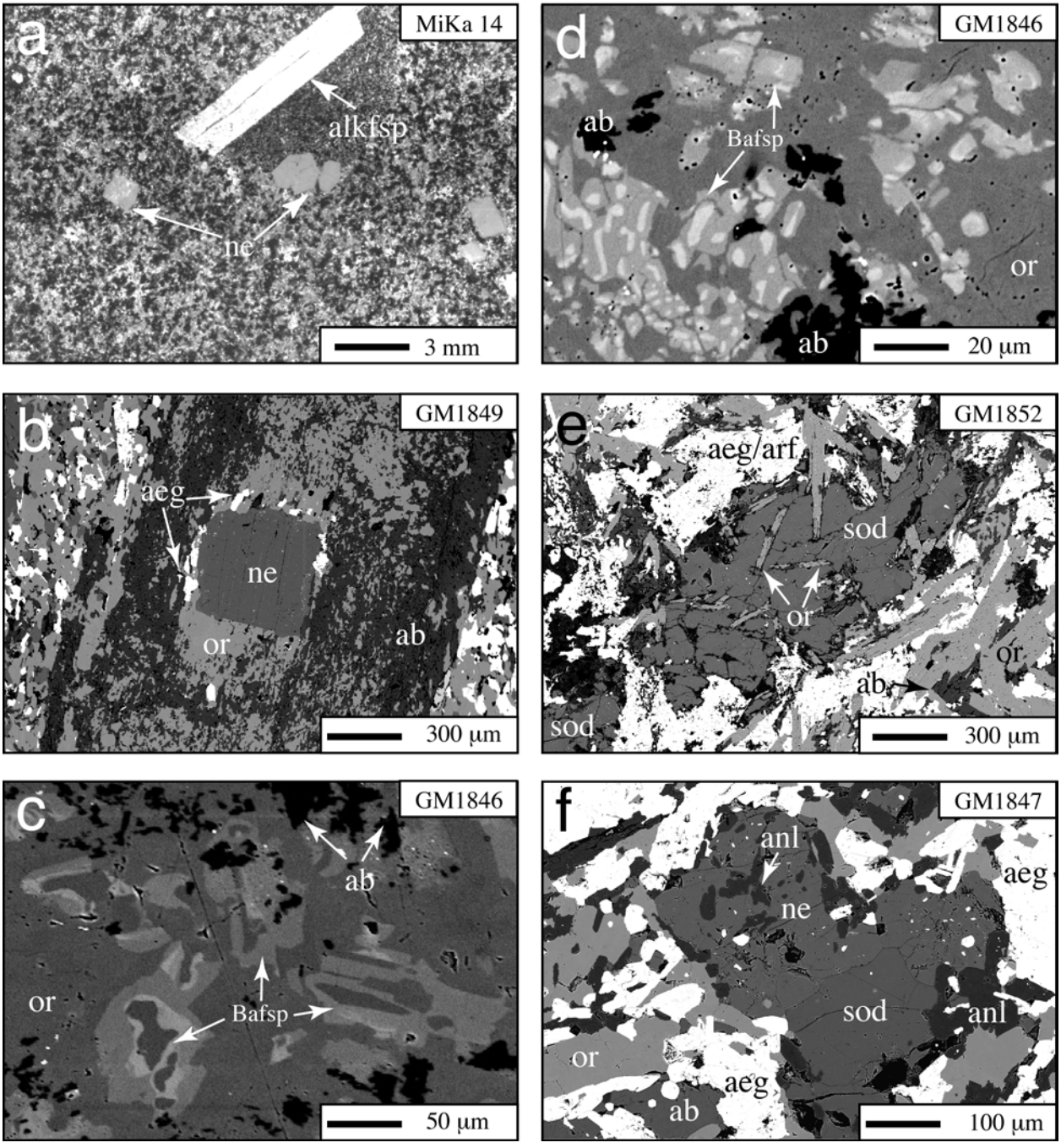
a
MiKa 14
alkfsp
ne
3 mm
d
GM1846
ab
Bafsp
or
ab
20 µm
b
GM1849
aeg
ne
or
ab
300 µm
e
GM1852
aeg/arf
sod
or
or
ab
sod
300 µm
c
GM1846
ab
or
Bafsp
50 µm
f
GM1847
anl
aeg
ne
sod
anl
or
aeg
ab
100 µm

Fig. 3

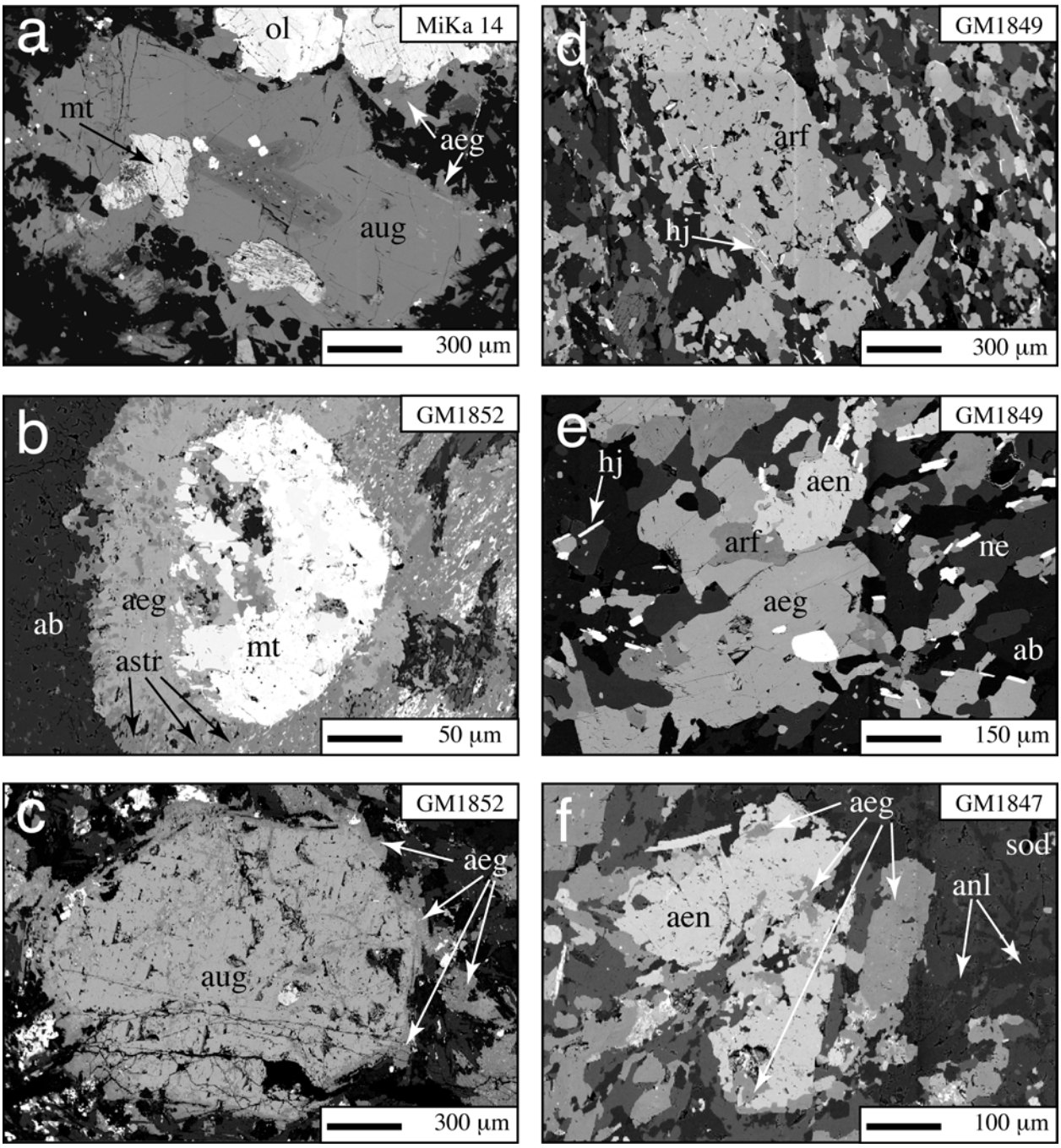
a
MiKa 14
ol
mt
aeg
aug
300 µm
d
GM1849
arf
hj
300 µm
b
GM1852
aeg
ab
mt
astr
50 µm
e
GM1849
hj
aen
arf
ne
aeg
ab
150 µm
c
GM1852
aeg
aug
300 µm
f
aeg
GM1847
sod
anl
aen
100 µm

Fig. 4

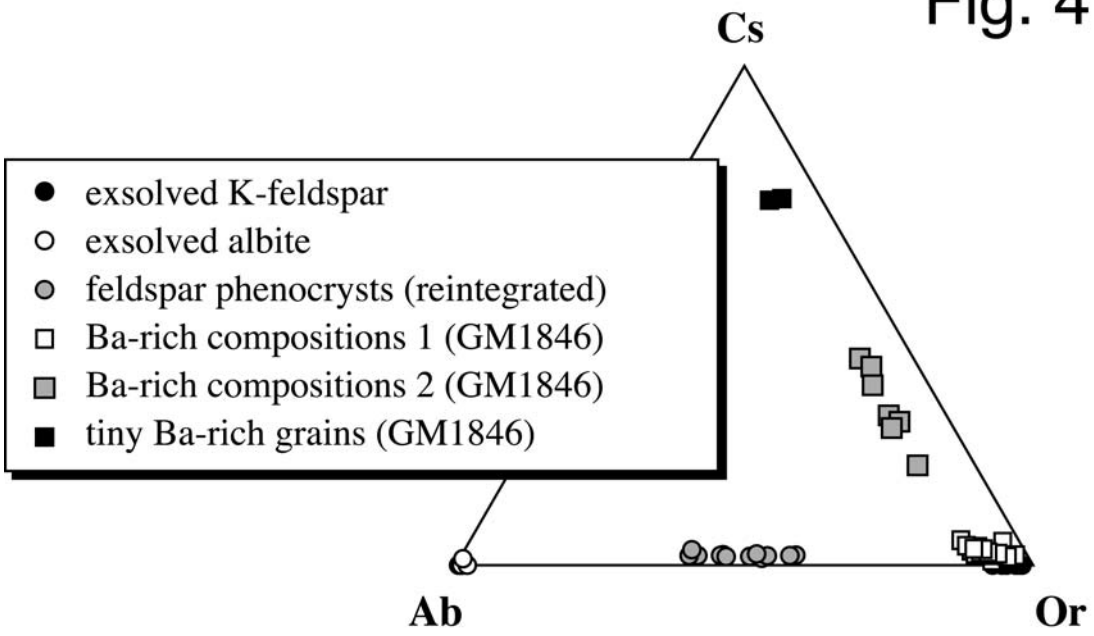
Cs
exsolved K-feldspar
exsolved albite
feldspar phenocrysts (reintegrated)
Ba-rich compositions 1 (GM1846)
Ba-rich compositions 2 (GM1846)
tiny Ba-rich grains (GM1846)
Ab
Or

Fig. 5

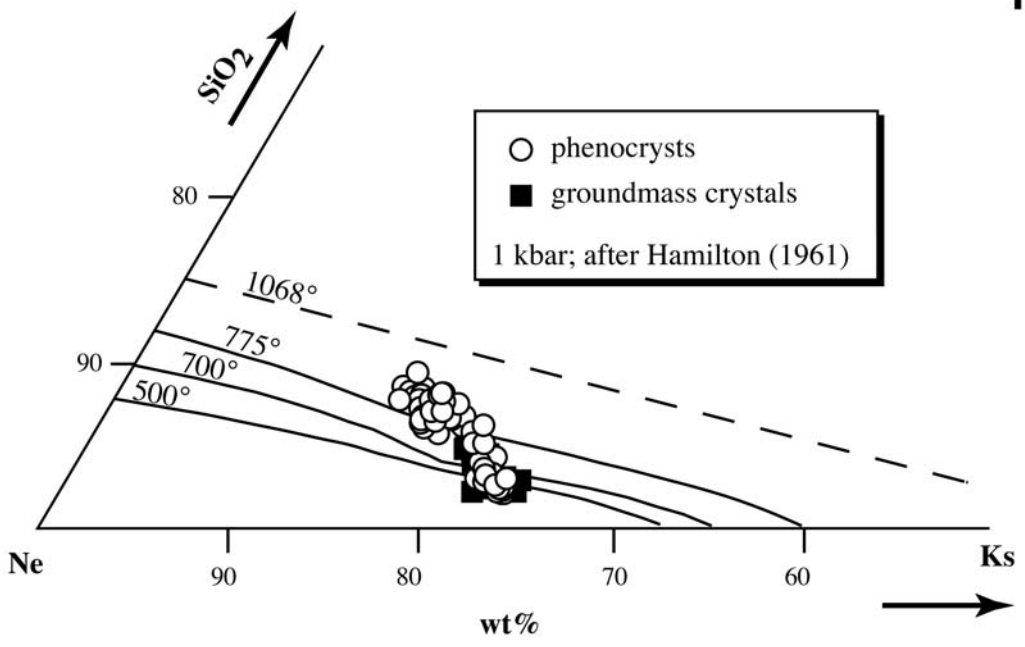
SiO2
80
90
1068°
775°
700°
500°
phenocrysts
groundmass crystals
1 kbar; after Hamilton (1961)
Ne
90
80
70
60
Ks
wt%

Fig. 6

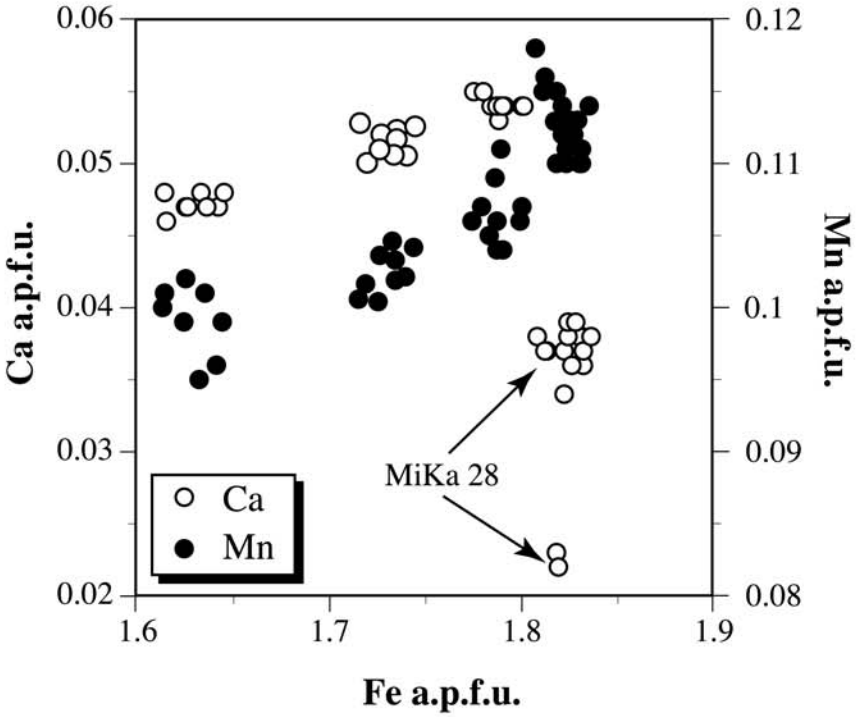
0.06
0.05
0.04
0.03
0.02
0.12
0.11
0.1
0.09
0.08
1.6
1.7
1.8
1.9
Ca a.p.f.u.
Mn a.p.f.u.
Fe a.p.f.u.
Ca
Mn
MiKa 28

Fig. 7

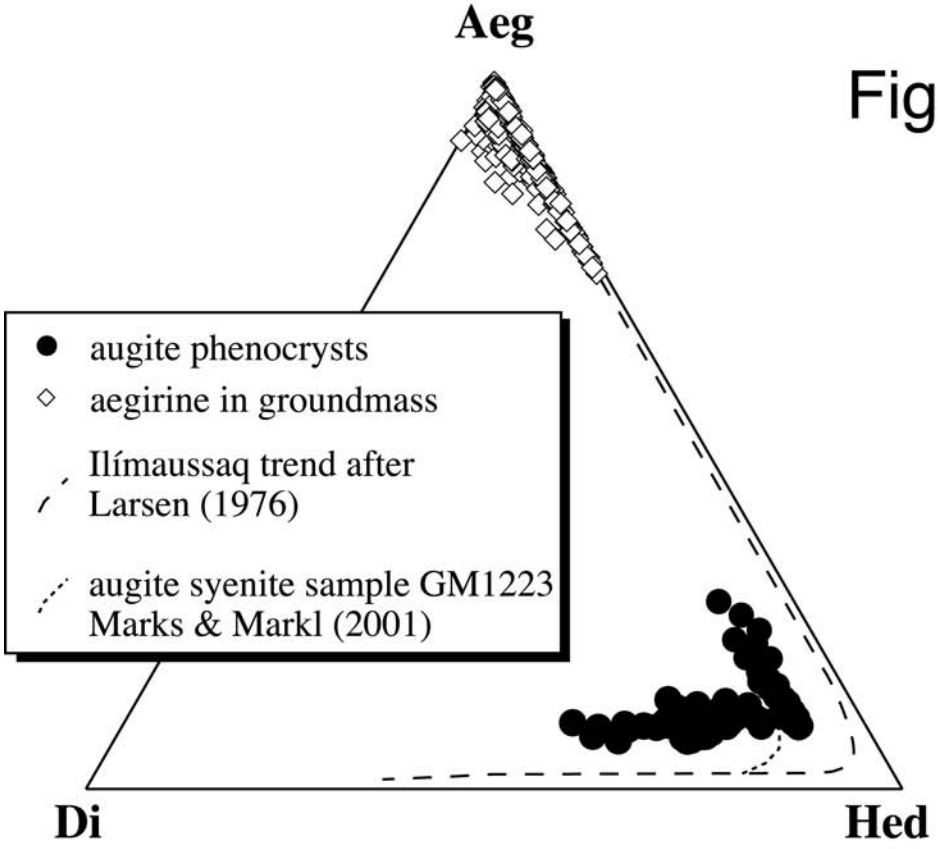
Aeg
augite phenocrysts
aegirine in groundmass
Ilímaussaq trend after Larsen (1976)
augite syenite sample GM1223 Marks & Markl (2001)
Di
Hed

Fig. 8

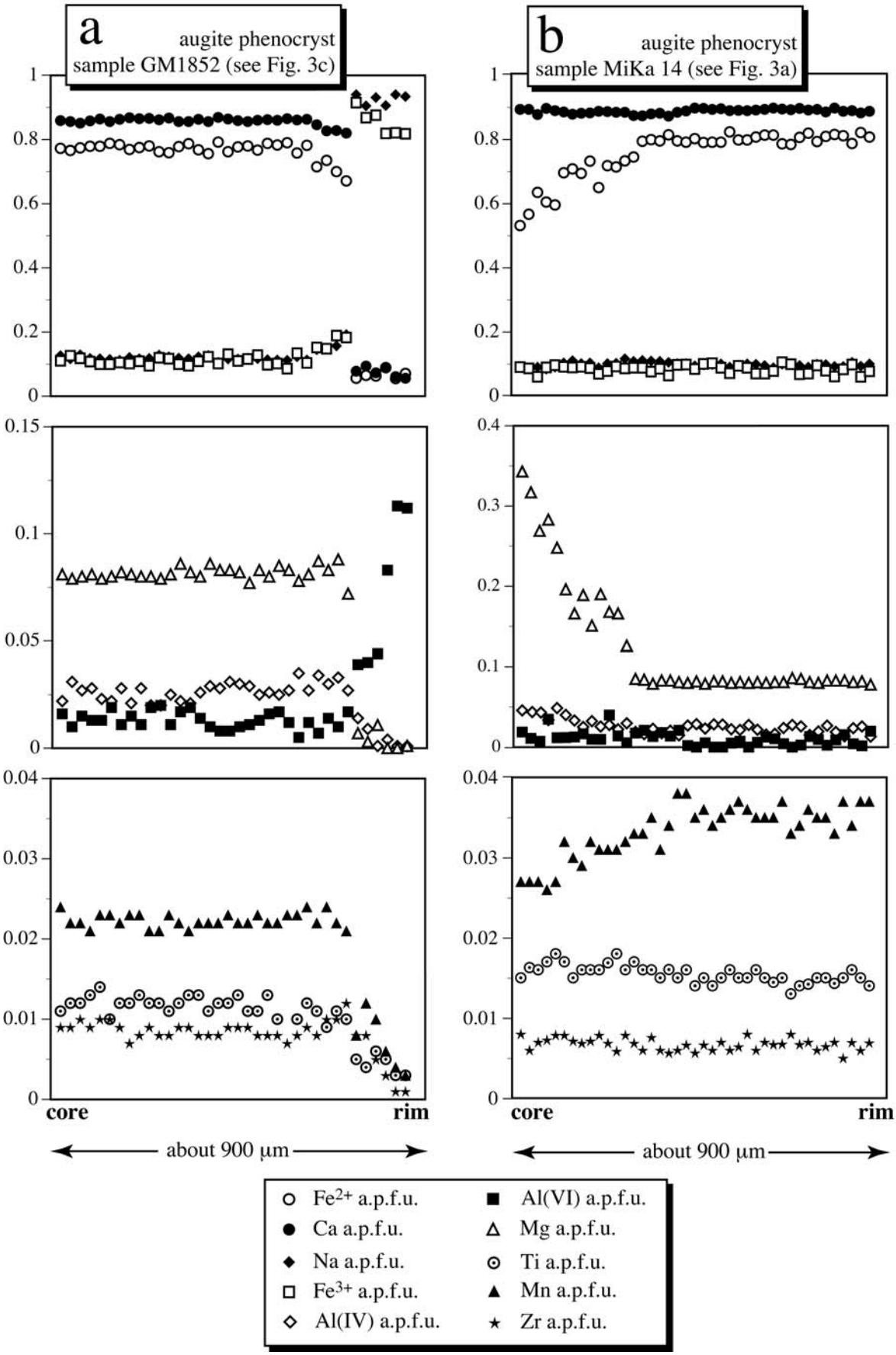
a
augite phenocryst
sample GM1852 (see Fig. 3c)
b
augite phenocryst
sample MiKa 14 (see Fig. 3a)
core
rim
about 900 μm
Fe2+ a.p.f.u.
Ca a.p.f.u.
Na a.p.f.u.
Fe3+ a.p.f.u.
Al(IV) a.p.f.u.
Al(VI) a.p.f.u.
Mg a.p.f.u.
Ti a.p.f.u.
Mn a.p.f.u.
Zr a.p.f.u.

Fig. 9

a

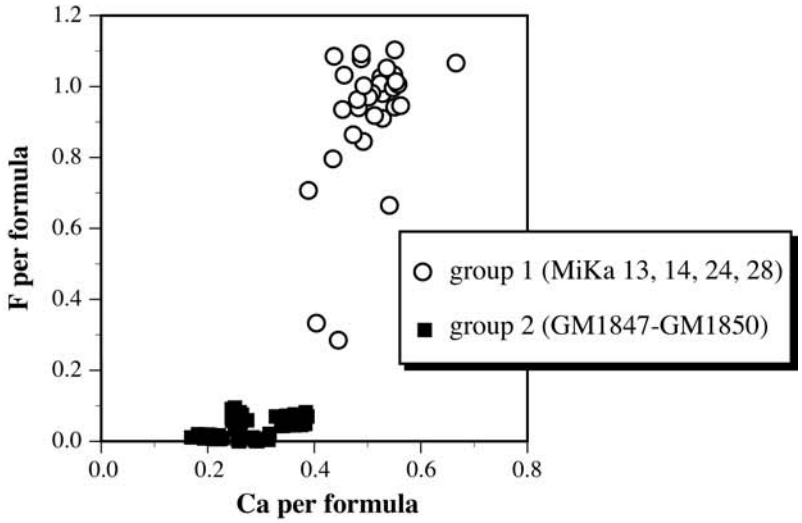
F per formula
Ca per formula
group 1 (MiKa 13, 14, 24, 28)
group 2 (GM1847-GM1850)

b

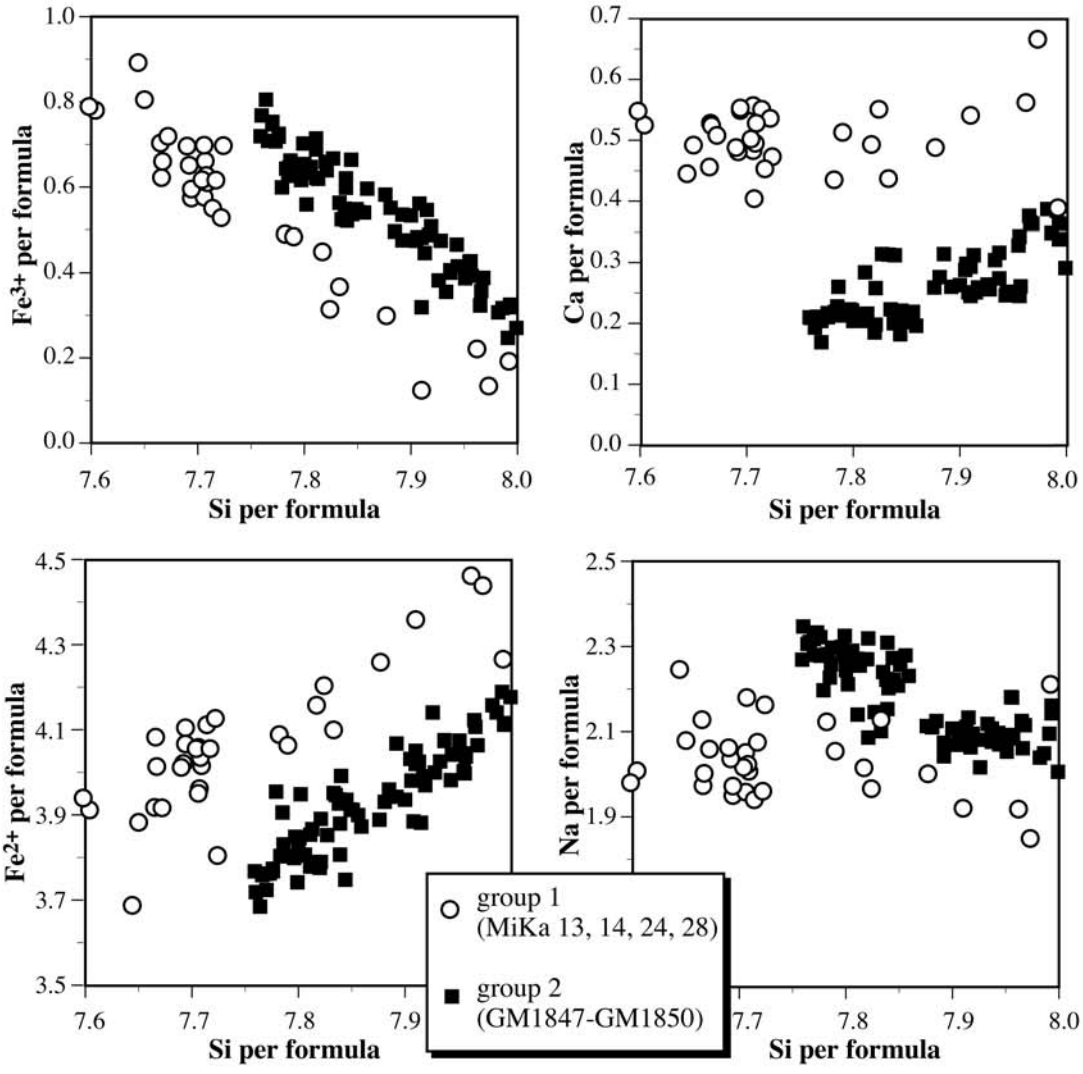
Fe3+ per formula
Ca per formula
Fe2+ per formula
Na per formula
Si per formula
group 1
(MiKa 13, 14, 24, 28)
group 2
(GM1847-GM1850)

Fig. 10

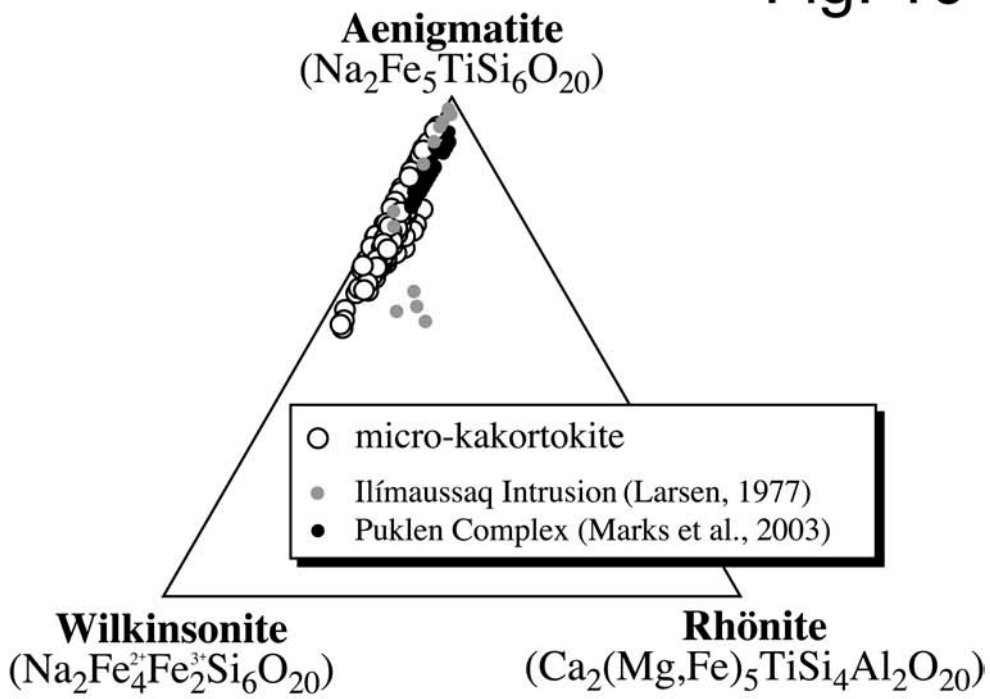
Aenigmatite
$(Na_2Fe_5TiSi_6O_{20})$
micro-kakortokite
Ilímaussaq Intrusion (Larsen, 1977)
Puklen Complex (Marks et al., 2003)
Wilkinsonite
$(Na_2Fe^{2+}_4Fe^{3+}_2Si_6O_{20})$
Rhönite
$(Ca_2(Mg,Fe)_5TiSi_4Al_2O_{20})$

Fig. 11

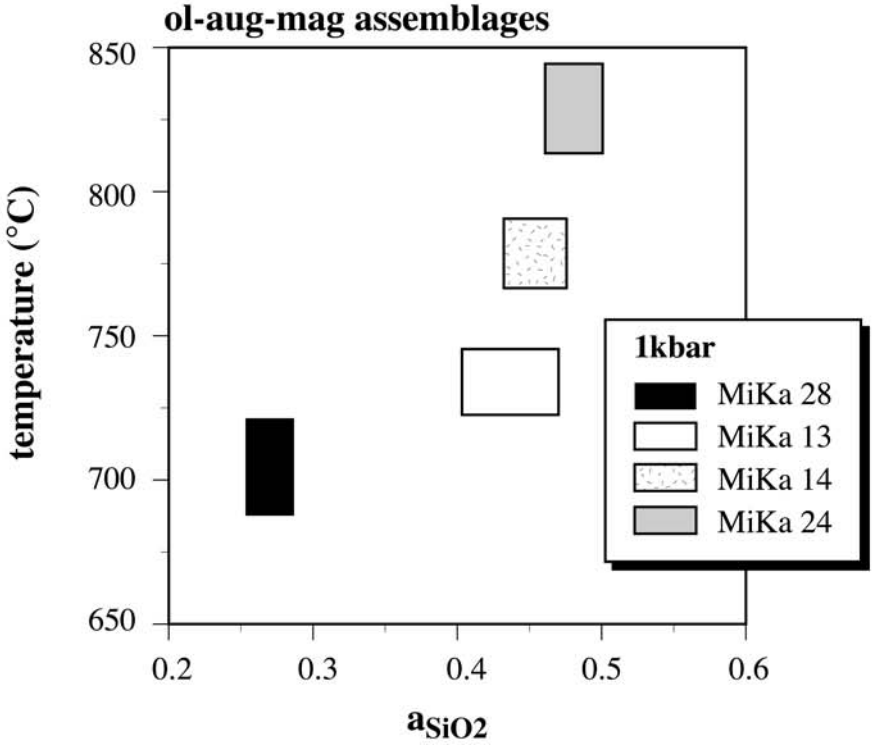
ol-aug-mag assemblages
temperature (°C)
850
800
750
700
650
0.2
0.3
0.4
0.5
0.6
a_{SiO2}
1kbar
MiKa 28
MiKa 13
MiKa 14
MiKa 24

Fig. 12

a

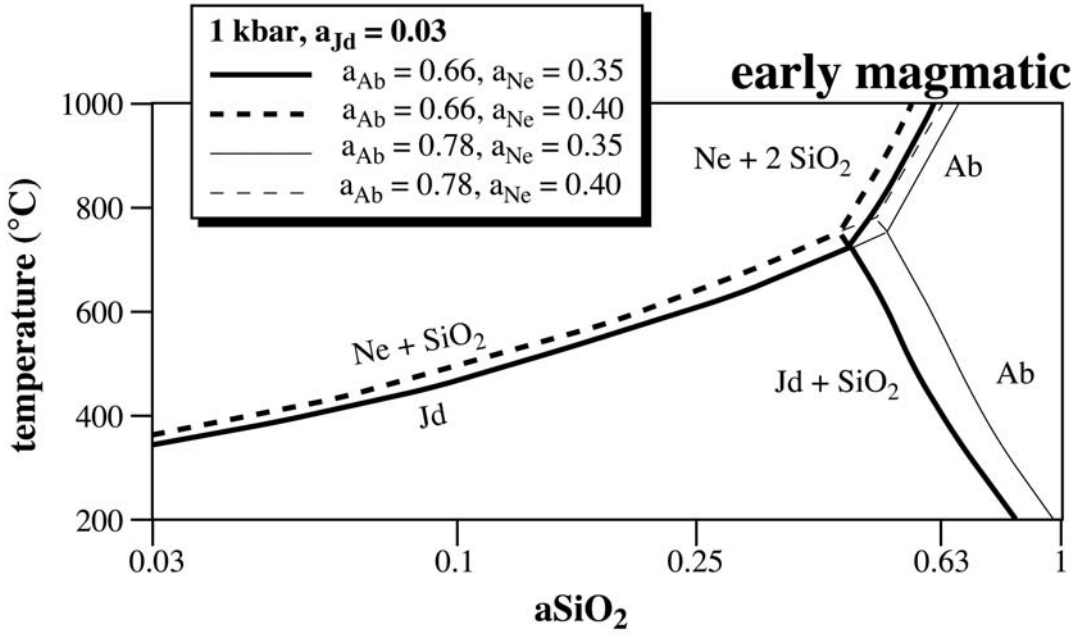
1 kbar, a_{Jd} = 0.03
a_{Ab} = 0.66, a_{Ne} = 0.35
a_{Ab} = 0.66, a_{Ne} = 0.40
a_{Ab} = 0.78, a_{Ne} = 0.35
a_{Ab} = 0.78, a_{Ne} = 0.40
early magmatic
Ne + 2 SiO2
Ab
Ne + SiO2
Jd
Jd + SiO2
Ab
temperature (°C)
1000
800
600
400
200
0.03
0.1
0.25
0.63
1
aSiO2

b

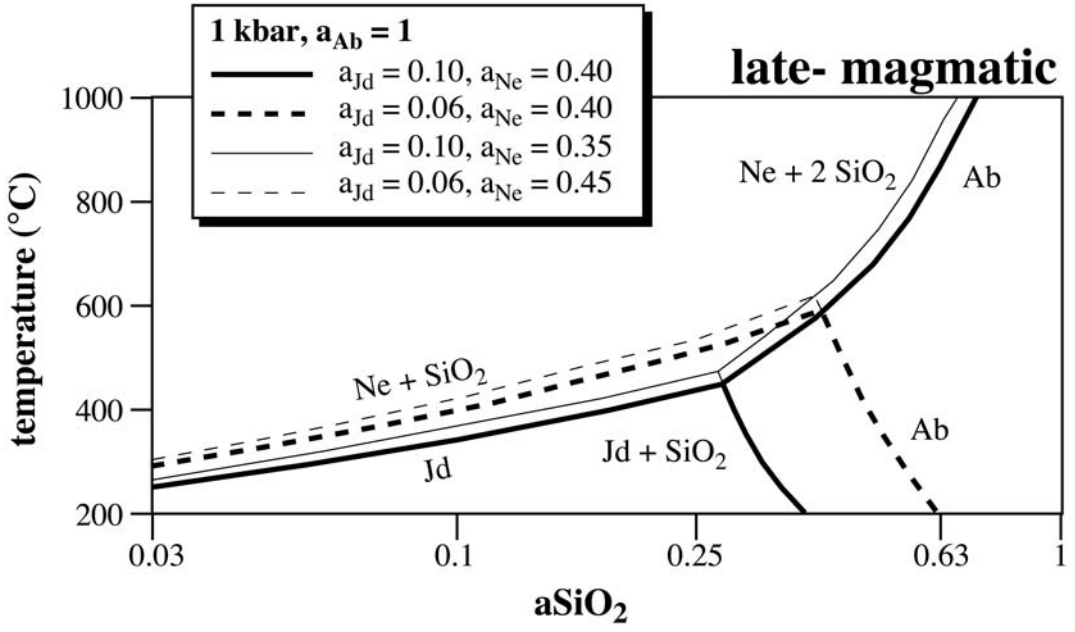
1 kbar, a_{Ab} = 1
a_{Jd} = 0.10, a_{Ne} = 0.40
a_{Jd} = 0.06, a_{Ne} = 0.40
a_{Jd} = 0.10, a_{Ne} = 0.35
a_{Jd} = 0.06, a_{Ne} = 0.45
late- magmatic
Ne + 2 SiO2
Ab
Ne + SiO2
Jd
Jd + SiO2
Ab
temperature (°C)
1000
800
600
400
200
0.03
0.1
0.25
0.63
1
aSiO2

Fig. 13

a

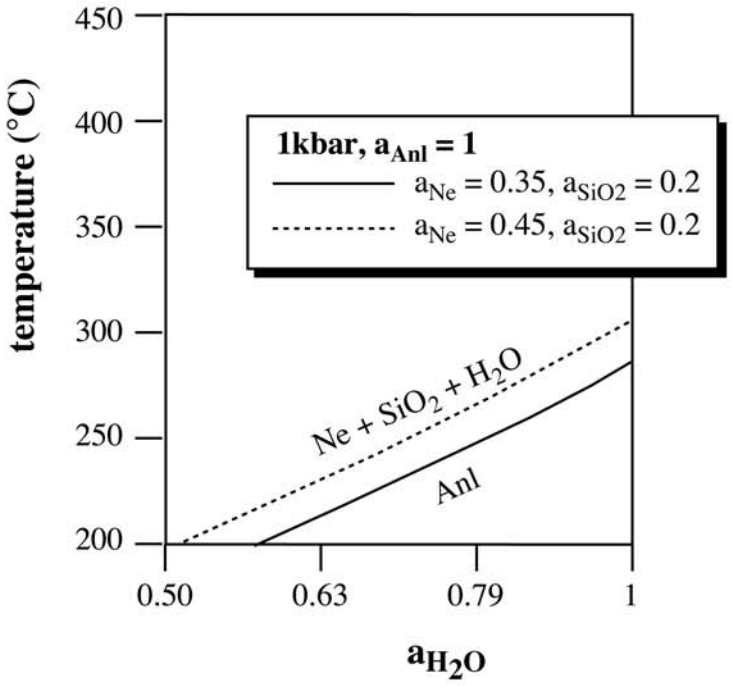
450
400
350
300
250
200
temperature (°C)
1kbar, a_{Anl} = 1
a_{Ne} = 0.35, a_{SiO2} = 0.2
a_{Ne} = 0.45, a_{SiO2} = 0.2
Ne + SiO_2 + H_2O
Anl
0.50
0.63
0.79
1
a_{H_2O}

b

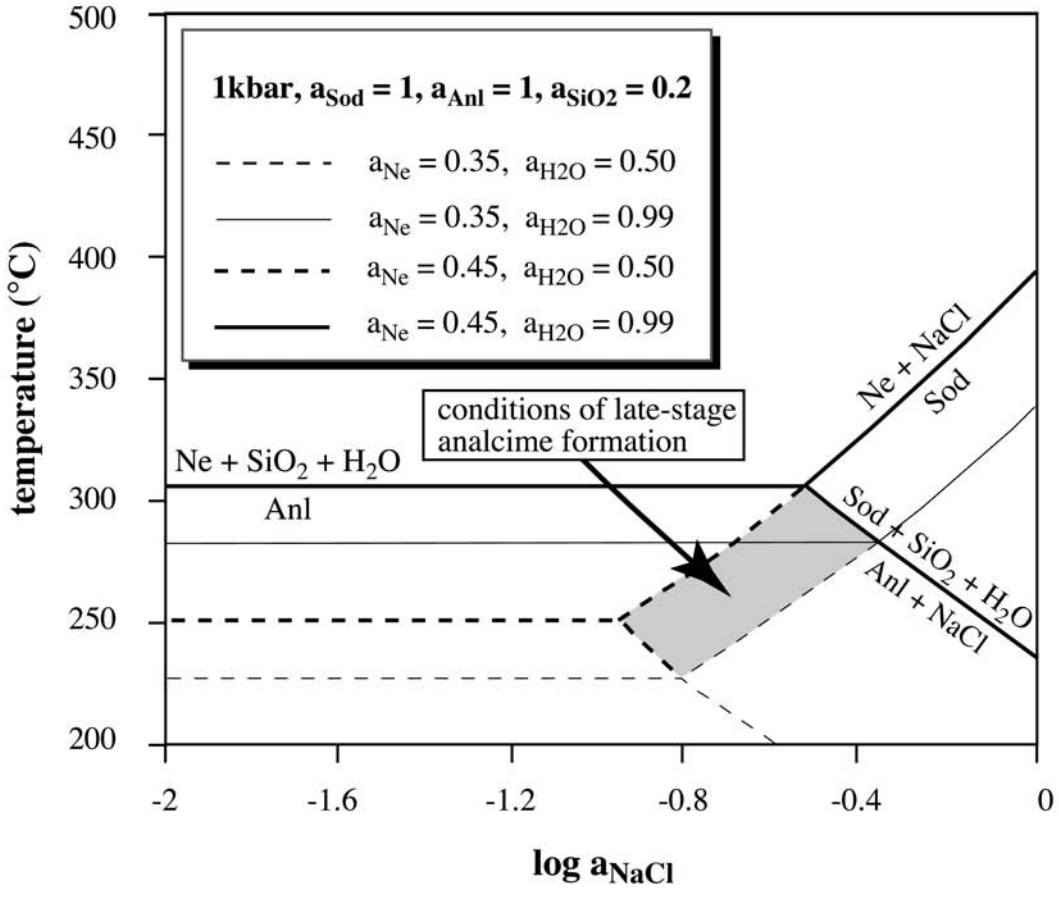
500
450
400
350
300
250
200
temperature (°C)
1kbar, a_{Sod} = 1, a_{Anl} = 1, a_{SiO2} = 0.2
a_{Ne} = 0.35, a_{H2O} = 0.50
a_{Ne} = 0.35, a_{H2O} = 0.99
a_{Ne} = 0.45, a_{H2O} = 0.50
a_{Ne} = 0.45, a_{H2O} = 0.99
conditions of late-stage analcime formation
Ne + SiO_2 + H_2O
Anl
Ne + NaCl
Sod
Sod + SiO_2 + H_2O
Anl + NaCl
-2
-1.6
-1.2
-0.8
-0.4
0
log a_{NaCl}

Kapitel 5: Spurenelementuntersuchungen an mafischen Mineralen (Amphibole, Pyroxene) dreier verschiedener Alkaligesteinsintrusionen der Gardar Provinz.

Manuskript-Titel:
TRACE ELEMENT VARIATIONS IN MAFIC MINERALS (AMPHIBOLE, CLINOPYROXENE) OF ALKALINE IGNEOUS ROCKS.

Autoren:
Michael Marks[1], Ralf Halama[1], Gregor Markl[1]

[1] Institut für Geowissenschaften, Eberhard-Karls-Universität Tübingen, Wilhelmstrasse 56, 72074 Tübingen.

Wird voraussichtlich eingereicht bei:
Geochimica et Cosmochimica Acta

Eigenanteile:

a) Idee	25 %
b) Probenbeschaffung	35 %
c) Datenbeschaffung	35 %
d) Auswertung und Interpretation	60 %
e) Ausarbeitung der Publikation	60 %

Abstract - We present a detailed laser ICP-MS study on trace element compositions of mafic minerals (clinopyroxene and amphibole) from three rift-related alkaline igneous complexes. The major element chemical composition of the investigated clinopyroxenes and amphiboles evolves from Ca-dominated via intermediate to Na-dominated members. In general, most trace elements are highly enriched compared to primitive mantle values, which is in accordance with the highly evolved character of the host rocks.

The major processes influencing the relative trace element abundances in both minerals are the chemical composition of the parental melts/fluids and crystal chemical controls. We found that the relative influence of these two factors varies for different groups of geochemically similar elements. The low abundances of large ion lithophile elements (Ba, Sr, Pb, Eu^{2+}) are interpreted to reflect prolonged feldspar fractionation, which is in accordance with petrographic and petrologic observations, and may therefore serve as an example for a melt compositional influence. However, factors like oxygen fugacity and crustal assimilation may also significantly affect the incorporation of Eu and Pb, respectively. In contrast, high field strength element (Ti, Zr, Hf, Sn, Nb, Ta) abundances appear to be mainly controlled by the major element composition of the host crystal which in turn determines the crystal site parameters. A crystal chemical control is also indicated for the REE, since clinopyroxenes and amphiboles show a continuous development from LREE-enriched patterns in the calcic minerals via wave-shaped pattern in the Ca-Na minerals towards a more pronounced HREE enrichment in the most Na-rich minerals. On the other hand, REE zoning profiles of individual minerals show the competing effects of compositional changes in the melt and the host crystals.

In general, the partitioning of most trace elements between clinopyroxene and co-genetic amphibole seems to be fairly independent of melt composition or major element composition of the host crystals. Most trace elements show a slight preference for amphibole, which is most pronounced for Nb, Ta, U, Th, Rb, Ba and Li. Exceptions to this general trend occur in rocks affected by late-stage fluid circulation resulting in the re-distribution of some mobile elements.

Keywords: trace elements; clinopyroxene; amphibole; alkaline rocks; Gardar Province

1. Introduction

Precise and accurate trace element data can be used to model and interpret magmatic processes. In situ determination of trace elements in minerals from both natural and experimental samples has become increasingly popular and many studies have been published concentrating on basaltic systems (e.g. Jeffries et al., 1995; Benoit et al., 1996; Coogan et al., 2000; Thompson & Malpas, 2000; Tiepolo et al., 2002), on ultramafic mantle rocks and on phases relevant to mantle melting (e.g. Nimis & Vanucci, 1995; Blundy & Dalton, 2000, Grégoire et al., 2000; Tiepolo et al., 2000). Studies on trace element partitioning and trace element contents in more evolved silicic systems are less frequent (Wörner et al., 1983; Lemarchand et al. 1987; Wood & Trigila, 2001), and especially the trace element concentrations of mineral phases in alkaline silicate plutonic rocks have not been studied in great detail (Larsen 1976; Shearer and Larsen 1994). However, alkaline plutonic complexes are common in rift-related provinces and they are often characterized by an enrichment of rare elements with economic potential (e.g. Kramm & Kogarko, 1994; Panneer Selvam & Suryanarayana Rao 1996; Platt, 1996; Digonnet et al., 2000). Since they represent highly fractionated mantle-derived melts (Kramm & Kogarko, 1994; Bea et al., 2001; Dunworth & Bell, 2001), they potentially provide insight into fractionation mechanisms and processes that lead to element enrichment processes.

The study of trace element contents of plutonic rocks faces a major difficulty: In contrast to volcanic rocks, whole-rock compositions are unlikely to reflect melt compositions due to accumulation processes of certain mineral phases. Additionally, many plutonic rocks are characterised by a multi-stage evolution and therefore whole-rock compositions may represent the result of a mixture of various processes (Marks et al., 2003). Both these problems are avoided by in situ measurements of trace element contents in minerals. However, experimental trace element partitioning studies between mafic minerals and alkaline silicate melts that would allow the calculation of melt compositions from mineral data are rare. The selection of suitable partition coefficients becomes even more difficult since processes of chemical differentiation are polythermal and often polybaric and thus, partition coefficients can vary for a single phase in the course of crystallisation (Blundy & Wood, 2003). Consequently, a lack of partition coefficient data suitable for alkaline plutonic rocks precludes the calculation of accurate melt compositions from the measurements of trace element contents in minerals.

Therefore, we compare the trace element contents of mafic minerals from three related, but petrologically different alkaline to peralkaline igneous complexes in order to investigate the partitioning behaviour of trace elements in natural alkaline silicate melts. Our study concentrates on clinopyroxene and amphibole because these two minerals can incorporate large amounts of

geochemically relevant trace elements (Blundy & Wood, 1997; Botazzi et al., 1999). The three complexes studied show an almost continuous spectrum in mafic mineral compositions from Ca-rich and Na-poor to Ca-poor and Na-rich. Recent studies have shown that the crystal chemistry exerts a major control on trace element partitioning (Blundy & Wood ,1991; Blundy & Wood, 1994; Wood & Blundy, 1997; Wood & Blundy, 2001). The size of ions relative to the site of interest and the charge of ions are critical factors in governing trace element behaviour, whereas the melt chemistry is thought to be of little significance (Blundy & Wood, 2003). However, melt structure becomes more important as polymerization of the melt increases (Sisson, 1994; Gaetani & Grove, 1995). Our comprehensive set of trace element data allows us to constrain the controlling factors on trace element partitioning and trace element abundances in a suite of petrologically and geochemically well studied alkaline igneous complexes. We also determine distribution coefficients for a wide range of elements between clinopyroxene and amphibole in alkaline igneous rocks. Distribution coefficients between minerals are unlikely to be controlled by absolute concentrations in the melt and might therefore be used to evaluate the crystal chemical control on trace element partitioning.

2. Regional geology

The Gardar Igneous Province (Fig. 1) in South Greenland represents a failed rift structure of Mid-Proterozoic (1.35 – 1.14 Ga) age (Upton & Emeleus, 1987; Upton et al., 2003). It comprises a sequence of interlayered basalts and sandstones (Eriksfjord Formation; Poulsen, 1964), a large number of dike rocks of variable chemical composition and twelve major alkaline to peralkaline igneous complexes. The basement rocks mainly consist of I-type calc-alkaline plutonic rocks (Julianehåb batholith) (van Breemen et al., 1974; Alaart, 1976; Kalsbeek & Taylor, 1985), which were emplaced between 1.85 and 1.80 Ga (Garde et al., 2002). Archaean country rocks occur in the northwestern part of the province.

The igneous complexes are mostly composite and show a range from relatively primitive gabbroic to highly evolved syenitic rocks. Fluid inclusion data (Konnerup-Madsen & Rose-Hansen, 1984) and the preserved contacts between supracrustal rocks and the Ilímaussaq intrusion (Poulsen, 1964) show that the magmas intruded into shallow crustal levels (< 5 km).

For this study, we selected three igneous complexes: 1.) The Puklen complex is evolving from silica-saturated syenites to alkali granites and represents a silica-oversaturated fractionation trend (Marks et al., 2003). 2.) The Ilímaussaq complex, evolving from alkaline, SiO_2-saturated syenites towards agpaitic nepheline syenites represents the silica-undersaturated trend (Markl et al.,

2001b). 3.) The Grønnedal-Ika complex represents an association of SiO_2-undersaturated syenite with carbonatite. In the following, we shortly review the petrogenesis of these three complexes.

2.1 The Puklen complex

The Puklen complex is situated in the western part of the Gardar Province (Fig. 1). The field geology was described in detail by Pulvertaft (1961) and Parsons (1972) and the petrology was investigated by Marks et al. (2003). The first magma pulse formed a suite of silica-saturated to oversaturated syenites. In the southern part of the intrusion, a fine-grained and leucocratic granophyre cuts the adjoining syenite. A second pulse of magma produced a homogeneous, coarse-grained peralkaline granite, which grades into, or may be locally intruded by fine-grained and leucocratic microgranite.

The primary mafic minerals in syenites are augite ± olivine + Fe-Ti oxide + calcic to sodic-calcic amphibole I. Secondary calcic amphibole II formed by late-stage autometasomatic reactions. In the granites, the primary mafic minerals are ilmenite and sodic amphibole, the latter is overgrown by late-stage aegirine. Detailed isotopic work (Marks et al., 2003) showed that the Puklen melts were primarily derived from a mantle source with variable amounts of crustal assimilation.

2.2 The Ilímaussaq complex

The formation of the Ilímaussaq complex (Fig. 1) involved three magma batches (Larsen & Sørensen, 1987; Konnerup-Madsen & Rose-Hansen, 1984). The earliest melt batch is represented by a shell of augite syenite, which was later intruded by a sheet of alkali granite in the north of the complex. The third intrusive phase comprises the major part of the complex and consists of different varieties and partly layered agpaitic nepheline syenites (Ferguson, 1964). The major mafic minerals in the augite syenite are augite + olivine + Fe-Ti oxide + calcic amphibole (Larsen 1976, 1977, 1981; Markl et al., 2001a+b; Marks & Markl, 2001). In the alkali granite and in the agpaites, sodic amphibole and aegirine occur in addition to high amounts of eudialyte (REE-rich Zr-silicate). Homogeneous oxygen and neodymium isotope compositions of mineral separates from the augite syenite and the agpaitic nepheline syenites indicate a closed system evolution of the complex and support a mantle derivation of the magma (Marks et al., submitted). The only exception is the alkali granite, which can be explained by higher amounts of crustal contamination compared to the other rock types (Marks et al., submitted).

2.3 The Grønnedal-Ika complex

The Grønnedal-Ika complex consists of partly layered silica-undersaturated nepheline syenites, which were intruded by a central plug of calcio-carbonatite (Emeleus, 1964; Bedford, 1989; Pearce et al., 1997). The major mafic mineral in the nepheline syenites is clinopyroxene, amphibole is very scarce (Bedford, 1989). The nepheline syenitic magmas of the Gronnedal-Ika intrusion are thought to be produced by fractional crystallisation of mafic magmas. Sr and Nd isotopic data indicate a fairly homogeneous mantle source for the syenitic and carbonatitic magmas. Crustal rocks were not significantly assimilated (Pearce et al., 1997; Halama and Markl, 2003).

3. Sample material and analytical methods

Several representative samples from each rock type were selected for this study. Most of the analysed samples have been part of previous petrological and geochemical studies on the respective igneous complexes (Markl et al., 2001b; Marks & Markl, 2001; Markl & Baumgartner, 2002; Marks et al., 2003; Halama & Markl, 2003; Halama et al., unpblished data). Selected samples and minerals analysed are summarised in Table 1.

In situ laser ablation inductively coupled plasma-mass spectrometer (LA-ICP-MS) analyses of REE and other trace elements were performed at the EU Large-Scale Geochemical Facility (University of Bristol) using a VG Elemental PlasmaQuad 3 + S-Option ICP-MS equipped with a 266 nm Nd-YAG laser (VG MicroProbe II). The laser beam diameter at the sample surface was approximately 20 µm. All measurements were made using Thermo Elemental PlasmaLab "time-resolved analysis" (TRA) data acquisition software with a total acquisition time of 100 s per analysis, allowing about 40 s for background followed by 50 s for laser ablation. NIST 610 glass was used for instrument calibration, and NIST 612 was used as a secondary standard. Si was used as an internal standard to correct the ablation yield differences between and during individual analyses on both standards and samples. To avoid analytical uncertainties due to variations in the concentrations of the internal standard, Si concentrations were quantitatively measured within 20 µm of the laser ablation pits using a JEOL 8900 electron microprobe (EMP) at the Universität Tübingen (see later). The precision of trace element concentrations, based on repeated analyses of standards, is approximately ± 5% for element concentrations >10 ppm and ±10 % for concentrations <10 ppm. Data processing was carried out offline using the same PlasmaLab software used for data collection and various custom-designed Excel spreadsheets. The limits of detection are defined as 3.28 standard deviations above background level, which equates to a 95% confidence that the measured signal is significantly above background. Typical detection limits are 1 - 20 ppm for Sc, V, Co, Cu, Zn, Ga, Rb and Ba, 0.2 - 1 ppm for Sr, Y, Zr, Nb, Sn, Cs, Hf and Pb

and 0.05 – 0.6 ppm for the REE, U, Th and Ta. Detection limits for Li are highly variable between 2 and 80 ppm depending on the specific setting during measurements.

Major element composition of minerals was determined using a JEOL 8900 electron microprobe at the Institut für Geowissenschaften at the Universität Tübingen, Germany. For calibration both natural and synthetic standards were used. The beam current was 15 nA and the acceleration voltage was 15 kV. The counting time on the peak was 16 s for major elements, and 30-60 s for minor elements (Mn, Ti, Zr, F, Cl). Background counting times were half of the peak counting times. The peak overlap between the Fe Lβ and F Kα lines was corrected for. Data reduction was performed using the internal ϕρZ procedures of JEOL (Armstrong, 1991).

4. Major element compositional trends of the mafic minerals (clinopyroxene, amphibole) from the three investigated complexes

4.1 Clinopyroxene

The pyroxene trends observed in the three investigated intrusive complexes are shown in Fig. 2. In all three complexes, the most primitive pyroxenes (in terms of X_{Fe}) are diopsidic in composition with low Na contents (< 0.1 a.p.f.u.). During fractionation, pyroxene composition gets more Fe- and Na-rich, reaching almost end-member aegirine composition in Puklen and Ilímaussaq (Larsen, 1976; Marks & Markl, 2001; Markl et al., 2001; Marks et al., 2003). Differences in the degree and timing of Na-and Fe^{3+}-enrichment can be attributed to oxygen fugacity during crystallization: The highly reducing conditions for the Puklen and Ilímaussaq complexes (below the FMQ buffer) allow a strong Fe-enrichment, but still low Na contents during fractionation (e.g. Larsen, 1976). In contrast, more oxidized conditions in the Grønnedal-Ika complex (Pearce et al., 1997) result in relatively high Na- and Fe^{3+}-contents at intermediate Fe/Mg ratios. A similar compositional trend found in the Puklen complex is the result of more oxidized (ΔFMQ = +1) conditions during late-magmatic autometasomatism (Marks et al., 2003).

4.2 Amphibole

Fig. 3 shows the amphibole trends observed in the three investigated intrusive complexes in the Ca_B vs Si diagram after Mitchell (1990). For the Puklen and Ilímaussaq intrusives, the trend is typical for magmatic alkaline to peralkaline rocks. Primary amphibole ranges in composition from almost pure Ca-amphibole (ferro-edenite, ferro-pargasite, hastingsite) with relatively high Al-contents in the early rock types and evolves via Na-Ca amphibole (katophorite, ferro-richterite) to Na-amphibole (nyböite, arfvedsonite, leakeite) in the most evolved rocks. Secondary amphibole in the Puklen rocks evolves from ferro-edenite towards ferro-actinolite, which is known only from silica-

oversaturated alkaline complexes (Mitchell, 1990). Amphiboles in the Grønnedal-Ika syenites are mainly sodic-calcic katophorites, sodic and calcic amphiboles are very scarce (Bedford, 1989).

5. Trace element compositions

Overall, more than 230 trace element analyses of clinopyroxene and 150 analyses of amphibole were performed. In order to present a good overview of the whole data set, we present the averages of analyses from the respective minerals of each sample studied. In cases of significant chemical zoning with respect to major and trace element composition within individual grains, representative zoning profiles are shown. Typical analyses of clinopyroxene and amphibole from the three investigated igneous complexes are summarized in Tables 2-3. All rare earth element (REE) and trace element (TE) patterns are normalized to primitive mantle values of McDonough & Sun (1995). The order of presentation for both clinopyroxenes and amphiboles follows the above-described major element trends starting with the Ca-rich endmembers.

5.1 Clinopyroxene

Augites of Puklen and Ilímaussaq

Figures 4 a & b show average REE and TE patterns from augites of Puklen and Ilímaussaq, which are characterized by low Na/Ca ratios < 0.15. Normalized REE concentrations for all augites are 10 to 200 times enriched relative to primitive mantle values and show strongly developed negative Eu anomalies (Eu/Eu* = 0.12 – 0.38 for Puklen, 0.31 and 0.42 for Ilímaussaq, respectively). Overall, the patterns are characterized by slight LREE-enrichments. In most samples, a smooth increase from La to Nd is followed by a decrease from Sm to Er and a further increase towards Lu. La_N/Yb_N values vary between 1.5 and 3.7 (Puklen) and between 2.1 and 2.3 (Ilímaussaq), respectively.

Most other incompatible elements are enriched by a factor of about ten to hundred compared to primitive mantle values. For all augites, relative depletions can be detected for the high field strength elements (HFSE; Ti, Zr, Hf, Nb, Ta). For the large ion lithophile elements (LILE), strong negative peaks are observed for Ba and Sr and also for Pb except for three Puklen samples, which will be discussed below. The transitional metals Sc, V, Co and Zn are generally less enriched (Sc and Zn) or even depleted (V and Co). Principally, the REE and TE patterns for augites from Puklen and Ilímaussaq are very similar. However, the negative peaks for Pb and Sr are stronger developed in the Ilímaussaq augites and those of Zr, Hf and Ti appear to be weaker than in Puklen augites. In augites from Puklen, a slightly positive anomaly for Li can be detected, which is less pronounced in the Ilímaussaq augites.

Fig. 5 shows representative zoning profiles (Na p.f.u., X_{Fe} and selected trace element contents) across an augite from Puklen (Fig. 5a) and Ilímaussaq (Fig. 5b), respectively. Both profiles show similar characteristics. With increasing fractionation (increase of X_{Fe} and Na content from core to rim), Sc decreases and Zn, Zr and the REE increase. Whereas the amount of enrichment of Zn is more or less equal in both augites, the enrichment of Zr and REE_{tot} is much more extensive in the Ilímaussaq than in the Puklen augite.

Aegirine-augites of Grønnedal-Ika

REE and TE patterns for aegirine-augites of Grønnedal-Ika are shown in Fig. 6. Their Na/Ca ratios vary between 0.2 and 2. The enrichment levels for REE and most other TE are in a similar range compared to augites. Besides the lack of a significant Eu anomaly (Eu/Eu* = 0.69 – 1.16) and stronger enrichment in Tm-Lu, the shape of the REE patterns is rather similar to that of augites (Fig. 6a). La_N/Yb_N ratios are quite variable with a range from 0.6 to 6.5.

As for augites, negative peaks are detected for some LILE (Ba, Pb, Sr), Ti, Ta and the transitional elements (Sc, V, Co). In contrast to augites, for Zr and Hf positive peaks are developed and the positive Li anomaly turned into a negative one in aegirine-augites. Furthermore, a striking positive anomaly for Sn appears in aegirine-augites, which is not present in augites.

In most samples, aegirine-augites are fairly homogeneous. However, in one sample (GM1496), aegirine-augites with a relatively low Na/Ca ratio of about 0.2 show a thin rim of distinctly more Na-rich compositions (Na/Ca ratio ~ 0.7). Mantle-normalized REE patterns and TE patterns of core and rim compositions for a typical crystal of this sample are shown in Fig. 6b. The core pattern is parallel to that of the rim from La to Gd but shows a strong decrease towards Lu. The rim pattern is similar in shape and relative enrichment to the other Grønnedal-Ika aegirine-augites (Fig. 6a). Furthermore, rim compositions are enriched in Zr, Hf, Sn and Zn but depleted in Li, Sc, V and Co compared to the core and are similar to the patterns of the other aegirine-augites.

Aegirines of Puklen and Ilímaussaq

Average mantle-normalized REE patterns for aegirines (Figs. 7) are rather variable in their level of enrichment, their extent of negative Eu anomalies (Eu/Eu* = 0.16 – 0.63) and their shape, especially for the Puklen aegirines. With the exception of one sample, all Puklen aegirines show a more or less pronounced enrichment of HREE, whereas all Ilímaussaq aegirines are enriched in both LREE and HREE. This results in a V-shaped pattern, which seems to be typical for aegirines (Larsen, 1979; Shearer & Larsen, 1994; Piilonen et al., 1998). La_N/Yb_N ratios are typically lower than in augites and aegirine-augites and vary from 0.1 to 2.9.

As for augites and aegirine-augites, multi-element diagrams for aegirines show more or less pronounced negative peaks for Ba, Sr, V and Co (Fig. 7). In contrast, normalized Pb concentrations are variable with some aegirines having a clear positive Pb peak and some showing slightly negative ones. As in aegirine-augites, positive peaks for Zr, Hf and Sn are present, whereas the negative Ti peak has disappeared in the aegirines. A positive Li anomaly can be found in most aegirines similar to most augites, but unlike the aegirine-augites.

5.2 amphibole

Ca and Na-Ca-amphiboles of Puklen, Ilímaussaq and Grønnedal-Ika

Average REE patterns of Ca- and Ca-Na-amphiboles are shown in Figs. 8 & 9. The Puklen amphiboles have strongly developed negative Eu anomalies (Eu/Eu* = 0.06 – 0.29), but two different patterns can be distinguished: Ferro-richterites show pronounced HREE-enrichment with La_N/Yb_N ratios between 0.47 and 0.45. In contrast, ferro-edenites are characterised by variably developed LREE-enrichment and a flat HREE section resulting in La_N/Yb_N ratios between 1.5 and 2.5. Secondary ferro-actinolites from Puklen syenites are heterogeneous in terms of enrichment level and shape with La_N/Yb_N ratios between 0.7 and 1.1. In some cases, they have lower REE contents compared to primary amphibole, whereas in other cases the opposite can be observed. REE patterns of Ilímaussaq ferro-pargasites from the augite syenite are characterized by significant negative Eu-anomalies (Eu/Eu* = 0.26 and 0.30), a LREE enrichment and a smooth decrease from Gd to Lu. La_N/Yb_N ratios vary from 5.3 to 8.6. The Grønnedal-Ika katophorites lack a significant Eu anomaly (Eu/Eu* = 0.70 – 0.71). They show slight enrichments in LREE and the heaviest REE (La_N/Yb_N = 4.4 and 7.1).

Most trace elements in Ca- and Ca-Na amphiboles are 5-300 times enriched compared to primitive mantle values. Characteristic features of most samples are negative anomalies for Ba, Sr, Ta, V and Co and positive ones for Nb, Sn and Li. Strong negative Pb anomalies are only present in amphiboles from Ilímaussaq and Grønnedal. Positive Zr-Hf peaks do not occur in the Ca-amphiboles, but in the Ca-Na amphiboles of Grønnedal.

Figure 10 shows a representative zoning profile from core to rim of a Ca-Na amphibole crystal from a Puklen syenite (GM1615). The contents of Zr, Zn and REE increase from core to rim. With increasing fractionation (increase in X_{Fe} and Na/Ca ratio), LREE (La as example) slightly decrease and HREE (Yb as example) strongly increase resulting in a decrease of the La_N/Yb_N ratio from about 1.2 - 1.3 in the core regions to about 0.13 at the rim of crystals. However, the Eu/Eu* value remains relatively constant at about 0.25.

Na-amphiboles of Puklen and Ilímaussaq

REE and TE spectra of arfvedsonites are shown in Fig. 11. Eu anomalies are strongly negative in the Puklen arfvedsonites Eu/Eu*= 0.04 and 0.19), but more variable in Ilímaussaq arfvedsonites (Eu/Eu*= 0.26 - 0.92). The enrichment of LREE and HREE is highly variable developed with La_N/Yb_N ratios < 1 to 4. TE patterns of arfvedsonites are highly heterogeneous within and among the Puklen and Ilímaussaq rocks. Highly variable concentrations can be observed for Th, U, Pb, Zr and Hf. Most Ilímaussaq Na-amphiboles have positive anomalies of Zr, Hf, Nb, Sn and Li, which are much less prominent in Puklen.

Principally, zoning profiles of arfvedsonite from Puklen and Ilímaussaq (Fig. 12) show similar characteristics as the profiles of Ca-amphiboles (Fig. 10) and augites (Fig. 5), except for the REE. Zn and Zr increase from core to rim and Sc decreases. However, the total content of REE decreases with fractionation, which is in contrast to the behaviour of augites and Ca-amphiboles. The behaviour of LREE and HREE in the two amphibole types is different: In Na-amphiboles, LREE and HREE have similar concentrations in the core regions. During fractionation, HREE contents remain fairly constant, whereas LREE concentrations strongly decrease. This is in contrast to Ca-amphiboles, where LREE contents slightly decrease and HREE strongly increase during fractionation. Both processes result in the same effect: a decrease of the La_N/Yb_N ratio with increasing fractionation.

6. Discussion

In principle, relative trace element abundances in minerals either reflect the composition and structure of the melts or fluid phases they crystallised from or the partitioning of the respective elements is mainly controlled by crystal-chemical effects, i.e. the major element composition of the crystals dominates the incorporation of these elements (e.g Blundy & Wood, 1991; Wood & Blundy, 1997). The absolute concentration of a particular trace element in a mineral also reflects its absolute concentration in the parental melt. In the following, we will discuss how these aspects are of variable significance for different groups of geochemically related elements.

6.1 Rare earth elements (REE): crystal chemical control and effect of eudialyte fractionation

All mafic minerals analysed have REE enriched mantle-normalised patterns and show a continuous development from LREE-enriched patterns in the calcic minerals via wave-shaped pattern in the Ca-Na minerals towards a more pronounced HREE enrichment in the most Na-rich minerals. These principal changes are reflected in the REE patterns of both amphiboles and chemically corresponding clinopyroxenes (Fig. 11).

- The enrichment in HREE in Ca-Na- and especially Na-rich mafic silicates might partly reflect a general preference for trivalent REE as the incorporation of Na^{+} requires charge balance with a trivalent ion, following the coupled substitution Na + REE <=> 2 Ca on the M2 site as proposed for REE partitioning in clinopyroxene (Wood & Blundy, 1997). However, this process should also affect the LREE, which do not show significant enrichment in the Na-rich minerals. Therefore, it seems more likely that there is a particular site preference of the HREE with smaller ionic radii into the optimal sites available in the more Na-rich minerals. HREE were also shown to be compatible in Na-bearing clinopyroxene on the spinel-lherzolite solidus (Blundy et al., 1998).
- For amphiboles, there are multiple crystal-chemical mechanisms for REE^{3+} incorporation and REE are distributed over more than one structural site (Botazzi et al., 1999) Additionally, it is known that the REE site-preference is mainly a function of major-element composition of the B-group sites in amphiboles (Tiepolo et al., submitted). This is in agreement with our data, where we observe distinct changes in REE patterns from calcic amphiboles (2 Ca^{2+} on B-site) via sodic-calcic amphiboles (B-site occupied by one Ca^{2+} and one Na^{+}) towards sodic amphiboles (2 Na^{+} on B-site).

However, the REE contents of the Ilímaussaq minerals indicate that there is also a melt compositional influence on their absolute REE_{tot} contents and the shape of the normalized REE patterns. Both, amphiboles and clinopyroxenes, show an evolution from a pronounced LREE enrichment in the most Ca-rich minerals towards roughly an order of magnitude lower values in the Na-rich compositions, contrary to the trend expected for incompatible trace elements. The same trend can be seen in single minerals, as exemplified in a representative zoning profile of a Na-amphibole from Ilímaussaq (Fig. 12), which shows a strong LREE depletion from core to rim, whereas HREE content stays more or less constant. This feature is probably best explained by the fractionation of eudialyte, which is a REE-bearing mineral with highly enriched LREE contents compared to HREE (Bailey et al., 2001) and which is ubiquitous in the agpaitic Ilímaussaq rocks.

6.2 The large ion lithophile elements (Ba, Sr, Pb, Eu^{2+}): effects of feldspar fractionation

With respect to Ba, Sr, Pb and Eu, the trace element patterns of clinopyroxene and amphibole from Ilímaussaq and Puklen are very similar. All patterns except that for calcic amphiboles of the Ilímaussaq augite syenite show strongly negative Ba anomalies. For Sr and Eu, in all patterns (except for arfvedsonite in the late-stage vein, sample GM1401) negative anomalies occur. Pb, however, shows variable behaviour with some samples showing a negative anomaly and some

samples with positive a one. In the Grønnedal samples, all patterns have negative anomalies for Ba, Sr and Pb, but lack a significant Eu anomaly.

Ba, Sr and to a lesser extent also Pb are compatible in alkali feldspar in silicic magmas (Nash and Crecraft, 1985; White, 2003). Thus, negative anomalies for these elements in mafic minerals are consistent with fractionation of feldspar. However, the variable behaviour of Pb compared to Ba and Sr implies that an additional process influences the incorporation of Pb into clinopyroxene and amphibole. This will be discussed later.

Negative Eu anomalies are mostly controlled by feldspar fractionation, particularly in felsic magmas where Eu (in the divalent state) is compatible in plagioclase and alkali feldspar (Drake & Weill, 1975). Thus, the strongly negative Eu anomalies in the Puklen and Ilímaussaq mafic minerals probably reflect the fractionation of large amounts of feldspar. Early fractionation of plagioclase in Gardar magmas is indicated by the abundant occurrence of anorthosite xenoliths throughout the province (Bridgwater, 1967; Bridgwater & Harry, 1968; Halama et al., 2002) and it is believed that the whole province is underlain by a large anorthosite body (Bridgwater, 1967). Strongly negative Eu anomalies are also typical for whole-rock samples of the earliest intrusive units form Ilímaussaq (Bailey et al., 2001), indicating that fractionation of feldspar occurred before final emplacement.

In contrast to Ilímaussaq and Puklen, aegirine-augites and amphiboles of Grønnedal lack a significant Eu anomaly. A general lack of Eu anomalies in the Grønnedal whole-rocks has also been demonstrated by Bedford (1989). This can be explained in two different ways: either there was no feldspar fractionation during the early evolution of the complex, or oxygen fugacity was significantly higher in the Grønnedal magma, leading to the destabilization of Eu^{2+} relative to Eu^{3+}, which is incompatible in feldspar. We prefer the latter interpretation since

- Aegirine-augites and Ca-Na amphiboles in Grønnedal have significantly negative anomalies for Ba, Sr and Pb, which can be interpreted to result from fractionation of feldspar and the partitioning of these elements is probably independent from oxygen fugacity.
- The alkali feldspar-rich nature of the Grønnedal rocks, similar to the two other complexes, indicates that feldspar played an important role during the magmatic evolution of the complex.
- It has been shown that Ilímaussaq and Puklen rocks crystallised under highly reduced conditions significantly below the synthetic FMQ buffer (Larsen, 1976; Marks & Markl, 2001, Markl et al., 2001b, Marks et al., 2003). For Grønnedal, the observed rarity of olivine and amphibole and the onset of Na and Fe^{3+} enrichment in pyroxenes at relatively high Mg contents indicate rather oxidized conditions (Pearce et al., 1997).

In general, partitioning of LILE into clinopyroxene and amphibole seems to be influenced by the melt composition. Because of fractionation of feldspar during early stages, these elements are

depleted in the residual melts and thus strongly depleted in the crystallizing clinopyroxenes and amphiboles.

6.3 The high field strength elements (Ti, Zr, Hf, Sn, Nb, Ta): crystal chemical controls

Ti, Zr, Hf and Sn show a systematic behaviour in terms of their normalized concentrations in the various pyroxene types. Their normalized concentrations relative to the neighbouring elements increase with increasing Na-content. This increase is most pronounced for Zr, Hf and Sn and weaker for Ti. In amphiboles, similar systematics for Zr, Hf and Sn can be observed, whereas Ti remains fairly constant and relatively less depleted throughout the amphibole series from calcic to sodic varieties. The overall similar geochemical behaviour of these elements is probably related to their similar ionic radii and charges (Shannon, 1976).

Generally, incompatible HFSE contents in clinopyroxene and amphibole increase from Ca-rich to Na-rich members. For instance, in Ilímaussaq rocks, Zr, Hf and Sn contents strongly increase from 250 ppm, 7 ppm and <1 ppm in augites to >2000 ppm, 60 ppm and 400 ppm in aegirines. The increase of Zr, Hf and Sn during fractionation within one single pluton may be attributed to enrichment of incompatible elements during closed system fractional crystallisation. However, several arguments favour a major element crystal-chemical control of the trace element contents:

- In two of the investigated complexes, significant amounts of Ti-rich magnetite and/or ilmenite crystallized early in their evolution (Larsen, 1976; Marks &Markl, 2001; Marks et al., 2003) and thus, probably much of the Ti initially present was incorporated into these minerals, causing a strong depletion of Ti in the evolving melt. However, in the Ilímaussaq clinopyroxenes, the resulting effect on Ti content in clinopyroxene is surprisingly small: Early augites contain only slightly more Ti (up to 5200 ppm) than later aegirines (up to 4200 ppm) and in the Puklen rocks, early augites are even poorer in Ti (maximum of 5200 ppm) than late-stage aegirines (up to 10500 ppm). Despite presumably decreasing Ti contents in the melt, Ti contents in the precipitated mafic silicates increase with fractionation.
- Ti-rich aegirines have been described from a number of peralkaline igneous rocks of the Gardar province (Larsen, 1976; Jones & Peckett, 1980; Shearer & Larsen, 1994; Ranløv & Dymek, 1991) and elsewhere (Nielsen, 1979; Piilonen et al., 1998; Njonfang & Nono, 2003). In contrast, Ti-rich augites in more primitive alkali basaltic lavas of the Gardar Province have not been reported so far despite relatively high whole-rock TiO_2 contents of 1.7-3.0 wt.% (Halama et al., in press) compared to the typically low TiO_2 contents (< 0.7 wt.%) in the highly fractionated agpaitic rocks of Ilímaussaq (Bailey et al., 2001).

- In the Ilímaussaq intrusion, late-stage hydrothermal mineralizations containing rare Sn silicates like sørensenite ($Na_4SnBe_2(OH)_4Si_6O_{16}$) are well known (Semenov et al., 1965). Thus, one could argue, that the high Sn contents in late aegirines compared to earlier augites are an effect of fractionation and enrichment of Sn. However, the relatively high Sn contents and striking positive Sn anomalies in the Grønnedal aegirine-augites argue against this, since these pyroxenes are invariably early magmatic phases.
- For an optimal site of about 0.70 Å in pyroxenes and amphiboles (Jensen, 1973; Bailey et al., 2001), Zr^{4+} (0.72 Å), Hf^{4+} (0.71 Å) and Sn^{4+} (0.69 Å) fit fairly well, whereas Ti^{4+} (0.605 Å) is considerably smaller (Shannon, 1976). This relatively large mismatch of Ti might contribute to the rather weak increase in Ti contents during fractionation compared to Zr, Hf and Sn. The latter are close to the optimal site size and might therefore react more sensitively than Ti on small crystal-chemical changes.

Normalized Nb contents in clinopyroxenes systematically increase from < 10 times enriched in calcic members to nearly 1000 times enriched in sodic ones. In amphiboles, Nb contents are slightly higher with normalized values between 100 and 1000 times enriched. In contrast, Ta is strongly depleted in both clinopyroxenes and amphiboles with normalized values between 0.01 and 0.6. Nb/Ta ratios in most clinopyroxenes vary between about 2 and 30 and are slightly lower than in amphiboles (10-80). Tiepolo et al. (2000) showed that in amphibole with high X_{Fe}, Nb is favoured relative to Ta, and explained this by an accompanied increase of the M1-site and Nb^{5+} having a radius 1 – 2 pm larger than Ta^{5+}. Thus, the high Nb/Ta ratios in the amphiboles investigated here can be explained by their high X_{Fe} (Marks et al., 2003). Comparable experimental work for clinopyroxenes is lacking, but our data indicate that similar reasons could be responsible for the fractionation of Nb from Ta in clinopyroxenes.

The association of the Grønnedal syenites with a carbonatite and the proposed liquid immiscibility relationship (Bedford, 1989) could also have an influence on the HFSE contents, because the HFSE are known to partition into the silicate liquid during liquid immiscibility with a carbonate liquid (Veksler et al., 1998). Zr and Hf have the lowest $D^{carbonate\text{-}silicate}$ values (0.016 and 0.0093, respectively) and should therefore be most enriched in the silicate liquid. Both the Grønnedal aegirine-augites and amphiboles have the most significant positive Zr and Hf peaks compared to the other complexes, which could be interpreted to reflect an enrichment in those elements in the silicate liquid during liquid immiscibility. However, similar peaks, although at lower enrichment levels, are also present in some Ilímaussaq minerals and there is no significant difference between the Grønnedal minerals and those of the other complexes for Nb and Ta. Thus, it

appears as if the crystal chemical control on HFSE partitioning could mask most of the possible previous enrichment during liquid immiscibility.

In summary, it seems likely that for the HFSE, the major element composition of the host crystal has a dominant control on the partitioning of these elements into clinopyroxene and amphibole. This is in contrast to the LILE.

6.4 The transitional metals (Co, V, Zn) and Sc: early precipitation of olivine and Fe-Ti oxides

Co and V are strongly depleted compared to primitive mantle values. Depletion reaches values down to 0.001. These elements are all compatible in olivine and/or spinel (Arth, 1976). Their low concentrations in the investigated clinopyroxenes and amphiboles may therefore be attributed to early precipitation of olivine and spinel. The presence of mafic cumulates underneath the exposed alkaline complexes is likely and confirmed by large positive gravity and magnetic anomalies centred on the Ilímaussaq area (Blundell, 1978; Forsberg & Rasmussen, 1978). Some samples from Puklen have significantly higher concentrations of Co and V, which will be discussed below.

Sc is compatible in clinopyroxene and amphibole within a large range of magma compositions (e.g., Arth, 1976; Mahood & Hildreth, 1983). Normalized Sc concentrations decrease systematically from calcic to sodic clinopyroxenes and amphiboles from relatively high values between 10 and 1 down to values < 0.1. A strong decrease of Sc during fractionation of augite is indicated by the zoning profiles shown in Fig. 5. This may indicate that fractionation of clinopyroxene was important for the evolution from early relatively Ca-rich rock types (augite syenites) towards later Na-rich and more evolved ones within one single complex, but probably not during ascent and fractionation of the parental basaltic magmas. This conclusion is consistent with experimental and petrological work of Upton (1971) and Upton & Thomas (1980) on gabbroic dike rocks from the Gardar Province, who found olivine and magnetite to be the dominant liquidus assemblage with only minor clinopyroxene.

In contrast to Co and V, normalized Zn contents in both clinopyroxene and amphibole are significantly enriched compared to primitive mantle. Enrichment factors in clinopyroxenes vary unsystematically between 1 and 20 and increase from <10 in Ca-amphiboles to about 100 in sodic amphiboles. In six-fold coordination, Zn^{2+} has an ionic radius of 0.74 Å, which is very similar to the ionic radius of Sc^{3+} (0.745 Å), whereas the radii of V^{2+} (0.79 Å), V^{3+} (0.64 Å), Co^{2+} (0.65 Å) and Co^{3+} (0.545 Å) are somewhat different (Shannon, 1976). Since the compatibility of Sc in clinopyroxene and amphibole is well-known, it is likely that the Zn^{2+} ion with a similar ionic radius may have a similar degree of compatibility, in contrast to V and Co. This indicates some influence of crystal-chemical effects on the partitioning behaviour of the transitional metals.

6.5 Lithium in clinopyroxenes: Influence of the melt composition

In the clinopyroxenes, Li behaves quite variable with flat patterns or small positive peaks in the mantle-normalised augite patterns, negative peaks in the aegirine-augites and positive peaks in the aegirines. The enrichment level is also quite different, depending on the complex: Clinopyroxenes from Ilímaussaq have medium values of ~ 20-40x, from Puklen ~ 100x and from Grønnedal < 7x primitive mantle values, apparently independent of the chemical composition. This indicates that Li contents in the clinopyroxenes are dependent of the melt composition. The Puklen melts were relatively most enriched in Li, whereas the Grønnedal melts had relatively low Li contents. The generally positive Li peaks in amphiboles, especially for the sodic members, are clearly an effect of preferential partitioning of Li into amphibole and it was shown by Hawthorne et al. (1993, 1994) that Li could be a major component in Na-amphiboles from peralkaline igneous rocks.

6.6 Puklen: How does crustal contamination influence the trace element patterns?

For the Ilímaussaq and Grønnedal rocks it has been shown that crustal assimilation is of only minor importance for the evolution of these complexes (Marks et al, 2003; Halama & Markl, 2003). This is in contrast to the Puklen samples, where crustal contamination plays a major role (Marks et al., 2003). By using Nd isotopic data as indicators for crustal contamination (Marks et al., 2003) we will discuss in the following how crustal assimilation influences the incorporation of specific elements into clinopyroxene and amphibole.

Syenites show a range of ε_{Nd} values between –3.8 and –7.2, and alkali granites vary between –5.9 and –9.6. Within the syenites, samples GM1593 (ε_{Nd} = -7.2) and GM1600 (ε_{Nd} = -6.4) are the most contaminated ones. Augites of these two samples have the highest contents in U, Pb, V and Zn but the lowest concentrations of Ti, Zr, and Hf. This is consistent with assimilation of crustal rocks, which have high contents of U, Pb, V and Zn and low contents of Ti, Zr and Hf compared to the primitive mantle (Rudnick & Fountain, 1995; McDonough & Sun, 1995). For Pb it can be observed that these two samples are those with positive Pb anomalies (Fig. 4). We defined a Pb/Pb* value, which was calculated similar to Eu/Eu* as the geometric mean $Pb/Pb^* = Pb_N \sqrt{(Ce_N \cdot \mathrm{Pr}_N)}$. This should be a useful parameter, since Ce and Pr normally have similar normalized values. The significant correlation between Pb/Pb* and ε_{Nd} values in Fig. 13 confirms the influence of crustal contamination on this parameter and provides evidence of a relation between trace element composition in minerals and assimilation processes during the magmatic evolution of an alkaline complex.

6.7 Partitioning of trace elements between coexisting clinopyroxene and amphibole

To establish meaningful intermineral partition coefficients, chemical equilibrium is required. However, chemical equilibrium is often difficult to evaluate (e.g. Chazot et al., 1996). We calculated clinopyroxene-amphibole trace element abundance ratios for selected samples where textural and isotopic criteria (Markl et al., 2001b; Marks et al., 2003) indicate equilibrium conditions (Figs. 14a-d, Table 4). These values might not strictly be interpreted as partition coefficients but can be used as useful guides for trace element partitioning during petrogenesis and will be used here as an approximation for equilibrium partition coefficients. They may serve as a test of equilibrium partitioning in further studies.

Calculated clinopyroxene-amphibole partition coefficients ($D_{cpx\text{-}amph}$) for the majority of trace elements vary for the Ilímaussaq augite syenites (Fig. 14a) between 0.1 and 0.6. In the Puklen syenites (Fig. 14b), they are slightly higher (between 0.6 and 1.7). In the Na-Ca system of Grønnedal (Fig. 14c), a larger range between 0.3 and 2.7 is observed. Finally, in the Na-dominated system of Ilímaussaq (Fig. 14d) they vary between 0.07 and 0.9. In comparison with $D_{cpx\text{-}amph}$ values from a xenolithic mantle-derived harzburgite (Grégoire et al., 2000), our patterns from alkaline rocks show some striking similarities both in general shape and in absolute values (Fig. 14c), despite major differences in mineral chemistry. Other experimentally determined and measured $D_{cpx\text{-}amph}$ values on natural samples of ultramafic (Vannucci et al., 1991; Chazot et al., 1996; Witt-Eickschen & Harte, 1994) and basanitic (Adam & Green, 1994) compositions also overlap with our data. This indicates that trace element partitioning between clinopyroxene and amphibole is not significantly influenced by the melt composition. In all, clinopyroxene-amphibole partition coefficients seem to be relatively independent of major element mineral compositions and no systematic variation of D values with increasing Na-content of clinopyroxene and amphibole can be observed. As expected, samples with similar major element chemical composition show similar patterns, despite certain differences in the absolute D values. Some elements exhibit some noteworthy features:

- Nb and Ta have always a strong preference for amphibole, which is in accordance with previous studies on mantle minerals (e.g., Witt-Eickschen & Harte, 1994; Chazot et al., 1996) and andesitic melts (Brenan et al., 1995).
- U and Th are also preferentially incorporated into amphibole except for the Puklen samples. However, both are relatively enriched in clinopyroxene compared to the neighbouring elements, which is consistent with a marked incompatibility in amphibole (Tiepolo et al., submitted).
- Rb and Ba are apparently less compatible in clinopyroxene than in amphibole, which has been shown by previous studies (e.g., Brenan et al., 1995; Chazot et al., 1996) and is caused by a

strong preference of these two elements for the A-site in amphibole (e.g. Dalpé & Baker, 2000), which has no equivalent position in pyroxene. As for U and Th, Rb and Ba in the Puklen syenites have significantly higher $D_{cpx\text{-}amph}$ values. This might be caused by secondary fluid circulation, which was shown to disturb the Rb/Sr isotopic system in the Puklen minerals (Marks et al., 2003).

- $D_{cpx\text{-}amph}$ values for Sr are characterized by small positive peaks in the Ca-rich system, but slight depressions in the Na-rich system. The two Puklen samples behave variable, which may be an effect of secondary metasomatism, as mentioned above (Marks et al., 2003).
- Zr, Hf and Sn develop a preference for clinopyroxene as the system evolves towards Ca-Na and Na-rich compositions, but absolute D_{Zr} and D_{Hf} values > 1 only occur in the Ca-Na system (Grønnedal). For Zr and Hf contradictory data from similar compatibilities in andesitic rocks (Brenan et al., 1995), to variable behaviour (Vannucci et al., 1991) and a preference for amphibole (Chazot et al., 1996) in ultramafic rocks exist.
- Li partitions preferentially into amphibole as the system becomes more Na-rich.

The $D_{cpx\text{-}amph}$ values of the REE are continuously increasing from the LREE towards the HREE for the Ilímaussaq and Grønnedal rocks. However, whereas in Ilímaussaq, all D_{REE} are always < 1, D_{REE} values in Grønnedal increase from D_{La} = 0.2 towards D_{Lu} = 2.7, i.e. the LREE partition preferentially into amphibole, but the HREE do not. In contrast, D_{REE} values for Puklen syenites are fairly constant. For the REE, Klein et al. (1997) assumed that as a consequence of nearly identical values of Young´s moduli and lattice site geometries of M4- and M2-sites in amphibole and clinopyroxene, respectively, $D_{cpx\text{-}amph}$ should be identical for all REE and consequently, REE patterns of clinopyroxenes and amphiboles should be subparallel. Measured REE partition coefficients between clinopyroxene and amphibole in mantle rocks (Witt-Eickschen & Harte, 1994; Chazot et al., 1996) partly confirm this assumption as our data for the Puklen syenites do (Figs. 4a, 8a and 14b). However, Witt-Eickschen and Harte (1994) also found a slight tendency of increase of $D_{cpx\text{-}amph}$ for the REE with increasing Na-content, which is not confirmed by our data. The tendency of increase of $D_{cpx\text{-}amph}$ values from La to Lu found by Witt-Eickschen and Harte (1994) in mantle rocks and by Irving and Frey (1984) for basanitic rocks is in accordance with our results for the Ilímaussaq and Grønnedal rocks, but not for the Puklen syenites, where $D_{cpx\text{-}amph}$ for the REE stay fairly constant from La to Lu.

7. Summary and concluding remarks

This comparative study on trace element contents in mafic minerals of three alkaline igneous complexes confirms that trace element contents of amphiboles and clinopyroxenes are influenced

mainly by two different factors: The major element composition of the host mineral exerts a dominant control on the partitioning, and the melt composition can lead to significant differences in absolute and/or relative concentrations.

- Naturally, elements compatible in early fractionating mineral phases results in the depletion of these elements in minerals precipitated during later stages. This is particularly true for the large ion lithophile elements (Ba, Sr, Pb, Eu^{2+}) and some of the transitional elements like V and Co, which reflect early fractionation of feldspar, olivine and spinel, respectively. In general, absolute concentrations of these elements in clinopyroxene and amphibole seem to be mainly influenced by the melt composition. Since these elements have been extracted from the residual melts they are strongly depleted in the crystallizing clinopyroxenes and amphiboles. However, we showed that other factors like oxygen fugacity (Eu-partitioning) or crustal assimilation (Pb-contents) may disturb such primary characteristics.
- The partitioning of some high field strength elements (Ti, Zr, Hf, Sn) seems to be mainly governed by the major element composition of the host crystal. Zr, Hf and Sn fit fairly well for an optimal site in clinopyroxene and amphibole, whereas Ti has a considerable mismatch. This results in rather weak effects on Ti partitioning in contrast to large changes of Zr, Hf and Sn contents with changing Na/Ca ratio in clinopyroxene and amphibole.
- For the REE, a crystal chemical control on partitioning is indicated, since clinopyroxenes and amphiboles show a continuous development from LREE-enriched patterns in the calcic minerals via wave-shaped pattern in the Ca-Na minerals towards a more pronounced HREE enrichment in the most Na-rich minerals.

However, major element mineral composition and melt composition cannot be regarded as two independent factors. The latter is influenced by primary characteristics derived from the melt source(s) and secondary processes such as the fractionation of trace element-rich phases, assimilation of crustal material or liquid immiscibility, and, together with intensive crystallisation parameters such as P, T and f_{O2}, determines the major element mineral composition.

The partitioning of most trace elements between clinopyroxene and co-genetic amphibole seems to be fairly independent of melt composition or major element composition of the host crystals. However, the $D_{cpx\text{-}amph}$ values of the REE are continuously increasing from the LREE towards the HREE for the Ilímaussaq and Grønnedal samples but are fairly constant from La to Lu for Puklen samples. Most trace elements show a slight preference for amphibole. This is most pronounced for Nb, Ta, U, Th, Rb, Ba and Li. However, in Puklen samples U, Th, Rb and Ba have significantly higher $D_{cpx\text{-}amph}$ values up to about 20, which might be explained by secondary fluid circulation and late-stage autometasomatism resulting in the re-destribution of these elements in the

Puklen rocks. In contrast, Zr, Hf and Sn develop a preference for clinopyroxene relative to the neighbouring elements, as the system evolves from a Ca-dominated to a Na-dominated one.

Acknowledgments - Laser ICP-MS measurements were carried out at the Large Scale Geochemical Facility supported by the European Community - Access to Research Infrastructure action of the Improving Human Potential Programme, contract number HPRI-CT-1999-00008 awarded to Prof. B. J. Wood (University of Bristol) which is gratefully acknowledged. Bruce Paterson provided invaluable help during these measurements. We also thank Thomas Wenzel for constructive criticism of the manuscript. Financial support for this work was funded by the Deutsche Forschungsgemeinschaft (grant Ma-2135/1-2).

References

Adam, J. and Green, T. H. (1994) The effects of pressure and temperature on the partitioning of Ti, Sr and REE between amphibole, clinopyroxene and basanitic melts. *Chemical Geology* **117**, 219-233.

Allaart, J. H. (1976) Ketilidian mobile belt in South Greenland. In: Escher, A. and Watt, W.S. (eds.), Geology of Greenland, Grønlands Geologiske Undersøgelse 121-151.

Armstrong, J. T. (1991) Quantitative elemental analysis of individual microparticles with electron beam instruments. In: Heinrich, K.F.J. and Newbury, D.E. (eds.), Electron Probe Quantitation. New York & London: Plenum Press. 261-315.

Arth, J. G. (1976) Behaviour of trace elements during magmatic processes-a summary of theoretical models and their applications. *Journal of Research of the U.S. Geological Survey* **4**, 41-47.

Bailey, J. C., Gwozdz, R., Rose-Hansen, J., and Sørensen, H. (2001) Geochemical overview of the Ilimaussaq alkaline complex, South Greenland. *Geology of Greenland Survey Bulletin* **190**, 35-53.

Bea, F., Arzamastsev, A., Montero, P., and Arzamastseva, L. (2001) Anomalous alkaline rocks of Soustov, Kola: evidence of mantle-derived metasomatic fluids affecting crustal materials. *Contributions to Mineralogy and Petrology* **140**, 554-566.

Bedford, C. M. (1989) The mineralogy, geochemistry and petrogenesis of the Grønnedal-Ika complex, south west Greenland. Unpublished PhD thesis, University of Durham

Benoit, M., Polvé, M., and Ceuleneer, G. (1996) Trace element and isotopic characterization of mafic cumulates in a fossil mantle diapir (Oman ophiolite). *Chemical Geology* **134** , 199-214.

Blundell, D. J. (1978) A gravity survey across the Gardar Igneous Province, SW Greenland. *Journal of the geological Society of London* **135**, 545-554.

Blundy, J. D. and Wood, B. J. (1991) Crystal-chemical controls on the partitioning of Sr and Ba between plagioclase feldspar, silicate melts, and hydrothermal solutions. *Geochimica et Cosmochimica Acta* **55**, 193-209.

Blundy, J. and Wood, B. (1994) Prediction of crystal-melt partition coefficients from elastic moduli. *Nature* **372**, 452-454.

Blundy, J. and Wood, B. (1997) A predictive model for rare earth element partitioning between clinopyroxene and anhydrous silicate melt. *Contributions to Mineralogy and Petrology* **129**, 166-181.

Blundy, J. and Dalton, J. (2000) Experimental comparison of trace element partitioning between clinopyroxene and melt in carbonate and silicate systems, and implications for mantle metasomatism. *Contributions to Mineralogy and Petrology* **139**, 356-371.

Blundy, J. and Wood, B. (2003) Partitioning og trace elements between crystals and melts. *Earth and Planetary Science Letters* **210**, 383-397.

Blundy, J. D., Robinson, J. A. C., and Wood, B. J. (1998) Heavy REE are compatible in clinopyroxene on the spinel lherzolite solidus. *Earth and Planetary Science Letters* **160**, 493-504.

Bottazzi, P., Tiepolo, M., Vannussi, R., Zanetti, A., Brum, R., Foley, S. F., and Oberti, R. (1999) Distinct site preferences for heavy and light REE in amphibole and the prediction of $^{Amph/L}D_{REE}$. *Contributions to Mineralogy and Petrology* **137**, 36-45.

Brenan, J. M., Shaw, H. F., Ryerson, F. J., and Phinney, D. L. (1995) Experimental determination of trace-element partitioning between pargasite and a synthetic hydrous andesitic melt. *Earth and Planetary Science Letters* **135**, 1-11.

Bridgwater, D. (1967) Feldspathic inclusions in the Gardar igneous rocks of South Greenland and their relevance to the formation of major Anorthosites in the Canadian Shield. *Canadian Journal of Earth Sciences* **4**, 995-1014.

Bridgwater, D. and Harry, W. T. (1968) Anorthosite xenoliths and plagioclase megacrysts in Precambrian intrusions of South Greenland. *Meddelelser om Grønland* **185** , 243.

Chazot, G., Menzies, M., and Harte, B. (1996) Determination of partition coefficients between apatite, clinopyroxene, amphibole, and melt in natural spinel lherzolites from Yemen: Implications for wet melting of the lithospheric mantle. *Geochimica et Cosmochimica Acta* **60**, 423-437.

Coogan, L. A., kempton, P. D., Saunders, A. D., and Norry, M. J. (2000) Melt aggregation within the crust beneath the Mid-Atlantic Ridge: evidence from plagioclase and clinopyroxene major and trace element compositions. *Earth and Planetary Science Letters* **176**, 245-257.

Dalpé, C. and Baker, D. R. (2000) Experimental investigation of large-ion-lithophile-element-, high-field-strength-element- and rare-earth-element-partitioning between calcic amphibole and basaltic melt: the effects of pressure and oxygen fugacity. *Contributions to Mineralogy and Petrology* **140**, 223-250.

Digonnet, S., Goulet, N., Bourne, J., Stevenson, R., and Archibald, D. (2000) Petrology of the Abloviak aillikite dykes, New Quebec; evidence for a Cambrian diamondiferous alkaline province in northeastern North America. *Canadian Journal of Earth Sciences* **37**, 517-533.

Drake, M. J. and Weill, D. F. (1975) Partitioning of Sr, Ba, Ca, Y, Eu2+, Eu3+ and other REE between plagioclase feldspar and magmatic liquid: an experimental study. *Geochimica et Cosmochimica Acta* **39**, 689-712.

Dunworth, E. A. and Bell, K. (2001) The Turiy massif, Kola peninsula, Russia: Isotopic and geochemical evidence for multi-source evolution. *Journal of Petrology* **42**, 377-405.

Emeleus, C. H. (1964) The Grønnedal-Ika alkaline complex, South Greenland. The structure and geological history of the complex. *Meddelelser om Grønland* **172** , 75.

Escher, A. and Watt, W. S. (1976) Geology of Greenland. Copenhagen: Geological Survey of Greenland. 603.

Ferguson, J. (1964) Geology of the Ilimaussaq alkaline intrusion, South Greenland. *Bulletin Grønlands Geologiske Undersøgelse* **39**, 82.

Forsberg, R. and Rasmussen, K. L. (1978) Gravity and rock densities in the Ilimaussaq area, South Greenland. *Rapport Grønlands Geologiske Undersøgelse* **90**, 81-84.

Gaetani, G. A. and Grove, T. L. (1995) Partitioning of rare earth elements betwee clinopyroxene and silicate melt: Crystal-chemical controls. *Geochimica et Cosmochimica Acta* **59**, 1951-1962.

Garde, A. A., Hamilton, M. A., Chadwick, B., Grocott, J., and McCaffrey, K. J. W. (2002) The Ketilidian orogen of South Greenland: geochronology, tectonics, magmatism, and fore-arc accretion during Palaeoproterozoic oblique convergence. *Canadian Journal of Earth Sciences* **39**, 765-793.

Grégoire, M., Moine, B. N., O´Reilly, S. Y., Cottin, J. Y., and Giret, A. (2000) Trace element residence and partitioning in mantle xenoliths metasomatized by highly alkaline, silicate- and carbonate-rich melts (Kerguelen Islands, Indian Ocean). *Journal of Petrology* **41**, 477-509.

Halama, R. and Markl, G. (2003) A Nd- and O isotopic study pf the carbonatite-syenite association in the Grønnedal-Ika complex, Gardar Province, South Greenland. *Geophysical Research Abstracts* **5**, 00808.

Halama, R., Waight, T., and Markl, G. (2002) Geochemical and isotopic zoning patterns of plagioclase megacrysts in gabbroic dykes from the Gardar Province, South Greenland: implications for crystallisation processes in anorthositic magmas. *Contributions to Mineralogy and Petrology* **144**, 109-127.

Halama, R., Wenzel, T., Upton, B. G. J., Siebel, W., and Markl, G. (in press) A geochemical and Sr-Nd-O isotopic study of the Proterozoic Eriksfjord Basalts, Gardar Province, South Greenland: Reconstruction of an OIB-signature in crustally contaminated rift-related basalts. *Mineralogical Magazine special volume*

Hawthorne, F. C., Ungaretti, L., Oberti, R., and Bottazzi, P. (1993) Li: An important component in igneous alkali amphiboles. *American Mineralogist* **78**, 733-745.

Hawthorne, F. C., Ungaretti, L., Oberti, R., and Cannillo, E. (1994) The mechanisms of [6]Li incorporation in amphiboles. *American Mineralogist* **79**, 443-451.

Irving, A. J. and Frey, F. A. (1984) Trace element abundances in megacrysts and their host basalts: Constraints on partition coefficients and megacryst genesis. *Geochimica et Cosmochimica Acta* **48**, 1201-1221.

Jeffries, T. E., Perkins, W. T., and Pearce, N. J. G. (1995) Measurements of trace elements in basalts and their phenocrysts by laser probe microanalysis inductively coupled plasma mass sepctrometry (LPMA-ICP-MS). *Chemical Geology* **121**, 131-144.

Jensen, B. B. (1973) Patterns of trace element partitioning. *Geochimica et Cosmochimica Acta* **37**, 2227-2242.

Jones, A. P. and Peckett, A. (1980) Zirconium-bearing aegirines from Motzfeldt, South Greenland. *Contributions to Mineralogy and Petrology* **75**, 251-255.

Kalsbeek, F. and Taylor, P. N. (1985) Isotopic and chemical variation in granites across a Proterozoic continental margin-the Ketilidian mobile belt of South Greenland. *Earth and Planetary Science Letters* **73**, 65-80.

Klein, M., Stosch, H.-G., and Seck, H. A. (1997) Partitioning of high field-strength and rare-earth elements between amphibole and quartz-dioritic to tonalitic melts: an experimental study. *Chemical Geology* **138**, 257-271.

Konnerup-Madsen, J. and Rose-Hansen, J. (1984) Composition and significance of fluid inclusions in the Ilimaussaq peralkaline granite, South Greenland. *Bulletin de Minéralogie* **107**, 317-326.

Kramm, U. and Kogarko, L. N. (1994) Nd and Sr isotope signatures of the Khibina and Lovozero agpaitic centres, Kola Province, Russia. *Lithos* **32**, 225-242.

Larsen, L. M. (1976) Clinopyroxenes and coexisting mafic minerals from the alkaline Ilimaussaq intrusion, south Greenland. *Journal of Petrology* **17**, 258-290.
Larsen, L. M. (1977) Aenigmatites from the Ilimaussaq intrusion, south Greenland: Chemistry and petrological implications. *Lithos* **10**, 257-270.
Larsen, L. M. (1979) Distribution of REE and other trace elements between phenocrysts and peralkaline undersaturated magmas, exemplified by rocks from the Gardar igneous province, South Greenland. *Lithos* **12**, 303-315.
Larsen, L. M. (1981) Chemistry of feldspars in the Ilimaussaq augite syenite with additional data on some other minerals. *Rapport Grønlands Geologiske Undersøgelse* **103**, 31-37.
Larsen, L. M. and Sørensen, H. (1987) The Ilimaussaq intrusion-progressive crystallization and formation of layering in an agpaitic magma. *In: Fitton, J.G. & Upton, B.G.J. (eds.), Alkaline Igneous Rocks, Geological Society Special Publication* **30**, 473-488.
Lemarchand, F., Villemant, B., and Calas, G. (1987) Trace element distribution coefficients in alkaline series. *Geochimica et Cosmochimica Acta* **51**, 1071-1081.
Mahood, G. and Hildreth, W. (1983) Large partition coefficients for trace elements in high-silica rhyolithes. *Geochimica et Cosmochimica Acta* **47**, 11-30.
Markl, G. and Baumgartner, L. (2002) pH changes in peralkaline late-magmatic fluids. *Contributions to Mineralogy and Petrology* **144**, 31-346.
Markl, G., Marks, M., and Wirth, R. (2001a) The influence of T, aSiO2, fO2 on exsolution textures in Fe-Mg olivine: an example from augite syenite of the Ilimaussaq Intrusion, South Greenland. *American Mineralogist* **86**, 36-46.
Markl, G., Marks, M, Schwinn, G., and Sommer, H. (2001b) Phase equilibrium constraints on intensive crystallization parameters of the Ilimaussaq Complex, South Greenland. *Journal of Petrology* **42**, 2231-2258.
Marks, M. and Markl, G. (2001) Fractionation and assimilation processes in the alkaline augite syenite unit of the Ilimaussaq Intrusion, South Greenland, as deduced from phase equilibria. *Journal of Petrology* **42**, 1947-1969.
Marks, M., Vennemann, T. W., Siebel, W., and Markl, G. (2003) Quantification of magmatic and hydrothermal processes in a peralkaline syenite- alkali granite complex based on textures, phase equilibria, and stable and radiogenic isotopes. *Journal of Petrology* **44**, 1247-1280.
Marks, M., Vennemann, T., Siebel, W., and Markl, G. (submitted) Decoupling of O and H isotopes in Fe-rich amphiboles and strong D-depletion during magmatic processes: an example from the peralkaline Ilimaussaq Intrusion, South Greenland. *Geochimica et Cosmochimica Acta*
McDonough, W. F. and Sun, S. S. (1995) The composition of the Earth. *Chemical Geology* **120**, 223-253.
Mitchell, R.H. (1990) A review of the compositional variation of amphiboles in alkaline plutonic complexes. *Lithos* **26**, 135-156.
Nash, W. P. and Crecraft, H. R. (1985) Partition coefficients for trace elements in silicic magmas. *Geochimica et Cosmochimica Acta* **49**, 2309-2322.
Nielsen, T. F. D. (1979) The occurence and formation of Ti-aegirines in peralkaline syenites; an example from the Tertiary ultramafic alkaline Gardiner complex, East Greenland. *Contributions to Mineralogy and Petrology* **69**, 235-244.
Nimis, P and Vannucci, R. (1995) An ion microprobe study of clinopyroxenes in websteritic and megacrystic xenoliths from Hyblean Plateau (SE Sicily, Italy): constraints on HFSE/REE/Sr fractionation at mantle depth. *Chemical Geology* **124**, 185-197.
Njonfang, E. and Nono, A. (2003) Clinopyroxene frome some felsic alkaline rocks of the Cameroon Line. centraö Africa: petrological implications. *European Journal of Mineralogy* **15**, 527-542.
Panneer Selvam, A. and Suryanarayana Rao, S. (1996) Geology and uranium mineralisation of the Proterozoic alkali syenite from Rasimalai, North Arcot Ambedkar District, Tamil Nadu, India *Exploration and Research for Atomic Minerals* **9**, 41-54.
Parsons, I. (1972) Petrology of the Puklen syenite-alkali granite complex, Nunarssuit, South Greenland. *Meddelelser om Grønland* **195**, 73.
Pearce, N. J. G., Leng, M. J., Emeleus, C. H., and Bedford, C. M. (1997) The origins of carbonatites and related rocks from the Grønnedal-Ika Nepheline Syenite complex, South Greenland: C-O-Sr isotope evidence. *Mineralogical Magazine* **61**, 515-529.
Piilonen, P. C., McDonald, A. M., and Lalonde, A. E. (1998) The crystal chemistry of aegirine from Mont Saint-Hilaire, Quebec. *Canadian Mineralogist* **36**, 779-791.

Platt, R. G. (1996) Nepheline syenite complexes - an overview. *In: R.H. Mitchell (Editor), Undersaturated alkaline rocks; mineralogy, petrogenesis, and economic potential.* Short Course Handbook vol. 24, 63-99.
Poulsen, V. (1964) The sandstones of the Precambrian Eriksfjord Formation in South Greenland. *Rapport Grønlands Geologiske Undersøgelse* **2**, 16.
Pulvertaft, T. C. R. (1961) The Puklen intrusion, Nunarssuit, SW Greenland. *Meddelelser om Grønland* **123**, 35-49.
Ranløv, J. and Dymek, R. F. (1991) Compositional zoning in hydrothermal aegirine from fenites in the Proterozoic Gardar Province, South Greenland. *European Journal of Mineralogy* **3**, 837-853.
Rudnick, R. and Fountain, D. M. (1995) Nature and composition of the Continental Crust: A lower crustal perspective. *Reviews of Geophysics* **33**, 267-309.
Semenov, E. I., Gerassimivsky, V. I., Maksimova, N. V., Andersen, S., and Peteresen, O. V. (1965) Sorensenite, a new sodium-beryllium-tin-silicate from the Ilimaussaq Intrusion, South Greenland. *Bulletin Grønlands Geologiske Undersøgelse* **61**, 19.
Shannon, R. D. (1976) Revised effective ionic radii and systematic studies of interatomic distances in halides and chalcogenides. *Acta Crystallographica* **A32**, 751-767.
Shearer, C. K. and Larsen, L. M. (1994) Sector-zoned aegirine from the Ilimaussaq alkaline intrusion, South Greenland: Implications for trace-element behavior in pyroxene. *American Mineralogist* **79**, 340-352.
Sisson, T. W. (1994) Hornblende-melt trace-element partitioning measured by ion microprobe. *Chemical Geology* **117**, 331-344.
Thompson, G. M. and Malpas, J. (2000) Mineral/melt partition coefficients of oceanic alkali basalts determined on natural samples using laser ablation-inductively coupled plasma-mass spectrometry (LAM-ICP-MS) *Mineralogical Magazine* **64**, 85-94.
Tiepolo, M., Vanucci, R., Oberti, R., Foley, S., Bottazzi, P., and Zanetti, A. (2000) Nb and Ta incorporation and fractionation in titanian pargasite and kaersurtite: crystal-chemical constraints and implications for natural systems. *Earth and Planetary Science Letters* **176**, 185-201.
Tiepolo, M., Tribuzio, R., and Vannucci, R. (2002) The compositions of mantle-derived melts developed during the Alpine continental collision. *Contributions to Mineralogy and Petrology* **144**, 1-15.
Tiepolo, M., Vannucci, R., Bottazzi, P., Oberti, R., Zanetti, A., and Foley, S. (submitted) Partitioning of REE, Y, Th, U and Pb between pargasite, kaersutite and basanite to trachyte melts: implications for percolated and veined mantle. *Geochem. Geophy. Geosys.*
Upton, B. G. J. (1971) Melting experiments on chilled gabbros and syenogabbros. *Carnegie Institute Washington Year Book* 112-118.
Upton, B. G. J. and Thomas, J. E. (1980) The Tugtutôq younger giant dyke complex, South Greenland: fractional crystallisation of transitional olivine basalt magma. *Journal of Petrology* **21**, 167-198.
Upton, B. G. J. and Emeleus, C. H. (1987) Mid-Proterozoic alkaline magmatism in southern Greenland: the Gardar province. *In: Fitton, J.G. & Upton, B.G.J. (eds.), Alkaline Igneous Rocks, Geological Society Special Publication* **30**, 449-471.
Upton, B. G. J., Emeleus, C. H., Heaman, L. M., Goodenough, K. M., and Finch, A. (2003) Magmatism of the mid-Proterozoic Gardar Province, South Greenland: chronology, petrogenesis and geological setting. *Lithos* **68**, 43-65.
van Bremen, O., Aftalion, M., and Allart, J. H. (1974) Isotopic and Geochronologic Studies on Granites from the Ketilidian Mobile Belt of South Greenland. *Bulletin of the Geological Society of America* **85**, 403-412.
Vannucci, R., Tribuzio, R., Piccardo, G. B., Ottolini, L., and Bottazzi, P. (1991) SIMS analysis of REE in pyroxenes and amphiboles from the Proterozoic Ikasaulak intrusive complex (SE Greenland): implications for LREE enrichment processes during post-orogenic plutonism. *Chemical Geology* **92**, 115-133.
Veksler, I. V., Petibon, C., Jenner, G. A., Dorfman, A. M., and dingwell, D. B. (1998) Trace element partitioning in immiscible silicate-carbonate liquid systems: an initial experimental study using a centrifuge autoclave. *Journal of Petrology* **39**, 2095-2104.
White, J. C. (2003) Trace-element partitioning between alkali feldspar and peralkalic quartz trachyte to rhyolite magma. Part II: Empirical equations for calculating trace-element partition coefficients of larg-ion lithophile, high field-strangth, and rare-earth elements. *American Mineralogist* **88**, 330-337.
Witt-Eickschen, G. and Harte, B. (1994) Distribution of trace elements between amphibole and clinopyroxene from mantle peridotites of the Eifel (western Germany): An ion-microprobe study. *Chemical Geology* **117**, 235-250.

Wood, B. J. and Blundy, J. D. (1997) A predictive model for rare earth element partioning between clinopyroxene and anhydrous silicate melt. *Contributions to Mineralogy and Petrology* **129**, 166-181.
Wood, B. J. and Blundy, J. D. (2001) The effect of cation charge on crystal-melt partitioning of trace elements. *Earth and Planetary Science Letters* **188**, 59-71.
Wood, B. J. and Trigila, R. (2001) Experimental determination of aluminous clinopyroxene-melt partition coefficients for potasic liquids, with applicatio to the evolution of the Roma province potassic magmas. *Chemical Geology* **172**, 213-223.
Wörner, G., Beusen, J.-M., Duchateau, N., Gijbels, R., and Schmincke, H.-U. (1983) Trace element abundances and mineral/melz distribution coefficients in phonolites from the Laacher See Volcano (Germany) *Contributions to Mineralogy and Petrology* **84**, 152-173.

Figure captions

Fig. 1: Sketch map of the alkaline igneous Gardar Province, South Greenland, with the three igneous complexes Puklen, Ilímaussaq and Grønnedal-Ika (modified after Escher and Watt, 1976).

Fig. 2: Major element compositional trends for clinopyroxenes of the three complexes studied, after data from Larsen (1976), Marks & Markl (2001), Markl et al. (2001b), Marks et al. (2003) and Halama et al. (in preperation).

Fig. 3: Major element compositional trends for amphiboles of the three complexes studied, after data from Larsen (1976), Marks & Markl (2001), Markl et al. (2001b), Marks et al. (2003) and Halama et al. (in preperation).

Fig. 4: Averaged primitive mantle-normalized REE and TE patterns for augites of (a) Puklen and (b) Ilímaussaq. Normalizing values are after McDonough & Sun (1995).

Fig. 5: Zoning profiles for selected elements and X_{Fe} from core to rim of augite from (a) Puklen and (b) Ilímaussaq.

Fig. 6: (a) Averaged mantle-normalized REE and TE patterns for aegirine-augites of Grønnedal. (b) Mantle-normalized REE patterns and TE patterns of core and rim compositions for an indivdual aegirine-augite of sample GM1496.

Fig. 7: Averaged mantle-normalized REE and TE patterns for aegirines of (a) Puklen and (b) Ilímaussaq.

Fig. 8: Averaged mantle-normalized REE and TE patterns for (a) ferro-edenites and ferro-richterites and (b) ferro-actinolites of Puklen.

Fig. 9: Averaged mantle-normalized REE and TE patterns for (a) ferro-pargasites of Ilímaussaq and (b) katophorites of Grønnedal.

Fig. 10: Zoning profile for selected elements, X_{Fe} and Na/Ca ratio from core to rim of ferro-richterite from Puklen.

Fig. 11: Averaged mantle-normalized REE and TE patterns for arfvedsonites of (a) Puklen and (b) Ilímaussaq.

Fig. 12: Zoning profile for selected elements from core to rim of arfvedsonite from Ilímaussaq.

Fig. 13: ε_{Nd} versus Pb/Pb* diagram for mineral separates of the Puklen rocks. ε_{Nd} data from Marks et al. (in press). See text for definition of Pb/Pb*.

Fig. 14: Clinopyroxene/amphibole partition coefficients for (a) Ilímaussaq augite syenites, (b) Puklen syenites, (c) Grønnedal syenites and (d) Ilímaussaq agpaites. For comparison, clinopyroxene/amphibole partition coefficients from a harzburgite (Grégoire et al., 2000) are shown in (c).

Table 1: Summary of samples and minerals analysed

Rock type	Sample	Analysed mafic minerals
Ilímaussaq:		
augite syenite	GM1331	augite, calcic amphibole
augite syenite	GM1333	augite, calcic amphibole
alkali granite	GM1303	aegirine, sodic amphibole
agpaite	GM1294	aegirine
agpaite	GM1305	aegirine
agpaite	GM1334	aegirine, sodic amphibole
agpaite	GM1336	aegirine
agpaite	GM1337	aegirine, sodic amphibole
agpaite	GM1344	aegirine
agpaite	GM1347	aegirine, sodic amphibole
agpaite	GM1370	aegirine, sodic amphibole
agpaite	GM1371	aegirine
agpaite	GM1396	sodic amphibole
late-stage vein	GM1401	sodic amphibole
pegmatite	GM1657	sodic amphibole
Puklen:		
syenite	GM1586	augite, calcic amphibole I
syenite	GM1589	calcic amphibole I, calcic amphibole II
syenite	GM1590	augite, calcic amphibole I
syenite	GM1600	augite, calcic amphibole I, calcic amphibole II
syenite	GM1603	augite, calcic amphibole I, calcic amphibole II
syenite	GM1615	augite, sodic-calcic amphibole
syenite	GM1616	augite, sodic-calcic amphibole
syenite	GM1635	augite
granophyre	GM1593	calcic amphibole I, calcic amphibole II
alkali granite	GM1587	aegirine, sodic amphibole
alkali granite	GM1605	aegirine, sodic amphibole
alkali granite	GM1608	aegirine
microgranite	GM1620	aegirine, sodic amphibole
microgranite	GM1627	aegirine, sodic amphibole
Grønnedal-Ika:		
nepheline syenite	GR01	aegirine-augite
nepheline syenite	GR13	aegirine-augite
nepheline syenite	GR15	aegirine-augite
nepheline syenite	GR44	aegirine-augite
nepheline syenite	GR63	aegirine-augite
nepheline syenite	GM1496	aegirine-augite
nepheline syenite	GM1526	aegirine-augite, sodic-calcic amphibole
nepheline syenite	GM1531	sodic-calcic amphibole

Table 2: Mean trace element contents of clinopyroxenes from Ilímaussaq, Puklen and Grønnedal-Ika

Complex	Ilímaussaq	Puklen	Puklen	Grønnedal-Ika	Grønnedal-Ika	Grønnedal-Ika	Grønnedal-Ika	Ilímaussaq	Ilímaussaq	Ilímaussaq	Puklen	Puklen
Rock type	augite syenite	syenite	syenite	nepheline syenite	nepheline syenite	nepheline syenite	nepheline syenite	alkali granite	agpaite	agpaite	alkali granite	microgranite
Sample No.	GM1331	GM 1586	GM1600	GR44	GM1526	GM1496	GM1496	GM1303	GM1294	GM1334	GM1587	GM1620
Clinopyroxene type	augite	augite	augite	aegirine-augite	aegirine-augite	aegirine-augite core	aegirine-augite rim	aegirine	aegirine	aegirine	aegirine	aegirine
No. of analyses	6	14	8	10	10	3	2	8	4	7	8	11
Cs	0.15	0.63	0.95	—	0.25	—	—	0.31	0.20	0.18	13.1	0.01
Rb	0.85	3.31	6.41	2.49	2.11	3.06	1.18	0.77	0.68	1.04	107	6.60
Ba	1.14	2.14	21.6	0.85	1.89	1.53	—	3.26	0.49	0.37	175	2.52
Th	0.98	0.26	4.90	0.29	0.19	—	0.10	1.19	0.49	0.14	15.8	0.35
U	0.44	0.36	1.62	0.08	0.08	0.04	—	0.46	0.14	0.05	14.5	0.23
Nb	1.01	0.79	8.23	2.96	9.02	2.40	3.69	27.0	74.9	4.67	371	48.0
Ta	n.a.	0.14	1.68	0.48	0.91	0.23	0.87	1.43	n.a.	n.a.	22.7	1.69
La	28.91	32.44	13.4	43.4	11.2	8.17	9.73	2.41	4.06	5.01	370	39.5
Ce	104.4	98.11	313	140	42.8	32.5	38.9	7.17	11.4	13.8	622	115
Pb	0.74	1.71	35.6	0.49	0.46	0.21	0.27	25.0	28.8	0.82	1172	2.20
Pr	16.45	17.54	45.6	22.9	8.19	5.90	7.60	1.17	1.82	1.97	76.6	18.2
Sr	27.65	5.80	43.2	205	56.9	589	352	2.01	2.44	4.62	38.0	6.50
Nd	75.81	92.74	219	106	41.2	33.5	41.6	5.72	7.89	8.38	368	86.5
Zr	243.1	199.1	90.3	1127	5721	127	6218	1338	982	1406	2303	234
Hf	7.26	6.74	3.98	29.4	145	3.01	116.1	54.2	18.7	29.0	51.1	7.52
Sm	19.42	23.32	53.0	23.1	10.4	9.13	12.5	3.43	1.83	1.48	76.1	19.5
Eu	2.35	1.72	1.93	4.80	2.03	3.48	3.28	0.20	0.20	0.15	3.99	0.99
Ti*	5348	3676	1280	1199	959	2098	1918	1325	3483	3473	5567	2400
Sn	1.43	1.95	4.64	8.11	54.7	1.32	45.3	97.3	265	169	125	2.06
Gd	14.97	19.69	44.8	15.6	6.81	7.09	7.29	4.08	1.59	0.99	77.0	15.0
Tb	2.62	3.15	7.63	2.12	1.26	0.94	1.14	1.14	0.30	0.15	11.7	2.48
Dy	15.16	17.67	45.9	11.5	6.91	4.65	7.19	9.11	1.61	0.92	60.3	15.2
Li	32.0	195.0	278	8.47	5.31	8.76	2.49	71.0	25.0	29.0	148	176
Y	68.90	84.57	228	42.9	23.4	13.8	24.3	35.5	7.62	4.38	429	78.0
Ho	3.03	3.70	9.11	1.97	1.37	0.61	1.44	2.47	0.27	0.21	13.4	3.18
Er	7.87	9.52	23.9	5.62	4.76	1.32	4.49	10.4	0.79	0.77	39.0	10.8
Tm	1.17	1.64	3.40	1.03	1.15	0.16	0.84	2.02	0.20	0.24	6.03	1.88
Yb	8.87	14.84	23.4	9.16	13.5	0.80	8.96	11.5	2.13	3.08	45.4	18.0
Lu	1.40	2.83	3.69	1.88	2.78	0.15	2.06	1.77	0.51	0.79	6.53	3.45
Sc	210.3	121.2	118	12.8	13.2	8.50	2.45	2.44	3.44	10.6	7.38	53.0
V	3.99	1.38	196	12.1	4.21	148	8.99	0.76	0.20	5.73	8.41	3.50
Co	n.a.	10.60	111	12.3	6.59	22.8	7.85	n.a.	n.a.	n.a.	7.90	5.31
Zn	199.9	276.4	487	247	306	89.2	322	376	61.6	130	1033	385
Ga	10.63	6.40	7.56	10.5	12.8	12.1	19.3	5.66	72.2	40.6	13.7	4.60

n.a. = not analysed; — = not detected; * = analysed by electron microprobe

Table 3: Mean trace element contents of amphiboles from Ilímaussaq, Puklen and Grønnedal-Ika

Complex	Ilímaussaq	Puklen	Puklen	Puklen	Puklen	Grønnedal-Ika	Ilímaussaq	Ilímaussaq	Puklen	Puklen
Rock type	augite syenite	granophyre	syenite	granophyre	syenite	nepheline syenite	alkali granite	agpaite	alkali granite	microgranite
Sample No.	GM1331	GM1593	GM1600	GM1593	GM1615	GM1526	GM1303	GM1334	GM1587	GM1620
Amphibole type	calcic ferro-pargasite	calcic I ferro-edenite	calcic I ferro-edenite	calcic II ferro-actinolite	sodic-calcic ferro-richterite	sodic-calcic katophorite	sodic arfvedsonite	sodic arfvedsonite	sodic arfvedsonite	sodic arfvedsonite
No. of ananlyses	6	8	9	4	7	1	14	7	7	5
Cs	0.02	1.43	1.01	—	0.39	—	—	0.20	14.8	0.69
Rb	19.4	105	12.3	—	28.9	18.7	53.4	41.3	192	13.2
Ba	303	161	13.5	2.90	2.85	3.37	1.20	3.18	79.5	2.17
Th	23.3	4.31	2.40	3.05	0.35	—	1.48	0.20	154	1.65
U	6.61	1.00	0.24	0.32	0.14	—	1.33	0.13	9.84	0.93
Nb	365	303	86.5	10.4	137	517	94.6	132.8	355	36.4
Ta	n.a.	7.57	1.93	0.88	2.11	20.4	1.22	n.a.	11.0	1.06
La	253	72.4	109	32.5	42.0	53.9	12.4	17.9	3986	104
Ce	557	264	407	57.9	103	145	44.2	44.1	7791	300
Pb	5.89	28.5	20.0	9.39	7.41	0.95	15.0	2.55	1260	24.0
Pr	168	37.1	57.8	7.47	15.0	20.1	4.74	5.67	1169	41.1
Sr	96.6	30.4	25.1	10.7	15.3	93.7	5.99	18.9	726	37.4
Nd	692	155	245	28.7	66.7	84.1	17.3	21.3	4993	186
Zr	1640	50.9	976	52.6	1087	1766	853	1472	1697	576
Hf	49.9	2.92	8.18	4.91	25.4	50.4	27.2	34.2	39.3	15.5
Sm	134	39.6	61.6	6.11	12.6	15.4	2.98	3.00	771	62.2
Eu	9.65	0.70	1.68	0.37	0.88	2.56	0.23	1.00	36.0	3.00
Ti*	18788	4000	7940	900	8871	6712	7428	5122	10514	4800
Sn	4.50	96.2	14.6	41.8	9.56	19.1	38.1	39.1	58.9	20.8
Gd	95.4	30.7	46.3	5.67	9.03	7.79	1.83	1.50	612	43.5
Tb	14.0	6.45	8.38	1.11	1.72	1.16	0.41	0.51	86.6	6.50
Dy	76.1	42.8	50.3	7.21	14.2	5.47	3.72	1.90	505	41.6
Li	29.0	722	167	240	1466	31.3	756	390	2895	288
Y	345	250	269	48.5	130	18.4	21.6	12.1	2494	177
Ho	14.7	9.28	10.0	1.64	4.87	0.92	1.49	0.73	122	9.51
Er	36.7	25.7	26.2	5.95	24.6	2.70	8.77	2.49	298	23.6
Tm	4.89	4.12	3.83	1.63	6.67	0.53	2.78	0.78	33.7	4.11
Yb	32.4	31.1	29.9	22.7	65.3	5.17	35.3	8.04	191	38.6
Lu	4.38	4.36	4.39	5.81	13.1	1.04	7.88	1.58	26.1	7.77
Sc	156	83.6	54.6	40.4	48.4	6.44	8.43	11.7	20.8	42.0
V	1.64	29.0	147	5.77	4.75	1.41	0.89	7.32	32.6	4.20
Co	n.a.	43.6	29.8	n.a.	17.6	19.8	3.23	n.a.	13.0	8.80
Zn	381	1381	1109	1927	1476	592	3287	956	4667	931
Ga	56.0	45.5	23.5	5.32	13.2	32.3	6.16	36.0	16.2	6.40

n.a. = not analysed; — = not detected; * = analysed by electron microprobe

Table 4: Clinopyroxene-amphibole partition coefficients for alkaline igneous rocks

Complex	Ilímaussaq	Ilímaussaq	Ilímaussaq	Ilímaussaq	Puklen	Puklen	Gronnedal-Ika
Rock type	augite syenite	augite syenite	agpaite	agpaite	quartz syenite	quartz syenite	nepheline syenite
Mineral pair	augite - ferro-pargasite	augite - ferro-pargasite	aegirine - arfvedsonite	aegirine - arfvedsonite	augite - ferro-edenite	augite - ferro-edenite	aegirine-augite - katophorite
Sample	GM 1331	GM 1333	GM 1334	GM 1337	GM 1600	GM 1603	GM 1526
Cs	7.50	1.57	0.90	0.25	0.94		
Rb	0.04	0.05	0.03	0.03	0.52	1.08	0.11
Ba	0.004	0.004	0.12	0.04	1.60	3.92	0.56
Th	0.04	0.36	0.70	0.01	2.04	22.10	
U	0.07	0.58	0.38	0.07	6.84	16.92	
Nb	0.003	0.003	0.04	0.01	0.10	0.03	0.02
Ta					0.87	0.04	0.04
La	0.11	0.11	0.28	0.07	1.23	1.55	0.21
Ce	0.19	0.15	0.31	0.12	0.77	1.52	0.29
Pb	0.13	0.30	0.32	0.22	1.78	2.28	0.48
Pr	0.10	0.20	0.35	0.15	0.79	1.59	0.41
Sr	0.29	0.60	0.24	0.11	1.72	0.34	0.61
Nd	0.11	0.26	0.39	0.15	0.90	1.76	0.49
Zr	0.15	0.17	0.96	0.52	0.93	0.76	3.24
Hf	0.15	0.19	0.85	0.80	0.49	0.57	2.88
Sm	0.15	0.33	0.49	0.18	0.86	1.52	0.67
Eu	0.24	0.35	0.15	0.11	1.15	1.48	0.79
Ti	0.28	0.45	0.68	0.66	0.16	0.28	0.14
Sn	0.32	0.05	4.32	1.92	0.32	0.23	2.87
Gd	0.16	0.37	0.66	0.18	0.97	1.52	0.87
Tb	0.19	0.34	0.29	0.15	0.91	1.36	1.09
Dy	0.20	0.35	0.48	0.19	0.91	1.39	1.26
Li	1.10	0.25	0.07	0.06	1.66	0.82	0.17
Y	0.20	0.33	0.36	0.18	0.85	1.46	1.28
Ho	0.21	0.35	0.29	0.12	0.91	1.59	1.49
Er	0.21	0.37	0.31	0.17	0.91	1.52	1.76
Tm	0.24	0.41	0.31	0.20	0.89	1.52	2.19
Yb	0.27	0.46	0.38	0.26	0.78	1.52	2.62
Lu	0.32	0.61	0.50	0.33	0.84	1.66	2.69
Sc	1.35	14.13	0.90	0.50	2.17	2.53	2.05
V	2.43	6.17	0.78	0.48	1.33	0.20	2.99
Co					3.72	1.67	0.33
Zn	0.53	0.50	0.14	0.06	0.44	0.59	0.52

Fig. 1

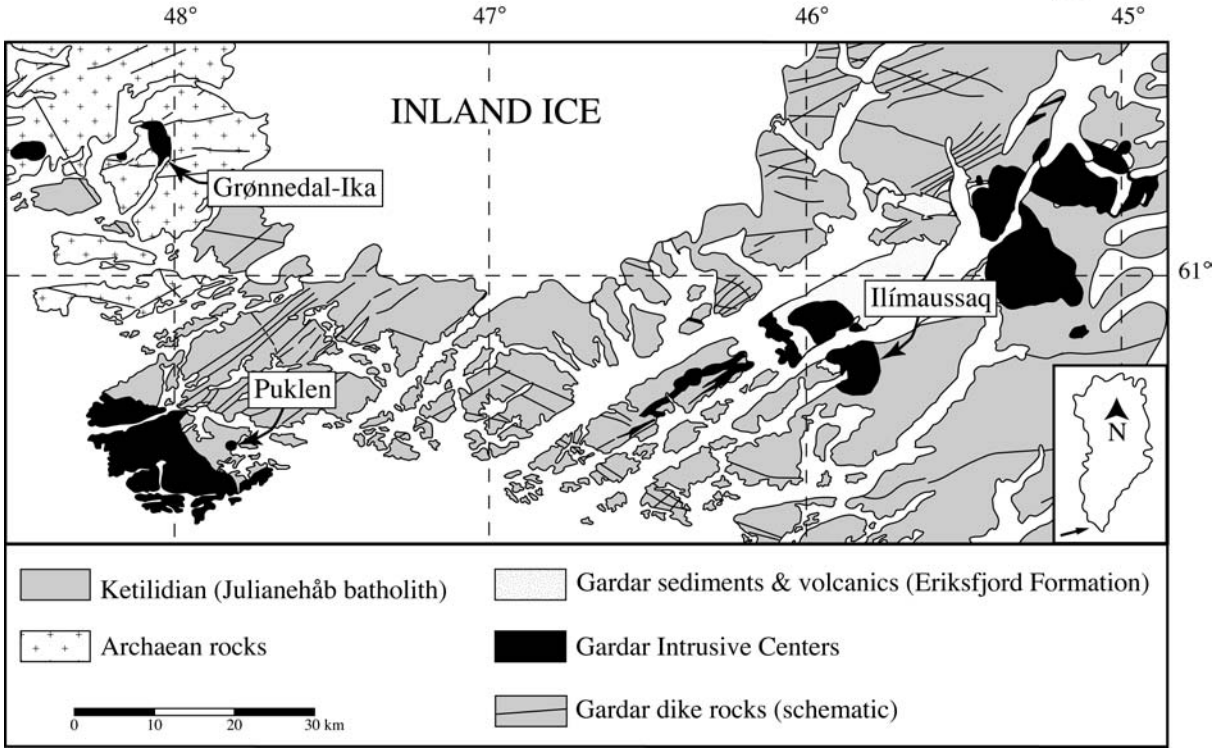
48°
47°
46°
45°
61°
INLAND ICE
Grønnedal-Ika
Puklen
Ilímaussaq
N
Ketilidian (Julianehåb batholith)
Archaean rocks
0
10
20
30 km
Gardar sediments & volcanics (Eriksfjord Formation)
Gardar Intrusive Centers
Gardar dike rocks (schematic)

Fig. 2

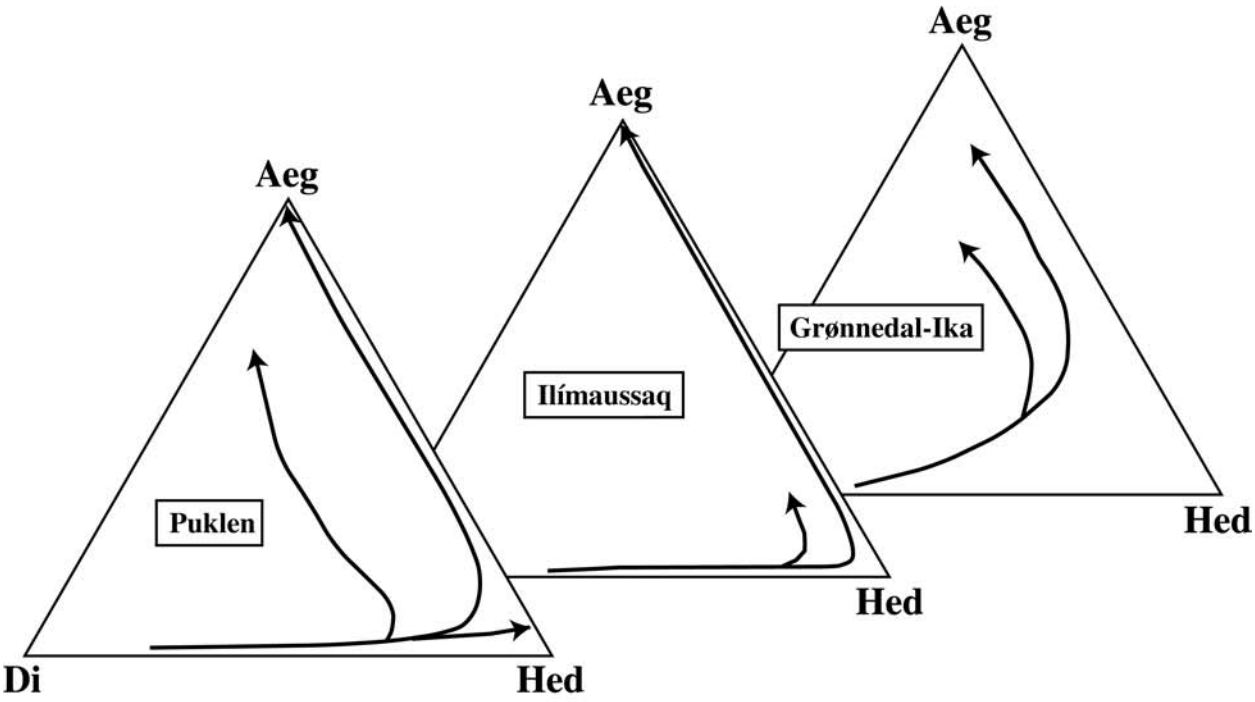
Aeg
Aeg
Aeg
Puklen
Ilímaussaq
Grønnedal-Ika
Di
Hed
Hed
Hed

Fig. 3

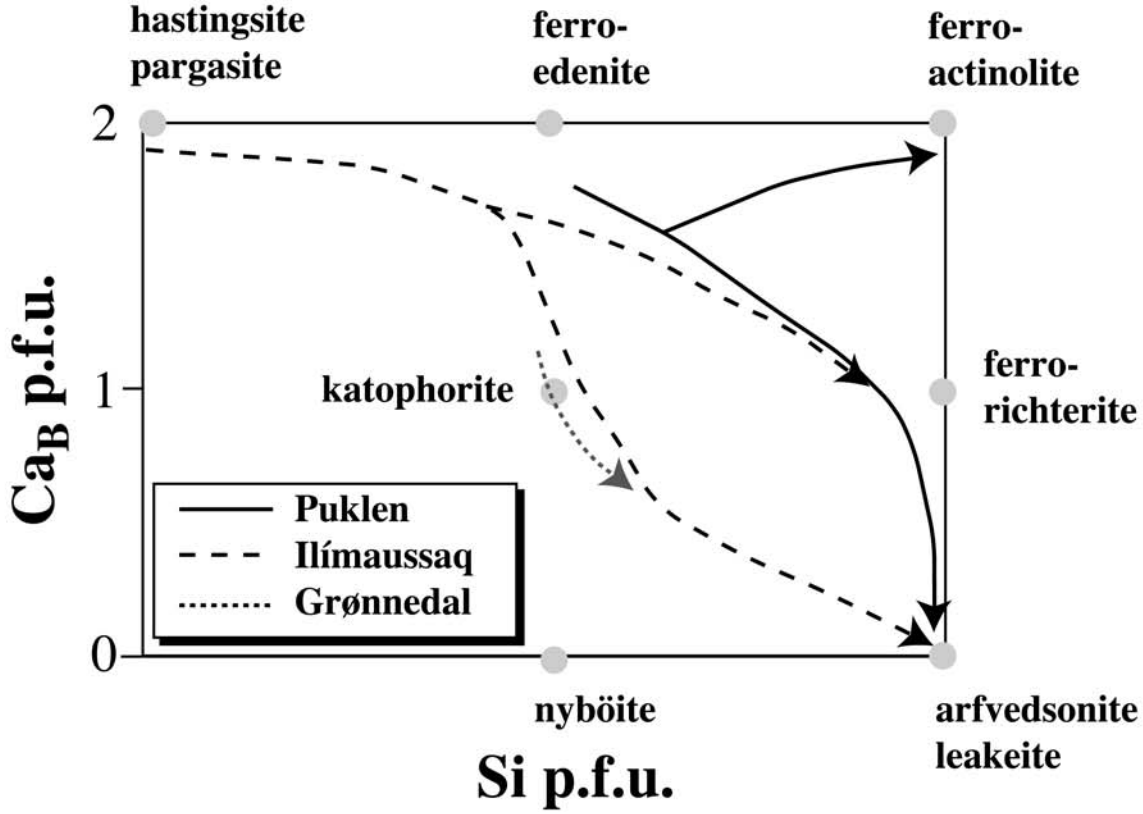
hastingsite
pargasite
ferro-
edenite
ferro-
actinolite
2
1
0
katophorite
ferro-
richterite
Puklen
Ilímaussaq
Grønnedal
nyböite
arfvedsonite
leakeite
Ca_B p.f.u.
Si p.f.u.

(a) Puklen augites

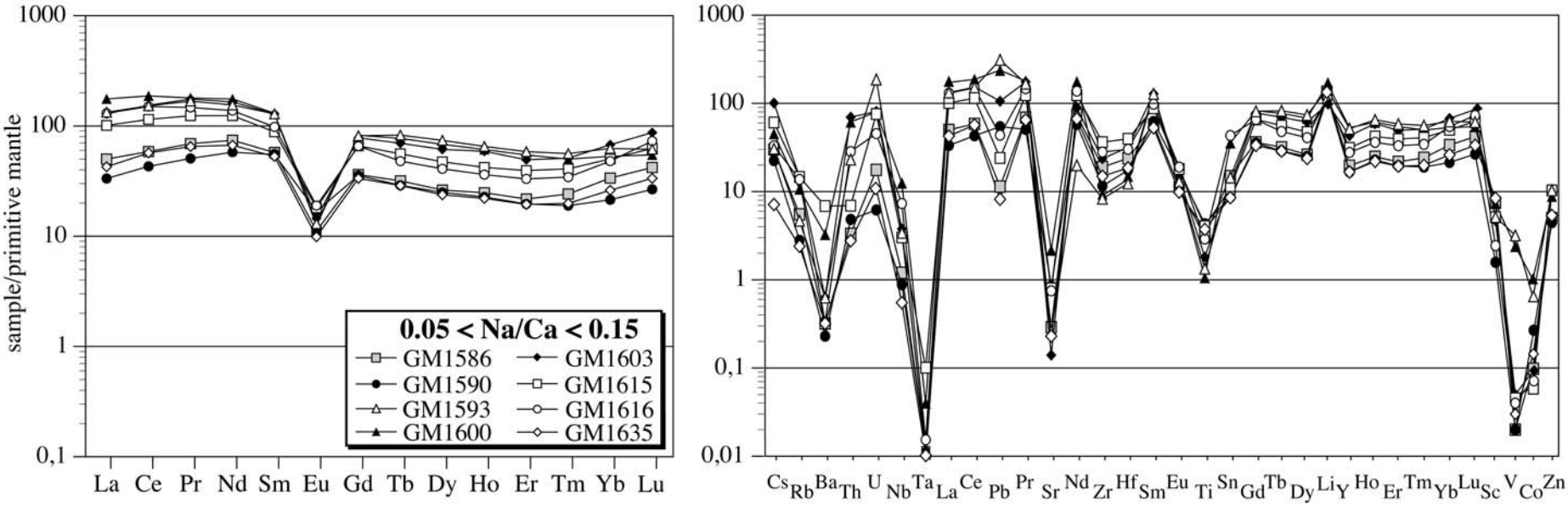

(b) Ilímaussaq augites

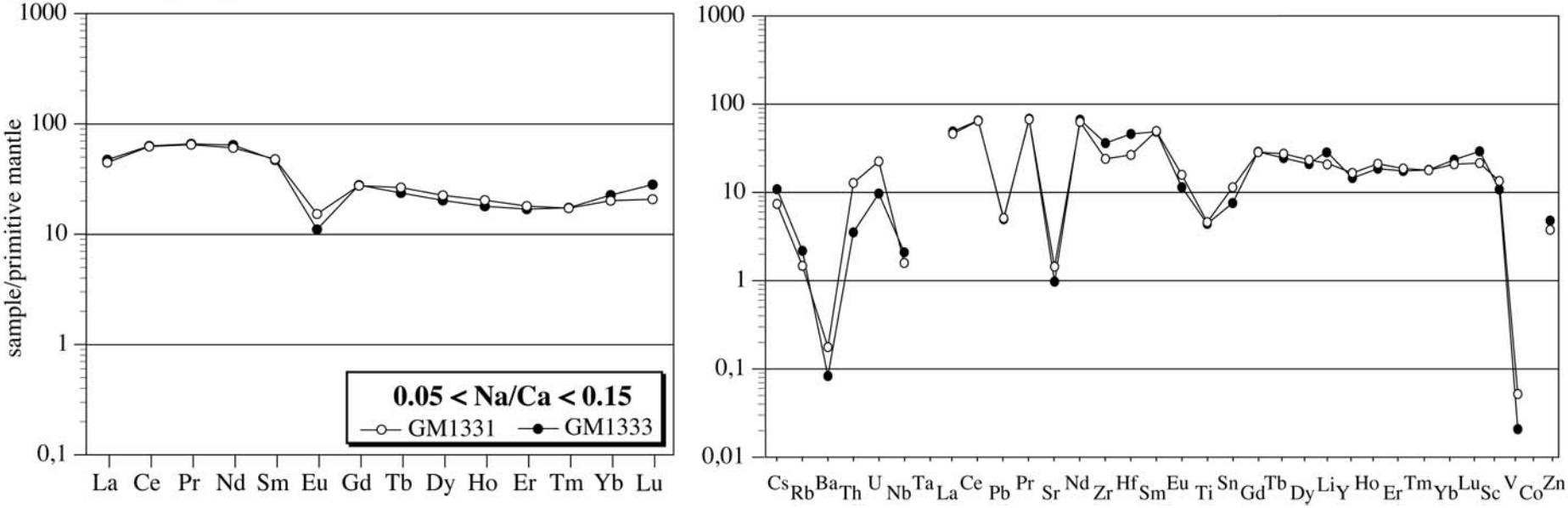

Fig. 4

Fig. 5

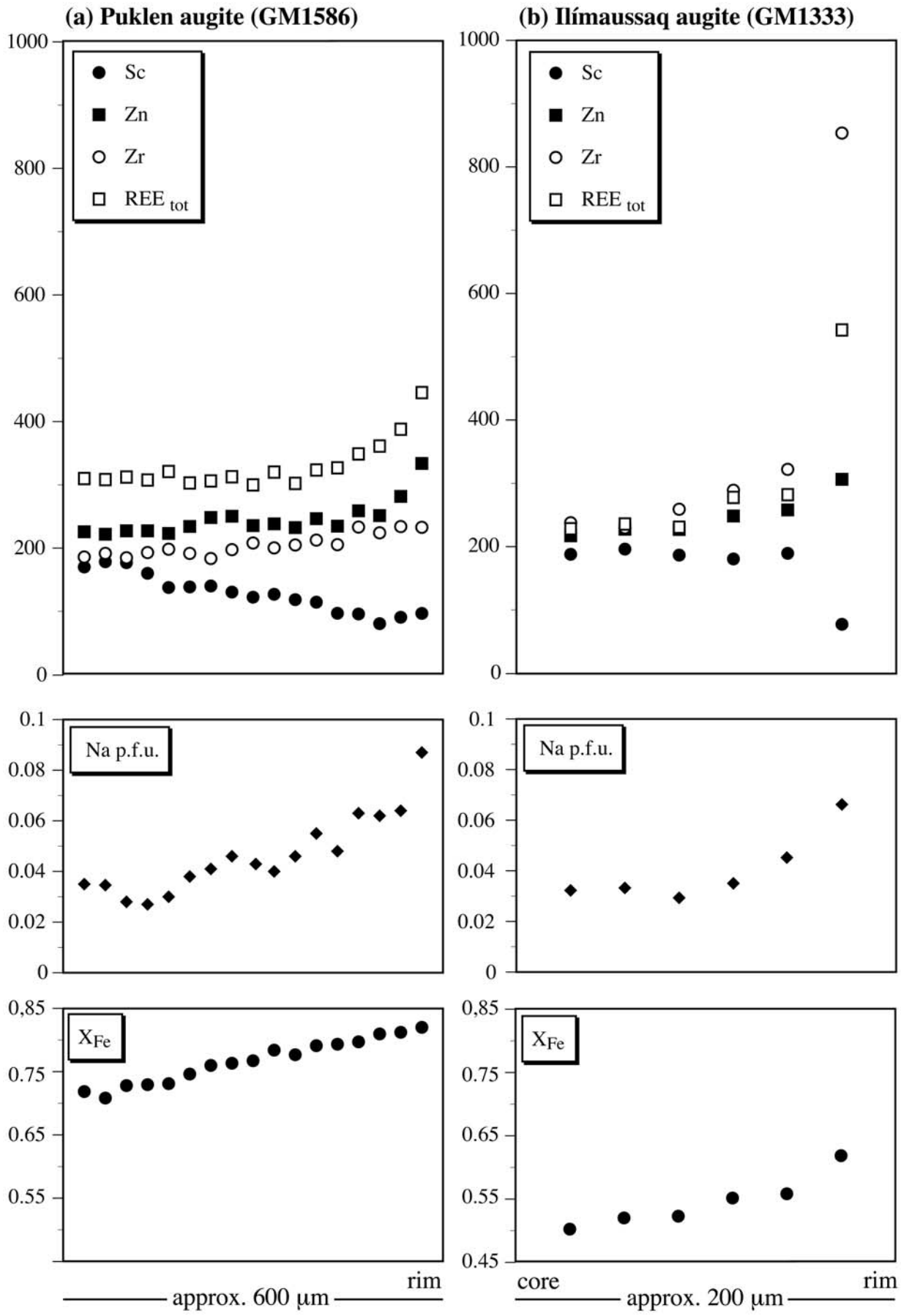
(a) Puklen augite (GM1586)
(b) Ilímaussaq augite (GM1333)
Sc
Zn
Zr
REE tot
Na p.f.u.
X Fe
core
rim
approx. 600 μm
approx. 200 μm

(a) Grønnedal-Ika aegirine-augites

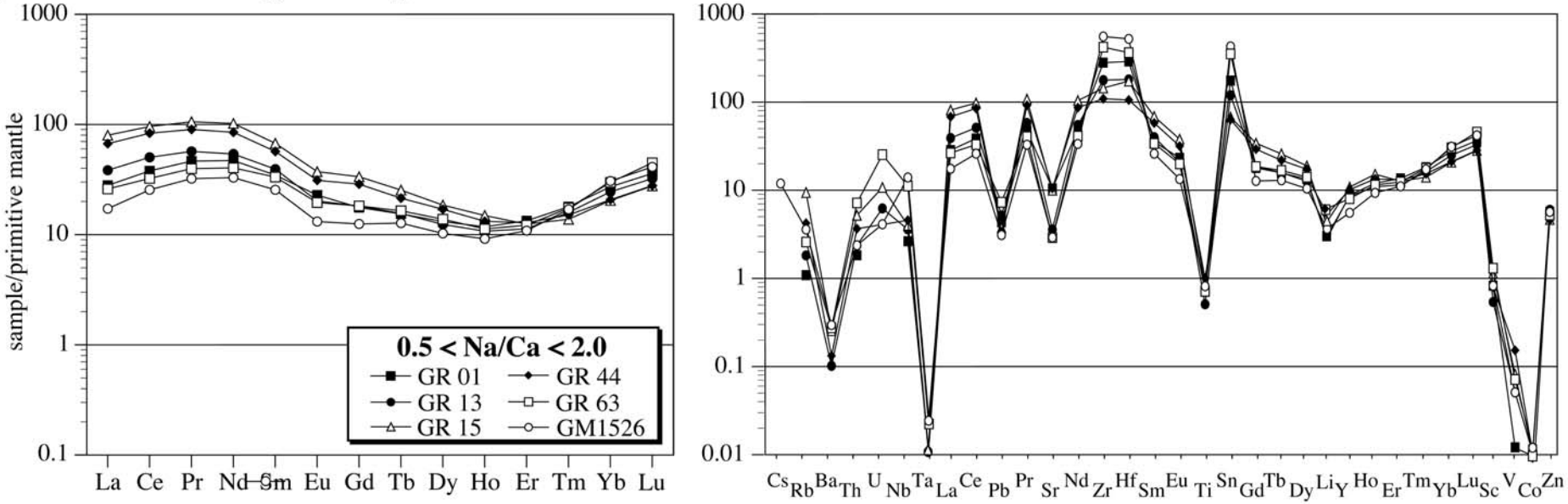

(b) Grønnedal-Ika aegirine-augites sample GM1496

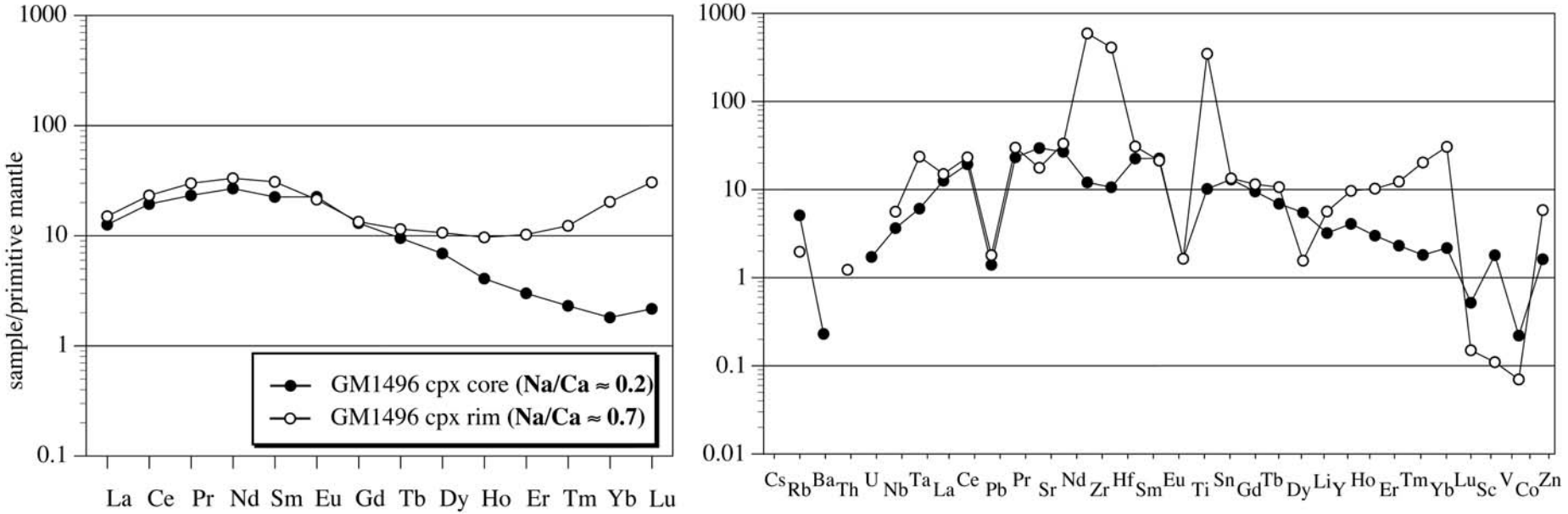

Fig. 6

(a) Puklen aegirines

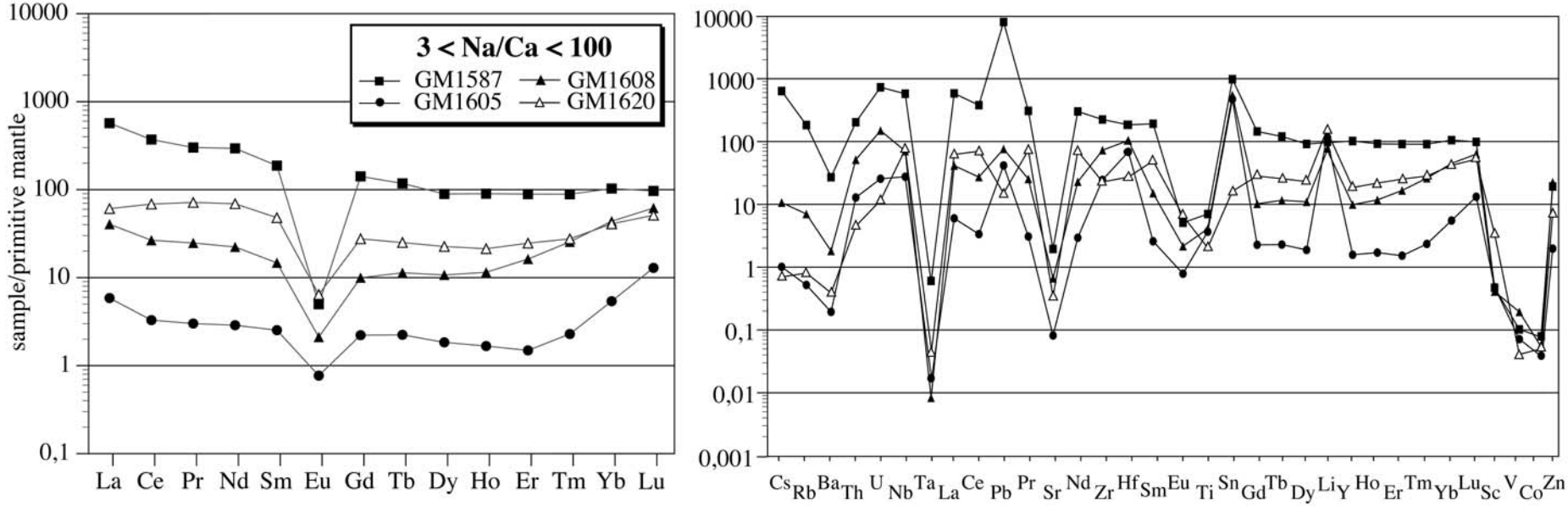

(b) Ilímaussaq aegirines

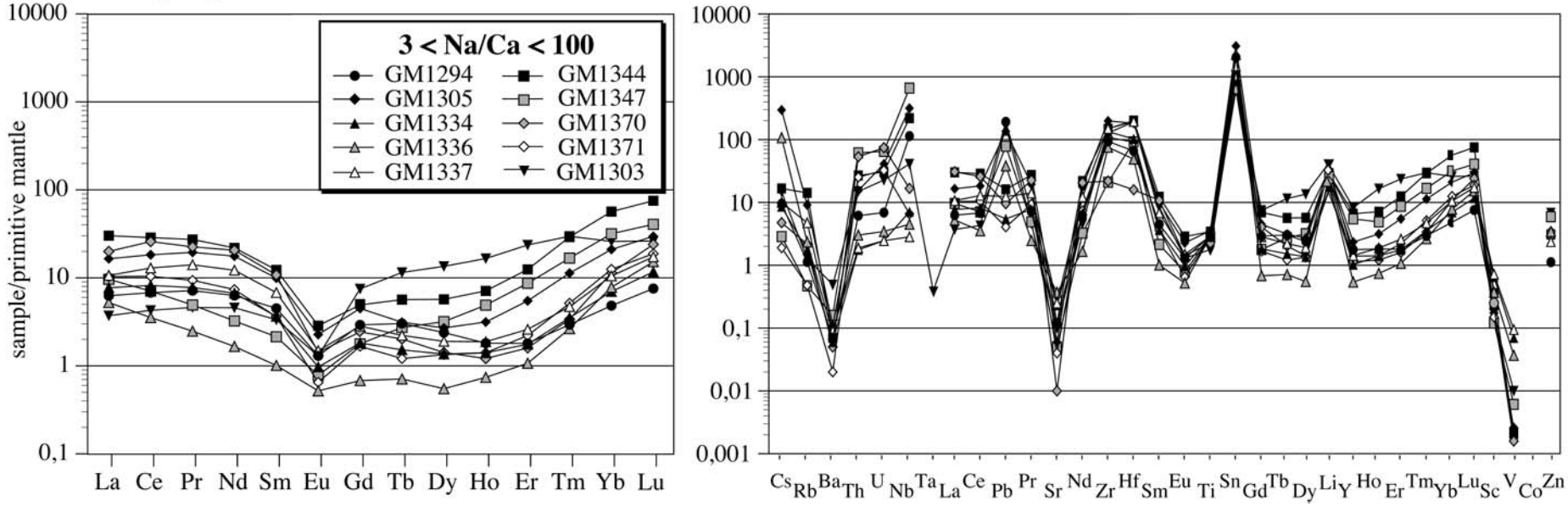

Fig. 7

(a) Puklen primary ferro-edenites and ferro-richterites

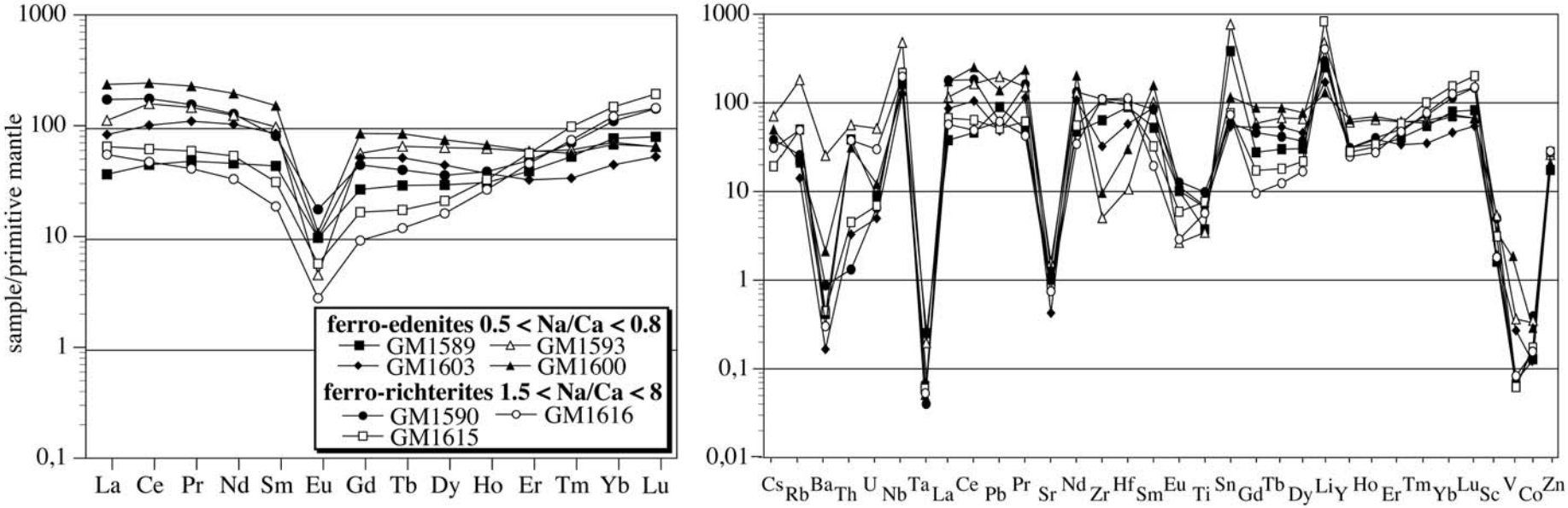

(b) Puklen secondary ferro-actinolites

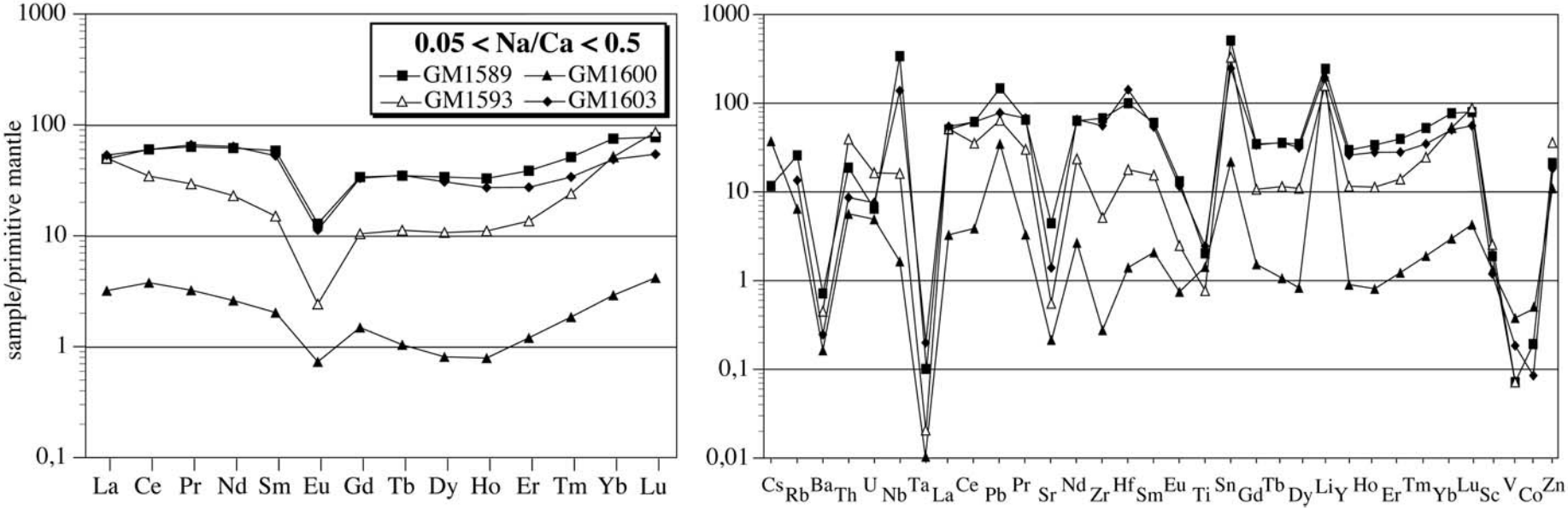

Fig. 8

(a) Ilímaussaq ferro-pargasites

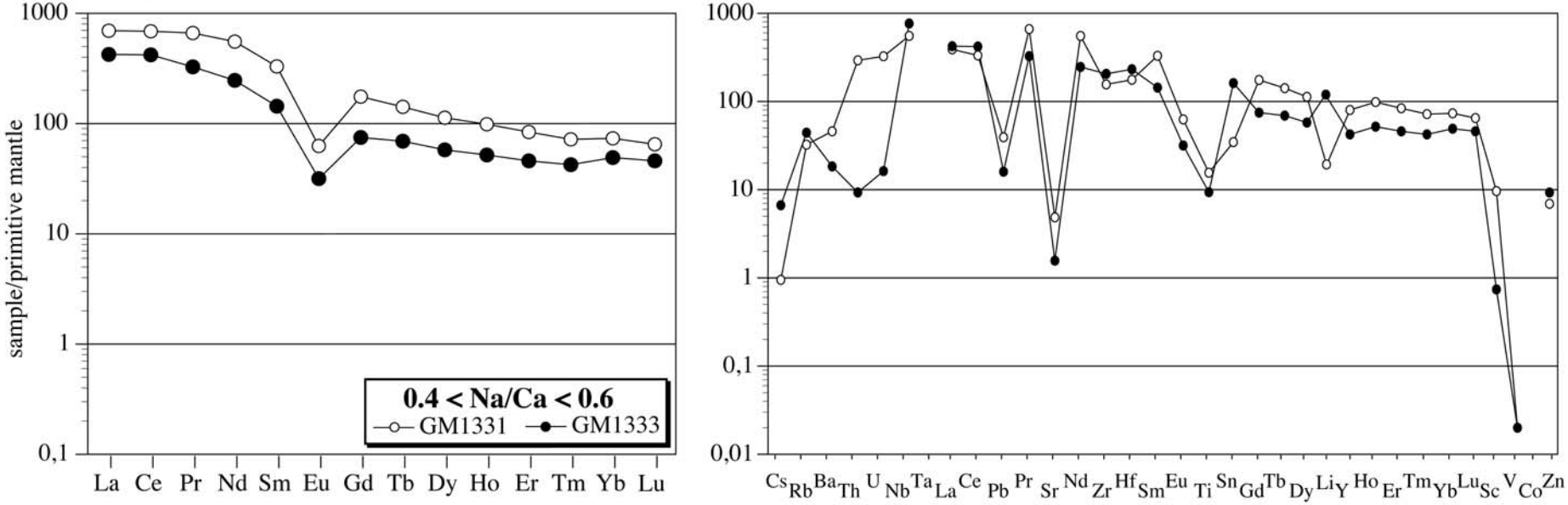

(b) Grønnedal-Ika katophorites

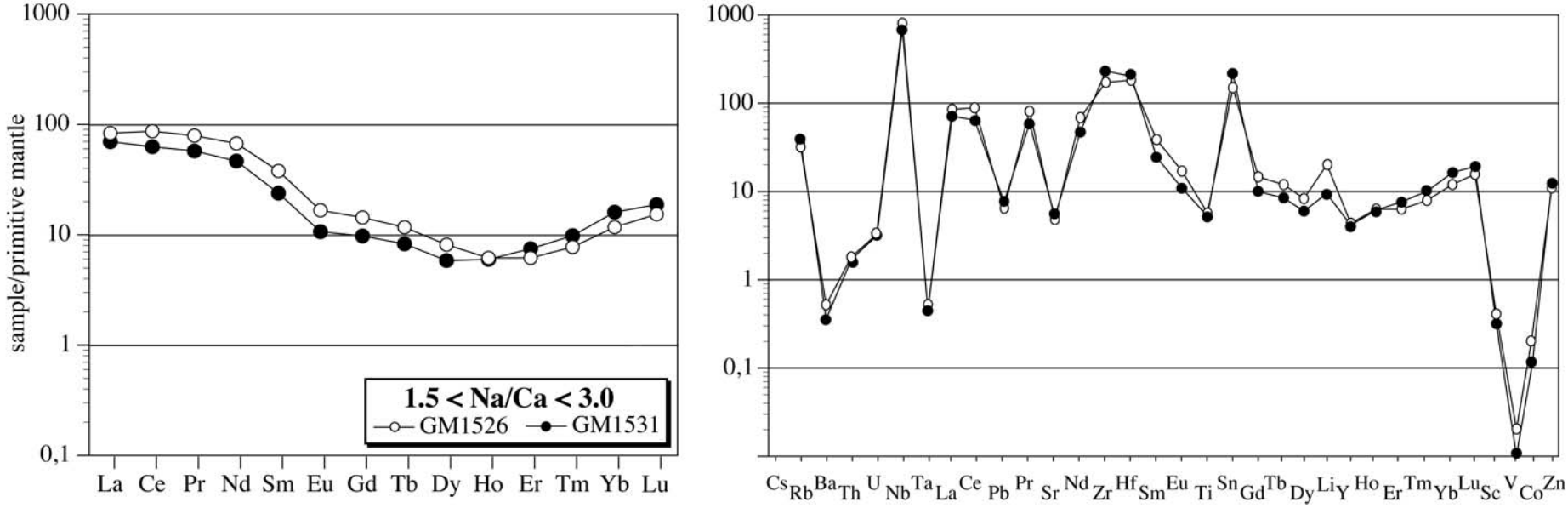

Fig. 9

Fig. 10

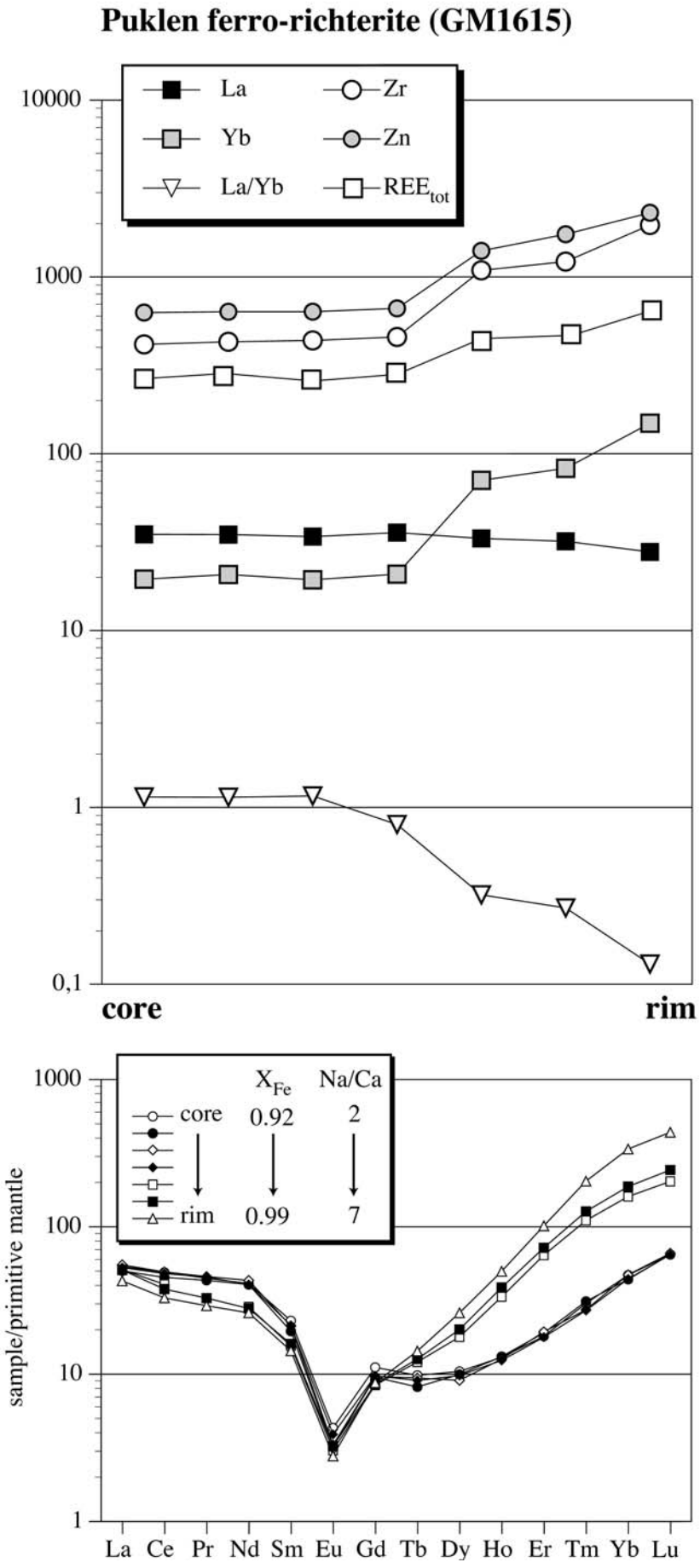
Puklen ferro-richterite (GM1615)
La
Zr
Yb
Zn
La/Yb
REE$_{tot}$
10000
1000
100
10
1
0,1
core
rim
X_{Fe}
Na/Ca
core
0.92
2
rim
0.99
7
1000
100
10
1
sample/primitive mantle
La Ce Pr Nd Sm Eu Gd Tb Dy Ho Er Tm Yb Lu

(a) Puklen arfvedsonites

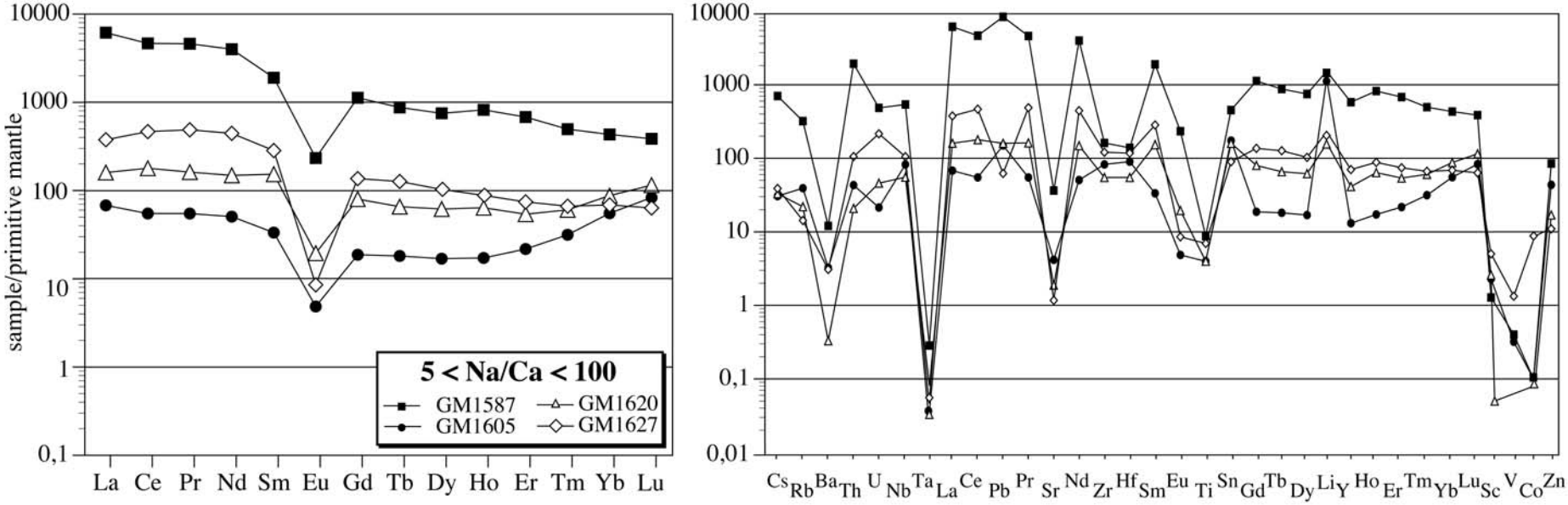

(b) Ilímaussaq arfvedsonites

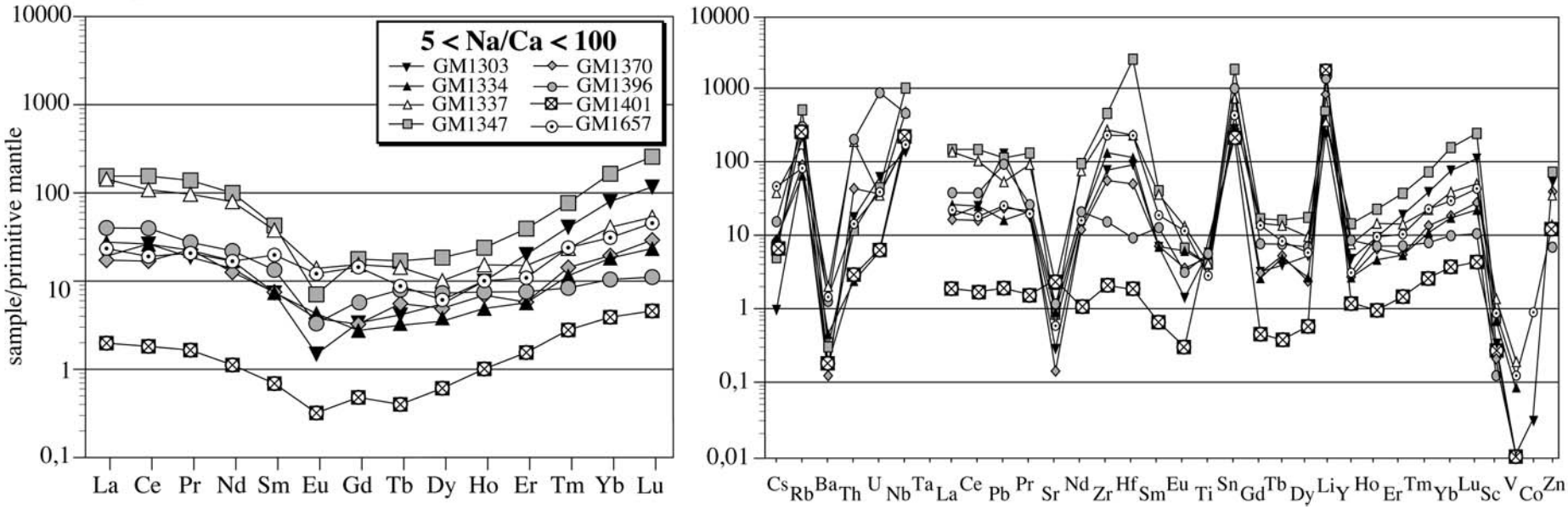

Fig. 11

Ilímaussaq arfvedsonite (GM1303)

Fig. 12

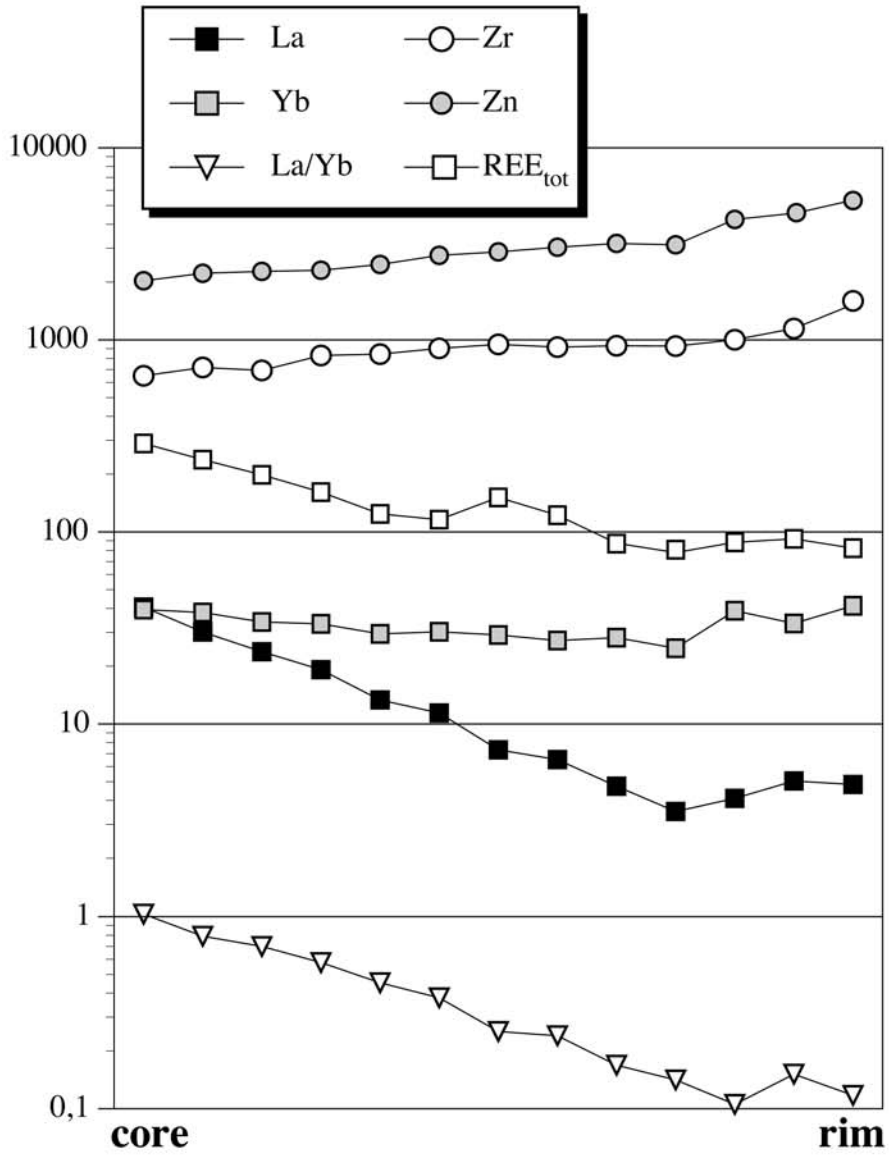

Fig. 13

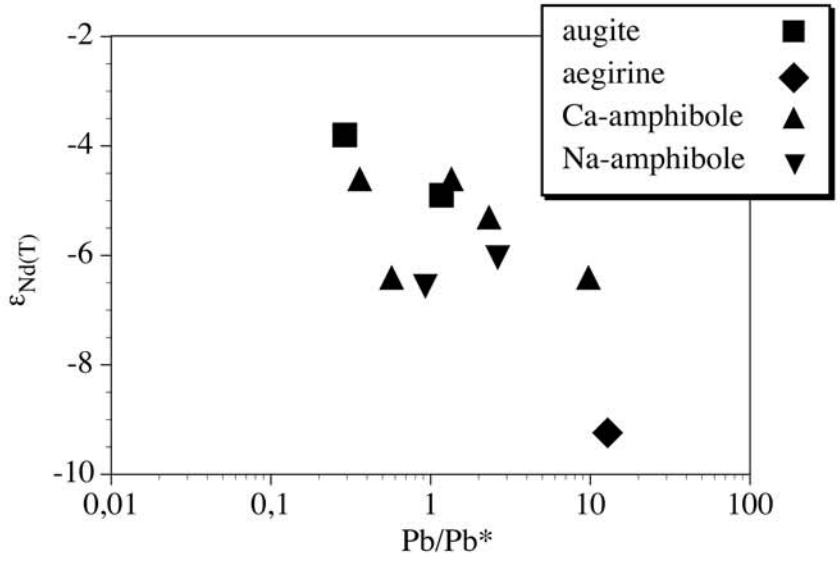

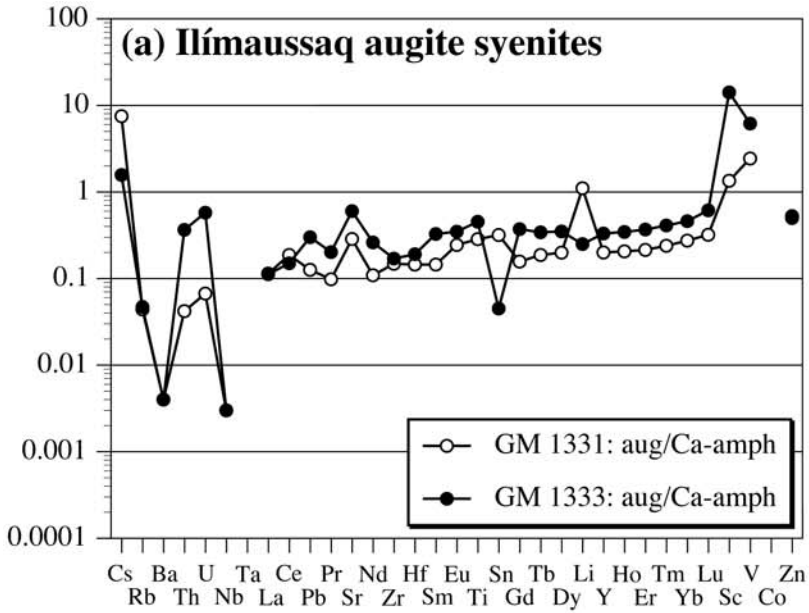
(a) Ilímaussaq augite syenites
100
10
1
0.1
0.01
0.001
0.0001
GM 1331: aug/Ca-amph
GM 1333: aug/Ca-amph
Cs Ba U Ta Ce Pr Nd Hf Eu Sn Tb Li Ho Tm Lu V Zn
Rb Th Nb La Pb Sr Zr Sm Ti Gd Dy Y Er Yb Sc Co

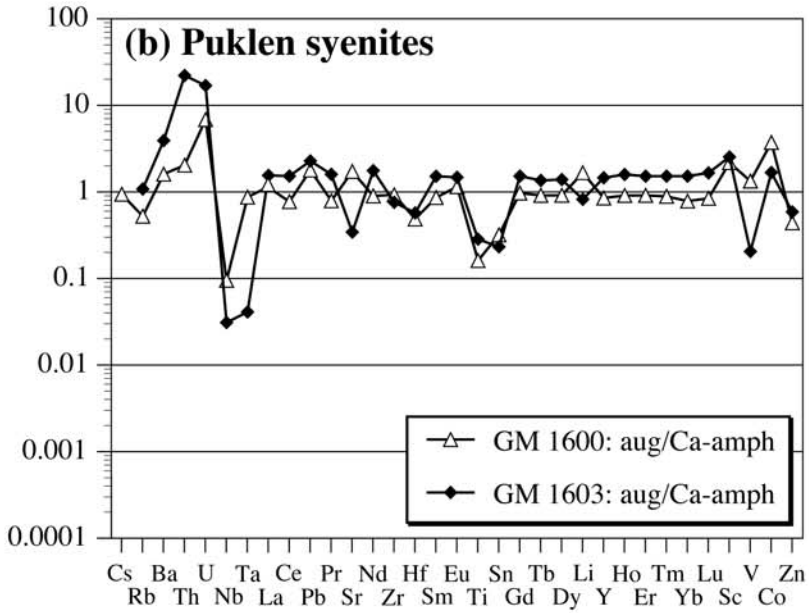
(b) Puklen syenites
100
10
1
0.1
0.01
0.001
0.0001
GM 1600: aug/Ca-amph
GM 1603: aug/Ca-amph
Cs Ba U Ta Ce Pr Nd Hf Eu Sn Tb Li Ho Tm Lu V Zn
Rb Th Nb La Pb Sr Zr Sm Ti Gd Dy Y Er Yb Sc Co

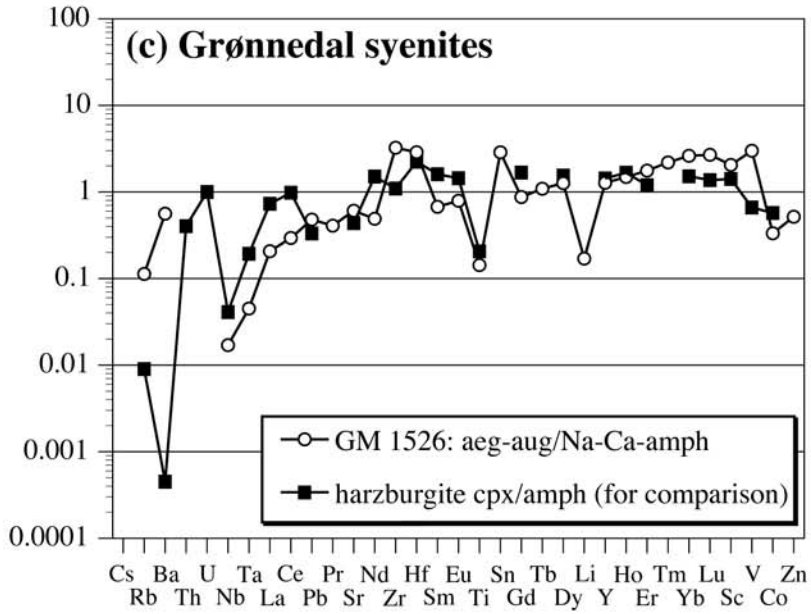
(c) Grønnedal syenites
100
10
1
0.1
0.01
0.001
0.0001
GM 1526: aeg-aug/Na-Ca-amph
harzburgite cpx/amph (for comparison)
Cs Ba U Ta Ce Pr Nd Hf Eu Sn Tb Li Ho Tm Lu V Zn
Rb Th Nb La Pb Sr Zr Sm Ti Gd Dy Y Er Yb Sc Co

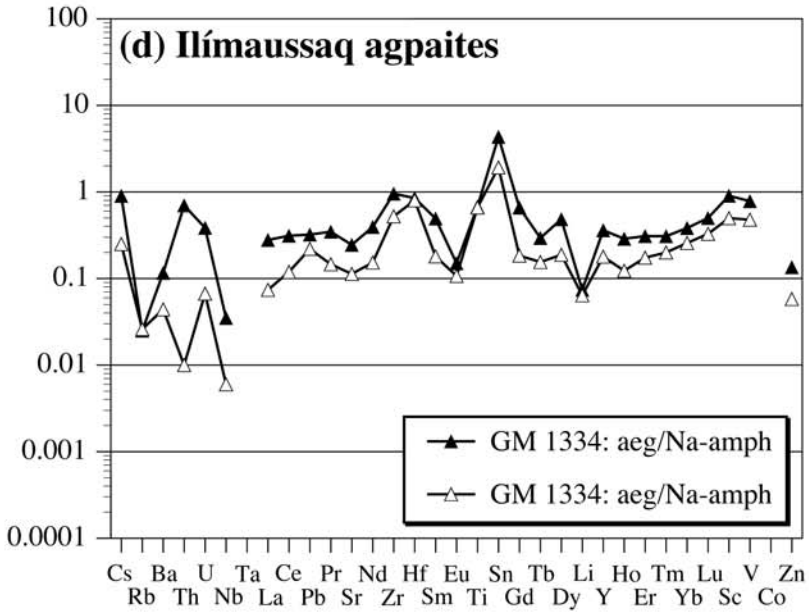
(d) Ilímaussaq agpaites
100
10
1
0.1
0.01
0.001
0.0001
GM 1334: aeg/Na-amph
GM 1334: aeg/Na-amph
Cs Ba U Ta Ce Pr Nd Hf Eu Sn Tb Li Ho Tm Lu V Zn
Rb Th Nb La Pb Sr Zr Sm Ti Gd Dy Y Er Yb Sc Co

Fig. 14

LEBENSLAUF

29.4.1974	Geburt in Lahr/Schwarzwald
1980-1984	Grundschule in Oberschopfheim
1984-1990	Realschule in Friesenheim, 1990 Mittlere Reife
1990-1993	Integriertes Berufliches Gymnasium Lahr, 1993 Abitur
1993-1995	Studium der Chemie an der Universität Freiburg, Vordiplomsprüfung September 1995
1995-1999	Studium der Mineralogie an der Universität Freiburg, Diplom im Dezember 1999 über syenitische Gesteine der Ilimaussaq Intrusion, Süd Grönland.
Seit 2000	Promotionsstudent an der Eberhard Karls Universität Tübingen. Promotion über Petrologie und Geochemie von Alkaligesteinen der Gardar Provinz, Süd Grönland.

EIDESSTATTLICHE VERSICHERUNG

Hiermit erkläre ich, dass ich die vorliegende Arbeit selbständig verfasst und keine anderen als die von mir angegebenen Quellen und Hilfsmittel benutzt habe.

Ferner erkläre ich, dass ich nicht anderweitig mit oder ohne Erfolg versucht habe, eine Dissertation einzureichen.

Tübingen, 7. Juli 2003

(Michael Marks)